Modelling of engine transmission systems for heavy vehicles the differential compound engine versus the turbocharged engine

Rezaeian, M.

Award date:
1988

Awarding institution:
University of Bath

MODELLING OF ENGINE TRANSMISSION SYSTEMS FOR HEAVY VEHICLES THE DIFFERENTIAL COMPOUND ENGINE VERSUS THE TURBOCHARGED ENGINE

Submitted by

M. REZAEIAN

for the degree of Ph.D.
of the University of Bath
1988

M. Rezaeian

ProQuest LLC
789 East Eisenhower Parkway
P.O. Box 1346
Ann Arbor, MI 48106-1346

DEDICATED

To My Mother

B. MIRZAKHANI

ACKNOWLEDGEMENTS

The author would sincerely like to acknowledge the help, care, advice and patience he has received during the course of this work.

Most of his appreciation and gratitude is directed towards his supervisor, Professor F.J. Wallace, who has shown extraordinary encouragement, sympathy and guidance and without whose help and endurance, the author could not have written this thesis.

The author also extends thanks to :

Dr. M. Wilson for his advice, help and encouragement throughout the work on computer programs and programming.

Dr. S.J. Charlton for his help in providing and running the computer program SPICE.

Dr. D. Prince and Mr. J. Hall for their guidance in the experimental part of the project.

Mrs. H.J. Ford for typing the thesis.

Finally, it would be an incomplete acknowledgement if the author did not express his appreciation to his Mother who, despite ill-health, withstood the separation from her son during a critical period.

C O N T E N T S

2. SURVEY OF THEORETICAL WORK

(page: 52-95)

SYMBOLS

a	turbine nozzle angle
A	frontal area of truck
A_c	the surface area on the coolant side of the wall
A_g	" " " " " gas " " " "
bmf	bypass mass flow
bhp(1)	(intended) engine brake power
C_1, C_2	shape factors in fuel burning rate equation
c	the stage terminal velocity at the turbine rotor entry
cgr	overall compressor gear ratio in the DCE
cgr'	sun to compressor step up gear ratio
C_m	mean piston linear speed
C_p	gas specific heat in constant pressure process
C_v	" " " " " volume "
d	pipe diameter
dN	derivative of shaft speed
dp	pressure drop across cooler
$\dot{E}_{fr}$	heat of the piston friction transferred to the liner
egr	basic epicyclic gear ratio
emf	engine air mass flow
enf	air flow through cooler
esl,esm	mean engine speed (intended, updated)
et	mean engine torque
F	force, equivalence ratio
f	fuel air ratio
f_c	cooler pressure drop coefficient
f_d	coefficient of air drag friction
f_r	coefficient of rolling friction
f_p	pipe pressure drop coefficient
ffrate	fuel flow rate
f_1	premixed burning function
f_2	diffusion " "

g	gravity acceleration
h	coefficient of heat transfer in convection
h_c	h on coolant side of the wall
h_g	h on gas side of the wall
h_{03}	stagnation enthalpy at inlet of turbine
h_{04}	" " " exit " "
HP	power
I	mass moment of inertia
ID	ignition delay
k	correction speeding-up factor
K	conduction heat transfer coefficient
K_w	K for wall material
K_1, K_2	shape factors in fuel burning rate equation
k_1, k_2, k_3	constants in Chen and Flyn friction model
ℓ	pipe length
m	trapped mass in a control volume
$\dot{m}_{sc}$	scavenge air flow (during overlap period)
$m_f(t)$	fuel mass (kg) at N.D. crank angle t
$\dot{m}_f(t)$	fuel mass burning rate (kg/$\dot{C}$A) at t
$M_f(y)$	N.D. fuel burnt at t
$\dot{M}_f(t)$	N.D. fuel burning rate at t
$\dot{m}$	gas flow rate (used with appropriate suffix)
m_t	total fuel mass (kg) per shot
m_{man}	mass of gas inside a manifold
N	speed (used with appropriate suffix)
N_0	engine speed at governor set point
N_{FL}	" " " full load at a fixed rack position
N_{NL}	" " " no load " " " " "
oge	output shaft gear efficiency
oge'	" " overall transmission efficiency

ogr	output shaft overall gear ratio
ogr'	planet carrier to output shaft step up gear ratio
ogft	output shaft static friction torque
P	pressure
P_{01}	stagnation compressor inlet pressure
P_{02}	" " outlet "
P_{03}	" turbine inlet "
P_{04}	" " outlet "
P_6	cylinder pressure at the start of blowdown
P_{ID}	" " during the delay period
P_{inl}	inlet manifold pressure (boosted)
P_{man}	manifold pressure
P_{max}	maximum cylinder pressure
Q_{cal}	fuel calorific value
QLF	engine heat loss factor input to program 'EMAT'
$\dot{Q}$	heat flow rate through a surface
R	thermal resistance (used with numeric suffixes)
R	gear pitch radius (used with alphabetic suffixes)
R_{air}	air gas constant
R_e	Reynolds number
R_{tyre}	dynamic tyre radius
RHM	pseudo manifold volume ratio for pulse model input to program 'EMAT'
r	gear ratio
r_b	back axle ratio
r_g	gearbox gear ratio
r', r"	new rack position during a transient
r_i, r_f	initial and final rack position
r_{min}, r_{max}	minimum and maximum rack position
rb_1, rb_2	boost ratios used for the boost compensator operation

$r_{overspeed}$	compressor overspeed ratio
rcl, rcm	mean boost pressure ratio
s_d	slope of speed droop line
T	temperature
T_1, T_2	predictor, corrector temperature
T_{01}	compressor inlet stagnation temperature
T_{03}	turbine inlet stagnation temperature
T_{04}	turbine exit stagnation temperature
T_6	cylinder temperature at the start of blowdown
T_c	coolant temperature
T_{cw}	engine cooling water temperature
T_{co}	engine cooling oil temperature
Tg	mean temperature of in-cylinder gases
T_{ID}	Tg during ignition delay
T_{inl}	inlet manifold temperature (boosted)
T_p	piston node temperature
T_{sc}	mean surface temperature on the coolant side
T_{sg}	" " " " " gas "
T_{man}	manifold temperature
T_{gov}	governor time constant
t	time (also N.D)
tge	turbine gear efficiency
tge'	turbine overall transmission efficiency
tgft	turbine static friction torque
tgr	turbine gear ratio
tt	turbine torque
u	peripheral velocity of the turbine rotor tip
$\bar{u}$	air flow mean velocity
v, V_{veh}	vehicle speed
v_o	head wind velocity

W	weight
$\dot{W}$	power (used with appropriate suffixes)
$\dot{W}_{Ltot}$	total gear losses
xk	combustion rate factor
x_L	fraction of the piston heat transferred to the liner (input to program 'SPICE')
x_{ang}	correction factor for turbine nozzle angle
x_{tmf}	control factor for turbine mass flow

SYMBOLS - Greek

α_N	turbine nozzle angle
α	combustion phase proportionality factor
β	combustion phase proportionality factor
γ	road slope angle
Δ	nominal burning duration (deg CA)
Δp	pressure drop
Δ	increment (in general)
$\Delta\psi$	increment of crank angle position
η_c	total to static compressor efficiency
$\eta_{B.th}$	engine brake thermal efficiency
η_{mech}	engine mechanical efficiency
η_{trans}	transmission efficiency
η_{vol}	volumetric efficiency
θ_i	crank angle at the start of comhustion
ρ	air density
σ	percentage decrease in engine speed from no load to full load condition at constant accelerator pedal position
τ	torque (used with appropriate suffixes)
ψ	angular crank position
ω	angular shaft speed

SUFFIXES

A	annulus
COMP	compressor
CYL	cylinder
C	coolant
D	drive train
e	exhaust
ENG	engine
EXH.ST	exhaust manifold storage
f	fuel
F	friction
i	inlet
in	in
INL.ST	inlet manifold storage
g	gas side
hg	head gas side
j	liner zone no. in 'SPICE'
ℓg	liner gas side
L	load
out	out
o/s	output shaft
pg	gas side of piston
P	planet
PC	planet carrier
S	sun wheel
tract	tractive
TURB	turbine

ABBREVIATIONS

AFBR	apparent fuel burning rate
AHRR	apparent heat release rate
ATDC	after top dead centre
BMEP	brake mean effective pressure
BSFC	brake specific fuel consumption
BTDC	before top dead centre
CA	crank angle

CI	compression ignition
DI	direct injection
EVC	exhaust valve closure
EVO	exhaust valve opening
FMEP	friction mean effective pressure
GIMEP	gross indicated mean effective pressure
IC	internal combustion
ID	ignition delay
IMEP	indicated mean effective pressure
ISFC	indicated specific fuel consumption
IVC	intake valve closure
IVO	intake valve opening
L10	Cummins L10 Diesel engine
LTC	limiting torque curve
ND	non-dimensional
NIMEP	net indicated mean effective pressure
PT	pressure-time
PMEP	pumping mean effective pressure
P-V	pressure-volume
T/C	turbocharged
TDC	top dead centre
TL11	Leyland TL11 Diesel engine

LIST OF FIGURES

CHAPTER ONE

CHAPTER TWO

CHAPTER THREE

CHAPTER FOUR

CHAPTER FIVE

CHAPTER SIX

CHAPTER SEVEN

CHAPTER EIGHT

SUMMARY

The thesis describes a predominantly theoretical investigation of the operating characteristics of a high output Diesel engine both in the form of an aftercooled turbocharged engine and a differential compound engine (DCE). Two types of programming based on a rapid prediction technique and a detailed step-by-step technique are applied to each of the two engine configurations.

Chapter 1 covers an overview of some of the requirements demanded for a modern power plant appropriate to a heavy goods vehicle. In Chapter 2, the programs and programming techniques applied in the course of the investigation are described in some detail.

Chapters 3 and 4 mainly deal with calibration of the program submodels to match the steady state engine performance predictions against the relevant initially available experimental results for the particular engine under investigation (Cummins L10 engine) in its aftercooled turbocharged configuration.

Chapters 5 and 6 are concerned with the steady state performance predictions of the same engine but in its DCE configuration, using the results of calibration in Chapters 3 and 4 respectively. In Chapter 6, the results are prepared by implementing a detailed step-by-step program and used as a more reliable prediction to validate what is prepared in Chapter 5.

Finally, the transient performance of the DCE compared with its turbocharged engine counterpart under the same type of load (in accelerating a 65000 lb truck from rest) is demonstrated in Chapter 7.

The existing test bed for the DCE incorporates a Leyland 520 Diesel engine. The corresponding experimental results are used to evaluate analytical predictions and this is covered in Chapter 8. Conclusions with respect to the programming techniques and comparison between the two configurations of engine as well as some recommendations for further work are presented in Chapter 9.

CHAPTER ONE

INTRODUCTION

1.1 GENERAL REQUIREMENTS FOR ENGINE-TRANSMISSION SYSTEMS FOR HEAVY GOODS VEHICLES

1.1.1 Alternatives for Tractive Power Plant

From a technical standpoint, the ideal power plant should be self-starting and should produce maximum torque at zero speed, with torque dropping to zero at the maximum speed at which the engine will turn. The engine should require only a minimum of power-consuming auxiliaries (fan, waterpump, transmission, muffler, etc.) and should achieve very nearly the same specific fuel consumption or conversion efficiency under conditions of low speed and heavy load as it does at high speed and no load. Finally, it should produce smooth, vibrationless power in the form of rotary motion, preferably transmitted directly to the wheels (to avoid the "universal" gears).

A change in automotive vehicle propulsion technology would be accompanied by changes in cost (initial cost and maintenance), operation and complexity, and performance. 'Performance' covers a multitude of subtleties, not merely power available on demand - that is, responsiveness acceleration, and speed. Since one can only rate power plants with respect to any given figure of merit if all other factors are equal, it is extraordinarily difficult to compare the various systems because they differ in very fundamental ways. However, they must be judged in the light of the existing literature, which is notably deficient in meaningful comparisons between different kinds of power plants, at least for automotive applications.

As was stated, for vehicular applications, the ideal performance characteristics of a power plant are constant power output over the full speed range. Consequently, the engine output torque varies with speed hyperbolically as shown in fig. 1.1. This will provide the vehicle with high tractive effort at low speeds where demands for acceleration, drawbar pull, or grade climbing capability are high. There are power plants that have power-torque-speed characteristics close to the ideal for vehicular applications, such as series-wound electric motors and

steam engines. The internal combustion engine has less favourable performance characteristics and can only be used with a suitable transmission. Despite this shortcoming, it has found the widest application in automotive vehicles to date, because of its relatively high power to weight ratio, good fuel economy, low cost and operational flexibility.

In addition to the continuous search for improving the efficiency, power-to-weight ratio, size and economy of vehicular powerplants, considerable emphasis has been placed on the control and reduction of undesirable exhaust emissions in recent years. Various technological options including further modification of the internal combustion engine are being investigated. In general, the two basic approaches to reducing undesirable emissions are to prevent them from forming and to remove them from the exhaust once formed.

Alternatives to the reciprocating internal combustion engine may be considered as (ref. 1)

i) Gas turbine engines
ii) Rankine-cycle external combustion engines
iii) Non-condensing external combustion (Stirling-cycle) engines
iv) Electric propulsion systems
v) Hybrid power systems (such as a combination of the internal combustion engine and electric propulsion).

The gas turbine has several advantages as a vehicular power plant. It has a favourable power to weight ratio and can be used with a wide range of fuels. The carbon monoxide and hydrocarbon in the exhaust of a gas turbine are lower than those of an equivalent gasoline engine. There is evidence to suggest that nitrogen oxide emissions could also be reduced. The gas turbine is, however, not without drawbacks as an automotive power plant. The greatest disadvantage is its low efficiency and poor fuel economy under idling or part load conditions which constitute a significant portion of the operation of automotive vehicles.

The Rankine vapour-cycle external combustion engine has torque-speed characteristics close to the ideal. Coupled with its high overload capacity, the Rankine-cycle engine would eliminate the need for a

transmission. It can use a wide range of hydrocarbon fuels and yet undesirable emissions including nitrogen oxides are very low. Among the disadvantages of this kind of power plant are the time required to put the engine into operation and relatively poor power-to-weight ratio.

The Stirling-cycle engine utilizes alternate heating and cooling of the working medium, such as compressed helium or hydrogen gas, at constant volume to develop useful mechanical work. To date, it has rather poor power-to-weight ratio and is mechanically complex. The emission characteristics of the Stirling engine are, however, extremely good. It also has excellent performance characteristics at higher speeds, which suggest its potential value in a hybrid power system for automotive vehicles where it could run continuously under optimum operating conditions.

Since the internal combustion engine is still the most commonly used power plant in automotive vehicles to date, it is appropriate to review the basic features of its characteristics that are essential to the prediction of vehicle performance. Representative characteristics of a gasoline engine and of a Diesel engine are shown in figs. 1.2 & 1.3 respectively. The internal combustion starts operating smoothly at a certain speed (the idle speed). Good combustion quality and maximum engine torque are reached at an intermediate engine speed. As speed increases further, the mean effective pressure decreases because of growing losses in the air induction manifolds, and the engine torque also declines. Power output, however, increases with increase of speed up to the point of maximum power. Beyond this point, the engine torque decreases more rapidly with increase of speed. This results in the decline of power output. In vehicular applications, the maximum permissible speed of the engine is usually set just above the speed of the maximum power output.

1.1.2 The Diesel Engine for Truck Application

The most important factor in the selection of an appropriate type of engine for commercial vehicles is the operating cost. The Diesel engine has continuously and steadily become dominant in the heavy goods transportation. This dominance is primarily due to the outstanding fuel

economy of the Diesel and, to a smaller extent, to its somewhat lower maintenance costs. Also, the cost of Diesel fuel has been lower than the cost of gasoline but the situation may change as markets change.

The other factor which is of great importance in the application of the Diesel engine in this field is the careful matching of the engine and transmission to one another as well as to the specific vehicle application; otherwise, the total package may be commercially unattractive. There are many considerations and compromises in selecting these components and proper matching is not a simple matter.

The commercial vehicles can be classified according to g.v.w (gross vehicle weight) and/or application severity. It is customary to characterize vehicle engines by the terms heavy, medium and light duty to indicate the severity of service required of the engine. The weight of the loaded vehicle is one, but only one, consideration in determining whether the vehicle application demands a heavy, medium or light duty engine. Table 1.1 gives a more detailed listing of important factors (ref.2).

Since heavy-duty engines have higher initial costs there is a natural tendency to choose an engine designed for less severe use. On the other hand, the horsepower and life required for the application may dictate a heavy duty engine. The decision as to the type of application is not trivial. It involves considerable judgement and knowledge of the proposed application and must be thoughtfully made if the selection is to be economical from the standpoint of first cost maintenance, fuel consumption and life, that is, total operating costs.

A comprehensive study of the application of both gasoline and Diesel engines shows that Diesel engines are routinely installed where both medium and heavy duty applications are required, although in medium duty applications there is a trade-off between using a Diesel and gasoline engine.

1.1.2.A <u>High Specific Output and Low Cost</u>

To improve the payload capacity of a truck of a particular gross weight,

the dry (unladen) weight of the truck has to decrease. Although use of light weight material for the chassis and body is a means of achieving this end, light weight power plant can also make a contribution.

Therefore, increased engine output is not an objective in itself. It has two main purposes:

(1) increased power to weight and power to bulk ratio in order to install more power in a given space (or to reduce axle load thus increasing payload).

(2) Reduced costs per horsepower to be more commercially attractive.

The latter argument is as important as the first, because it is the only means of offsetting the high cost of labour. If the total swept volume of a Diesel engine is kept constant, output can be increased by :

- Increasing rotational speed
- Increasing BMEP

It is not rotational speed but piston speed which is a limiting factor for engine design. As stroke to bore ratio is more or less fixed within a certain range, rotational speed can be increased without affecting piston speed only by using smaller cylinder dimensions. For operational reasons, the number of cylinders is somewhat restricted so that increased rotational speed will not be the most effective means of achieving higher power.

The other alternative, namely increased BMEP, is therefore the area where most research and development work is concentrated. Higher BMEP means more fuel must be burnt, but this necessitates an increased combustion air mass flow rate. A higher air intake pressure results in a higher maximum pressure within the cylinder. With existing engine designs max. pressure is limited to approx. 150 bar (limited firing pressure to give good reliability).

This value can only be kept constant when combustion air flow is increased, by reducing the compression ratio, or by retarding injection. To illustrate, the weight of a typical naturally aspirated engine is approx. 4.4 kg/hp compared with the turbocharged version of the same engine which is 3.6 kg/bhp, an experimental engine with a lower

compression ratio has a weight of 2.8 kg/bhp, and with aftercooling of 2.5 kg/bhp (Ref. 3).

A low compression ratio engine, however, is normally difficult to start under adverse conditions and idling tends to be erratic due to incomplete combustion. During recent years, engine manufacturers throughout the world have evolved different methods to overcome these starting and idling problems; however, the systems used so far have been rather complex.

For example, in one method, with the charge transfer system, a non-firing cylinder is used to increase the pressure of its opposite number in the other bank (in vee bank arrangement). By means of an externally controlled valve, compressed air is transferred via a small pipe to the corresponding cylinder. Thus the pressure in the 'power' cylinder is increased to enable proper starting (ref. 4).

Another operational problem connected with high mean effective pressure is the comparatively narrow range of operation which can be allowed due to turbocharger matching.

1.1.2.B Good Engine Torque Back Up and Tractive Effort

A torque curve that rises as speed falls reduces the number of gearbox ratios and gear changes required. Such a torque curve is said to have good 'torque back up'. Torque back-up may be defined as :

$$\frac{\text{maximum torque - torque at maximum speed}}{\text{torque at maximum speed}}$$

With good torque back up, the vehicle will benefit from high torque at low speeds to provide a margin for acceleration and to allow the vehicle to lug up very steep hills. There are marked differences in percent torque rise and percent change in engine speed between different engines. It is misleading merely to compare the power output of engines at rated speed. However, if two engines have the same rated horsepower but different torque back up they will not have the same horsepower at lower engine speeds and therefore, will not necessarily have the same performance in trucks with their variable engine speed application.

As will be seen in fig. 1.7 most Diesel engines have their torque peak at about two-thirds rated engine speed. Engines designed with an unusually high percentage torque rise (over 20%) are called power torque or high torque engines and typically have a greater operating speed range between rated and peak torque points. The tractive effort needed by vehicle is quite far from what a Diesel engine provides, fig. 1.13. In order to generate a continuously increasing tractive effort to zero vehicle speed, a multi-ratio gearbox and clutch is required. This transforms engine torque into a cascade curve, fig. 1.10 consisting of a series of mini-torque curves, each one a function of the overall drive-line ratio in that gear. The ideal would thus be a continuously variable transmission (CVT), but until it is applicable in practice, the multi-ratio gearboxes will continue to be used for the foreseeable future.

As is discussed in the section on multi-ratio gearboxes, Section 1.2.3A, a wider engine speed range with greater torque back up leads to fewer discrete ratios and provides a better driveability, reduced journey time, and hence better system economy.

1.1.2.C Good Fuel Economy

(A) General

In this era of energy uncertainty, the overall efficiency of every major fuel consumer has to be taken into careful consideration; whether it be production of goods, home heating and cooking or transportation. Clearly, automotive transportation is one of the most important factors in the energy use equation. Nowadays, transport vehicles and prime movers are considerably better than those of the past. These include safety, ride, handling, interior noise level, comfort, emission performance, and of course, fuel economy. Many factors are responsible for the recent rapid improvement in fuel economy, and these same factors will continue to be important in the dramatic fuel economy improvements expected in the near future. These factors include : tyre improvements, reduced aerodynamic drag, the application of new lightweight materials, more efficient automotive structures and greatly improved engines and total drive trains.

In each component area, whether engines, transmissions or tyres, the rate of progress is slowing as we approach the ultimate limits for a given technology. Very early on in the development of engines, for example, rather rapid progress was made in improving both power and fuel economy. However, with maturing technology the incremental gains have slowed dramatically as the fundamental limits are approached.

In many instances, the theoretical limits of performance are difficult to define. Certainly, this is true of aerodynamic losses. In the internal combustion engine, however, for a given set of operating parameters such as compression ratio and fuel-air ratio, the laws of thermodynamics place a rather specific limit on thermal efficiency.

Fuel economy of vehicles is substantially influenced by performance targets and driving cycle by which they are rated. Power-train optimization for fuel economy, disregarding performance, can result in poor customer acceptance. Trade-offs must be made between fuel economy, performance, and driving cycle ratings. Vehicle performance is rated according to :

a) acceleration
b) gradeability
c) maximum speed
d) driveability

In the first place, there are two limiting factors to the performance; one is the maximum tractive effort that the tyre ground contact can support, the other is the tractive effort that the engine torque with a given transmission can provide. The smaller of these two will determine the performance potential of the vehicle.

Gradeability is related to fuel economy because it establishes limits for the overall drive-train ratio coverage. Gradeability refers to the capability of the vehicle to climb hills. A grade capability is established as a minimum on which the vehicle must accelerate upwards from rest in both forward and reverse gears. This grade is typically 25% for trucks.

The desired maximum speed of the vehicle relates to fuel economy in that

it will determine the engine horsepower and the final drive ratio.

Driveability is based upon a subjective jury evaluation of the vehicle, which rates power-train response, noise and vibration.

Returning to engine factors for improving fuel economy, a brief description of these is given below:

B. Means of reducing engine losses

The partially reducible losses are divided into closed period, open period, including exhaust blowdown and pumping losses, and mechanical friction. The closed period losses can be further separated into combustion loss and heat loss. The combustion loss is associated with the inability to burn instantaneously, the heat loss is related to the heat transfer primarily during combustion and expansion.

Of the open period losses, the exhaust blow down loss is the small loss in useful work because of early opening of the exhaust valve. Experiments have shown that the total effect of eliminating these three cycle losses is an efficiency gain of less than 20%. The so-called "pumping loop" associated with the exhaust and intake processes, causes additional piston work in induction of the fresh air and discharging the exhaust gases against the various flow resistances in the exhaust system. This is called the pumping work.

The difference between the work output and the work delivered to the piston face (indicated work) is called the mechanical friction which is mainly composed of piston ring rubbing, bearing and gear drive losses.
All factors are being studied by engine designers in their attempt to improve efficiency and fuel economy, and one of their most important new tools in this quest is the growing availability of electronic controls. This technology is permitting a greater degree of system optimization than in the past. A host of other technologies related to fuel preparation, valve timing, combustion chamber shape, intake and exhaust manifold design as well as many other aspects are under continuous investigation to provide fuel economy improvements.

1.1.2.D Reliability

The time needed for maintenance is an important factor, since labour costs are becoming increasingly expensive. Also, we must accept that the quality of labour varies greatly throughout the world. In designing a modern Diesel engine, both of these factors must be recognized. There is a direct relationship between servicing and reliability and the former must be considered part of the cost of reliability.

Each engineer may have his own view of reliability but perhaps the following formal definition will summarize these views :
"Reliability is the ability of an item or system to perform a required function under stated conditions for a stated period of time, expressed as a probability".

Reliability R(t) is:

$$= \frac{\text{Number of items surviving at time 't'}}{\text{Number of items present at start of test (i.e. t=0)}}$$

Planning for reliability is an important element of new product policy. In other words "get the specification right for the job it has to do". The potential reliability of a product is created during its design, development and test period. An accurate assessment of "in-service" vehicle and engine reliability is essential, if the new product planning base is to be sound. This reliability assessment is best conducted by systematic analysis of operators' records on earlier, related products.

Failures are analysed into three categories:

i) those failures which totally disable the vehicle/engine, that is, critical items.

ii) those failures which disrupt the operation of the vehicle/engine, but do not disable it, that is, major items

iii) those failures of a minor nature which do not disrupt the operation of the vehicle, but can be repaired at some future convenient time.

Having established the key reliability target for an engine system, the next crucial stage in achieving the new product reliability targets is

the design and development stage.

During the development phase, combustion performance, system performance (e.g. cooling), structure and dynamic performance (e.g. cylinder block, head, main and gudgeon pin bearing), are closely monitored against their individual performance targets.

Finally, in the validation stage, as indeed during the later stages of the development phase, engines are subject to overstressed conditions to
a) reduce testing times, and
b) to verify an acceptable safety margin
which will accommodate some deviation in either production or service or both.

During the development and validation test phase records of different failures will be obtained for each engine sub-system or component.

At that stage, when the items are beginning to wear out, the failure rate increases with time. From the data obtained and studied at this stage, one could have a correct judgement about the reliability of a new designed product. The final validation test for reliability usually consists of the following, for a completely new design :

- bench tests of a certain period of time mixed cycle
- bench tests of a certain period of time thermal cycles
- bench tests of a certain period of time overload and overspeed m/s
- road test of say 60,000 and 200,000 km

However, confidence in new engine-transmission systems is obtained by accelerated endurance testing which incorporates periods of running with 5 per cent overload and 10 per cent overspeed, and periods with high coolant temperatures, alternatively thermal shock cycles caused by admitting cold water to the hot cooling system. Such treatment can be expected to uncover any weakness within a much shorter time than normal service.

Reliability of high specific output engines is dependent upon the durability of the highly loaded engine system parts. With the increased output being achieved by increased brake mean effective pressure, the

power producing or supporting parts are subjected to higher temperatures and pressures. These parts include : the cylinder head, cylinder head to liner seal, valves, piston, piston ring, cylinder liner, cylinder jacket, connecting rods, crankshaft, bearings, main frame, turbine and compressor shafts and impellers, and all the associated fasteners. It is these parts that receive attention during the up-grading process.

As a result of the increased cost and the need to conserve fuel, improving fuel economy has become a major development objective inevitably in a heat engine some of the factors which can be altered to improve fuel economy also affect durability, such as increasing peak cylinder pressure, BMEP, operating temperatures, etc.

In the future the continued demand to improve fuel economy can be expected to result in higher component temperatures. This becomes very evident when the operating characteristics of turbo-compounding and adiabatic systems are considered. The introduction and success of these systems will depend on providing durability to ensure reliability under the associated extreme operating conditions.

Diesel engine power range covers a very wide field. In a classification, the engines most suited to traction purposes may be categorized into four classes. The reliability needed for different types of heavy commercial vehicle power plant may be interpreted from major overhaul life as listed in table 1.2, (ref. 5).

1.1.2.E Acceptable Emission Characteristics

Automotive engines are subject to legislation intended to make them environmentally acceptable to the general public. The major legal requirements for truck engines are related to exhaust smoke and gaseous emissions, and vehicle noise. British Standard AU 141a 1971 established smoke levels for full power operation over a speed range from rated speed down to 45 per cent of that speed or 1000 rev/min., whichever is the bigger.

In Diesel engines, a number of features in the fuel injection system contribute to clean combustion. High rates of injection enable the fuel

to be injected in a short time span, as near as possible to the ideal timing. In this way, smoke is minimised. A second important feature is the use of "controlled flow" injectors. After manufacture to the normal close tolerances, all injectors are finally quality checked to ensure that they give the correct flow within tight tolerances.

There is no current European emission legislation for truck engine gaseous emission, although one was in preparation for introduction in 1984/85. However, there are two standards for gaseous emission levels in the U.S.A., the Federal standard and the California standard (ref. 6). These tests use a complex routine of tests simulating 13 modes of operation and the specific weight of gaseous emissions is recorded and must meet the standards. The elements of gaseous emission are unburnt hydrocarbons (HC), carbon monoxide (CO) and different nitrogen oxides (NO_x). It has been found that in Diesel engines, when HC decreases, NO_x increases and vice versa. Thus regulations for HC and NO_x are typically expressed as the sum of NO_x and HC (in terms of grams/hp.hr).

There are many sources of noise in a vehicle engine, viz. fan, exhaust, air intake, tyres, body etc. Most noise measurements are made during "drive by" at a distance of 50 ft (~15m) under specified speed and loading conditions and are expressed in units of dBA, (ref. 7). Although the subject is quite complex, one should always consider that the engine is the most important source of vehicle noise.

Smoke emission

Fig. 1.4 depicts the current legislation in Europe, (ref. 8), ie:

BS AU 141a 1971

The figure also shows smoke level in Hartridge units, for a bus engine. In practice smoke or soot (carbon) particles are formed when air/fuel mixtures are less than about 130% of stoichiometric, when local combustion temperatures are high enough to crack the fuel, yielding acetylene and near pure carbon molecules. These can be reburnt during the expansion cycle in the excess air. Perfect mixing and combustion cannot actually be achieved; hence excess air is required to ensure that all fuel is burnt efficiently.

Competitive engines in the automotive classes considered will usually have smoke levels 15-20 Hartridge units below the stated legislation, and in most cases smoke is barely visible.

Turbocharged engines are still smoke limited between maximum torque and low idle and are still vulnerable to acceleration smoke penalties despite further efforts to reduce turbocharger lag. The following factors will reduce smoke:

i) advanced injection timing

ii) lower compression ratios

but the trade off against (i) and (ii) could be increased combustion noise due to increased ignition delay. Also lowering compression ratio below 10 raises difficulty in the engine starting or part load operation and high SFC over the power range.

It is expected that future turbocharged engines equipped with adequate sensors will achieve enhanced engine smoke limited performance between idle (~500 rpm) and peak torque.

Engine mounted sensors will control injection rate to maintain an acceptable in-service smoke performance. This will penalise the poorly maintained Diesel engine and thus the operator.

Idle smoke

There is also a tendency for blue/white smoke to occur during long periods of idle and for considerable blue/black smoke to occur on pulling away. This results from incomplete combustion of fuel and lubrication oil during idling, some of which appears in the exhaust as a fine spray and is visible as blue/white smoke.

Two separate approaches have been applied to alleviate this problem, both successful. In the first place the compression ratio should be as high as possible without resulting in excessive maximum cylinder pressure. For highly turbocharged engines the compression ratio is of the order of 14:1 and for charge cooled engines somewhat lower to keep P_{max} limited to approx. 125 bar.

The first approach has been to recognise that at idle delayed injection timing improves the white/blue smoke very considerably. Normal dynamic timing for power is approx. 24° BTDC but the optimum timing for smoke free idling is approx. 14° BTDC. A cost effective and simple solution has been found within the fuel pump itself. Using such a fuel system design, the closure of the injection port is controlled at the beginning of pumping and end of injection timing is fixed. Therefore the timing varies with rack opening and is retarded by approx. 10° at idle fuelling.

On charge cooled engines, although the compression ratio is a little lower, air temperature rises in the charge cooler under idle conditions. Since the charge cooler is circulated with water from the engine jacket at say, 80°C it acts as a cooler for the boost air, typically at 160°C leaving the turbocharger, when the engine operates on full rack, but warms the intake air at idle when the turbocharger is contributing very little. This behaviour reduces idle smoke in the charge cooled turbocharged engine.

Noise

The robust construction, low maximum engine speed, and turbocharging favourably influence noise level, and this may prove to be a vital factor since a legislative proposal concerning maximum noise has been announced (ref. 7).

The characteristically harsh noise of the Diesel engine which is caused by the instantaneous combustion of a large part of the fuel injected during the ignition delay is considerably reduced with a higher brake mean effective pressure, since the higher pressure and temperature brought about by turbocharging reduce the ignition delay. A higher brake mean effective pressure gives a smaller engine for a given output, and this in turn implies a smaller area of the noise-transmitting surfaces which simplifies the insulation of noise in the design of the vehicle. A considerable damping of induction and exhaust noise is obtained by turbocharging; the turbocharger itself does not suffer from noise problems.

1.1.3 Engine Selection Process

The engine selected must meet the severity of service if reasonable life and maintenance costs are to be attained. Other considerations in the engine selection process are :
An engine with sufficient horsepower is required to provide the specified performance, i.e. to achieve and maintain acceptable road speed under the conditions at which the truck will operate. Sufficient power must be provided to cover accessories as well as drive-train losses. Fig. 1.5 indicates a typical order of magnitudes of power consumption by various accessories. Operating conditions must include road grade, wind and altitude conditions. At cruising speed, (about 10% below maximum speed), good fuel economy should be achieved.

The engine must also have sufficient torque to start the vehicle under the most severe conditions at which the truck will operate as well as to achieve good gradibility. Gradibility is normally based on the maximum torque of the engine, while startability is normally based on torque at clutch engagement, i.e. in the 800-1000 rpm range.

The engine selected must be ecologically acceptable under all operating conditions - it must not put out unacceptable exhaust emissions or noise while providing the performance demanded of it. The engine demands certain services from the vehicle. Since the vehicle must provide torque multiplication, the engine and transmission must be considered together. The vehicle must also provide cool, clean air, oil, fuel and water, proper control of the temperature of the engine, removal of exhaust gases, adequate support for the engine, etc.

1.2 CONVENTIONAL SYSTEMS

1.2.1 Supercharging the Diesel Engine

Supercharging is defined as the pre-compression of the charge outside the working cylinder. The charge is thus compressed both outside and inside the cylinder. The purpose of supercharging is to increase the charge density and thereby the power above that of the naturally aspirated engine. For all internal combustion engines operating at a given air/fuel ratio, the indicated power is roughly proportional to the air consumption. As a general rule, increasing the indicated power of an engine with substantially constant friction losses leads to improved mechanical efficiency. It is thus apparent that boosting or supercharging in which the intake air density is increased gives the prospect of enhancing both the specific power output and the specific fuel consumption of a given engine. The engineering problem then becomes that of providing the boost in a manner suitable for the engine type and application without unacceptable penalties.

Improved specific power

As stated above, the increased air intake density allows increased indicated power while the frictional losses increase only slightly and thus improved brake power is also possible. Thus an engine of a given swept volume operating at a given speed will yield higher specific brake power.

Improved specific fuel consumption

This is achieved as a direct result of the enhanced brake power without the penalty of excessive friction losses. If the engine is running at the same or at a higher air/fuel ratio the indicated specific fuel consumption will remain substantially unchanged or slightly reduced while the improved mechanical efficiency already referred to automatically brings with it an improved brake specific fuel consumption.

Reduced smoke

Most boost systems can be arranged to provide excess air at full load and speed and thus it is frequently possible to arrange for the engine to run at a higher air/fuel ratio and thus give lower smoke emission than a naturally aspirated engine.

Increased torque back up

In order to obtain the maximum potential from a naturally aspirated engine attempts are usually made to match the fuelling curve to the air consumption of the engine so that it is always running close to its smoke limited air/fuel ratio. As a result, the torque curve of a naturally aspirated engine is directly related to the volumetric efficiency and the associated fuelling curves. In the case of a boosted engine if sufficient torque can be made available at the lower speed, the fuelling can be reduced at higher speeds, so that improved torque back up is obtained while the engine still gives adequate rated power.

Reduced noise

Boosting generally gives both a reduced delay period and smoother initial combustion patterns so that the noise generating forces within the engine are reduced. An immediate consequence of this is that boosted engines can be developed to produce significantly lower drive-by noise levels than naturally aspirated engines.

Reduced emission

The ability to run at higher air/fuel ratios at rated conditions means that a boosted engine can be adjusted to give lower hydrocarbon emissions and the reduced delay period allows injection retard so that reduced NO_x emission can also be obtained.

Advantages and disadvantages of supercharging summary

Hence for a given output power, the advantages of supercharging could be summarised as follows:-

(1) Reduced space requirements (fewer cylinders, shorter engine)
(2) Lower weight, better specific weight
(3) Better efficiency with exhaust-turbocharging (flatter fuel consumption characteristics)
(4) Lower cost per unit output, in particular for larger engines
(5) Smaller radiator: lower percentage heat loss
(6) Exhaust noise reduction by the exhaust turbine
(7) Less derating with reduced ambient air density
(8) Lower emissions with certain controlled combustion processes.

The disadvantages of supercharging are :

(1) Greater mechanical and thermal loads

(2) Greater complexity

(3) Poor acceleration only with turbocharging

1.2. 2 Classification of supercharging systems

Supercharging systems can be classified according to :

i) The method of driving the compressor

ii) The design of the compressor

iii) The type of connection between the supercharging unit and the engine, or the type of power transfer

iv) The type of engine

(i) Compressor drive

a) externally powered (auxiliary engine, electrical motor) : external supercharging

b) powered by the engine with drive from crankshaft : mechanical supercharging

c) powered by exhaust-driven turbine : exhaust turbocharging

d) no compressor, but compression-wave supercharging with vaned rotor (COMPREX)

(ii) Compressor design

a) positive displacement type : linear or rotary piston such as Roots blower, screw compressor

b) flow type : aerodynamic compressor of radial, axial or mixed flow design

(iii) Coupling and power transfer

a) compressor connected to engine crankshaft, power drive from engine shaft, no turbine : mechanical supercharging

b) compressor connected to turbine, free-running and mechanically separate from engine : exhaust turbocharging

c) compressor, turbine and engine shaft coupled mechanically : compound engine

d) compressor and engine coupled mechanically, power drive from turbine shaft : gas generator

(iv) Type of engine

a) petrol engine or diesel engine

b) four-stroke or two-stroke engine

1.2.2.A Exhaust driven superchargers (Turbochargers)

At present, virtually all boosted diesel engines use the turbocharger as the means of obtaining the required intake air density. A turbine placed in the exhaust gas flow is connected directly to a compressor which can thus supply the increased density intake air to the engine. The compressor is almost invariably of the centrifugal type but the turbine may be either an inward flow radial or an axial flow type depending upon the size and application. Most smaller Diesel engines use inward flow radial turbines while larger engines such as those used for marine and stationary purposes, tend to use axial flow turbines.

In practice, the typical turbine can only work effectively over a relatively limited mass flow range compared with the compressor. There are several consequences of these characteristics of the turbocharger :

a) If the turbine is sized to give good low speed boost, the boost will be too high at full speed and the engine will carry a severe penalty due to back pressure caused by the small turbine.

b) The rising boost characteristic means that good torque back up depends on careful selection of turbine and control of the fuelling curve.

c) The limited flow range of turbomachinery means that obtaining boost over a wide speed range is very difficult.

d) The compressor flow range is limited and the engine demand may be such that too little air is requested at high pressure ratios when the compressor will stall and surging occurs or engine air flow at high speed may be beyond the zone of good compressor efficiency such that inefficient turbocharger operation results.

e) The fact that the turbocharger speed is independent of crankshaft speed means that under transient conditions turbocharger lag can be a problem.

f) A beneficial consequence of the independence of turbocharger shaft and

crankshaft, however, is that a fair degree of altitude compensation is available since the reduced turbine back pressure at altitude makes more turbine work available so that more power is fed to the compressor to offset the lower air density.

g) Overspeeding of the turbocharger at altitude may be a problem due to this effect but there is generally sufficient reserve available with modern turbochargers for it not to be a major consideration.

1.2.2.B
Turbocharging truck type engines

Since the work reported in this thesis relates to truck type engines, turbocharging of this type of engine is considered first. For truck applications the main aims are those of obtaining adequate torque back up over a wide enough speed range while still giving the required maximum power and acceptable specific fuel consumption.

Thermal and mechanical loading, noise, smoke and emission constraints apply throughout the engine operating range. The characteristics of the turbocharger imply that some compromise is necessary in that selection of the ideal turbocharger build for the peak torque condition always involves a sacrifice of turbocharger efficiency at higher speeds. The normal practice is to select the compressor and turbine to give the required boost at the desired peak torque speed. This, therefore, means that the best turbocharger efficiency should be aimed for in this region. Below this speed, boost will fall off rapidly due to the combination of reduced available exhaust energy and falling turbocharger efficiency. Beyond this speed, boost will climb at least linearly due to the rapidly increasing available exhaust energy. The only way of limiting the boost at high speed with fixed turbocharger geometry is by reducing the fuelling and careful fuelling curve development is therefore required to give the desired torque back up and also control the boost at the rated speed. The usual compromise reached is somewhere between a torque back up of 10 to 20 per cent at a speed of 60 to 70 per cent of the engine rated speed (ref. 11).

The usual limit to the degree of turbocharging is set by the levels of cylinder pressure and hence the compression ratio is the first parameter used to control this, followed by retard of injection timing which is also useful as a means of emission control. A compromise must be reached

between power and a suitably shaped torque curve for the turbocharged automotive Diesel engine. Fig. 1.7 shows a typical torque curve for a turbochaged automotive Diesel engine limited (for reliability) by maximum values of (ref. 37)

- cylinder pressure
- exhaust temperature
- exhaust smoke level
- turbocharger speed

As shown in fig. 1.7 these limits can be superimposed on the torque (or BMEP) curve, where the maximum possible torque curve is shown. However, for a turbocharged engine the position of most of these limiting lines will move if the turbocharger match is changed.

It is clear from fig. 1.7 that the factor that is most restrictive when trying to achieve desirable torque characteristics is the low speed smoke limit. Because of the natural characteristic of the turbocharger, boost pressure rises with speed and hence, the smoke limit is set by insufficient boost pressure and air flow at low engine speeds.

In order to achieve an acceptable torque curve, the fuel delivery (per cycle) is held relatively constant over the speed range and efforts are made to raise boost pressure at low speeds.

In conclusion, in selecting a boost device and the appropriate characteristics for small to medium power Diesel engines the following outcomes can be drawn :

a) the ideal exhaust driven supercharger is not available and each application requires a balance of performance,emissions, installation and cost factors.
b) with turbochargers, the main problems are associated with obtaining sufficient low speed boost without excessive boost or turbine back pressure at the engine rated speed.

1.2.2.C Variable Geometry Turbocharging

The standard truck Diesel engine turbocharger with its relatively simple basic components suffers from two inherent limitations, namely:-

i) a comparatively narrow compressor map, particularly as pressure ratio is raised.

ii) the tendency of the radial inflow turbine towards increasing swallowing capacity with decreasing rotational speed, i.e. under part load conditions.

Both limit the scope for good torque back up, the former due to the tendency for the limiting torque line in the compressor map to run close to the surge line and the latter by the resultant inability of the turbocharger to maintain a sufficiently high rotational speed under engine part speed conditions to give boost pressure ratios required for high torque back up.

On the other hand, in the early stages of the transient response of the engine to suddenly increased power demand, fuelling has to be limited because of initially low air available and also need of turbocharger acceleration through a very wide speed range. These limitations of the simple turbocharger have been discussed in a number of papers suggesting different solutions which all give rise to new operational problems. Watson (ref. 9) indicated in his paper that one of the most promising approaches towards overcoming the limitations of the standard turbocharger would be the introduction of variable geometry devices, particularly as applied to the turbine.

In an extensive theoretical and experimental investigation of single stage turbocharging, Wallace et al (ref.10) showed that the use of variable geometry features in turbine provides a very significant improvement in torque characteristics and specific fuel consumption of the engine. From this report, operating characteristics for aftercooled continuously variable geometry and standard non-aftercooled fixed geometry turbocharging are given in fig. 1.8. Comparison of characteristics of these two builds shows the following improvements:

	Fixed Geometry	Variable Geometry
Torque back up	14% at 70% max.speed	50% at 50% max.speed
Peak torque BMEP	12-18 bar	16.75 bar
Max.brake thermal eff.%	37.8	38.3
Air/fuel ratio at 1400 rpm	16.52	22.2

In this paper, the beneficial effects on overall engine-transmission performance resulting from improved engine torque characteristics, achieved by simulated variable turbine geometry with aftercooling, were clearly shown. Variable geometry turbocharging offers substantial benefits not only in improved steady state performance but also with respect to greatly enhanced transient response due to the ability of the turbocharger to accelerate more rapidly, leading in turn to a more rapid build up in boost, with improved air fuel ratios and reduced smoke and higher torque.

Despite these very promising features of variable geometry turbocharging, it is not as yet, a well established technique, partly because the cost of the equipment with its control system is still high.

1.2.3 Transmission Characteristics

In vehicle performance prediction, power consumption of all accessories over the full engine speed range should be evaluated and subtracted from the gross engine power to obtain the effective power available to the transmission input shaft (fig. 1.5).

As mentioned earlier, the power-torque-speed characteristics of the internal combustion engine are not suited for direct vehicle propulsion. A transmission, therefore, is required to provide the vehicle with the tractive effort-speed characteristics that will satisfy the load demands under all conditions. The term transmission includes all those systems employed for transmitting the engine power to the driven wheels or sprockets.

For over-the-road trucks, the maximum required transmission torque multiplication ranges from 8 to 10 with a further rear axle torque ratio of between 4 and 6.

1.2.3.A Multi-ratio Gear Transmission

The manually operated, multi speed gear transmission usually consists of a clutch, a gearbox, a propeller shaft, and a drive axle (fig. 1.9). As a

general rule, the drive axle has a constant gear reduction ratio which is determined by the common practice requiring direct drive (non-reducing drive) in the gearbox in the highest gear. For vehicles requiring extremely high torque at low speeds, an additional reduction gear (final drive) may be placed at the driven wheels. The gearbox provides a number of gear reduction ratios ranging from three to five for passenger cars and more for heavy commercial vehicles.

The gear ratio of the highest gear (i.e. the smallest ratio) is determined by the maximum vehicle speed required. The maximum tractive effort or the maximum gradability specified, on the other hand, determines the gear ratio of the lowest gear (i.e. the largest reduction ratio). Ratios between these two limits should be spaced in such a way that they will provide the tractive effort-speed characteristics as close to the ideal as possible, as shown in fig. 1.10.

For maximum life, the engine should not be operated above rated speed. Also if the speed drops below the speed for peak torque, a decrease in vehicle speed (engine rpm) causes a further decrease in torque which may then cause a further decrease in vehicle speed (fig. 1.10).

In the first iteration, gear ratios between the highest and the lowest gear may be selected using the geometric progression rule. The basis for this method for selecting gear ratios is to have the engine operating within the same speed range in each gear, as shown in fig. 1.11. This would ensure that in each gear the fuel economy characteristics are similar.

For a four-speed gearbox, the following relationship can be established:

$$\frac{r_2}{r_1} = \frac{r_3}{r_2} = \frac{r_4}{r_3} = \frac{n_{e2}}{n_{e1}} = R$$

and

$$R = \sqrt[3]{\frac{r_4}{r_1}}$$

where r_1, r_2, r_3 and r_4 are the gear ratios of the first, second, third and fourth gear, respectively. In a more general case, if the ratio of the highest gear r_n and that of the lowest gear r_1 have been determined

and the number of speeds of the gearbox n_g is known the ratio R can be determined by

$$R = \left(\frac{r_n}{r_1}\right)^{\frac{1}{n_g - 1}}$$

and

$$r_n = R\, r_{n-1}$$

For commercial vehicles, the gear ratios in the gear box are often arranged in geometric progression with respect to sequential gear split (percent step) changes in the transmission. The gear split is defined as

$$\text{Gear split} = \frac{\text{higher gear ratio - lower gear ratio}}{\text{lower gear ratio}} \times 100$$

If the gear split is more than the percent change in the engine speed range of operation (with torque back up) the engine will not be able to operate successfully. If there is an insufficient number of gear splits, certain engine speeds outside the permissible range may occur. Thus, the normal speed range over which the vehicle operates should be taken into account in selecting gear splits. Equal gear splits are not a requirement, but closer gear splits may be used in a particular vehicle speed range to enhance the performance.

The development of high duty trucks leads to the manufacture of vehicles with ever increasing load capacity. A large load capacity requires more powerful engines with more sophisticated gearboxes. The latter are characterized by larger input torques and an increase in the number of gears. The larger input torques mean more liberally dimensioned gears (operating with synchromesh). At the same time, there is an increased demand for short-duration gear changes.

1.2.3.B Synchromesh Mechanism for Heavy Truck Gearboxes

To make driving safe and comfortable, synchronizers have been incorporated in the manual gearboxes of trucks. The synchromesh mechanisms make the gear change independent of the skill of the driver, and increase the average life of the gearbox. For these reasons, the

synchromesh type of truck gearbox is being used extensively and rapid progress is being made in the development of better synchronizers.

Easy gear changing refers to the condition where only a low level of force is required to change gear. It influences the time taken to change and, consequently, adds to the ease of driving. Easy gear changing can result in clash during gear changing. Analysis of the problem of clash shows that it is influenced by many factors, even with a theoretically correct design of synchronizer. In practice, another form of clash called 'partial clash' may also be encountered. The partial clash may be caused for several reasons and some of them may be unavoidable. However, it is necessary at the design stage to allow for the influence of parameters like oil temperature, otherwise, the life of the synchronizer may be greatly reduced.

Difficult gear changing may occur when a larger changing force is necessary than normal. This may depend on design factors or oil and clutch drag. There are designs where the gear changing is made with the help of air or oil pressure and the shifting forces are limited, but other problems may arise.

As is implied synchronization is made with the help of friction. Unfortunately, where there is friction there is also wear and in this case it causes progressive decrease of the synchronization force. The life of synchronizer elements depends on many factors such as :
materials, quality of friction surfaces, size of the friction surfaces, oil and clutch drag and basic design.

1.2.3.C Automatic Gearboxes for Trucks

Economic pressures, increasing traffic densities, etc., will lead to greater use of fully automatic transmissions in buses. In the trucking field, economic considerations are also creating a trend to larger and more powerful vehicles which will demand ease and certainty of control, and thus a place for fully automatic transmissions. An examination of the format of commercially successful fully automatic hydrokinetic truck and bus transmissions reveals that transmission designers have made extensive use of epicyclic gearing.

Although the highway truck will always make the greatest possible use of motorways, it is inevitable that part of the journey will be on regular roadways and more than likely that its journey will begin and end in a built-up area. It follows that the driver will be subjected to all the problems arising from increased traffic density and, accordingly, an automatic transmission would be welcome, reducing driver fatigue and enhancing safety and efficiency.

Epicyclic gearing has a very extensive use in semi- and fully-automatic transmission because of high efficiency and constructional advantages. The high efficiency of power transmission of the epicyclic is due to the following:

(1) The speed of tooth engagement is relatively low
(2) No external journal loads arise from gear tooth action, since the gear separating forces are balanced and self-contained.
(3) The transmitted tooth load is carried by a multiplicity of gear teeth, resulting in moderate unit loadings.

The constructional advantages of the epicyclic are :

(1) It is constant mesh gearing
(2) It is a three element gear set providing a good control over speed ratios.

While the low relative speed of tooth engagement, the absence of external loads, and moderate unit loading contribute to high efficiency, there are other advantages which arise from these characteristics.

The low relative speed of tooth engagement makes a very significant contribution to the attainment of a satisfactory noise level without recourse to unduly high standards of accuracy. The absence of external journal loads relieves the gearcase of the bursting forces which parallel shaft gearing imposes, and makes possible the use of simple light weight casings. Moderate unit loading and the constant-mesh nature of the epicyclic gearing are the underlying reasons for the long life and durability which is expected of, and usually given by the automotive epicyclic gearset.

Not withstanding the advantages associated with automatic transmissions, the need for additional cooling, the higher first cost and often lower efficiency (especially because of torque converter incorporated) has limited the application of epicyclic gearsets. Under high torque conditions a torque converter is relatively inefficient in comparison with stepped gears, and the excessive heat generated must be removed by the cooling system. There are some techniques such as lock-up mechanisms in selected forward gear ranges and the use of an auxiliary high reduction gearbox to be engaged in first gear close to the stall position which make it possible to avoid converter efficiencies below 70%, but all these modifications lead to higher initial cost and greater complication.

1.2.3.D CVT Transmission

Stepped transmissions allow utilization of full engine output at several road speeds by changing the ratio between engine and rear wheels. Several steps are available which are shifted after disconnecting the engine and rear wheels by means of the clutch. Interruption of the power flow is undesirable because of the power loss involved during declutching, and can even become dangerous with heavy vehicles. Only infinitely variable drives would perform as desired and follow the ideal torque-speed curve without interruption. A variable drive has the following advantages over a stepped transmission:

a) the power flow is not interrupted when the ratio is changed,
b) ratio change is accomplished smoothly since there are no steps, avoiding jerks which are uncomfortable to passengers and dangerous on slippery roads,
c) there is no unexpected shifting, as occurs with automatic transmissions, and
d) the engine speed does not vary unless the accelerator pedal position is altered, therefore, a ratio change due to road load has no effect on engine speed.

1.2.4 Power-train Matching and Fuel Economy

Drive-train elements in a modern vehicle, apart from the engine are the transmission (including the clutch or torque converter), the drive shaft (including universal joints), the differential and final drive assembly,

and axle shafts (fig. 1.9)

The transmission and final drive/differential are the two most important drive components in terms of fuel consumption. Various losses incurred in the transmission of power can be substantial particularly with automatic transmissions with their relatively inefficient torque converter and in the hypoid gears of a rear drive differential assembly. Losses in the bearings, universal joints, and other elements are less important. In current automotive transmissions either of the automatic or manual shift type, a finite number of gear ratios is available. Therefore, it is impossible to match the engine and vehicle perfectly across the operating range of the engine.

Power-train matching is a technique for optimizing vehicle fuel economy through the process of determining the best overall combination of power-train parameters compatible with all of the given constraints. Figure 1.12 shows the fuel consumption characteristics of a typical Diesel engine as a function of BMEP and engine speed superimposed upon islands of constant BSFC, as well as the line representing lowest fuel consumption throughout the power range, the so-called economy curve.

Engine losses, including cycle losses, pumping losses and mechanical friction losses are least, in percentage terms, at high BMEP and low rpm. Low rpm minimises engine friction from the bearings, pistons, valve gear and auxiliary drives, including the cooling fan and alternator (fig.1.5). The role of the transmission is thus vital in providing the optimum gear ratios and gear shift points to follow the economy line as closely as practical.

A manual transmission, however, must compromise the ideal because it must employ a limited number of discrete gear ratios. These ratios, including the final drive ratio, and the steps between ratios are selected to effect the best overall compromise between :

i - economy
ii - performance
iii - maximum speed
iv - driveability

Excessive numbers of ratios, or close steps between ratios could result in too frequent shifting. Also the interruption of power during the shift interval, and excessive operation of the accelerator pedal, adversely affects performance and economy, respectively.

Figure 1.10 illustrates that maximum performance is achieved when the transmission is upshifted where the falling torque (BMEP) or acceleration curve for a gear ratio intersects the curve for the next higher ratio. The truck transmission demands a careful study of overall ratio and the number of ratios available within that overall range. It is not unusual for passenger cars to have a power to weight ratio of 80 bhp/ton. In these circumstances unless the ultimate in performance is required three ratios are sufficient for normal driving and the vehicle will remain flexible over a wide speed range in each gear. The truck, however, has a much lower power to weight ratio, normally of the order of 6-9 bhp/ton. In order to obtain an acceptable performance the relative lack of power must be compensated by the provision of a greater number of gear ratios so that in any condition of operation a ratio is available which allows the engine to work in a narrow speed band which gives high torque and efficiency.

The vehicle manufacturer has the problem of deciding what overall reduction ratio is necessary between the engine and driving wheels, and how and where this overall reduction should be achieved. At the maximum governed speed of the engine, the gearing should give the vehicle a top speed of 55-60 mph. At the other end of the range, the gearing should give the vehicle a capability of climbing at least a 20% (1 in 5) grade. To achieve this kind of performance, the British medium truck requires an overall ratio of about 55:1 (ref.31). Since the maximum economical first gear ratio in the gearbox is about 8:5:1 and the maximum single step through the axle bevel gearing is about 7:1, it is clear that a single-speed axle is barely adequate for present use and will certainly be inadequate for future vehicles.

These considerations affect the design of the rear axle, and various combinations of gearbox and axle are emerging.

1 - 5-speed gearbox and single speed axle

2 - 8- or 10-speed gearbox and single speed axle

3 - 5-speed gearbox and 2-speed axle

4 - 5-speed gearbox and 3-speed tandem axle

From the standpoint of vehicle operation and performance, a 15-speed combination is much more efficient than a 5-speed one. In all operations, other than high speed or motorway running there is a fairly narrow band of engine speed where the balance of fuel economy and engine torque available results in the most economical use of the engine. On a typical large truck engine this speed band is from 1300 to 1600 rpm. The higher the number of ratios available, the narrower is the band of engine speed variation in the course of gear changing.

Referring to fig. 1.12, the best economy line for all power levels can only be followed with a transmission providing an infinite number of ratios. The control system for such a CVT would seek the engine speed and BMEP level corresponding to the best BSFC condition over the power range. Thus the CVT ratio and the engine fuelling would be under full control. The control strategy would essentially optimize fuel economy for any typical driving cycle. A start-up device such as a clutch, fluid coupling, or torque converter is required since CVT mechanisms of the traction drive or friction drive type do not possess start-up capability and are also limited in ratio coverage. Hydrostatic or hydromechanical systems are often considered for automotive application, but past developments have been plagued by noise and other problems.

Efficiency characteristics and ratio coverage of the CVT mechanism are critical in achieving a fuel economy advantage over automotive conventional transmissions. Since the CVT mechanism operates full time and at lower efficiency levels than geared ratios and direct drive, it starts with an efficiency disadvantage. However, the potential gain in engine efficiency can more than offset lower transmission efficiencies.

Recent developments in continuously variable transmissions (CVT) hold promise, and if they prove acceptable in terms of cost, durability, manufacturability and other considerations it is projected that they would yield a 10% fuel economy improvement over the best of current designs. Unfortunately, the technology of the CVT is by no means certain.

Axle ratio is also an important consideration in the matching of the engine to the vehicle. The lower axle reduction ratio causes the engine to operate at a higher load factor but at a reduced rpm with an attendant reduction in engine pumping losses and friction.

Apart from the question of engine-drive train match-up, the various component efficiencies are important. The torque converter in an automatic transmission in particular has been a serious problem over the years because of rather significant slippage between the input and output shafts. This device nevertheless remains despits its inefficiences, one of the elements of modern automatic transmission. Under stall conditions the torque converter efficiency is zero, and even under optimum conditions torque converter efficiency rarely exceeds 95%. Of course, some of the inherent disadvantages of the simple torque converter are being ameliorated with the advent of lockup or divided path designs in which some or all of the power is transmitted through a mechanical system under certain operating conditions. In the future, most automatic transmissions will employ some form of lockup mechanism.

1.2.5 Limitations of a Conventional System

Regarding the turbocharged Diesel engine in combination with multi-ratio transmission with manual gear selection as the conventional power plant of heavy goods vehicle, although it is well established and used in common practice, there are several limitations and inefficiencies associated with it, as follows :

i) The system has a considerable transient inefficiency associated with the fact that system efficiency is zero during a gear change.

ii) Driveability of the vehicle is poor, since a driver is involved in too many gear changes, involving considerable effort in clutch pedal operation and gear selection.

iii) The system requires well trained drivers to make correct decisions for economical driving. Although the problem may be solved by the use of automatic gearboxes, the latter imply high initial and maintenance costs.

iv) Weight and size of the clutch-gearbox construction included in the system reduce the payload capacity of the vehicle.

v) The condition of compressor-turbine power balance in the

turbocharger limits the use of boost and prevents the utilization of potential excess turbine power at high BMEP levels.

vi) Turbocharger lag leads to poor transient response and emission characteristics of the engine. In particular, smoke is a problem under transient operating conditions.

vii) Although HC and NO_x can be closely controlled by special techniques applied, they are always a problem in T/C engines.

1.3 UNCONVENTIONAL SYSTEMS

1.3.1 Differentially Supercharged Diesel Engine (DDE)

In surveying the possible ways of directing Diesel-engine development towards the ideal constant horsepower vehicle engine, Dawson et al (ref.11), proposed the concept of the differentially supercharged engine. This idea was not completely new when the concept was developed in detail by Dawson etal in 1963 (ref.11). Patent literature had contained a number of references to this system, amongst the earliest being Invernizzi in 1925 and Weber in 1927. In the early nineteen fifties, further work was done by Geislinger in France, Larbon and Stalblad in Sweden and Glamann in Germany and France. Glamann's work with Berliet at that time, was probably the first example of the application of the CVT principle to a road vehicle.

Referring to the earlier sections of this chapter, inadequate torque back up of turbocharged engines calls for a complicated gearbox with many step ratios to cover the requirements of road vehicles. The LTC of such an engine is constrained by several parameters including smoke emission at lower engine speeds. The resultant deficiency of air due to turbocharger characteristics in lower speeds restricts the permissible fuel delivery and thus the available torque. If a system can provide higher turbocharger speed and hence air flow, it will overcome the low speed torque deficiency.

Differential supercharging is done in such a way that compressor and output shaft are differentially connected leading to maximum boost at low engine/output shaft speeds with a self adjusting falling boost characteristic along the LTC as the engine/output shaft speed is increased (figs. 1.15 and 1.16).

Basically the system consists of an epicyclic gear used as a differential interposed between a Diesel engine and the output shaft with the engine driving the planet carrier, the output shaft being driven by the annulus and the sunwheel driving a supercharger through a step-up gear train, the supercharger feeding the engine (fig. 1.14). It is important to recognize that, as indicated in fig. 1.14, this is a torque-dividing or torque

balancing system. Despite fixed ratios between system shaft torques, there is a varying speed relationship between the three members of the differential train, the speeds depending on the torque reactions at each shaft at any instant of time.

Dawson and his co-workers carried out the development in three phases, starting with the simplest possible unit comprising a Diesel engine, a lobe type compressor, a friction clutch, a differential gearbox and a three-speed gearbox. Ultimately, the combination of the differential gearbox, modified injection equipment, torque converter with adequate stall ratio and screw type compressor with a heat exchanger was developed. The target was a BMEP of 255 psi at 1200 rpm with a limiting torque curve suitable for a 20 ton truck, the engine being controlled under all conditions, including starting from rest, by the use of two pedals only. Figs. 1.15, 1.16 show the performance characteristics of the scheme at the final stage of its development, fitted with a 2 stepped gearbox, having ratios of 1:1 and 1.8:1.

A comparison of the performance of the turbocharged and differentially supercharged engines with the same nominal horsepower was provided by fitting them into two vehicles of the same load carrying capacity. The result is shown in fig. 1.17. Gear ratios were chosen to give both vehicles approximately the same top speed of 55 mph. The curves indicate that, use of the DD engine with a two-speed gearbox gives superior performance over the turbocharged engined vehicle under all driving conditions.

From the work carried out by Dawson et al, it was possible to obtain a good assessment of the unit, at least in general terms as follows :

1.3.1.A Advantages and Potentials

1) Better performance. Because of substantial improvement in specific power of the DD engine over that of the T/C engine with stepped transmission, an increase of 45 per cent in payload for a 20 ton truck was experienced.

2) Better selection of characteristics. A much greater range of power unit output characteristics is available to meet particular vehicle requirements by using the DD engine and gearbox rather than the conventional engine and gearbox.

3) Better economy. The DD engine shows improved fuel economy over a major portion of its operating range, particularly where high speeds are required. Charge cooling lowers the exhaust temperature markedly raising specific output even by 15%.

4) Longer life. Unlike the conventional engine and gearbox, the DD engine operates at lower speeds to achieve a given average road speed. Also, because of the favourable air/fuel ratio at which the DD engine operates, component temperatures are lower.

5) Better vehicle driveability. A vehicle fitted with the DD engine operates under two pedal controls. The combination of this with the uprating of the engine makes it superior to vehicles powered by turbocharged engines with automatic gearboxes.

6) Lower overall cost. Bringing down the cost of the torque converter and supercharger by reasonable production quantity, should make the overall cost competitive with a conventional engine and transmission and cheaper than a conventional engine coupled to an automatic transmission.

1.3.1.B Disadvantages and Impotentials

Although the DDE scheme appeared to be admirable in respect of suitable geometric layout, it was less so in respect of suitable step-up ratio between the sunwheel and the compressor drive so that the compressor overspeed ratio imposed was beyond what the system required. On the other hand, the power absorbed by the compressor became an increasing proportion of engine power as output shaft speed decreased, and this fact made the very flat fuel consumption curves. One would expect that, in the case of the differentially supercharged engine, unlike the differential compound engine (which will be dealt with in more detail later), the increasing torque with decreasing output shaft speed is achieved by

increasing the engine BMEP with corresponding deterioration in specific fuel consumption. It was expected that some recovery of compressor work in the form of positive loop work during the exhaust and suction strokes was possible, and with small valve overlaps this was a distinct possibility.

As will be described later, even with limited work recovery as indicated above, the differential compound engine shows better part load efficiency than the DD engine unit owing to the much more efficient use of exhaust energy in the separate exhaust turbine as opposed to positive 'loop work' as a method of recovering compressor work.
Although much was learned from the limited DDE development programme, many aspects require further investigation:-

1) Truck retardation capabilities compared with the conventional stepped gearbox truck.
2) Special driving techniques and requirements.
3) The comparative handling characteristics on undulating and/or congested trunk roads and in town traffic.
4) The side effects of noise and smoke emission.
5) The thermal loading of the engine in terms of requirements created for better charge cooling.

1.3.2 Differential Compound Engine (DCE)

As has already been shown, in the case of turbocharged engines for traction purposes with mechanical transmission systems, there is a tendency to match the turbocharger so as to give maximum engine torque (or BMEP) at approximately half to two-thirds of maximum engine speed; this inevitably leads to surplus air being available from the turbocharger at maximum engine speed, with the resultant necessity for bypassing surplus air or, alternatively, incurring excessive port or valve pressure drop.

The chief mechanical limitation of the turbocharged engine is the impossibility of achieving satisfactory torque-speed characteristics for traction applications without the use of complicated transmission systems. These include mechanical multi-ratio gearboxes using either spur

or epicyclic gearing, combinations of mechanical with hydrodynamic units, hydrostatic units, and finally, electrical systems in off-highway and rail traction.

In the compound engine arrangement a mechanical connection exists between engine, compressor and turbine (fig. 1.18) and is largely free from the thermodynamic limitations of the turbocharged engine, owing to the fact that power can circulate freely between the members of the aggregate.

The use of infinitely variable or differential gearing between the members of the compound engine aggregate enhances both thermodynamic performance and flexibility. Such an aggregate is intended primarily for traction purposes and is shown to combine the thermodynamic advantages of the compound engine with torque-speed characteristics approaching the ideal hyperbolic relation, thus eliminating the necessity for complex external transmission arrangements. This is achieved by coupling the members of the aggregate and the output-shaft through the medium of differential or epicyclic gearing, (fig. 1.19).

Various compound engine arrangements with differential rather than fixed ratio gear connection between the members of the aggregate have been investigated by Hooker, (ref. 12), Chatteron, (ref. 13), and Wallace, (ref. 14) , for more than 30 years. Wallace has shown, in the course of a 25 year development that such units meet to a very high degree the specific requirements of the traction application, namely :

1. High unit power achieved by the use of high boost pressures.
2. Torque-speed characteristics approaching the ideal hyperbolic law, and permitting drastic simplification of the external transmission system.
3. Good part-load efficiency - superior to the turbocharged or other schemes like gas generator engines - made possible by the free power flow between the members of the aggregate.
4. High degree of engine assisted braking, and
5. Good response to sudden changes in load demand.

1.3.2.A Evolution of Wallace's DCE Scheme

In the very early stages of developing the free floating compound schemes, in 1963, (ref. 14), Wallace presented an assessment of the best possible arrangement of the components. Two possible coupling arrangements satisfying the essential conditions were considered. Figs. 1.19 and 1.20 show the general and more detailed arrangements of the components, respectively. The role of the auxiliary turbine in both schemes is the recovery of energy of compressed air in excess of engine requirements by feeding it back to the shaft system.

Using similar tentative power distributions between engine, main turbine and compressor at the design point, together with epicyclic gear ratios, the operating characteristics of these two schemes were examined. The results showed that, at maximum engine speed with reduction in output shaft speed, the compressor speed increases, resulting in higher engine boost and hence in higher engine and turbine, as well as compressor power. Hence, provided the degree of compressor overspeeding and additional engine loading implied are acceptable, output shaft power will be such as to give continuous increase in torque with decreasing output shaft speed, as required in traction units. The results showed that even without the contribution of the auxiliary turbine, the stall torque conversion (the ratio of output shaft torque at stall to design point) for both schemes was of the order of 3.0, while part load efficiency decreases from a common maximum of approximately 38 per cent near the design point.

The comparison between these two schemes disclosed that :

i) At maximum output shaft speed, engine idling speed in scheme "b" is of the order of 80 per cent of that in scheme "a", providing a wider range of engine speed, for the latter.

ii) The degree of compressor overspeeding (as output shaft speed decreases from design point to stall, keeping engine speed constant at its design point) in scheme "b" is of an order of 70 per cent of that in scheme "a". Hence, loss of efficiency under off-design conditions is rather lower in scheme "b" than in scheme "a", owing to the much lower degree of bypassing in the former.

Apart from the slightly more complex stall-turbine layout for scheme "b", it was the preferred arrangement, because of a lesser degree of compressor overspeeding and lesser degree of engine and main turbine bypassing with resultant improvement in thermal efficiency.

The thermodynamic loss implicit in bypassing is recovered partially by the use of the stall turbine. The use of the stall turbine permits an increase in stall torque ratio from approx. 3 to 10 for both schemes.

As the second step, in 1966 (ref. 15), Wallace presented his compound engine scheme based on an opposed piston 2 stroke engine (scheme "b") in more detail approaching nearly constant horsepower with decreasing output-shaft speed. Again, the basic arrangement is shown in line diagram form in fig. 1.21, where the functional relation between the various components is seen. The engine drives the annulus of the epicyclic gear train, the sunwheel drives the positive displacement type compressor (two in parallel in the prototype engine, since it was designed to use standard proprietary units), while the planet carrier drives the output shaft, into which are geared both the main power turbine and the auxiliary (or stall) turbine.

The air from the compressor normally passes through the intercooler and engine to the power turbine, the latter providing the back pressure necessary for high supercharging and also making a direct contribution to the total output power and torque of the unit.

The general operating characteristics of the unit were governed by the choice of the design point, that is, the condition of normal maximum output shaft speed and power. The constant power characteristic was achieved by employing the stall turbine at low output shaft speeds, in addition to the exhaust gas turbine. The decrease in output shaft speed from design speed to zero was accompanied by an increase in compressor speed. This overspeeding to a large extent determined the choice of compressor in that :

i) the compressor rotor stress level must have not exceeded the permissible maximum.

ii) the increase in compressor speed must have been accompanied

by a corresponding increase in compressor mass flow in order to realise the potentialities of the differential compound concept.

These considerations virtually dictated the choice of a positive displacement (screw type) compressor. Both the mass flow and acceptable efficiency range of single-stage centrifugal compressors at the high pressure ratios envisaged being too limited, due to surge at the lower, and choking at the higher speed limit and maximum speeds resulting from the proposed method of operation, leading to excessively high stress levels.

The unit therefore was expected to be utilised under virtually constant boost pressure and engine power conditions, with the engine speed fixed at its design point value, and with the torque rising continuously with decrease in output shaft speed, due first to the increasing torque of the main power turbine, and then much more rapidly due to the major contribution of the auxiliary turbine. Nevertheless, the theoretical ideal of a constant output shaft power envelope was not fully realized, mainly for the following reasons :

i) the increase in compressor speed and consequently increase in air mass flow as the stall operating point was approached caused progressively lower turbine inlet temperatures and hence a correspondingly lower rate of increase of power from the main turbine. This condition was accentuated by the fact that the power turbine efficiency, after an initial increase fell off fairly rapidly as stall was approached.

ii) when the stall turbine was first coupled into the output shaft its efficiency was low. It was evident that the shape of the power envelope was critically affected by the matching, in terms of the turbine output shaft gear ratio, both of the main and auxiliary turbines. This match should have been systematically optimized.

iii) the part load efficiencies were affected by compressor efficiency

to a large extent. For example, an improvement of compressor efficiency from 62% to 75% improved the overall efficiency from 34.2% to 37.5%.

Similarly, with improved matching of both power, and stall turbine, a closer approximation to the ideal constant horsepower envelope could have been expected. However, in this latest prototype form, the unit represented a very considerable advance over previously attempted solutions for a constant power unit and the attainment of a stall torque nearly seven times the normal design torque by the differential coupling method adopted, made possible the elimination of any form of change speed transmission except in the most stringent conditions.

The proposed method of coupling of a multistage axial flow stall turbine for the prototype could, with advantage, have been replaced by one in which a single-stage radial flow turbine similar to the power turbine geared into the output shaft through a small separate torque converter. Fig. 1.22 shows a comparison of the original prototype design and the improved design. As shown, the resultant improvement in torque conversion was from 6.75 to nearly 10:1, this being sufficient to eliminate any form of change speed gearbox under all conditions.

At a later stage in 1971, (ref. 16), considerable modifications both of the original concept and of the hardware actually constructed were made with a view to improving specific performance aspects mainly under the headings :

1) Higher stall torque ratio
2) Improved part load efficiency
3) Improved matching of engine, compressor and turbine.

This was reported by Wallace et al (ref. 16) and the schematic of transmission scheme is shown in fig. 1.23 as embodied in the hardware being tested. This new scheme was proposed to solve two weaknesses of the previous schemes as follows :

i) The torque converter representing an undesirable complication.
ii) The swallowing characteristics of the radial power turbine being

such that the very rapid increase in gas flow associated with progressive reduction of output shaft speed, due to speeding up of the compressor could not be accommodated by the turbine without exceeding reasonable limits of boost pressure. Hence some blowing off of air through the auxiliary turbine via the air control valve, had to be accepted.

The torque converter was therefore removed and both turbines were equipped with variable nozzle gear in order to vary their swallowing capacity in accordance with optimum matching requirements. The nozzle angle was varied from zero (complete closure) to approximatly 30 deg.

Fig. 1.23 shows the two modes of operation. The LH diagram applies to the output shaft speed in excess of approximately $^1/_3$ of its maximum speed, when the power turbine is operative (with variable nozzle control) while the auxiliary turbine is declutched with its nozzle completely closed and acting as a shut off valve. The RH diagram applies to the low output shaft speed regime with power turbine still connected, but nozzles completely closed; stall turbine clutched in and under variable nozzle control. The control valve was that employed in the earlier schemes, this time employed as an engine bypass in order to prevent excessive pressure drops across the engine when unnecessarily large quantities of scavenging air would otherwise be used. In each mode of operation exhaust gas from the engine and bypass air direct from the compressor mixed in a plenum chamber upstream either of the power or the stall turbine.

The main differences between the original hardware scheme A and the developed scheme B may thus be summarised as shown in table (1.3).

The chief operating advantages of the developed scheme over the original one were as follows :-

1) Variable nozzle control of both turbines in conjunction with engine bypass control enabled precise matching of engine, compressor and turbines to be achieved, that is, the unit could operate on an optimized schedule of engine speed, boost pressure, scavenge ratio and trapped air fuel ratio.

2) Wasteful blow off of compressor air necessitated by inadequate swallowing capacity of the fixed nozzle turbines in the original scheme was avoided.

3) Use of hot gas in the stall (auxiliary) turbine rather than compressor air increased its torque contribution and permitted elimination of the torque converter.

4) The provision of variable turbine nozzles made possible the adoption of nozzle reversal (that is swinging the nozzles). This possibility showed that very substantial braking or reversing effort could have been achieved.

5) With the extreme flexibility obtained by combined turbine nozzle and engine bypass control, power level could be significantly raised (by about 30 per cent) at maximum output shaft speed. Uprated operation was made possible by the combined effect of increased turbine power and engine power, the former resulting from lower scavenge ratio (down to 1.3 from 1.4) and the latter resulting from the increased boost pressure (being kept high throughout the range of output shaft speed).

The choice of a two-stroke engine in the original DCE scheme had been dictated by two considerations:

i) the ability of the two-stroke engine to accommodate large throughflows without incurring the penalty of excessive pressure drops and hence loss of potential turbine power.
ii) the expectation that a two-stroke engine would have significantly higher power/weight and power/bulk ratios than an equivalent four-stroke engine.

Operating experience with high-output high-speed two-stroke engines has shown (refs.15, 16) that thermal loading limitations are severe and that BMEP is limited to approximately 160-165 psi even with piston cooling. Hence four-stroke engines operating with BMEPs of the order of 250 psi and at less severe thermal loadings can actually show better power/weight

ratios.

The changeover from the fixed turbine nozzle scheme with an auxiliary turbine using air at low output shaft speeds, to the scheme with variable nozzles for the power and auxiliary turbines, with the latter accepting a mixture of engine exhaust gas and bypass air, made it possible to substitute a four-stroke engine for a two-stroke engine, primarily due to the ability to adjust bypass ratio in accordance with engine "swallowing capacity".

The combination of variable turbine nozzles and choice of bypass ratio confers on the DCE scheme the advantage of completely flexible choice of engine ratings and general operating conditions. This also has an important bearing on control of emission characteristics by judicious choice of maximum cycle pressure and temperature.

1.3.2.B Final Layout and Type of Components

In 1983, (ref. 17), Wallace presented his DCE scheme in its present form. The basic layout of the plant is shown in fig. 1.24. A Leyland 500 four-stroke Diesel engine of 8.2 l displacement drives the ring gear of a fully floating epicyclic gearbox. The planet carrier is geared to the output shaft which, in turn, receives a direct power input from the only turbine incorporated in the system (of the inward radial variable geometry type) connected by continuous variable transmission. The supercharging compressor (of the improved rotary positive displacement type) is driven by the sunwheel member of the epicyclic gear train via a step up ratio gearing. The speed relationships for the engine-compressor-output shaft train incorporated in the experimental rig are given in fig. 1.25. and show the well-known trend of all differential gear trains, namely, speeding up of the compressor shaft when the output shaft is slowed down, while the engine speed is kept constant. The arrangement makes it possible for the engine to operate under optimum conditions for any given level of power demanded, irrespective of output shaft speed, and provides the basis for very high torque back-up.

The gas flow path is also indicated in fig. 1.24. Air delivered by the

Lysholm-type compressor divides into two flows : to the engine through a charge cooler and direct to the turbine through a bypass line controlled by a bypass valve. The engine exhaust gases combine with the bypass flow and then pass through the single stage, inward radial flow exhaust turbine which has been specially equipped with fully variable nozzles.

Control of the unit is thus through three simultaneous inputs, namely, fuel rack setting for controlling power, bypass valve and turbine nozzle angle settings for controlling boost level, which enables any load demand (that is, combination of output shaft speed and torque) to be met so as to satisfy certain external constraints, such as optimum overall efficiency.

The thermodynamic linkage between engine, compressor and turbine imposed by the epicyclic gear train, enables the system as a whole to be optimized for any demanded output shaft and torque combination. This optimization is achieved by control of 3 variables which determine the speed and torque relations of the plant, viz. fig. 1.24.

a) Power turbine nozzle setting - this primarily affects the boost level at which the plant operates.
b) Turbine CVT setting - this allows the turbine to operate at its best efficiency under all conditions.
c) Injection timing - this allows the engine to operate either at maximum torque on the plant limiting torque curve (LTC) without exceeding permissible maximum cylinder pressure or, at its best efficiency under part load conditions.

All 3 controls are interactive and therefore demand a common control strategy (fig. 1.26). Although fig. 1.24 also shows a variable bypass valve, its use is limited to transient operation, being always wide open under steady state conditions for best efficiency. Each of the 3 devices listed above is under electrohydraulic control operated, in turn, by analogue control loops, receiving their voltage input either from manually operated potientometers (for purposes of initial manual optimization) or via A/D converters from the central microprocessor which stores the numerical arrays representing the optimum control

voltages for each of the 3 devices as a function of input variables as shown in fig. 1.26, i.e. output shaft speed and fuel rack position, expressed as analogue voltages.

It is anticipated that the system will have to be supplemented under fast transient conditions, by the provision of special transient controls. This is shown diagramatically in fig. 1.27. The main feedback signals are still output shaft speed and fuel rack position. Under steady state conditions these would result in a uniquely determined engine speed which can also be stored as a numerical array in the central microprocessor. This desired speed is compared with the instantaneous actual speed, and the difference signal is used to close a transient switch in the auxiliary boost control system, which demands a boost level lower than the steady state value consistent with adequate air fuel ratio but designed to permit more rapid system acceleration. This desired value is compared with the actual measured value and applied as a supplementary transient signal to the turbine nozzle actuator. However, it is the function of the microprocessor operated control system to implement these optimum schedules, via fuel pump governor, turbine nozzle actuator and the CVT operating lever.

1.3.3 Features of the Present Form of the DCE Scheme

1.3.3.A Steady State Performance Characteristics

The performance characteristics represented in this section are taken from the work presented by Wallce et al, (ref. 17) in 1983. Fig. 1.28 illustrates output shaft torque versus speed characteristics of the DCE unit itself, with superimposed contours of overall efficiency. It is based on computer predictions using a comprehensive simulation package with well tested engine, compressor, turbine and gear subroutines, and represent fully optimized steady state operation. In the preparation of overall efficiency figures, allowance was made for epicyclic gear and turbine CVT losses.

It is evident that the output shaft torque gives a continuous and steep rise of approximately 3.07:1 over the output shaft speed range of 5:1. Fig. 1.29 shows the tractive effort versus speed field for the complete

38 ton truck, with superimposed constant gradient lines and some individual specific fuel consumption figures relative to back axle horsepower. It should be noted that the gap between output shaft stall and $^1/_5$ of its maximum value is bridged in vehicle applications by the output torque converter (fig. 1.24) which has a built-in torque ratio of 3.25, giving an overall torque ratio between stall and rated conditions of about 10. Fig. 1.30 shows the corresponding power envelope and demonstrates that power is held substantially constant over the upper 80 per cent of the speed range. The only constraint to keep the engine running at rated speed and hence at constant rated power at different output shaft running conditions is that of compressor speed. This constraint imposes the need to allow the engine to run along a short LTC, from rated speed to the peak torque speed. If the power can be maintained nearly constant along this curve, the original concept of constant power can also be retained. However, since the torque rise is achieved steplessly system flexibility will nevertheless be superior to that of a conventional turbocharged engine coupled to a multi speed gearbox. On the other hand, the system efficiency contours must be considered very satisfactory, with the 35% contour covering well over one third of the total operating field.

1.3.3.B Transient Performance Characteristics

Due to the fact that torque balance must at all times be maintained within the epicyclic gear train, a step input of fuel in response to a sudden load demand will result in the first instance, in rapid acceleration of the low inertia parts of the system, that is, the engine and compressor. The resultant rapid attainment of high engine power and boost levels favourably reacts on the overall system response compared with a conventional system, in which engine and output shaft speeds are in a fixed ratio, with consequent less rapid pick up of engine power.

The main objective in transient control is to achieve more rapid acceleration demanding a lower level of boost during the initial period than the steady state value, consistent with a minimum acceptable air-fuel ratio. The resultant reduced compressor torque demand is transmitted through the epicyclic gear train as a reduced engine torque

demand, and hence gives rise to more rapid engine acceleration.

Figs. 1.31 and 1.32 show transient response for a fuel step from 50% to 100% of full load at three constant output shaft speeds with respect to output shaft torque and trapped air-fuel ratio. The extremely rapid response (over no more than 0.5 sec), illustrates the superiority of the DCE, with respect to transient response, over highly turbocharged engines, where typically the response time would be of the order of 2.5 to 3 sec.

The only adverse feature is the sudden drop in trapped air-fuel ratio within 0.1 sec of application of the fuel step, which would call for some modification of the fuelling schedule during the early part of the transient particularly at higher output shaft speeds. However, the extremely rapid recovery of air fuel ratio to acceptable levels within less than 0.5 sec is quite apparent. A powerful method of modulating transient response lines in bypass control. A sudden closure of the normally fully open bypass valve, during the transient, makes trapped air-fuel ratio recover even more rapidly, with a consequent drastic reduction in transient smoke. Thus the differential connection, coupled with inherently generous trapped A/F ratio under all operating conditions gives the unit a distinct advantage over all alternative transport prime movers.

Optimization of CR and P_{max} and Pollution

The compound engine, as opposed to the turbocharged engine, is particularly flexible in the range of effective compression ratios and maximum cylinder pressures which can be adopted. Thus if low compression ratios appear attractive from the standpoint of emissions, they can be tolerated more readily than in the turbocharged engine, since starting difficulties are greatly eased by the combination of mechanically driven compressor and variable turbine nozzles which allow high boost pressures to be attained even during starting. Likewise, the loss of engine efficiency usually associated with low compression ratios and maximum pressures can be offset by the gain in the turbine power contribution due to higher engine exhaust and hence turbine inlet temperatures.

Investigations have shown that low maximum cylinder pressure and low compression ratio (≃ 10), should be conducive to the lowest possible NO concentrations. Similar remarks apply also to CO and smoke, even at the highest rating at which the unit has been operated experimentally, no exhaust smoke has been observed.

1.3.3.c Reliability and Some Other Features

Since the DCE uses only proven components, a high level of reliability is expected. Engine component failures, particularly piston failures due to excessive thermal and mechanical loadings, are directly related to engine rating (bhp/piston area) which is limited by considerations similar to those of the turbocharged engine, noting the fact that, lower engine compression ratios can be adopted more readily in the DCE.

Turbine power feedback to the output shaft in the DCE provides the basis for good fuel economy at higher output shaft speeds. As a matter of fact, because of the relatively low compressor efficiency and the considerable quantities of excess air to be diverted through the bypass at lower output shaft speeds, the fuel economy tends to be worse under these conditions. However, low engine speeds under these conditions reduce bypass flow to acceptable levels.

Engine ratings for the DCE are similar to those achieved in very highly turbocharged Diesel engines, subject primarily to thermal and mechanical limits. In terms of specific weight, the DCE constitutes a complete engine transmission system and shows far lower figures (~ 3 lb/bhp) than an equivalent turbocharged engine associated with a mechanical, hydrokinetic, hydrostatic or electrical transmission system.

First cost is one of the most important aspects and possibly the most problematic. However, since the DCE consists entirely of standard and proven types of components, it seems that both capital and maintenance costs should be quite close to those of the well established turbocharged engine in association with a conventional transmission.

Characteristic	Severity of Service		
	Heavy	Medium	Light
Average fuel rate ---------- (%)	up to 90	below 50	15 - 40
Maximum fuel rate Annual mileage (thousands)	above 60 - 70	10 - 60	5 - 25
GVW (thousands of lb)	30.9 - 97.0	24.3 - 33.1	7.7 - 22.05
Average GVW ---------- (%)	80 - 90	50 - 75	50 - 75
Maximum GVW Engine Power (hp)	above 250	150 - 250	100 - 200
Life before major overhaul (thousands of miles)	300 - 500	125 - 200	100

TABLE 1.1 Characteristics of different truck application

Classification	Heavy commercial vehicle engine power range	Major overhaul " km "
Class I	70 - 170 hp (52 - 127 kW)	200,000
Class II	150 - 250 hp (112 - 186 kW)	350,000
Class III	250 - 350 hp (186 - 261 kW)	500,000
Class IV	350 hp upwards(261 kW upwards)	800,000

TABLE 1.2 Classification of heavy vehicle engines

	Scheme " A "	Scheme " B "
Power Turbine 1	1) Fixed nozzles 2) Uses exhaust gas	1) Variable nozzles 2) Uses mixture of exhaust gas and bypass air
Auxiliary Turbine 2	1) Fixed nozzles 2) Uses air 3) Drives planet carrier through 10:1 step down gearbox and torque converter	1) Variable nozzles 2) Uses mixture of exhaust gas and bypass air 3) Drives planet carrier through 10:1 step down gearbox only

TABLE 1.3 Summary of differences in hardware of scheme " A " and " B "

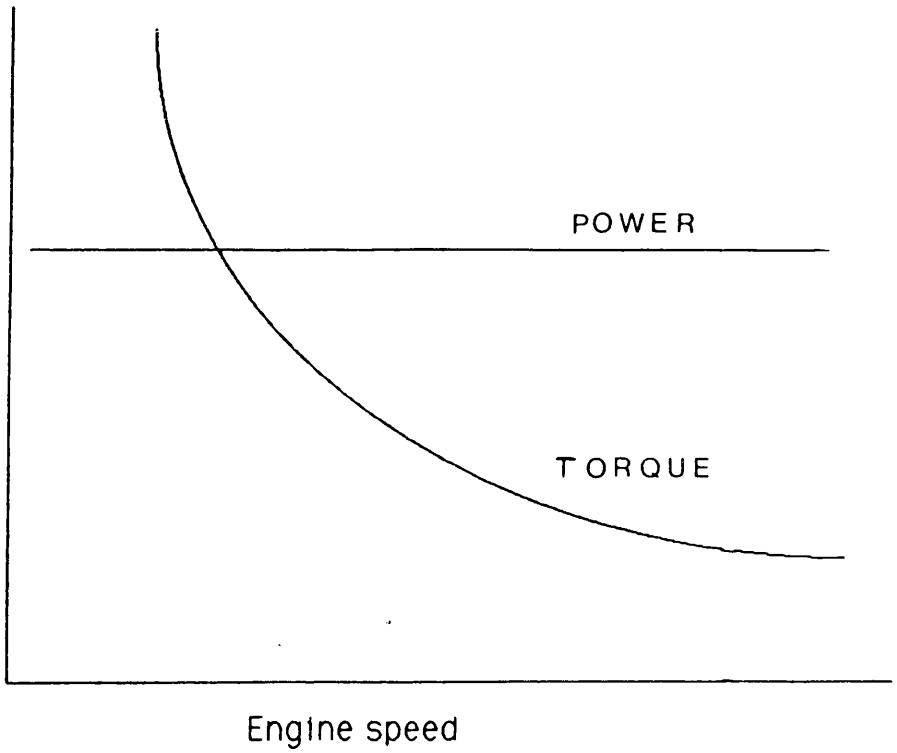

Fig. 1.1 Ideal torque-speed characteristices for tractive purposes

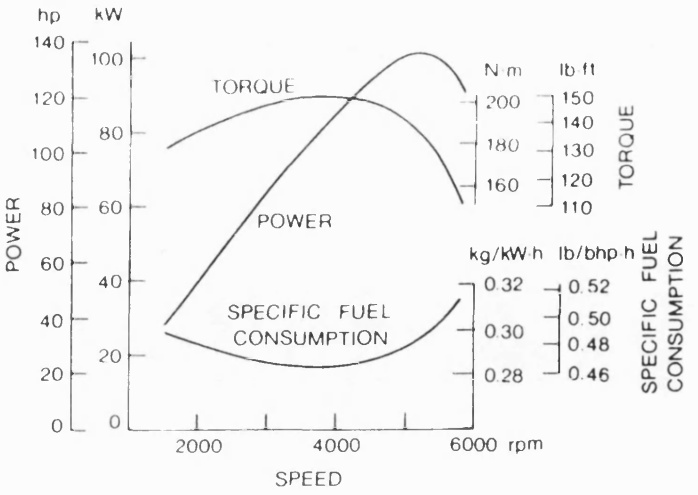

Fig. 1.2 Performance characteristics of a gasoline engine

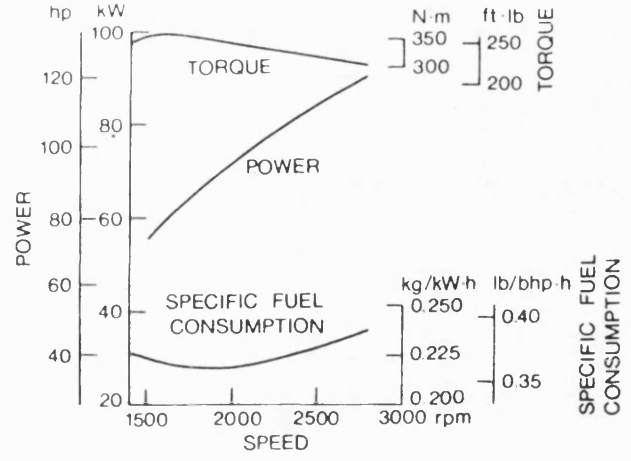

Fig. 1.3 Performance characteristics of a Diesel engine

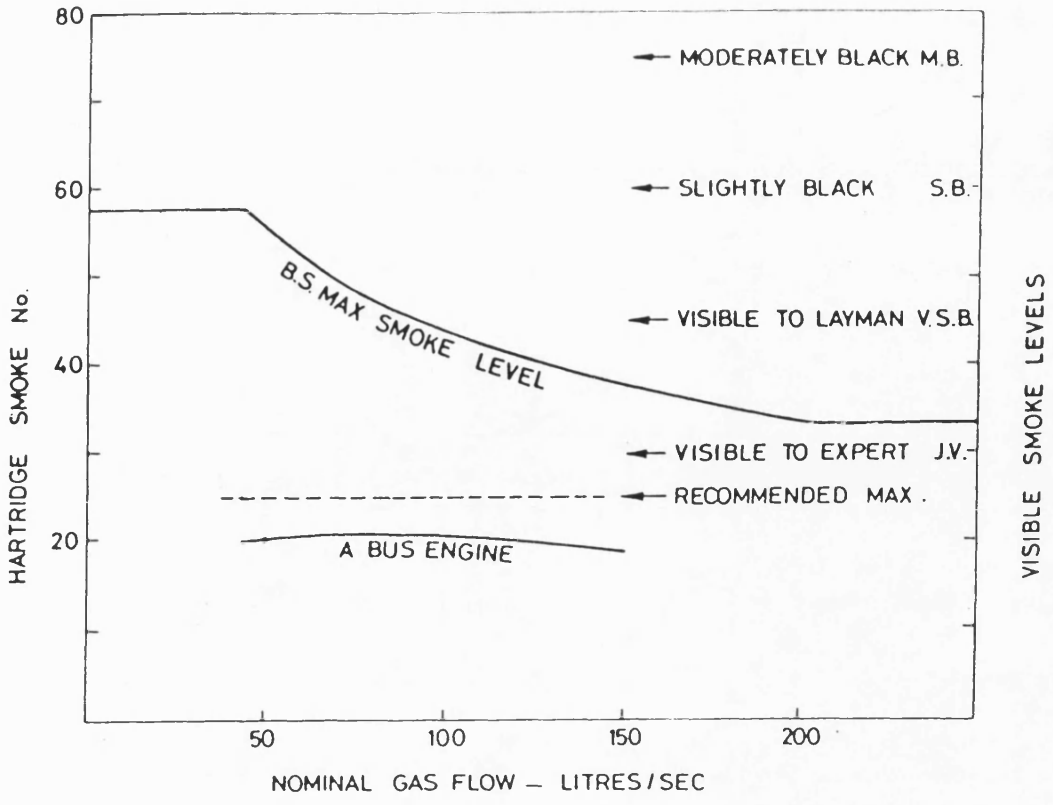

Fig. 1.4 BS standard for max. smoke level

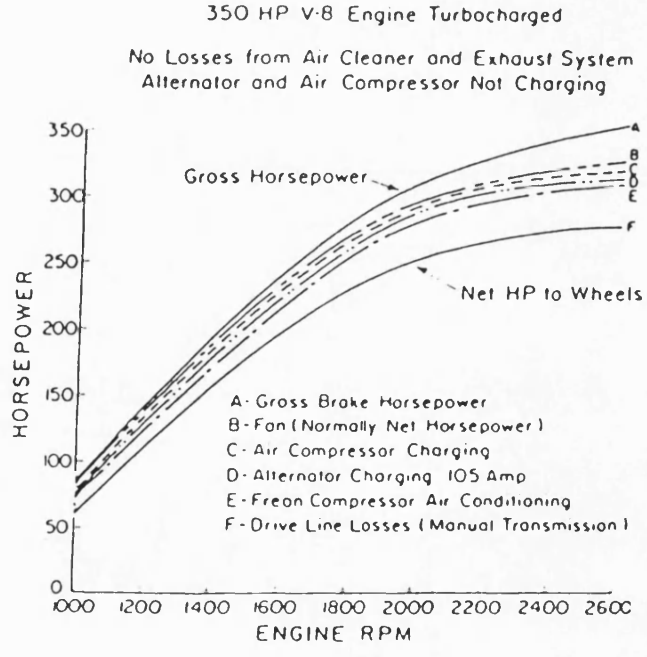

Fig. 1.5 Power losses in an engine installation

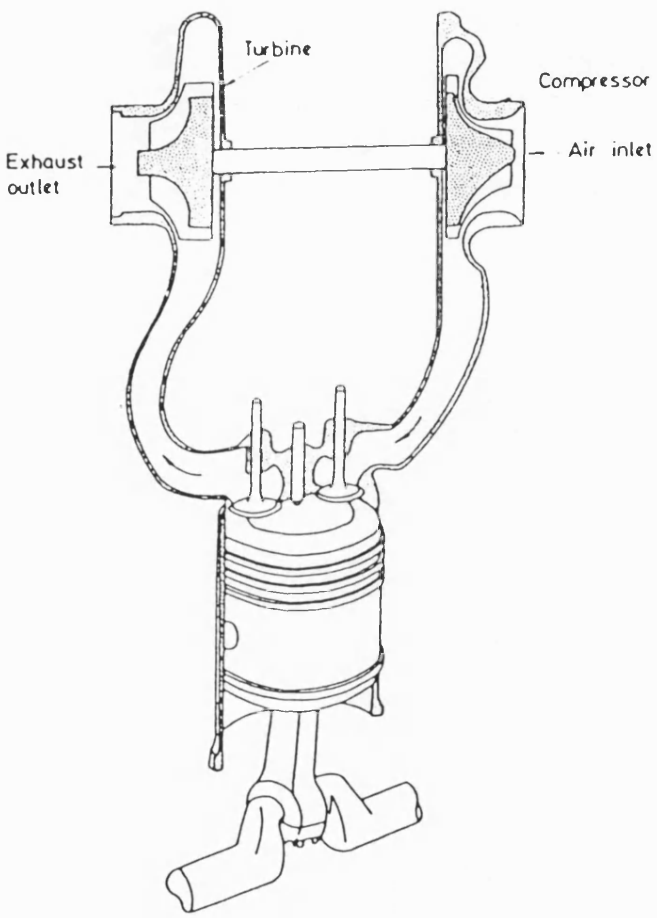

Fig. 1.6 Principles of turbocharging

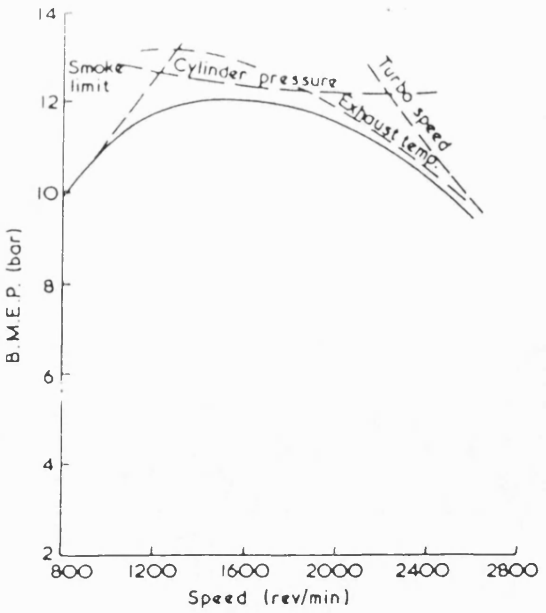

Fig. 1.7 Turbocharged truck engine torque curve showing limits to BMEP

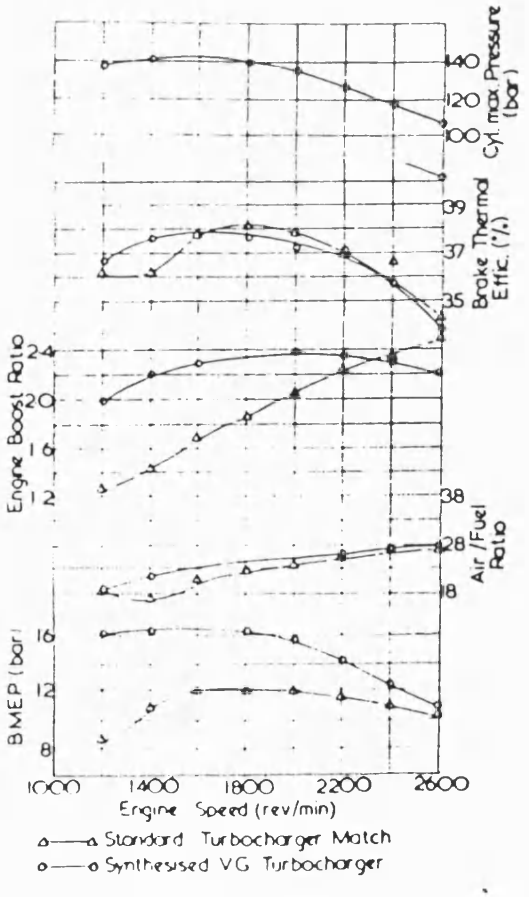

Fig. 1.8 Performance of a Diesel engine using synthesised variable geometry turbocharger

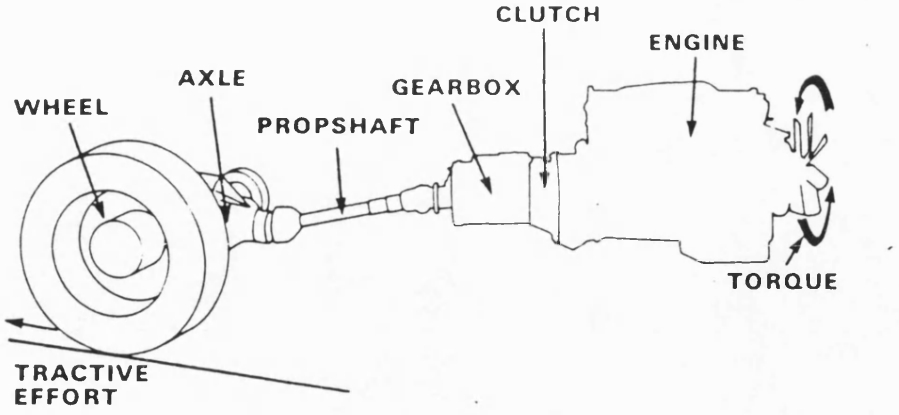

Fig. 1.9 Silhouette of typical conventional automotive power plant

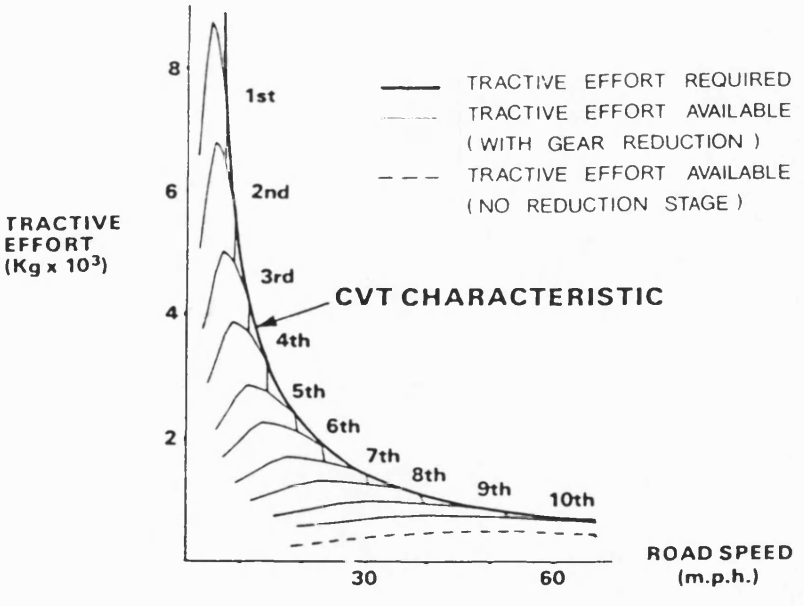

Fig. 1.10 Tractive effort-speed characteristics of a vehicle

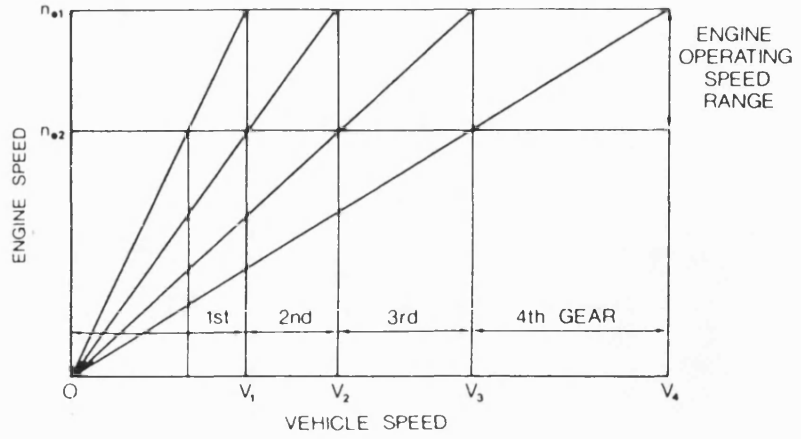

Fig. 1.11 Selection of gear ratios based on geometric progression rule

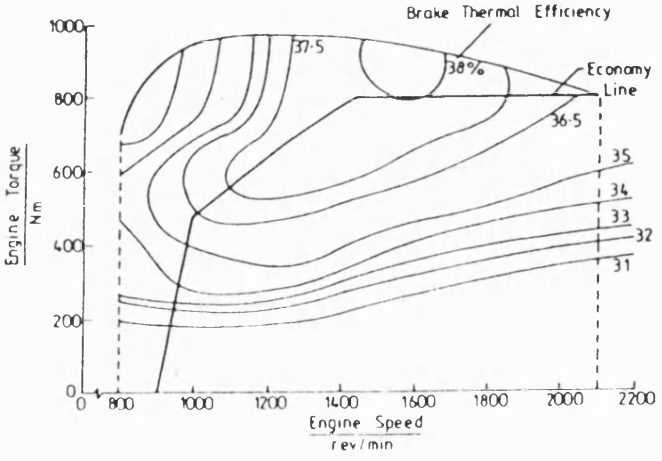

Fig. 1.12 Performance map of a turbocharged Diesel engine

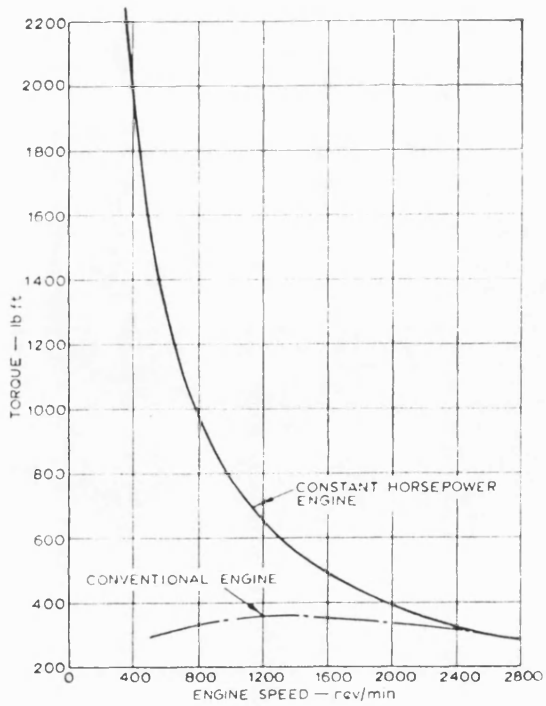

Fig. 1.13 Typical torque curve for conventional and constant power engine

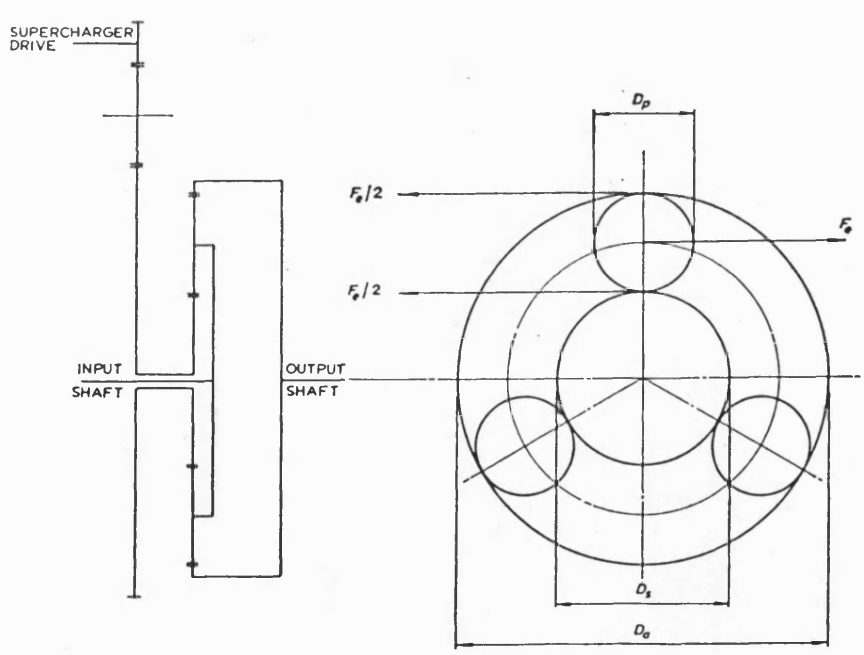

Fig. 1.14 Differential gear arrangement

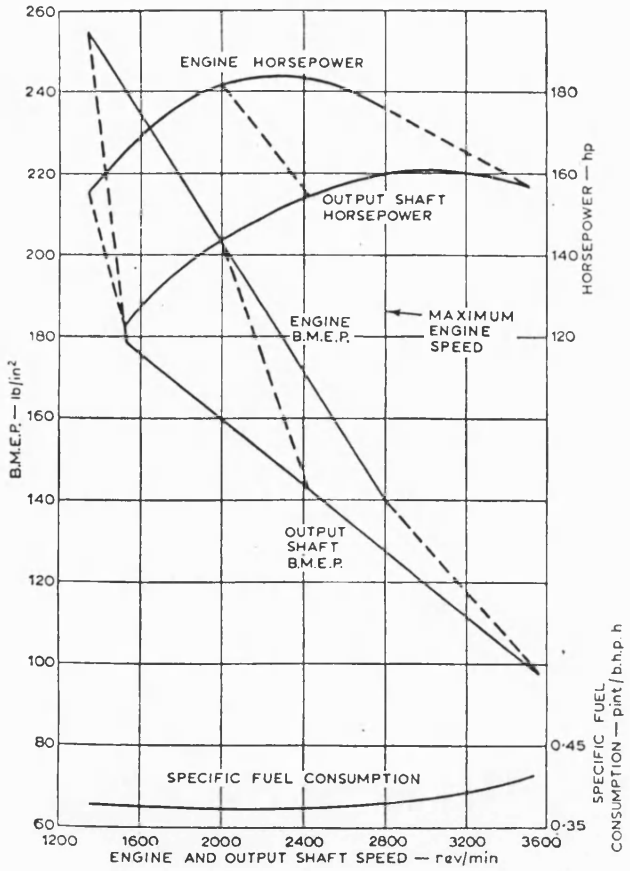

Fig. 1.15

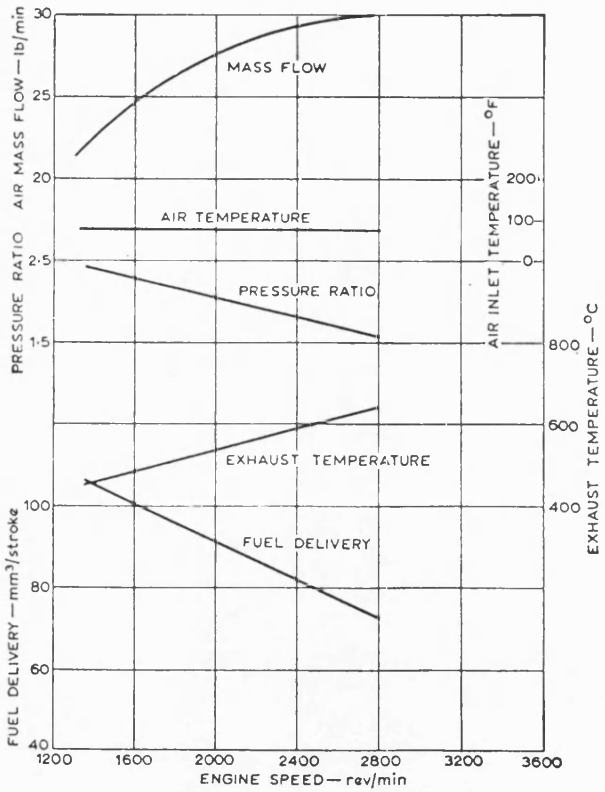

Fig. 1.16

Differential Diesel engine performance "third development phase"

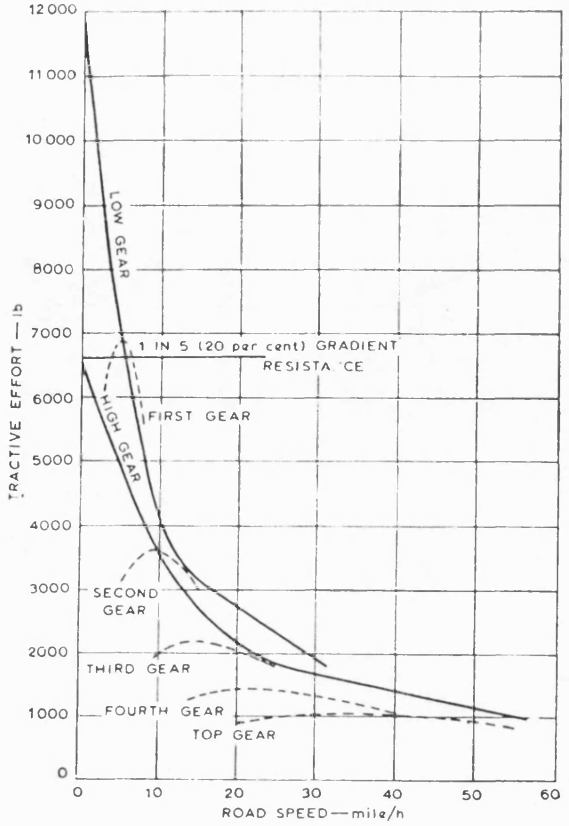

——— Differential engine.
– – – – – Conventional engine/transmission.

Calculated performance comparison between turbocharged 6·354 and 6·354 DD engine in a truck of 31 400 lb gross weight. Vehicle details: frontal area 65 ft² (air resistance 0·14 (mile/h)²); rolling resistance 12 lb/1000 lb; axle ratio, 7·17/1 for DD engine and 5·95/1 for turbocharged engine; gear ratios for turbocharged engine 1·0, 1·47, 2·24, 3·78 and 7·08; gear efficiency, turbocharged, 90 per cent direct gear, 85 per cent indirect; DD engine, 90 per cent low gear, 95 per cent high.

Fig. 1.17 Tractive effort : differential supercharged engine "third development phase"

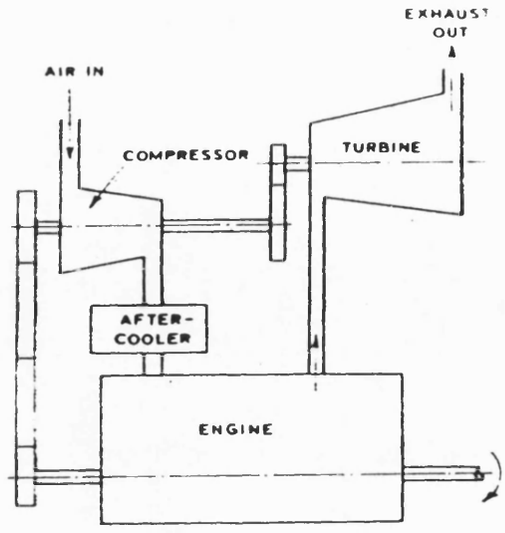

Fig. 1.18 Compound engine

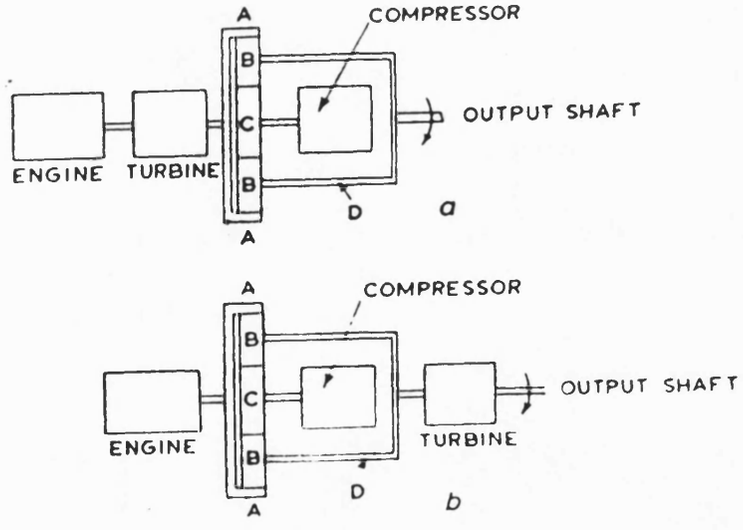

Fig. 1.19 Simple sketches of two possible ways of connecting the components of the differential compound engine

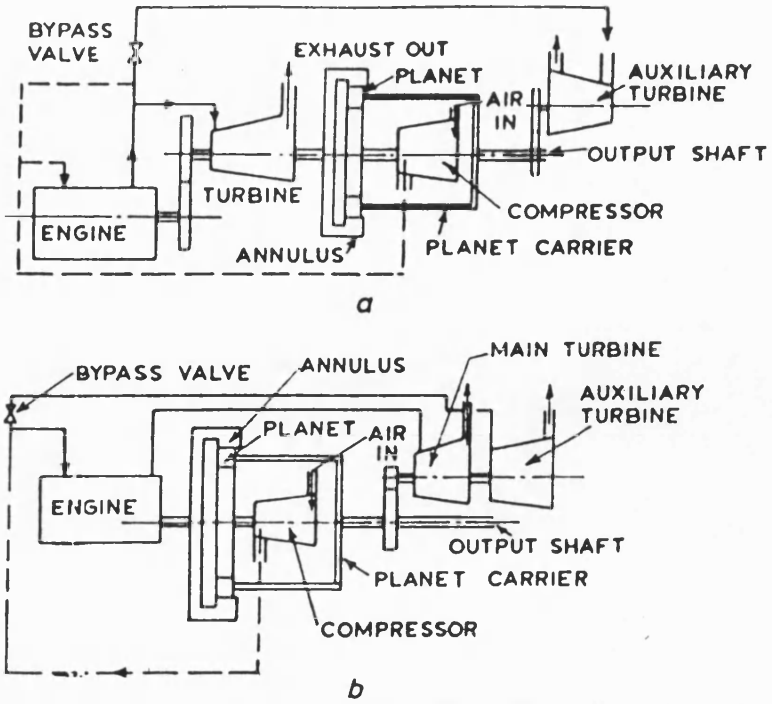

a Scheme (a) with auxiliary turbine.
b Scheme (b) with auxiliary turbine.

Fig. 1.20 Two different schemes for the differential compound engine with respect to the location of power turbine

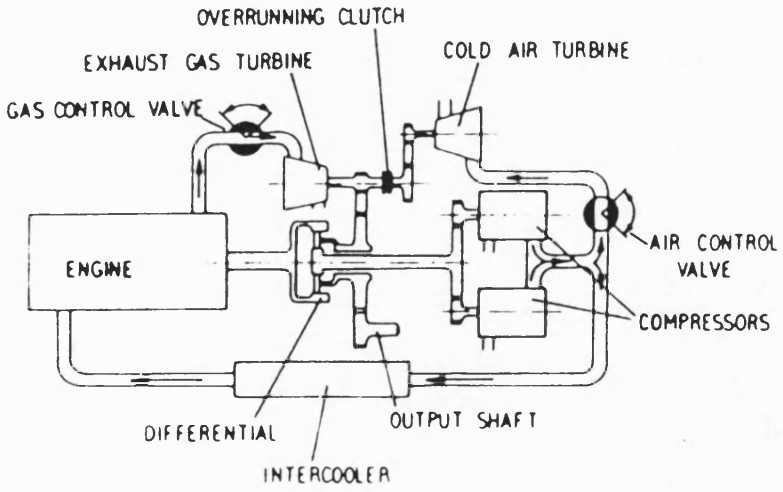

Fig. 1.21 General basic arrangement of the differential compound engine (DCE)

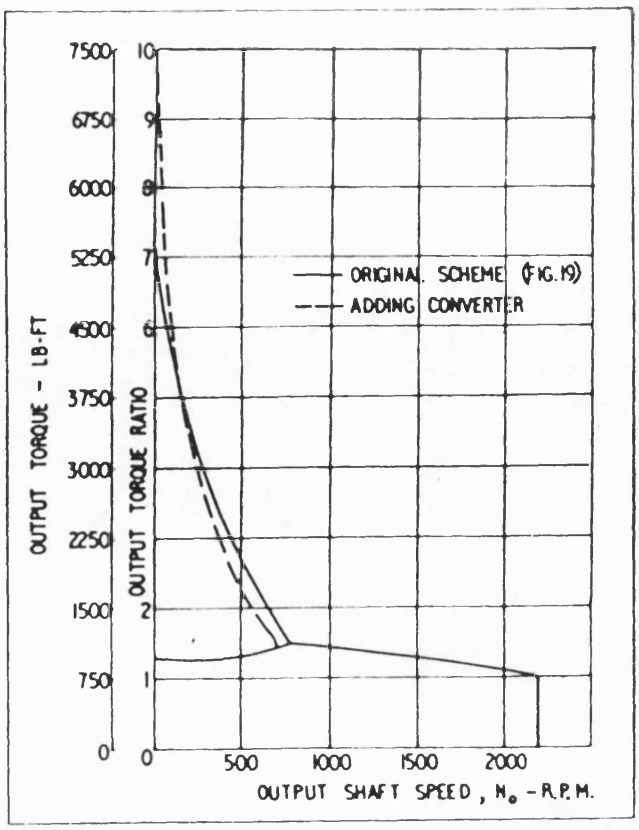

Fig. 1.22 Torque-speed characteristics of the original DCE versus converter addition

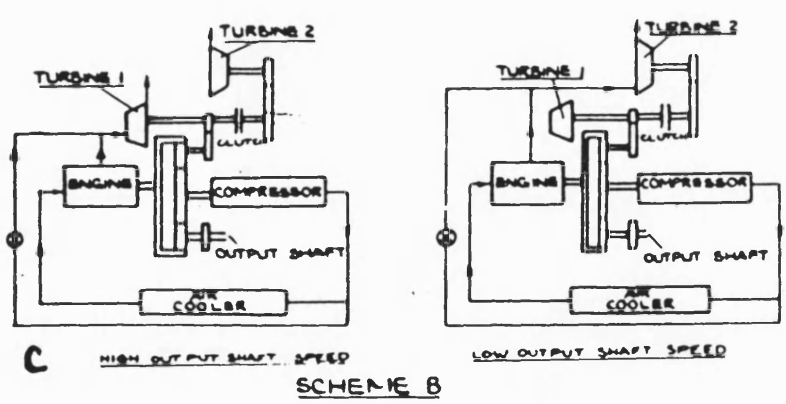

Fig. 1.23 Schematics of transmission schemes

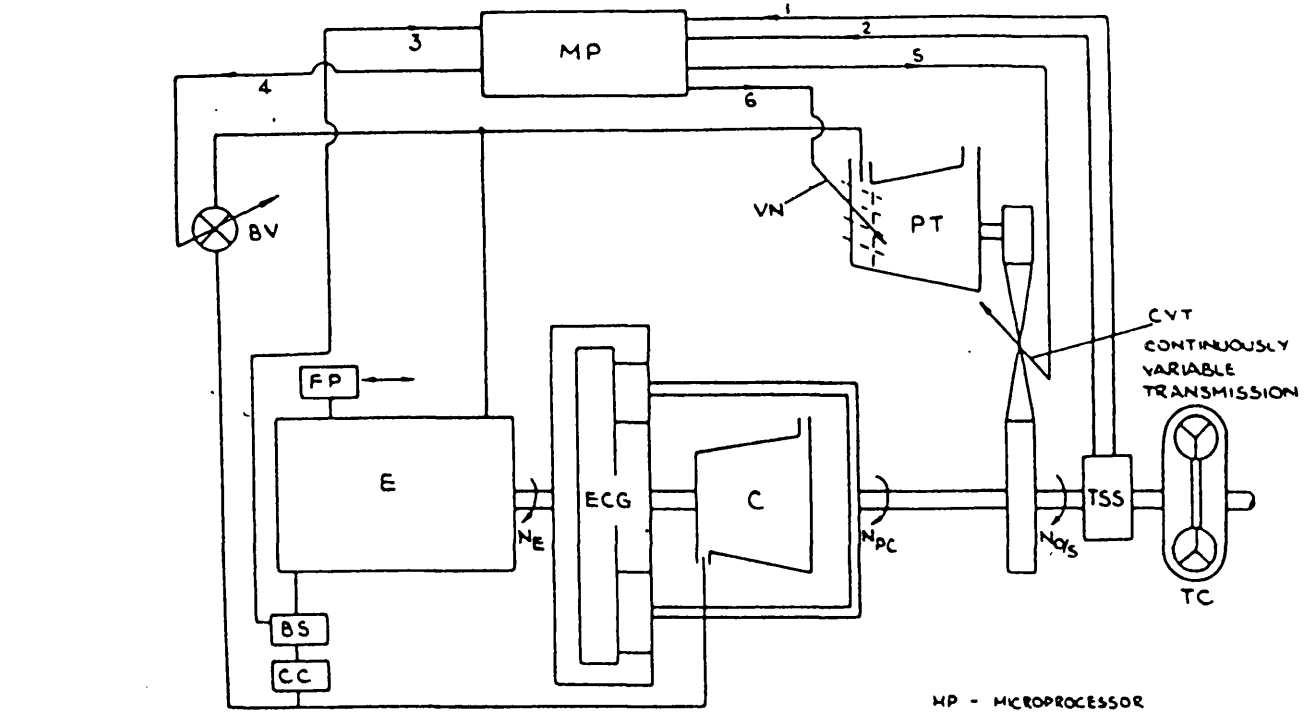

Fig. 1.24 Final version of the DCE layout

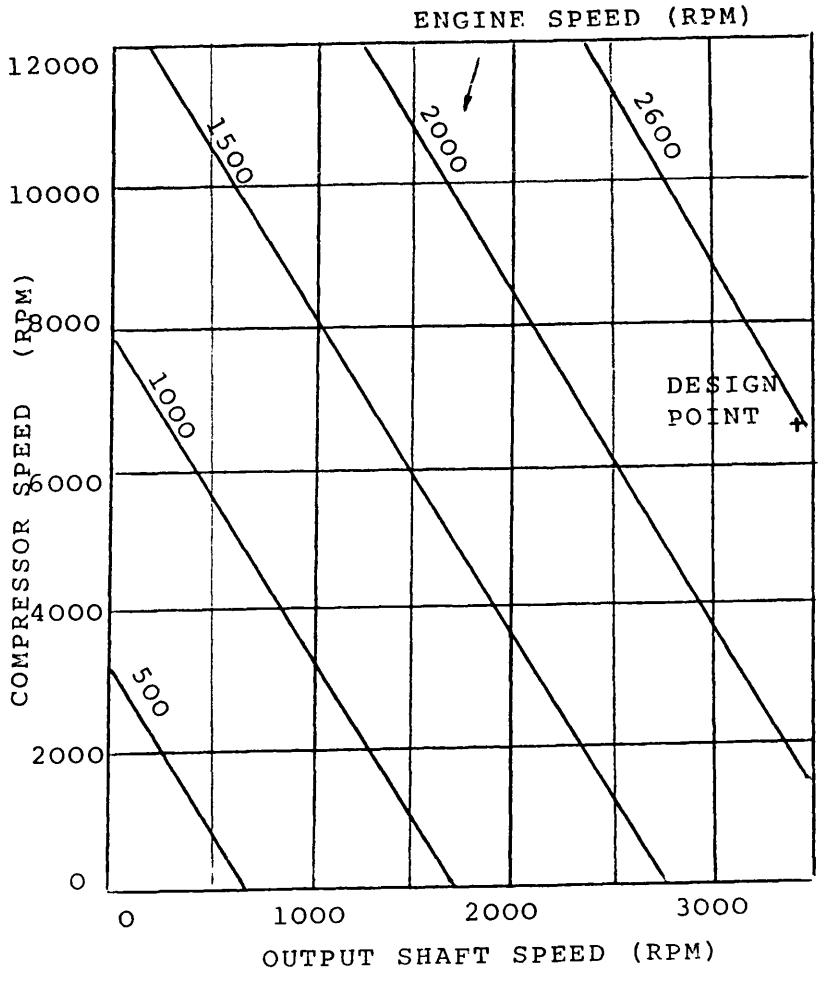

Fig. 1.25 Engine, compressor and output shaft speeds (in the DCE)

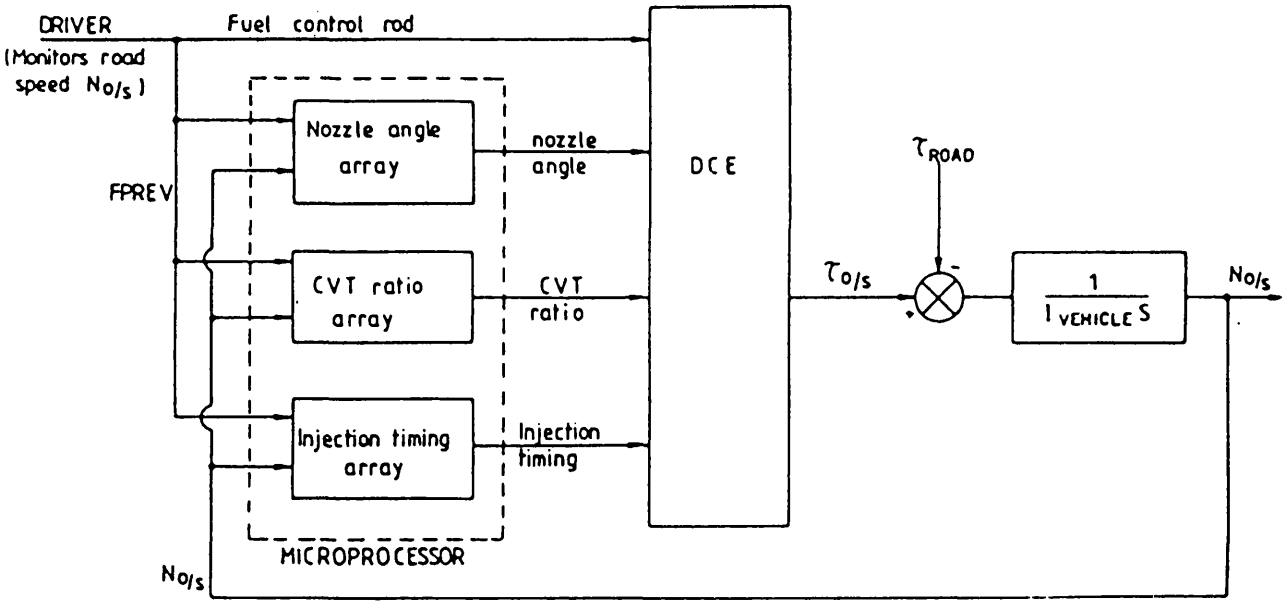

Fig. 1.26 Steady state control scheme for the DCE

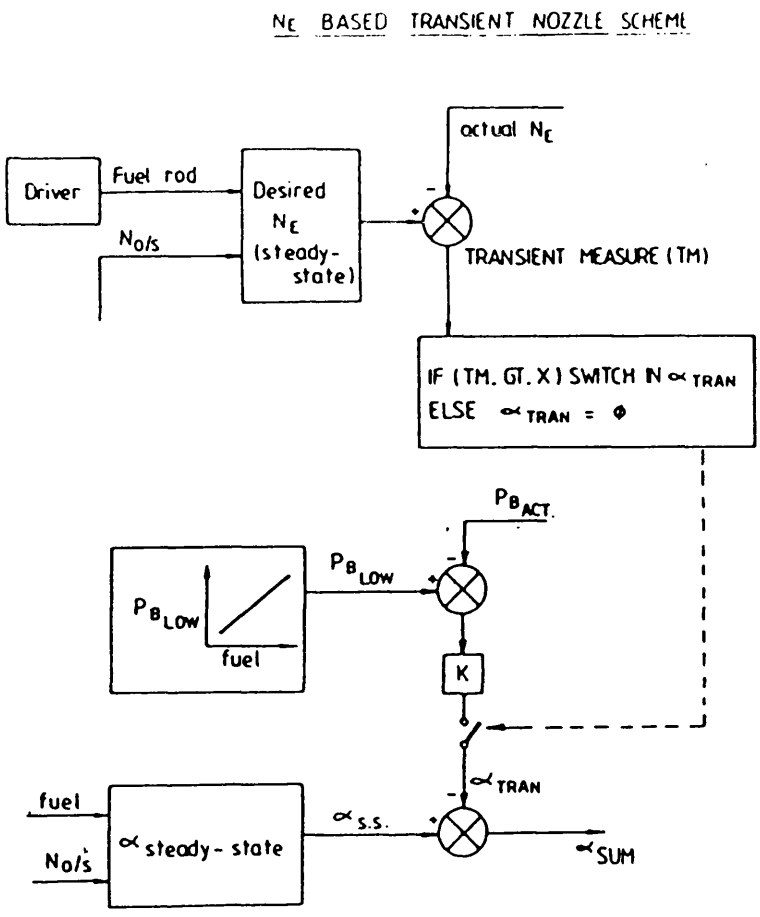

Fig. 1.27 Transient control scheme for the DCE adjusting turbine nozzle angle

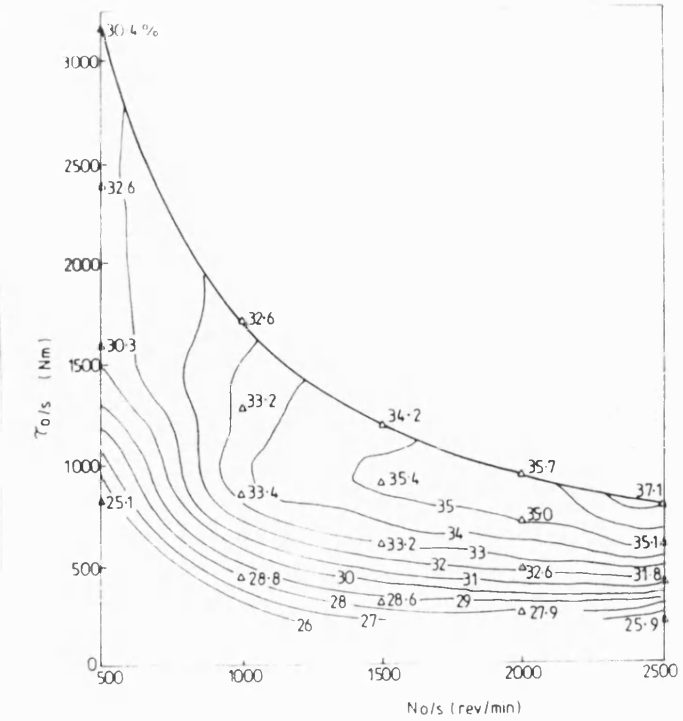

Fig. 1.28 DCE torque characteristics with efficiency contours

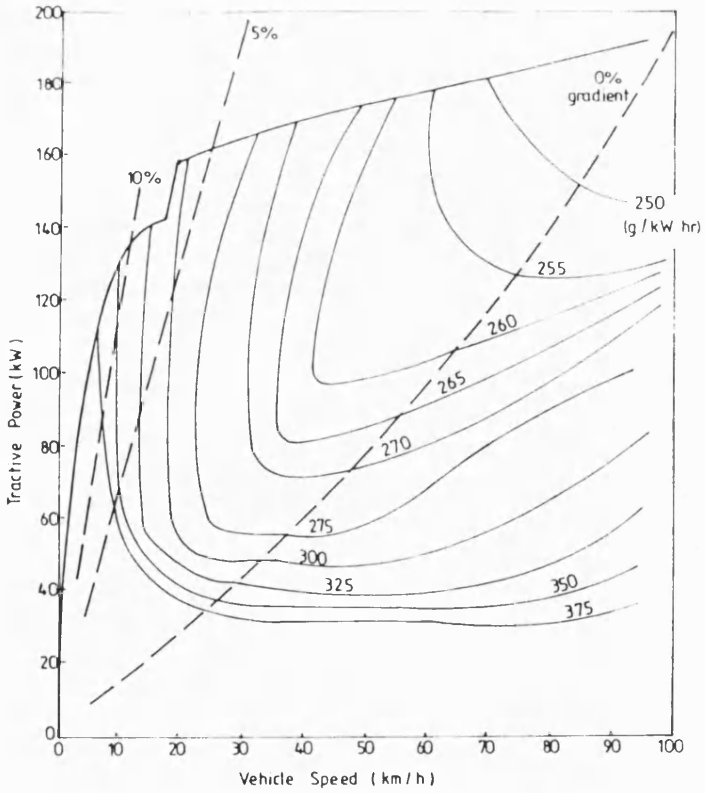

Fig. 1.30 Tractive power charactieristcis with SFC contours for a 38 ton truck equipped with the Perkins T6 354-DCE

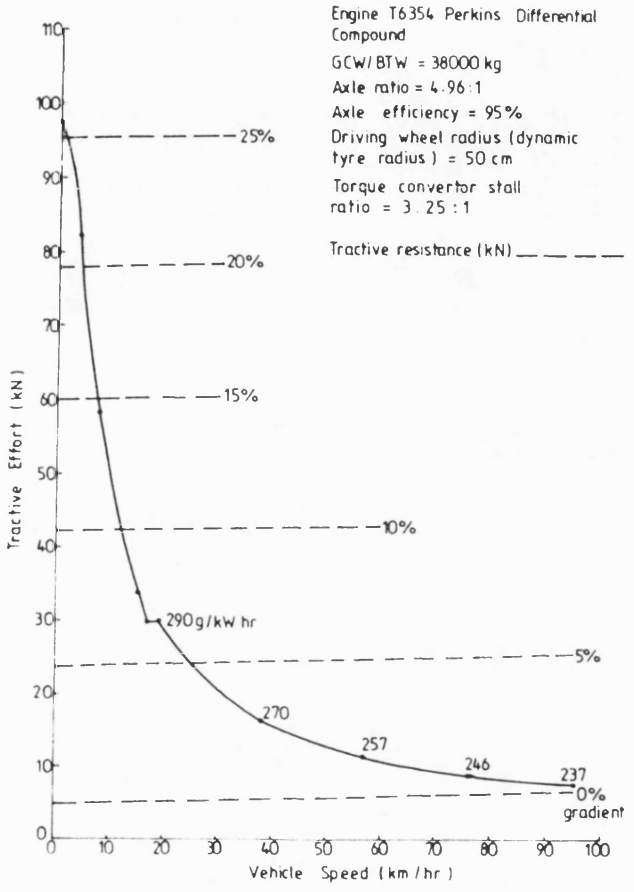

Fig. 1.29 Tractive torque characteristics for a 38 ton truck equipped with the Perkins T6 354-DCE

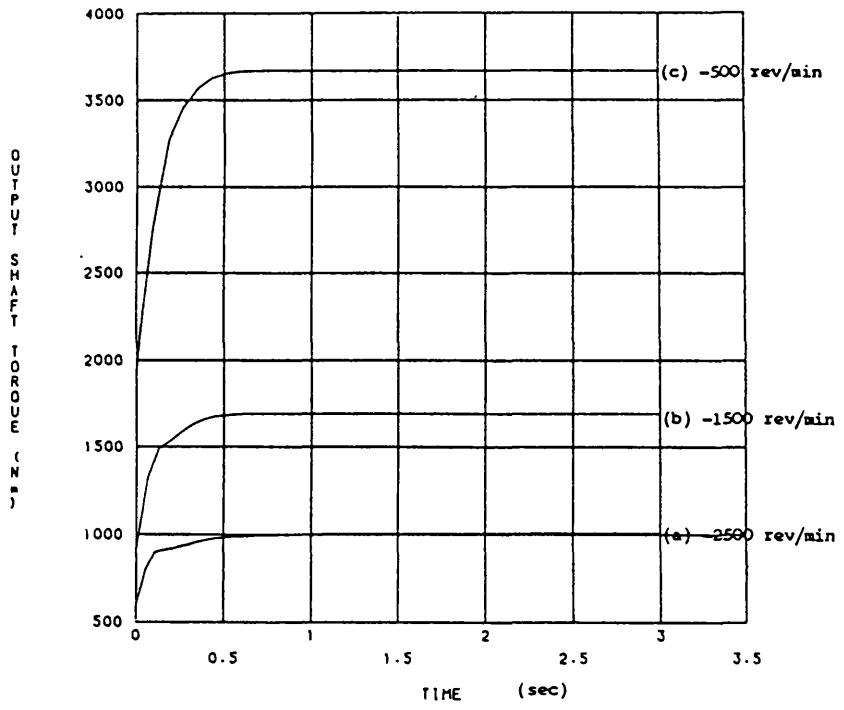

Fig. 1.31 Typical transient response of output shaft torque of the DCE at different constant output shaft speeds

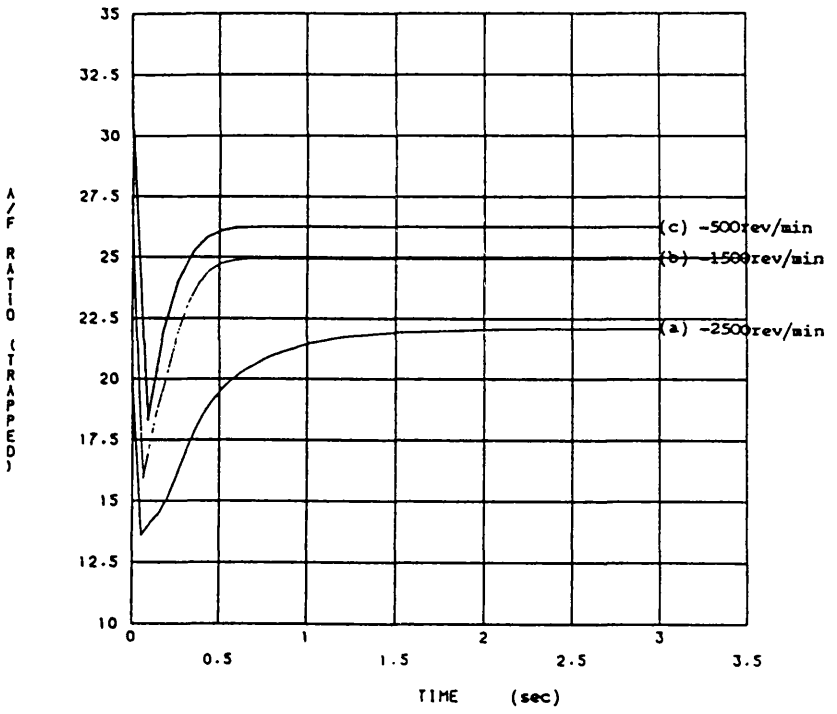

Fig. 1.32 Typical transient response of the DCE with respect to air/fuel ratio at different constant output shaft speeds

CHAPTER TWO

SURVEY OF THEORETICAL WORK

2.1 INTRODUCTION

The application of computer techniques is essential in the early stages of engine design, in particular in providing a tool for sensitivity study of design variables and reducing the required engine testing time. Also engine simulation clearly outlines those areas in which our knowledge is deficient as different aspects of cycle have to be expressed mathematically.

The ultimate goal in this thesis is to investigate theoretically the superiorities of transient performance characteristics of an engine in its DCE over those of its turbocharged configuration. The Cummins L10 engine was taken for this purpose as it is typical in developing power to meet heavy duty truck requirements. However, to achieve the goal, several other steps had to be taken which mainly support the reliability of the results of the comparison.

Several computer programs of two different degrees of complexity were used in this respect. Each of the programs has modular structure with subroutines representing the individual components and phenomena and a master or linking program specific to the particular configuration being modelled. As far as the overall system performance prediction is concerned, the simple programs based on simplified engine cycle can satisfactorily be used. However, the predictions of more complex programs based on application of well known filling and emptying method are not only more realistic but also very informative in terms of in-cycle phenomena and variations of performance parameters. The only problem is that the program of this kind is very costly to run. Therefore, the bulk of the work is carried out with the simple (rapid matching) programs and is validated at some selected running conditions by the detailed programs.

In order to establish a reliable basis for performance characteristic predictions for the L10 engine in its DCE configuration, it was necessary

to examine both types of the program predictions and tune up their input data and submodels for the L10-T/C engine to match the results against the available manufacturer's test data.

In this chapter, a brief description for each of the programs used throughout the theoretical work is given in the form of subsections dealing with the relevant subroutines, flowchart, input data with respect to the Cummins L10 Diesel engine specification and requirements. The programs and the general purpose of their applications are :

1. The program 'EMAT' for simple steady-state simulation of T/C Diesel engines.
2. The program 'SPICE' for detailed steady-state simulation of any configuration of internal combustion engines.
3. The program 'TRANIC' for simple transient simulation of T/C Diesel engines.
4. The program 'DCE2' for simple steady-state simulation of the DCE.
5. The program 'CSPDCE' for detailed steady-state simulation of the DCE.

2.2 SIMPLE STEADY-STATE SIMULATION OF THE L10-T/C DIESEL ENGINE USING PROGRAM 'EMAT'

2.2.1 Brief description of program 'EMAT'

The steady-state engine matching computer program 'EMAT' (Ref. 19) has been used very successfully at Bath for many years and has been modified to simulate other configurations such as two stage, variable geometry turbocharged and compound engines.

This program has a modular structure, with a series of subroutines describing the individual components and for mathematical calculations as follows (for the components): (see fig. 2.2.a)

a) Engine
b) Compressor
c) Turbine
d) Cooler

(for the gas properties):

a) Enthalpy
b) Specific heats
c) Gamma

(and for the mathematical calculations):

a) Interpolation
b) Iteration

Program 'EMAT' links all these subroutines together, and the matching condition is established by iteration, to obtain turbocharger equilibrium conditions. A quasi-steady approach is used, all equations being algebraic. The program is highly dependent on detailed empirical knowledge of a particular engine and employs experimental matching coefficients to achieve good agreement over a wide range of operation. In the case of other components incorporated in the system, their performance is represented by their steady state characteristics, which could be obtained experimentally. These components are connected by the air flow passing through them and by the pressure ratios across them. No mass accumulation is allowed between the various components.

Steady State Prediction

Fig. 2.1 shows schematically a single stage after-cooled T/C engine driving a load under steady state conditions, speed N_E, torque τ_E while fuel is supplied at the rate m_f.

In the application of steady state, the T/C version of the program 'EMAT' fuel flow rate, m_f, and demanded engine speed, N_E, are used as inputs and all other relevant operating conditions, in particular the output torque, τ_E, and the turbocharger operating point in terms of speed and flow characteristics are determined.

The program draws on all the subroutines (just mentioned) and calls them sequentially, as shown in the flow chart, figs. 2.2.a and 2.2.b. The program has been found to give accuracies very little inferior to experimental results, while run times are of the order of about one tenth of the step-by-step programs. However, care has to be taken when extrapolating the data beyond the valid range.

2.2.2 Subroutines of Program 'EMAT'

2.2.2.A The engine model

The mathematical representation of C.I. engine cycles has undergone a rapid revolution in recent years. The engine model used in engine matching program is based on a substantially modified air standard cycle. This approach has been developed at Bath by Way (Ref. 18) and still divides the cycle into a relatively small number of discrete steps, retaining some of the computational speed and simplicity. Fig. 2.3 is a schematic diagram.

The modifications which have been introduced, allow for :

1) change of chemical composition and effect on gas properties,
2) throttling losses through valves by adjustment of induction and exhaust pressure levels and allowance for pumping work,
3) heat transfer based on detailed experimental investigations,
4) departure from idealised constant volume and/or constant pressure combustion by use of injection timing and duration, and modified

by heat transfer, based on detailed experimental investigations,

5) consideration of gas exchange process by taking details of valve timing and valve lift curves into account, and dealing realistically with pressure differences across the engine.

The engine model is composed of two distinct periods, viz. the closed and open period

a) Closed period

Referring to fig. 2.3, this period is that part of the cycle with no air flow through the cylinders and refers to the discrete calculation steps for :

Compression 1-2 (assumed adiabatic)

Combustion 2-5 (by heat release model with heat transfer to coolant)

Expansion 5-6 (again assumed adiabatic)

Combustion is calculated as a mixing controlled process, in three discrete steps corresponding to :

i) constant volume applied between 5° BTDC and 5° ATDC with a small correction for the piston work during the period,

ii) constant pressure, and

iii) a transition period between constant pressure and adiabatic expansion.

Actual values for heat transfer are obtained from empirical correlations apropriate to a particular engine. The heat release proportions in parts (ii) and (iii) are considered to be equal.

Finally, the release condition P_6 and T_6 are determined with completion of the closed period through adiabatic expansion process 5-6.

b) Open period

This period is again divided into several discrete subphases as follows : (6-7) blow down, (7-8) exhaust, (8-9) overlap, (9-10) suction and, (10-1) supercharge.

By making the initial assumption of constant mean valve areas and cosntant mean inlet and exhaust manifold pressure P_{im} and P_{em}, it is

possible to arrive at estimates of the cylinder pressure $P_7 = P_8$ during exhaust and $P_9=P_{10}$ during suction, as well as of the scavenge air mass flow, m_{sc}, during the overlap period.

Completion of the open period calculations finally yields the trapped conditions P_1, T_1 as well as equivalence ratio, as a function of retained residual gases.

2.2.2.B The compressor model

Centrifugal compressors invariably have characteristics of the type shown in fig. 2.4. Two-dimensional numerical arrays are used to represent given characteristics of the form of fig. 2.4. These give for fixed dimensionless speeds ($N/\sqrt{T_{o1}}$) and at (evenly) spaced mass flow increments ($m\sqrt{T_{o1}}/P_{o1}$) values of pressure ratio (P_{o2}/P_{o1}) and of total to static efficiency (η_c).

2.2.2.C The turbine model (fig. 2.5)

In contrast to the compressor model, the nozzled turbine subroutine used is of the analytical type. This has the advantage that the effects of changes in turbine build or of variable geometry can be taken into account without the necessity for preparing separate numerical arrays for each possible build.

2.2.2.D The heat exchanger model

In their most general form the heat exchanger models provide a relationship between pressure ratio (on the gas side) and dimensionless inlet mass flow, and for effectiveness as a function of its design point value and the ratio of actual to design point dimensionless mass flow.

2.2.2.E The simple iteration subroutine

During the course of an iteration, this subroutine is used to find the next value of the relevant variable. The iteration proceeds in three

stages. Before iteration starts the error terms are set to zero in the main program. In the course of calculations, error terms are established to obtain two points with errors of opposite signs. In the second stage, a third mid point between these points is found. The third stage is carried out when the subroutine has three points at its disposal to find a final value of the variable so as to converge around the zero error axis of a rectangular hyperbola through the previous three points.

2.2.3 Flowchart for Program 'EMAT'

Due to the number of unknown variables, it is not possible to obtain a matched result without iteration. In fact, without initial guesses it is not possible to enter any of the subroutines representing the physical components. The iteration structure is determined by the requirements of the subroutines in terms of which variables are required as inputs and which as outputs.

Fig. 2.2.b shows the flowchart for the program 'EMAT'. The initial statements are concerned with the reading and sorting of input data. At the start of calculations, the interpolation routine is called to obtain, as a first guess, the engine delivery ratio corresponding to equal inlet and mean exhaust pressures. The first guess for turbocharger speed is made corresponding to values given as data.

At this stage, flow calculations begin by calling the compressor subroutine. The use of compressor subroutine demands knowledge of compressor speed and mass flow. Other compressor variables like pressure ratio, efficiency, torque, etc. are calculated subsequently. With the control marker in the program, the subroutine will choose a first guess for mass flow corresponding to the mid point between surge and choke for the given speed. On exit from the compressor subroutine the cooler subroutine is entered. Using the compressor mass flow and cooler outlet conditions, the engine delivery ratio, 'DRS', is then calculated for comparison with the value previously obained from the data, 'DRSX'.

At this stage the compressor flow is matched to the engine flow by means of the delivery ratio, which is given as data as a function of engine

speed and the ratio of mean exhaust pressure to inlet pressure. The engine and compressor cannot be matched without a value for the mean exhaust pressure which can only be obtained by reference to the turbine characteristics. Therefore, the error bound for delivery ratio at this stage is relatively large, as the interpolated value of 'DRSX' is only an approximation which will have to be corrected later when the mean exhaust pressure is known. The iteration subroutine is repeatedly entered, giving a new value of compressor mass flow each time for the next compressor calculation, until the error is within the permitted tolerance.

As soon as the delivery ratio criterion is satisfied the engine subroutine can be entered. From the matching point of view the principal purpose of the engine subroutine is to provide the exhaust conditions. But this requires an estimate for the minimum exhaust pressure ratio (REX) which is used to calculate the open period work.

The turbine subroutine requires as input values of turbine speed, inlet pressure ratio and inlet temperature. From these and the turbine geometry, the flow, efficiency and power are calculated. In this program the use of the turbine subroutine is complicated by the exhaust pulse model in which turbine inlet conditions are represented by 5 values of pressure ratio corresponding to different stages of the pulse. Iteration is needed to match the exhaust flow with the engine exhaust flow and the turbine power with the compressor power.

In the absence of any calculated value of 'REX' an initial guess is taken as the square root of the compressor pressure ratio. The important point for the iteration logic is that the minimum pulse pressure ratio (REX) is unknown until the iteration is complete; this pressure ratio affects the pressure ratio at all points of the pulse. The calculations are set out in such a way that the total flow through the turbine over the pulse period, divided into 5 steps must match the engine exhaust flow.

However, if the pressure ratio during the pulse is too high the turbine flow rate will be high so the pulse will take a shorter time than say 120° crank angle degrees alloted to it for a six cylinder engine. This period of the pulse is therefore the control parameter needed to find the

corrected value for the pressure ratio 'REX'. Iteration is carried out to obtain an error in the pulse period less than one degree crank angle.

As soon as a new value of the mean exhaust pressure is obtained, it requires an alteration of engine delivery ratio usually as a result of modification of the compressor air flow. A further and more accurate delivery ratio check is made and these iterations continue until the delivery ratio criterion and the exhaust pulse criterion are both satisfied.

The calculation so far performed have been with the guessed value for turbocharger speed. This leads to an error in the turbocharger power balance. This error is compared with the minimum acceptable error and if not acceptable, a new value of turbocharger speed is obtained by the iteration subroutine. The whole of the previous iteration procedure is then repeated until satisfactory values are obtained for delivery ratio, exhaust pulse period and turbocharger power balance.

The matching calculation is then complete and the results are stored in the output array.

2.2.4 The EMAT Input Data to Simulate the L10-T/C Engine along its LTC

In the first step of the simulation of the steady state performance characteristics of the Cummins L10 engine, the engine matching program EMAT was used in its single stage T/C version.

The input data of the program is described in the input format given in table 2.1, in the order of values as they are entered. The figures in the table show the Cummins L10 engine and its turbocharger particulars, and also the running conditions at engine speeds of 1000, 1200, 1600, 1900 and 2100 rpm with a fuelling schedule such as to yield an engine performance close to the LTC.

Comments on Input Data

Crank angle convention. Crank angles for valve opening or injection timing are expressed in degrees between zero and 720, with zero

corresponding to top dead centre for the open period. Thus the start of injection is 343 degrees (17 BTDC).

Engine empirical factor for combustion rate. The program uses an empirical equation to calculate combustion rate with an adjustable factor XK. This should have a value of the order of 0.01 to 0.1.

Referring to the typical P-v diagram used by the EMAT program (fig. 2.3) and the concept behind the combustion process assumptions, when injection timing is well before 5 deg BTDC, the combustion rate factor XK determines what portion of fuel is due to be converted into released heat in each phase of the combustion period.

In the empirical equation, that portion of fuel (α : alpha) which is due to burn during constant volume phase of combustion is a function of injection timing, XK and injection duration. Figs. 2.6.a and b give the value of α as a function of the injection timing and duration for two extreme cases of XK = 0.01 and 0.1.

Any increase in XK implies greater heat release during the constant volume phase of combustion rather than the other two phases. As a consequence the maximum cylinder pressure and temperature increase with any increase in the combustion rate factor. Therefore, the combustion rate factor plays an important role in determining the P-v diagram and its net area.

Engine empirical factor for heat transfer. Similarly the heat loss correlation has an adjustable factor 'QLF'. The empirical equation for heat loss assumes that the heat transfer is largely a function of air flow, while the mean temperature difference is controlled by the inlet manifold temperature, the air-fuel ratio and the water temperature. The equation is not strictly dimensionless, so the factor QLF will have a value dependent on the system of units used, and also to a small extent on the engine and its running condition. Using the metric system the factor has a value of the order 1.0 to 1.5.

'QLF' was examined over several running conditions using the L10

experimental data. Table 2.2 shows the variation of this factor over the running conditions of minimum BSFC.

Pseudo manifold volume ratio for pulse model. This variable, 'RHM' does not represent the true geometric volume but is merely an empirical value to obtain the correct turbine power under pulsing conditions. The value is usually about 8-10 cylinder volumes - far larger than the actual manifold. The value of RHM may be set to a very large value - say 1000 - to represent constant pressure turbocharging.

Arrays of empirical engine factors. The range of 5 engine speeds should cover the speed range of the engine from the lowest to the highest. The 5 values of diagram factor, FMEP and guessed turbine speed should correspond to these engine speeds. The 5 values of exhaust/inlet pressure ratio should cover a range above and below 1, typically between 0.8 and 1.2. The 25 values of delivery ratio form a two dimensional array in terms of speed and exhaust/inlet pressure, the first 5 values corresponding to the first (lowest) value of engine speed.

Turbine data (analytical subroutine) The numbers correspond to flow stations through the turbine, 1) at the stator nozzle, 2) at the rotor entry, 3) at rotor exit. The program may accept data for either a vaned or vaneless stator. For the vaneless type, the diameter at the nozzle, is twice the distance from the centre to the mean point of the volute entry throat. The area at the volute throat is given while the width at the nozzle vanes must be set to zero. For a vaned turbine, the calculation starts at the vanes (the volute is not represented). The diameter at exit from the vanes, and the passage width are given while the throat area is now replaced by the nozzle angle in degrees.

The pitch of the blade at exit is the axial displacement by rotating the turbine by one revolution with the blade exit following a helical path. This dimension is more easily obtained from the drawing than the exit angle which varies over the blade height. By setting the blade thicknesses to zero, the number of blades is not required. The empirical flow loss factor has a value of about 0.8 for small turbines. The mechanical friction loss factor gives a friction power loss proportional

to the square of turbocharger speed. This gives credible results with values of the order of 0.05-0.1 depending on turbine size.

2.3 STEADY STATE SIMULATION OF THE L10-T/C ENGINE USING PROGRAM 'SPICE'

2.3.1 Brief Description of Program 'SPICE'

The computer program 'SPICE' is a large FORTRAN based simulation program for internal combustion engines. The program has a well organized modular structure and is designed to be flexible and adaptable to user's needs. Any type of volume, flow and mechanical junction with new required characteristics may be written and added to the program in a modular way. Therefore, a model can be constructed with almost unrestricted freedom. Some of the systems that may be modelled using SPICE are given in fig.2.7.

The program is based on the 'Filling and emptying' concept in which, for example, a turbocharged engine is treated as a series of control volumes with simultaneous inflow and outflow, and the governing equations are solved as a system of simultaneous differential equations. A set of first order non-linear coupled ordinary differential equations for stagnation temperature, mass and equivalence ratio results for each control volume of the system and is solved at discrete time steps (ref. 20). The mathematical model describing the system also comprises of flow junctions and shafts which are governed again by differential equations. The basis of these equations are the conservation principles for energy, mass and momentum.

'SPICE' uses sub-models to determine the terms required in the solution of the differential equations. Ignition delay, heat release and heat transfer are modelled empirically using relatively simple, but effective models based on engine parameters and variables. If accuracy of simulation is required, it is necessary to fine tune these empirical models using the available correlation constants within each to match the simulated performance to the known performance of an engine.

The numerical method used by 'SPICE' is the modified Euler predictor-corrector scheme which has the advantage of computational simplicity and speed. If the number of iterations to meet the required convergence criteria, at any stage, exceeds a prescribed number (usually

four), the step size may be further reduced by half until a solution is found.

2.3.2 The Program Structure

In execution of the program SPICE, use is made of several subroutines at each stage of reading input data, performing calculations, or storing and printing out of results (fig. 2.8.a). The program is modularly constructed so that the new subroutines can be added to the main program to meet any new modelling requirement. At present, the program comprises more than a hundred subroutines, some of them acting merely as linking routines. Every individual parameter involved in defining system variables is assigned to a component of an array, and hence there are a number of multi-dimensional arrays, some of them acting as intermediate arrays. In the course of computations, the values of stored array components undergo modifications until a final solution for the system is found.

A main linking routine is used to read in and initialise all the elements of the arrays and finally to call another major linking routine for finding numerical solution to the sets of system differential equations (fig. 2.8.a). In numerical solution, the major use is made of different predictor and corrector routines to reach mechanical and thermodynamic equilibrium for the system. Other subroutines, in turn, defining the shaft system (incorporated in the aggregate) are used for shaft predictor or corrector routines.

Flow modelling is performed by the use of two major predictor and corrector routines, each of which draws on several other subroutines to model a control volume which may be a cylinder, a manifold or a prechamber, one at a time. For cylinder modelling provision is made for all thermodynamic phenomena covering heat and mass transfer and hence the model incorporates different submodels (subroutines) to calculate:

a) The instantaneous cylinder volume, exposed liner surface area and rate of change of each of them;

b) The instantaneous rate of heat release according to a simple Wiebe function (ref. 21) or Watson-Marzouk model (ref. 22);

c) The ignition delay using Watson adaptation of Wolfer's (ref. 23);

d) The rate of heat transfer from the cylinder contents to chamber wall, using semi-empirical correlations due to Woschni (ref. 24), Hohenberg (ref. 25), Eichelberg (ref. 26), or Annand (ref. 27) with two alternative options of constant wall temperature or resistance modelling. The liner temperature is calculated at this stage. Adiabatic modelling is also possible;

e) The gas properties, viz. specific heats, gamma, gas constant, enthalpy, internal energy and rate of change of internal energy, as a function of gas temperature and fuel-air ratio (ref. 28);

f) The gas flow rate, enthalpy and fuel air ratio passing through a junction next to a control volume by diverting the solution to another appropriate subroutine depending on the junction type, e.g. poppet valve, port, simple orifice, etc. Essentially the flow at these junctions is modelled as an isentropic expansion through a throat, the area of which is taken as the product of the instantaneous geometric area and a discharge coefficient normally derived from steady state flow tests;

g) The operating point of a compressor or turbine regarding either as a type of junction having a particular governing map to be entered, for interpolation of the turbomachinery flow and efficiency as a function of its speed and pressure ratio;

The manifold and prechamber models are covered by the same subroutines as the cylinder, but omitting the volume change routine for both models as well as heat release routine in the case of manifolds.

In the case of insufficient input data or any other program run failure, a number of error messages appear. As already mentioned, ignition delay, heat release and heat transfer are modelled empirically and hence, if

accuracy of simulation is required, it is necessary to fine tune these models to match the simulated performance to the known performance of an engine.

2.3.3 Flowchart for Program 'SPICE'

Figs. 2.8.b and 2.8.c are flowcharts of program 'SPICE' in two parts, the latter being used inside the former. The numerical solver is based on the predictor and corrector technique and examines convergence criteria applied to temperature, T, equivalence ratio, F, mass, m, and shaft speeds, N_E and $N_{T/C}$. Fig. 2.8.c shows the overall flowchart of the predictor-corrector of the program. Although the temperature is specifically shown in the predictor-corrector part (loop) of the flowchart, the other variables share the same procedure. The different subroutines in this respect are called 'THPRED' and 'THCORR' for variables T,F and m, and 'SHPRED' and 'SHCORR' for variables N_E and $N_{T/C}$ (fig. 2.8.a).

Parameter ψ is the angular crank position of cylinder under consideration, and is incremented by the crank step $\Delta\psi$. ψ is checked for the end of each cycle. The convergence of a variable is not expected to be satisfied until at least two iterations has been completed. If after a number of say, six times, (as shown) further iterations are still needed, the calculation step size is halved and the iteration counter is set to zero for a restart. All control volumes incorporated in the system are treated according to their particular type in every iterative loop.

All criteria concerning the variables T,F,m,N_E and $N_{T/C}$ should be met before the crank angle is incremented and a check must be made whether step size needs to be doubled (where it has previously been halved).

During and after a cycle calculation, the input control codes determine whether the results are to be written into output files. In any case, the instantaneous conditions of control volumes and shafts at the end of a cycle are used as initial conditions for the start of the next cycle.

Fig. 2.8.c is the flow chart for a control volume to find solutions to the differential equations for the thermodynamic variables. As mentioned in Section 2.3.2, depending on whether the type of control volume is a cylinder, three submodels of variable volume, heat release and heat transfer are used additionally.

Flow modelling consists of calculations of the rate of mass flow through a junction before or after a control volume, and is an essential preliminary before the system of thermodynamic differential equations are solved. The method of calculation adopted depends on the type of a junction. If the junction is defined as a type of orifice, viz. simple orifice, poppet valve, port, reed valve or any other type of valve, its area is taken as the product of the instantaneous geometric area and a discharge coefficient normally derived experimentally.

The simplest type is the orifice which is normally assumed to have a constant flow area. Valves and ports are represented as a table of effective flow area against crank angle, and three scale factors are available to allow easy manipulation of the data. These factors allow the opening time of the valve to be advanced or retarded and flow area or the period of opening to be scaled.

The flow rate is determined assuming one dimensional isentropic flow between the stagnation conditions in the control volumes at entry and exit. If alternatively, the junction is a turbocharger compressor or turbine, its instantaneous rate of flow is considered to be a function of the rotor speed and the pressure ratio. Tabulated performance maps are provided as a part of input data and used to evaluate the mass flow rate and isentropic efficiency.

Having calculated heat and mass transfer for a control volume, the gas properties as well as the differentials of internal energy with respect to temperature and equivalence ratio, are evaluated. The gas properties, mass, equivalence ratio, and rate of heat release and heat loss constitute the thermodynamic differential equations which are solved by the method illustrated in the flowchart, fig. 2.8.c.

2.3.4 The SPICE input data and modelling to simulate the L10-T/C engine

The model for the L10 engine in its turbocharged configuration is shown in fig. 2.9. The engine is modelled as the full six cylinders with one intake manifold and two exhaust manifolds feeding the twin entry turbocharger turbine. The intercooler is represented by a pressure loss and a thermal effectiveness. The poppet valves are modelled by tabulated values of crank angle and effective flow area. The effective flow area is determined by the valve area and the corresponding discharge coefficient.

The heat transfer correlation chosen is due to Woschni with the gas side wall temperature controlled by a thermal resistance model. Due to lack of information, initially, about heat release and engine friction, an arbitrary model was first used for each of them. The model used for heat release was due to Watson and Marzouk (ref. 22) in conjunction with the Wolfer-Watson ignition delay model (ref. 23). Hydraulic injection delay was based on the time for a pressure wave in the fuel line to travel from the pump to the injector.

The Cummins L10 engine is equipped with a patented fuel injection system [ref.37] having integrated fuel pump-injector units. The very slight hydraulic delay associted with the unit injector is modelled as a pipe having a length of 10 mm. Experimental heat release diagrams and engine friction data were used as the basis for modified computer models. The heat release model applies Wiebe functions with appropriate coefficients in conjunction with specified zero injection and ignition delay, and adjusted starts of combustion.

Tables 2.3 and 2.4.a & b, show a typical input data set for one operating point of the Cummins L10 T/C Diesel engine. Input data to the program basically consists of engine, compressor and turbine specifications and relevant maps.

a) The engine input data file (table 2.3) consists of :

1) Control codes for the type of control volume and flow junctions with connecting arrangements.
2) Control codes for submodels and associated data files (to be

created and attached).

3) Engine and flow junction geometric data.
4) Fuel and fuel injection data.
5) Shaft data.
6) Combustion chamber heat transfer data.
7) Effective flow area map of intake and exhaust valves in conjunction with the scale factors to control timing, opening period and flow area.
8) Ambient conditions.
9) Initial conditions of control volumes providing simulation start condition.

The engine geometric data is in accordance with the manufacturers' information. Table 2.5 shows the summary of the engine geometric and heat transfer data.

b) The compressor and turbine input data files (2.4.a & b)

Each of these data files consists of geometric data and relevant map, having scale factors to enable the user to scale (up and down) the pressure ratio, mass flow and efficiency of the turbocharger elements. In this case, the maps and specifications supplied by the engine manufacturer for the A2 Trim Holset turbine with 25 Cm^2 casing area and the H2C 8650 Holset compressor were used. The compressor and turbine scale factors applied are both equal to 1.

The rated running point of the L10 engine in the first runs is at 290 hp at an engine speed of 2100 rpm and in the case of matching the heat release model is at 250 hp at the same engine speed. These two different ratings were applied, to conform to two sets of data supplied by the manufacturer.

2.3.4.A Computer runs using the Watson heat release model

The running conditions arbitrarily chosen include five points each for full load, for part load and for low load at engine speeds of 1000, 1200, 1600, 1900 nd 2100 rpm, synthesizing the experimental results obtained from the manufacturer. Because of the Watson-Marzouk high swirl heat

release model incorporated in the program, it was necessary to change the injection timing from its real value for example from 17 deg. BTDC to a retarded timing 8 deg. BTDC to achieve better agreement with the experimental results. Table 2.6.a gives the fuelling schedules over these runs.

2.3.4.B Computer runs using the Wiebe function heat release model

Referring to the experimental heat release diagrams, supplied by the manufacturer, the required data for combustion modelling, using the Wiebe model, is available for the following engine running conditions:

1) At engine speed of 1000 rpm at 700 lb.ft (i.e. 100% load)
2) At engine speed of 1260 rpm at 190, 375, 560 and 750 lb.ft (i.e. 25%, 50%, 75% and 100% load).
3) At engine speed of 1500 rpm at 750 lb.ft (i.e. 100% load).
4) At engine speed of 1800 rpm at 700 lb.ft (i.e. 100% load)
5) At engine speed of 2100 rpm at 160, 310, 470 and 625 lb.ft (i.e. 25%, 50%, 75% and 100% load).

Table 2.6.b gives the applied fuelling schedule and combustion timing obtained from the experimental heat release data.

2.4 TRANSIENT SIMULATION OF THE L10-T/C ENGINE USING PROGRAM USING PROGRAM 'TRANIC'

2.4.1 Brief Description of Program 'TRANIC'

The main purpose of the program TRANIC is to simulate the transient response of a T/C Diesel engine, although it is also applicable to steady state simulation.

In providing transient running conditions, use is made of two receivers (plenums) between compressor and engine and also between engine and turbine, to allow for differences in mass flow rates between these components. Fig. 2.10 shows a schematic diagram of the physical model. Differential equations are used to define both the mass and energy continuity conditions for these plenums.

The engine model used is based on the five point engine cycle similar to that in program EMAT, to yield, under instantaneous inlet and fuelling conditions, all other engine variables including the exhaust conditions and engine torque. The fuel flow is under the control of a governor and can be changed according to any desired schedule.

In the course of a transient simulation, the torque differences between the mechanically linked components, i.e. between compressor and turbine and between engine and load, cause changes in turbocharger and engine speed, as functions of their respective inertias and the length of the time step. Eventually such a simulation arrives at constant shaft speeds corresponding to a balanced torque condition, provided that sufficient simulation time is available. Although the transient simulation can start using guessed initial conditions, it is also possible to establish an equilibrium condition.

Fig. 2.11.a shows the structure of program TRANIC and its subroutines which are called upon to perform the necessary calculations for the turbocharger and engine. The position of the newly developed subroutine 'ROAD' is also shown in this figure. The other subroutines deal respectively with engine and turbine modelling, gas property calculations and numerical methods applied for linear interpolations and

Runge-Kutta integrations, while the road subroutine defines aerodynamic, frictional and gradient resistances for a complete vehicle.

2.4.2 Subroutines of Program 'TRANIC' (Fig. 2.11.a)

In general, the models for engine and turbine, gas property calculations and the numerical interpolation method used by program TRANIC are the same as described in Section 2.2.2 for program EMAT, as follows :-

a) The model of the engine is based on the five point cycle, in conjunction with empirical relationships as already defined.
b) The model of the turbine defines the analytical steady state thermodynamic behaviour of a radial inflow turbine.
c) The compressor thermodynamic behaviour is predicted by the use of interpolation on numerical arrays describing the compressor map.
d) The cooler model is based on empirical formulae, using cooler effectiveness and air flow to provide cooler exit conditions (in terms of arrays of pressure and temperature).
e) One and two dimensional interpolation techniques are used, and
f) Several small routines are applied to evaluate gas properties, viz. gamma, specific heats and enthalpy.

In addition, three subroutines which are specifically written for program TRANIC are described below.

2.4.2.A Subroutine defining differential equations (DERIV)

Fig. 2.12 is a flowchart of subroutine DERIV. This routine defines the energy and mass continuity equations for the receivers between adjacent components, and the equations describing the dynamics of the shaft between the engine and load, and of the turbocharger rotor. In defining these differential equations, the component models and the numerical techniques described above, are used.

2.4.2.B The integrator subroutine (RUNKUT)

This routine is used to provide the solution to the first order

differential equations defined in the other routine. The method of integration is based on the standard Runge-Kutta method, of any desired order between 1 and 4, as specified in the data input.

2.4.2.C Subroutine 'ROAD'

This subroutine makes it possible to simulate the transient road behaviour of a vehicle equipped with a stepped transmission, and having scheduled successive gear changes, without any interruption of program runs. Fig. 2.13 shows the flowchart of the subroutine.

The subroutine provides the modified program 'TRANIC' and in particular subroutine 'DERIV' with updated values of equivalent road resistance imposed on the engine (with respect to the overall transmission ratios) in each gear and also determines the vehicle speed over each time step. During gear change periods the vehicle decelerates while the engine is declutched, and road resistance continues to act on the vehicle.

Control codes are used to determine whether the engine is declutched or, if not, what the engaged gear number is.

2.4.3 Flowchart for Program 'TRANIC'

Figs. 2.11.b and 2.12 respectively show the flowcharts of program TRANIC and of the differential equation solver "DERIV". TRANIC is mainly a linking program and hence the main calculations are performed by its subroutines. The most important parts of the program deal with :

1 - Reading in the general input data and operating conditions.
2 - Calculations to set up complementary data.
3 - Initialization of certain variables, for every set of new initial conditions.
4 - Use of subroutines to perform main calculations.
5 - Updating cumulative variables.
6 - Examining the convergence criteria when true initial steady-state conditions at the start of a transient are required.

7 - Storing the end results of a specified number of step calculations in output arrays and writing them into output files,
8 - Use of control statements to direct the sequence or to control the end of calculations.

In the setting up of a part of the complementary data use is made of the analytical turbine subroutine to supply the program with turbine mass flow, torque and efficiency arrays. This provides a shorter run time for the program as the quick interpolations (using turbine arrays) will be performed in place of the lengthy calculation at each time step based on the analytical subroutine. The number of time steps in the course of complete simulation may reach tens of thousands.

In other parts of initial calculations the components of the compressor mass flow arrays are modified with respect to altered ambient condition, the cooler exit pressure and temperature arrays are set up with respect to the compressor maps and, the engine volume at defined points of the modified air standard cycle is calculated.

Although the program TRANIC simulates transients it can also handle steady state running conditions for any given engine speed and load, using the relevant control code in the input data. This is normally done whenever an actual rather than a guessed initial steady state is required prior to transient simulation. Four convergence criteria have to be satisfied to establish whether steady state exists. These consist of two mass flow criteria (concerning compressor, engine and turbine flow balance) and two torque criteria (concerning turbine and compressor, as well as engine and load torque balance).

Several sets of initial conditions can be provided as input data as the starting conditions for different transient simulations, one at a time. Therefore, a big loop in the program covers the initialization of the system variables for each of these sets.

The integrator subroutine 'RUNKUT' is used to solve the differential equations for turbocharger and engine speed and for temperature and pressure of the receivers in the system. For this purpose other

instantaneous system variables have already been updated. The differential equations are located at the end of the subroutine 'DERIV' and are called by the main linking program (TRANIC), for the next step calculations.

The cumulative variables such as elapsed (simulated) time, resettable step counter (np), road distance or consumed fuel are calculated after return to the TRANIC program for the start of the next time-step calculations. As already stated, the time step length in comparison with the simulation time is very small. Therefore, to avoid the need for huge output file space, the results are stored in the output array only for every tenth time step (nsp). A check is also made to purge the output array into output file once the former is filled in up.

In the case of the road simulation, before the start of the next time step calculations, it is important to examine whether the engine speed is within set limits. The engine operates between rated and permissible minimum speed both during up-changes, i.e. engine acceleration in successive gears with engine deceleration while declutched; and during down-changes, i.e. engine deceleration in successive gears with engine acceleration while declutched. The gear change during up-change is thus faced by rated engine speed and during downchanges by minimum engine speed. During acceleration, it is the road resistance torque and equivalent engine load inertia which are applied to the engine, running under boost controlled maximum rack position. During deceleration, however, the only resistane torque and inertia are due to the engine itself and the engine is run in the minimum rack position.

The flowchart of the ROAD subroutine shown in fig. 2.13 has been developed to evaluate road dependent variables during acceleration (downshift) and deceleration (upshift) of the engine.

Although only a single type of road condition (in terms of rolling friction coefficient, road slope and wind velocity) was simulated by the original program TRANIC, in its modified form using the ROAD subroutine no such limitations exist. As indicated in Section 2.4.1, this routine is called by subroutine 'DERIV' to update some of the variables used in

the solution of differential equations.

Fig. 2.12 shows the flowchart for subroutine 'DERIV' with all events fully described.

2.4.4 Input Data for Program 'TRANIC'

The detailed description of input data is given in table 2.7.b. The data comprises two parts, one being relevant to system components and the other to the simulation operating conditions.

The general input data for the first part include:

i) Engine geometric data and empirically based physical data.
ii) The control scheme including fuel schedule and governor specification.
iii) Compressor pressure ratio and efficiency maps as a function of speed and mass flow and also arrays of air flow at surge and choke as a function of speed.
iv) Turbine geometric data and loss factors.
v) Aftercooler data.

The operating data is essentially composed of :

i) Control codes for different purposes.
ii) Ambient condition.
iii) Load data in terms of array or road-vehicle data.
iv) A number of sets of guessed initial conditions to start the transient simulation.

Table 2.7.a shows the input data echo relevant to the transient simulation of a 65000 lb truck equipped with the Cummins L10 turbocharged engine. The turbocharger is essentially the same as that used for the T/C-L10-290 (hp) but is run at a higher level of speeds to cope with a hypothetical T/C-L10-240(kW) engine. As will be seen the object is to compare the performance of this uprated engined truck with a similar DCE equipped truck of the same nominal power.

Simulation of the transient performance of the L10 engine on a 65000 lb

truck has been performed using a 7-speed stepped transmission with specified gear ratios. For the first series of calculations, the road simulations in the different gears were performed separately, followed by individual engine decelerations.

The arrays of truck equivalent loads and inertias to be applied to the engine crankshaft in different gears are given in table 2.8. To avoid this tedious procedure, the road subroutine was developed to perform continuous calculations covering vehicle acceleration in subsequent gears and engine deceleration in the periods of gear changes. The truck and road particulars are now given as input data instead of the equivalent load and inertia array and are given in table 2.7.a.

2.5 SIMPLE STEADY STATE SIMULATION OF THE L10-DCE USING PROGRAM DCE2

2.5.1 Brief Description of the Program

Program DCE2 is a simple program which is applied for steady state simulation of the differential compound engine. As indicated in Section 2.2.1, the program structure closely resembles that of 'EMAT' and uses the same quasi-steady approach.

The program is of modular structure, the subroutines being similar to those in EMAT, but contains additional subroutines 'PIPE' and 'ORIF' to model system pipe losses and bypass orifice flow [see fig. 2.16]. Fig. 2.14.a shows the program structure.

Program DCE2, however, is a linking program which defines the particular relationships of the 'DCE', that is, the torque and speed relationships, the epicyclic gearbox and the engine bypass flow mixing with exhaust gases to pass through a variable nozzle radial flow turbine. The method of solution is by iteration and is applied to compressor air flow, engine and bypass flow, engine fuelling and turbine nozzle angle respectively, to establish a match condition.

The program is used to find all the system variables based on demanded engine torque, as well as engine and output shaft speeds. A further facility is the use of the program over a range of turbine gear ratios to determine the best match in terms of best overall system efficiency.

The program predictions, in comparison with experimental results, prove to be quite satisfactory while computer run times are less than one tenth of the corresponding step-by-step program, CSP-DCE (see Section 2.6).

2.5.2 Flowchart for Program DCE2

Fig. 2.14.b shows the flowchart for DCE2. The initial statements of the program are concerned with reading in general and running data. The latter are defined primarily by engine torque and speed and output shaft speed.

The program itself is structurally composed of four iteration loops; the first, to find the compressor operating point, the second to find the engine and bypass flow, the third to fix the fuelling requirement and the fourth to determine turbine nozzle angle. As is implied, the operating conditions of the system components are fixed progressively according to the normal gas flow direction, starting with the compressor.

The calculations start with preparation of some of the engine data, e.g. swept volume and FMEP, input geometric and empirical data, as well as estimated compressor operating conditions. Then the iteration loops perform as follows:

1) Finding the compressor running condition based on the known engine torque and speed and also output shaft speed:

In finding the compressor operating point, use is made of a compressor subroutine based on maps, which has to be provided with known pressure ratio and speed. The compressor speed is a direct function of the engine and output shaft speed, but its pressure ratio needs to be iterated for a matched condition. Because of torque balance between engine and compressor (dictated by the epicyclic gearing), the compressor torque is determined once the engine torque is known.

To find the compressor operating point, the compressor subroutine is entered. As pressure ratio determines compressor torque, while on the other hand this torque is already determined by engine torque, an iteration loop for pressure ratio is called. In this loop a compressor torque error term is used to modify the initially guessed pressure ratio, using an array of guessed compressor pressure ratio as a function of engine torque. As implied, compressor mass flow, cmf, is also determined in the course of the first iteration loop and together with compressor pressure ratio makes it possible to determine upstream cooler pressure, rcx.

2) Engine and bypass flow calculations based on the bypass valve area and pipe losses with respect to a matched delivery ratio, drs.

This is the second iteration loop which finds a matched engine delivery

ratio, and fixes the engine and bypass mass flows. The delivery ratio may be calculated by interpolation based on the engine speed, es, and the inlet to exhaust pressure ratio, rex. This procedure could yield engine flow, emf, as well as bypass flow, omf, readily if the inlet and exhaust conditions were available. But neither of these conditions are known at the beginning. Hence based on some assumptions regarding the pressure ratio across the engine, rxx, all of these are first estimated.

Only if the bypass area, A, is less than 100 sq. cm, the bypass flow, omf, will be determined by the bypass area as well as its pressure difference. Otherwise, omf is determined by the difference between cmf and emf. Therefore, when bypass valve is wide open (A>100) a preliminary emf is estimated by assuming :

i) Exhaust pressure = cooler inlet pressure
ii) Pressure drop across the cooler = 5%
iii) Cooler effectiveness = 0.8

It should be noted that (i) and (ii) yield an assumed rxx which together with es estimates drs. This, in turn, together with (ii) and (iii) leads to an estimated emf and hence omf (=cmf-emf).

However, if bypass is restricted (A<100) a preliminary omf is estimated by assuming:
exhaust pressure = cooler inlet pressure/1.3.

This, together with the bypass area, yield an estimated omf and hence emf (=cmf-omf).

As soon as the flow distribution between the engine and bypass is estimated, the pipe pressure losses from the cooler inlet and from the exhaust manifold to turbine inlet (dpc and dpb respectively) can be evaluated. These loss values are used to modify the early assumption of the exhaust pressure.

On the other hand, having estimated emf, cooler routine can be entered to yield a better estimation for inlet manifold conditions. At this stage, using the modified inlet and exhaust condition, drs is evaluated

by two different methods:

i) Calculation using the estimated emf and modified inlet condition.

ii) Interpolation using the engine speed, es, and modified, rxx.

The error detected by the drs values from the above methods leads to appropriate modification with the initially assumed exhaust pressure. This calculation process is repeatedly performed until an acceptable error is resulted.

3) Fixing the engine fuel flow to meet the engine torque requirement (with respect to the conditions of engine manifolds).

This is the third iteration loop and fixes the engine fuel flow to provide the desired torque level. Before the loop starts, an estimate is made for injected fuel based on indicated engine torque. The loop begins by fixing the fuel injection variables using given maps of injection timing and duration (as a function of engine speed and injected fuel) provided as input data. With the manifold conditions as previously determined and the estimated fuel injection data, the engine subroutine is called to yield engine torque, which is compared with the desired engine torque. The engine torque error allows a simple iteration loop to be entered until torque balance is achieved.

Before the next stage of the program calculations start, the turbine speed and inlet conditions, based on engine running conditions, are found.

4) Fixing the turbine nozzle angle to meet required turbine running conditions (i.e. the set of turbine speed, mass flow and pressure ratio).

The fourth and last iteration loop deals with turbine nozzle angle to be compatible with the turbine running conditions imposed by the preceding calculations. The iterations start with an assumed turbine nozzle angle, and use the analytical turbine subroutine to calculate turbine mass flow. The flow is compared with the previously determined compressor airflow and fuel flow. The error is applied to the fourth iteration

loop, and a new turbine nozzle angle is found based on its previous value and the mass flow error. When balance is reached, turbine torque and power are also calculated.

To finish the program calculations, output shaft, torque, power and brake thermal efficiency are calculated. An output array capable of handling eight running conditions is used to store the program results.

2.5.3 The DCE2 Subroutines

As mentioned in Section 2.5.1, all the subroutines of program 'EMAT' described in Section 2.2.2 are used for program DCE2. The compressor, however, is of the positive displacement type and a typical map of such a compressor is shown in fig. 2.15. A brief description of the additional subroutines 'PIPE' and 'ORIF' is given below:

2.5.3.A Subroutine 'PIPE'

The simulation model considered in DCE2 shown in fig. 2.16 takes into account the effect of pressure losses in four connecting pipes. The losses are calculated by the subroutine 'PIPE' based on the effect of the length, diameter and relative surface roughness of the pipes a,b,c and d. This consideration provides more realistic simulation.

2.5.3.B Subroutine 'ORIF'

To model gas flow through bypass valve, a subroutine called 'ORIF' is used. This routine calculates the gas mass flow rate through an orifice area which is subject to known upstream and downstream conditions.

2.5.4 The DCE2 Input Data to Simulate the L10-DCE

The input data for 'DCE2' is similar to that for 'EMAT' due to the use of similar submodels. However, the gearing system requires extra input data (see fig. 2.16). The input data file includes the following additional data compared with that for 'EMAT' as described in Section 2.2.4:

a) Gear ratios (of epicyclic and direct gearing connections involved in the system),
b) Vector of guessed values of compressor pressure ratio as a function of engine torque,
c) Pipe losses from compressor outlet to cooler inlet, from cooler inlet to turbine plenum through bypass piping and from exhaust manifold to turbine plenum, (fig. 2.16),
d) Required running condition in terms of engine torque and speed and also output shaft speed.

The engine fuelling, hence, is to be calculated rather than being given as input data (as was the case in the operating data of program EMAT). A typical input data set together with descriptions is given in table 2.9.a.

Outline of cases run.

The rapid matching program DCE2 in which the engine subroutine has been calibrated against turbocharged performance data supplied by Cummins Engine Co., using program EMAT (Section 2.2) is used to predict the DCE performance characteristics with the L10 engine.

In preparing the input running conditions in terms of system gear ratios, engine torque and speed and output shaft speed, some general guidelines regarding the best choice of design point operating conditions were applied, to provide optimum rated performance and torque back up. These were as follows :

a) The engine rating was chosen to be high, but not excessive, in order to allow an ample margin for the increase in boost and BMEP on the limiting torque curve without which the high torque ratio of the DCE cannot be realized. This in turn implies :
   i - Air-fuel ratios of the order of 27 to 29:1
   ii - Boost ratios of the order of 2.8 to 3:1
   iii - BMEP of the order of 13-14 bar
b) The engine to compressor power ratio at the design point which is a function of the epicyclic gear train ratios as well as of the choice of output shaft speed relative to engine speed was fixed in the range 3.0 to 3.8:1. If it is too low, air flow will be in excess of engine

demand. If it is too high, the compressor will speed up excessively as output shaft speed is reduced.

c) The bypass flow at the rated point should not be more than between 5 and 7 per cent of total flow.

d) On the limiting torque curve, the compressor should operate in its region of best efficiency.

However, the engine has been uprated compared with the aftercooled L10 in turbocharged form (L10-250T/C) to give 240 kW (322 hp) rather than 186 kW (250 hp). The calculations were carried out over the full output shaft speed range from 2200 rev/min to 440 rev/min and at 100, 75, 50 and 25 per cent load. Input operating data is given in table 2.9.b.

2.6. STEADY-STATE SIMULATION OF THE L10-DCE USING PROGRAM 'CSPDCE'

2.6.1 Brief Description of Program 'CSPDCE'

Like program SPICE (Section 2.3), the cycle simulation program (CSP) is based on the filling and emptying concept, in which the inlet manifolds, the engine cylinders and the exhaust manifolds are treated as control volumes with simultaneous inflows and outflows. Different versions of CSP are available at Bath University, one of them being designed specifically to simulate the differential compound engine, abbreviated as "CSPDCE". The program is broken down into certain linked components (or models of specific processes) in terms of different subroutines. Nevertheless, the main program, in addition to its linking function, also solves the major coupled differential equations. Fig. 2.17.a shows the program structure.

The subroutines used in CSPDCE define the models of different components or processes. The components include :

a - Compressor
b - Charge cooler
c - Inlet and exhaust manifolds
d - Cylinders
e - Inlet and exhaust valves
f - Turbine
g - Gearbox

and the processes include :

a - Combustion (heat release)
b - Heat transfer from the hot gases to the cylinder wall
c - Property relationships for the working gas

The model (fig. 2.18), therefore, comprises a series of thermodynamic control volumes linked by mass or energy transfer, viz:

i) the inlet manifold connected directly to the compressor and through the inlet valves to the cylinders,
ii) the cylinders connected through inlet and exhaust valves to the manifolds, with the processes of heat release by combustion, heat transfer through the combustion chamber walls and work transfer to or from the piston,

iii) the exhaust manifolds connected to the cylinders through exhaust valves and directly to the turbine, with heat transfer through the walls to the surroundings.

Like 'SPICE', 'CSP' is capable of realistically handling complex unsteady phenomena but in a more specific way. This is achieved by assuming quasi-steady flow behaviour at any instant. The calcultions usually proceeds in a series of very short time steps, it being assumed that the rate of change of mass, etc. remains constant for that time step only. The error introduced by this assumption is difficult to estimate, the numerical error of course, could be reduced by a shorter time step or a number of iterations.

The numerical method used by 'CSP' is the modified Euler's predictor-corrector with two iteration at any stage giving computer run time an order of magnitude shorter than SPICE. Although a specified accuracy is only achieved by provision of unlimited repeated iterations, sufficient accuracy can be provided by using good relaxation factors based on past experience. The solution procedure is to integrate three differential equations for temperature, mass and fuel-air ratio in each control volume in parallel for equal increments of crank angle, using the information obtained at each previous step. The shaft speeds also change as a result of application of thermodynamic and mechanical equations. The complete cycle calculation is repeated with the revised initial values until sufficient convergence is obtained. Depending on the original estimates, convergence to the steady state conditions will occur within 3 to 5 cycle repetitions. The results of the last two cycles can be used to check the required convergence.

2.6.2 Subroutines of Program 'CSPDCE'

All of the different subroutines of 'CSPDCE' are introduced in fig. 2.17.a where their locations are shown with respect to each other. The following subsections deal with short descriptions of these subroutines.

2.6.2.A The compressor model (COMLY) - FIG. 2.15

The subroutine 'COMLY' defines performance characteristic maps of a Lysholm positive displacement compressor. The maps are defined in terms of two 2-dimensional arrays of mass flow and power as functions of speed and pressure ratio. Hence this routine is used by the main program, 'CSPDCE', to calculate the instantaneous operating parameters of the compressor based on the updated values of compressor speed and plenum pressure at every new crank position.

2.6.2.B Subroutine 'COMPMAP'

The subroutine 'COMPMAP' is used to create an output file which can generate the compressor maps with optional combinations of speed, pressure ratio, mass flow, power, torque and efficiency. This routine is used only by the modified version of 'CSPDCE', and enables the user to examine the compressor characteristics.

2.6.2.C The turbine model (TURBW4, TURBW)

Unlike the compressor, the turbine is modelled analytically by either of the subroutine 'TURBW4' used in the original version of 'CSPDCE' or 'TURBW' in the modified version. These subroutines are essentially the same as that described in Section 2.2.2.C.

'TURBW4' is used to generate the maps of turbine mass flow and efficiency at a fixed nozzle angle once in the beginning of the main program outside the cycle calculations. These maps are repeatedly used in cycle calculations. However, 'TURBW' is used for the same purpose but inside the cycle calculations at every new nozzle angle demanded by the adopted control strategy. These maps are also written into an output file for graphical purposes.

2.6.2.D The flow junction model (ORIFICE)

The gas mixtures flowing into or out of the combustion chamber (cylinder) is represented by one dimensional flow through an orifice.

The realistic non-isentropic effects are accounted for by the application of a variable discharge coefficient to the actual valve area. The flow direction and velocity are determined by the conditions of state in the control volumes located at either end of the junction.

2.6.2.E The combustion model (WIEBE, or ARHR)

Mathematical equations (shape functions) that conform to experimental heat release diagrams are used for the combustion modelling. Although it is purely an experimental approach with only limited fundamental theoretical support, it avoids the need for complicated multi-dimensional thermal/chemical combustion modelling. Heat release rate is essentially taken equivalent to the fuel burning rate, being identified from a diagram at any crank angle.

The combustion model is potentially a major source of error as it influences all other thermal exchanges. Two types of heat release diagram with and without premixed burning spike are shown in figs. 4.1,c and 4.2,b. These models are due to Watson-Marzoul (Ref. 22) and Wiebe (Ref. 21) respectively.

2.6.2.F The combustion gas properties routine (GASPROP)

The mathematical expressions for the internal energy and gas constants as functions of temperature, pressure and equivalence ratio obtained by Krieger and Borman (Ref. 33) are used for the required thermodynamic property evaluation of the products of combustion and air. The lean side formulation is in terms of single equations for internal energy and gas constants. The rich side formulation is also in terms of single equations with variable coefficients depending on a selected number of equivalence ratios (viz. 1.1, 1.2, 1.4 and 1.6).

2.6.2.G The heat transfer model (HEAT,RESIST)

Unlike the heat release model, the spatial and time average heat transfer model has a theoretical basis which is modified by empirical constants. This model is used as part of the energy equation and

predicts the heat transfer to the individual cylinder components, that is, piston, liner and cylinder head. These components are represented by a network of constant thermal resistances (fig. 4.4,b) in which the heat flows are iteratively adjusted to balance at the network junctions.

The formula adopted in the current cycle program is that of Woschni (Ref.24) representing convection only, but with adjustable coefficients. It considers the gas velocity as a part of the pressure head and applies suitable empirical values for the required constants.

2.6.2.H The crank mechanism model (MECH)

This subroutine analyses piston movement and evaluates the mean piston velocity and instantaneous position to determine the cylinder volume and its rate of change with respect to crank angle.

2.6.2.I The engine friction model

The power loss due to engine friction is used to calculate the brake power output from indicated work generated at the piston working face. The formula adopted within the program is that of Chen and Flyn (Ref. 29) developed for turbocharged engines. In the formula use is made of the effects of maximum cylinder pressure and mean piston velocity with empirical constants for a particular engine.

2.6.2.J The epicyclic gearbox model (EPGEAR,EPIC)

Using the kinematic and dynamic equations governing the epicyclic gearing, the gearbox model simulates the dynamic performance characteristics of the DCE epicyclic gearbox. The model updates the system shaft speeds as a function of instantaneous applied torque taking into account the component inertias and the load dependent and viscous friction losses. There are three components in the gear set; any two of them can be moved entirely independently of the third. However, with respect to a defined speed relationship, three component accelerations are required when the gearing system is subjected to three shaft torques. In order to provide such a condition use is therefore made of a

speed error correction algorithm to modify slightly the component accelerations found, so that those components which are going too fast are slowed down, and those which are lagging are speeded up.

2.6.3 Flowchart for Program 'CSPDCE'

Fig. 2.17.b is the concept flow chart and fig. 2.17.c, together with fig. 2.17.d is the detailed flowchart of 'CSPDCE'. In the detailed flowchart the same variable notation has been used as in the program listing. Table 2.11 gives the notation.

The program has four major loops : the first (outermost) loop keeps the program running up to the number of cycles required (input), the second controls the completion of each cycle, the third examines the convergence criteria and the fourth or innermost loop, handles the thermodynamics and gas exchange processes of the cycle.

Before the loops start, the initial statements are concerned with the reading and sorting of input data. As part of input data, the turbine maps are produced in terms of two-dimensional arrays of mass flow and efficiency as functions of speed and pressure ratio, using the analytical turbine subreoutine, 'TURBW4'. On completion of the sorting of input data, the compressor speed, time step, number of cycle steps and finally the intake and exhaust valve area arrays (in case of the optionally input valve lift instead of valve area) are calculated.

The first major loop starts by counting the cycle number and setting the cyclic cumulative values of the variable to zero. Then the second major loop begins by incrementing the crank angle in steps of specified length to complete a cycle. After completion of a cycle, the cumulative values of performance parameters such as mass flow, torque and power of the different components as well as pressure and temperature of the plenums are converted into their cyclic average values, and also certain other variables such as FMEP, BMEP, engine brake thermal efficiency and system energy balance are calculated. Before the next cycle starts, the summary of performance parameters is stored as a one-dimensional array which can be written into the result file, otherwise the array is overwritten by

that for the next cycle.

A complete cycle calculation is performed in crank step increments within the second major loop and proceeds stage by stage within different appropriate loops to determine values of all the variables such as pressure, temperature, trapped mass, equivalence ratio and gas properties as well as rate of change of them for each control volume. Initially, the predicted temperature, equivalence ratio and mass for each control volume in the first cycle are based on guessed values and read from input data. The volume and combustion data for each cylinder are calculated using two subroutines 'MECH' and 'WIEBE' (optionally ARHR) at early stage of the loop. Using suitable relaxation factors, the predicted shaft speeds are established.

The third loop now starts for iteration and includes the main body of the second loop covering the thermodynamic and gas exchange processes in a cycle. The iteration is carried out at each new crank position. The convergence criteria are examined with respect to the temperature, trapped mass and equivalence ratio for each of the control volumes at the end of the loop. If the criteria are not satisfied, the calculations will be performed only once more with substituted predicted values by corrected ones of the first iteration. Before the gas exchange calculations start, the gas properties and their differentials are determined by calling the gas property subroutine 'GASPROP'. This is followed by setting the rate of change of trapped mass and enthalpy of all the control volumes to zero (no gas flow through junctions). This leads the program to the stage of gas flow consideration.

The fourth or innermost loop is considered to repeat the gas exchange calculations for all the control volumes. At the beginning of the loop, the instantaneous area for intake and exhaust valves are updated. These, together with pressure differences across them are used in the subroutine 'ORIFICE' to calculate mass flow rates from a cylinder into a manifold or vice versa. In general, the gas exchange calculations for a cylinder are divided into three distinct phases, viz. exhaust, overlap and intake. Each phase is identified by valve areas and the calculation is directed to the appropriate section of the program by "IF" and "GO

TO" statements.

To update predictor values of rate of change of mass enthalpy and equivalence ratio in the inlet and exhaust manifolds, operating conditions of the compressor and turbine are to be determined. These are done by using the instantaneous pressure of the relevant plenums and the updated speeds. Therefore, the gas exchange loop draws not only on the cylinders but also on the manifolds, compressor and turbine. Furthermore, updating the enthalpy is part of thermodynamic calculations of the cycles. For the purpose of finding overall performance parameters, the cumulative values of compressor/turbine mass flow, torque, power, speed and efficiency as well as the temperature and pressure of the manifolds are also stored but only if the final iteration is being executed.

Immediately after the turbomachinery calculations, the flow is determined with respect to magnitude and flow direction; also its cumulative value at the time of last iteration is stored.

The gas exchange process is now completed. In order to complete the remainder of the thermodynamics of the cycle, the combustion chamber heat transfer and heat release are determined and the thermodynamic differential equations are set up. The heat transfer routine, 'HEAT', calculates the heat transfer coefficients and together with the heat transfer network model of the subroutine 'RESIST' determines the instantaneous and cumulative heat transfer to the liner, cylinder head and piston. The heat transfer coefficients can also be scaled by an input scaling factor.

In the course of setting up the differential equations for all of the control volumes, new predictors of rate of change of equivalence ratio and temperature are also established. However, the main sets of differential equations comprise two parts, one being concerned with correctors and the other with new predictors both for gas temperature, equivalence ratio, mass and pressure. If sufficient accuracy is achieved, the new predictor values will be the solution, otherwise the next iteration is called for starting from gas property estimations.

Before the crank step calculations are completed the dynamic epicyclic gear routine 'EPGEAR' is called. At this stage the instantaneous torques and speeds of the epicyclic shafts are used and new values of shaft speeds and planet carrier torque are established. The new planet carrier torque determines a new output shaft torque. The new crank step starts after the cumulative values of;

engine work, torque, speed and also output shaft speed and burnt fuel have been calculated. The maximum cylinder pressure and temperature are determined by comparing the relevant values in every crank step computations with those in the previous one.

2.6.4 The CSPDCE System Modeling and Input Data

The block diagram for the L10-DCE is given in Fig. 2.18. The 6 cylinder engine is modelled as shown with one intake manifold fed by the positive displacement compressor,

and one exhaust manifold feeding the radial inward flow turbine. The intercooler is represented by a pressure loss and a cooler effectiveness. The poppet valves are modelled by tabulated values of crank angle, area and discharge coefficient.

The uncooled bypass air passes through the bypass valve which is modelled as an orifice, to the exhaust manifold where it mixes with exhaust gases before entering the turbine. In order to remove possible adverse effect of exhaust pressure pulses from different cylinders on each other, the exhaust manifold is represented by a large volume. This calls for a longer simulation time to arrive at a final steady state condition from the guesses initial condition.

Heat release and friction modelling are based on the engine in its T/C configuration (Section 2.3.4) using the adjusted Wiebe function (Ref. 21) and the modified Chen and Flyn model (Ref. 29). The heat transfer correlation due to Woschni (Ref. 24) with the gas side wall temperature controlled by a thermal resistance network is again applied.

As shown in Fig. 2.18,the engine drives the ring gear (annulus-shaft # 1)

of the fully floating epicyclic gearbox; the planet carrier (shaft # 2) is geared to the output shaft (shaft # 4) which, in turn, receives a direct power input from the exhaust turbine.The turbine shaft (shaft # 6) is connected to the output shaft (# 4) by direct spur reduction gearing. The supercharger compressor (shaft # 5) is driven by the sunwheel (shaft # 3) of the epicyclic gear train. Shaft and shaft junction data consist of : shaft moment of inertias, efficiencies and speed ratios of meshing gear pairs.

Table 2.10 shows a typical input data set for steady state simulation of one operating point. The input data to the program consists of specifications and relevant data arrays for engine, compressor, turbine and gear set and also some miscellaneous data, including :

i) the engine firing order
ii) the geometric data and maps of engine and intake and exhaust valves
iii) the geometric data and interconnection arrangements for inlet and exhaust manifolds,
iv) the scale factors for compressor mass flow and efficiency
v) the turbine geometric data
vi) the gearing system data
vii) the running condition required (in terms of engine speed and fuelling)
viii) ambient conditions and engine oil/cooling water temperature
ix) guessed initial conditions for pressure, temperature and equivalence ratio in each control volume and the temperatures of liner, piston and cylinder head.

```
CUMMINS L10 T/C DIESEL ENGINE
Engine data
------------
no. of cyls.*bore*stroke*con.rod length*inl.&exh. valve dia.*comp.ratio
6.0       0.1250    0.1360    0.217900  0.05650   0.05650   16.30
angle of exh.&inl. valve closing and opening*combustion rate factor
ratio of manifold to cyl. volume*empirical heat loss factor
3.0       193.0     495.0     701.0     0.01      8.00      1.00
five values of engine speed
1000.0    1300.0    1500.0    1800.0    2200.0
five values of exh./inl. manifold pressure ratio
0.8       0.91      1.0       1.11      1.25
25 values of delivery ratio as a function of above two variables
.845  .845  .845  .845  .845  .85   .85   .85   .85   .85   .855  .855  .855
.855  .855  .86   .86   .86   .86   .86   .865  .865  .865  .865  .865
five values of engine diagram efficiency
1.00      0.96      0.92      0.90      0.89
five values of FMEP as a function of engine speed
0.476     0.68      0.885     0.952     1.088
five values of T/C speed as a function of engine speed
50000.    60000.    70000.    80000.    90000.
Turbine data
------------
turbine diameter at nozzle outlet : rotor tip entry : exit (outer&inner)
throat area*rotor blade entry angle : exit pitch : entry thickness
0.0976    0.09000   0.0700    0.0254    0.0046    1.5708    0.18      0.000
max. nozzle length*rotor entry : width at up&downstream ; cone angle
polytropic eff.*bearing loss factor*blade thickness at exit (outer&inner)
0.0135    0.0135    0.0135    1.5708    0.8       0.004
turbine dia. at volute inlet and nozzle outlet*six different loss factors
0.184     0.097
gas constant*fuel cal.value*ambient press.&temp.*coolant temp. no. of T/Cs
0.287     43150.0   0.93      294.5     350.0     1.00
max. restriction required*boost ratios at which throat is fully open&restricted
0.00      2.0       1.5
program control markers
00011111
Input data ( engine running conditions )
---------------------------------------
eng.speed*fuel per rev.*max.cyl. press.*inj.timing & duration*turb.noz.angle
1000.0    .000261   0.000     343.0     14.25     26.0
1200.0    .000276   0.000     343.0     15.25     26.0
1600.0    .000318   0.000     343.0     17.80     26.0
2000.0    .000329   0.000     343.0     21.30     26.0
2100.0    .000315   0.000     343.0     23.00     26.0
0.0
```

Table 2.1 The 'EMAT' input data based on the Cummins L10-T/C engine particulars

speed	BSFC	hc		amd		fuel rate		rt	tm		tw	
rpm	lb/hp.hr	BTU/min	kJ/min	lb/min	kg/min	lb/hr	gr/rev	(A/F)	F	K	F	K
800.	0.361	2182.	2302.	6.6	2.99	26.9	0.250	14.8	122	323	81.7	300
1000.	0.341	2756.	2907.	10.9	4.94	36.4	0.275	18.0	125	324	82.5	301
1200.	0.335	4081.	4305.	18.9	8.57	53.5	0.336	21.2	127	325	89.4	305
1400.	0.327	4435.	4680.	24.3	11.0	61.1	0.330	23.9	132	328	91.9	306
1600.	0.323	6258.	6602.	35.1	15.9	91.2	0.430	23.1	142	334	108.	315
1800.	0.323	6580.	6942.	40.1	18.2	96.3	0.404	25.0	147	337	112.	317
2200.	0.340	6401.	6753.	45.3	20.5	91.5	0.314	29.7	152	340	112.	317

$$hc = 22.116\ qlf * (vs . cyl)^{0.6} * amd^{0.4} * (1.13\ tm + 21000/rt - tw)$$

where :

hc	heat transfer to coolant	[kJ/min]
qlf	empirical heat loss factor	
amd	air mass flow delivered	[kg/min]
tm	inlet manifold temperature	[K]
rt	trapped air to fue ratio	
tw	cooling water temperature	[K]
vs	cylinder swept volume	[m]
cyl	number of cylinders	

for the L10 engine ;

$$qlf = hc / [\ 1.397\ amd^{0.4}\ (1.13\ tm + 21000/rt + tw)\ ]$$

= 1.34 as an average for a speed range 800 - 2200 rpm
= 1.45 " " " " " 1000 - 2200 rpm
= 1.55 " " " " " 1200 - 1800 rpm

Table 2.2 Calculation of empirical heat loss factor for the Cummins L10-T/C Diesel engine

```
_DUA1:[REZAIAN.SPICE]L10ENG1.2100;8                                    20-NOV-1987 20:58
* SP1/W.F: CUMMINS L10 SIX CYL T/C DIESEL ENGINE - AT Ne=2100 rpm AND FULL LOAD
* CONTROL DATA:
* no. of: cycles,step deg.,control volumes,junctions,shafts & sets of heat release,geometric,heat transfer ar
6 1 9 14 2 1 4 1 2
* PRINT AND PLOT CONTROL DATA:
* printout cycle result no., crank ang. interval of printout & plot ,no. of volumes,junctions and shafts in r
1 30 2 1 4 4 1
1            *LINER DATA FOR CYLINDER 1
1 4 5 9      *PLOT DATA AVAILABLE FOR VOL # 1 ONLY
1 2 3 4      *PLOT DATA AVAILABLE FOR JUN # 1 ONLY
2            *PLOT DATA AVAILABLE FOR SHAFT # 2 ONLY
* VOLUME DATA ( each line being devoted to a cotrol volume ) :
* the no. for volume type,geo. data set,heat rel. data set,heat tran. data set,shaft connected (cyls. only)
* relative angular crank position, no. of strokes
* the model no. of ignition delay,heat release,heat transfer,engine friction
0 1 1 1 1 0   4 1 2 11 4
0 1 1 1 1 480 4 1 2 11 4
0 1 1 1 1 240 4 1 2 11 4
1 2 0 0 1 0   0 0 0  0 0
1 3 0 0 1 0   0 0 0  0 0
0 1 1 1 1 600 4 1 2 11 4
0 1 1 1 1 120 4 1 2 11 4
0 1 1 1 1 360 4 1 2 11 4
1 4 0 0 1 0   0 0 0  0 0
* JUNCTION DATA ( each line being devoted to a junctin ) :
* no. for junction type,geometric data set,no. of turb.entries,volumes. at entry/exit to/from a junction,T/C
2 2 0 0 0 0 0 4 2
1 1 0 4 0 0 0 1 0
1 2 0 1 0 0 0 5 0
3 3 2 5 9 0 0 0 2
1 1 0 4 0 0 0 2 0
1 2 0 2 0 0 0 5 0
1 1 0 4 0 0 0 3 0
1 2 0 3 0 0 0 5 0
1 1 0 4 0 0 0 6 0
1 2 0 6 0 0 0 9 0
1 1 0 4 0 0 0 7 0
1 2 0 7 0 0 0 9 0
1 1 0 4 0 0 0 8 0
1 2 0 8 0 0 0 9 0
* SHAFT DATA ( each line being devoted to a shaft ) :
* shaft type no.,mech. eff.,mech. work overhead(mep) for crank shaft or rotor inertia for T/C shaft
0 1 0
1 1 .0001
* HEAT RELEASE SETS ( line no. = set no. )
* (0=dynamic version),static inj. timing,dur. of burning,fuel cal. value,fuel inj./shot,fuel pipe,Wiebe coef:
0 -15.5 62.5 42.8E+6 101.4E-6 0 1.4 7.0
* GEOMETRIC DATA SETS ( line no. = set no. ) :
* FOR A CYLINDER : bore,stroke,compression ratio,connecting rod length, zero
* FOR A MANIFOLD : volume,surface area,heat trans. coeff.,heat sink temp.,emisivity of surface
.125  .136 16.3 .2179 0
.0040 .40  25 310 .5
.0024 .15  25 310 .5
.0024 .15  25 310 .5
* CHAMBER SURFACE AREAS AND TEMPERATURES :
* no. of entries ( piston,cyl. head,three parts of liner )
5
* coolant-side heat tran. coeff. and bulk temp.,chamber wall thickness:conductivity:thermal resistance:area:
* fraction of heat from piston to liner/ distance of liner region edges to liner top
1900 370 .018 160 0  .016 520 .3
1900 320 .016 40  0  .012 520 .0
1900 320 .010 40  0  .010 400 .025
1900 320 .008 40  0  .043 400 .136
1900 320 .006 40  0  .041 400 .240
* VALVE DATA SETS :
* no. of map points,timing shift angle, duration and area scale factor
24 0 1 0.45
* crank angle timing array
341 347 353 361 371 381 391 401 411 421 431 437
441 451 461 471 481 491 501 511 521 531 541 553
* area array
0 85E-6 200E-6 435E-6 847E-6 1342E-6 1827E-6 2197E-6 2380E-6
2492E-6 2525E-6 2529E-6 2525E-6 2496E-6 2402E-6 2240E-6 1957E-6
1531E-6 1050E-6 621E-6 309E-6 132E-6 48E-6 0
* ( as above but for second valve data set )
24 0 1 0.45
135 145 155 165 175 185 195 209 225 235 245 255
265 275 285 295 305 315 325 335 345 351 357 363
0 248E-6 730E-6 1135E-6 1460E-6 1706E-6 1844E-6 1955E-6 1995E-6
2008E-6 2013E-6 2009E-6 1996E-6 1973E-6 1943E-6 1852E-6 1725E-6
1495E-6 1197E-6 865E-6 413E-6 221E-6 86E-6 0
* ENTRY AND EXIT CONDITIONS :
* pressure and temperature
97E+3 305 97E+3 305
* INITIAL SHAFT SPEEDS :
* engine and turbocharger
2100
83946
* CONTROL VOLUME INITIAL CONDITIONS ( line no.= vol. no. ) :
* pressure,temperature,fuel/air ratio
192000    350    8.1E-4
188700    670    3.5E-2
1430000  1180    3.5E-2
196000    330    3.5E-12
181000    710    3.5E-2
189000    353    1.8E-3
```

Table 2.3 The 'SPICE' input data based on the Cummins L10-T/C Diesel engine particulars

COMPRESSOR INPUT DATA FILE OF SPICE

```
* COMPRESSOR TR86B KU40  H2C 8650 TRIM - HOLSET
* CONTROL DATA:NO. SPEED CURVES, SCALING FACTORS:RP,N,E,M
5,1,0.0575,1,1.323E-6
* INTERCOOLER DATA
3200,320,0.90
* TABULATED COMPRESSOR MAP
40000
1.24,6.4,.66
1.22,11.8,.74
1.20,15.4,.76
1.17,18.4,.73
1.15,22.0,.67
1.14,23.1,.64
*
60000
1.55,11,.62
1.55,19,.75
1.51,25,.77
1.46,30,.75
1.39,34,.69
1.34,38,.64
*
80000
2.06,16,.62
2.06,27,.72
2.00,35,.74
1.93,41,.75
1.81,47,.70
1.66,52,.63
*
100000
2.74,24,.61
2.79,35,.67
2.73,44,.70
2.69,51,.71
2.38,61,.67
2.11,64,.58
*
120000
3.68,43,.60
3.71,49,.62
3.63,60,.64
3.42,64,.63
3.26,66,.61
2.52,68,.49
```

Table 2.4,a The compressor input data file of the program "SPICE" for the Cummins L10-T/C Diesel engine

TURBINE INPUT DATA FILE OF SPICE

```
* TURBINE A2 TRIM HOLSET HOL  CASING = 25 CM2 ) / TEST NO. 787
* CONTROL DATA  NO. SPEED CURVES  ROTOR DIA.  SCALING: RP N E M
5 .085 1 .0575 1 1.323E-6
* TABULATED TURBINE MAP: P-RATIO M EFF
10000
1.2 30 .40
1.4 38 .32
1.6 43 .28
2.0 47 .22
2.8 51 .16
4.4 56 .12
*
30000
1.2 26 .68
1.4 37 .70
1.6 42 .67
2.0 47 .62
2.8 51 .48
4.4 56 .38
*
50000
1.2  5 .00
1.4 26 .48
1.6 36 .67
2.0 44 .74
2.8 50 .74
4.4 56 .60
*
70000
1.2  0 .00
1.4  0 .00
1.6 20 .21
2.0 32 .52
2.8 43 .60
4.4 53 .69
*
85000
1.2  0 .00
1.4  0 .00
1.6 14 .21
2.0 28 .52
2.8 40 .60
4.4 51 .69
*
```

Table 2.4,b The turbine input data file of the program 'SPICE'

for the Cummins L10-T/C Diesel engine

CUMMINS L10 T/C DIESEL ENGINE	
GEOMETRIC DATA :	
Bore	125.0 mm
Stroke	136.0 mm
Connecting rod length	218.5 mm
Compression ratio	16.3 -
Inlet manifold volume	2.4 l
Inlet manifold surface	1200.0 cm^2
Exhaust manifild volume	2*2.4 l
Exhaust manifold surface	1200.0 cm^2
AVERAGE THICKNESSES :	
Piston crown	18.0 mm
Cylinder head	16.0 mm
Upper section of the liner	10.0 mm
Mid section of the liner	8.0 mm
Lower section of the liner	6.0 mm
Distance from the liner top -to the lower edge of each - liner region	25 , 136 & 240 mm
HEAT TRANSFER DATA :	
Heat trans. coef. of manifold walls	25 W/m^2K
Emisivity of manifold surfaces	.5
Coolant-side convection coef.	1700 W/m^2K
Piston conductivity	160 W/mK
Cylinder head/liner conductivity	40 W/mK
Fraction of heat transferred from - the piston to the liner through - the ring pack and skirt	0.3

Table 2.5 Summary of the ' SPICE ' input data based on the L10-T/C engine

ENGINE SPEED [rpm]	1000.0	1200.0	1600.0	1900.0	2100.0
INJECTED FUEL [mg/shot]	91.7	112.0	102.0	128.0	118.0

(a) Applied in the Watson heat release model at injection timing of both 17 and 8 deg BTDC

ENG.SPEED [RPM]	FUEL/SHOT [mg]	START OF COMBUSTION [deg. BTDC]
1000.0	116.4	17.0
1260.0	120.4	18.0
	90.0	12.0
	62.2	8.0
	35.8	4.5
1500.0	117.7	17.0
1800.0	110.1	16.5
2100.0	101.4	15.5
	79.4	12.3
	56.7	9.0
	35.5	5.0

(b) Using the Wiebe function heat release model together with appropriate start of combustion

Table 2.6 Fuelling schedule applied in the steady state detailed simulation of the L10-T/C diesel engine

```
CUMMINS L10 turbocharged engine
   nes  nxpr nfprev  nps nrack
     5     5     3     9     7
    bore        strk        conlen      cr          cyl         dvi         dve
     0.1250      0.1360      0.2180     16.3000      6.0000      0.0560      0.0560
    xevc        xivc        xevo        xivo        volcc       volce       dpce        dpet
     3.0000    193.0000    495.0000    701.0000      0.0100      0.0100      0.0700      0.0700
    xk          qlf         tw          pulsf       calval      xjel
     0.1000      1.5000    350.0000     10.0000  43152.0000      3.0000
    vxpr        array of values of delivery ratio vdrs
     1.2500      0.8650      0.8650      0.8650      0.8650      0.8650
     1.1100      0.8600      0.8600      0.8600      0.8600      0.8600
     1.0000      0.8550      0.8550      0.8550      0.8550      0.8550
     0.9100      0.8500      0.8500      0.8500      0.8500      0.8500
     0.8000      0.8450      0.8450      0.8450      0.8450      0.8450
    vfprev      array of values of start of injection vxinj
     0.0005    340.0000    339.0000    338.0000    338.0000    339.0000
     0.0003    343.0000    342.0000    341.0000    341.0000    342.0000
     0.0001    346.0000    345.0000    344.0000    344.0000    344.0000
    vfprev      array of values of duration of injectio vdinj
     0.0005     13.0000     16.0000     19.0000     22.0000     27.0000
     0.0003     10.0000     12.0000     14.0000     17.0000     20.0000
     0.0001      7.0000      8.0000      9.0000     11.0000     13.0000
                array of values of engine speed ves1, engine friction vfmep, &diagram factor ved
               1000.0000   1300.0000   1500.0000   1800.0000   2100.0000
                  0.9000      1.1500      1.5000      1.7000      1.9300
                  1.0000      0.9600      0.9200      0.9000      0.8900
    deltas      dtgov       rmax        rmin        rmaxl       rbl         rb2         pscale
    250.0000      0.0100      5.0000      0.0000      1.6000      1.0000      2.2000      1.7000
    vrack       array of values of fuel per stroke vfps
      6.0000     90.0000     99.8000    103.4000    103.0000     99.8000     95.3000     89.8000     85.3000
      5.0000     75.0000     83.9000     88.9000     88.5000     85.8000     80.8000     75.8000     71.0000
      4.0000     64.0000     71.2000     74.9000     74.0000     69.9000     64.9000     60.3000     56.3000
      3.0000     52.0000     59.4000     61.7000     60.0000     54.7000     47.6000     44.0000     41.3000
      2.0000     39.0000     44.9000     44.5000     40.8000     35.4000     31.8000     29.5000     27.7000
      1.0000     20.0000     22.6000     22.2000     19.5000     17.2000     15.4000     14.1000     13.1000
      0.0000      0.0000      0.0000      0.0000      0.0000      0.0000      0.0000      0.0000      0.0000
                array of values of fuel pump speed vps
               300.0000    400.0000    500.0000    600.0000    700.0000    800.0000    900.0000   1000.0000
HOLSET COMPRESSOR DATA    Model : H2C 8650 TR BU 40
    ncs    nmf nunitm nslope
      5     9     1     0
     scfa        pas         tas         xjtc
      1.1000      1.0000    302.0000      0.001200
     vcs        array of values of pressure ratio vpr
 120000.0000      3.7700      3.7600      3.7500      3.7400      3.7300      3.7200      3.6000      3.3000
 100000.0000      2.8300      2.8200      2.8100      2.8000      2.7950      2.6900      2.4600      1.9400
  80000.0000      2.0800      2.0700      2.0650      2.0620      2.0200      1.7200      1.4200      1.2100
  60000.0000      1.5700      1.5600      1.5530      1.4850      1.3700      1.1400      1.0600      1.0200
  40000.0000      1.2600      1.2500      1.2100      1.0900      1.0500      1.0300      1.0200      1.0100
     vcs        array of values of efficiency vef
 120000.0000      0.4300      0.4500      0.4900      0.5350      0.5650      0.6300      0.6400      0.6100
 100000.0000      0.4800      0.5100      0.5600      0.6100      0.6600      0.7400      0.6900      0.5300
  80000.0000      0.4500      0.5000      0.6000      0.7200      0.7600      0.6600      0.4400      0.2700
  60000.0000      0.4500      0.5700      0.6780      0.7900      0.6750      0.5500      0.3000      0.2600
  40000.0000      0.5500      0.6500      0.7680      0.5800      0.5700      0.5600      0.4000      0.3100
                array of values of mass flow vmf
                  0.0000      2.2700      6.8030     12.2900     15.9640     23.3110     27.2110     30.0680
    array of values of mass flow at surge vsl
      2.9020      5.0340      7.4370     10.8840     19.5920
    array of values of mass flow at choke vcl
     16.7610     22.1070     28.1900     31.0210     31.0220
    xloss       xeff        coefficients in cooler equations
     -1.0000     90.0000
turbine data
     dl          d2t         d3o         d3i         bb1         bb2s        bb2r
      0.0976      0.0900      0.0700      0.0254      0.0135      0.0135      0.0135
     a           b2          psi         bp3         xnb         bt2         bt3o        bt3i
     24.0000      1.5708      1.5708      0.1800     24.0000      0.0000      0.0000      0.0000
     ff          fric
      0.8000      0.1000
running data
   iesi   ies   ilds    iw itran itype norder  iroad    nyear  ig
      1     1     8     0     2     2     1     1     7     1
 npage   nsp    np   iout   imax   iplot
    10   100     0     2    50     99
    esmin       torqmn      pa          ta          tolm        tolt        szerol      ovratio
    800.0000     30.0000      0.9930    294.4000      0.0300     10.0000   2350.0000
    step        timend
      0.0020      8.0000
    array of subsequent vehicle gear ratio
     10.1300      5.9900      3.5600      2.5700      1.8400      1.3500      1.0000
    vehicle particulars: raxle,mass,1st/g l.inrtia,rtyre,area,gbx.effcy.,gear-change(rtd) eng.spd.
      3.7000  14509.0000      2.6880      0.5011      7.9330      0.9800   2100.0000
    road speeftion : rolling fric.coef., rd.slope,wind  vel., drag coef.
      0.0120      0.0000      0.0000      1.1070
    arrays of initial values of speed and load, ves,vtorq
  1000.0000
     0.0000
    arrays of first guesses of tc speed & reciever conditions, vcsn,vpcc,vpce,vpet,vtcc,vtce,vtet
 22000.0000
     1.0100
     1.0600
   290.0000
   370.0000
```

Table 2.7,a The 'TRANIC' input data for road simulation

```
input data

engine data
***********
icomm      comment in a4 format to specify engine type.
           ---------------------------
           card holding array sizes. 20i4 format.
nes        number of engine speeds relating to empirical factors.
nxpr       number of inlet/exhaust pressure ratios for del rat arrays
nfprev     number of fuelling values for injection timing arrays.
nps        number of fuel pump speeds for pump charactrristics.
nrack      number of values of fuel rack or metering valve position.
           ------------------------------
           2 cards of engine physical dimensions. 10f8.0 format.
bore       cylinder bore diameter                          metres
strk       piston stroke                                   metres
conlen     connecting rod length                           metres
cr         compression ratio                               nominal
dvi        effective internal diameter of inlet port       metres
dve        effective internal diameter of exhaust port     metres
           ------------------------
xevc       angle of exhaust valve closing          degrees atdc open
xivc       angle of inlet valve closing            degrees atdc open
xevo       angle of exhaust valve opening          degrees atdc open
xivo       angle of inlet valve opening            degrees atdc open
volce      volume between compressor and engine cyls.     sq metres
volet      volume between engine cyls and turbine.        sq metres
dpce       mean pipe diameter of volume volce                metres
dpet       mean pipe diameter of volume volet                metres
           ------------------------------
           one card of miscellaneous engine data.  format10f8,0
xk         empirical combustion rate factor. value usually 0.05 - 0.10
qlf        empirical heat transfer factor.   value usually 1.0  - 1.4
tw         coolant water temperature for h.t.calculation usually 350 k
pulsf      empirical factor for exhaust pulse calculation.
           value about 10 if realistic value of volet used.
calval     lower calorific value of fuel.                  kj/kg
xjel       inertia of engine-load system                   kg.sq metre
           ------------------------------
           arrays of delivery ratio and injection timing as a
           function of speed and pressure ratio or fuel per rev
           arrays of friction & diagram factor, function of nes.
vxpr       inlet/exhaust pressure ratio      nxpr values
vdrs       delivery ratio                    nxpr * nes values
vfprev     fuel/revolution *10e6  kg         nfprev values
vxinj      start of injection deg atdc open  nfprev * nes values
vdinj      duration of injection degrees     nfprev * nes values
ves1       array of engine speeds     rpm     nes values
vfmep      friction mean effective pressure. nes values
ved        diagram correction factor.         nes values
           ---------------------------------------
           fuel pump and governor data.  format(10f8.0)
deltas     speed difference for full rack movement
dtgov      time constant for governor transient response. rpm
rmax       maximum rack position. arbitrary units, usually mm
rmin       minimum rack position.
rmax1      reduced maximum rack position under boost control.
rb1        boost ratio below which rmax1 applies.
rb2        boost ratio above which rmax applies.
           ---------------------------------------
           arrays of fuel pump characteristics. format(10f8.0)
vrack      rack or metering valve positions. usually in mm
vfps       fuel per stroke for a given rack and speed,*10e6 kg
vps        array of pump speeds (half engine speed). rpm.

           compressor data
           ***************
icomm      comment in a4 format to specify compressor type.
           ------------------------------------------------
           dimensions of data arrays and code for units. format 2014
ncs        number of compressor speeds.  maximum value 8
nmf        number of values in mass flow array. maximum 9
nunitm     code for mass flow units:- 1 for kg/min
           2 for lbm/min              3 for cu ft/min
nslope     code = 0 for mass flow or volume flow values.
                  1 for function (flow/pressure ratio).
           ------------------------------------------------
           1 card of miscelleneous compressor values.
scfa       scale factor in case an incorrect map is used.
pas        manufacturers standard inlet pressure.       bar
tas        manufacturers standard inlet temperature.    k
xjtc       inertia of complete rotating assembly.    kg.sq m
           ------------------------------------------------
           compressor performance arrays.
vcs        compressor speeds.                              rpm
vpr        pressure ratio as function of speed & flow.
vef        efficiency as function of speed and flow.
vmf        flow, as mass flow or volume flow according to nunitm.
vsl        flow at surge as function of speed.
vcl        flow at choke as function of speed.
           ------------------------------------------------
           aftercooler coefficients.
xloss      pressure loss coefficient. no of dynamic heads lost.
xeff       effectiveness coefficient. pseudo n.d.flow for eff=0.8
```

Table 2.7,b The notation used in table 2.7,a

	turbine data.	
	**********	
icomm	comment in a4 format to specify turbine type.	
	---	
	3 cards of dimensions and empirical data in format(10f8.0)	
d1	diameter at nozzles or at volute tongue.	metres
d2t	rotor tip diameter.	metres
d3o	outer (shroud) diameter at exit.	metres
d3i	inner (hub) diameter at exit.	metres
bb1	passage width at nozzles. vaned turbine only. must be zero for vaneless turbine.	metres
bb2s	passage width just before rotor entry.	metres
bb2r	passage width just after rotor entry. bb2s and bb2r usually equal.	metres
	---	
a	nozzle angle. vaned turbine only.	degrees
	volute throat area. vaneless turbine only.	sq metres
b2	blade angle at entry rel to tangent. usually 90	degrees
psi	cone angle at rotor entry. usually 90	degrees
bp3	axial pitch at exit treated as a screw.	metres
xnb	number of rotor blades.	
bt2	rotor blade thickness at entry.	metres
bt3o	rotor blade thickness at exit outer diameter.	metres
bt3i	rotor blade thickness at exit inner diameter.	metres
	---	
ff	thermodynamic loss factor. (polytropic efficiency)	
fric	bearing loss coefficient.	
	---	
	running conditions.	
	**********	
icomm	comment in a4 format to specify run.	
	---	
	control integers on two cards in 20i4 format	
ies1	number of run at which calculation is to start.	
ies	number of runs for which data is supplied.	
ilds	number of values in load torque vs speed arrays.	
iw	code for diagnostic printout if required.	
	0 for final results only.	
	1 for full diagrostics.	
	-1 for printout of pseudo transient in steady state calculation.	
itran	set to 0 to get initial steady state matching.	
	set to 1 or 2 (= itype) for instant transient from guesses.	
itype	type of transient.	
	1 for load change with no change of governor set point.	
	2 for a change of governor set point.	
norder	order of runge kutta integration method, 1 - 4	
	---	
npage	number of output data sets printed across page.	
nsp	number of calculation steps for each printout.	
np	number of initial steps printed at full rate before nsp applies.	
iout	code for output units. 1 for imperial, 2 for si.	
imax	max number of steady state loops before failure assumed.	
	---	
	two cards of miscellaneous running data. format(10f8.0)	
esmin	minimum engine speed for steady state t/c speed matching.	
torqmn	minimum engine torque for steady state t/c speed matching. if both speed & torque below these values initial guess for turbocharger speed is retained in steady state.	
pa	ambient pressure at inlet to compressor.	bar.
ta	ambient temperature at inlet to compressor.	k.
tolm	tolerance on steady state mass flow. fraction of flow.	
tolt	tolerance on steady state engine torque. abs value in nm. tolerance on t/c torque balance is taken as tolt/200.0	
szero1	governor set point for fuel step transient.	
	---	
step	calculation time step.	seconds.
timend	total time of transient.	seconds.
	---	
	arrays of torque vs speed characteristic during transient.	
vldt	array of load torque. ilds values.	n.m.
vlds	array of load speeds. ilds values.	rpm
	---	
	arrays of speed & torque values for steady state matching.	
ves	array of engine & load speeds. ies values.	rpm
vtorq	array of engine & load torques. ies values.	n.m.
	---	
	arrays of first guesses of steady state t/c speed and manifold conditions. ies values each. format(10f8.0).	
vcsn	turbocharger speed.	rpm
vpce	inlet manifold (cooler to engine) pressure.	bar
vpet	exhaust manifold (engine to turbine) pressure.	bar
vtce	inlet manifold temperature.	k
vtet	exhaust manifold temperature.	k

Table 2.7,b (cont')

gear mesh no.	overal gear ratio	eng.+load inertia (N.m)	equivalent road resistance torque (N.m) at engine at diff. Ne(rpm)							simulation time (sec)
			1000.	1200.	1400.	1600.	1800.	2000.	2200.	
1 st.	37.48	7.2	46.7	46.8	46.9	47.0	47.1	47.2	47.3	1.4
2 nd.	22.16	17.2	79.5	79.8	80.2	80.6	81.0	81.5	82.1	2.4
3 rd.	13.17	45.35	135.5	136.9	138.6	140.5	142.7	145.2	147.9	4.7
4 th.	9.51	85.34	192.4	196.2	200.6	205.8	211.7	218.2	225.5	5.5
5 th.	6.81	164.75	280.2	290.5	302.8	316.9	332.9	350.8	370.6	10.5
6 th.	4.92	313.66	417.4	444.8	477.2	514.7	557.1	604.5	656.9	25.3
7 th.	3.7	553.40	616.8	683.5	759.8	847.9	947.7	1059.2	1182.5	--
declutchg.	--	1.83	0.0	0.0	0.0	0.0	0.0	0.0	0.0	--

TABLE 2.8 Operating condition data for the program ' TRANIC ' to simulate a 65000 lb truck in different gears

```
------------------------------------------------------------------------------
CUMMINS L10 DCE
Engine data
-----------
* no. of cyls.
* bore
* stroke
* connecting rod length
* inlet & exhaust valve diameters
* compression ratio
* max.engine torque
    6.0       0.4102    0.4462    0.7145    0.1857    0.1857   16.3     1700.0
..............................................................................
* crank angle at exhaust & inlet valve closing and opening
* combustion rate factor
* bypass orifice area
* empirical heat loss factor
    3.0     193.0     495.      701.0       0.01      110.0     1.0
..............................................................................
* gear   ratio   of compressor ; turbine and output shaft
* ger efficiency  "      "           "      "    "       "
* friction torque "      "           "      "    "       "
    9.55     14.67      1.445     .98       .931      .98      10.       10.       10.
..............................................................................
* initial speed and five values of engine speed
 0000.000  1000.0    1300.0    1500.0    1800.0    2200.0
..............................................................................
* array of delivery ratio based on five values of engine speed
  for five ratio of exhaust to inlet pressure
    0.8       0.845     0.845     0.845     0.845     0.845
    0.91      0.85      0.85      0.85      0.85      0.85
    1.0       0.855     0.855     0.855     0.855     0.855
    1.11      0.86      0.86      0.86      0.86      0.86
    1.25      0.865     0.865     0.865     0.865     0.865
..............................................................................
* five values of injection timing as a function of fuel/rev.
    0.0003  346.0000  345.0000  344.0000  344.0000  345.0000
    0.0007  343.0000  342.0000  341.0000  341.0000  342.0000
    0.0010  340.0000  339.0000  338.0000  338.0000  339.0000
..............................................................................
* five values of injection duration as a function of fuel/rev.
    0.0003    12.       12.       13.       14.       15.
    0.0007   17.       18.       19.       20.       22.
    0.0010   23.       24.       25.       26.       27.
..............................................................................
* five values of diagram factor based on five engine speeds
    1.0       0.96      0.92      0.90      0.89
..............................................................................
* five values of FMEP based on five engine speeds
    7.        10.       13.       14.       16.
..............................................................................
* five values of ratio of output shaft speed to engine speed
    0.0000    1.0000    1.5000    2.0000    3.0000
..............................................................................
* five values of ratio of output shaft torque to engine torque
    3.0000    2.2000    1.2000    0.8000    0.6000
..............................................................................
* five values of engine torque
    0.0000  150.0000  300.0000  450.0000  600.0000
..............................................................................
* five values of boost pressure ratio
    1.0000    1.5000    2.0000    2.5000    3.0000
..............................................................................
```

Table 2.9,a The 'DCE2' input data based on the L1O-DCE particulars

```
.....
Turbine data
------------
* turbine diameter at nozzle outlet ; rotor tip entry ; outer & inner of exit
* throat area*rotor blade entry angle ; exit pitch ; entry thickness
    0.6000    0.5815    0.4600    0.1200   20.0000    1.5708    0.8000    0.0000
.....
* passage depth at rotor entry
* width at stator exit and rotor entry
* cone angle
* fluidic and mechanical friction factor
* blade thickness at exit (outer & inner)
    0.0542    0.0542    0.0542    1.5708    0.8000    0.1000    0.0000    0.0000
.....
* gas constant
* fuel cal.value
* ambient press.&temp.
* cooler temp.&eff.
* inj.delay
* comp.scale factor
   53.3000 18550.      14.4     530.      630.        0.8000    12.5      1.18
.....
* position factor of comp.efficiency contours on the map
   1.2       2.0
.....
* Program control markers
-------------------------
000101
.....
* limit on number of iterations for each loop
   30
0.0       0.0       0.0       1.5
.....
* piping loss data  ( pipe a , b , c , d )
-----------------------------------------
0.0       0.0       0.0       1.5
0.0       0.0       0.0       1.5
0.0       0.0       0.0       1.5
.....
* Required system runing conditions
-----------------------------------
* output shaft speed *engine torque&speed *range of turbine gear ratio *inj.delay
440.      1258.5    1350.       95.      110.          1.
 0.0
 0.0
-------------------------------------------------------------------------------
```

The ' DCE2 ' input data based on CUMMINS L10 DCE specification

Table 2.9,a (cont')

output shaft speed (rpm)	engine torque (N.m)	engine speed (rpm)	range of turbine gear ratio (min.-max.)	
440.	1258.5	1350.	95.	110.
440.	1020.0	1250.	85.	99.
440.	739.0	1150.	68.	80.
440.	386.0	1100.	20.	32.
500.	1214.0	1400.	85.	98.
500.	944.0	1350.	72.	85.
500.	708.0	1200.	56.	70.
500.	385.5	1100.	20.	30.
1050.	1134.0	1500.	40.	50.
1050.	945.0	1350.	36.	46.
1050.	680.4	1250.	25.	40.
1050.	386.6	1100.	11.	26.
1600.	1000.6	1700.	24.	36.
1600.	797.0	1600.	20.	35.
1600.	586.5	1460.	10.	26.
1600.	303.8	1400.	4.	15.
1900.	890.5	1900.	18.	30.
1900.	718.7	1775.	15.	27.
1900.	515.5	1670.	11.	24.
1900.	270.0	1570.	4.	15.
2200.	801.0	2100.	17.	30.
2200.	638.2	2000.	13.	24.
2200.	447.8	1900.	10.	20.
2200.	280.2	1800.	2.5	10.

Table 2.9,b steady state operating conditions input to the program 'DCE2' to simulate the Cummins L10 engine

```
                                        >> CUMMINS L10 DCE <<
                * ifire = firing order
153624
.....................................................................................
                ENGINE DATA
                -----------
                * type differential compound
                * ncyl = no. of cylinders
 6
.....................................................................................
                * bore = cyl. bore
                * stk  = piston stroke
                * conlen = connecting rod length
                * cr   = compression ratio
125.      136.      217.8     16.3
.....................................................................................
                * phi(i) , i=1,ncyl  == phase angle between cylinders (degrees)
0.      -480.    -240.    -600.    -120.    -360.
.....................................................................................
                VALVE DATA
                ----------
                * nl   = no. of inlet valve data points
                * mark = 0 valve lift input data , 1 valve effective area input data
                * div  = inlet valve head dia.
                * sai  =  ""      ""  seat angle (degrees)
                * swi  =  ""      ""   "   width
                * vlmi =  ""      ""  max. lift
                * vsfi =  ""      ""  scaling factor
                * TIVO =  ""      ""  open (degree crank angle)
                * TIVC =  ""      ""  close (degree crank angle)
23 0 56.    30.      5.15    20.0    1.0     341.    553.
.....................................................................................
                * tiv(i) , i=1,nl  == inlet valve non-dimensional crank angle
0.       .02830  .05660  .09434  .14151  .18868  .23585  .28302  .33019  .37736
.42453  .47170  .51887  .56604  .61321  .66038  .70755  .75472  .80189  .84906
.89623  .94340  1.0
.....................................................................................
                * aiv(i) , i=1,nl  == inlet valve non-dimensional valve lift
0.         .0336      .0792      .1722      .3352      .5311      .7230      .8694
.9418      .9861      1.00       1.00       .9877      .9505      .8864      .7744
.6058      .4155      .2457      .1306      .0522       .0190     0.0
.45        .44167     .43731     .43011     .41809     .40536     .39996     .39469
.....................................................................................
                * cdiv(i) , i=1,nl  == inlet valve coeff. of discharge
.39231     .39096     .39046     .39046     .39078     .39204     .3942      .39811
.40405     .41242     .42475     .4248      .44001     .44226     .45
.....................................................................................
                * n2,mark,dev,sae,swe,vlme,vsfe,tevo,tevc
                (outlet valve data;descriptions are the same as for inlet valve data)
23 0 56.    30.      5.0      16.0    1.0      135.     363.
.....................................................................................
                * tev(i) , i=1,n2
0.       .04386  .08772  .13158  .17544  .21930  .26316  .32456  .39473  .43860
.52631  .57017  .61403  .65790  .70175  .74561  .78947  .83334  .87720  .92105
.94737  .97370  1.0
.....................................................................................
                * aev(i) , i=1,n2
0.0        .1234      .3632      .5647      .7264      .8487      .9174      .9726
.9925      1.00       1.00       .9931      .9816      .9667      .9214      .8582
.7438      .5955      .4303      .2055      .1100      .043       0.0
.....................................................................................
                * cdev(i) , i=1,n2
.45        .43105     .4167      .40536     .40086     .39757     .39550     .39379
.39325     .39289     .39289     .39325     .39352     .39402     .39532     .39726
.40045     .40378     .41319     .42624     .43182     .43384     .45
.....................................................................................
                MANIFOLD DATA
                -------------
                * nim , vim(i) , i=1,nim  == no. and volume of inlet manifolds
 1 10.
.....................................................................................
                * nem , vem(i) , i=1,nem , aem  == no. , volume and area of exhaust manifolds
 1 40.      1200.
.....................................................................................
                * control volume interconnection code numbers
 1 7 8
 2 7 8
 3 7 8
 4 7 8
 5 7 8
 6 7 8
.....................................................................................
```

Table 2.10 The 'CSPDCE' input data based on the L10-DCE particulars

```
                * ach  = cylinder head heat transfer area
                * apc  = piston crown area
                * al   = liner area at TDC
                * htc  = exhaust manifold heat transfer coeff.
                * swl  = swirl ratio in Woschni formula
123.0     170.0     76.0      25.0
                * friction scaling factor and,  Wiebe function scaling factors
1.0       1.0       1.0       1.4       7.0
                COMPRESSOR MAP
                --------------
                * icomp = compressor mode factor : 1 for compressor map , 0 for subroutine
 0
                * cmsf = compressor mass scale factor
                * cesf =    ""      eff.  ""    ""
1.1       1.
                TURBINE DATA
                ------------
                * iturb = turbine mode factor
 0
                * tmsf,tesf  = turbine scale factors
                * xtmf       =   ""    varable geometry relaxation factor
.75       1.0       3.0       3.0
                * ntp , nts  = no. of turbine pressure ratio and speed points for maps
17 7
                * vtp  = vector for turbine pressure ratio points
5.0     4.75    4.5     4.25    4.0     3.75    3.5     3.25    3.0     2.75
2.5     2.25    2.0     1.75    1.50    1.25    1.01
                * vts  = vector for turbine non-dim. speed points
500.      750.      1000.     1250.     1500.     1750.     2000.
                * dl   = dia. at nozzle entry (mm)
                * d2t  = dia. at rotor tip (mm)
                * d3o  = dia. at rotor exit (shroud)
                * d3i  =  "   "    "     "   (hub)
                * a    = nozzle angle ( degrees)
                * b2   = blade angle at rotor entry (rad. to tangential)
                * bp3  = blade pitch at exit
                * bt2  = blade thickness at rotor entry (mm)
.183      .177      .1402     .0366     8.886     1.5708    .2438     0.
                * bbl  = nozzle width
                * bb2s = width just upstream of rotor entry
                * bb2r =  ""     "   downstream of  "    "
                * psi  = cone angle at rotor entry (rad)
                * ff   = flow loss factor ; =1 for no loss
                * tfric = turbine shaft friction factor
                * bt3o = blade thickness at rotor exit at tip (mm)
                * bt3i =  ""      ""     "    "    "   "  root (mm)
.01650    .01650    .01650    1.5708    .800      .1        0.        0.
                GEARING SYSTEM DATA
                -------------------
                * egr  = epicyclic gear ratio
                * cgr  = compressor step-up gear ratio
                * tgr  = turbine step-down gear ratio
                * ogr  = output shaft gear ratio
                * oge  =   "      "    "   efficiency
                * tge  = turbine gear efficiency
                * crge = carrier  "       ""
                * cge  = compressor "     ""
                * sge  = sun      "       ""
                * age  = annulus  "       ""
3.074     3.1067    22.50     1.915     0.94      0.98      0.98      0.98
0.94      0.98
                * ja,je,jc,jcr,jp,js,jt,jo
                inertia of annulus,engine,compressor,carrier,planet,sun,turbine,output shaft
.376      3.09      .0089     .268      .0064     .3207     .0076     100000.
                * xj   = scale factor for shaft inertias
1.
```

Table 2.10 (cont')

```
                * byp  = bypass flow area
                * oslt = output shaft torque
                * oss  =  ""     "   speed
.003       1022.     2200.
                 RUNNING CONDITION
                 -----------------
                * control markers
 0 0 1
                * es   = engine speed ( rpm )
                       =  ""   power ( kw )
                * ffrate= fuel flow rate ( kg/s )
                * calval= fuel calorific value ( kj/kg )
                     =  "   adjustment relaxation factor
2100.     240.      .01396    43152.    0.0
                * ta   = ambient temp. ( deg K )
                * pa   =    "    press. (KN/m**2)
                * tw   = cooling water temp. ( deg K )
                * tch  = temp. of cylinder head
                * tp   =  "     "  piston crown
                * tl   =  "     "  liner
                * pb   =  back press. ( KN/m**2 )
                * pin  = intake press.    ""
                * tin  =  ""   temp.
294.4   99.     480.    500.    553.    450.    100.0   100.    294.4
                * tcw  = cooling water average temp. ( deg K )
                * tco  =  ""     oil     "     "        "
                * r2,r4,r5,...= heat transfer resistances
                * rlx  = relaxation factor for iteration
350.    350.    1.5     34.51   2.69    43.44   21.28   15.     .50
                * sinj = static injection setting ( deg BTDC )
                * dinj = injection delay due to mechanical factoras ( deg )
                * bdur = duration of burning

-19.0   0.5     65.0    135.0
                * step = crank angle increment ( deg )
2.
                * cfl,cfa,cfv,cfm = conversion factors for length, area, volume and mass
.001      .0001     .001      .001
                * temp(i), i=1,ncv  first estimate of temp. in each control volume
                * pr(i)  , i=1,ncv    "      ""    "  press. "   "     "       "
                * eq(i)  , i=1,ncv    "      ""    "  eq. ratio  "     "       "
450.    1000.   800.    1000.   400.    800.    400.     800.
210.    800.    1000.   7000.   150.    220.    225.    230.
.02     .5      .5      .02     .02     .5      0.       .5
                * iecho  = 1 for data echo prior to output result file
 1
                * ncyct  = no. of simulation cycles
50
90000     .0003
                * rlx3,rlx4  = relaxation factors for iteration
1.00      1.00
2.        .000001   .00001
.1        1.0       319.
```

The ' CSPDCE ' input data based on the CUMMINS L10-DCE specification

Table 2.10 (cont')

a	turbine nozzle angle
arbf	apparent rate of burning fuel
ave	exhaust valve effective area
avi	intake valve effective area
ca	crank angle
cao	" " of first cylinder
caeb	" " at end of burning
ceff	compressor efficiency (instantaneous)
ce	" " (cycle avg. value)
cmass	compressor mass flow (instantaneous)
cmf	" " " (cycle avg. value)
cpower	compressor power (instantaneous)
cpw	" " (cycle avg. value)
cs	compressor speed (instantaneous)
csm	" " (mean value)
ctorq	compressor torque (instantaneous)
ctq	" " (cycle avg. value)
dinj	injection delay
dmass	rate of change of mass in a control volume
dmassp	predicted 'dmass'
dmh	rate of change of enthalpy
dvol	rate of change of cyl. volume
dyinj	dynamic injection timing
emf	engine mass flow rate
eq	equivalence ratio
eqc	corrected 'eq'
eqp	predicted 'eq'
es	engine speed (instantaneous)
esm	" " (cycle avg. value)
esp	predicted 'es'
et	engine torque
exhe	exhaust energy
ffrate	fuel mass flow rate
flow	gas mass flow rate
h	enthalpy
icv	index representing number of control volume
irl	index (referring to inlet manifold)
ir2	" (" " exhaust ")
istep	" (" " number of a step)
iter	" (" " " " iteration)
mass	mass of gas into cylinder
massc	corrected "mass"
massp	predicted "mass"
mf	mass of fuel burnt at a cetain crank angle
ncyl	no. of cylinders
nstep	total no. of steps
oss	output shaft speed
pb	turbine back pressure
pexh	exhaust manifold pressure
phi	phase angle between cylinders
pim	inlet manifold pressure
pmax	max. cylinder pressure
pr	pressure in any control volume
pratio	compressor pressure ratio
prt	mean turbine expansion ratio
r	air gas constant
rc	compressor mean press. ratio
rdf	dr/df [partia differential] (f: equivalence ratio)
rdp	dr/dp [" "] (p: pressure)
rdt	dr/dt [" "] (t: temperature)
sk	vertical position of piston with respect to TDC
teff	turbine efficiency (instantaneous)
te	" " (cycle avg. value)
temp	temperature in a control volume
tempc	corrected "temp"
tempp	predicted "temp"
texh	exhaust manifold temperature
tim	inlet manifold temperaure
tmass	turbine mass flow (instantaneous)
tmf	" " " (cycle avg. value)
tmsf	" " scale factor
tpower	" power (instantaneous)
tpw	" " (cycle avg. value)
ts	" speed (instantaneous)
tsm	" " (cycle avg. value)
tstep	time step (seconds)
ttorq	turbine torque (instantaneous)
ttq	" " (cycle avg. value)
u	internal energy
uc	u/c for turbine
udf	du/df [partial derivative]
udp	du/dp [" "]
udt	du/dt [" "]
vm	piston mean velocity
vol	cylinder volume
vte	vector for turbine efficiency
vtmf	" " " mass flow
vtp	" " " pressure ratio

Table 2.11 The notation used in the detailed flowchart for 'CSPDCE'

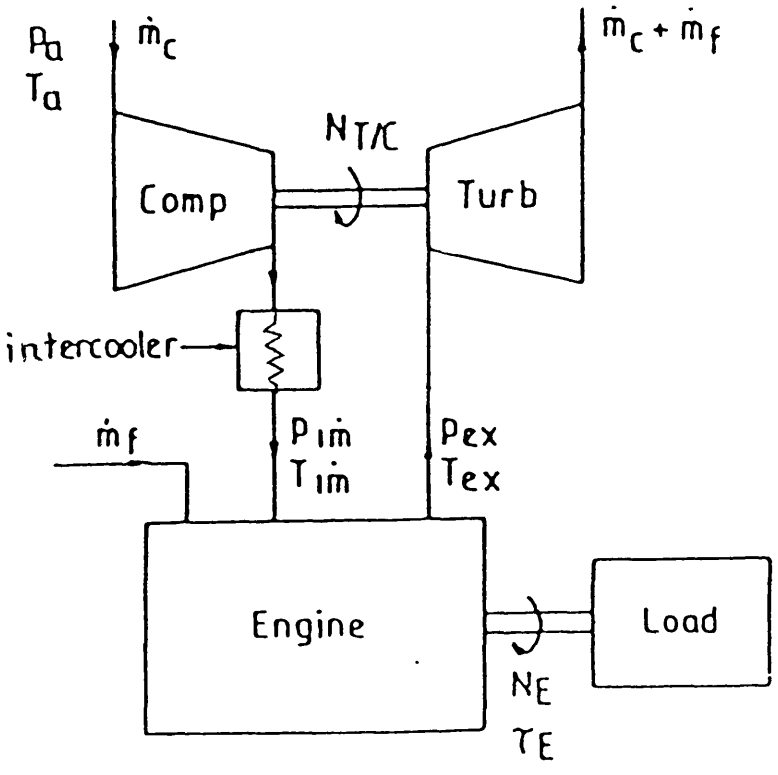

Fig. 2.1 Single stage intercooled turbocharged engine

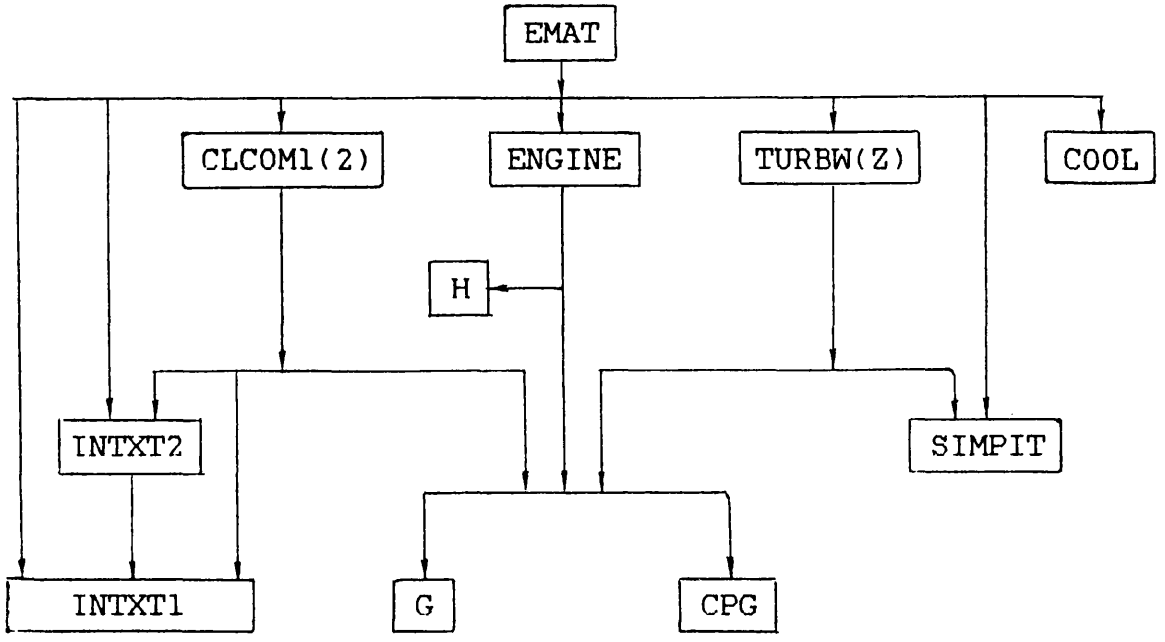

Fig. 2.2,a General layout for the program EMAT

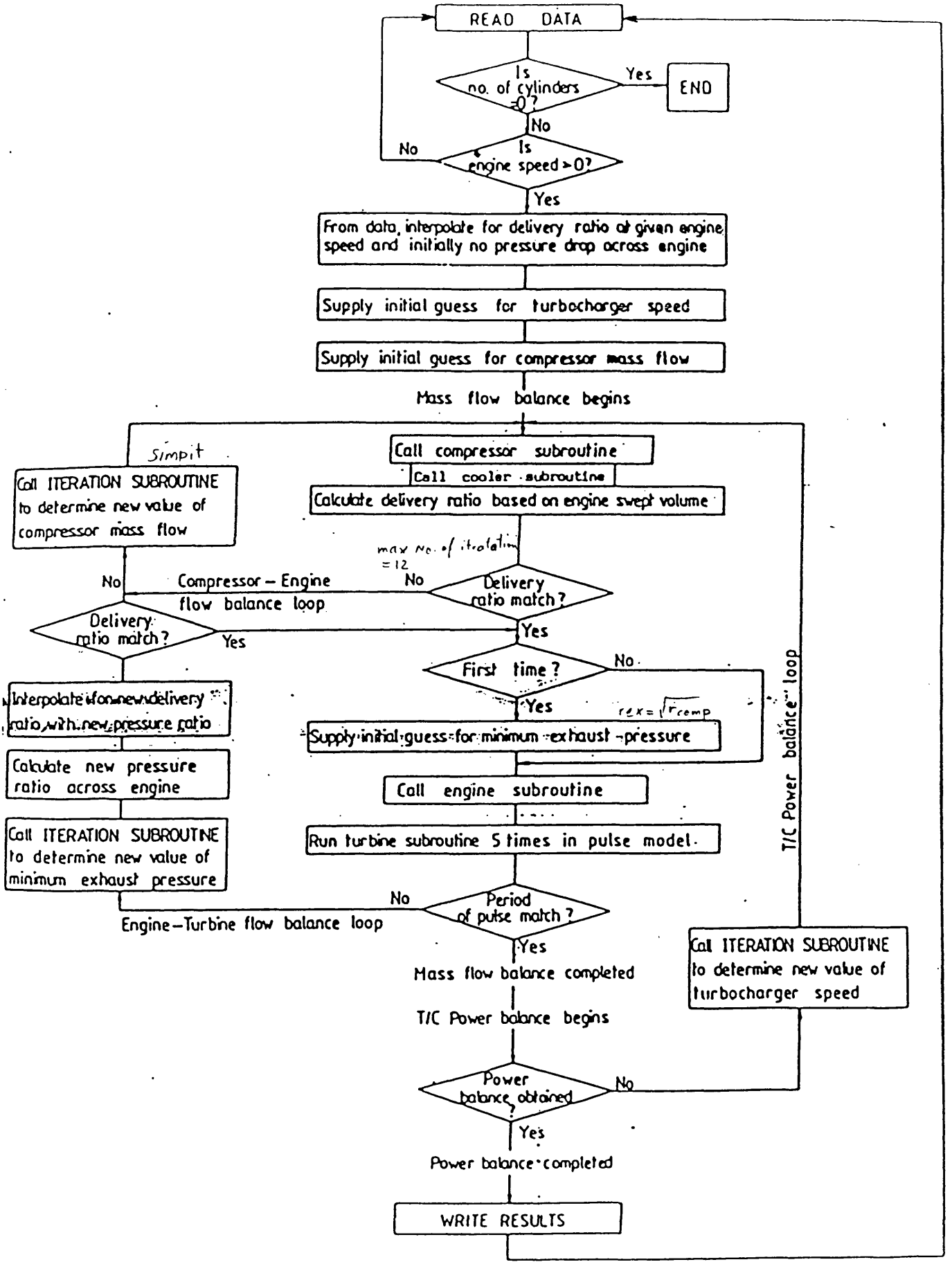

Fig. 2.2,b Flow diagram for single-stage T/C Diesel engine matching program EMAT

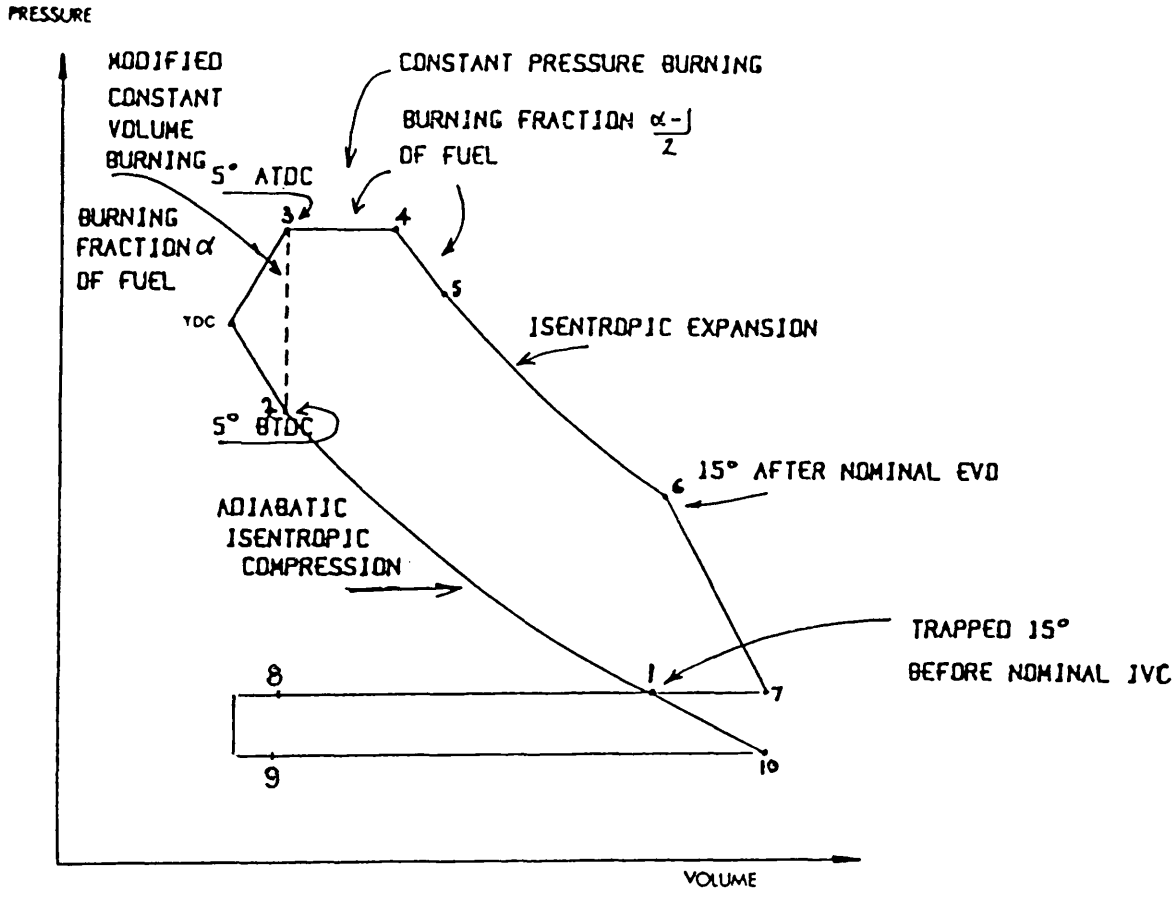

Fig. 2.3 Simplified engine cycle

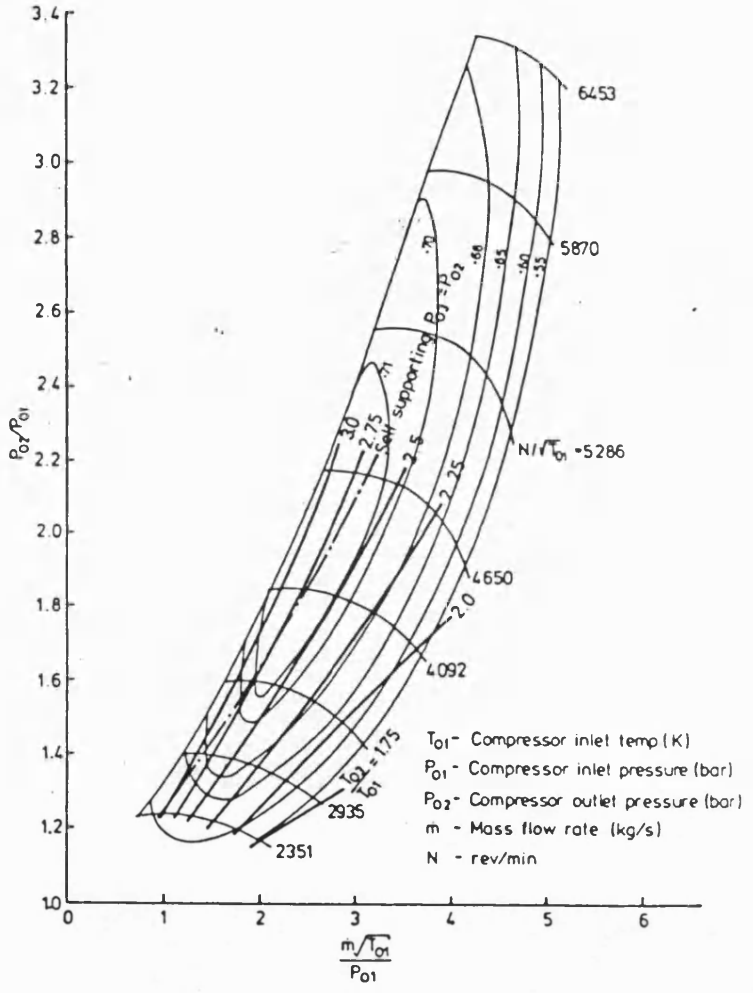

Fig. 2.4 Typical map for centrifugal compressor

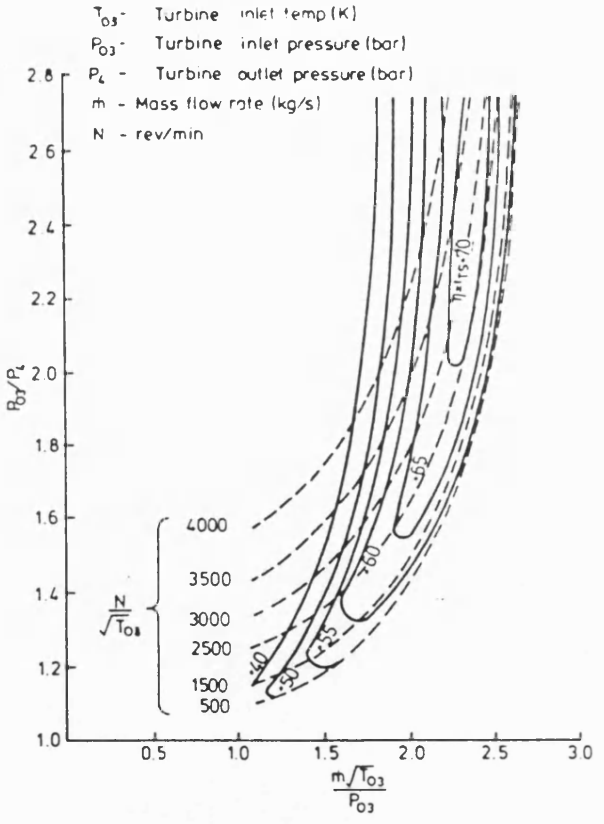

Fig. 2.5 Typical radial inward flow turbine map

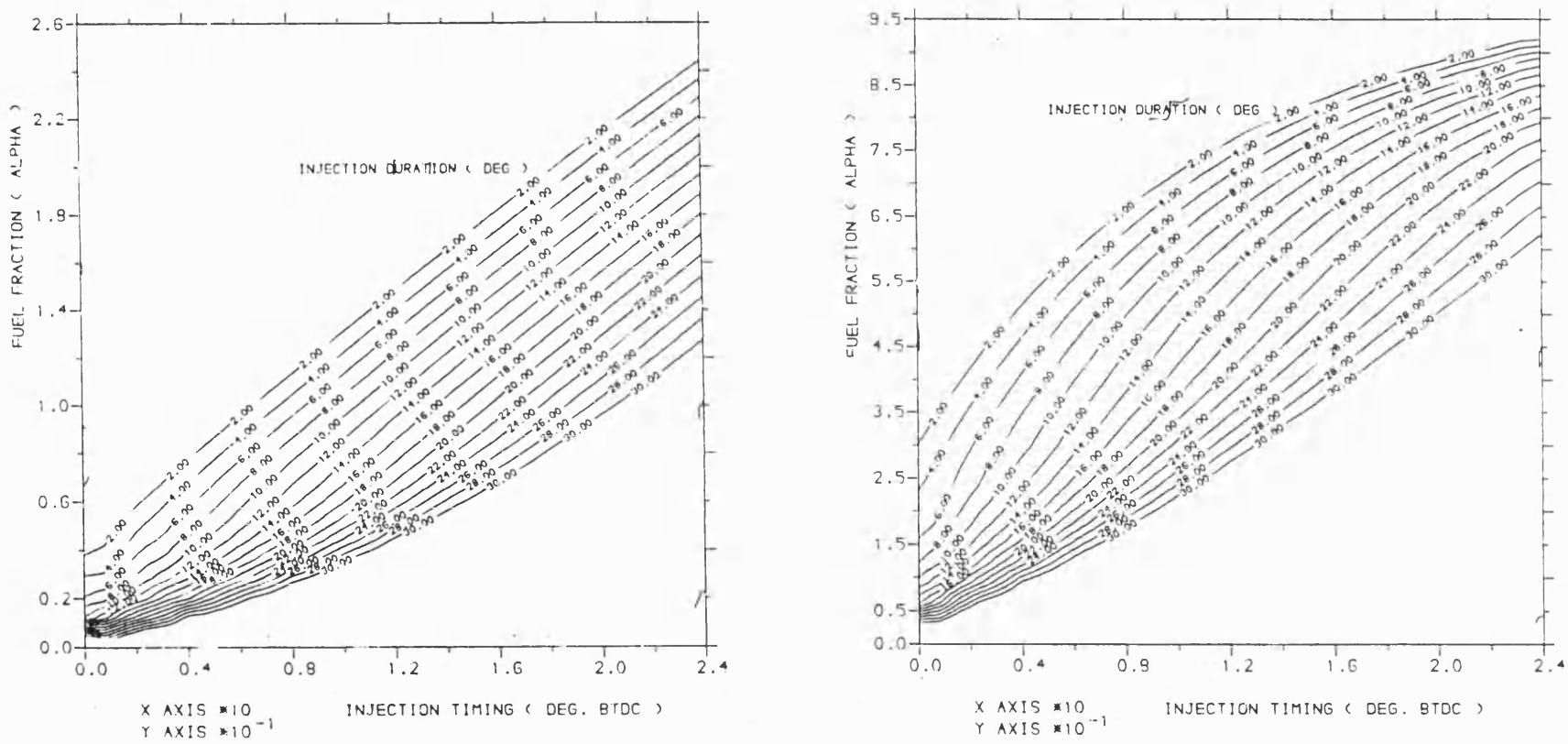

Fig. 2.6 Fraction of fuel burnt during constant volume part of combustion as a function of injection timing and duration (combustion model used in program ' EMAT ')

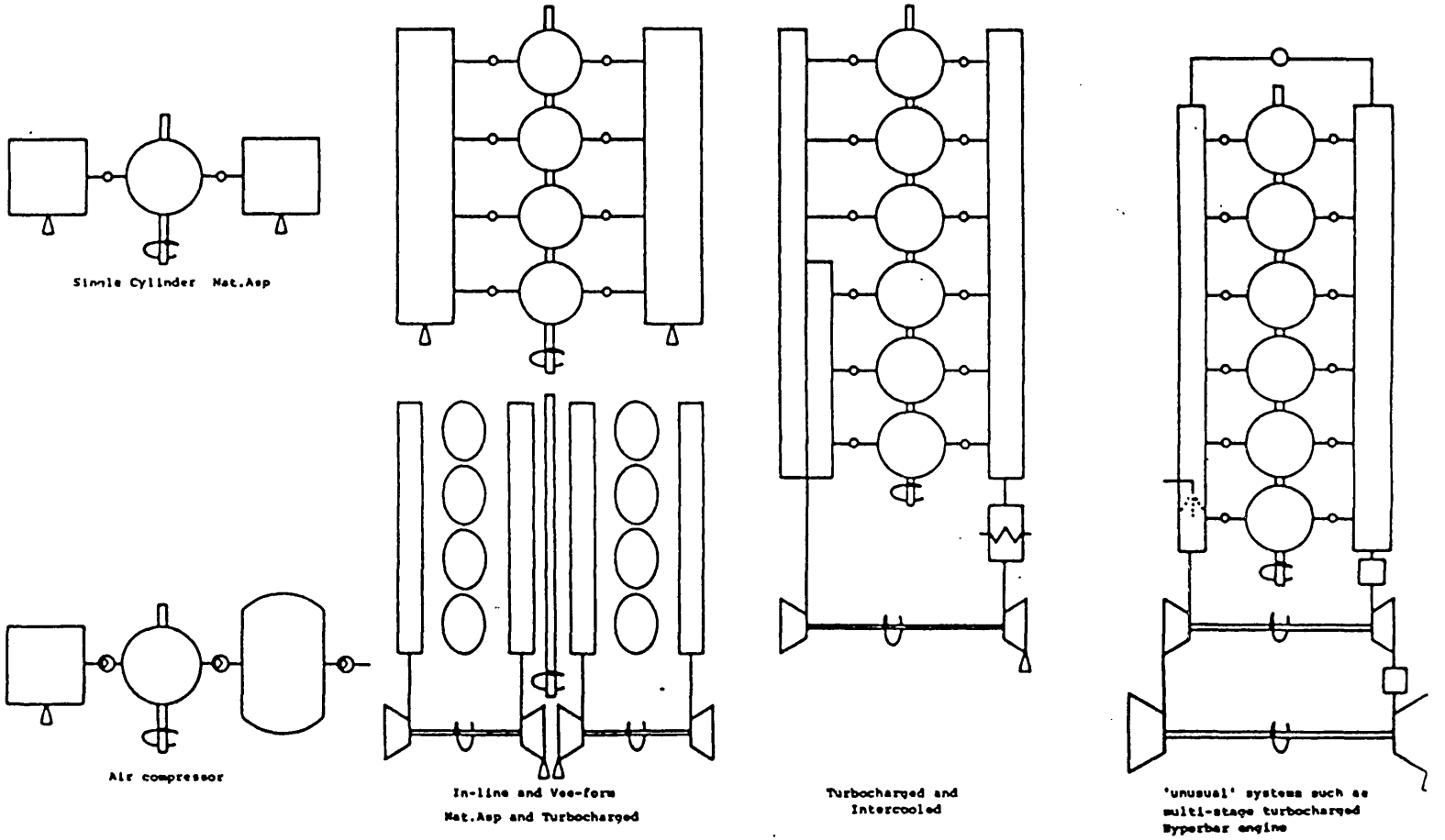

Fig. 2.7 Some of the systems that may be modelled using 'SPICE'

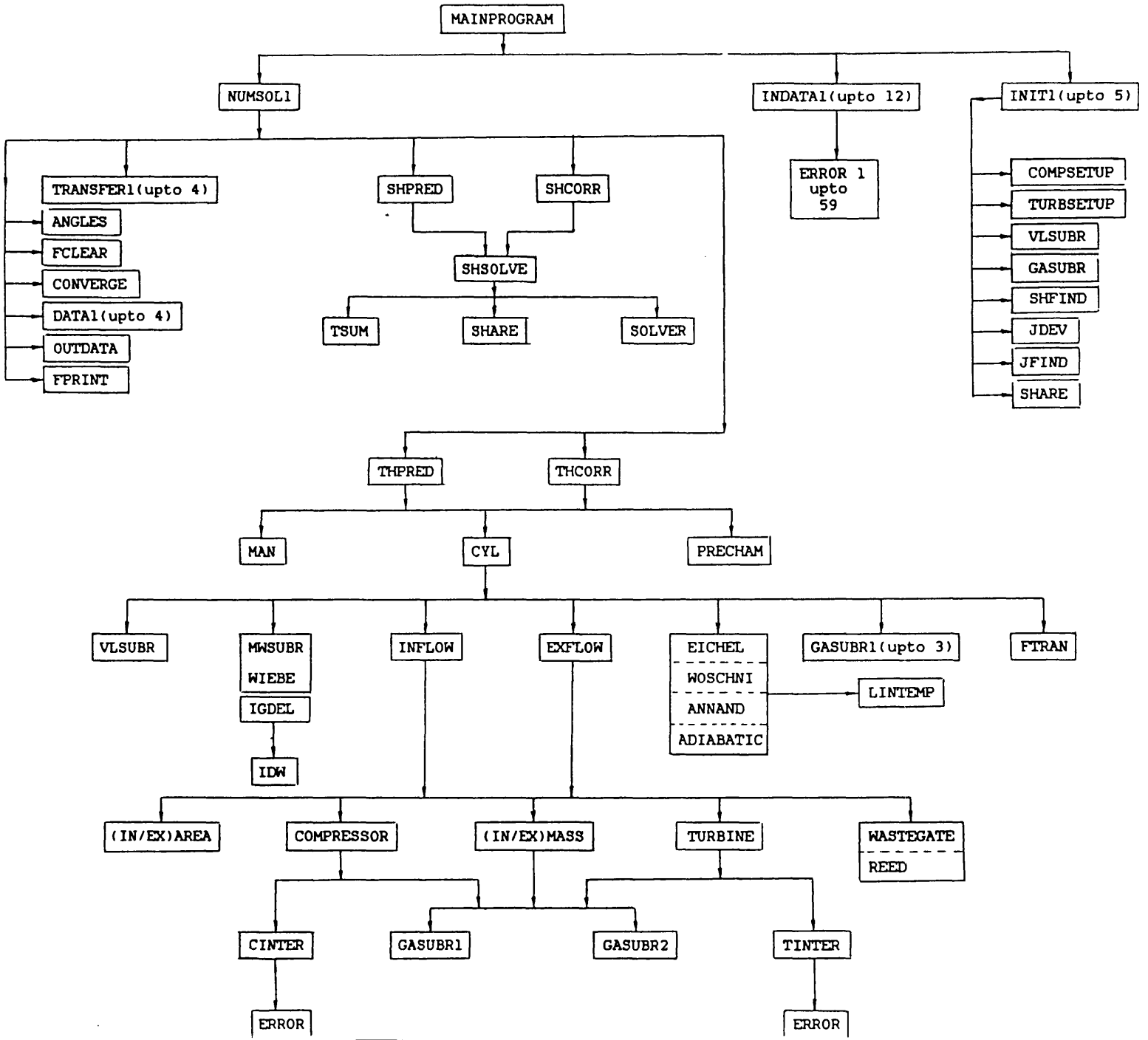

Fig. 2.8,a General layout for the program 'SPICE'

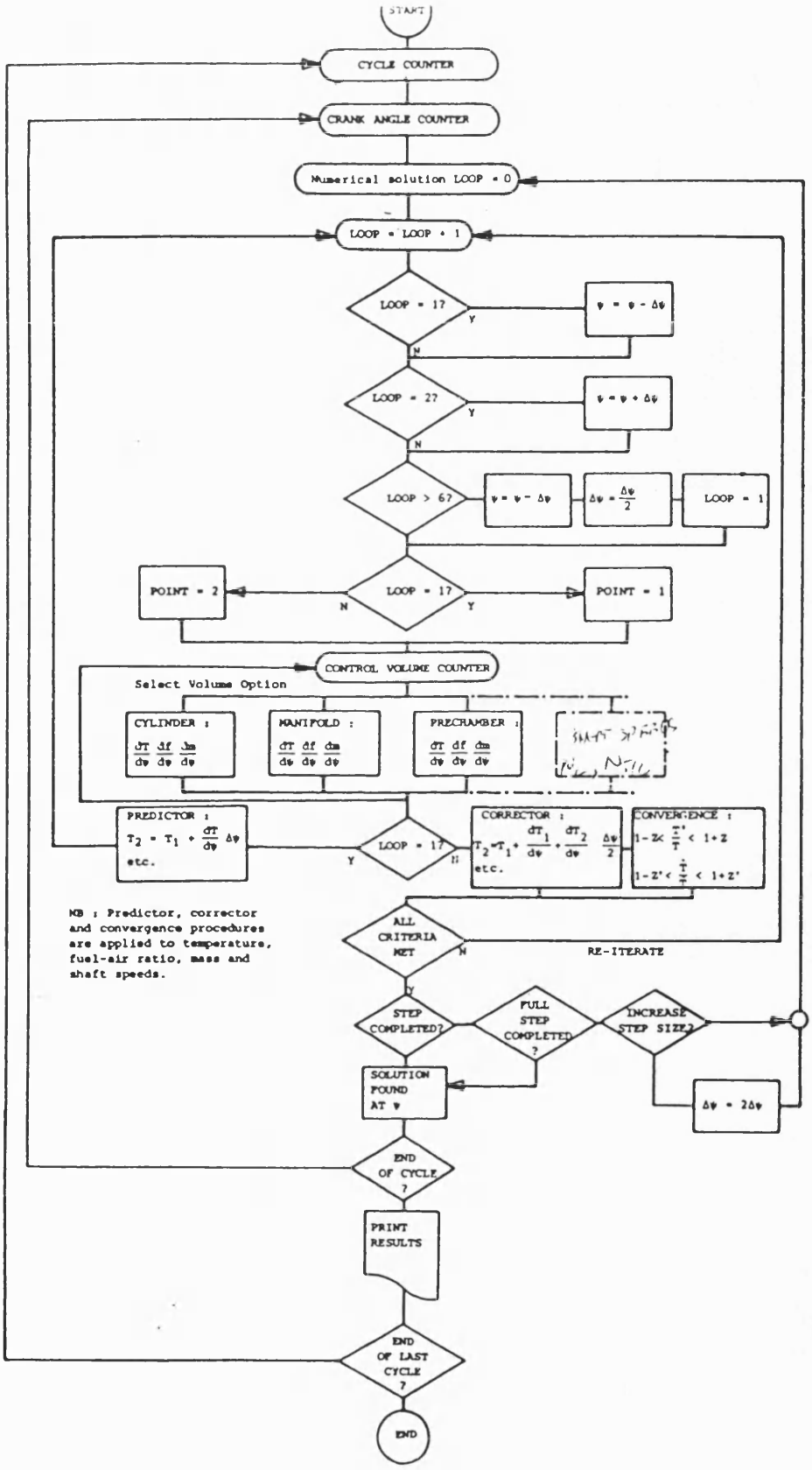

Fig. 2.8,b Flow diagram for simulation program for internal combustion engines 'SPICE'

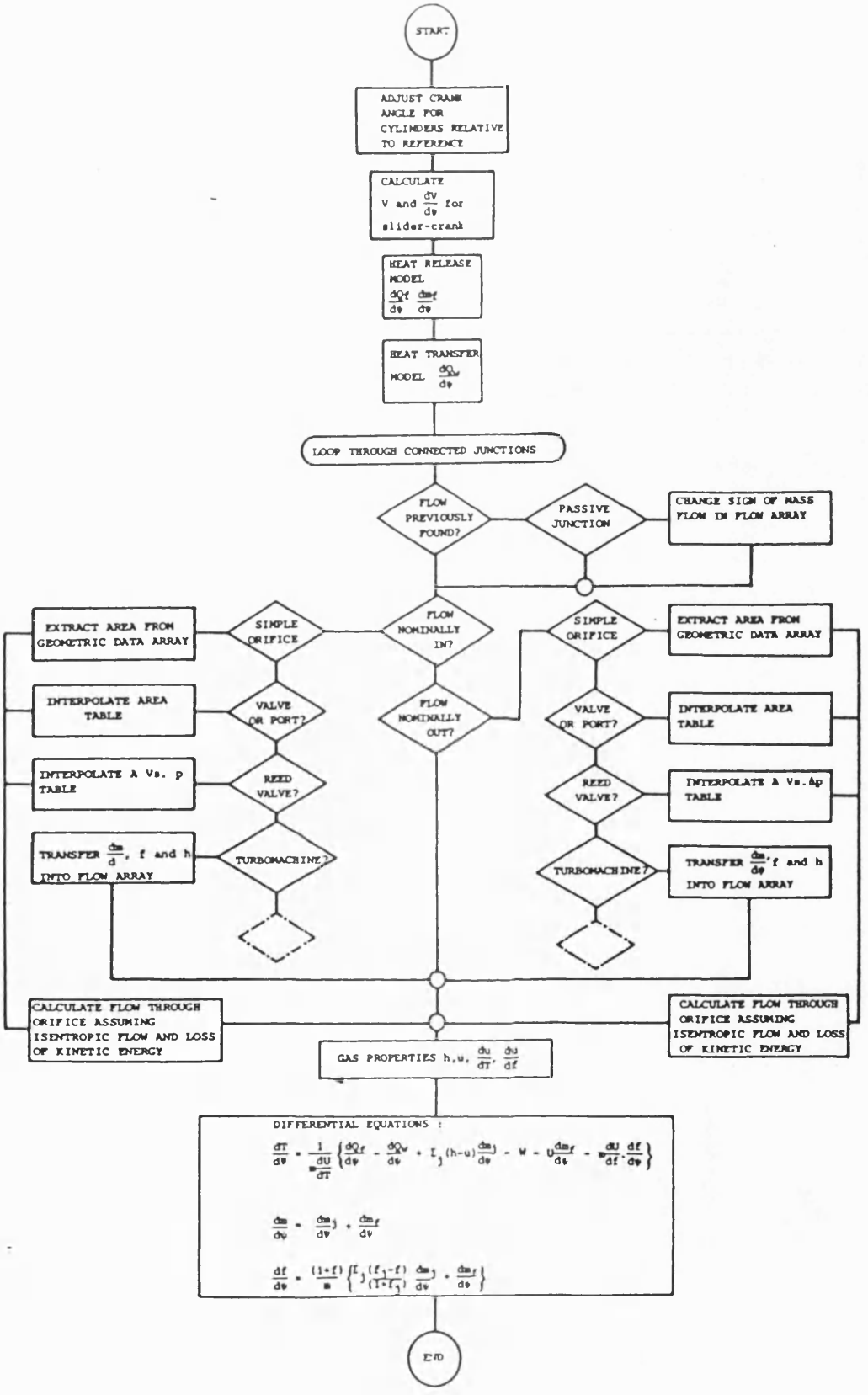

Fig 2.8, c Control volume flow diagram

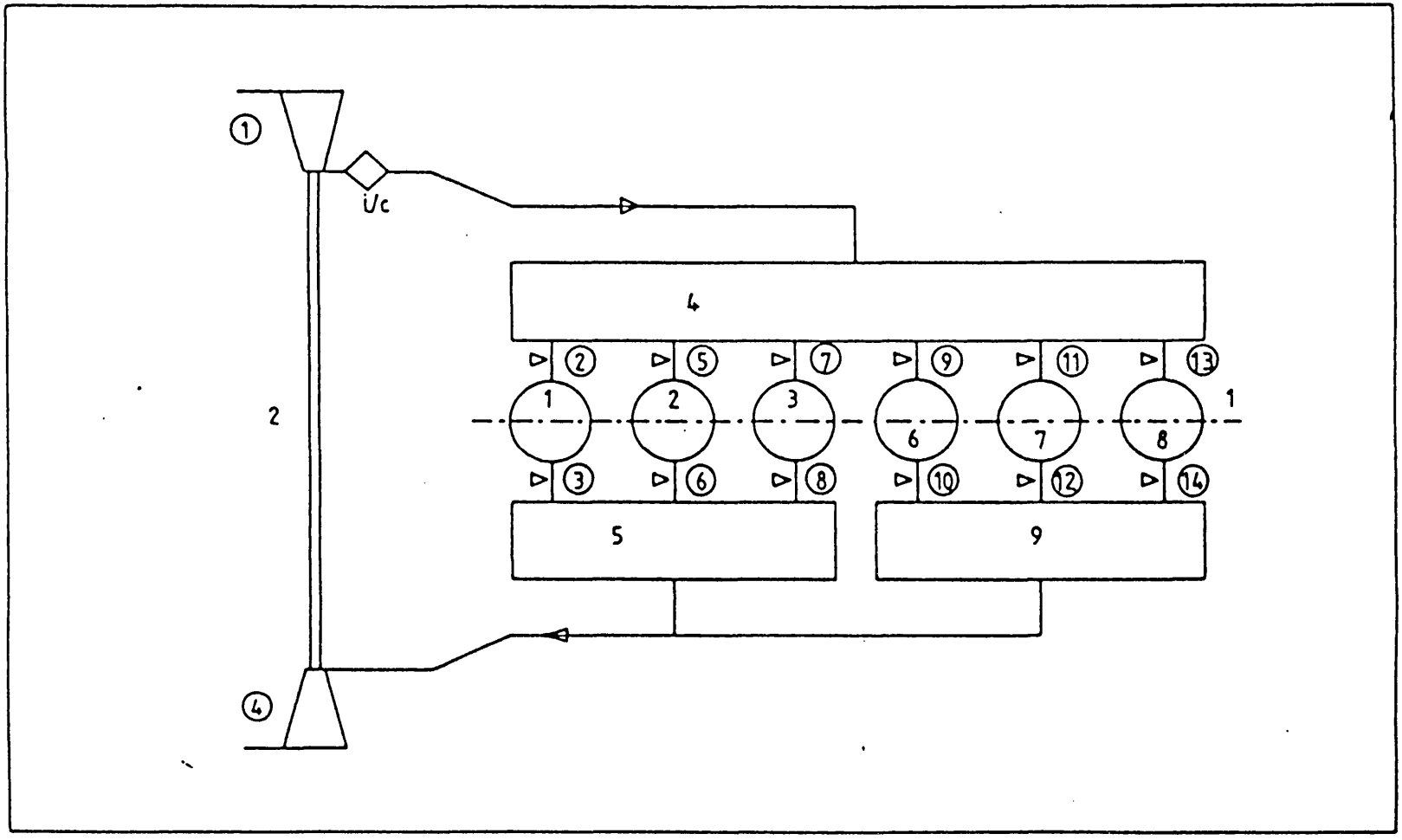

Fig. 2.9 Control volume model for the Cummins L10-T/C Diesel engine

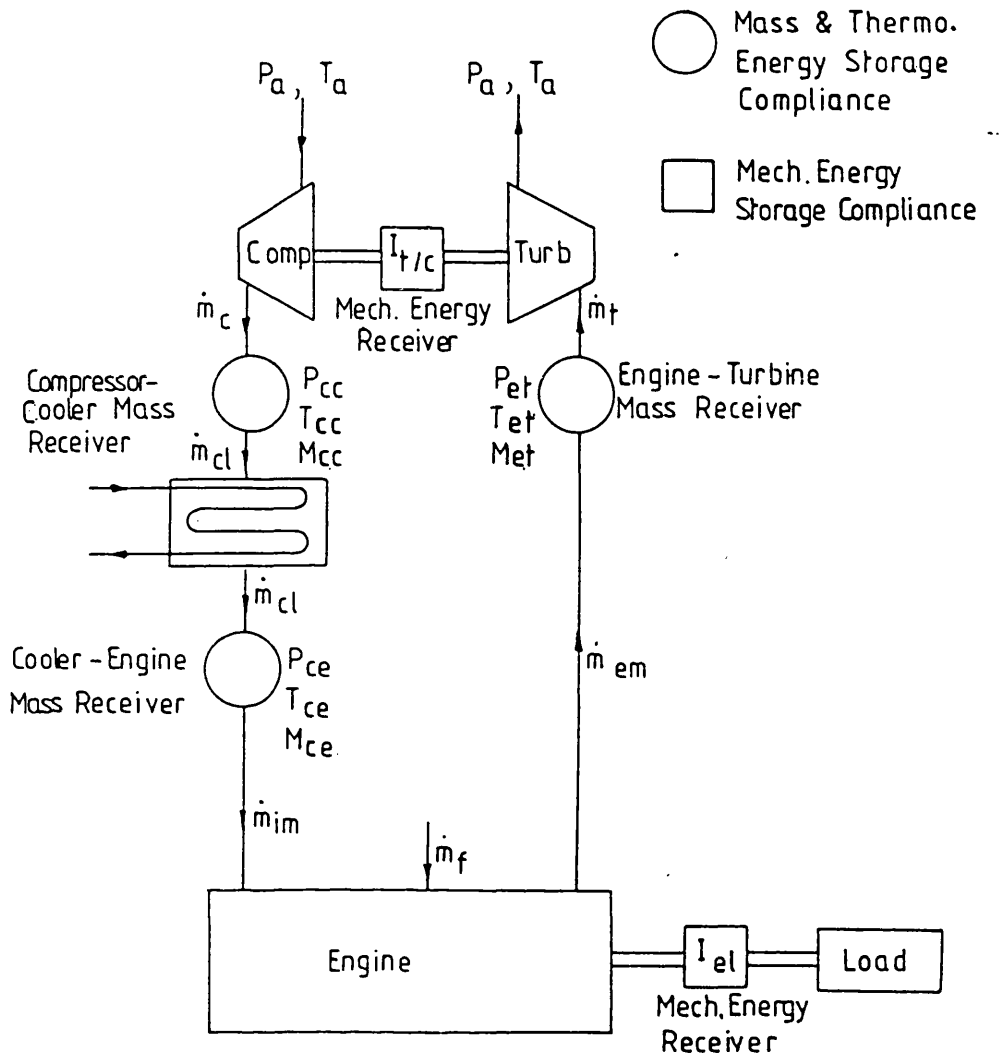

Fig. 2.10 Turbocharged engine model used for integrative system applied in the program 'TRANIC'

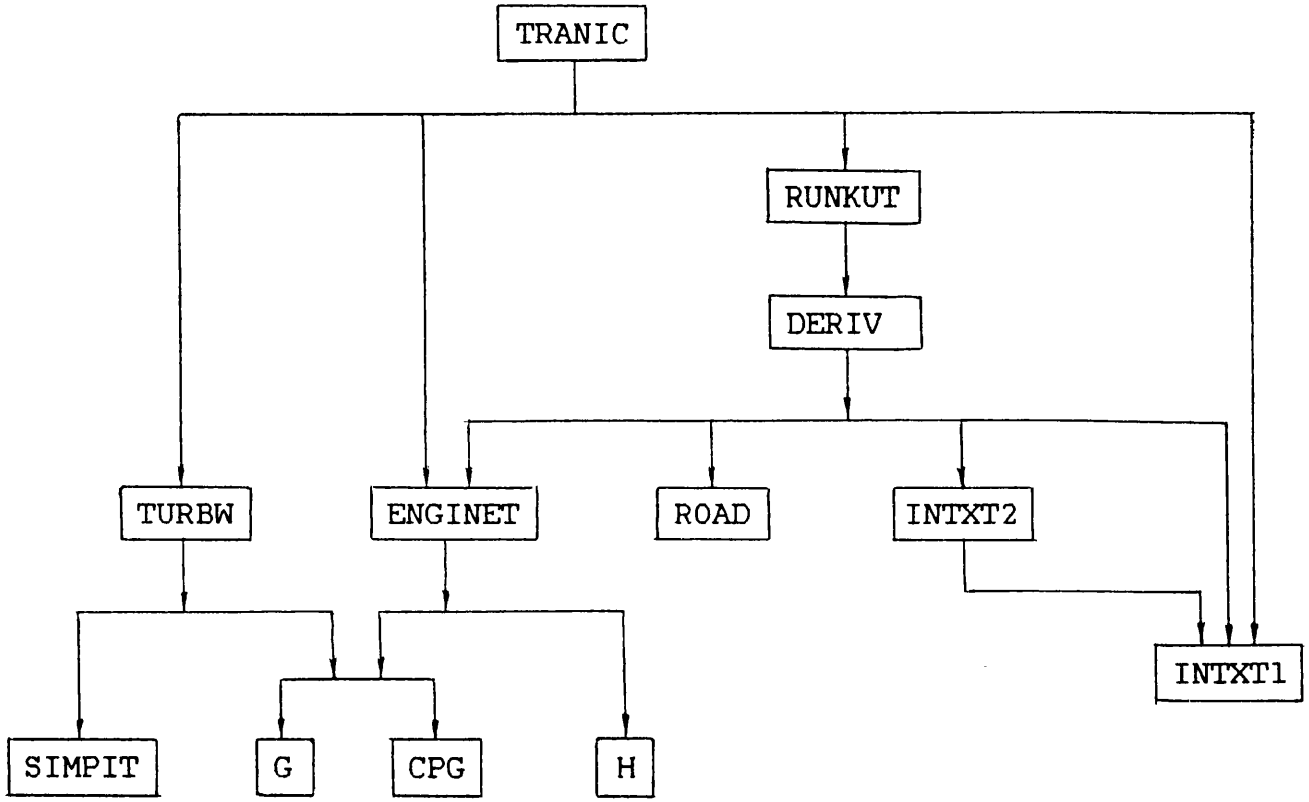

Fig. 2.11,a General layout for the program TRANIC

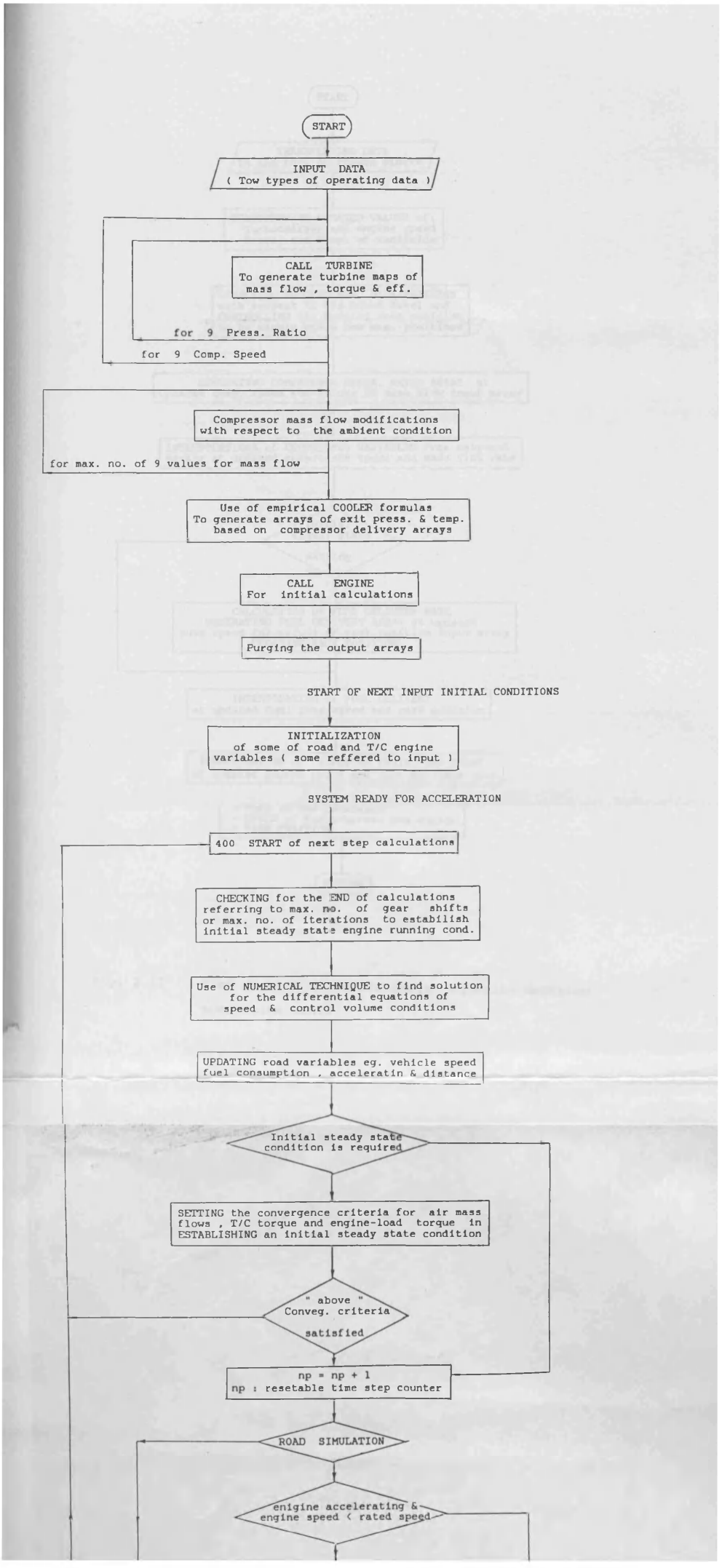
START
INPUT DATA
(Tow types of operating data)
CALL TURBINE
To generate turbine maps of
mass flow , torque & eff.
for 9 Press. Ratio
for 9 Comp. Speed
Compressor mass flow modifications
with respect to the ambient condition
for max. no. of 9 values for mass flow
Use of empirical COOLER formulas
To generate arrays of exit press. & temp.
based on compressor delivery arrays
CALL ENGINE
For initial calculations
Purging the output arrays
START OF NEXT INPUT INITIAL CONDITIONS
INITIALIZATION
of some of road and T/C engine
variables (some reffered to input)
SYSTEM READY FOR ACCELERATION
400 START of next step calculations
CHECKING for the END of calculations
referring to max. no. of gear shifts
or max. no. of iterations to estabilish
initial steady state engine running cond.
Use of NUMERICAL TECHNIQUE to find solution
for the differential equations of
speed & control volume conditions
UPDATING road variables eg. vehicle speed
fuel consumption , acceleratin & distance
Initial steady state
condition is required
SETTING the convergence criteria for air mass
flows , T/C torque and engine-load torque in
ESTABLISHING an initial steady state condition
" above "
Conveg. criteria
satisfied
np = np + 1
np : resetable time step counter
ROAD SIMULATION
enigine accelerating &
engine speed < rated speed

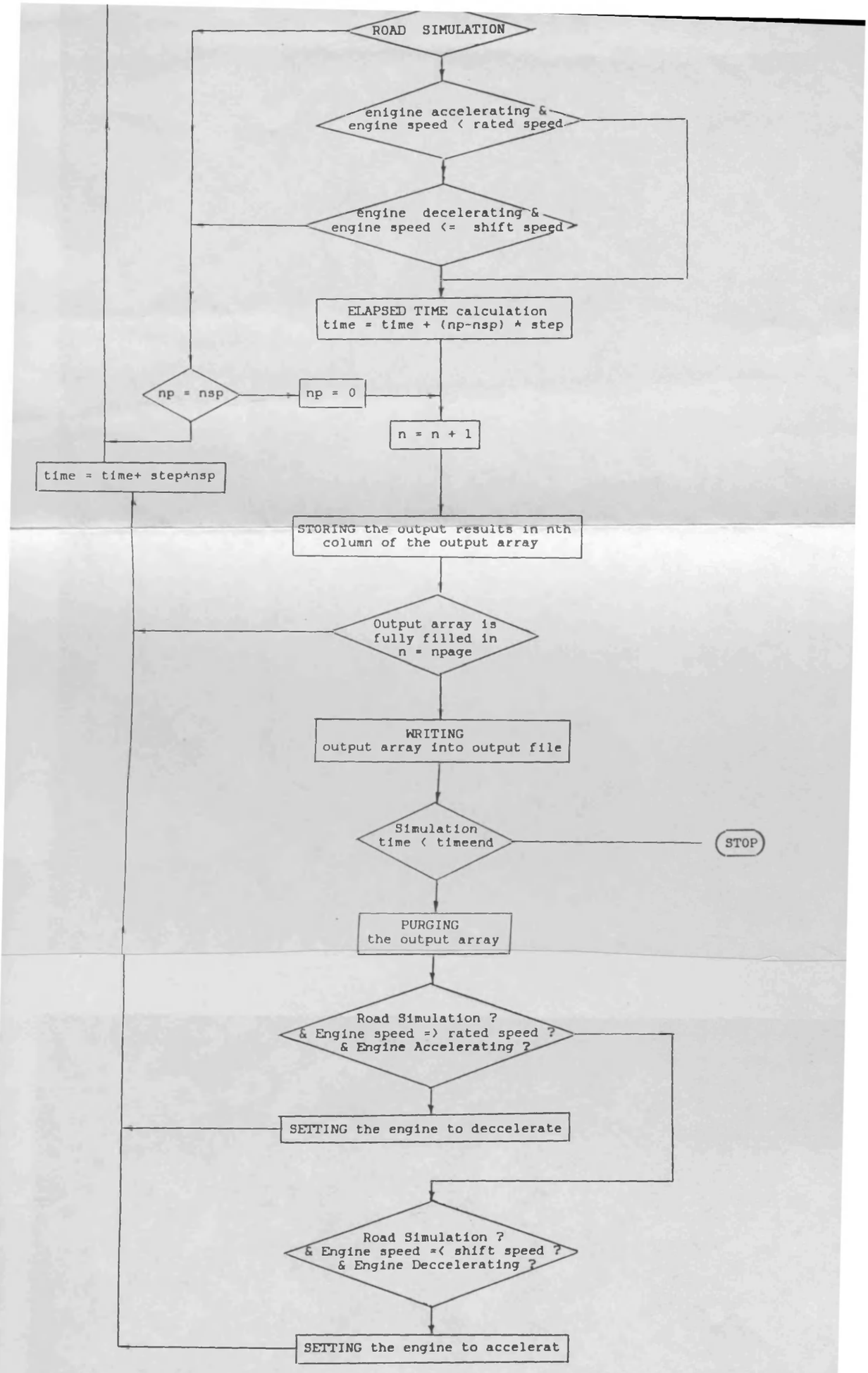

Fig. 2.11,b Flow diagram for transient simulation program TRANIC

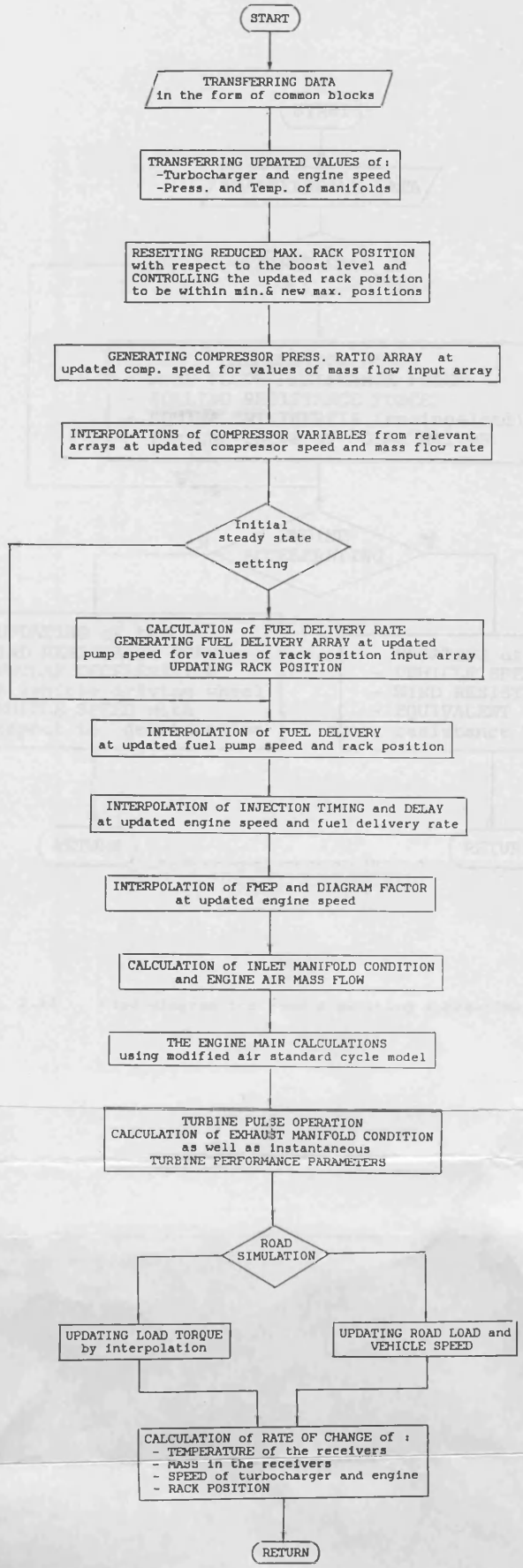

Fig. 2.12 Flow diagram for differential equation defining subroutine DERIV

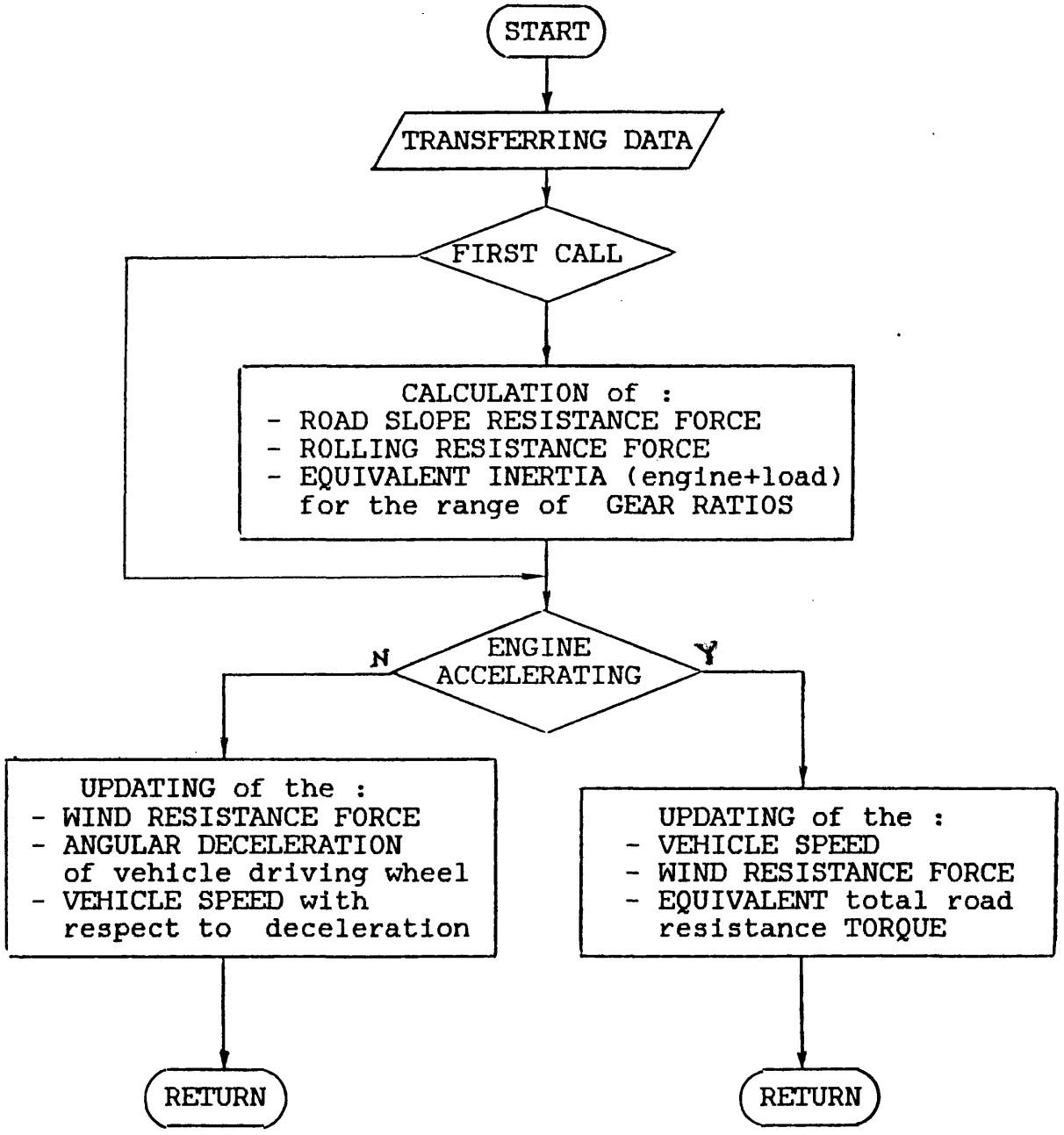

Fig. 2.13 Flow diagram for road simulating subroutine ROAD

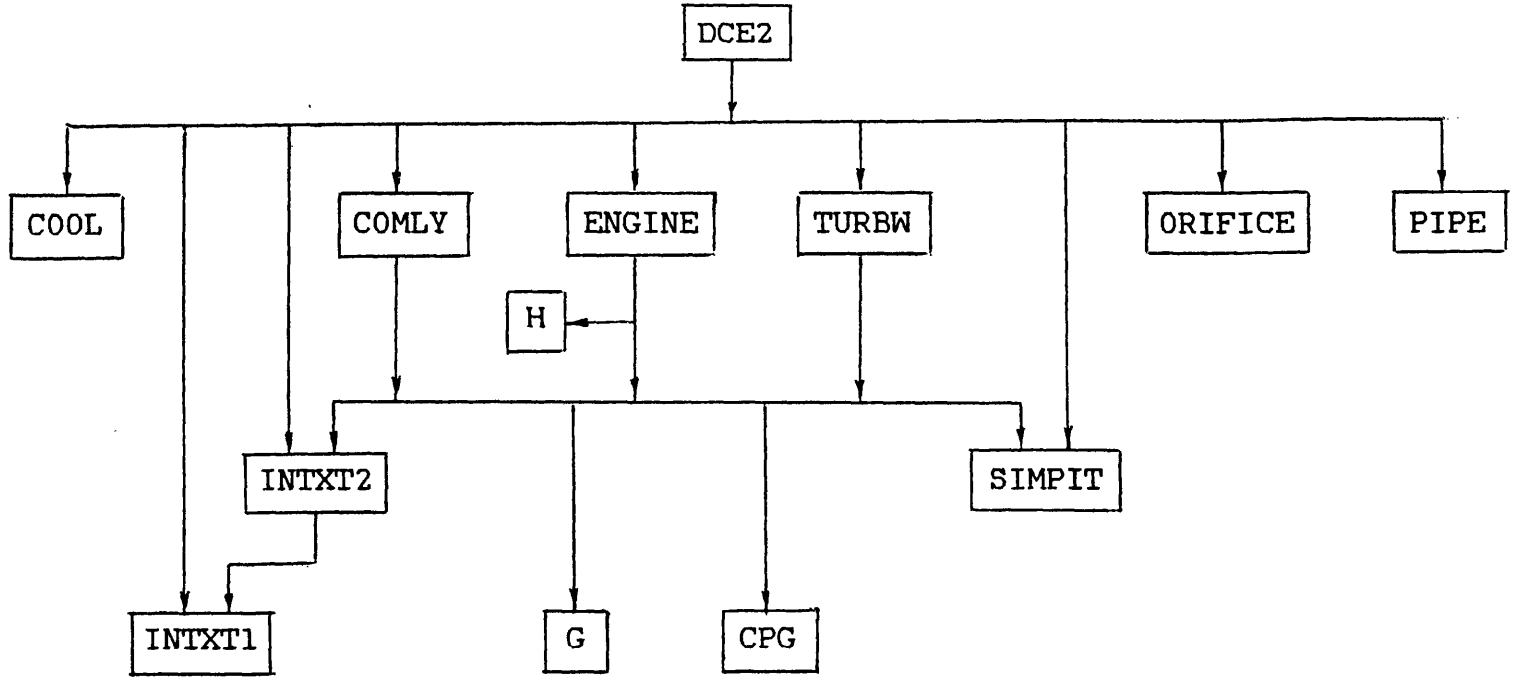

Fig. 2.14,a General layout for the program DCE2

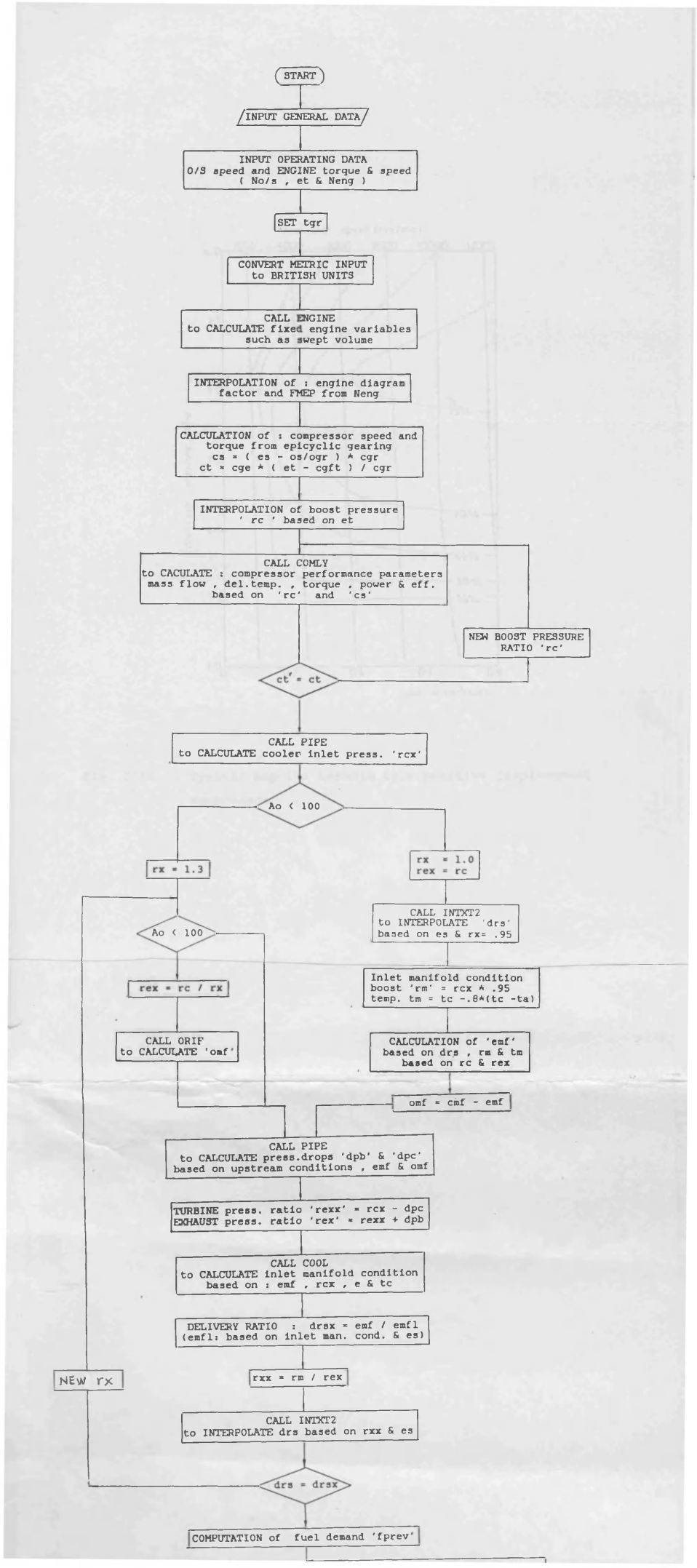
START
INPUT GENERAL DATA
INPUT OPERATING DATA
O/S speed and ENGINE torque & speed
(No/s , et & Neng)
SET tgr
CONVERT METRIC INPUT
to BRITISH UNITS
CALL ENGINE
to CALCULATE fixed engine variables
such as swept volume
INTERPOLATION of : engine diagram
factor and FMEP from Neng
CALCULATION of : compressor speed and
torque from epicyclic gearing
cs = (es - os/ogr) * cgr
ct = cge * (et - cgft) / cgr
INTERPOLATION of boost pressure
' rc ' based on et
CALL COMLY
to CACULATE : compressor performance parameters
mass flow , del.temp. , torque , power & eff.
based on 'rc' and 'cs'
NEW BOOST PRESSURE
RATIO 'rc'
ct' = ct
CALL PIPE
to CALCULATE cooler inlet press. 'rcx'
Ao < 100
rx = 1.3
rx = 1.0
rex = rc
Ao < 100
CALL INTXT2
to INTERPOLATE 'drs'
based on es & rx= .95
rex = rc / rx
Inlet manifold condition
boost 'rm' = rcx * .95
temp. tm = tc -.8*(tc -ta)
CALL ORIF
to CALCULATE 'omf'
CALCULATION of 'emf'
based on drs , rm & tm
based on rc & rex
omf = cmf - emf
CALL PIPE
to CALCULATE press.drops 'dpb' & 'dpc'
based on upstream conditions , emf & omf
TURBINE press. ratio 'rexx' = rcx - dpc
EXHAUST press. ratio 'rex' = rexx + dpb
CALL COOL
to CALCULATE inlet manifold condition
based on : emf , rcx , e & tc
DELIVERY RATIO : drsx = emf / emf1
(emf1: based on inlet man. cond. & es)
NEW rx
rxx = rm / rex
CALL INTXT2
to INTERPOLATE drs based on rxx & es
drs = drsx
COMPUTATION of fuel demand 'fprev'

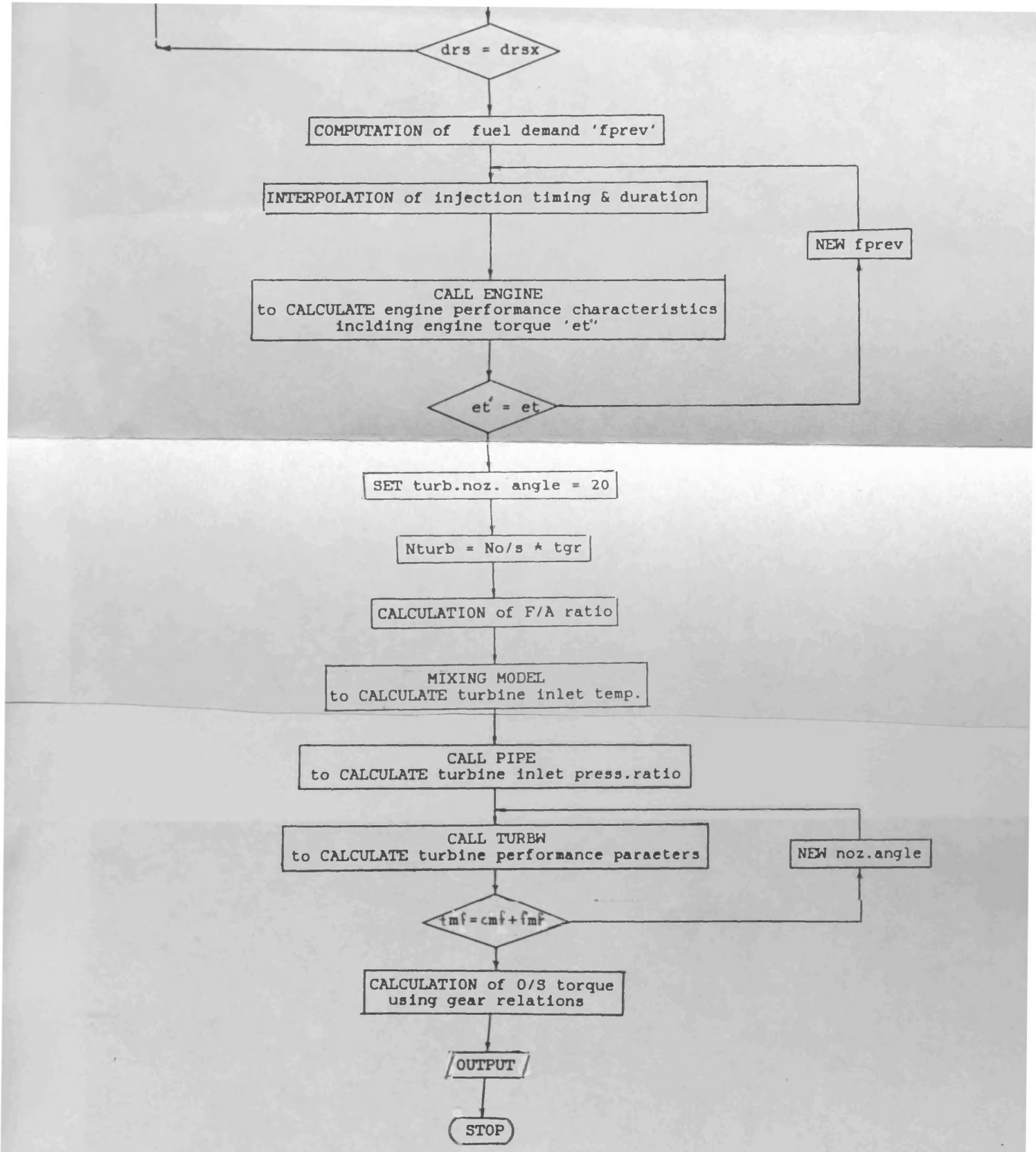

Fig. 2.14,b Flow diagram for the steady state DCE simulation program DCE2

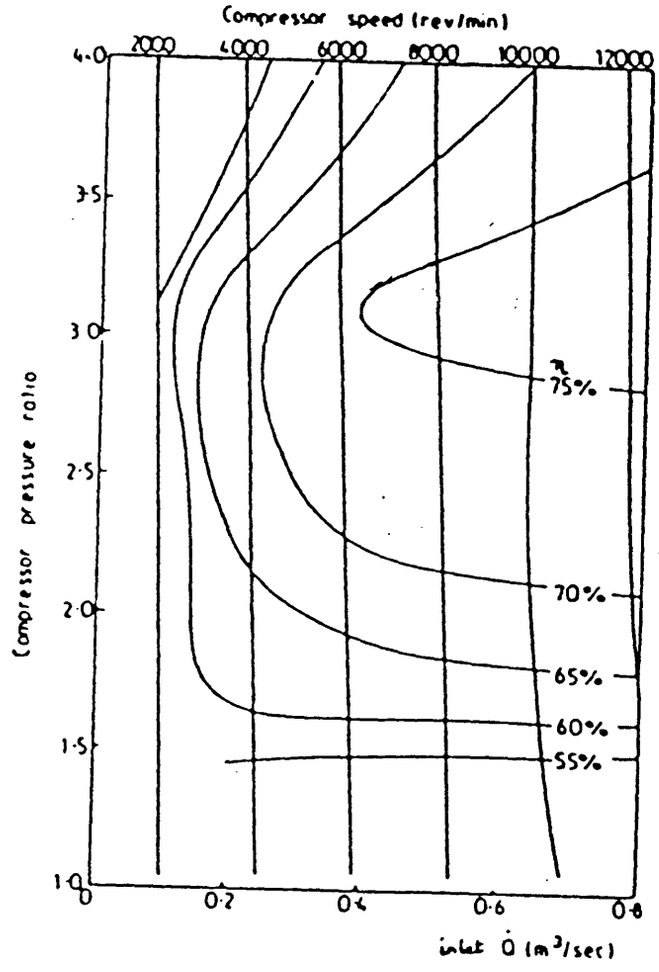

Fig. 2.15 Typical map for Lysholm type positive displacement compressor

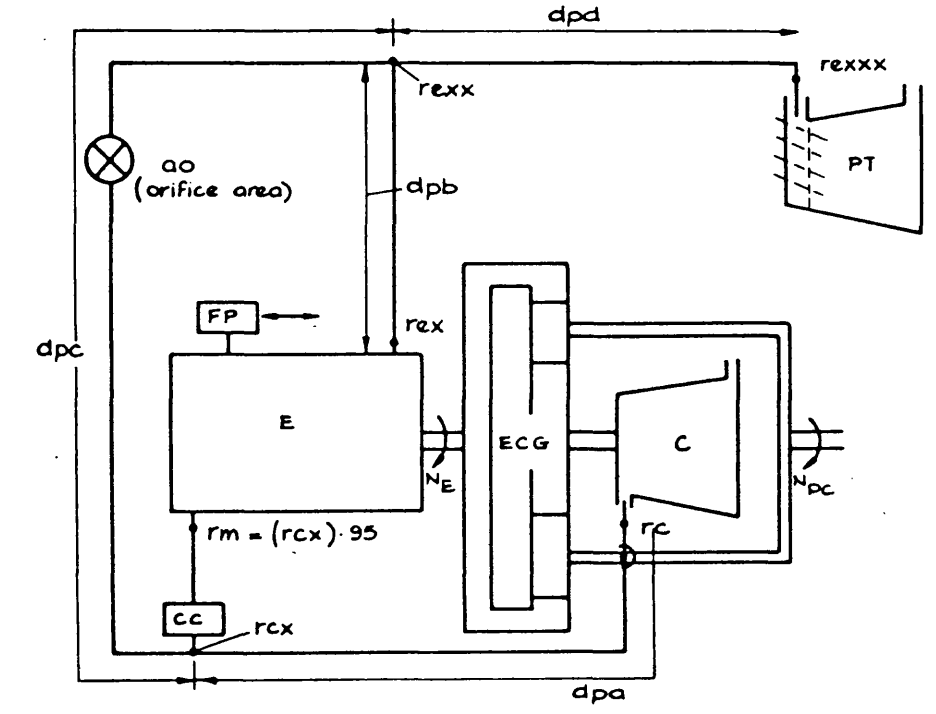

PRESSURE NOTATION : Compression to junction ≡ pipe a
Bypass pipe ≡ pipe c
Engine to exhaust junction ≡ pipe b
Exhaust junction to turbine ≡ pipe d

Fig. 2.16 DCE model applied in the program DCE2

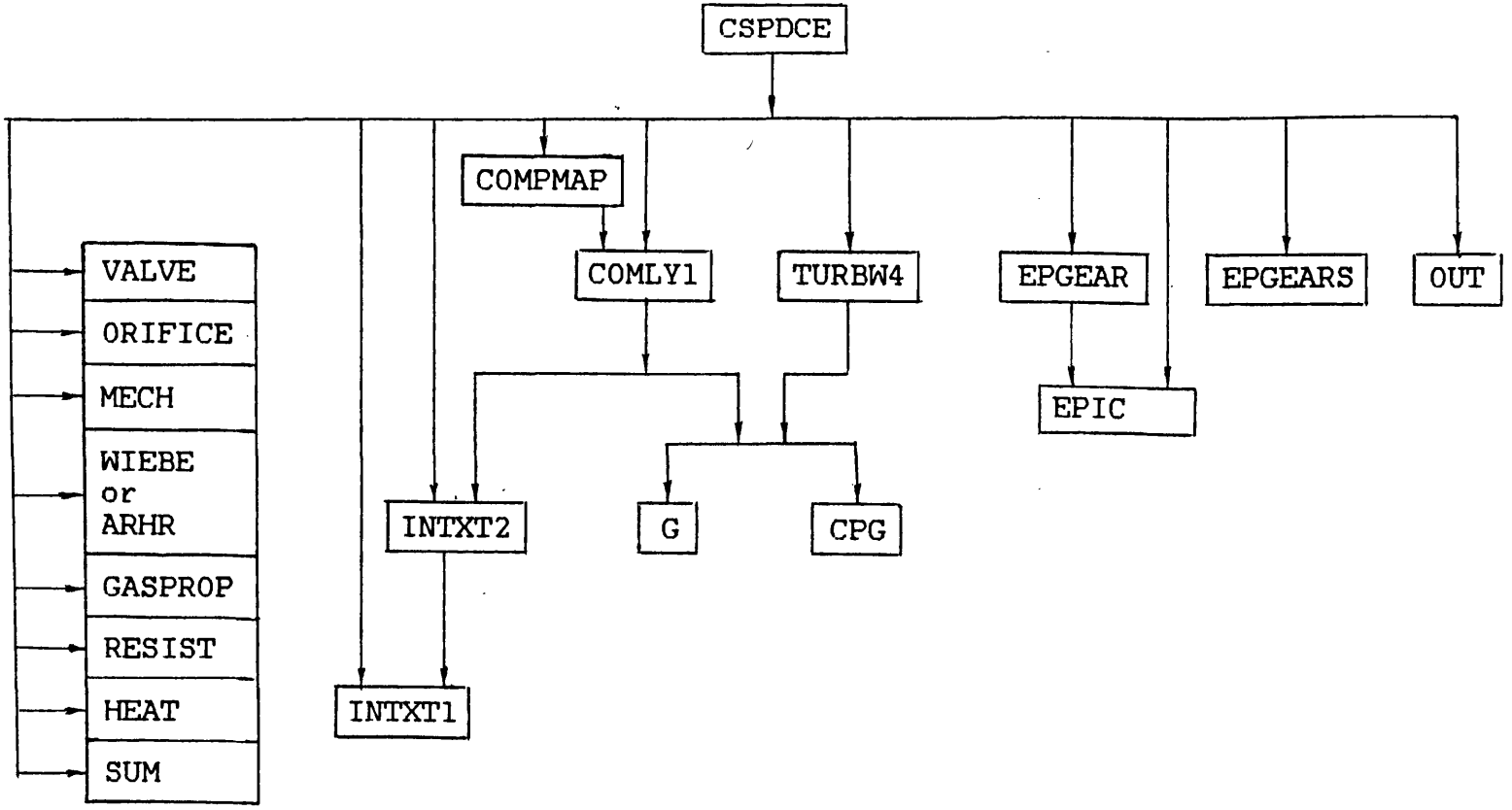

Fig. 2.17,a General layout for the program CSPDCE

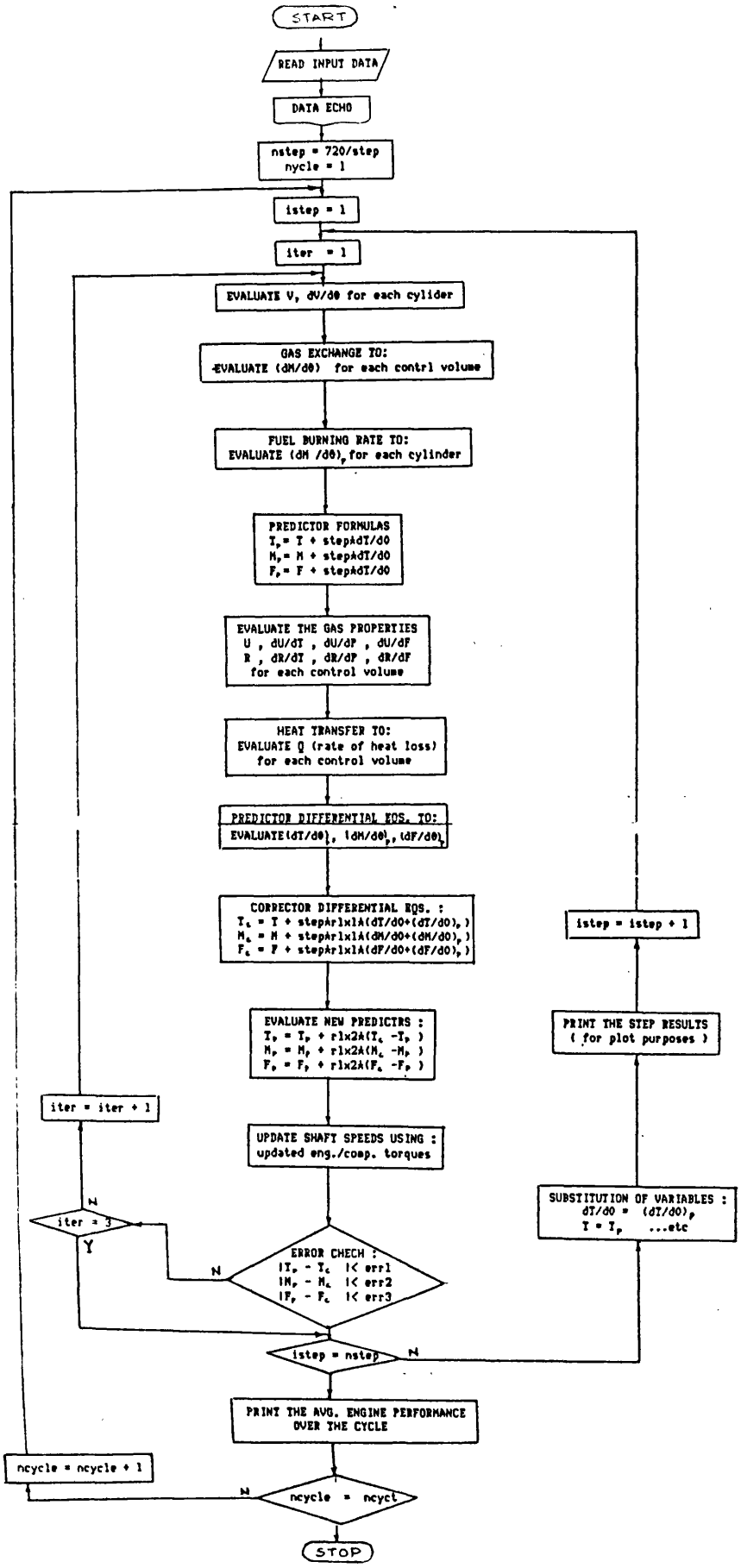

Fig. 2.17,b Flow diagram for the program CSPDCE

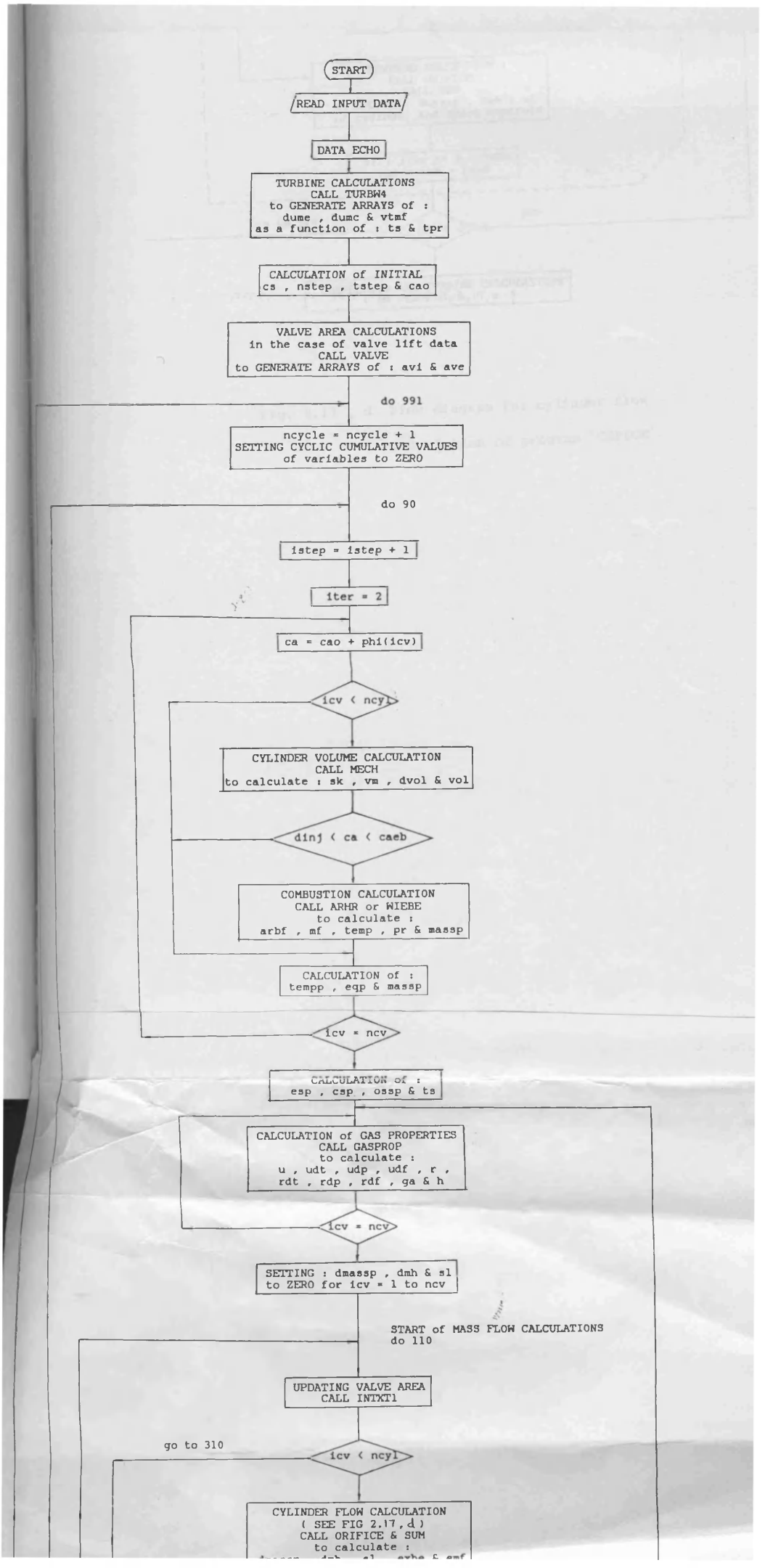
START
READ INPUT DATA
DATA ECHO
TURBINE CALCULATIONS
CALL TURBW4
to GENERATE ARRAYS of :
dume , dumc & vtmf
as a function of : ts & tpr
CALCULATION of INITIAL
cs , nstep , tstep & cao
VALVE AREA CALCULATIONS
in the case of valve lift data
CALL VALVE
to GENERATE ARRAYS of : avi & ave
do 991
ncycle = ncycle + 1
SETTING CYCLIC CUMULATIVE VALUES
of variables to ZERO
do 90
istep = istep + 1
iter = 2
ca = cao + phi(icv)
icv < ncyl
CYLINDER VOLUME CALCULATION
CALL MECH
to calculate : sk , vm , dvol & vol
dinj < ca < caeb
COMBUSTION CALCULATION
CALL ARHR or WIEBE
to calculate :
arbf , mf , temp , pr & massp
CALCULATION of :
tempp , eqp & massp
icv = ncv
CALCULATION of :
esp , csp , ossp & ts
CALCULATION of GAS PROPERTIES
CALL GASPROP
to calculate :
u , udt , udp , udf , r ,
rdt , rdp , rdf , ga & h
icv = ncv
SETTING : dmassp , dmh & sl
to ZERO for icv = 1 to ncv
START of MASS FLOW CALCULATIONS
do 110
UPDATING VALVE AREA
CALL INTXT1
go to 310
icv < ncyl
CYLINDER FLOW CALCULATION
(SEE FIG 2.17,d)
CALL ORIFICE & SUM
to calculate :

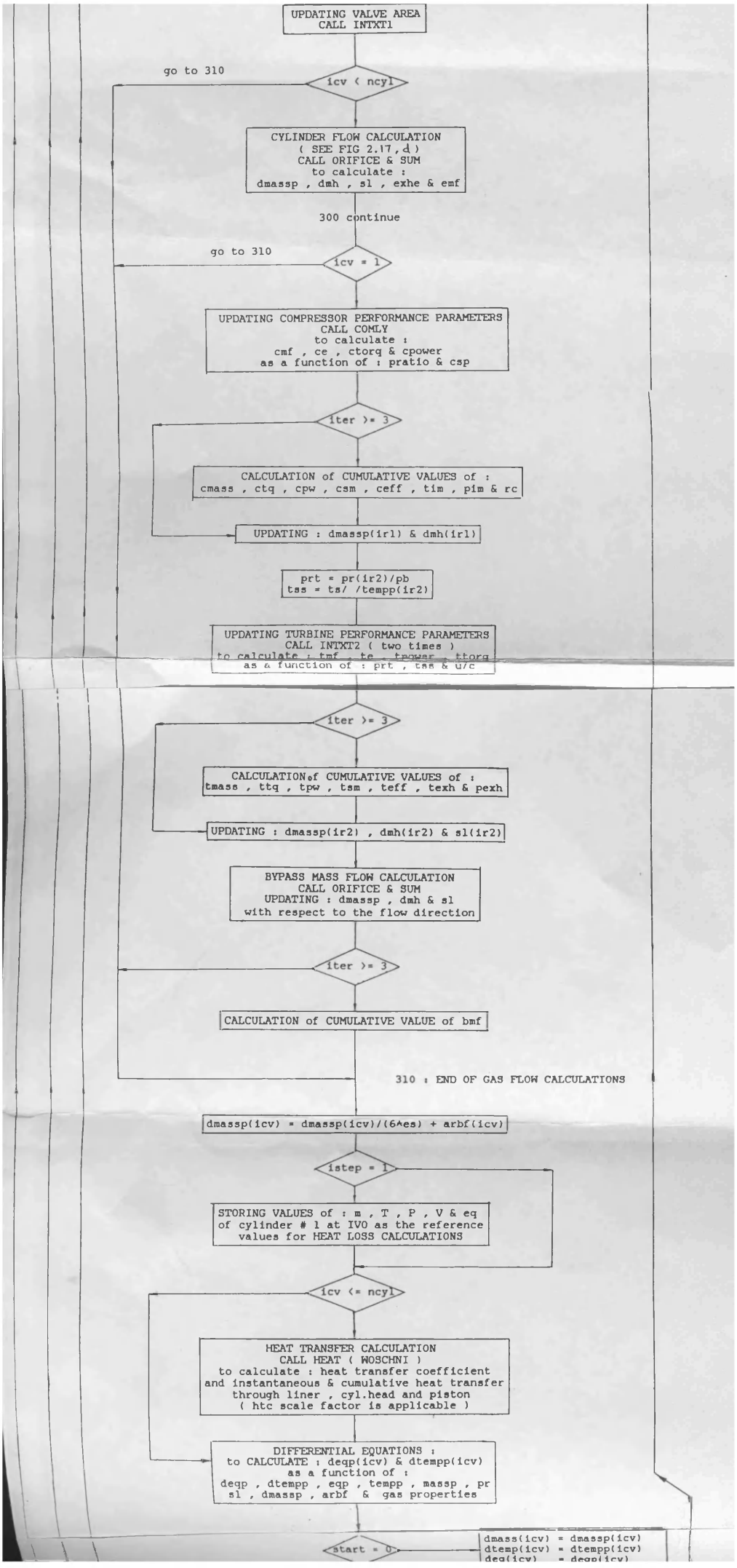
UPDATING VALVE AREA
CALL INTXT1
go to 310
icv (ncyl
CYLINDER FLOW CALCULATION
(SEE FIG 2.17, d)
CALL ORIFICE & SUM
to calculate :
dmassp , dmh , sl , exhe & emf
300 continue
go to 310
icv = 1
UPDATING COMPRESSOR PERFORMANCE PARAMETERS
CALL COMLY
to calculate :
cmf , ce , ctorq & cpower
as a function of : pratio & csp
iter)= 3
CALCULATION of CUMULATIVE VALUES of :
cmass , ctq , cpw , csm , ceff , tim , pim & rc
UPDATING : dmassp(ir1) & dmh(ir1)
prt = pr(ir2)/pb
tss = ts/ /tempp(ir2)
UPDATING TURBINE PERFORMANCE PARAMETERS
CALL INTXT2 (two times)
to calculate : tmf , te , tpower , ttorq
as a function of : prt , tss & u/c
iter)= 3
CALCULATION of CUMULATIVE VALUES of :
tmass , ttq , tpw , tsm , teff , texh & pexh
UPDATING : dmassp(ir2) , dmh(ir2) & sl(ir2)
BYPASS MASS FLOW CALCULATION
CALL ORIFICE & SUM
UPDATING : dmassp , dmh & sl
with respect to the flow direction
iter)= 3
CALCULATION of CUMULATIVE VALUE of bmf
310 : END OF GAS FLOW CALCULATIONS
dmassp(icv) = dmassp(icv)/(6^es) + arbf(icv)
istep = 1
STORING VALUES of : m , T , P , V & eq
of cylinder # 1 at IVO as the reference
values for HEAT LOSS CALCULATIONS
icv (= ncyl
HEAT TRANSFER CALCULATION
CALL HEAT (WOSCHNI)
to calculate : heat transfer coefficient
and instantaneous & cumulative heat transfer
through liner , cyl.head and piston
(htc scale factor is applicable)
DIFFERENTIAL EQUATIONS :
to CALCULATE : deqp(icv) & dtempp(icv)
as a function of :
deqp , dtempp , eqp , tempp , massp , pr
sl , dmassp , arbf & gas properties
start = 0
dmass(icv) = dmassp(icv)
dtemp(icv) = dtempp(icv)
deq(icv) = deqp(icv)

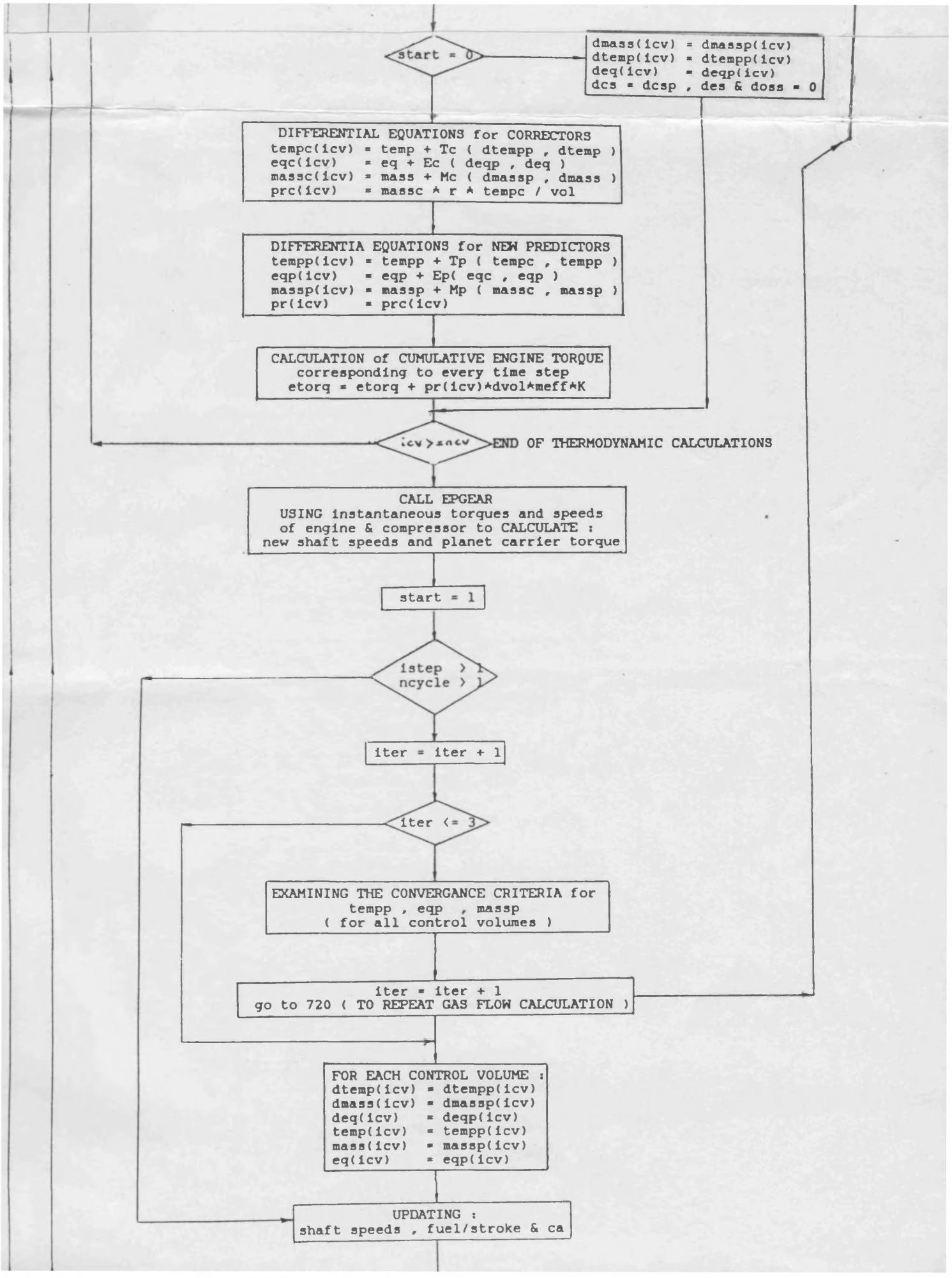
start = 0
dmass(icv) = dmassp(icv)
dtemp(icv) = dtempp(icv)
deq(icv) = deqp(icv)
dcs = dcsp , des & doss = 0
DIFFERENTIAL EQUATIONS for CORRECTORS
tempc(icv) = temp + Tc (dtempp , dtemp)
eqc(icv) = eq + Ec (deqp , deq)
massc(icv) = mass + Mc (dmassp , dmass)
prc(icv) = massc * r * tempc / vol
DIFFERENTIA EQUATIONS for NEW PREDICTORS
tempp(icv) = tempp + Tp (tempc , tempp)
eqp(icv) = eqp + Ep(eqc , eqp)
massp(icv) = massp + Mp (massc , massp)
pr(icv) = prc(icv)
CALCULATION of CUMULATIVE ENGINE TORQUE
corresponding to every time step
etorq = etorq + pr(icv)*dvol*meff*K
icv > =ncv
END OF THERMODYNAMIC CALCULATIONS
CALL EPGEAR
USING instantaneous torques and speeds
of engine & compressor to CALCULATE :
new shaft speeds and planet carrier torque
start = 1
istep > 1
ncycle > 1
iter = iter + 1
iter <= 3
EXAMINING THE CONVERGANCE CRITERIA for
tempp , eqp , massp
(for all control volumes)
iter = iter + 1
go to 720 (TO REPEAT GAS FLOW CALCULATION)
FOR EACH CONTROL VOLUME :
dtemp(icv) = dtempp(icv)
dmass(icv) = dmassp(icv)
deq(icv) = deqp(icv)
temp(icv) = tempp(icv)
mass(icv) = massp(icv)
eq(icv) = eqp(icv)
UPDATING :
shaft speeds , fuel/stroke & ca

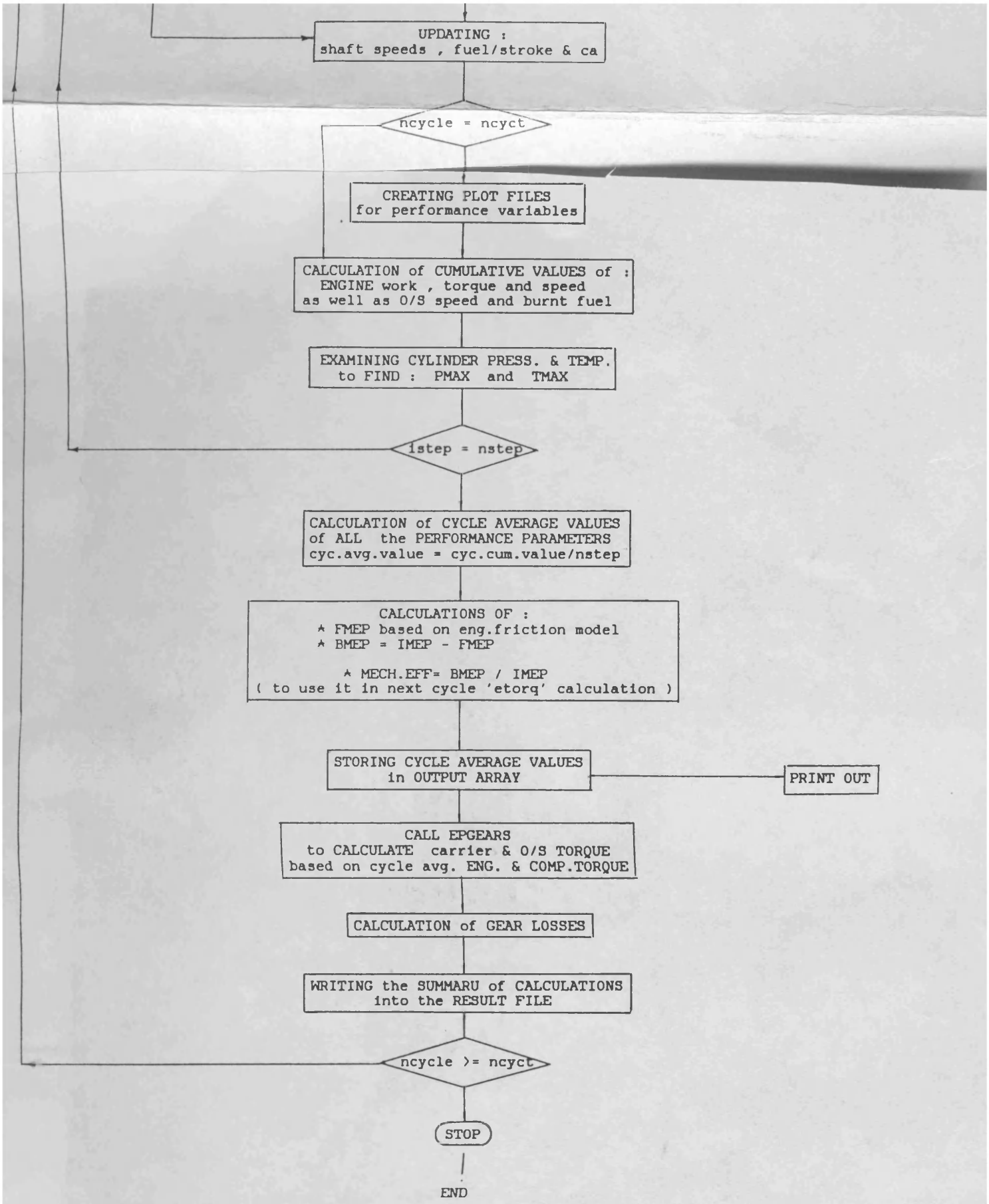

Fig. 2.17,c Detailed flow diagram for 'CSPDCE'

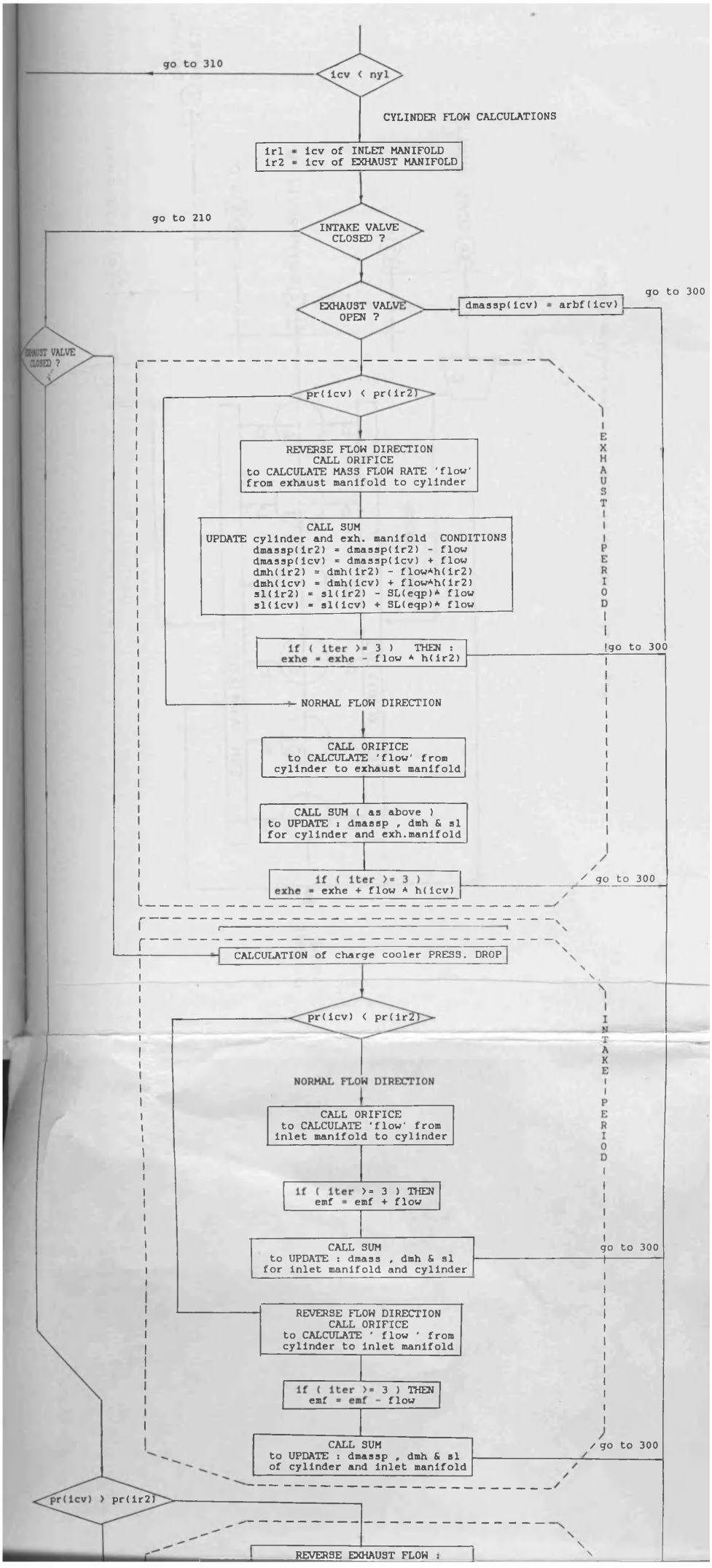
go to 310
icv < nyl
CYLINDER FLOW CALCULATIONS
ir1 = icv of INLET MANIFOLD
ir2 = icv of EXHAUST MANIFOLD
go to 210
INTAKE VALVE CLOSED ?
EXHAUST VALVE OPEN ?
dmassp(icv) = arbf(icv)
go to 300
EXHAUST VALVE CLOSED ?
pr(icv) < pr(ir2)
REVERSE FLOW DIRECTION
CALL ORIFICE
to CALCULATE MASS FLOW RATE 'flow'
from exhaust manifold to cylinder
CALL SUM
UPDATE cylinder and exh. manifold CONDITIONS
dmassp(ir2) = dmassp(ir2) - flow
dmassp(icv) = dmassp(icv) + flow
dmh(ir2) = dmh(ir2) - flow*h(ir2)
dmh(icv) = dmh(icv) + flow*h(ir2)
sl(ir2) = sl(ir2) - SL(eqp)* flow
sl(icv) = sl(icv) + SL(eqp)* flow
if (iter >= 3) THEN :
exhe = exhe - flow * h(ir2)
go to 300
EXHAUST PERIOD
NORMAL FLOW DIRECTION
CALL ORIFICE
to CALCULATE 'flow' from
cylinder to exhaust manifold
CALL SUM (as above)
to UPDATE : dmassp , dmh & sl
for cylinder and exh.manifold
if (iter >= 3)
exhe = exhe + flow * h(icv)
go to 300
CALCULATION of charge cooler PRESS. DROP
pr(icv) < pr(ir2)
NORMAL FLOW DIRECTION
CALL ORIFICE
to CALCULATE 'flow' from
inlet manifold to cylinder
if (iter >= 3) THEN
emf = emf + flow
CALL SUM
to UPDATE : dmass , dmh & sl
for inlet manifold and cylinder
go to 300
INTAKE PERIOD
REVERSE FLOW DIRECTION
CALL ORIFICE
to CALCULATE ' flow ' from
cylinder to inlet manifold
if (iter >= 3) THEN
emf = emf - flow
CALL SUM
to UPDATE : dmassp , dmh & sl
of cylinder and inlet manifold
go to 300
pr(icv) > pr(ir2)
REVERSE EXHAUST FLOW :

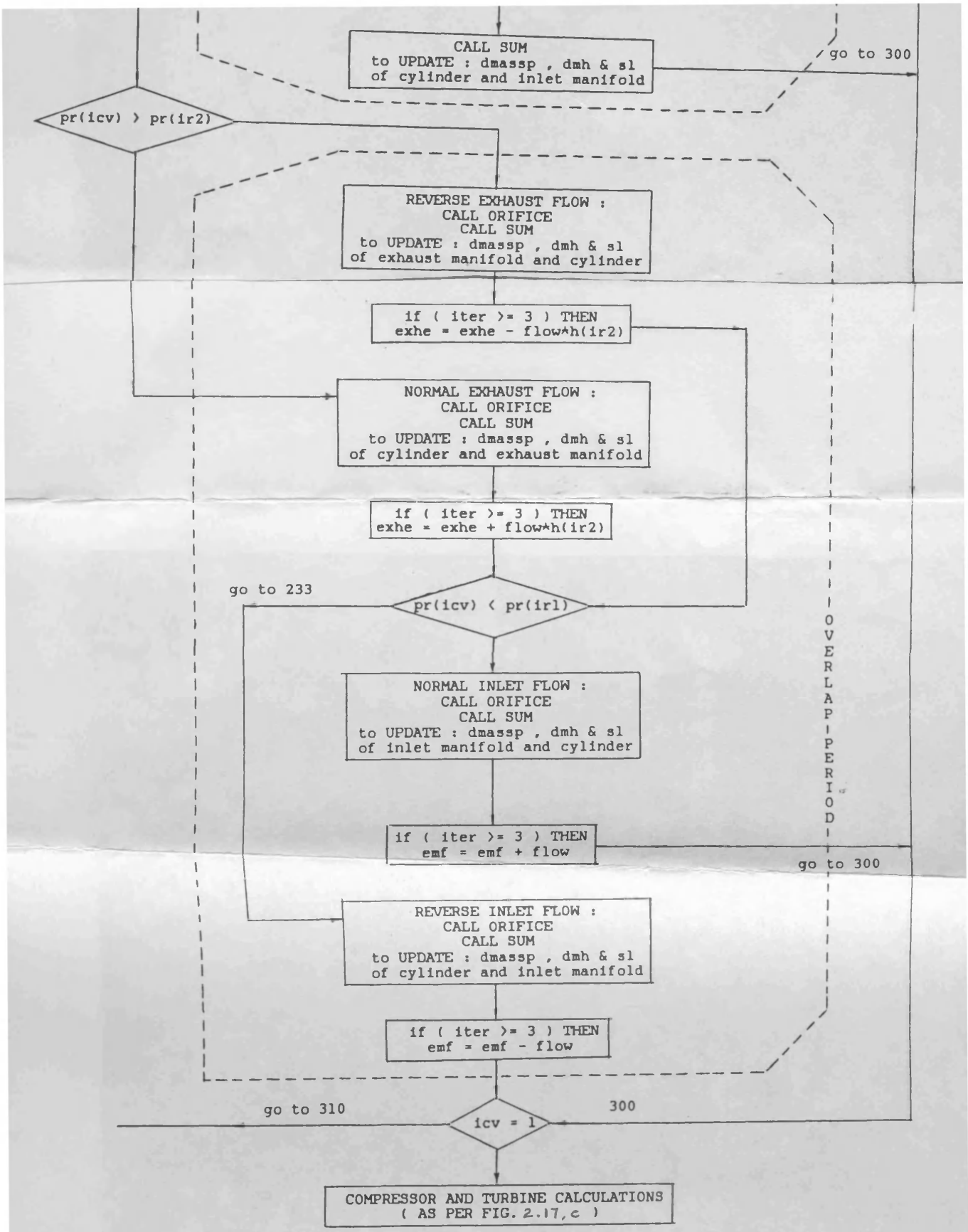

Fig. 2.17 , d Flow diagram for cylinder flow calculation of program 'CSPDCE'

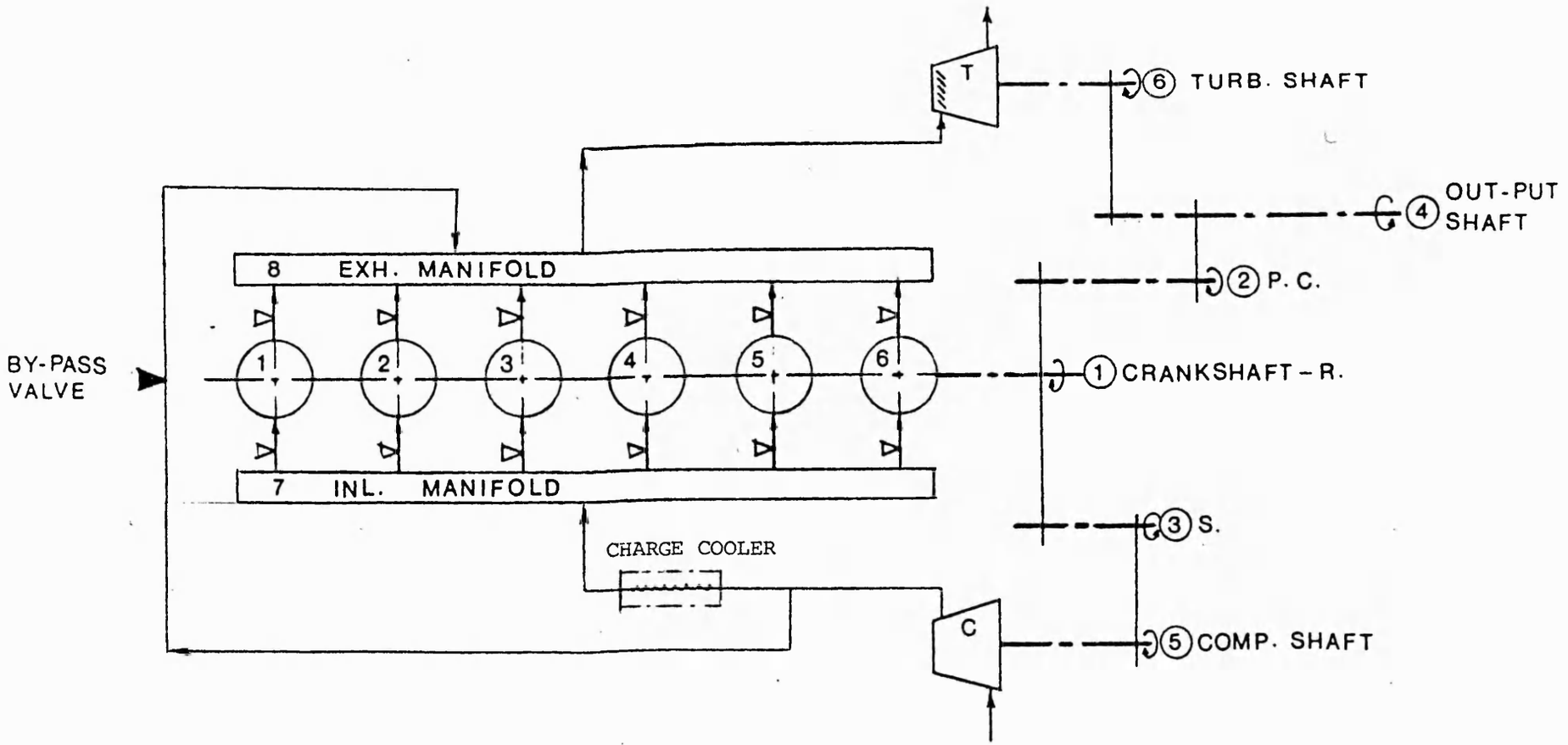

Fig. 2.18 DCE model applied in the program CSPDCE

CHAPTER THREE

SIMPLE STEADY-STATE SIMULATION OF THE L10-T/C ENGINE USING PROGRAM 'EMAT'

3.1 INTRODUCTION

In order to establish a reliable basis for theoretical performance assessment of the L10 engine in its DCE configuration compared with that of the T/C engine over their respective ranges of application, it is necessary to examine the 'EMAT' results and tune up the input data for the L10-T/C engine to match the results against the available experimental test data, since the DCE programs applied in the investigations use almost exactly the same engine subroutine as that in 'EMAT'. The programs include these, dealing with the design and steady state performance assessment of the L10-DCE (program DCE2) and with the transient response of a 65000 lb truck equipped either with the T/C or DCE versions of the L10 engine (program 'TRANIC' and 'DCE-TRAN').

3.2 THE TURBINE NOZZLE ANGLE

In order to study the effects of some of the input variables on predicted engine performance, it was decided to calibrate the program using existing Bath data for the Leyland TL11 engine, for which accurate input data had been prepared. TL11 is an engine having cylinder capacity, working range and engine performance quite close to those of the Cummins L10 engine. The results of these calculations were used for fine tuning of the data for the L10 engine in its T/C configuration.

One of the important input variables examined was turbine nozzle angle as it has a marked effect on engine and turbocharger characteristics. The same fuel variation schedule versus engine speed as given in table 2.1 for the LTC was used with nozzle angles of 22,26 and 30 deg. The rest of the input data was left unchanged.

Referring to fig. 2.5 which shows typical radial turbine characteristics, it is realized that, although the flow range of a particular turbine trim is large, operation away from the design point results in a loss of efficiency. As important is the fact that the expansion ratio of the turbine will vary greatly with mass flow rate. Since compressor pressure ratio and turbine expansion ratio are directly related, boost will be low at low mass flow rates and vice versa.

Fig. 3.1 shows the variation of turbocharger performance characteristics for three different matches 1,2 and 3 with nozzle angles of 22, 26 and 30 deg. By closing down the turbine nozzles, their throat areas decrease and for a given mass flow, the expansion ratio across the turbine is forced to increase (fig. 3.1,a) which in turn makes the turbine generate higher power (fig. 3.1,b) and causes higher turbocharger speed (fig. 3.1,d). Hence the compressor air flow increases (fig. 3.2,d) causing an additional effect in raising the pressure ratio throughout the system. Therefore, the turbine operating point shifts towards its choke condition because of higher flow rates and expansion ratios resulting, in turn, in higher turbine efficiencies (fig. 3.1,c) over the entire engine speed range. However, the compressor operating line in the compressor map (fig. 3.4) indicates that match 2 gives the most favourable conditions, the LTC

line passes through the best efficiency region of the map, with marginally safer maximum speed.

Figs. 3.2 and 3.3 show the variations of engine performance characteristics for three different matches. Higher air mass flow rates through the engine (fig. 3.2,d) as the nozzles are closed down provide the engine with higher air-fuel ratio (fig. 3.2,b) which is beneficial in meeting smoke limit requirements at lower engine speeds and in providing lower thermal loading through lower maximum cylinder temperature (fig. 3.3,c) at lower speeds and lower exhaust temperature (fig. 3.3,b) at high speeds. However, higher boost ratio causes higher inlet air temperatures (fig. 3.3,d) and higher maximum cylinder pressures (fig. 3.3,a) which call for a higher charge cooling capacity (when a cooler is fitted) and reduced engine fuelling to remain within the operating limits of the engine. For a fixed geometry turbocharger, the benefit of higher boost and air-fuel ratio at low speeds is accompanied by excessive turbine boost pressure at high speed, (fig. 3.1,a), when the air flow is greatest (fig. 3.2,d). Thus the piston must pump the exhaust gases out against high pressure, resulting in excessive negative loop work, i.e. lower BMEP (fig. 3.2,a) and higher BSFC (fig. 3.2,c).

In general, a compromise is called for to find the best match (when a fixed geometry turbocharger is in use). In the case of adjustable turbine nozzles, the LTC operating line can be arranged to coincide with the best efficiency region in the compressor map, providing higher air-fuel ratio at low speeds and avoiding excessive boost and maximum cylinder pressure at high speeds.

3.3 JUSTIFICATION OF TYPE OF COMPRESSOR USED FOR THE L10 ENGINE

One of the aims of using 'EMAT' was to examine how correct and accurate its predictions are. At the beginning of the work as full turbocharger data were not available, the map of the Holset H2C 8640 compressor was used, as fitted to engines of similar size to the L10. The compressor actually used for the L10 is the Holset type H2C 8650. When the correct map became available, the program was re-run with a new compressor array in order to improve the correlation between theoretical and experimental results (which is dealt with in detail in the next section of this chapter). Furthermore, it was another chance to realise whether the program prediction justifies what has been experienced in matching different compressor sizes with a certain engine.

Again, the same fuelling schedule as given in table 2.1 is applied, the results being shown in fig. 3.6,a. The turbine data is essentially the same as used in section 3.1 with the nozzle angle fixed at 26 deg. The engine data coresponds to the L10 specification (table 2.1).

Fig. 3.5 shows the variation of four compressor performance characteristics at different engine speeds for both compressor trims. Use of the slightly larger compressor type H2C 8650 results in more of the operating region experiencing higher compressor efficiencies (fig. 3.5,b), with higher mass flow (fig. 3.5,d) but potentially with a less generous surge margin. As the maximum compressor efficiency occurs at lower pressure ratios, low speed boost is higher (fig. 3.5,c) as the result of higher turbine torque and turbocharger speed (fig. 3.5,a).

Therefore, the choice of the H2C 8650 compressor while retaining a sufficient surge margin (fig. 3.12) and also giving operating points at maximum torque and power having reasonable speed and efficiency (figs. 3.5,a and b) is fully justified. It is noticeable that by deliberately matching into a rather inefficient region at maximum engine speed and load (fig. 3.5,b), boost pressure (fig. 3.5,c) and therefore maximum cylinder pressure (fig. 3.6,b) are held down. However, this is accompanied by lower BMEP, mass flow and also by higher exhaust temperature (figs. 3.6,c and 3.5,d).

3.4 ASSESSMENT OF THE EMAT PERFORMANCE PREDICTIONS FOR THE L10 ENGINE COMPARED WITH EXPERIMENTAL RESULTS

In this section, detailed comparison between EMAT predictions and experimental test results are given. The investigation is made both with and without a charge cooler together, using the same compressor (Holset H2C 8650) as used in practice.

The input data is given in table 2.1 and the EMAT simulation results for these two modes of operation are given in tables 3.1 and 3.2. The graphical representations of results are given in figs. 3.7 to 3.12. Relevant experimental test results for the L10-T/C aftercooled engine were obtained from the Cummins company, part of which is shown in table 3.3. The required data for comparison was linearly interpolated from these test results. The upper part of table 3.4 shows the location of interpolation made from the original experimental test results and the interpolated values in the column in between. The lower part of the table 3.4 shows the final interpolation results in metric units ready for comparison with theoretically computed results.

The parameters to be investigated are the engine and turbocharger performance characteristics.

3.4.1 Effect of Charge Air Cooling

The temperature increase of the charge air across a compressor depends on its pressure ratio and isentropic efficiency. If the pressure ratio is large, and if the air is not cooled, the temperature of the compressed air becomes high, which is detrimental to the engine in two ways:

a) the amount of charge admitted into the cylinder is directly related to the density before the intake valves. The adverse effect of the temperature increase on charge density could possible offset the desirable effects of boost. As indicated in tables 3.1 and 3.2, although without charge cooling, the compressor pressure ratio and in particular the boost is higher, mass flow rate (fig. 3.7,a) is lower because of higher inlet air temperature (fig. 3.8,d). In other words, any

temperature decrease in the charge taken into cylinders results in an increase in the volumetric efficiency calculated based on ambient conditions, i.e. independently of engine load and speed and also of charge air density and turbocharger design.
b) The thermal loading of the engine considerably increases with charge air temperature, since the whole temperature level of the cycle (maximum cylinder temperature shown in fig. 3.8,b and exhaust temperature shown in fig. 3.9,b), is directly related to the charge temperature at the beginning of compression. On the other hand, higher combustion temperature in the charge non-cooled engine increases formation of nitrogen oxides which is regulated by legislation.

In spite of the benefits of charge cooling, there are some disadvantages associated with it, as follows :

a) the pressure loss across the cooler will partially offset the density increase from cooling (table 3.2).

b) if the boost pressure is low and the available coolant relatively warm (such as engine cooling water), charge cooling will produce only marginal benefit at full power.

c) in low rated engines the extra cost of equipment outweighs the benefits of charge cooling.

As will be seen in the following sections, the effect of charge cooling on engine performance has been found to be reduced heat transfer, higher air-fuel ratio and higher thermal efficiency over the entire range of engine speed.

3.4.2 Maximum Cylinder Temperature (T_{max})

Fig. 3.8,b shows the maximum cylinder temperature predicted with EMAT. Variation of this parameter can best be explained with respect to the variation of the inlet temperature (fig. 3.8,d), fuel burned during constant volume combustion (fig. 3.8,a) and air-fuel ratio (fig. 3.8,c)

over the speed range. The values generating the curve in fig. 3.8,a are based on the fuelling schedule (gr/rev) and the fuel fraction burned during constant volume combustion which can be found by entering the map given in fig. 2.6.

The inlet manifold temperature is fairly constant over the speed range when the charge cooler is applied. However, the fact that "T_{max}" follows exactly the same trend as that of released heat during constant volume combustion (fig. 3.8,a) is due to the increase in air-fuel ratio (fig. 3.8,c) with increase in engine speed. Although this applies when no charge cooling is used, the increase in inlet air temperature with increase in engine speed not only cancels the effect of increasing air-fuel ratio but also causes "T_{max}" to be higher than the levels which would be expected based only on constant volume heat release particularly at high speeds.

3.4.3 Engine Heat Transfer (Losses)

Only a part of the heat of combustion of the fuel is converted into mechanical work, while the remainder appears mainly as exhaust enthalpy and heat loss to coolant. Although the coolant load is affected by the friction work of the engine, it is mainly due to transfer of heat from the hot gases. The transfer of heat between a gas and a surface depends upon many variables, such as temperature, temperature difference, area, density, viscosity, thermal conductivity, heat capacity, gas velocity, surface finish and geometry. All of these variables are continually changing in value since engine operation is cyclical, and hence a time averaged relations are used in simple calculations such as those performed by EMAT.

The heat transfer in an IC engine is mainly due to convection and conduction rather than radiation, and hence the turbulence within the combustion chamber plays an important role. Despite the complexity of the real process, certain generalizations will be made for the overall process to assist in understanding the trend in engine characteristics. The heat transfer between gas and surface will be considered to be

increased by any increase in in-cylinder gas velocity or density, and also any increase in exposed surface area or temperature difference between gas and surface.

The gas velocity is considered to be dependent on piston speed and the gas density on boost or, in turn, on engine load. Therefore, the variables affecting heat loss reflect the engine operating conditions.

In studying the limiting torque curve (LTC) of the L10-T/C engine, both engine speed and load are changed. Although with increased speed the various processes are exposed to heat losses for shorter periods of time per cycle, a proportionally greater number of cycles takes place in exact compensation. However, in practice, the scrubbing action of the gases on the wall which is very detrimental on engine heat losses is mainly dependent on audible knock rather than piston velocity.

In the T/C-CI engine, any increase in load is usually accompanied by higher boost, since the injected fuel per cycle and hence exhaust gas energy available at turbine entry increases. Therefore, the density of working air and gases throughout the cycle increases with increase in load resulting in a higher rate of heat transfer, though not in direct proportion to the increase in input energy. Hence the percentage heat loss decreases slightly with increased load (fig. 3.10,b).

The above reasoning is in good agreement with the predictions of program EMAT for percentage heat transfer either with or without charge cooling (see fig. 3.10).

Without charge cooling, higher cycle temperatures result in higher percentage heat transfer along the LTC. The difference in heat transfer between these two conditions increases as the difference between inlet manifold temperature increases.

The experimental results of heat transfer measurements do not seem to be very accurate since the changes do not conform with what is expected. However, in order to have a simulation adequately balanced around experimental results the relevant curves are considered to cross each

other at approximately mid engine speed (fig. 3.10,b).

3.4.4 Brake Thermal Efficiency

Fig. 3.10,c shows the brake thermal efficiency curves determined experimentally and calculated theoretically with the program 'EMAT'.

Comparison between the curves shows that those for the charge cooled engine are fairly close around their maxima, but not at high and low speeds. Modifications of the engine friction losses are needed to bring these curves into closer agreement, since the engine friction expressed as a function of speeds as entered in input data was based on the values relating to a similar but not identical engine. However, by manipulating the engine friction losses for lower and higher speeds very good agreement between the theoretical and experimentsl results could be obtained. This was deferred until more experimental data was obtained from the manufacturer. The same data was subsequently applied in the comprehensive step-by-step calculation program 'SPICE' to be described in the next chapter.

The effect of charge cooling on the brake thermal efficiency is also shown in fig. 3.10,c. As shown by fig. 3.10,b, the percentage heat loss decreases with charge cooling. It should be noted that a given percentage reduction in heat loss is not directly reflected in an equal percentage in efficiency (or reduction in BSFC) since exhaust enthalpy is also affected by any change in percentage heat loss (see figs. 3.10,a and c).

3.4.5 Air Consumption and Engine Power or Torque

As has already been mentioned, for a CI engine operating at a given air-fuel ratio, the indicated power is roughly proportional to the air consumption. From figs. 3.11,a and 3.7,a which respectively show the LTC power and air mass flow rate, the trends of these curves are very similar, although they diverge somewhat at higher engine speeds. The cause can be sought under three headings, viz. the variation of friction loss, heat transfer and in particular air-fuel ratio (fig. 3.8,c) as the engine speed increases.

Comparison between EMAT predictions and experimental results for air flow, BMEP, and subsequently torque and power shows that the curves for the aftercooled L10 engine are in very good agreement particularly in the mid engine speed region. In the light of the earlier analysis of discrepancies in measured and calculated brake thermal efficiency as a function of engine friction, better results with BMEP throughout the speed range could be achieved.

The effect of the assumed charge cooler effectiveness of 0.8 has been found to be a 3 to 5 percent increase in power from high to low engine speed which makes charge cooling of the L10 profitable in any of its many applications.

3.4.6 Indicated and Brake Specific Fuel Consumption (ISFC and BSFC)

In a case where the fuel-air ratio and percentage heat transfer are kept constant over a range of engine speeds, the indicated specific fuel consumption (ISFC) would be substantially independent of speed but the percentage heat loss decreases appreciably with speed increase (see fig. 3.10,b); hence producing a falling curve to lower values at higher speeds for 'ISFC'.

The mechanical efficiency decreases with increasing speed making a trend oppose to trend of heat loss in the case of 'BSFC', (fig. 3.10,d). Tests on the real engine confirm that the friction loss is the significant factor in raising fuel consumption at high speeds, while heat losses are the significant factor at low speeds.

For these reasons, the BSFC curve for the reciprocating CI engine can be quite flat at low speeds (because of the counterbalancing effect of heat loss and friction loss trends) and can rise at high speeds as the effect of increasing friction and pumping loss overtakes that of decreasing heat loss. Fig. 3.10,d shows the experimental L10 BSFC curves and those calculated using program EMAT. As was seen, modifications with friction loss input to the program would match the calculated results of brake thermal efficiency to those of the test results, which, in turn, would decrease the discrepancies in between the BSFC curves.

WITH COMPRESSOR H2C 8650, WITHOUT CHARGE COOLER

COMMINS L10 DIESEL ENGINE, HOLSET H2C TURBOCHARGER 122 94 470

number of cylinders	6.0	bore (m)	0.12500	stroke (m)	0.13600			
con-rod length (m)	0.21790	inlet valve closing (degs)	200.0	compressor scaling factor	1.000			
ambient temperature (deg k)	305.0	max. pressure limit (bar)	0.0000	ambient pressure (bar)	0.94560			
compression ratio	16.30	exhaust valve opening (degs)	499.0	turbine flow loss factor	0.8000			
engine speed(r.p.m)	1000.00	1200.00	1600.00	2000.00	2100.00	0.00	0.00	0.00
boost pressure ratio	1.242	1.342	1.763	2.174	2.194	0.000	0.000	0.000
trapped a/f ratio	20.765	20.816	21.855	24.449	26.261	0.000	0.000	0.000
delivery ratio	0.878	0.889	0.900	0.914	0.934	0.000	0.000	0.000
manifold temp (deg k)	331.955	341.933	376.471	407.135	408.635	0.000	0.000	0.000
engine power (k w.)	66.90	89.69	147.34	179.79	175.48	0.00	0.00	0.00
engine torque (n.m.))	638.85	713.75	879.36	858.45	797.96	0.00	0.00	0.00
b.m.e.p (bar)	8.0169	8.9568	11.0351	10.7726	10.0136	0.0000	0.0000	0.0000
s.f.c. (kgs/kw hr)	0.234	0.222	0.207	0.220	0.226	0.000	0.000	0.000
b.thermal eff.	0.3564	0.3759	0.4027	0.3794	0.3689	0.0000	0.0000	0.0000
fuel / rev (kg.)	2.610	2.765	3.180	3.295	3.150	0.000	0.000	0.000
max cyl pressure (bar .)	103.37	114.60	139.98	149.92	145.30	0.00	0.00	0.00
max cyl temperature(deg k)	2176.38	2276.66	2318.09	2220.37	2136.21	0.00	0.00	0.00
exhaust temperature(deg k)	763.23	802.69	873.78	929.49	914.09	0.00	0.00	0.00
percentage heat to coolant	36.46	31.87	24.93	20.87	20.15	0.00	0.00	0.00
compressor pressure ratio	1.2416	1.3422	1.7629	2.1743	2.1939	0.0000	0.0000	0.0000
delivery temperature(deg k)	331.95	341.93	376.47	407.13	408.64	0.00	0.00	0.00
delivery pressure (bar)	1.173	1.270	1.666	1.926	1.976	0.000	0.000	0.000
compressor speed (r.p.m.)	41274.2	48407.9	70000.0	84936.2	86352.8	0.0	0.0	0.0
volume flow (cu m / min)	5.02	6.39	10.29	14.92	16.08	0.00	0.00	0.00
compressor power (kw.)	2.443	4.266	13.290	27.510	30.096	0.000	0.000	0.000
compressor efficiency	0.726	0.728	0.755	0.746	0.745	0.000	0.000	0.000
turbine speed (r.p.m)	41274.2	48407.9	70000.0	84936.2	86352.8	0.0	0.0	0.0
turbine power (kw)	2.517	4.363	13.522	27.816	30.270	0.000	0.000	0.000
effective turbine efficiency.	0.643	0.637	0.625	0.606	0.600	0.000	0.000	0.000
fract of flow thro turbine.	1.000	1.000	1.000	1.000	1.000	0.000	0.000	0.000
first step press. ratio(entry 1)	1.294	1.369	1.674	2.065	2.136	0.000	0.000	0.000
press. ratio(entry 2)	0.000	0.000	0.000	0.000	0.000	0.000	0.000	0.000
n.d. torque	1.3921	1.5604	1.9180	2.1318	2.1225	0.0000	0.0000	0.0000
n.d. mass flow.	253.7882	267.9107	295.5289	308.0868	307.9964	0.0000	0.0000	0.0000
n.d.speed	1379.7440	1578.9250	2222.5522	2717.6699	2808.7615	0.0000	0.0000	0.0000
efficiency.	0.660	0.662	0.648	0.616	0.609	0.000	0.000	0.000
final step press. ratio(entry 1)	1.078	1.119	1.350	1.716	1.800	0.000	0.000	0.000
press. ratio(entry 2)	0.000	0.000	0.000	0.000	0.000	0.000	0.000	0.000
n.d. torque	-0.0023	0.0800	0.6160	1.2761	1.3713	0.0000	0.0000	0.0000
n.d. mass flow.	60.5714	101.5480	203.9423	265.3341	272.0571	0.0000	0.0000	0.0000
n.d.speed	1411.2024	1618.2328	2280.9141	2778.4911	2867.2745	0.0000	0.0000	0.0000
efficiency.	-0.016	0.250	0.519	0.575	0.575	0.000	0.000	0.000
compressor mass flow(kg/min).	5.42	6.91	11.12	16.11	17.37	0.00	0.00	0.00
delevered air to fuel ratio	20.76	20.82	21.86	24.45	26.26	0.00	0.00	0.00
v.g. nozzle width (m.m.)	13.5000	13.5000	13.5000	13.5000	13.5000	0.0000	0.0000	0.0000
cooler effectiveness	0.0000	0.0000	0.0000	0.0000	0.0000	0.0000	0.0000	0.0000
engine diagram factor	0.9800	0.9700	0.9400	0.8900	0.8800	0.0000	0.0000	0.0000
turbine nozzle angle (degs)	26.0000	26.0000	26.0000	26.0000	26.0000	0.0000	0.0000	0.0000

TABLE 3.1 RESULTS OF USING H2C 8650 HOLSET COMPRESSOR AND : qlf=1.45 ; xk=0.10 ; noz.ang=26 deg
(WITHOUT CHARGE COOLING)

WITH COMPRESSOR H2C 8650, & COOLER

CUMMINS L10 DIESEL ENGINE, HOLSET H2C TURBOCHARGED 227 137 685

number of cylinders	6.0	bore (m)	0.12500	stroke (m)	0.13600			
con-rod length (m)	0.21790	inlet valve closing (degs)	200.0	compressor scaling factor	1.000			
ambient temperature (deg k)	305.0	max. pressure limit (bar)	0.0000	ambient pressure (bar)	0.94560			
compression ratio	16.30	exhaust valve opening (degs)	499.0	turbine flow loss factor	0.8000			
engine speed(r.p.m)	1000.00	1200.00	1600.00	2000.00	2100.00	0.00	0.00	0.00
boost pressure ratio	1.176	1.277	1.626	1.828	1.949	0.000	0.000	0.000
trapped a/f ratio	22.097	23.197	26.026	31.479	30.503	0.000	0.000	0.000
delivery ratio	0.879	0.907	0.938	1.062	0.927	0.000	0.000	0.000
manifold temp (deg k)	295.858	297.918	303.942	308.769	310.204	0.000	0.000	0.000
engine power (k w.)	69.81	94.32	152.42	184.26	180.10	0.00	0.00	0.00
engine torque (n.m.))	666.68	750.59	909.68	879.76	818.98	0.00	0.00	0.00
b.m.e.p (bar)	8.3661	9.4192	11.4156	11.0401	10.2774	0.0000	0.0000	0.0000
s.f.c. (kgs/kw hr)	0.224	0.211	0.200	0.215	0.220	0.000	0.000	0.000
b.thermal eff.	0.3719	0.3953	0.4165	0.3898	0.3786	0.0000	0.0000	0.0000
fuel / rev (kg.)	2.610	2.765	3.180	3.295	3.150	0.000	0.000	0.000
max cyl pressure (bar .)	105.82	119.81	144.39	157.80	144.05	0.00	0.00	0.00
max cyl temperature(deg k)	2096.24	2140.36	2026.66	1832.97	1846.07	0.00	0.00	0.00
exhaust temperature(deg k)	728.00	746.31	780.46	787.07	802.26	0.00	0.00	0.00
percentage heat to coolant	33.69	28.38	20.62	15.83	16.14	0.00	0.00	0.00
compressor pressure ratio	1.2381	1.3442	1.7120	1.9238	2.0516	0.0000	0.0000	0.0000
delivery temperature(deg k)	331.29	341.59	371.71	395.85	403.02	0.00	0.00	0.00
delivery pressure (bar)	1.172	1.272	1.545	1.824	2.076	0.000	0.000	0.000
compressor speed (r.p.m.)	41222.3	48905.6	69806.6	83395.6	85501.6	0.0	0.0	0.0
volume flow (cu m / min)	5.34	7.12	12.26	19.20	18.68	0.00	0.00	0.00
compressor power (kw.)	2.536	4.710	14.772	31.509	33.065	0.000	0.000	0.000
compressor efficiency	0.734	0.739	0.764	0.694	0.713	0.000	0.000	0.000
turbine speed (r.p.m)	41222.3	48905.6	69806.6	83395.6	85501.6	0.0	0.0	0.0
turbine power (kw)	2.619	4.806	14.983	31.898	31.986	0.000	0.000	0.000
effective turbine efficiency.	0.642	0.635	0.615	0.586	0.582	0.000	0.000	0.000
fract of flow thro turbine.	1.000	1.000	1.000	1.000	1.000	0.000	0.000	0.000
first step press. ratio(entry 1)	1.302	1.395	1.753	2.295	2.291	0.000	0.000	0.000
press. ratio(entry 2)	0.000	0.000	0.000	0.000	0.000	0.000	0.000	0.000
n.d. torque	1.4011	1.5884	1.9074	2.1086	2.0603	0.0000	0.0000	0.0000
n.d. mass flow.	255.0175	271.0795	296.8967	307.9360	305.9982	0.0000	0.0000	0.0000
n.d.speed	1413.1847	1662.9113	2394.8176	2980.7654	3011.7616	0.0000	0.0000	0.0000
efficiency.	0.662	0.664	0.640	0.594	0.591	0.000	0.000	0.000
final step press. ratio(entry 1)	1.083	1.139	1.430	1.955	1.978	0.000	0.000	0.000
press. ratio(entry 2)	0.000	0.000	0.000	0.000	0.000	0.000	0.000	0.000
n.d. torque	0.0034	0.1230	0.7403	1.4694	1.4803	0.0000	0.0000	0.0000
n.d. mass flow.	65.6346	115.6339	219.6835	279.1915	279.9521	0.0000	0.0000	0.0000
n.d.speed	1406.0570	1705.3697	2456.1786	3041.2292	3067.4550	0.0000	0.0000	0.0000
efficiency.	0.021	0.309	0.528	0.566	0.565	0.000	0.000	0.000
compressor mass flow(kg/min).	5.77	7.70	13.24	20.74	20.18	0.00	0.00	0.00
delevered air to fuel ratio	22.10	23.20	26.03	31.48	30.50	0.00	0.00	0.00
v.g. nozzle width (m.m.)	13.5000	13.5000	13.5000	13.5000	13.5000	0.0000	0.0000	0.0000
cooler effectiveness	0.8000	0.8000	0.8000	0.8000	0.8000	0.0000	0.0000	0.0000
engine diagram factor	0.9800	0.9700	0.9400	0.8900	0.8800	0.0000	0.0000	0.0000
turbine nozzle angle (degs)	26.0000	26.0000	26.0000	26.0000	26.0000	0.0000	0.0000	0.0000

TABLE 3.2 RESULTS OF USING H2C 8650 HOLSET COMPRESSOR AND : qlf=1.45 ; xk=0.10 ; nox.ang=26 deg

(WITH CHARGE COOLING)

11/22/85 18:52

TEST TITLE: L10 LFC TCP /TRANSDUCERS CALIBRATED 10/30/84

TESTCELL: 113 TESTID: AL10TCPD

DATE	30JUL85	30JUL85	30JUL85	30JUL85	30JUL85	30JUL85	30JUL85	30JUL85	30JUL85	30JUL85	
TIME	17:04:00	17:14:00	17:16:00	17:18:00	17:28:00	17:30:00	17:32:00	17:41:00	17:43:00	17:45:00	
POINT NUMBER	326	327	328	329	330	331	332	333	334	335	
VALIDATION	UNVALID	UNVALID	UNVALID	UNVALID	UNVALID	UNVALID	UNVALID	UNVALID	UNVALID	UNVALID	
BASIC ENGINE PERFORMANCE											
ENG SPD	2102.	2101.	2102.	2102.	2101.	2101.	2102.	2102.	2102.	2100.	RPM
ENG TORQ	823.	747.	746.	745.	522.	521.	522.	296.	297.	298.	LB-FT
FUEL RATE	108.1	98.7	98.8	98.7	72.6	72.2	72.3	45.6	45.6	45.8	LB/HR
AEXH PRT T	1044.	1008.	1007.	1007.	903.	903.	904.	760.	760.	760.	DEG F
BRK PWR	329.	299.	299.	298.	209.	208.	209.	118.	119.	119.	HP
BSFC	.328	.330	.331	.331	.348	.346	.346	.385	.384	.384	LB/HP-HR
BMEP	203.	184.	184.	184.	129.	129.	129.	73.	73.	74.	PSI
CUBMILSTROKE	155.	141.	141.	141.	104.	103.	103.	65.	65.	66.	MM3
AIRHANDLING - SINGLE STAGE, AFTERCOOLED											
TOT AIR MF	48.1	45.5	45.5	45.5	38.9	38.7	38.7	30.1	30.1	30.0	LB/MIN
VOL EFF MNF	.93	.93	.92	.92	.92	.92	.92	.88	.88	.88	UNITLESS
VOL EFF AMB	1.83	1.73	1.73	1.73	1.47	1.47	1.47	1.14	1.14	1.14	UNITLESS
PHI	.56	.54	.54	.54	.47	.47	.47	.38	.38	.38	UNITLESS
A/F	26.7	27.7	27.6	27.7	32.1	32.2	32.1	39.6	39.6	39.4	UNITLESS
CMP EFF	.72	.72	.72	.72	.72	.72	.72	.70	.70	.71	UNITLESS
TUR EFF	.80	.79	.79	.79	.77	.77	.78	.73	.72	.72	UNITLESS
CMP COR SPD	94323.	90317.	90247.	90237.	77900.	77850.	77840.	61739.	61783.	61793.	RPM
CMP COR MF	50.7	47.7	47.7	47.7	40.2	40.0	40.0	30.8	30.8	30.7	LB/MIN
TUR COR SPD	97418.	94386.	94352.	94341.	84628.	84559.	84548.	71040.	71134.	71152.	RPM
TUR COR MF	23.9	23.4	23.4	23.4	21.8	21.7	21.7	18.3	18.3	18.3	LB/MIN
TRB EFF	.55	.54	.54	.54	.53	.53	.53	.48	.48	.49	UNITLESS
TUR PR	1.87	1.81	1.80	1.80	1.62	1.62	1.62	1.42	1.43	1.43	UNITLESS
CMP PR	2.29	2.16	2.16	2.15	1.80	1.80	1.80	1.44	1.44	1.45	UNITLESS
AC AIR DP	-1.1	-1.0	-1.1	-1.2	-.6	-.7	-.6	-.2	-.3	-.2	IN HG
GAS SYSTEM ENERGY BALANCE											
GSEB CYL	.188	.193	.195	.194	.212	.211	.211	.259	.257	.261	UNITLESS
GSEB AC	.049	.046	.045	.045	.035	.035	.035	.017	.018	.017	UNITLESS
GSEB ITUR	.097	.092	.092	.092	.080	.080	.080	.064	.065	.064	UNITLESS
GSEB EXH	.328	.329	.328	.329	.338	.338	.338	.347	.346	.343	UNITLESS
GSEB SFT	.424	.421	.420	.420	.400	.401	.402	.361	.362	.362	UNITLESS
GSEB UNAC	.011	.012	.011	.012	.015	.015	.015	.016	.017	.017	UNITLESS
TOTAL ENGINE HEAT REJECTION											
FRAC CLNT	.228	.233	.232	.231	.234	.235	.236	.249	.250	.250	UNITLESS
FRAC EXH	.328	.329	.328	.329	.338	.338	.338	.347	.346	.343	UNITLESS
FRAC SFT	.424	.421	.420	.420	.400	.401	.402	.361	.362	.362	UNITLESS
FRAC UNAC	.020	.017	.020	.020	.028	.026	.025	.043	.042	.045	UNITLESS
FRAC FCLR											UNITLESS
CLNT HRJ	7516.	7014.	6984.	6953.	5192.	5168.	5200.	3469.	3480.	3495.	BTU/MIN
CLNT SP HRJ	.54	.55	.55	.55	.59	.58	.59	.69	.69	.69	UNITLESS
EXH HRJ	10817.	9905.	9895.	9890.	7478.	7439.	7449.	4819.	4806.	4793.	BTU/MIN
FCLR HRJ											BTU/MIN
FLOW											
TOT AIR MF	48.1	45.5	45.5	45.5	38.9	38.7	38.7	30.1	30.1	30.0	LB/MIN
CLNT MTR0 VF	16.3	14.9	14.8	14.7	9.1	9.0	9.0	5.4	5.4	5.4	GAL/MIN
CLNT MTR1 VF	16.3	14.9	14.8	14.7	9.1	9.0	9.0	5.4	5.4	5.4	GAL/MIN
CLNT MTR0 MF	139.7	127.9	127.0	126.1	78.3	77.4	77.4	46.1	46.1	46.1	LB/MIN
CLNT MTR1 MF	139.7	127.9	127.0	126.1	78.3	77.4	77.4	46.1	46.1	46.1	LB/MIN

HRJ

PART OF EXPERIMENTAL RESULTS OF CUMMINS L10-290 T/C ENGINE OBTAINED FROM MFG. COMPANY

Table 3.3

11/22/85 18:53
TEST TITLE: L10 LFC TCP /TRANSDUCERS CALIBRATED 10/30/84
TESTCELL: 113 TESTID: AL10TCPD

DATE	30JUL85	30JUL85	30JUL85	30JUL85	30JUL85	30JUL85	30JUL85	30JUL85	30JUL85	30JUL85	
TIME	17:04:00	17:14:00	17:16:00	17:18:00	17:28:00	17:30:00	17:32:00	17:41:00	17:43:00	17:45:00	
POINT NUMBER	326	327	328	329	330	331	332	333	334	335	
VALIDATION	UNVALID	UNVALID	UNVALID	UNVALID	UNVALID	UNVALID	UNVALID	UNVALID	UNVALID	UNVALID	
Z											
AC AIR MRJ	-1609.	-1378.	-1365.	-1366.	-777.	-773.	-774.	-242.	-249.	-242.	BTU/MIN
AC M MRJ	-4579.	-4520.	-4271.	-4133.	-1765.	-1614.	-1485.	-575.	-537.	-460.	BTU/MIN
AC MRJ ERR	1.35	1.30	1.32	1.33	1.44	1.48	1.52	1.42	1.46	1.53	UNITLESS
AC EFT	-3.45	-4.32	-4.05	-3.87	-2.96	-2.63	-2.35	-3.56	-3.05	-2.51	UNITLESS
OC M MRJ											BTU/MIN
HEADS MRJ											BTU/MIN
CLNT MRJ	7516.	7014.	6984.	6953.	5192.	5168.	5200.	3469.	3480.	3495.	BTU/MIN
CF AC	-.61	-.64	-.61	-.59	-.34	-.31	-.29	-.17	-.15	-.13	UNITLESS
CF OC											UNITLESS
CF HEADS											UNITLESS
CF UNAC											UNITLESS
PRESSURE											
RAIL	191.	164.	164.	164.	103.	103.	103.	53.	53.	53.	PSI
CMP OT	33.2	29.9	29.8	29.7	20.8	20.7	20.7	11.4	11.4	11.5	IN HG
FPMP IN	-6.2	-6.2	-6.2	-6.2	-6.2	-6.2	-6.2	-6.2	-6.2	-6.2	IN HG
OILRFL	31.	31.	32.	32.	32.	32.	32.	33.	32.	32.	PSI
M PMP OT	5.5	5.5	5.5	5.5	5.5	5.5	5.5	5.5	5.5	5.5	PSI
BLOW-BY	9.7	8.5	8.8	8.5	6.4	6.6	6.6	4.5	4.6	4.5	IN H2O
AIR MTR	-2.1	-1.9	-1.9	-1.9	-1.4	-1.4	-1.3	-.8	-.8	-.8	IN H2O
CMP IN	-19.9	-17.8	-17.9	-17.8	-12.6	-12.5	-12.5	-7.8	-7.8	-7.8	IN H2O
TUR OT	2.5	2.1	2.1	2.2	1.5	1.5	1.5	.9	.9	.9	IN HG
INT MNF	35.9	32.4	32.5	32.5	22.8	22.7	22.7	12.6	12.7	12.7	IN HG
TUR FI	26.3	24.0	24.0	24.0	17.9	17.9	17.9	12.1	12.1	12.1	IN HG
TUR RIP	26.5	24.2	24.1	24.1	18.2	18.2	18.2	12.5	12.6	12.6	IN HG
OIL PUMP	54.	54.	54.	54.	53.	53.	53.	52.	52.	52.	PSI
AC AIRIN	36.3	33.0	33.0	32.9	23.5	23.4	23.5	13.4	13.4	13.5	IN HG
AC M OT	7.5	7.4	7.4	7.4	7.7	7.7	7.7	7.9	7.9	7.9	PSI
MPMP IN	7.	7.	7.	7.	8.	8.	8.	8.	8.	8.	PSI
ENG M IN	13.	13.	13.	13.	12.	12.	12.	11.	11.	11.	PSI
ENG M OT	19.2	18.4	18.4	18.3	14.5	14.5	14.4	12.2	12.1	12.1	PSI
BAROMETER	29.355	29.355	29.355	29.359	29.369	29.369	29.368	29.368	29.368	29.368	IN HG 32
VAP PRESS	.782	.782	.782	.790	.790	.790	.801	.801	.801	.801	IN HG
TEMPERATURE											
CMP IN	89.	89.	89.	89.	88.	88.	88.	88.	89.	89.	DEG F
OILRFL	233.	229.	229.	229.	222.	221.	221.	216.	216.	216.	DEG F
CMP OT	292.	276.	275.	275.	226.	226.	227.	174.	175.	175.	DEG F
INT	155.	152.	152.	152.	144.	144.	145.	141.	141.	142.	DEG F
AC M OT	140.	140.	140.	140.	136.	136.	137.	137.	137.	138.	DEG F
AC M IN	179.	182.	180.	179.	163.	161.	160.	152.	151.	150.	DEG F
PAN	248.	245.	244.	244.	235.	235.	235.	227.	226.	227.	DEG F
CELL	132.	131.	129.	130.	125.	126.	124.	116.	116.	116.	DEG F
MP OT	177.	175.	175.	175.	174.	174.	174.	175.	176.	176.	DEG F
TUR OT	913.	889.	889.	888.	807.	807.	807.	698.	698.	697.	DEG F
TUR RI	1092.	1054.	1053.	1053.	948.	947.	947.	804.	805.	804.	DEG F
TUR FI	1141.	1104.	1103.	1103.	980.	981.	981.	817.	818.	818.	DEG F
EXH PRT1	1061.	1024.	1024.	1022.	916.	915.	916.	766.	767.	766.	DEG F
EXH PRT2	1070.	1033.	1033.	1033.	916.	916.	916.	762.	762.	763.	DEG F
EXH PRT3	1054.	1020.	1018.	1018.	907.	908.	908.	763.	763.	763.	DEG F

Table 3.3 (cont')

11/22/85 18:53
TEST TITLE: L10 LFC TCP /TRANSDUCERS CALIBRATED 10/30/84
TESTCELL: 113 TESTID: AL10TCPD

DATE	30JUL85	30JUL85	30JUL85	30JUL85	30JUL85	30JUL85	30JUL85	30JUL85	30JUL85	30JUL85	
TIME	17:04:00	17:14:00	17:16:00	17:18:00	17:28:00	17:30:00	17:32:00	17:41:00	17:43:00	17:45:00	
POINT NUMBER	326	327	328	329	330	331	332	333	334	335	
VALIDATION	UNVALID	UNVALID	UNVALID	UNVALID	UNVALID	UNVALID	UNVALID	UNVALID	UNVALID	UNVALID	
TEMPERATURE (CONTINUED)											
EXH PRT4	1011.	972.	971.	971.	869.	869.	869.	734.	734.	735.	DEG F
EXH PRT5	1054.	1016.	1016.	1016.	916.	915.	916.	785.	786.	784.	DEG F
EXH PRT6	1012.	981.	980.	980.	896.	895.	897.	749.	751.	752.	DEG F
FPMP IN	104.	103.	104.	103.	103.	104.	105.	104.	104.	104.	DEG F
AIR MTR	85.	85.	85.	85.	83.	84.	84.	83.	84.	85.	DEG F
DYNO	103.	102.	102.	102.	95.	95.	95.	89.	89.	89.	DEG F
FDBRG	154.	158.	158.	159.	160.	161.	161.	162.	162.	162.	DEG F
RDBRG	151.	155.	156.	157.	159.	160.	161.	161.	162.	162.	DEG F
ENG H IN	123.5	119.1	118.7	118.4	102.2	101.6	101.2	89.6	89.3	89.0	DEG F
ENG H OT	187.9	184.8	184.7	184.6	182.3	182.3	182.3	181.0	181.0	181.0	DEG F
ENG H DT	64.2	65.6	65.8	66.0	79.9	80.5	81.0	91.2	91.5	91.9	DEG F
MISCELLANEOUS											
FLOTRON	106.0	97.9	98.0	97.9	71.7	70.9	71.8	45.1	45.1	45.3	LB/HR
RTD	837.	838.	841.	841.	843.	844.	846.	847.	848.	849.	UNITLESS
EXP SMK	58.1	45.1	58.0	58.6	55.6	61.6	37.2	43.5	73.4	56.7	UNITLESS
CELESCO	.1	.1	.0	.1	.1	.1	.1	.1	.1	.1	% OPAC
RPM	2097.	2098.	2097.	2098.	2099.	2100.	2100.	2100.	2099.	2098.	RPM
TOT REVS	3499.	3831.	3828.	3830.	3469.	3488.	3488.	2763.	2763.	2752.	REV
ELAPSED TIME	1.664	1.823	1.821	1.822	1.651	1.660	1.659	1.314	1.314	1.310	MIN
ENG SPD	2102.	2101.	2102.	2102.	2101.	2101.	2102.	2102.	2102.	2100.	RPM
ENG TORQ	823.	747.	746.	745.	522.	521.	522.	296.	297.	298.	LB-FT
CLNT MTR OP	152.	139.	138.	137.	85.	84.	84.	50.	50.	50.	HZ
PTUR SPD	0.	0.	0.	0.	0.	0.	0.	0.	0.	0.	0.35*RPM
TOTFL MTR OP	0.	0.	0.	0.	0.	0.	0.	0.	0.	0.	HZ
TUR SPD	94640.	90620.	90550.	90540.	78090.	78040.	78030.	61890.	61990.	62000.	RPM
AIR MTRO OP	446.	422.	422.	422.	359.	357.	358.	277.	277.	278.	HZ
FUEL RATE	108.1	98.7	98.8	98.7	72.6	72.2	72.3	45.6	45.6	45.8	LB/HR
FUEL WT	3.000	3.000	3.000	3.000	2.000	2.000	2.000	1.000	1.000	1.000	LB
SPEED VAR	6.	4.	4.	6.	4.	8.	7.	5.	5.	6.	RPM
TORQ VAR	31.	21.	19.	19.	19.	16.	21.	15.	15.	15.	LB-FT
FUEL VAR	12.8	4.0	5.0	4.2	7.2	9.0	7.8	2.1	1.8	1.3	LB/HR
CETANE	45.0	45.0	45.0	45.0	45.0	45.0	45.0	45.0	45.0	45.0	UNITLESS
LOG TIME	0.	0.	0.	0.	0.	0.	0.	0.	0.	0.	SEC
TEST TIME	217.2	217.3	217.4	217.4	217.6	217.6	217.7	217.8	217.8	217.9	HR

Table 3.3 (cont')

ENGINE												
Speed	rpm	1000.0			1200.0			1600.0			2100.0		
Fuel Flow	lb/hr	36.4	34.5	21.3	53.5	43.8	31.3	91.2	67.3	64.6	98.7	87.6	72.6
Torque	lb.ft	560.0	530.0	318.0	696.0	566.0	399.0	925.0	675.0	647.0	745.0	650.0	522.0
Power	hp	107.0	101.0	61.0	159.0	129.0	91.0	282.0	206.0	197.0	298.0	260.0	209.0
B.M.E.P.	psi	138.0	130.0	78.0	172.0	140.0	98.0	228.0	167.0	160.0	184.0	160.0	129.0
B. Th. Eff.	%	40.7	40.5	39.6	41.4	41.0	40.5	43.0	42.5	42.4	42.0	41.2	40.0
B.S.F.C.	lb/hphr	0.341	0.342	0.351	0.336	0.339	0.343	0.323	0.327	0.328	0.331	0.338	0.348
Air/Fuel		18.0	19.0	25.6	21.1	24.0	27.8	23.1	26.0	26.3	27.7	29.6	32.1
Inlet Temp.	F	125.0	125.0	130.0	127.0	126.0	129.0	142.0	137.0	136.0	152.0	148.0	144.0
Exhaust Temp.	F	863.0	837.0	664.0	963.0	877.0	768.0	1054.0	941.0	929.0	1007.0	964.0	903.0
Heat Loss	%	24.8	24.6	23.3	24.6	24.7	24.9	22.5	23.2	23.3	23.1	23.2	23.4
COMPRESSOR													
Speed	rpm	50520.0	48770.0	36660.0	60880.0	53370.0	43700.0	84160.0	71560.0	70140.0	90540.0	85245.0	78090.0
Press. Ratio		1.31	1.29	1.15	1.48	1.36	1.22	2.02	1.68	1.65	2.15	2.00	1.80
Air Flow	lb/min	10.9	10.6	9.1	18.8	16.9	14.5	35.1	29.1	28.4	45.5	42.7	38.9
Efficiency	%	63.0	62.7	61.0	66.0	66.0	66.0	70.0	70.9	71.0	72.0	72.0	72.0
TURBINE													
Efficiency	%	89.0	87.0	73.0	88.0	82.3	75.0	83.0	81.2	81.0	79.0	78.0	77.0

" a "

ENGINE					
Speed	rpm	1000.00	1200.00	1600.00	2100.00
Fuel Flow	g/Rev	0.261	0.276	0.318	0.329
Torque	Nm	718.00	767.00	915.00	881.00
Power	kW	74.30	95.00	151.60	191.40
B.M.E.P	bar	8.84	9.52	11.36	10.90
B. Th. Eff.	%	40.50	41.00	42.50	41.20
B.S.F.C	kg/kWh	0.210	0.209	0.201	0.208
Air/Fuel		19.00	24.00	26.00	29.60
Inlet Temp.	K	324.00	325.00	331.00	337.00
Exhaust Temp.	K	720.00	742.00	778.00	790.00
Heat Loss	%	24.60	24.70	23.20	23.20
COMPRESSOR					
Speed	rpm	48770.00	53370.00	71560.00	85245.00
Press. Ratio		1.29	1.36	1.68	2.00
Air Flow	kg/min	4.81	7.66	13.20	19.40
Efficiency	%	62.70	66.00	70.90	72.00
TURBINE					
Efficiency	%	87.00	82.30	81.20	78.00

" b "

TABLE 3.4 Interpolated experimental data of the L10-T/C engie used for comparison with the ' EMAT ' performance predictions

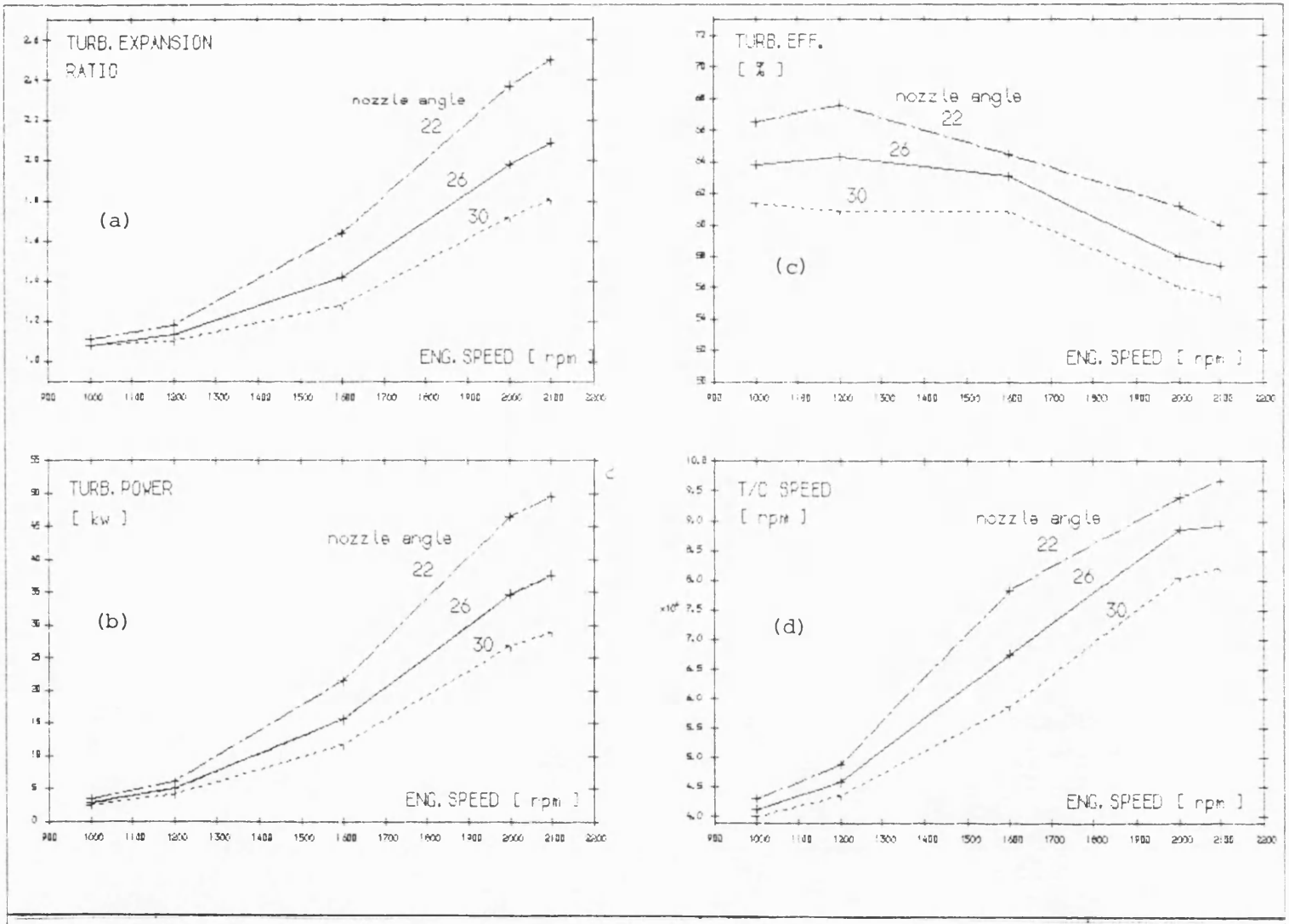

Fig. 3.1 Effect of turbine nozzle angle adjustments on turbine performance characteristics in turbocharging the Leyland TL11 Diesel engine

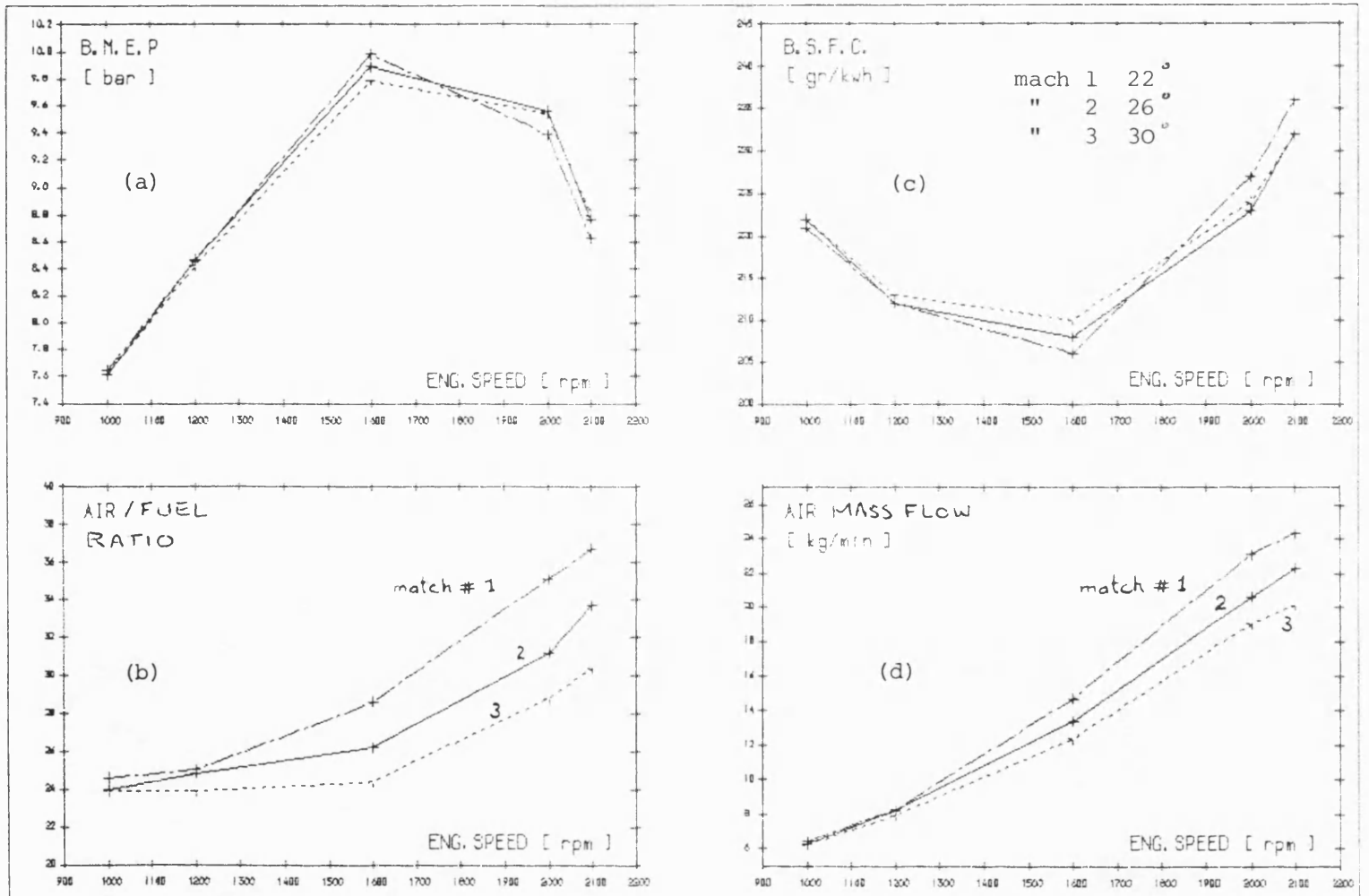

Fig. 3.2 Effect of turbine nozzle angle adjustments on performance characteristics of the Leyland TL11-T/C Diesel engine

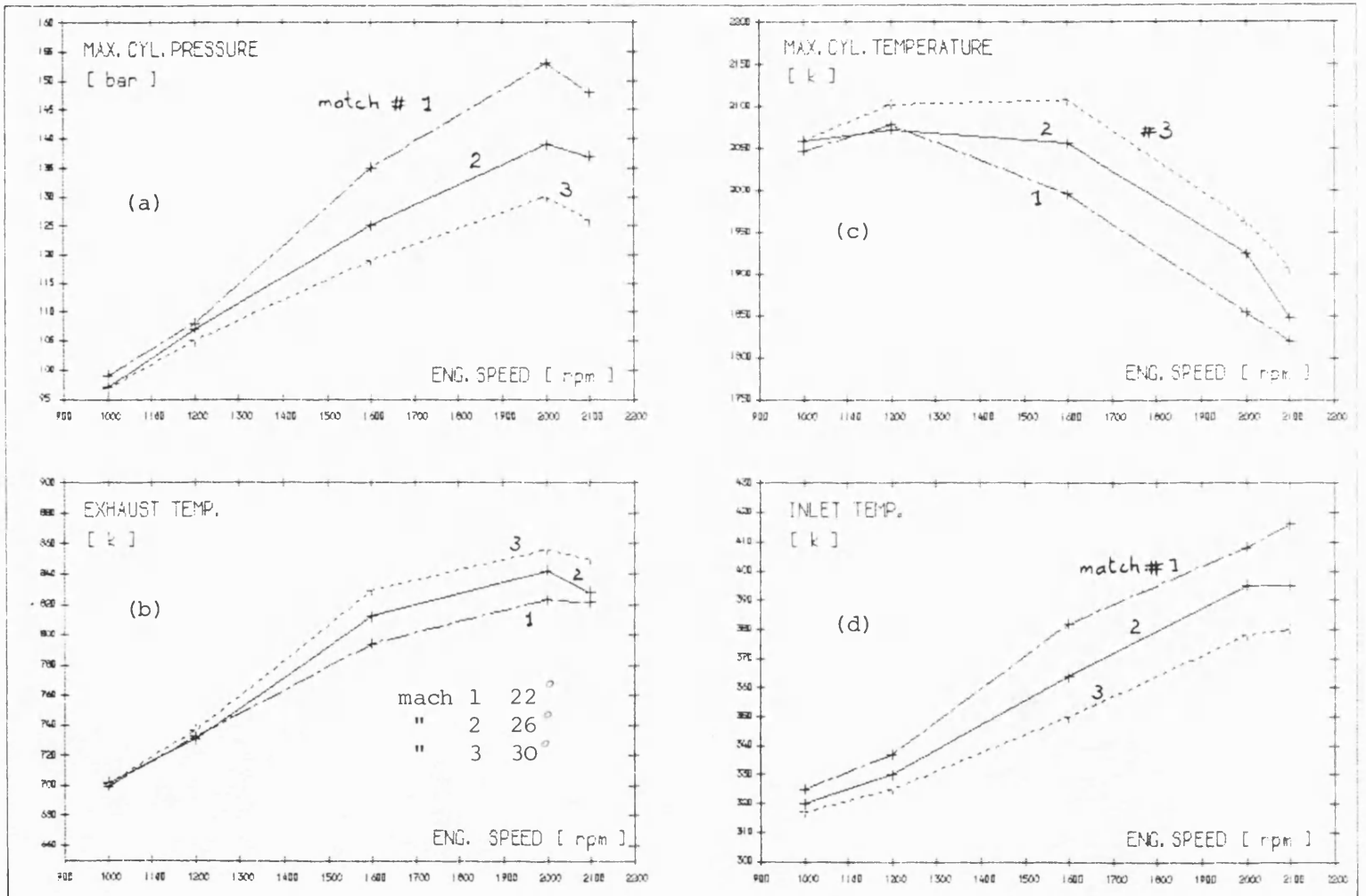

Fig. 3.3 Effect of turbine nozzle angle adjustments on performance characteristics of the Leyland TL11-T/C Diesel engine

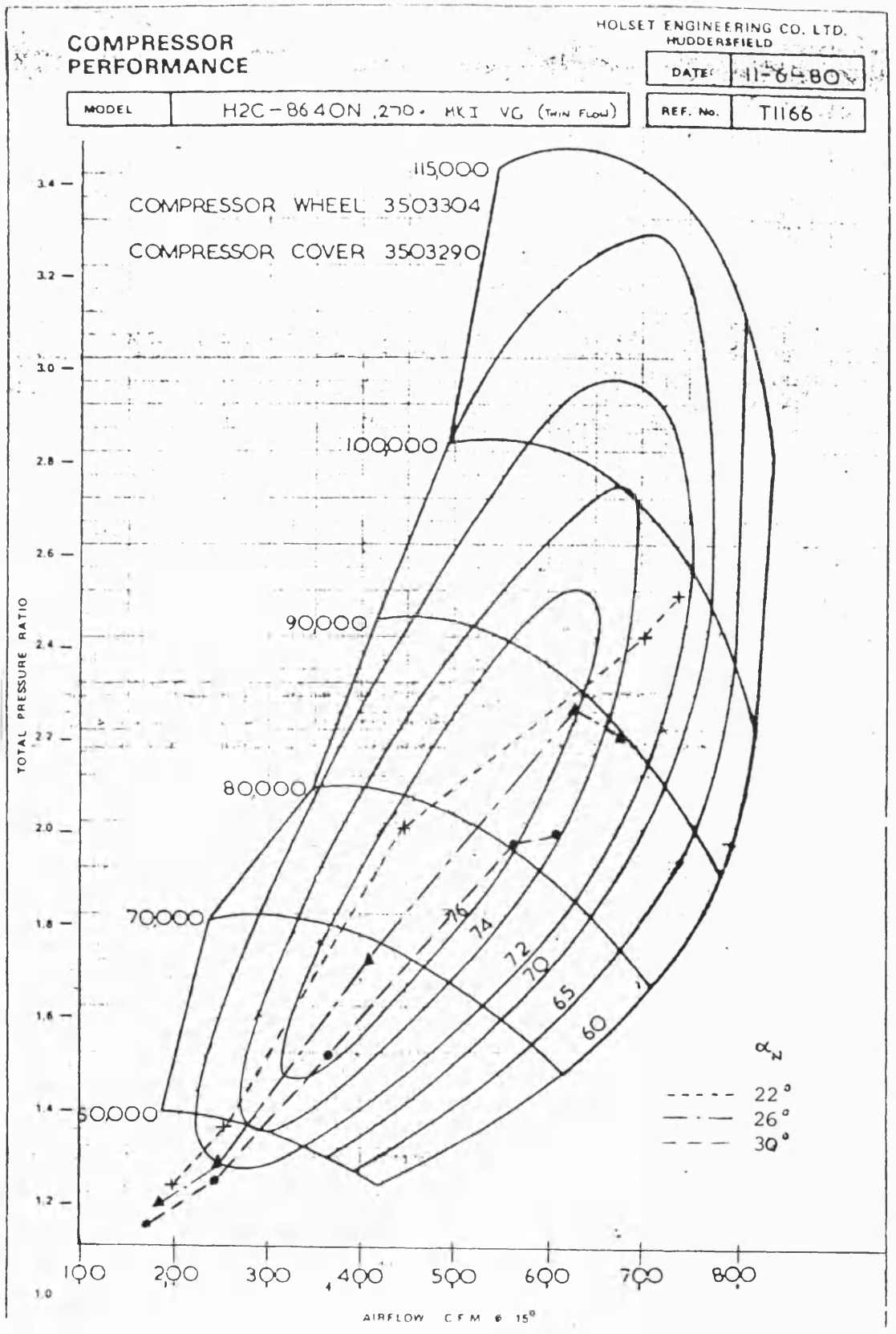

Fig. 3.4 Holset H2C 8640 compressor map and the operating lines of the Leyland TL11-T/C engine at different turbine nozzle angle adjustments

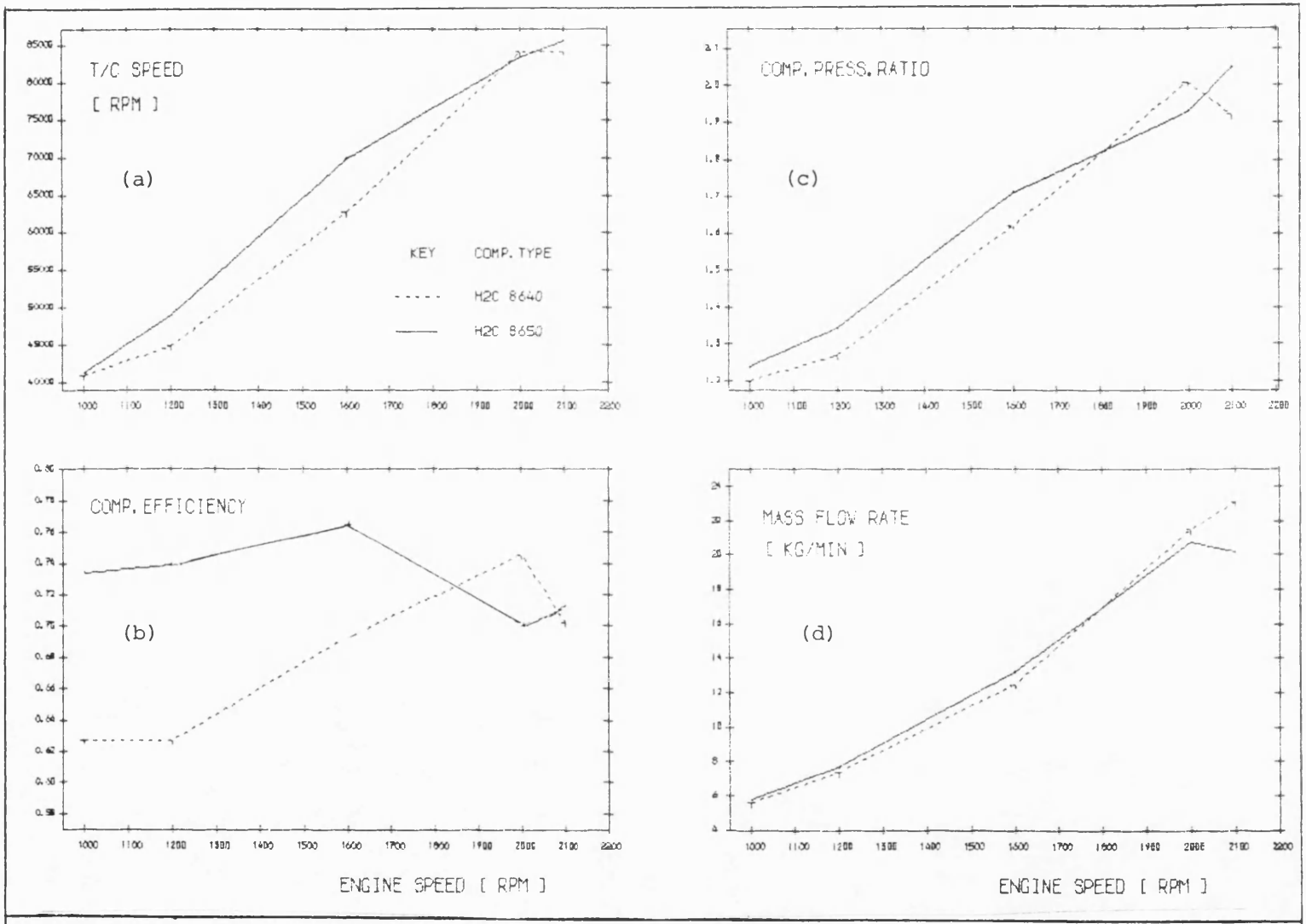

Fig. 3.5 Effect of compressor size on flow characteristics in Turbocharging of the Cummins L10-T/C Diesel engine using the same turbine

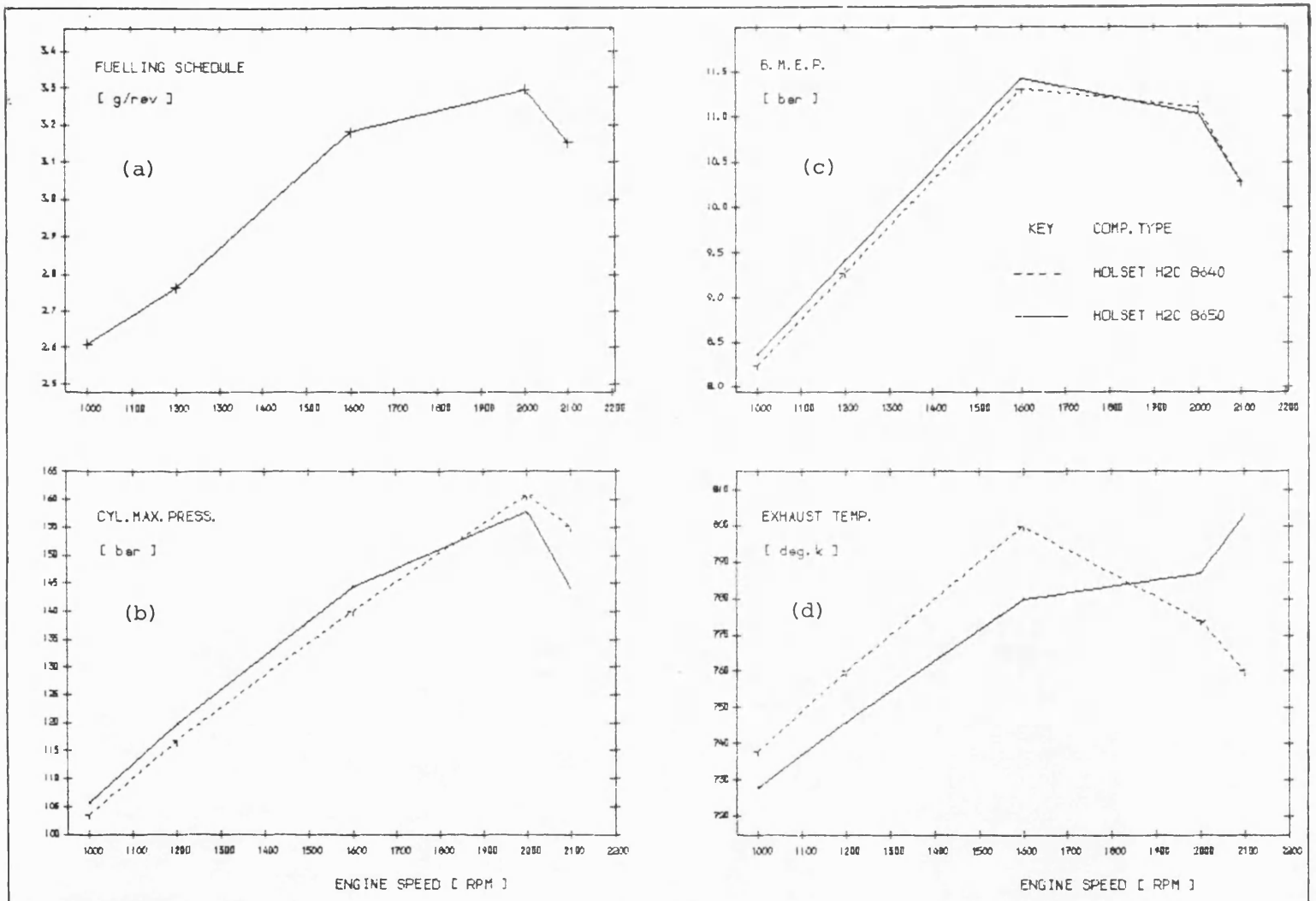

Fig. 3.6 Effect of compressor size on the L10-T/C engine performance characteristics

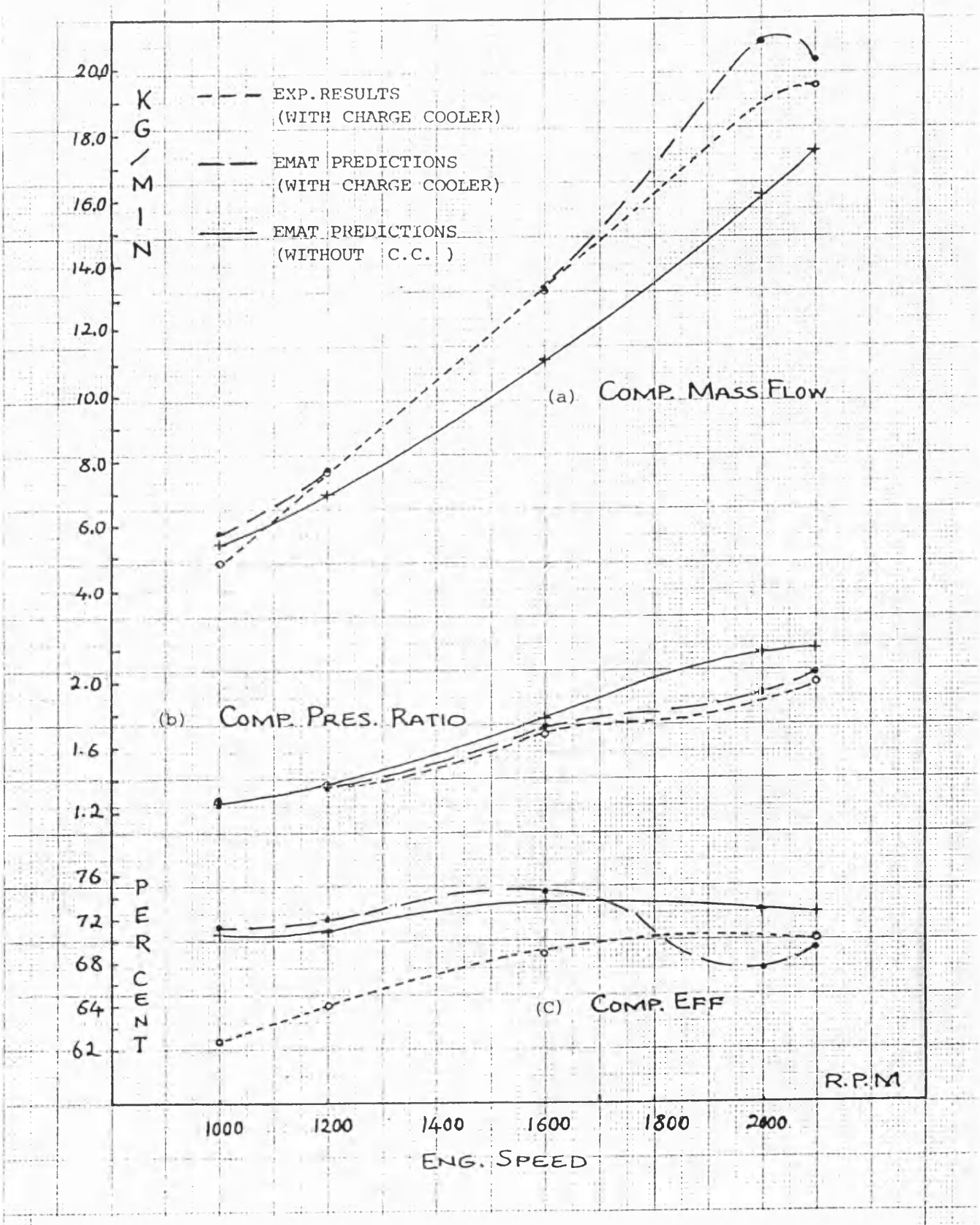

Fig. 3.7 Comparison of EMAT predictions with experimental results for the Cummins L10-T/C Diesel engine performance characteristics

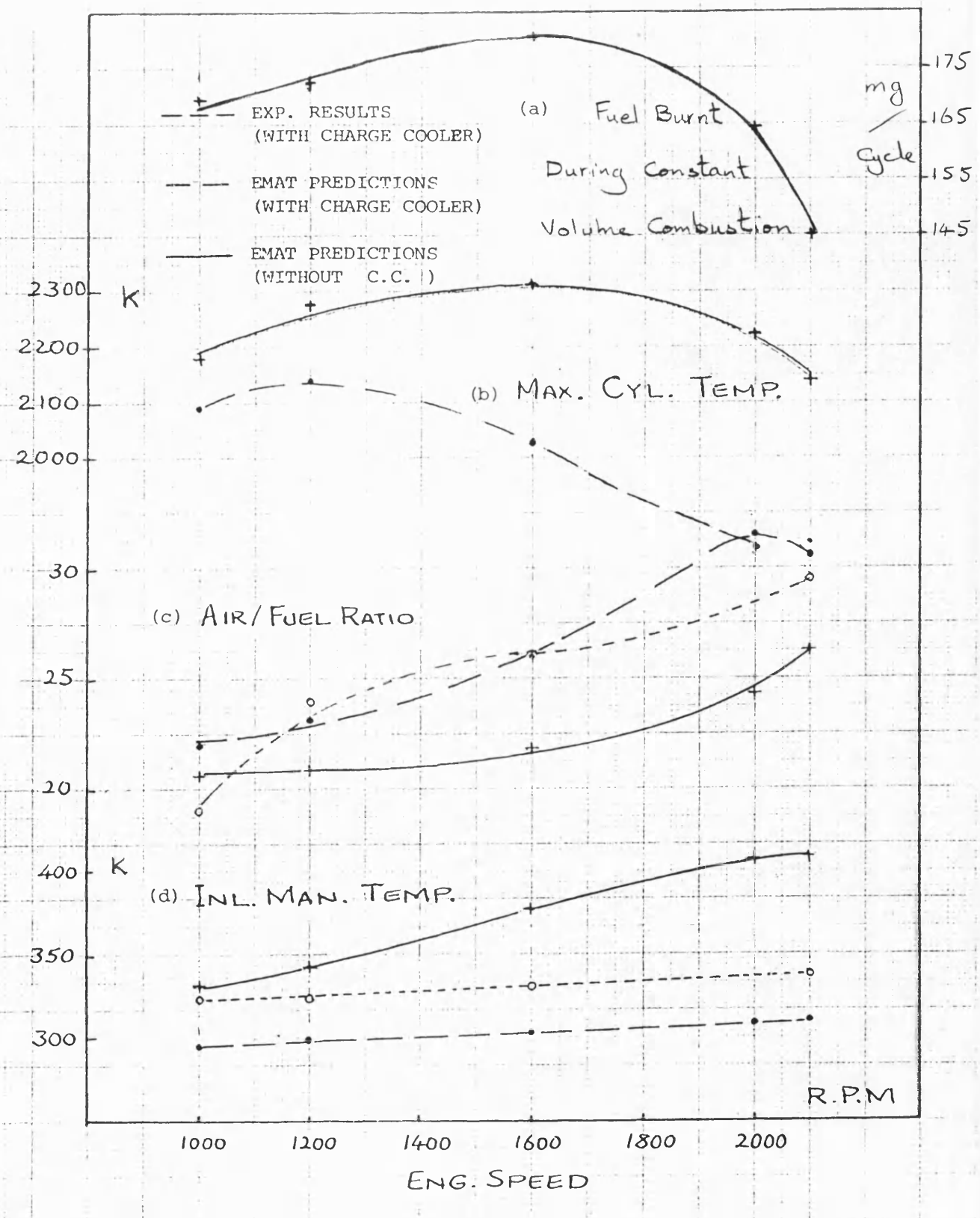

Fig. 3.8 Comparison of EMAT predictions with experimental results for the Cummins L10-T/C Diesel engine performance characteristics

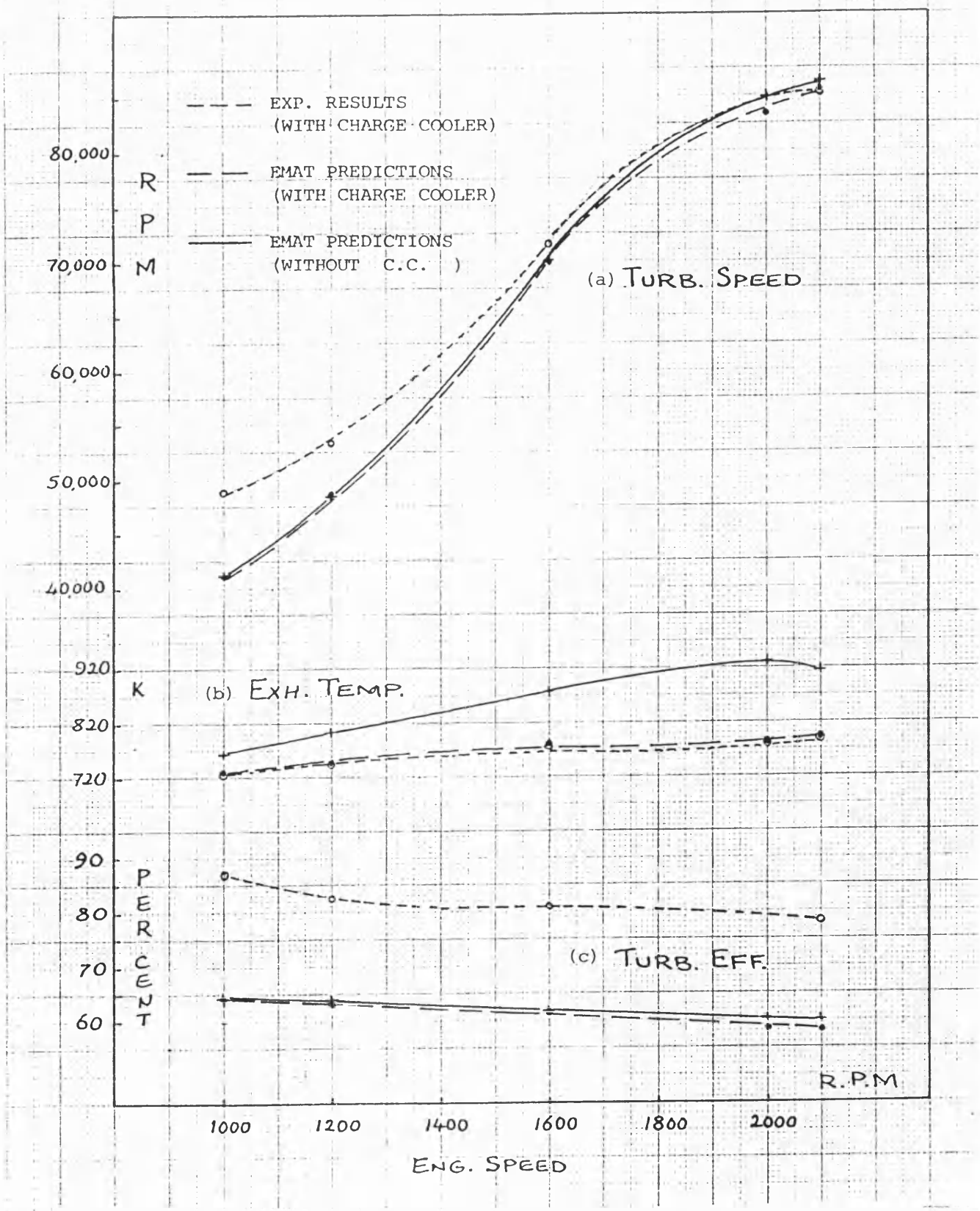

Fig. 3.9 Comparison of EMAT predictions with experimental results for the Cummins L10-T/C Diesel engine performance characteristics

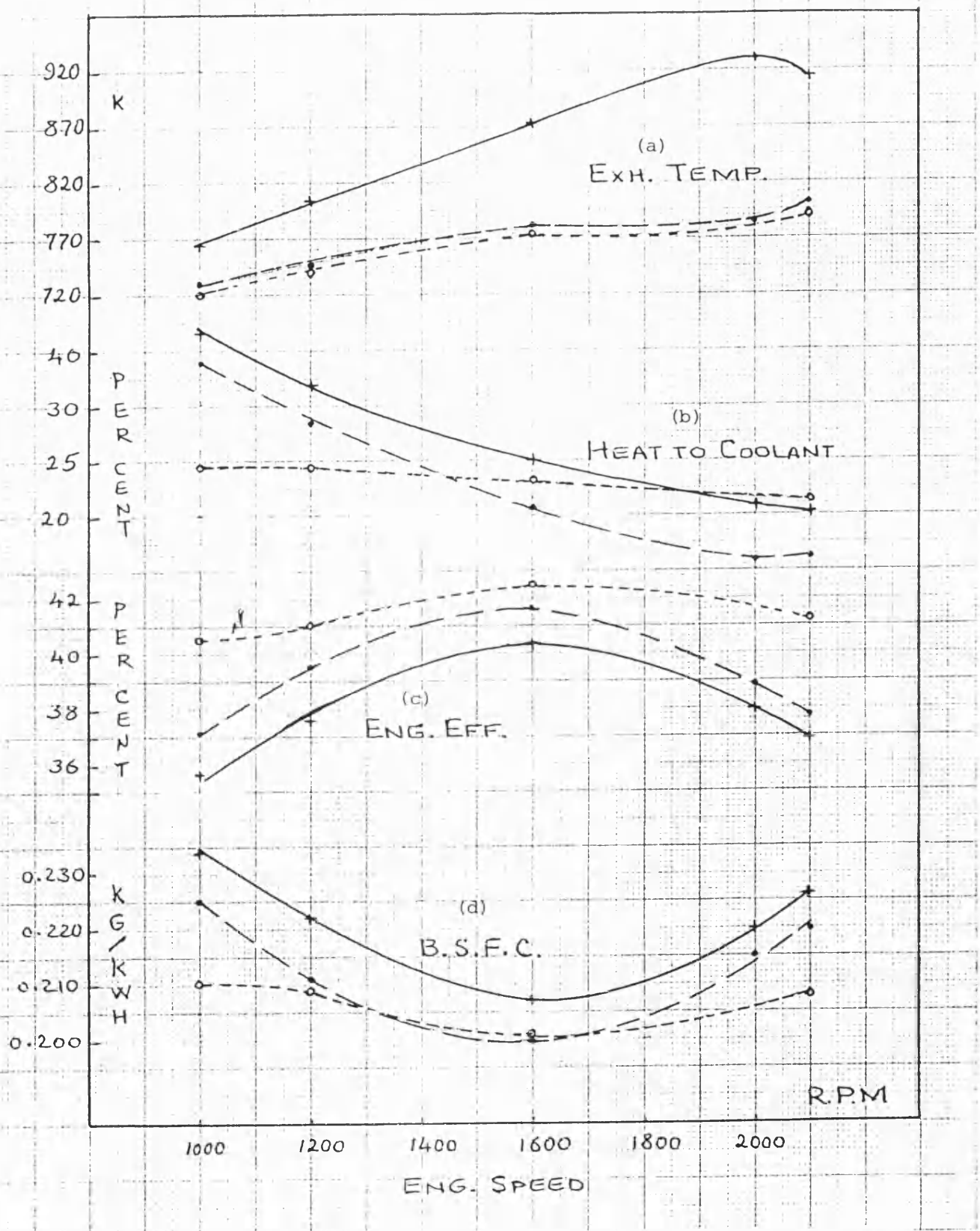

Fig. 3.10 Comparison of EMAT predictions with experimental results for the Cummins L10-T/C Diesel engine performance characteristics

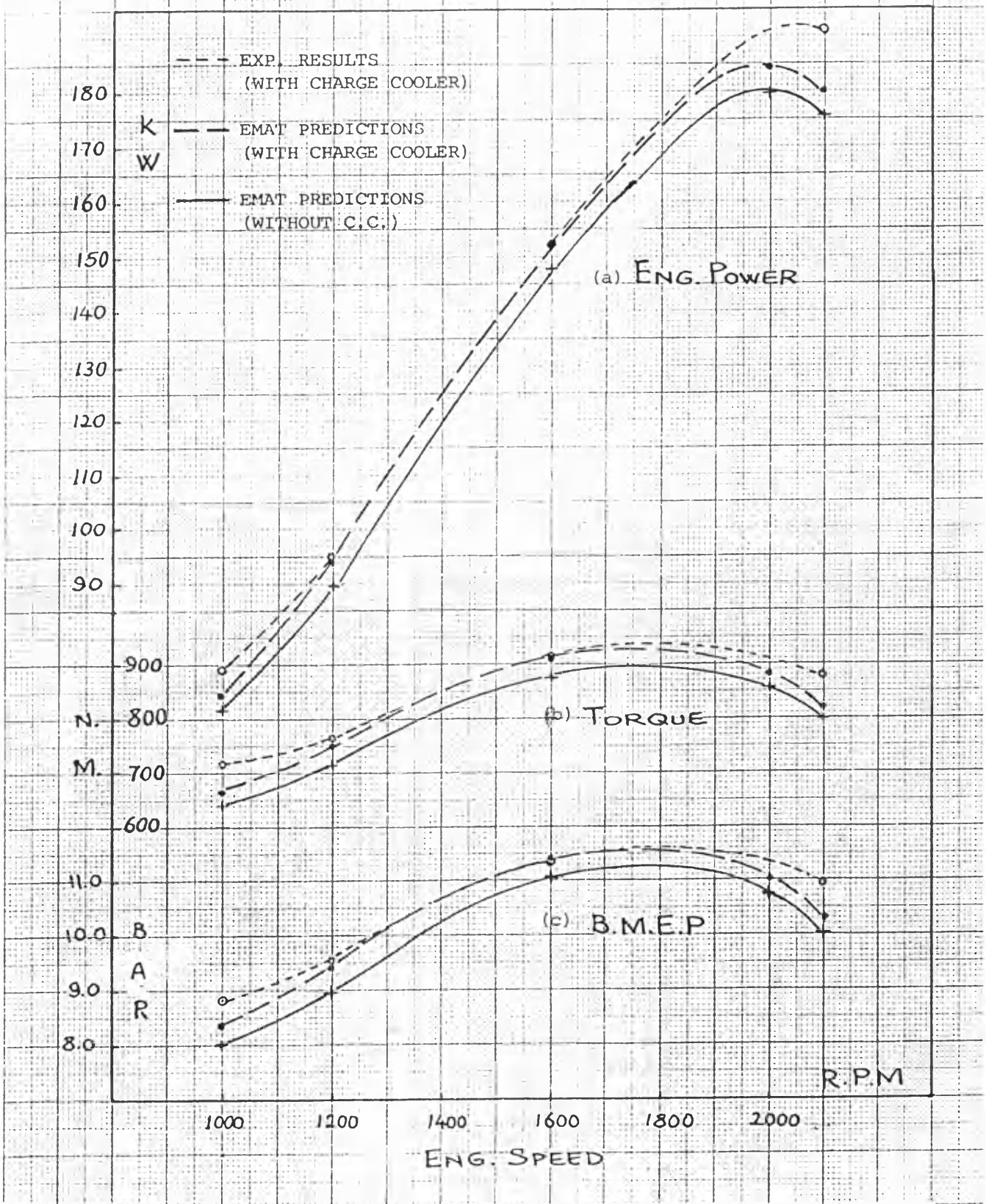

Fig. 3.11 Comparison of EMAT predictions with experimental results for the Cummins L10-T/C Diesel engine performance characteristics

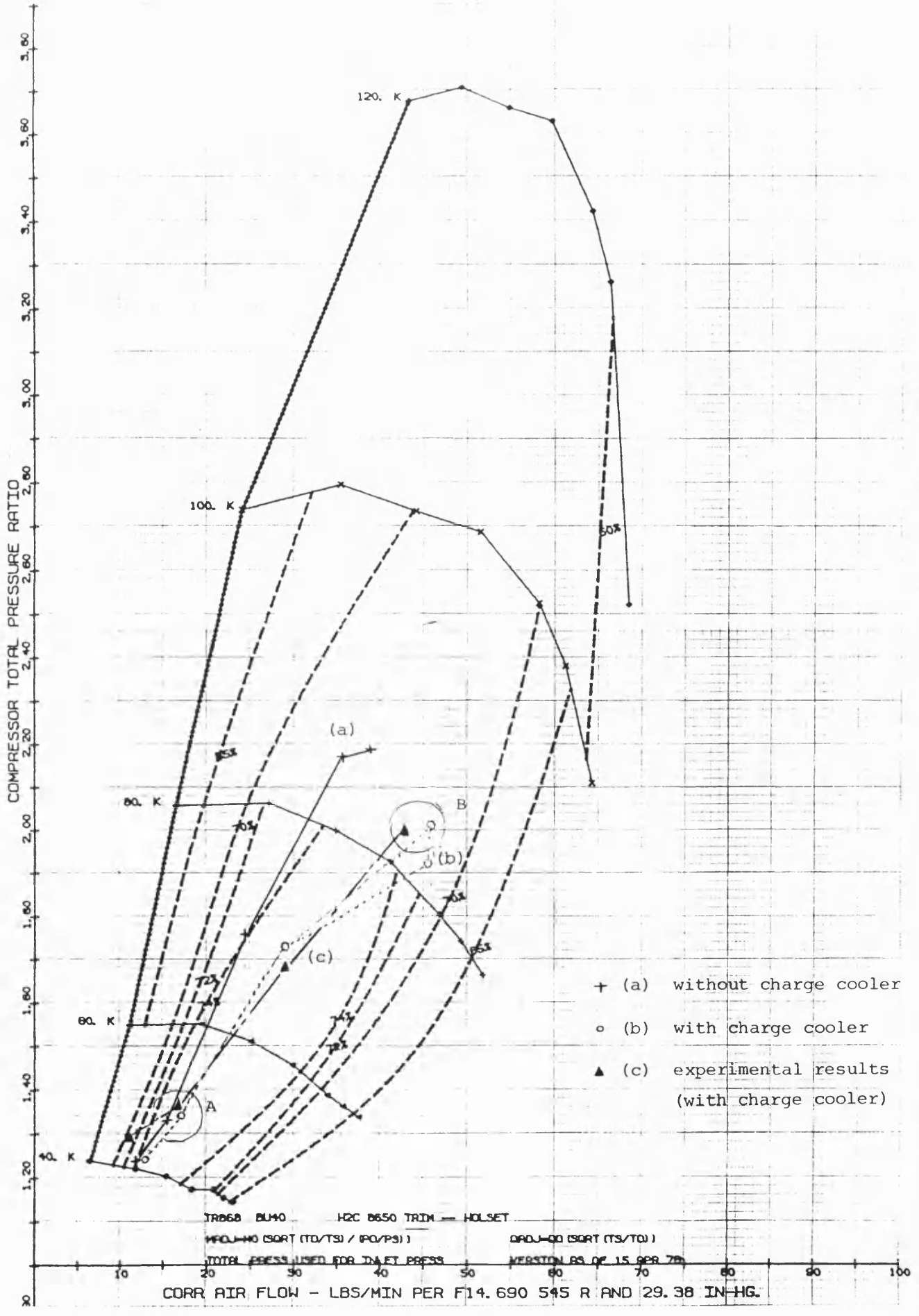

Fig. 3.12 Holset H2C 8650 compressor map superimposed with the experimental and predicted operating lines of the L10-T/C engine

CHAPTER FOUR

COMPREHENSIVE STEADY STATE SIMULATION OF THE CUMMINS L10-T/C ENGINE USING PROGRAM SPICE

4.1 INTRODUCTION

It has been well established that for investigations of the effect of changes in design and operating conditions, the method of "filling and emptying" is sufficiently accurate even for high-speed engines. Calculations are performed over successive small crank angle (i.e. time) intervals, quasi-steady flow being assumed (i.e. momentarily steady flow) during the crank angle step, such that the rate of change of properties is constant during that step.

To investigate the performance characteristics of the L10 engine in its DCE configuration by means of comprehensive simulation, it is necessary to finely tune different submodels of the programs in use for this type of engine. For such tuning, the conventional turbocharged configuration of the engine was simulated, since the necessary detailed experimental test results were available in that configuration. This chapter describes the steps taken to carry out this stage of modelling with the use of the comprehensive step-by-step calculation SPICE program. All major in-cycle phenomena are thereby taken into consideration.

4.2 THEORY

4.2.1 The Need for Accurate Heat Release Models

To predict Diesel engine performance over its operating range by means of cycle simulation, a detailed knowledge of heat release is necessary. The heat released by burning of the fuel determines the state of the working gases at each crank angle increment after combustion begins. However, the combustion process calculations are undoubtedly the weakest link in the chain leading to the prediction of engine performance.

A Diesel combustion simulation requires models of compressible viscous air motion, fuel spray penetration, droplet break-up and evaporation, air entrainment, chemical kinetics, turbulent diffusion, etc. To make provision for the spatial and temporal variations in composition and burning rate, the model should be three dimensional and unsteady. Progress is being made on simplified models but current results are qualitative rather than quantitative.

A relatively successful approach to the problem of combustion modelling within an engine cycle simulation has been to represent the overall thermal effects of the combustion process by an apparent heat release rate (AHRR). While this approach cannot replace fundamental combustion research, because it tells us nothing about the details of the process involved, it does represent the overall effects of combustion enabling predictions to be made of engine performance parameters required by the designer. The difficulty, hence, has partly been overcome by the development of an empirical correlation simulating the combustion process via an analytical expression whose governing parameters are linked to in-cylinder conditions.

However, the method relies on a wealth of knowledge concerning the "AHRR" derived from experimental cylinder pressure diagrams recorded under appropriate conditions, for any particular engine, or engine type.

4.2.2 Apparent Fuel Burning Rate (AFBR)

A simplified single zone combustion model has been widely applied to

engine cycle simulations. This approach considers the cylinder contents to be a homogeneous mixture of ideal gases which are always in thermodynamic equilibrium, and free of temperature and property gradients, pressure waves, etc. Combustion is modelled as a uniformly distributed heat source, which produces instantaneously burning fuel at a rate equivalent to a specified time varying pattern, known as the apparent fuel burning rate (AFBR).

The relationship between the "AFBR" and the resultant "AHRR" is based on the assumption that thermodynamic and chemical equilibrium exist at all times. All the fuel injected is considered to react irrespective of the equivalence ratio. Beyond the stoichiometric equivalence ratio, any increase in the amount of reacting fuel leads to a reduction in the specific cumulative heat release. Thus formulation of a correlation based on the 'AFBR' rather than the AHRR greatly simplifies handling of rich fuel-air mixtures.

The procedure to derive 'AFBR' diagrams from experimental cylinder pressure diagrams is to conduct an instantaneous energy balance of the cylinder contents during the closed cycle period. This, in effect, is the reverse of the normal cycle calculation, when combustion rate is an input parameter and the resultant cylinder pressure diagram is calculated. Unfortunately, even this simple calculation usually requires very accurate pressure diagrams and a careful calculation procedure to produce realistic and useful results.

Before describing such a combustion model in detail, it is appropriate to review different catagories of combustion chambers since they play a major role in this respect.

4.2.3 Open Combustion Chamber and Air Motion

The trend in medium- to high-speed Diesel engines has been towards the direct-injection or open chamber Diesel. An open chamber Diesel has the entire compression volume in one chamber between the piston and head.

The differences in combustion chamber design lie in the method of

achieving efficient and controlled combustion of a range of fuel-air mixtures. At one extreme, combustion is almost entirely controlled by high swirl and turbulence of the air, either before or after the combustion and at the other extreme, by the fuel injection equipment. Swirl is a rotary motion of the gases in the chamber, more or less about the chamber axis, while turbulence denotes a random motion of the gases.

In fact, whatever a combustion system is, it should ensure a better combustion quality so that an increase of IMEP, engine output and efficiency can be gained with better control of the combustion. For high-speed engines, additional air movement inside the chamber is usually desirable to accelerate the combustion process. However, high hot gas velocity in a combustion chamber increases the thermal impingement on the combustion chamber walls, thus limiting the maximum permissible mean effective pressure. For large slow-speed engines this additional air movement is unnecessary as a relatively long time is available for combustion.

Therefore, the open chamber design may be subdivided into three classes having overlap:

1) High-swirl open chambers
2) Medium-swirl open chambers
3) Semiquiescent and low-swirl open chambers

4.2.3.A Combustion chamber design for swirl induction

It is helpful to distinguish between primary and secondary swirl and turbulence. The primary ones are induced before combustion on the inlet and compression strokes by the flow geometries of the inlet passage ways and the chamber; the secondary ones arise from the combustion process and are directed by the flow geometry of the combustion chamber and containing walls. However, the problem is to generate a rotational swirl in the cylinder roughly proportional to engine speed. It should be emphasized that, although swirl action helps the mixing process of air with fuel, the objective is not to achieve an ultimate maximum in swirl, rather, the objective is to match swirl, fuel and injection

characteristics to yield the desired rate of pressure rise (and maximum pressure). Swirl induced on the intake stroke is obtained by sacrificing a gain in volumetric efficiency, and swirl, however induced, will increase the heat losses.

Two different types of swirl inducer are shown in fig. 4.1,a. Fig. 4.1,b shows a typical medium-swirl open chamber in which the combustion chamber has the shape of a deep bowl with special features to encourage the swirl action. A typical "AFBR" pattern of this type is shown in fig. 4.1,c in which two phases of combustion are involved.

4.2.3.B Quiescent type combustion

Requirements in highly turbocharged engines toachieve high mean effective pressure together with the short time available for burning - part from the need for economical fuel consumption and clear exhaust - makes two demands on the whole combustion system:

1. Low thermal impingement of the components surrounding the combustion space,
2. Low peak pressures

which require minimized air motion during combustion and also comparatively lower compression ratio while ensuring high thermal efficiency and smoke free exhaust. This will not be achieved unless a high combustion rate is provided. This type of combustion is called 'quiescent'; the injection system has to provide a high fuel-air mixing rate by:

1) A rapid fuel delivery or short duration of injection.
2) An increase of the contact between the injected fuel and the combustion air by means of a high degree of atomization over the whole load and speed range particularly at partial load or at high speeds.
3) A rapid and uniform distribution of the finely atomized fuel throughout the combustion space which can be ensured by a central multi-hole nozzle adapted to the combustion chamber geometry.

Fig. 4.2,a shows a typical quiescent combustion chamber., As is seen neither inlet port nor piston induces any air motion. Fig. 4.2,b illustrates a typical 'AFBR' pattern for this type of combustion chamber. As is seen, unlike the swirl type of combustion, it constitutes only one phase of combustion.

4.2.4 Application of Wiebe Function to the AFBR Modelling

Shipinski et al (ref. 30) were the pioneers in correlating the AHRR with the rate of injection by fitting a Wiebe function to experimentally determined heat release diagrams over a range of engine test conditions. Now it has been well established that for a mathematical representation of the results, the actual heat release diagrams could be replaced by simplified "Wiebe" heat release diagrams, which have the same beginning and duration of combustion so that if they are used for cycle simulations, the calculated values of peak cylinder pressure, power output and specific fuel consumption are in agreement with the measured data.

Such a simplified Wiebe heat release diagram is characterised by several parameters, viz. the beginning and duration of combustion, the Wiebe parameters and the equivalence ratio. Empirical correlations should be established whereby it is possible to predict variations of these parameters with altered operating conditions.

The Wiebe function for cumulative fuel burnt can be expressed as :

$$M_f(t) = \frac{m_f(t)}{m_t} = 1-\exp\ (-C_1 t^{C_2}) \qquad [4.1]$$

or in differential form (rate of fuel burning):

$$\dot{M}_f(t) = C_1 C_2 t^{C_2-1} \exp\ (-C_1 t^{C_2}) \qquad [4.2]$$

where $\dot{M}_f(t) = \dot{m}_f(t).\Delta/m_t$ [4.3]

C_1, C_2 shape factors in fuel burning rate equations

$m_f(t)$ fuel mass (kg) at t

$\dot{m}_f(t)$ fuel mass burning rate (kg/°CA) at t

$M_f(t)$ non dimensionalised fuel burnt at t

$\dot{M}_f(t)$ non dimensionalised fuel burning rate at t

t non dimensionalised crank angle

Δ nominal burning duration (°CA)

m_t total fuel mass (kg)

The "AFBR" is uniquely defined by :

a) the total mass of fuel burnt m_t as independent variable.

b) the start of combustion, θ_i, which can be related to the start of fuel delivery, the injection delay and the ignition delay.

c) the combustion duration (Δ), which is found to be a function of equivalence ratio and engine speed.

d) the Wiebe shape parameter C_1 and C_2.

Shipinski et al (ref.30) tried to link C_1 and C_2 to the fraction of total fuel injected during the delay period and the overall air-fuel ratio. Parameter C_1 can be considered as a combustion efficiency term, since selection of an appropriate value ensures that the expotential burning rate integrates to 100% fuel burnt at the end of combustion.

This AFBR correlation itself can be successfully used for the modelling of the quiescent type of combustion, (fig. 4.2,b). Therefore in order to have all the injected fuel burned at the end of combustion (where t = 1 and $M_f(t) = 1$), the value of the parameter C_1 in eqn. 4.1 should be as large as possible. However, it is kept within a limit between 6 and 10 for certain reasons as follows :

1) In a real combustion there is always some unburnt fuel at the end of the process.

2) The slope of rise and decay of a Wiebe curve very much depends on this parameter (fig. 4.2,b) which, in turn, determines the details of the AFBR curve.
3) As was stated earlier, there is a tendency to correlate this parameter to engine running condition parameters like air-fuel ratio.

As regards the modelling of the high swirl type of combustion, there are several approaches; among them the Watson et al (ref. 22) correlation is potentially more accurate, but is also more complex. The important feature of the model is that it divides the expression for fuel burning rate into two functions. These represent the initial 'pre-mixed combustion spike' and a slower 'diffusion burning controlled' phase, the sum at any instant being the instantaneous fuel burning rate (fig. 4.1,c). Thus:

$$\dot{M}_t(t) = \dot{M}_p(t) + \dot{M}_d(t) \qquad [4.4.a]$$

where the suffixes t,p and d denote total, premixed and diffusion respectively.

Dividing the non-dimensionalized burning rate into two components gives :

$$\dot{M}_t(t) = \beta . f_1(t) + (1-\beta) f_2(t) \qquad [4.4.b]$$

where :

f_1 = 'pre-mixed' burning function

f_2 = 'diffusion' burning function

β = proportionality factor

Thus the burning rate curve is expressed as the sum of two dimensionless distribution components weighted by the phase proportionality factor "β". The general equations describing these components are :

$$f_1(t) = k_1 k_2 (t)^{k_1 - 1} (1 - t^{k_1})^{k_2 - 1} \qquad [4.5.a]$$

$$f_2(t) = C_1 C_2 t^{C_2 - 1} \exp(-C_1 t^{C_2}) \qquad [4.5.b]$$

where f_2 is exactly the same diffusion burning function as was described in eqn. 4.2, but f_1 is a function capable of producing very steep rates of rise and decay, similar to that in the first stage of a high swirl type of combustion.

Values of the parameters k_1, k_2, C_1 and C_2 and their correlations with engine operating conditions are, therefore, to be experimentally determined for a particular type of engine. Referring to Watson's experiments (ref. 32) and as used, initially, for the Cummins L10 engine, these factors are as follows :

$$k_1 = 2.0 + 1.25 \times 10^{-8} \, (ID.N)^{2.4} \qquad [4.6.a]$$

$$k_2 = 5000 \qquad [4.6.b]$$

$$C_1 = 14.2 \quad F^{-0.644} \qquad [4.6.c]$$

$$C_2 = 0.791 \, C_1^{0.248} \qquad [4.6.d]$$

$$\text{Also } \beta = 1 - 0.926 \, F^{0.37}/ID^{0.26} \qquad [4.6.e]$$

where ID is ignition delay in 'msec', N is engine speed in 'rpm' and, F is equivalence ratio.

4.2.5 Ignition Delay

Ignition delay is the time which elapses between the start of fuel injection and the start of combustion indicated by a rapid rise in one of the indications of combustion, i.e. illumination, temperature rise or pressure rise. Whatever reference is made, the ignition delay is mainly due to physical changes associated with evaporation of the fuel and, to a lesser extent, due to chemical reactions needed to make a preflame reaction take place.

From the literature review, it can be noticed that different delay periods were measured in a variety of combustion chambers under different operating conditions. However, from an engineering point of view the pressure rise delay is the most important since the useful work calculation is based on pressure-volume variations. Therefore, amongst

the different correlations available, the Wolfer model (ref.23) predicting the pressure rise delay is the most appropriate.

The Wolfer model in use suggests a correlation as follows :

$$ID = \frac{3.52}{P_{ID}^{1.022}} \exp\,(2100/T_{ID}) \qquad [4.7]$$

where ID is the ignition delay in "ms", and P_{ID} and T_{ID} are the gas pressure and temperature during the delay period in "bar" and "deg.K".

Both the physical and chemical components of delay are therefore taken into account as they are features of the instantaneous cylinder pressure and temperature at the point of injection, i.e. the higher the cylinder pressure or temperature the shorter the ignition delay, for the following reasons:-

1) The self-ignition temperature of the fuel drops at higher pressures.
2) The availability of oxygen increases at higher pressure.
3) The heat transfer rate from the air to the fuel droplets increases as the density and also temperature of air increases.

which all contribute to a shorter delay period in one way or another. Although the effect of air motion is not taken into account, the correlation is assumed to be valid for a limited range of air-swirl.

4.2.6 Heat Transfer in an Engine and its Modelling

In the practical operation of Diesel engines, the difference between heat of combustion and total useful engine work (including work to drive accessories) leaves the system in the form of exhaust gas energy and heat losses. The study of engine heat losses is important not only from the point of view of efficiency but also for cooling system design and, perhaps, most important of all, for an understanding of the effect of heat flow on the operating temperatures of engine parts.

Heat is lost in different ways as follows :

1. Directly from the working fluid
   a) during the compression, combustion and expansion periods to the cylinder structure,
   b) during the exhaust process to the porting and ducts, and
   c) during the combustion period due to leakage into the crankcase.

2. Indirectly by mechanical and fluid friction work which causes higher component temperatures.

Heat losses are transferred to cooling medium which is mainly the engine circulating water and lubricant, although engine surroundings may play some minor role. Most of the heat which flows between the working fluid and the engine parts and between the engine parts and the cooling fluid is transferred by forced convection. However, radiation can play an appreciable role in the heat transfer process during combustion and expansion, i.e. when the gases are inflamed. Conduction is the mechanism by which heat flows through the engine structure.

The process of heat flow between the working fluid and the cooling medium of an engine can be approached by means of the assumption that it is analogous to the heat flow process in a heat exchanger. In spite of a number of differences between the two, the governing heat transfer formulations are the same, and it is worth recalling them for the case of a simple heat exchanger (fig. 4.3) passing hot gas and coolant separated by a solid wall. To introduce the heat being transferred the following symbols are used.

T_g	the mean temperature of the gas
T_c	the mean temperature of the coolant
A_g, A_c	the surface area on the gas side and the coolant side of the wall
T_{sg}, T_{sc}	the mean surface temperature of the gas side and the coolant side of the wall

k_w the conductivity coefficient of the wall material

h_g, h_c the coefficient of heat transfer in convection

t the thickness of the wall between A_g and A_c

$\dot{Q}$ the heat flow rate through the surfaces A_g and A_c

The heat flow rate from the gas to the area A_g, from there to the area A_c and from this area to the coolant can be written successively as follows:

$$\dot{Q} = h_g A_g (T_g - T_{sg}) \qquad [4.8]$$

$$\dot{Q} = \frac{k_w}{t} A_g (T_{sg} - T_{sc}) \qquad [4.9]$$

$$\dot{Q} = h_c A_c (T_{sc} - T_c) \qquad [4.10]$$

which constitute a set of three simultaneous equations.

Some of the ways in which the heat transfer in an engine differs from that in a heat exchanger, may be listed as follows :

1 - the radiation from engine combustion flames,
2 - the complex and varying geometry of the engine flow system,
3 - the gas side unsteady rate of fluid flow,
4 - the variation of temperature on both sides with crank angle,
5 - the effect of additional heat transferred to the cylinder wall due to piston friction,
6 - the heat flow along the cylinder walls,
7 - the variation of the wall conductivity with location, due to the amount of oil and deposit on the inside and outside of the wall.

In the cycle simulation programs in use (SPICE and CSP), although the simple equations 4.8 to 4.10 are applied, some well known heat transfer correlations and models are also employed to modify the variables with respect to the differences just mentioned. However, neither of the programs considers the heat flow along the cylinder walls or the effect of varying oil film and deposit thicknesses on the walls.

The correlation adopted within these cycle programs for simulation of the L10 engine is that of Woschni (ref. 24) who develops the heat transfer coefficient of gas side convection so as to cover the effect of some of the phenomena such as the flame radiation and the variation of gas velocity and viscosity, taking place in a real engine. As regards eqn. 4.8, as soon as a modified h_g is calculated, the heat flow rate through the surrounding walls of the combustion chamber, i.e. the cylinder head, the liner and piston surfaces can be readily calculated provided that the updated values of other variables are also available. Using crank mechanism and thermodynamic differential equations, the variables A_g (for the liner) and T_g are updated at each crank angle position, whereas for updating the wall temperatures a different approach based on the use of a one dimensional heat transfer model is applied at the end of each cycle. The model assumes the wall surfaces to be of a constant uniform temperature and heat transfer coefficient, free of any deposit build up or other time dependent changes in surface conditions.

As a simpler approach, the resistance model used in the program CSP is described first. The model whose schematic diagram is shown in fig. 4.4 which calculates the heat transfer to different chamber walls each being represented by three constant resistance values at any crank angle. The liner surface area and also h_g and T_g will be subject to updating at each calculation step. As in an electrical circuit, the heat flow rate is analogous to current (I) and the temperature difference to an electric potential difference (V). Hence referring to eqns. 4.8 to 4.10 the thermal resistance (R) becomes :

$$R = t/K.A \quad \text{"in conduction"} \qquad [4.11.a]$$

$$\text{or} \quad = 1/h.A \quad \text{"in convection"} \qquad [4.11.b]$$

Therefore, a network of thermal resistances analogous to an electrical network as shown in fig. 4.4 is set up; an electric current balance at each network junction can be established, so that there is a heat flux balance at each junction. The heat transfer through cylinder head, piston and liner which are shown in fig. 4.4 as $\dot{Q}_{hg}$, $\dot{Q}_{pg}$ and $\dot{Q}_{lg}$ represent

instantaneous rate of heat transfer. The component resistances (R_2, R_4, R_5, R_7 and R_9) are functions of the component geometry and thermal conductivity (R_4 controls the amount of heat transfer from the piston to the liner) whereas the interface resistances (R_1, R_8 and R_{10}) between liquid and metal are functions of the coolant heat transfer coefficient h_c, and the exposed area A_c (i.e. $R = 1/h_c\ A_c$). $\dot{E}_{fr}$ is considered to be the equivalent heat of piston friction transferred to the liner which in the CSP program amounts to 25% of the total engine friction.

Working out the governing network formulas, one may derive the piston node temperature (T_p) and gas side wall temperatures (T_{pg}, T_{lg} and T_{hg}) in the form of general functions as follows :

$$T_p = \Psi_{1p}\ (\dot{Q}_{pg},\ \dot{Q}_{\ell g},\ \dot{E}_{fr},\ R_i,\ T_{cw},\ T_{co}) \qquad [4.12]$$

$$T_{pg} = T_p + \dot{Q}_{pg} * R_5 \qquad [4.13]$$

$$T_{\ell g} = \Psi_{1_\ell}\ (\dot{Q}_{pg},\ R_i,\ T_p,\ T_{co}) \qquad [4.14]$$

$$T_{hg} = \Psi_{1h}(\dot{Q}_{hg},\ R_i,\ T_{cw}) \qquad [4.15]$$

where 'T_p' is the piston node temperature at which part of the piston heat transfer is directed to the liner, the suffix "i" for R indicates a combination of different resistances in the model, the suffixe 'pg', 'ℓg' and 'hg' stand for gas sides of piston, liner and cylinder head, and T_{cw} and T_{co} are cooling water and oil temperatures.

As regards the program 'SPICE', no piston node temperature is defined as such and a constant fraction (X_L as an input) of the piston heat transfer is considered to be a part of the total heat transferred to the liner and value of $\dot{E}_{fr}$ amounts to 50% of the total mechanical friction. Therefore the thermal network shown in fig. 4.4,b is broken at the connection made

by R_4 and as is shown in fig. 4.5 each of the walls will have its own separate circuit. Rewriting the heat transfer formulas, the gas side wall temperatures will be as follows :

$$T_{pg} = \Psi_{2p} \ (\dot{Q}_{pg}, \ R_i, \ T_{co}) \qquad [4.16]$$

$$T_{\ell g} = \Psi_{2\ell} \ (\dot{Q}_{pg}, \ \dot{Q}_{\ell g}, \ \dot{E}_{fr}, \ R_i, \ T_{cw}) \qquad [4.17]$$

$$T_{hg} = \Psi_{2h} \ (\dot{Q}_{hg}, \ R_i, \ T_{cw}) \qquad [4.18]$$

There is now no need to calculate a piston node temperature. However, the liner model is developed in a more realistic fashion considering three different thicknesses at the top, middle and bottom part each with its cooling boundary condition defined in input data (fig. 4.6). Even more realistic, the liner is divided into 15 zones along its length having their own temperatures during a cycle. Therefore, the simple liner circuit of fig. 4.5 now becomes a detailed network which is presented in fig. 4.7. The suffix "j" in this figure attributes to different zones of the liner and hence equations 4.8 and 4.17 in their general form for the liner zones become :

$$\dot{Q}_{\ell g_j} = h_g \ A_{\ell g_j} \ (T_g - T_{\ell g_j}) \qquad [4.19]$$

$$T_{\ell g_j} = \Psi_{2\ell} \ (\dot{Q}_{pg}, \ \dot{Q}_{\ell g_j}, \ \dot{E}_{fr}, \ R_i, \ T_{cw}) \qquad [4.20]$$

where $\dot{Q}_{\ell g_j}$ is the instantaneous rate of heat transfer from the gas to each liner zone. Those zones which are nearer to TDC are exposed to higher gas temperatures and for a longer time.

4.2.7 The Effects of Important Variables on the Friction Power Loss

As regards the nature of the friction power loss, it seems that only a detailed analysis of the effect of individual component losses in the engine can provide a complete knowledge. However, a study of the effect of engine running condition, viz. lubricant viscosity, engine speed and load, can provide cycle simulation programs with useful information.

A) The Effect of Engine Speed

Fig. 4.8 shows a number of results quoted by Dutcher (ref. 34) covering a period of about 70 years and including both petrol and C.I. engines.

Dutcher points out that there are two independent systems of frictional forces operating within any reciprocating engine, viz. rotating and sliding system. Although he and some others agree that frictional drag of the bearings is a function of speed of rotation varying almost directly with rubbing speed, in considering piston friction alone, there are different view points. However, as regards fig. 4.8, linear dependency of FMEP upon mean piston speed over a major speed range of many different reciprocating engines has been substantiated.

B) The Effect of Load (Cylinder Pressure)

Cylinder pressure affects the side thrust of the piston against the cylinder wall and also radial loading of the piston rings which, in turn, affects friction losses. Summarising the changes in power loss with load, Ricardo (ref. 35) states that, for piston friction, "viscous friction appears to be very important; it increases rapidly with speed, but is nearly independent of the gas loading; of equal importance is piston ring friction, which is nearly independent of speed but nearly proportional to gas pressure".

Although, this effect in a rigid high speed engine does not seem to be as important as the effect of inertia forces, there is some evidence that, even for these engines gas pressure behind the rings have an effect on engine friction. The effect of cylinder pressure on the FMEP at a range of selected speeds was thoroughly investigated by Dutcher (ref. 34) and it can be seen in fig. 4.9 that the FMEP changes almost linearly with cylinder pressure at any speed.

C) The Effect of lubricant Viscosity

Crankshaft journal friction (for plain bearings) and piston ring/cylinder wall friction during part, at least, of the cycle of operation under fluid film lubrication. Viscous friction is caused by shearing of the oil film and has a substantial influence on the FMEP.

Oil viscosity is dependent upon the oil grade and working temperature. Mueller and Pfundstein (ref. 36) show by means of fig. 4.10 obtained from a test on a truck engine, that the effect of a given change in water jacket temperature is more than twice as great as the same change in the oil temperature. This result is understandable because the friction between the piston and cylinder, which is a considerable proportion of the total engine friction, probably depends on the temperature of the oil on the cylinder walls, which takes the temperature of the governing water temperature.

4.3 FIRST STAGE OF TUNING THE SUBMODELS FOR THE L10 ENGINE

Before proceeding with analysis of submodel tuning requirements and simulation of the L10-T/C engine, it should be noted that the investigation was performed in two different stages. At each stage, the same specification and experimental results with respect to the overall performance characteristics as obtained from the manufacturer were used. However, detailed experimental data with respect to the different processes such as the engine heat release, heat transfer and friction were needed to justify the type and tuning of the corresponding submodels applied in the simulation. This did not become available until a later stage. Hence due to this initial lack of information, arbitrary models had to be used for friction, heat release and heat transfer.

The models employed were the same as those in use for the Leyland TL11 engine having 11.0 ℓ swept volume and a high swirl type of combustion chamber. The model used for heat release was due to Watson and Marzouk (ref. 22) in conjunction with the modified Wolfer (ref. 23) expressive for ignition delay. The heat transfer correlation chosen was due to Woschni (ref. 24).

As regards the first set of manufacturer's experimental data for the L10 engine, a rated power of 290 hp (215 kW) at an engine speed of 2100 rpm was assumed. As described in Section 2.3.4, and shown in fig. 2.9, the engine was modelled in its turbocharged configuration having two exhaust manifolds as used in practice (2 x 2.4ℓ) to take full advantage of pulse turbocharging.

The running conditions included five points for full load, five points for part load and five points for low load at engine speeds of 1000, 1200, 1600, 1900 and 2100 rpm, the object being to synthesize the experimental test results. The experimental and theoretical calculation results for full load (five points of the LTC) are given in table 4.1.

Referring to the first set of the L10 engine information an injection timing of 17 deg BTDC was certain at least for the design point, but for other conditions, it was necessary to assume the characteristics of a

conventional fuel injection system, in the absence of detailed data. The comparison of the theoretical and experimental results showed that the predicted brake thermal efficiency ($\eta_{B.TH}$) was on average, about 2.2% (based on total fuel energy) less than for the test results, whereas the predicted maximum cylinder pressure (P_{max}) exceeded a level of 150 bar near the design point.

A) Lowering P_{max}

Once a high swirl type of combustion chamber is assumed, it may be considered that air-fuel mixing is of the wall mixing rather than of the airborne type, i.e. the fuel is first deposited on the wall to be removed later by the air swirl. Most of the behaviour of an engine with this type of combustion can only be understood if reference is made to the phenomenon of ignition delay which more than in quiescent combustion systems plays a significant part. The length of the ignition delay controls the pattern of burning. The fuel injected during the delay mixes with air and forms a premixed rapidly burning flame giving rise to a rapid heat release and rise of cylinder pressure. The amount of heat released in the premixed burning phase is proportional to the amount of fuel injected during the delay period which is, in turn, proportional to the length of, and the rate of injection during the delay period. Therefore, ignition delay is one of the most important parameters in controlling the maximum cylinder pressure (P_{max}).

Motoring has shown that although the maxima of cylinder pressure and temperature (without firing) do not occur at the same crank angle position, they are quite close to TDC (after about 5 deg. BTDC). Therefore, in order to lower P_{max} of the simulated L10 engine at this stage of matching, it was considered to retard timing so as to take advantage of higher cylinder pressure and temperature during ignition delay to shorten the delay period. This strategy was found to be quite effective in lowering P_{max} and hence retardation of the injection time from 17 deg. BTDC was continued until fairly satisfactory results were achieved at a timing of 8 deg. BTDC. Table 4.2 gives the gross engine performance results based on the modified timing showing the comparison

with experimental results for engine running conditions along the LTC.

B) Improvement in $\eta_{B.TH}$

It must be noted that there were indeed two reasons for employing retarded timing, both leading to the required improvement in brake thermal efficiency:

i) For each injection rate, there is an optimum injection timing where the centroid of the heat release diagram falls on TDC and indicated thermal efficiency reaches its maximum. Also a higher injection rate calls for a more retarded injection timing and vice versa.

ii) In applying the friction correlation based on the Chen and Flyn model (ref. 29 and as demonstrated in section 4.6), the FMEP decreases with P_{max} resulting in an improvement in mechanical efficiency and hence brake thermal efficiency.

C) Other Performance Parameters

Table 4.3 gives a comparison between the SPICE predictions for the engine performance parameters based on two different injection timings. As shown, engine running conditions in terms of engine speed and fuelling for both cases are the same. However, there are some minor discrepancies between the air flows which are due to the differences in available energy at the turbine entry as the timing retards.

Table 4.3 shows that the retarded timing brings about an average of 30% increase in mean cylinder pressure during the delay period (fig. 4.11,a) while there is no major change in the inlet manifold pressure. Also an average increase of 3.7% in mean cylinder temperature during the delay period (fig. 4.11,b) is resulted whereas the inlet manifold temperature is reduced. Referring to the Wolfer correlation (eqn. 4.7) adopted in the program, this combination yields some decrease in ignition delay over the operating range (fig. 4.11,c). Consequently, the portion of the total fuel that burns in the premixed phase of combustion (β as given in eqn. 4.6,e) is reduced by an average of 45% (fig. 4.12,a). As a result, P_{max}

decreases by an average of about 23 bar (fig. 4.12,b) as was intended. A decrease in maximum cylinder temperature (T_{max}) of the order of 90 deg.K was also experienced (fig. 4.12,d).

Fig. 4.13 illustrates the trends of identical MEPs of the two cases of timing for comparison. As shown due to retarded timing, a higher IMEP (by an average of 2.8%) and lower FMEP (by an average of 5.8%) resulted from retarded timing, which in turn led to an improvement of $\eta_{B.TH}$ by an average of about 5.7% at low speeds and about 2.8% at high speeds (equal to average of 2.2% and 1.4% based on total fuel energy). This is shown in fig. 4.14 where other improvements in indicated thermal efficiency as well as mechanical efficiency over the operating range are illustrated.

As far as the improvement in gross IMEP is concerned it must be considered that although P_{max} for retarded timing is reduced, it occurs about 4 deg. c.a. later [at about 9.0 c.f. 5.0 deg ATDC as shown in fig. 4.12,c] which is due to the later start of combustion of about 7.5 deg. c.a [at about 4.5 c.f. 12.0 deg. BTDC as shown in fig. 4.11,d]. On the other hand, because of the shorter ignition delay, more fuel is burned in the diffusion phase of combustion and hence a more rounded cylinder pressure-crank angle diagram results with a higher level of cylinder pressure over the expansion period. (This could also be an implication of having the centroid of the heat release diagram closer to TDC). As shown in fig. 4.13,b PMEP is reduced, this in turn contributes to $\eta_{B.TH}$ yielding an even higher indicated efficiency (fig. 4.14,a).

Figs. 4.15 to 4.17 show, for all speeds, the superimposed diagrams of predicted in-cylinder conditions versus crank angle along the LTC as follows:

Fig. 4.15 Heat release diagram
Fig. 4.16 In-cylinder gas temperature
Fig. 4.17 In-cylinder gas pressure

The rate of temperature increase (in fig. 4.16) after combustion starts,

can be explained by the rate of heat release (fig. 4.15). Hence the temperature curves and their maxima (from 1759 deg.K to 1908 deg.K) for the different running conditions remain within a rather narrow range due to the almost constant slope of the leading edge of the different heat release curves. On the other hand, fig. 4.17 shows that the maximum cylinder pressures cover a rather wide range (from 94 bar to 137 bar), mainly because of the wide range of boost pressure ratios (from 1.33 to 2.11).

Although, by means of retarded injection timing, the brake thermal efficiency was satisfactorily matched with that of the experimental results while maximum cylinder pressure was lowered to a more acceptable range, the variations of in-cylinder performance parameters were by no means certain. Later experimental information with respect to the heat release, pumping work (PMEP) and mechanical friction (FMEP), made it possible to look into the details of in-cycle variations of thermodynamic parameters and also to establish a better match between the computer program submodels and different aspects of the real engine.

4.4 FURTHER EXPERIMENTAL TEST RESULTS OBTAINED FROM THE MANUFACTURER

The second set of the Cummins' report which became available at a later stage, mainly gives detailed experimental heat release diagrams and engine friction. The heat release diagrams have been prepared with sufficient accuracy using digitized dynamic cylinder pressure. The information has been recorded, using a "Biomation Waveform Recorder" in conjunction with the automated test cell computer system at Cummins.

The Biomation unit is capable of digitizing, storing and displaying a waveform and transferring the digital data to the automated test cell computer for further manipulation. The unit requires an accurate crank angle reference system to trigger the data storage. The system yields samples of data at intervals of 0.874 deg. C.A. Ten repetitions of the data recording process were performed for each test point and a computer summed the information to yield a ten cycle average.

The L10 engine was configured as described in table 4.4 for different tests. The test results are summarized in table 4.5. As is realized a power of 250 h.p (186.5 kW) is considered to be developed. The matrix of test points includes five points along the limiting torque curve (full load) and six points at reduced load. The cylinder pressure data integrated over the 720 degree cycle to yield a net indicated effective pressure (NIMEP). The "FMEP" (friction) of an engine is defined as the difference between "NIMEP" and "BMEP" and it is evident from table 4.5 that the calculated "FMEP" is at times negative. Fig. 4.18 is a comparison of the "FMEP" trend of the data and that expected from motoring dynamometer tests. According to the report, the needed correction on the data was made based on one of the probable errors attributed to the timing of the triggering circuit. After several attempts, retardation by 0.874 crank degrees appeared to be appropriate to bring the friction in line with the expected levels. Fig. 4.19 depicts the friction trend when applying a 0.874 crank degree displacement of the data. The friction levels are more acceptable and also justify the dependency of FMEP on load.

Pumping mean effective pressures (PMEP) are summarised in table 4.6. The

net pumping work is seen to increase as a function of load in fig. 4.20. The manifold pressure differential (difference between inlet and exhaust pressures) is largely responsible for this trend. It should be noted that the crank angle shift has negligible effect on PMEP. Another possible flaw in the data was discovered in the 1800 RPM region where PMEP is lower than expected. The "NIMEP" which was mentioned earlier takes the effect of the "PMEP" into account.

Finlly, the assessment and correction of the recorded cylinder pressure data yielded non-dimensional apparent heat release diagrams showing the effects of load and speed. The effect of speed is given in fig. 4.21 and that of load for engine speeds of 2100 rpm and 1260 rpm are shown in figs. 4.22 and 4.23.

4.4.1 The Semi-quiescent Low Swirl Open Chamber of the Cummins DI L10 Engine

The combustion chamber of the L10 engine is compact, with minimal wall area (per unit volume) surrounding the compressed air. The chamber has the shape of a shallow dish formed by the piston top (Mexican hat) as illustrated in fig. 4.24,a. Although air movement in the chamber is never entirely quiescent, the simplicity of the chamber and the contours of the inlet passageway (fig. 4.24,b) do not induce strong turbulence or swirl. Therefore, the problem of mixing the fuel and air and controlling the combustion rate, falls upon the injection system (ref. 37). In the L10 engine, the nozzle is located in the centre of the chamber with six or more orifices, each jet or spray contributing to a spray pattern that covers most of the combustion chamber. The nozzle is located so that the spray pattern fits the combustion chamber without impinging on the walls or piston. Thus for the L10 chamber a flat multiple-spray pattern from the nozzle has been designed, with air between each spray. The spray contains a range of droplet sizes to obtain various degrees of penetration, along with gradual vaporization, to find the air throughout the chamber without forming overrich mixtures near the nozzles. It follows that the timing, rate and pressure of fuel injection, size of each orifice, viscosity and ignition quality of the fuel and engine speed dictate the trend of pressure rise and completeness of combustion.

As was indicated in Section 4.2.5, ignition delay is mainly due to physical causes and, in turn, it will be the question of how quickly a combustible mixture is formed. In most cases it is difficult to distribute the fuel sufficiently evenly solely by controlling the shape of the jet. This is why it is necessary to make use of the turbulence caused by the suction process, or to create an artificial air movement in the cylinder for the mixture. As was seen in Section 4.3, organized air movement is the main feature of the high swirl type of combustion chamber and is utilised to achieve good distribution of the fuel.

However, as soon as very high injection pressure, together with a number of injection orifices are applied, a good distribution of finely atomized fuel will be achieved. This not only eliminates the need for any further air movement but also makes the ignition delay much shorter.

Table 4.7 based on manufacturer's information, gives a typical set of injection pressure values varying from 420 bar at an engine speed of 1000 rpm to 1034 bar at a speed of 2400 rpm applied by the "pressure-time" or "P.T" fuel system of the L10 engine. The associated ignition delay becomes so short that unlike that simulated in the first stage (Section 4.3, fig. 4.15), the experimental heat release diagrams (given in figs. 4.21, 4.22 and 4.23) reveal no spiky premixed phase for combustion.

4.4.2 Methods of Determining the Friction Mean Effective Pressure (FMEP) of the L10 Engine

Some of the different methods for determining engine friction which have been used to study the FMEP of the L10 engine are briefly described with reference to Ricardo (ref. 35) as follows :

4.4.2.A Use of indicator diagram

By this method, the indicated horse-power of an engine is measured with an indicator, and the power output with some type of dynamometer. Using the difference between the two determines the FMEP. Although this method is one of the best ways of determining real FMEP under firing conditions, the great difficulty is that the phase relationship of indicator diagrams

is not sufficiently accurate. As is stated by Ricardo (ref. 35), since the peak pressure rise of the diagram is crowded into the region of firing TDC, a phase error of only 1 deg. may vary the area of the diagram by as much as 5% or even more. Besides measurement of areas on the diagrams leads to further difficulties.

As described in Section 4.4 this problem was experienced in the analysis of experimental MEP values of the L10 engine.

4.4.2.B Motoring tests

Motoring tests have also been extensively used in practice. By this method, the engine is motored under conditions resembling firing conditions as closely as possible. The power required to drive the engine is taken to determine the FMEP. It cannot be claimed that the frictional losses or air pumping work are the same when motoring as when firing, hence corrections have to be made when motoring results are applied. Ricardo (ref. 35) states that motoring tests always overestimate the frictional losses due to loss of heat to cylinder walls during the compression and expansion strokes. It has been established that a higher compression ratio or swirl of an engine calls for a higher correction to be applied to motoring results.

There are further factors causing friction when running under power to differ from that when motoring, two of the more important ones being :
a) effect of cylinder pressure, and
b) effect of piston and cylinder wall temperature
which are difficult to control when motoring.

4.4.2.C The "Willans Line" method

In this method which is mainly applicable to C.I. engines, the line of gross fuel consumption against BMEP is extrapolated to cross the BMEP axis. This point then gives the power required to drive the engine, i.e. the power loss. Since the Willans line is rarely straight, there is some uncertainty as to the slope of the extrapolated line.

Fig. 4.25 shows the L10 fuelling map, from which the friction torque curve has been calculated, as shown at the bottom of this figure.

As explained in Section 4.4 the FMEP of the L10 engine has been measured using motoring and also indicator diagrams. Fig. 4.19 shows the FMEP test results based on these two methods, on which also are superimposed the FMEP obtained from the Willans line.

4.5 HEAT RELEASE MODELLING APPLIED TO THE SEMIQUIESCENT COMBUSTION CHAMBER OF THE L10 ENGINE

In the study of the heat release diagrams of the Cummins L10-250 T/C engine, which became available at a later stage of investigation, it was found that the Wiebe function itself (eqn.4.2) could be fitted with good agreement.

The effects of the Wiebe parameters on the shapes of resultant curves are illustrated in fig. 4.26. A recommended range from 0.5 to 1.5 and from 6 to 10 for the parameters C_1 and C_2 respectively in four combinations was examined. As is seen, these combinations show typical heat release diagrams having the same beginnings and endings. It is also seen that height and slope of the leading edge of the diagram increase with decrease in C_1 from 1.5 to 0.5 and with increase in C_2 from 6 to 10.

For the purpose of curve fitting, the experimental heat release diagrams were tabulated in the form of arrays to be transferred into the computer files. The diagrams are relevant to the following working conditions (as given in tables 4.5a and b):-

1) 1000 rpm at 700 lb.ft (i.e. 100% load)
2) 1260 rpm at 190, 375, 560 and 750 lb.ft (i.e. 25%, 50%, 75% and 100% load)
3) 1500 rpm at 750 lb.ft (i.e. 100% load)
4) 1800 rpm at 700 lb.ft (i.e. 100% lod)
5) 2100 rpm at 160, 310, 470 and 625 lb.ft (i.e 25%, 50%, 75% and 100% load)

Fig. 4.27 shows the experimental non-dimensionalised heat release diagrams for the conditions numbered 5, as above, after transfer into the computer files. This figure is equivalent to fig. 4.22. A computer program was written to find the best fit Wiebe functions for each of the eleven experimental heat release diagrams. The program looks for the best values of the four Wiebe parameters (i.e. the start and duration of combustion and also C_1 and C_2) to match the leading edge and maximum value of the Wiebe curves with the

experimental values. Figs. 4.28,a to 4.28,k show the results of curve-fitting for all the above running conditions. Table 4.8 indicates the values found for the parameters involved.

In this study it was also found that the width of the main portion of the heat release diagram increases slightly as the speed is increased (fig. 4.21). Another observation was that the centroid of the diagram is retarded slightly as the speed is increased. This can be best described by taking into consideration the increase in fuelling per cycle with the PT fuel system as the speed decreases. Thus a slight advance in the start of injection is mainly due to the higher level of fuel in the injection cup (ref. 37). The shape of the diagram is, however, almost unchanged.

The effects of load are shown in either figs. 4.22 or 4.27 and 4.23 for the engine operating at 2100 rpm and 1260 rpm respectively. Both of these sets display an increase in heat release duration, a decrease in heat release rate maxima and an advance of the centroid of the diagram with increasing load (fuelling). Again, this is consistent with the PT fuel system where the end of injection is essentially fixed and the start of injection advances with increased load (again because of the increased height of the fuel column). However, the manufacturer suggests that one heat release diagram can be used for the simulation of all operating conditions if proper scaling and timing shift are applied. Table 4.9 shows the results of their experience with the application of the heat release diagrams at two other conditions, i.e. at 2100 rpm at quarter load and at 1260 rpm at full load to the simulation of the running condition at 2100 rpm at full load. The results of simulation show an error of less than 4 per cent in maximum cylinder pressure and of less than 0.2 per cent in the "BMEP".

Despite the fact that, as described above, individual heat release diagrams show only small differences in Wiebe parameters (table 4.8), 'fine tuning' of C_1 and C_2 was used inthe simulation of the L10 engine.

4.6 FRICTION MODELLING OF THE L10 ENGINE

To provide the simulation programs in use (SPICE and CSP) with an appropriate friction model of the L10 engine, it is necessary to find a correlation between the FMEP and the engine running conditions. Firstly, it was decided to use the experimental results based on the application of indicator diagrams (fig. 4.19), since some information about the effect of cylinder pressure as well as engine speed on FMEP could be extracted.

Of the different friction models available, the one proposed by Chen and Flyn (ref. 29) was considered since it takes account of the effect of engine running condition in terms of both the engine speed and maximum cylinder pressure. The model proposes the following general formula for FMEP:

$$FMEP = k_1 + k_2 P_{max} + k_3 C_m \qquad [4.21]$$

where k_1, k_2 and k_3 are constants, P_{max} is the maximum cylinder pressure and C_m is mean linear piston speed.

With respect to the FMEP test results (fig. 4.19) it is clear that the model gave good agreement with experiments. Table 4.10 gives the numerical values of FMEP against P_{max} at peak torque and design point as extracted from test results given in table 4.5a.

To determine the factors in equation 4.21, the FMEP values relevant to constant C_m or constant P_{max} were used.

The value of k_2 was calculated based on using the FMEP values at constant engine speeds of 1260 and 2100 rpm at different loads. To work out an average value for k_2, each engine loading was taken as a reference for others to be compared with, one at a time. The formula is

$$k_2 = (FMEP_{ref} - FMEP)/(P_{max_{ref}} - P_{max}) \qquad [4.22]$$

The result of these calculations is presented in table 4.11. An average value of 0.005 for k_2 was then calculated.

To work out an average value for k_3 the same procedure as above (i.e. at constant P_{max} and two different speeds of 1260 and 2100 rpm) was applied. However, referring to fig. 4.19, since the motoring line seems to be an average line passing through the scattered FMEP values, its slope was used to yield k_3. A value of 0.139 $(\frac{bar}{m/sec})$ for k_3 was then calculated. As soon as k_2 and k_3 were determined k_1 was calculated using the FMEP values at full load as follows :

$$k_1 = FMEP - (0.005\ P_{max} + 0.139\ C_m) \qquad [4.23]$$

at 2100 rpm at full load:

FMEP = 1.448 bar

P_{max} = 129.3 bar

C_m = 9.52 m/s

k_1 = -0.522

at 1260 rpm at full load:

FMEP = 0.8793 bar

P_{max} = 97.73 bar

C_m = 5.712 m/s

k_1 = -0.328

In the end an adjusted value for k_3 was applied and the equation 4.21 in its specific form for the L10 engine was then considered to be :

$$FMEP = -0.5 + 0.005\ P_{max} + 0.139\ C_m \qquad [4.24]$$

where, as already implied, FMEP and P_{max} are in "bar" and C_m is in "m/sec".

In spite of the good agreement with experimental indicator diagram results given by this formula, as will be seen in section 4.8, the results given by the Willans line method were found to be preferable in order to achieve satisfactory predictions for BMEP. The results of the Willans method in terms of FMEP (bar) are also shown in fig. 4.19 which is an interpretation of the friction torque results shown in fig. 4.25. Fig. 4.19 shows that, not only the FMEP values, but also their rate of increase with engine speed based on the Willans method is higher than the values based on either motoring or the use of indicator diagrams for the running conditions along the LTC. However, in modifying equation 4.24 with respect to the Willans method results, the term representing the effect of cylinder pressure on the FMEP was retained as it is available only when using experimental indicator diagrams. The other two terms were, therefore, changed and the correlation based on the Willans line method was as follows :

$$FMEP = -0.375 + 0.005\ P_{max} + 0.15\ C_m \qquad [4.25]$$

4.7 COMPUTER RUNS BASED ON TUNED HEAT RELEASE AND FRICTION MODELS

The program "SPICE" together with the tuned Wiebe functions described in section 4.5 as heat release models and the modified Chen and Flyn friction model described in section 4.6, was used to simulate the Cummins L10-250 T/C Diesel engine. The different running conditions of load and speed were the same as those described in section 4.5.

Rate of fuel flow as one of the essential input values was interpolated linearly using the tables of experimental results (table 3.3 as a typical example) based on the torque levels given in table 4.5 at each running condition. However, as the fuel calorific value used in the input data was slightly different from the fluctuating experimental values, the interpolations of performance parameters based on the test results were modified in terms of the heat of combustion used in the computations.

Timing and combustion duration as the other basic input variables were based on the results of the Wiebe curve fitting summarised in table 4.8. The timing was taken as the start of combustion rather than injection timing. This was indeed a direct application of experimental heat release diagrams since insufficient information regarding injection timing versus fuelling was available. There was, therefore, no need to use any ignition delay model. Besides, the Wolfer model was not applicable to the semiquiescent type of combustion chamber. The heat transfer network was the same as that for the high swirl type of combustion chamber and coolant temperatures were based on experimental mean values.

As described in section 4.7 two sets of runs were performed based on the assumption of two different valve area maps both for the exhaust and the intake values. In the first set of runs, it was assumed that table 4.12 obtained from the manufacturer applies to a single intake and exhaust valve as in the case of the earlier runs for the high swirl type of combustion chamber (section 4.3), the values in table 4.12 being doubled when used for the four valve cylinder head. Finally to meet engine performance matching requirements, a scale factor of 0.45 was applied to both doubled intake and exhaust valve area maps, in a further set of runs. The implied ambiguity in the valve data as supplied is unfortunate.

4.8 NUMERICAL RESULTS, GRAPHICAL REPRESENTATION AND DISCUSSION

4.8.1 Results for Complete Engine-Turbocharger System

Tables 4.13 to 4.15 summarize the theoretical predictions (based on application of normal valve areas) and experimental results for the overall performance parameters of the L10-250 T/C engine.

Graphical representations of the results are given in figs. 4.29 to 4.52 for five running conditions at full load, viz. 1000, 1260, 1500, 1800 and 2100 rpm. Fig. 4.29 shows the fuelling schedule in terms of "mg/stroke" . Figs. 4.30 to 4.32 show the superimposed diagrams of the predicted in-cylinder conditions versus crank angle for the 5 points along the LTC as follows :

Fig. 4.30 Heat Release Rate
Fig. 4.31 Cylinder Temperature
Fig. 4.32 Cylinder Pressure

The slope of the leading edge of any heat release rate diagrams plays a major role in determining the rate of temperature increase. This slope is determined by the Wiebe shape factors, the value of fuel/shot and the burning duration. Since the combustion duration over the entire speed range - except at 1000 rpm where it is even shorter - remains constant (table 4.8) more fuel per cycle (fig. 4.29) results in a steeper leading edge for the heat release diagram as well as higher maxima as engine speed decreases. Slight differences in Wiebe shape factors (table 4.8) could also be taken into consideration, but they are of little effect. As shown in figs. 4.30 and 4.31 a higher slope of heat release rate causes a higher rate of cylinder temperature increase. However, the higher maximum temperature of the in-cylinder gases can be regarded as mainly due to higher injected fuel mass per cycle. The variation of cylinder temperature after combustion also follows the same trend as the heat release rate, descending from different maxima at different engine speeds.

As given in table 4.13 boost pressure ratio increases with engine speed and, as a result maximum cylinder pressure is expected to follow the same

trend. However, the lower rates of temperature rise counteract this effect. Hence, as shown in fig. 4.32, cylinder pressure-crank angle diagrams at different engine speeds are quite separate during compression stroke due to differences in boost pressure ratio, but they nearly coincide as soon as combustion starts. Therefore, the maxima of cylinder pressure unlike cylinder temperature are confined within a narrow range.

Figs. 4.33 and 4.34 show BMEP and brake thermal efficiency, each comparing predicted and measured results. The brake thermal efficiency shows maxima of 43.8% and 42.5% in the mid speed range of 1500 rpm to 1800 rpm, for the theoretical and experimental results respectively. Limited variation of the brake thermal efficiency above an engine speed of 1260 rpm (in particular with simulation results) makes the BMEP follow the same trend as that for the fuelling schedule (fig. 4.29). Hence torque back up as measured by BMEP is about 19% as against 18% increase in the extent of fuel per cycle at 60% of the design speed. However, any discrepancy between BMEP and fuelling within this speed range can be ascribed to differences in the brake thermal efficiencies from one engine speed to another.

As shown in fig. 4.33 an average downward shift of 0.37 bar is needed to match the predicted BMEPs with experimental results. Several alternatives are available; one being a revision of the heat transfer network. Fig. 4.35 shows the predicted and measured specific heat rejection in terms of Btu/Hp.min of the engine under investigation. No major adjustment of the heat network is demanded, particularly as only a fraction of any change in heat loss (about the value of thermal efficiency $\simeq$ 0.4) affects the output efficiency.

Another possible way of lowering BMEP values (particularly at a constant average value) is the use of higher FMEP values. This has already been done in applying one of the two friction correlations presented in section 4.6 (that due to Willans method (eqn. 4.25) with higher FMEP predictions (fig. 4.36) was used). Referring to eqn. 4.25, the first term implying a constant FMEP over the entire range of engine operating conditions is attributed to overhead friction such as accessories. Nevertheless, a positive value would be expected for this term, rather

than a negative one. On the other hand, the average demanded decrease in BMEP of 0.37 bar could well bring the constant term in the FMEP correlation (eqn.4.25) down to zero, this being more acceptable than a negative value.

Before further discussion on the FMEP modification, another modification was considered as having the potential of resolving some other problems. Fig. 4.37 shows air-fuel ratio based on both simulation and experiments. Except at an engine speed of 1000 rpm with a probable theoretical overestimate and experimental underestimation, the simulation yielded an average of 7.5% (about 1.8 points of air-fuel ratio) excess air flow over experimental results. As shown in fig. 4.38 the predicted exhaust gas temperature is about 6% (about 45 deg.K) less than that of the test results, which is a direct consequence of the higher predicted air-fuel ratio along the speed range. Looking into the inlet and exhaust pressure levels (table 4.13) reveals that, although the predicted pressure drop across the engine is generally lower than that in test results, calculated air flow through the engine is higher. This led to some doubt as to whether the correct valve area map had been used. Figs. 4.39 and 4.40 show the predicted and experimental operating lines superimposed on the compressor and turbine maps. Provided that a correct turbine and compressor map is applied, there would remain no other cause for high air throughput beyond the expected level rather than excessive valve areas.

Figs. 4.41 and 4.42 show the trends of the PMEP and volumetric efficiency respectively. Each of the figures contains the predicted and measured values and indicate that the discrepancies are not very big.

Although the reduction in valve areas as planned was liable to make the above discrepancies bigger, it could result in some decrease in air flow through the engine and hence higher predicted exhaust gas temperatures, both in line with what was required for a better match with experimental results.

Scaling of the valve areas was carried out by the application of a scale factor of 0.45 for both intake and exhaust valves. Some adjustments of cooler pressure drop and effectiveness were made so as to provide similar

inlet manifold conditions for simulation as reported in the experimental results.

Tables 4.16 to 4.18 give the simulation results based on reduced valve areas for the same eleven running conditions as in section 4.5. Again the same turbine and compressor map as before were applied. The heat release diagrams shown in fig. 4.30 are essentially valid for the new runs since the same combustion information given in table 4.8 was used. Figs. 4.43 and 4.44 show the variations of in-cylinder gas pressure and temperature during a cycle. The trends of these variables are very similar to those for the earlier runs when the valve areas were not subject to reduction. However, the maximum cylinder pressure as shown in fig. 4.45 is now much closer to test results whereas the maximum temperature particularly at the lower speeds has increased (fig. 4.44).

Fig. 4.37 shows that the predicted air flow is now in better agreement with the test results as is also the exhaust gas temperatures (fig. 4.38). The variation of the volumetric efficiency is shown in fig. 4.42, where a considerable decrease over the speed range is evident. As is shown in fig. 4.41, the PMEP values have undergone a substantial decrease with increase in engine speed, over and above experimental values because of the reduction in valve areas.

BMEP's are now very much in line with test results (fig. 4.33). As shown in fig. 4.34 calculated brake thermal efficiency is now also in good agreement with test results.

Fig. 4.47 and 4.48 show the predicted and experimental operating lines on the compressor and turbine maps. The lines on the compressor map coincide more closely than those on the turbine map which implies that the predicted operating conditions for the compressor are more realistic than those for the turbine. This of course may be regarded as a consequence of the reduced valve areas, particularly as the predicted pressure ratios are higher than test results. Reference to the similar maps and operating lines shown in figs. 4.39 and 4.40 (when normal valve areas were applied) reveals similar discrepancies; however, the above explanation is not available in this case.

It is worth noting that the last results given in table 4.16 show good agreement between the predicted and experimental speed and air flow for the turbocharger but not the pressure ratios. This can only be explained in terms of discrepancies between the actual and assumed compressor and turbine maps.

The distance between operating lines on each of the maps shown in figs. 4.47 and 4.48 indicates that either the applied compressor map in the simulation should be scaled down or the turbine map should be scaled up to obtain better agreement. Nevertheless, as the inlet manifold conditions both in the simulation results and those of the experiments are closely comparable, the engine performance parameters themselves could be studied excluding turbocharger and charge cooler operating conditions to investigate whether different aspects of the engine are well modelled. This is done in the following.

4.8.2 Results for engine alone

In the case of the result of energy balance calculation given in table 4.16 the system boundary (# 1) encloses only the engine even without its manifolds. Therefore, the gas conditions entering and leaving the system are considered to be those in the intake and exhaust manifolds (fig. 4.49).

The heat to coolant as a part of the energy balance is made up of the engine friction and apparently the engine heat transfer. The calculation of the exhaust gas energy is based on the difference between the enthalpies of the exhaust gas (before entering the turbine) and the fresh air leaving the inlet manifold. Fig. 4.49 shows how the exhaust gas energy is evaluated for the two alternative system boundaries.

The present method focuses attention on the engine itself, by excluding the running conditions of the turbocharger and also the heat transfer from intercooler and exhaust manifolds. All the percentage values in the energy balance are based on the total energy input crossing the system boundary (# 1) including the air enthalpy of engine intake above that of ambient condition. Figs. 4.50 to 4.52 show the exhaust gas energy, engine

heat loss and shaft work respectively. The percentage value of shaft work is now slightly lower than the brake thermal efficiency which is still based on taking the complete system, i.e. with the turbocharger and cooler inside the system boundary (# 1).

4.9 IN-CYCLE PHENOMENA DURING OPEN PERIOD

Use of the 'filling and emptying' method in the program "SPICE" based on small crank angle increments makes it possible to investigate in detail different phenomena occurring in a cycle. To examine in-cycle processes during the open period two sets of graphical representation of variations of different variables versus crank angle at peak torque running condition (1260 rpm) and at the design point (2100 rpm) have been prepared which are denoted by a and b on figure numbers respectively. In this investigation, the simulation of the L10-250 engine with reduced valve sizes are considered. Figs. 4.53 and 4.55 show the variation of pressure and temperature in the cylinder and inlet and exhaust manifold. Fig. 4.54 shows the P-v diagram.

The intake and exhaust valve flow data are shown in figs. 4.56 to 4.58 viz. fig. 4.56 shows variations of valve areas and pressure ratios, fig. 4.57 shows variations of Mach number and gas velocity through the valves and fig. 4.58 shows variations of mass flow rate through the valves.

On figs. 4.53 to 4.58 points of particular interest are denoted by capital letters with suffices c, i and e denoting cylinder, inlet and exhaust manifolds.

The open period starts at EVO as a continuous sequence of gas exchange processes. Referring to program "SPICE", since the firing TDC is taken as zero crank angle position, EVO of the L10 engine occurs at 135 deg. (point A, A_e or A_c). At this point since the pressure ratios across the exhaust valves (fig. 4.56) lie considerably above the critical (5.2 and 4.2 c.f. approx. 1.7), the exhaust flow occurs initially in the supercritical range. When the exhaust valves are first open, although velocities are high (sonic velocity in fig. 4.57), there is very little flow, due to the initially very small apertures (fig. 4.56), so that no sudden drop of pressure occurs within the cylinder (fig. 4.54). This condition persists from point A to point B quite close to point C at BDC where Mach number (fig. 4.57) first departs from the value of 1. During this period, in-cylinder gas temperature (fig. 4.55) drops about

150 deg.K which causes a decrease in exhaust gas velocity (fig. 4.57). Since a certain time is essential for the acceleration of the gases in the exhaust manifold, it also follows that, from point A_e to B_e, the inflow of gases from the cylinder will be more rapid than the outflow of the gases through the turbine.

It is desirable to open the exhaust valve as fast as possible. This not only ensures that the cylinder is at a lower pressure when the piston starts moving upward (lower pumping work), but also increases the energy available to the turbine. In such a case exhaust manifold peak pressure is expected to take place before BDC; this has not been achieved with the L10 engine (fig. 4.53) in particular at reduced valve areas, the design engine speed of 2100 rpm.

The second part of blowdown occurs in the subsonic range (fig. 4.57) with throttling, between points B_e and D_e where the exhaust peak pressure also occurs (fig. 4.53), and in the cylinder between points B_c and D_c, producing a gradual transition from the expansion line to the exhaust pressure line.

In the next phase of the exhaust action which occurs at subcritical pressure ratio between points D and E in fig. 4.57 there occurs, in most cases, a simultaneous expansion both in the cylinder and in the exhaust manifold, so that there is a common pressure drop with slightly higher pressure in the cylinder of the order of approx. 0.1 to 0.15 bar caused by the throttling effect (fig. 4.53). This subcritical flow process takes place during the wide open period of the exhaust valve (fig. 4.56). In an ideal case this process is expected to be accomplished as fast as possible to contribute to lowering pumping losses and can be more clearly seen at low engine speed of 1260 rpm (fig. 4.53a) rather than at the design speed of 2100 rpm (fig. 4.53b).

Since the cylinder pressure does n ot fall after the point "E" during the exhaust stroke, this point may be regarded as the end of the extended blowdown period. With restricted exhaust apertures, this process often covers the greater part of the exhaust stroke which in the case of the

L10-T/C engine is approximately 60% of the exhaust open period.

Corresponding to these pressure variations of the exhaust gases there are temperature variations which are shown in fig. 4.55. Although not predicted by the exhaust discharge equation, flow through the exhaust valve and also into the exhaust pipe is accompanied by a process of transformation of kinetic energy into heat, due to turbulence similar to throttling. At the same time, however, due to the high velocity, there is intense heat transfer to the walls.

As shown in fig. 4.56, from point E, i.e. end of blowdown, to point F i.e. inlet opening, the exhaust valve is rapidly closing while piston speed decreases from its maximum. This combination leads to almost constant cylinder pressure at the low engine speed of 1260 rpm (fig. 4.53,a). However, at 2100 rpm the flow rate through the closing exhaust valve is so small relative to piston displacement that as shown in fig. 4.53,b a compression like process occurs in the cylinder. On the other hand, the trapped gases at design point running condition is 1.09 times of that at peak torque (table 4.16).

As soon as the intake valves open (at point F, at crank position of 341 deg), the scavenging process starts. Satisfactory combustion chamber scavenging depending very largely on the extent of valve overlap. With small overlap, as is the case with the L10 engine (EVC-IVO = 22 deg. ca.) the time available is so small that only a small quantity of air is scavenged through. As shown in table 4.16, the scavenge ratio over the speed range is about 1.007. As fig. 4.53,a shows at low engine speed (1260 rpm), even with this small overlap, there is little compression caused by throttling at the end of the exhaust stroke. However, this condition no longer exists when engine speed increases. Fig. 4.53b shows the adverse effect of small overlap in causing in-cylinder compression at high engine speed (2100 rpm). As a result, not only is there no scavenging flow but also, as shown in fig. 4.57,b, there is back flow from the cylinder into the inlet manifold. From the point of IVO, in-cylinder gas temperature starts to fall (fig. 4.55,a) due to scavenging while gas velocity through the exhaust valves increases (fig. 4.57,a) due to the increasing pressure drop (fig. 4.56,a). Therefore,

exhaust gas Mach number has a relatively sharp rise during the overlap period due to this double effect at the engine speed of 1260 rpm, because of the considerable pressure difference across the intake valves, intake flow starts with higher velocity.

After the point of EVC, at both engine speeds (1260 and 2100 rpm), cylinder temperature approaches that of the inlet manifold as more fresh air mixes with exhaust residual gases; however, it never falls to the inlet manifold temperature (fig. 4.55). The most interesting fact is that the air velocity passing through the intake valves is almost proportional to engine speed (fig. 4.57) when adjusted by the pressure difference created across the valves, (fig. 4.53), by the piston speed

$$\left(\text{i.e. } \frac{105}{175} \text{ m/s} = \frac{1260}{2100} \text{ rpm}\right).$$

The trend of cylinder pressure at the design speed of 2100 rpm between points E_c and J_c in fig. 4.53,b is undesirable since it shows excessive compression during the exhaust period (from point E_c to H_c) and an excessive depression during the intake period (from point H_c to J_c). On the other hand the maximum pressure in the exhaust manifold occurs undesirably after BDC during the upward movement of the piston. These facts justify the assumption that the valve area maps given in table 4.12 refers to a single valve.

The trends of pressure variations at the design speed but with valve area maps based on twice those in table 4.12 are shown in fig. 4.53,c. As is seen in other part of this figure, the trends of Mach number of the flows through the exhaust and intake valves are quite reasonable, the undesirable cylinder pressure variations as described above are avoided, and maximum pressure in the exhaust manifold again occurs at about BDC.

4.10 CONCLUSION

The discussion in sections 4.8 and 4.9 suggests that the simulation results (table 4.13) for the L10-T/C engine are based on inaccurate turbine and valve area maps. However, as soon as the intake manifold condition and air flow through the engine are adjusted in the simulation to match those of test results, an excellent match of maximum cylinder pressure (fig. 4.45), exhaust temperature (fig. 4.38) and of the different components of the energy balance is achieved.

Thus the program "SPICE" has been matched in all important aspects to the L10 engine itself, therefore providing a sound basis for all subsequent detailed matching studies concerned with the DCE configuration.

	EXP.	SPICE	EXP.	SPICE	EXP.	SPICE	EXP.	SPICE	EXP.	SPICE
ENG. RUN. COND.										
Nom Speed RPM	1000.00	1000.00	1200.00	1200.00	1600.00	1600.00	1900.00	1900.00	2100.00	2100.00
Load %	100.00	100.00	100.00	100.00	100.00	100.00	100.00	100.00	100.00	100.00
Fuel Flow kg(lb)/h	(36.40)	16.51	(53.50)	24.26	(64.60)	29.30	(96.80)	43.90	(98.70)	44.76
Fuel/Shot mg	91.70	91.70	112.00	112.00	102.00	102.00	128.00	128.00	118.00	118.00
Timing BTDC deg		17.00		17.00		17.00		17.00		17.00
ENGINE RESULTS										
Torque N.m	751.52	704.73	937.10	891.27	865.40	834.37	1106.00	1080.58	1000.67	974.03
Brk. Power kW	78.7	73.8	117.76	112.0	145.00	139.8	220.06	215.0	220.06	214.2
BMEP bar	9.4	8.8	11.7	11.2	10.88	10.5	13.87	13.6	12.52	12.2
Brk Th Eff %	40.70	37.67	41.40	39.19	42.40	40.08	42.90	41.36	42.10	40.46
BSFC g/kWh	209.90	223.3	206.20	214.6	202.00	209.9	199.42	203.4	203.10	207.9
*										
Max Cyl P bar		111.		127.		131.		165.		156.
Max Cyl T K		1892.		1991.		1855.		1886.		1843.
*										
Air Flow kg/min	4.95	6.98	8.54	9.36	12.85	13.77	19.55	20.53	20.63	21.89
Ovrl. A/F Ratio	18.0	25.40	21.10	23.15	26.30	28.21	26.85	28.07	27.70	29.34
*										
Inl Man P bar	1.33	1.34	1.48	1.52	1.63	1.71	2.04	2.20	2.17	2.15
Exh Man P bar		1.21		1.37		1.57		2.04		2.11
Inl Man T degK	325.00	329.00	326.00	331.00	331.00	333.00	337.00	337.00	340.00	337.00
Exh Man T degK	735.00	703.00	790.00	775.00	791.00	745.00	821.00	784.00	815.00	780.00
TURBOCHARGER										
Speed RPM	50520.00	50609.00	60950.00	61137.00	70150.00	70257.00	88320.00	88393.00	90620.00	88510.00
Turb Power kW		4.9/4.8		9.6/8.8		17.0/16.4		39.7/37.4		42.6/39.1
*										
Turb PR -	1.22	1.29	1.32	1.48	1.45	1.68	1.73	2.16	1.81	2.20
Turb Eff %	53.00	59.50	54.00	53.81	55.00	60.79	56.00	66.12	54.00	67.01
*										
Comp PR -	1.31	1.40	1.48	1.58	1.65	1.77	2.12	2.28	2.16	2.22
Comp Eff %	63.00	73.51	66.00	74.66	71.00	75.18	72.00	72.99	72.00	72.00
BALLANCES										
Mass Flow -	--	1.00	--	1.00	--	1.00	--	1.00	--	1.00
T/C Power -	--	1.02	--	1.09	--	1.03	--	1.06	--	1.08
Energy : -	--	.997	--	1.00	--	1.00	--	1.00	--	1.00
Coolant %	24.80	28.34	25.00	24.83	23.30	21.28	23.00	20.15	23.30	19.50
Exhaust %	21.30	28.14	28.10	29.95	31.00	30.99	32.40	31.01	32.90	31.38
Work %	40.70	37.67	41.50	39.19	42.40	40.07	43.00	41.35	42.10	40.46
Friction %	--	6.09	--	5.77	--	7.53	--	7.19	--	8.14
Unaccuntd. %	13.2	--	5.4	--	3.3	--	1.6	--	1.7	--

Table 4.1 Comparison between the ' SPICE ' predictions, based on use of the WATSON high swirl heat release model, with experimental results for CUMMINS L10.290-T/C egine at full load running conditions

(Timing = 17 deg.BTDC)

	EXP.	SPICE	EXP.	SPICE	EXP.	SPICE	EXP.	SPICE	EXP.	SPICE
ENG. RUN. COND.										
Nom Speed RPM	1000.00	1000.00	1200.00	1200.00	1600.00	1600.00	1900.00	1900.00	2100.00	2100.00
Load %	100.00	100.00	100.00	100.00	100.00	100.00	100.00	100.00	100.00	100.00
Fuel Flow kg(lb)/h	(36.40)	16.51	(53.50)	24.26	(64.60)	29.30	(96.80)	43.90	(98.70)	44.76
Fuel/Shot mg	91.70	91.70	112.00	112.00	102.00	102.00	128.00	128.00	118.00	118.00
Timing BTDC deg		8.00		8.00		8.00		8.00		8.00
Burn Dur Angle		125.00		125.00		125.00		125.00		125.00
ENGINE RESULTS										
Torque N.m	751.52	753.43	937.10	945.37	865.40	866.60	1106.00	1115.75	1000.67	1001.30
Brk. Power kW	78.7	78.9	117.76	118.8	145.00	145.2	220.06	222.0	220.06	220.2
BMEP bar	9.4	9.45	11.7	11.9	10.88	10.9	13.87	14.0	12.52	12.6
Brk Th Eff %	40.70	40.00	41.40	41.27	42.40	41.65	42.90	42.58	42.10	41.53
BSFC g/kWh	209.90	210.0	206.20	203.8	202.00	202.0	199.42	197.5	203.10	202.5
*										
Max Cyl P bar		94.		107.		110.		137.		129.
Max Cyl T K		1800.		1908.		1765.		1796.		1759.
*										
Air Flow kg/min	4.95	7.17	8.54	9.62	12.85	14.07	19.55	20.90	20.63	22.15
Ovrl. A/F Ratio	18.0	26.00	21.10	23.80	26.30	28.80	26.85	28.56	27.70	29.70
*										
Inl Man P bar	1.33	1.34	1.48	1.51	1.63	1.69	2.04	2.17	2.17	2.11
Exh Man P bar		1.20		1.35		1.54		1.96		2.01
Inl Man T degK	325.00	321.00	326.00	322.00	331.00	324.00	337.00	328.00	340.00	328.00
Exh Man T degK	735.00	710.00	790.00	780.00	791.00	743.00	821.00	781.00	815.00	778.00
TURBOCHARGER										
Speed RPM	50520.00	50572.00	60950.00	61110.00	70150.00	70151.00	88320.00	88346.00	90620.00	88465.00
Turb Power kW		5.2/4.9		10.0/8.9		16.9/16.5		38.9/37.5		41.2/39.
*										
Turb PR -	1.22	1.29	1.32	1.47	1.45	1.65	1.73	2.10	1.81	2.12
Turb Eff %	53.00	59.83	54.00	53.81	55.00	58.70	56.00	64.57	54.00	65.65
*										
Comp PR -	1.31	1.40	1.48	1.58	1.65	1.76	2.12	2.25	2.16	2.18
Comp Eff %	63.00	74.27	66.00	75.33	71.00	75.32	72.00	72.70	72.00	71.08
BALLANCES										
Mass Flow -	--	1.00	--	1.00	--	1.00	--	1.00	--	1.00
T/C Power -	--	1.07	--	1.12	--	1.02	--	1.03	--	1.05
Energy : -	--	1.00	--	1.00	--	1.00	--	1.00	--	1.00
Coolant %	24.80	24.16	25.00	21.70	23.30	19.40	23.00	18.58	23.30	18.16
Exhaust %	21.30	29.34	28.10	31.32	31.00	32.02	32.40	31.96	32.90	32.34
Work %	40.70	40.03	41.50	41.26	42.40	41.65	43.00	42.58	42.10	41.53
Friction %	--	5.69	--	5.39	--	7.13	--	6.75	--	7.69
Unaccuntd. %	13.2	--	5.4	--	3.3	--	1.6	--	1.7	--

Table 4.2 Comparison between the ' SPICE ' predictions, based on using the WATSON high swirl heat release model, with experimental results for the CUMMINS L10.290-T/C engine at full load running conditions

(Timing = 8 deg.BTDC)

Eng.Speed (rpm)		1000	1200	1600	1900	2100
Fuel/Shot (mgr)		91.7	112.	102.	128.	118.
[TIMING]						
Inlet Pm (bar)	17	1.34	1.52	1.71	2.20	2.15
	8	1.34	1.51	1.69	2.17	2.11
Inlet Tm (k)	17	329.	331.	333.	337.	337.
	8	321.	322.	324.	328.	328.
Scav. Ratio	17	1.0180	1.0140	1.0089	1.0083	1.0083
	8	1.0175	1.0120	1.0088	1.0085	1.0087
Vol.Eff (%)	17	97.0	96.5	95.3	94.1	93.0
	8	97.5	96.9	95.7	94.5	93.5
Trap. A/F Ratio	17	25.3	23.1	28.1	28.0	29.4
	8	25.9	23.6	28.7	28.5	29.7
PmID (bar)	17	42.8	48.6	54.3	69.8	67.7
[During Ign.Delay]	8	55.9	63.4	71.1	90.1	87.6
TmID (k)	17	890.	906.	909.	929.	929.
[During Ign.Delay]	8	923.	938.	945.	963.	966.
Ign.Delay (msec)	17	0.83	0.70	0.60	0.45	0.46
	8	0.57	0.48	0.42	0.32	0.32
Ign.Delay (deg)	17	4.97	5.02	5.78	5.15	5.75
	8	3.40	3.45	4.05	3.59	4.08
Crank Ang.Comb.	17	-12.0	-11.9	-11.2	-11.8	-11.2
	8	- 4.6	- 4.5	- 3.9	- 4.3	- 3.8
Beta	17	0.2099	0.1457	0.1738	0.1096	0.1274
	8	0.1352	0.0660	0.1012	0.0284	0.0504
Pmax (bar)	17	111.	127.	131.	165.	156.
	8	94.	107.	110.	137.	129.
Crank Ang. at Pmax	17	+4.0	+5.0	+5.0	+6.0	+6.0
	8	+8.0	+9.0	+9.0	+9.0	+9.0
Tmax (k)	17	1892.	1991.	1855.	1886.	1843.
	8	1800.	1908.	1765.	1796.	1759.
Gross IMEP (bar)	17	10.01	12.67	12.25	15.80	14.76
	8	10.60	13.14	12.51	16.03	14.89
PMEP (bar)	17	0.19	0.23	0.15	0.11	-0.06
	8	0.21	0.26	0.19	0.17	0.01
Net IMEP (bar)	17	10.2	12.9	12.4	15.9	14.7
	8	10.8	13.4	12.7	16.2	14.9
FMEP (bar)	17	1.43	1.65	1.97	2.36	2.46
	8	1.34	1.55	1.86	2.22	2.32
BMEP (bar)	17	8.77	11.25	10.43	13.54	12.24
	8	9.46	11.85	10.84	13.98	12.58
G.Ind.Th.Eff (%)	17	43.00	44.14	47.07	48.26	48.79
	8	44.82	45.76	48.06	48.82	49.15
N.Ind.Th.Eff (%)	17	43.81	44.93	47.65	48.57	48.59
	8	45.66	46.67	48.79	49.34	49.19
Mech.Eff. (%)	17	86.08	87.16	84.19	85.20	83.26
	8	87.56	88.54	85.38	86.32	84.38
Brk.Th.Eff. (%)	17	37.67	39.19	40.08	41.36	40.46
	8	40.00	41.27	41.65	42.58	41.53
	exp.	40.70	41.50	42.40	43.00	42.10

Table 4.3 Comparison of the ' SPICE ' predictions based on using the WATSON-MARZOUK high swirl heat release model at two at two different injection timings for the CUMMINS L10.290-T/C Diesel engine

ENGINE CONFIGURATION

ENGINE MODEL Blue #5 TEST CELL 104

ENGINE SERIAL NO. 10601833 BUILD NO. 29

SAME AS BUILD 25

	HOURMETER	DATE
TEST START	8112.9	2/20/78
TEST END	8128.0	3/6/78

COMPONENT	PART NO.	COMMENT
PISTON	3008937A	Hi Ring Cast Iron COMP.RATIO 16.3
RING COMP		A9558
INT	3009433A	1/8 Grooved Back/B1200
OIL	3009434A	Low Tension 13 Pounds (Koppers)
CYLINDER HEAD	3008485	#6 Cylinder Pressure
CAMSHAFT	3013958	F1144 Beryllium Copper Push Rod

CAM TIMING .120 /.2032 DYNAMIC TIMING 17° BTC

VALVE LASH: INTAKE .040 EXHAUST .040

INJECTOR ADJUSTMENT 7 inch pounds @75° ATC

INJECTOR: SPRAY HOLES 10 - .006 - 12 °

NOZZLE FLOW 147 PPH

TOPSTOP SETTING .220

CALIBRATION FLOW 110 CC AT 1000 STROKES

TURBO ASSEMBLY H2C H3 267 NOZZLE AREA 3.25 TRIM T2

FUEL PUMP CODE OPEN

COMMENTS: Biomation Cylinder Pressure and Exhaust Pressure Runs #1 to 20

SUMMARY OF RESULTS

EP.TESTOP DATA	
RPM	KEY
2100	530
1260	550
TQ CRV	510

	RPM	BHP	BSFC
RATED	2100	250	.329
TORQUE PEAK	1260	180	.337

EMISSION TEST NO. _____

$BSNO_2$ _____ BSHC _____

COLD START PPM AT 20 MIN. _____

Table 4.4 Typical engine configuration data sheet for the L10-T/C engine (obtained from the manufacturer)

TABLE I

BIOMATION DATA SUMMARY

INDICATED MEAN EFFECTIVE PRESSURES

TEST CELL 104 3/6/78 H3-267(3.25)T2 TURBO

BIOMATION RUN NO.	SPEED (RPM)	LOAD (LB_F-FT)	BMEP (PSI)	IMEP CASHIFT=0 (PSI) [FMEP]	IMEP CASHIFT=.874 (PSI) [FMEP]	PEAK CYL PRESSURE (PSI) AC ONLY
10	2100	625	153.6	160.6 [7.0]	174.6 [21.0]	1874
1	2100	470	115.4	123.3 [7.9]	134.9 [19.5]	1503
12	2100	310	76.0	83.0 [7.0]	92.3 [16.3]	1154
13	2100	160	39.0	46.2 [7.2]	53.8 [14.8]	913
14	1800	700	172.1	175.4 [3.3]	189.2 [17.1]	1915
15	1500	750	184.4	186.7 [2.3]	200.0 [15.6]	1915
16	1260	750	184.4	184.4 [0]	197.1 [12.7]	1853
17	1260	560	137.6	139.4 [1.8]	149.4 [11.8]	1617
18	1260	375	92.0	93.2 [1.2]	101.0 [9.0]	1031
19	1260	190	46.3	47.7 [1.4]	53.9 [7.6]	739
20	1000	700	172.2	170.8 [-1.4]	182.3 [10.1]	1740

(a)

TABLE II

BIOMATION DATA SUMMARY

INDICATED MEAN EFFECTIVE PRESSURES

TEST CELL 104 3/7/78 & 3/8/78 H3-267(3.6)T3 TURBO

BIOMATION RUN NO.	SPEED (RPM)	LOAD (LB_F-FT)	BMEP (PSI)	IMEP CASHIFT=0 (PSI) [FMEP]	IMEP CASHIFT=.874 (PSI) [FMEP]	PEAK CYL PRESSURE (PSI) AC ONLY
21	2100	625	153.6	161.1 [7.5]	174.0 [20.4]	1730
22	2100	470	115.5	123.4 [7.9]	134.0 [18.5]	1372
23	2100	310	76.0	83.4 [7.4]	92.0 [16.0]	1051
24	2100	160	39.0	46.0 [7.0]	53.0 [14.0]	848
25	1800	700	172.2	173.7 [1.5]	186.6 [14.4]	1792
26	1500	750	184.4	181.5 [-2.9]	194.3 [9.9]	1849
27	1260	750	184.4	180.1 [-4.3]	192.4 [8.0]	1825
28	1260	560	137.5	138.6 [1.1]	148.3 [10.8]	1378
29	1260	375	92.0	93.7 [1.7]	101.3 [9.3]	1007
30	1260	190	46.4	47.6 [1.2]	53.6 [7.2]	714
31	1000	700	172.2	168.1 [-4.1]	179.6 [7.2]	1740

(b)

Table 4.5 Data summary for experimental MEPs of the L1O-T/C engine based on two different turbine swallowing capacities

BIOMATION DATA SUMMARY

PUMPING MEAN EFFECTIVE PRESSURES

TEST CELL 104 3/6/78 H3-267(3.25)T2 TURBO

BIOMATION RUN NO.	CALC IMEP 0-180° (PSI)	CALC IMEP 540-720° (PSI)	NET PUMPING (PSI)
10	7.83	-7.67	.16
11	6.49	-8.37	-1.88
12	3.74	-7.28	-3.54
13	2.85	-7.71	-4.86
14	10.94	-10.31	+ .63
15	11.06	- 4.63	6.43
16	12.90	- 5.96	6.94
17	7.23	- 3.55	3.68
18	4.71	- 2.85	+1.86
19	1.78	- 1.87	- .09
20	13.86	- 6.94	+6.92

(a)

BIOMATION DATA SUMMARY

PUMPING MEAN EFFECTIVE PRESSURES

TEST CELL 104 3/7/78 & 3/8/78 H3-267(3.6)T3 TURBO

BIOMATION RUN NO.	CALC IMEP 0-180° (PSI)	CALC IMEP 540-720° (PSI)	NET PUMPING (PSI)
21	7.43	-5.84	+1.59
22	4.85	-5.38	- .53
23	2.82	-5.30	-2.48
24	1.89	-6.00	-4.11
25	8.09	-7.59	+ .5
26	10.69	-5.98	4.71
27	12.39	-6.36	6.03
28	7.24	-3.28	3.96
29	3.93	-2.25	1.63
30	1.74	-1.57	.17
31	15.71	-9.48	6.28

(b)

Table 4.6 Data summary for experimental PMEPs of THE L1O-T/C engine based on use of two different turbine trims

L10 Injection System

(from oscill.photos)

Configuration	Speed/Load (rpm/ft-lb)	Injection Pressure (psia)	Cylinder Pressure (psia)	Fueling (Cu.MM.)	Injection Start of (^{O}btc)	Injection Duration (ca^{O})
•Turbocharged Only	2100/625	13300	1880	121.1	18	27
•H2C 8640 U22Q3	1800/700	11300	1960	132.0	20	27
•Bohn mid-rg pist.(15.1 CR)	1500/750	9800	2020	142.9	20	26
•.070/.2032 st.tim.	1260/750	7400	1960	148.7	19	24
• F1170 Cam 3/8 in.PTD DFF	1000/700	4900	1800	146.1	19	23
•10-.0065-12 (180 pph flow)						
Same Except	2400/525	15000	1860	109.1	-	-
•H2C 8650 U22Q3	2100/625	14200	2000	121.8	-	-
•Bohn mid-rg pist. (15.9 CR)	1800/684	12200	1940	131.3	-	28.1
•.080/.2032	1500/740	10400	1970	142.3	-	26.1
	1300/750	8300	1920	148.5	-	26.5
	1000/700	6100	1720	146.7	-	26.4

Table 4.7

CUMMINS L10-250 T/C DIESEL ENGINE
RESULTS OF USING WIEBE FUNCTION AS HEAT RELEASE MODEL

ENG-SPEED RPM	LOAD %	FUEL/SHOT mg	COMB-TIM DEG-BTDC	COMB-DUR DEG	A/F	C1	C2
1000	100	116.4	17.0	52.5	21.9	1.35	6.75
1260	100	120.4	18.0	62.5	23.2	1.35	7.00
	75	90.0	12.0	52.5	27.2	1.35	7.00
	50	62.2	8.0	50.0	34.8	1.40	7.25
	25	35.8	4.5	47.5	54.2	1.40	7.00
1500	100	117.7	17.0	62.5	25.8	1.35	7.25
1800	100	110.1	16.5	62.5	28.6	1.40	7.00
2100	100	101.4	15.5	62.5	32.3	1.40	7.00
	75	79.4	12.3	60.0	36.1	1.40	7.25
	50	56.7	9.0	52.5	42.9	1.50	6.75
	25	35.5	5.0	50.0	58.4	1.50	7.00

Table 4.8

COMPARISON OF DCS RESULTS
FOR BLUE ENGINE AT
2100 RPM, 1/4 LOAD

	2100 RPM FULL LOAD HEAT RELEASE	2100 RPM 1/4 LOAD HEAT RELEASE	1250 RPM FULL LOAD HEAT RELEASE	
FUEL RATE	1.36	1.36	1.36	BTU/CYL/CYCLE
AIRFLOW	4.78	4.79	4.78	LBS/CYL/MIN
BSFC	.500	.500	.492	LBS/BHP/HR
BMEP	34.7	34.7	35.2	LBS/IN^2
PMEP	8.2	8.2	8.2	LBS/IN^2
IMEP	49.5	49.5	50.0	LBS/IN^2
EXHAUST TEMPERATURE	1003	994	1004	^oR
PEAK CYLINDER PRESSURE	884	869	901	LBS/IN^2
C.A. OF P.C.P.	365	365	366	$^oC.A.$

Table 4.9

ENG.SPEED [rpm]	FMEP [bar]	Pmax [bar]
2100.0	1.448	129.30
	1.345	103.65
	1.121	79.58
	1.017	62.96
1260.0	0.879	127.80
	0.810	97.73
	0.621	71.10
	0.534	50.96

Table 4.10 Selected FMEP values from table 4.5,a

k2					
@ 2100 rpm			@ 1260 rpm		
		-	-		
	-	0.0041	0.0023	-	
-	0.0093	0.0065	0.0045	0.0071	-
0.0066	0.0080	0.0065	0.0045	0.0059	0.0043

Table 4.11 Result of calculation for k2

```
13:32 OCT 15 '85 EXH-L10-V1188-026.CR81RMB

C='V1188 Entered by CR81RMB .BROOKS   at 14:56 SEP 25, 85                    ',
C='Exhaust valve for the L10       engine family.                            ',
C='Valve lash setting -> 026                                                 ',
C='Flow area data used:                                                      ',
C='Lift ->     .000   .100   .200   .300   .400   .500   .600                ',
C='Area ->     .000   .700  1.080  1.340  1.500  1.560  1.590                ',
C='Peak valve lift =  .5011 at 605.3 c.a. ',
NPTS=115, CAINC=2.0, CABEG= 495.3, UNITS='ENGLISH',*END*
   .0000   .0034   .0471   .1195   .1597   .1929   .2666   .3464
   .4004   .4676   .5657   .6553   .7162   .7678   .8282   .8800
   .9292   .9887  1.0496  1.0949  1.1316  1.1731  1.2120  1.2464
  1.2834  1.3220  1.3500  1.3698  1.3910  1.4115  1.4294  1.4472
  1.4656  1.4823  1.4972  1.5047  1.5103  1.5152  1.5198  1.5246
  1.5289  1.5326  1.5363  1.5400  1.5430  1.5459  1.5486  1.5511
  1.5531  1.5550  1.5567  1.5581  1.5591  1.5599  1.5602  1.5603
  1.5603  1.5601  1.5596  1.5586  1.5574  1.5558  1.5540  1.5519
  1.5495  1.5468  1.5438  1.5407  1.5372  1.5335  1.5295  1.5254
  1.5209  1.5161  1.5112  1.5059  1.5004  1.4857  1.4697  1.4529
  1.4353  1.4172  1.3983  1.3788  1.3587  1.3368  1.3023  1.2672
  1.2315  1.1952  1.1586  1.1218  1.0850  1.0335   .9802   .9277
   .8760   .8254   .7765   .7292   .6702   .5907   .5157   .4454
   .3801   .3202   .2655   .2160   .1717   .1324   .0976   .0670
   .0403   .0172   .0000
```

```
13:31 OCT 15 '85 INI-L10-V1224-013.CR81RMB

C='V1224 Entered by CR81RMB .BROOKS   at 14:53 SEP 25, 85                    ',
C='Intake  valve for the L10       engine family.                            ',
C='Valve lash setting -> 013                                                 ',
C='Flow area data used:                                                      ',
C='Lift ->     .000   .100   .200   .300   .400   .500   .600                ',
C='Area ->     .000   .590  1.150  1.650  1.920  2.060  2.140                ',
C='Peak valve lift =  .4286 at 797.2 c.a. ',
NPTS=107, CAINC=2.0, CABEG= 701.2, UNITS='ENGLISH',*END*
   .0000   .0039   .0306   .0664   .0873   .1108   .1550   .2006
   .2350   .2779   .3376   .3959   .4482   .5114   .5865   .6568
   .7241   .8012   .8850   .9635  1.0404  1.1247  1.2036  1.2739
  1.3431  1.4163  1.4880  1.5539  1.6188  1.6690  1.7028  1.7335
  1.7636  1.7933  1.8202  1.8444  1.8679  1.8901  1.9092  1.9232
  1.9315  1.9387  1.9445  1.9494  1.9537  1.9568  1.9586  1.9597
  1.9600  1.9591  1.9571  1.9545  1.9510  1.9463  1.9408  1.9346
  1.9274  1.9195  1.9012  1.8824  1.8619  1.8396  1.8160  1.7910
  1.7642  1.7362  1.7069  1.6764  1.6400  1.5793  1.5169  1.4529
  1.3875  1.3213  1.2544  1.1869  1.1151  1.0385   .9624   .8874
   .8139   .7424   .6731   .6065   .5425   .4816   .4246   .3717
   .3234   .2795   .2400   .2049   .1740   .1468   .1231   .1026
   .0848   .0697   .0575   .0472   .0377   .0292   .0221   .0156
   .0090   .0030   .0000
```

Table 4.12 Exhaust and intake valve area maps

	EXP.	SPICE	EXP.	SPICE	EXP.	SPICE	EXP.	SPICE	EXP.	SPICE
ENG. RUN. COND.										
Nom Speed RPM	1000.00	1000.00	1260.00	1260.00	1500.00	1500.00	1800.00	1800.00	2100.00	2100.00
Load %	100.00	100.00	100.00	100.00	100.00	100.00	100.00	100.00	100.00	100.00
Fuel Flow lb/h	46.34	46.34	60.20	60.20	70.10	70.10	78.67	78.67	84.50	84.50
Fuel/Shot mg	116.74	116.74	120.40	120.40	117.74	117.74	110.10	110.10	101.40	101.40
Fuel Engy J/Cycle	29930.4	29771.0	30836.14	30672.0	30226.45	30066.0	28249.38	28130.0	26017.30	26099.0
Timing BTDC deg		17.00		18.00		17.00		16.50		15.50
Burn Dur Angle		52.50		62.50		62.50		62.50		62.50
ENGINE RESULTS										
Torque N.m	951.00	973.7	1020.10	1045.8	1022.21	1046.6	953.50	980.4	849.98	889.5
Brk. Power kW	99.62	102.0	134.60	138.0	160.57	164.4	179.73	184.8	186.92	195.6
BMEP bar	11.94	12.2	12.80	13.1	12.83	13.2	11.96	12.3	10.67	11.1
Brk Th Eff %	39.95	41.07	41.56	42.79	42.51	43.81	42.42	43.86	41.05	43.13
BSFC g/kWh	210.54	205.9	202.38	197.6	197.98	193.0	198.24	192.8	204.89	196.10
*										
Max Cyl P bar	120.00	132.	125.86	131.	127.52	135.	123.58	130.	119.31	127.
Max Cyl T K		2127.		2019.		1933.		1826.		1718.
*										
Air Flow kg/min	5.92	7.73	9.73	10.62	12.82	13.73	15.90	17.11	19.02	20.43
Ovrl. A/F Ratio	18.08	21.90	21.45	23.30	24.21	25.80	26.85	28.70	30.02	32.30
*										
Inl Man P bar	1.46	1.45	1.59	1.61	1.73	1.77	1.83	1.86	2.14	1.97
Exh Man P bar	1.25	1.25	1.36	1.40	1.45	1.55	1.55	1.69	1.84	1.88
Exh Man P bar	1.28	1.25	1.38	1.40	1.47	1.55	1.57	1.69	1.85	1.88
Inl Man T degK	324.00	323.00	326.00	325.00	330.00	327.00	334.00	328.00	341.00	330.00
Exh Man T degK	788.00	735.00	805.00	766.00	796.00	753.00	792.00	743.00	784.50	723.00
TURBOCHARGER										
Speed RPM	57790.00	57760.00	64987.00	65068.00	72568.00	72554.00	78047.00	78388.00	83863.00	83892.00
Turb Power kW		6.6/6.7		11.6/11.3		17.5/17.5		24.8/23.8		31.8/32.3
*										
Turb PR -	1.27	1.36	1.35	1.53	1.47	1.68	1.57	1.80	1.70	1.96
Turb Eff %	56.40	51.23	55.00	51.90	55.00	58.00	54.50	64.37	53.50	64.75
*										
Comp PR -	1.43	1.52	1.56	1.67	1.71	1.84	1.85	1.93	1.96	2.04
Comp Eff %	63.00	72.95	67.00	74.90	69.00	74.74	71.50	74.65	72.00	72.30
BALLANCES										
Mass Flow -	--	1.00	--	1.00	--	1.00	--	1.00	--	1.00
T/C Power -	--	0.99	--	1.03	--	1.00	--	1.04	--	0.98
Energy : -	--	1.00	--	1.00	--	1.00	--	1.00	--	1.00
Coolant %	34.48	31.74	25.57	27.55	21.86	25.94	19.43	25.37	18.40	25.71
Exhaust %	25.92	27.19	33.37	29.66	36.32	30.25	39.02	30.77	41.75	31.16
Work %	39.60	41.07	41.06	42.79	41.82	43.81	41.55	43.86	39.85	43.13

Table 4.13 Comparison between the ' SPICE ' predictions, based on using the WIEBE function heat release model and modified CHEN & FLYN friction model, with experimental results for the CUMMINS L10.250-T/C Diesel engine (normal valve area) at full load running conditions

		EXP.	SPICE	EXP.	SPICE	EXP.	SPICE	EXP.	SPICE
ENG. RUN. COND.									
Nom Speed	RPM	2100.00	2100.00	2100.00	2100.00	2100.00	2100.00	2100.00	2100.00
Load	%	100.00	100.00	75.00	75.00	50.00	50.00	25.00	25.00
Fuel Flow	lb/h	84.50	84.50	66.10	66.10	47.10	47.10	29.60	29.60
Fuel/Shot	mg	101.40	101.40	79.40	79.40	56.50	56.50	35.50	35.50
Fuel Engy	J/Cycle	26017.30	25879.00	20348.90	20265.00	14492.00	14465.00	9109.20	9060.00
Timing BTDC	deg		15.50		12.30		9.00		5.00
Burn Dur Angle			62.50		60.00		52.50		50.00
ENGINE RESULTS									
Torque	N.m	849.98	889.5	639.80	679.3	420.35	455.6	219.18	237.4
Brk. Power	kW	186.92	195.6	140.70	149.4	92.44	100.2	48.20	52.2
BMEP	bar	10.67	11.7	8.03	8.5	5.27	5.7	2.75	3.0
Brk Th Eff	%	41.05	43.13	39.51	42.06	36.44	39.48	30.23	33.11
BSFC	g/kWh	204.89	196.1	214.10	201.1	231.96	214.2	279.52	255.4
Max Cyl P	bar	119.31	127.	94.62	100.	72.48	75.	58.48	55.
Max Cyl T	K		1718.		1607.		1473.		1262.
Air Flow	kg/min	19.02	20.43	16.69	18.04	13.89	15.18	11.57	12.96
Ovrl. A/F Ratio		30.02	32.30	33.25	36.10	38.88	42.90	51.54	58.40
Inl Man P	bar	2.15	1.97	1.70	1.70	1.45	1.44	1.26	1.23
Exh Man P	bar	1.84	1.88	1.56	1.66	1.42	1.48	1.32	1.33
Exh Man P	bar	1.86	1.88	1.58	1.66	1.44	1.48	1.33	1.33
Inl Man T	degK	341.00	330.00	335.00	337.00	334.10	325.00	335.00	323.00
Exh Man T	degK	784.50	723.00	740.00	681.00	683.00	625.00	604.60	549.00
TURBOCHARGER									
Speed	RPM	83863.00	83892.00	74282.00	74200.00	62796.00	62912.00	51070.00	51179.00
Turb Power	kW		31.8/32.3		21.7/21.9		12.2/13.0		6.3/7.2
Turb PR	-	1.70	1.96	1.57	1.73	1.43	1.53	1.33	1.36
Turb Eff	%	53.50	64.75	76.84	65.68	73.30	59.80	65.11	56.63
Comp PR	-	1.96	2.04	1.71	1.77	1.46	1.50	1.27	1.29
Comp Eff	%	72.00	72.30	71.00	73.14	70.10	72.21	69.15	68.17
BALLANCES									
Mass Flow	-	--	1.00	--	1.00	--	1.00	--	1.00
T/C Power	-	--	0.98	--	0.99	--	0.93	--	0.88
Energy	-	--	1.00	--	1.00	--	1.00	--	1.00

Table 4.14 Comparison between the ' SPICE ' predictions, based on using the WIEBE function heat release model and modified CHEN & FLYN friction model , with experimental results for the CUMMINS L10.250-T/C Diesel engine at various loads at engine speed of 2100 rpm

	EXP.	SPICE	EXP.	SPICE	EXP.	SPICE	EXP.	SPICE
ENG. RUN. COND.								
Nom Speed RPM	1260.00	1260.00	1260.00	1260.00	1260.00	1260.00	1260.00	1260.00
Load %	100.00	100.00	75.00	75.00	50.00	50.00	25.00	25.00
Fuel Flow lb/h	60.20	60.20	45.42	45.20	31.25	31.08	18.03	17.92
Fuel/Shot mg	120.40	120.40	90.82	90.40	62.50	62.20	36.05	35.80
Fuel Engy J/Cycle	30836.14	30889.40	22765.00	22965.00	15864.00	15872.00	9122.60	9137.40
Timing BTDC deg		18.00		12.00		8.00		4.50
Burn Dur Angle		62.50		52.50		50.00		47.50
ENGINE RESULTS								
Torque N.m	1020.10	1045.8	763.60	792.4	511.66	546.6	261.73	291.6
Brk. Power kW	134.60	138.0	100.61	104.4	67.40	72.0	34.46	38.4
BMEP bar	12.80	13.1	9.58	9.9	6.42	6.8	3.28	3.6
Brk Th Eff %	41.56	42.79	41.44	43.38	40.21	43.07	36.10	39.95
BSFC g/kWh	202.38	197.6	204.74	195.0	210.27	196.3	237.31	211.4
*								
Max Cyl P bar	125.86	131.	95.04	101.	69.45	73.	49.24	52.
Max Cyl T K		2019.		1869.		1625.		1302.
*								
Air Flow kg/min	9.73	10.62	8.32	9.28	7.07	8.15	5.82	7.38
Ovrl. A/F Ratio	21.45	23.30	24.23	27.20	29.91	34.80	42.74	54.20
*								
Inl Man P bar	1.59	1.61	1.40	1.39	1.24	1.22	1.12	1.10
Exh Man P bar	1.36	1.40	1.28	1.28	1.21	1.18	1.16	1.13
Exh Man P bar	1.38	1.40	1.29	1.28	1.23	1.18	1.18	1.13
Inl Man T degK	326.00	325.00	327.60	322.00	328.00	320.00	332.00	319.00
Exh Man T degK	805.00	766.00	757.00	706.00	671.00	633.00	573.00	529.00
TURBOCHARGER								
Speed RPM	64987.00	65068.00	54894.00	54947.00	44770.00	44998.00	33780.00	33671.00
Turb Power kW		11.6/11.3		7.0/6.9		4.1/3.95		1.9/2.1
*								
Turb PR -	1.35	1.53	1.28	1.36	1.22	1.21	1.16	1.15
Turb Eff %	55.00	51.90	81.74	54.58	74.29	64.75	63.00	61.54
*								
Comp PR -	1.56	1.67	1.38	1.45	1.23	1.28	1.12	1.15
Comp Eff %	67.00	74.90	66.00	75.97	66.30	75.83	63.50	72.63
BALLANCES								
Mass Flow -	--	1.00	--	1.00	--	1.00	--	1.00
T/C Power -	--	1.03	--	1.01	--	1.04	--	0.89
Energy -	--	1.00	--	1.00	--	1.00	--	1.00

Table 4.15 Comparison between the ' SPICE ' predictions, based on using the WIEBE heat release model and modified CHEN & FLYN friction model , with experimental results for the CUMMINS L10.250-T/C Diesel engine (normal valve area) at various loads at speed of 1260 rpm

		EXP.	SPICE	EXP.	SPICE	EXP.	SPICE	EXP.	SPICE	EXP.	SPICE
ENG. RUN. COND.											
Nom Speed	RPM	1000.00	1000.00	1260.00	1260.00	1500.00	1500.00	1800.00	1800.00	2100.00	2100.00
Load	%	100.00	100.00	100.00	100.00	100.00	100.00	100.00	100.00	100.00	100.00
Fuel Flow	lb/h	46.34	46.34	60.20	60.20	70.10	70.10	78.67	78.67	84.50	84.50
Fuel/Shot	mg	116.74	116.74	120.40	120.40	117.74	117.74	110.10	110.10	101.40	101.40
Fuel Engy	J/Cycle	29930.4	29944.80	30836.14	30889.40	30226.45	30228.40	28249.38	28251.70	26017.30	26019.30
Timing BTDC	deg		17.00		18.00		17.00		16.50		15.50
Burn Dur Angle			52.50		62.50		62.50		62.50		62.50
ENGINE RESULTS											
Torque	N.m	951.00	968.30	1020.10	1032.23	1022.21	1027.50	953.50	951.74	849.98	856.71
Brk. Power	kW	99.62	101.4	134.60	136.2	160.57	161.4	179.73	179.4	186.92	188.4
BMEP	bar	11.94	12.1	12.80	13.0	12.83	12.9	11.96	12.0	10.67	10.7
Brk Th Eff	%	39.95	40.63	41.56	42.07	42.51	42.74	42.42	42.40	41.05	41.35
BSFC	g/kWh	210.54	207.0	202.38	199.9	197.98	196.8	198.24	198.4	204.89	203.4
FMEP	bar		0.95		1.12		1.30		1.47		1.65
*											
Max Cyl P	bar	120.00	130.	125.86	128.	127.52	130.	123.58	124.	119.31	119.
Max Cyl T	K		2165.		2076.		2008.		1923.		1833.
*											
Scav Ratio	-	-	1.0067	-	1.0066	-	1.0066	-	1.0072	-	1.0083
Air Flow	kg/min	5.92	7.37	9.73	9.98	12.82	12.62	15.90	15.35	19.02	18.15
Ovrl. A/F Ratio		18.08	21.14	21.45	22.04	24.21	23.95	26.85	25.98	30.02	28.63
*											
Inl Man P	bar	1.46	1.46	1.59	1.60	1.73	1.76	1.83	1.86	1.92	2.00
Exh Man P	bar	1.25	1.22	1.36	1.36	1.45	1.49	1.55	1.61	1.70	1.75
Exh Man P	bar	1.28	1.22	1.38	1.36	1.47	1.49	1.57	1.61	1.85	1.75
Inl Man T	degK	324.00	323.00	326.00	325.00	330.00	329.00	334.00	333.00	341.00	341.00
Exh Man T	degK	788.00	752.00	805.00	794.00	796.00	793.00	792.00	796.00	784.50	787.00
TURBOCHARGER											
Speed	RPM	57790.00	57651.00	64987.00	64978.00	72568.00	72475.00	78047.00	78292.00	83863.00	83906.00
Turb Power	kW		5.8/6.4		10.4/10.6		15.6/16.3		21.9/22.1		28.6/29.3
*											
Turb PR	-	1.27	1.33	1.35	1.49	1.47	1.63	1.57	1.73	1.70	1.86
Turb Eff	%	87.00	53.14	83.00	54.12	83.00	58.85	80.00	64.13	78.00	66.33
*											
Comp PR	-	1.43	1.51	1.56	1.66	1.71	1.83	1.85	1.94	1.96	2.08
Comp Eff	%	63.00	72.64	67.00	74.83	69.00	74.49	71.50	74.39	72.00	74.02
BALLANCES											
Mass Flow	-	--	.999	--	.999	--	.999	--	1.00	--	.999
T/C Power	-	--	.903	--	.975	--	.957	--	.993	--	.975
Energy :	-	--	.997	--	.998	--	.997	--	.998	--	.997
Coolant	%	34.48	30.77	25.57	25.12	21.86	22.36	19.43	20.40	18.40	19.71
Exhaust	%	25.92	29.04	33.37	33.33	36.32	35.58	39.02	38.04	41.75	40.09
Work	%	39.60	40.19	41.06	41.55	41.82	42.06	41.55	41.56	39.85	40.20

Table 4.16 Comparison between the ' SPICE ' predictions, based on the WIEBE heat release model and modified CHEN & FLYN friction model, with experimental results for the CUMMINS L10.250-T/C Diesel engine (reduced valve area) at full load running conditions

	EXP.	SPICE	EXP.	SPICE	EXP.	SPICE	EXP.	SPICE
ENG. RUN. COND.								
Nom Speed RPM	2100.00	2100.00	2100.00	2100.00	2100.00	2100.00	2100.00	2100.00
Load %	100.00	100.00	75.00	75.00	50.00	50.00	25.00	25.00
Fuel Flow lb/h	84.50	84.50	66.10	66.10	47.10	47.10	29.60	29.60
Fuel/Shot mg	101.40	101.40	79.40	79.40	56.50	56.50	35.50	35.50
Fuel Engy J/Cycle	26017.30	26019.30	20348.90	20348.90	14492.00	14492.00	9109.20	9109.20
Timing BTDC deg		15.50		12.30		9.00		5.00
Burn Dur Angle		62.50		60.00		52.50		50.00
ENGINE RESULTS								
Torque N.m	849.98	856.71	639.80	652.07	420.35	431.08	219.18	223.72
Brk. Power kW	186.92	188.4	140.70	143.4	92.44	94.8	48.20	49.2
BMEP bar	10.67	10.7	8.03	8.0	5.27	5.4	2.75	2.8
Brk Th Eff %	41.05	41.35	39.51	40.21	36.44	37.45	30.23	30.70
BSFC g/kWh	204.89	203.4	214.10	209.2	231.96	224.6	279.52	274.0
FMEP bar		1.65		1.53		1.41		1.31
*								
Max Cyl P bar	119.31	119.	94.62	95.	72.48	71.	58.48	52.
Max Cyl T K		1833.		1688.		1552.		765.7
*								
Scav Ratio -	-	1.0083	-	1.0104	-	1.0136	-	1.0191
Air Flow kg/min	19.02	18.15	16.69	16.27	13.89	13.72	11.57	11.67
Ovrl. A/F Ratio	30.02	28.63	33.25	32.94	38.88	39.12	51.54	53.20
*								
Inl Man P bar	2.15	2.00	1.70	1.77	1.45	1.50	1.26	1.28
Exh Man P bar	1.84	1.75	1.56	1.62	1.42	1.45	1.32	1.32
Exh Man P bar	1.86	1.75	1.58	1.62	1.44	1.45	1.33	1.32
Inl Man T degK	341.00	341.00	335.00	336.00	334.10	337.00	335.00	333.00
Exh Man T degK	784.50	787.00	740.00	731.00	683.00	672.00	604.60	796.00
TURBOCHARGER								
Speed RPM	83863.00	83906.00	74282.00	74040.00	62796.00	62629.00	51070.00	50795.00
Turb Power kW		28.6/29.3		18.8/20.4		10.3/12.0		5.5/6.6
*								
Turb PR -	1.70	1.86	1.57	1.65	1.43	1.46	1.33	1.32
Turb Eff %	53.50	66.33	76.84	63.98	73.30	58.38	65.11	56.76
*								
Comp PR -	1.96	2.08	1.71	1.80	1.46	1.53	1.27	1.31
Comp Eff %	72.00	74.02	71.00	74.98	70.10	75.32	69.15	72.29
BALLANCES								
Mass Flow -	--	.999	--	.999	--	.998	--	.999
T/C Power -	--	.975	--	.919	--	.858	--	.822
Energy -	--	.997	--	.994	--	.993	--	.992

Table 4.17 Comparison between the ' SPICE ' preddictions, based on using the WIEBE heat release model and modified CHEN & FLYN model , with experimental results for the CUMMINS L10.250-T/C Diesel engine (reduced valve area) at various loads at 2100 rpm

	EXP.	SPICE	EXP.	SPICE	EXP.	SPICE	EXP.	SPICE
ENG. RUN. COND.								
Nom Speed RPM	1260.00	1260.00	1260.00	1260.00	1260.00	1260.00	1260.00	1260.00
Load %	100.00	100.00	75.00	75.00	50.00	50.00	25.00	25.00
Fuel Flow lb/h	60.20	60.20	45.42	45.20	31.25	31.08	18.03	17.92
Fuel/Shot mg	120.40	120.40	90.82	90.40	62.50	62.20	36.05	35.80
Fuel Engy J/Cycle	30836.14	30889.40	13849.00	13849.00	9532.00	9532.00	5493.60	5493.00
Timing BTDC deg		18.00		12.00		8.00		4.50
Burn Dur Angle		62.50		52.50		50.00		47.50
ENGINE RESULTS								
Torque N.m	1020.10	1032.23	763.60	787.81	511.66	431.08	261.73	287.09
Brk. Power kW	134.60	136.2	100.61	103.8	67.40	70.8	34.46	37.8
BMEP bar	12.80	13.0	9.58	9.9	6.42	6.7	3.28	3.6
Brk Th Eff %	41.56	42.07	41.44	42.59	40.21	42.24	36.10	39.05
BSFC g/kWh	202.38	199.9	204.74	197.5	210.27	199.1	237.31	215.4
FMEP bar		1.12		0.97		0.83		0.73
*								
Max Cyl P bar	125.86	128.	95.04	98.	69.45	70.	49.24	50.
Max Cyl T K		2076.		1937.		1690.		1358.
*								
Scav Ratio -	-	1.0066	-	1.0080	-	1.0104	-	1.0156
Air Flow kg/min	9.73	9.98	8.32	8.63	7.07	7.56	5.82	6.78
Ovrl. A/F Ratio	21.45	22.04	24.23	25.50	29.91	32.53	42.74	50.88
*								
Inl Man P bar	1.59	1.60	1.40	1.38	1.24	1.22	1.12	1.11
Exh Man P bar	1.36	1.36	1.28	1.24	1.21	1.15	1.16	1.10
Exh Man P bar	1.38	1.36	1.29	1.24	1.23	1.15	1.18	1.10
Inl Man T degK	326.00	325.00	327.60	326.00	328.00	327.00	332.00	331.00
Exh Man T degK	805.00	794.00	757.00	737.00	671.00	662.00	573.00	555.00
TURBOCHARGER								
Speed RPM	64987.00	64978.00	54894.00	54894.00	44770.00	44741.00	33780.00	33576.00
Turb Power kW		10.4/10.6		6.2/6.5		3.6/3.64		1.6/2.0
*								
Turb PR -	1.35	1.49	1.28	1.33	1.22	1.21	1.16	1.15
Turb Eff %	55.00	54.12	81.74	56.87	74.29	66.97	63.00	60.64
*								
Comp PR -	1.56	1.66	1.38	1.44	1.23	1.27	1.12	1.16
Comp Eff %	67.00	74.83	66.00	75.66	66.30	75.78	63.50	73.14
BALLANCES								
Mass Flow -	--	.999	--	.999	--	1.00	--	.999
T/C Power -	--	.975	--	.953	--	.987	--	.804
Energy -	--	.998	--	.998	--	.999	--	.996

Table 4.18 Comparison betwwen the ' SPICE ' predictions, based on using the WIEBE function heat release model and modified CHEN & FLYN friction model, with the experimental results for the CUMMINS L10.250-T/C Diesel engine (reduced valve area) at various load at 1260 rpm

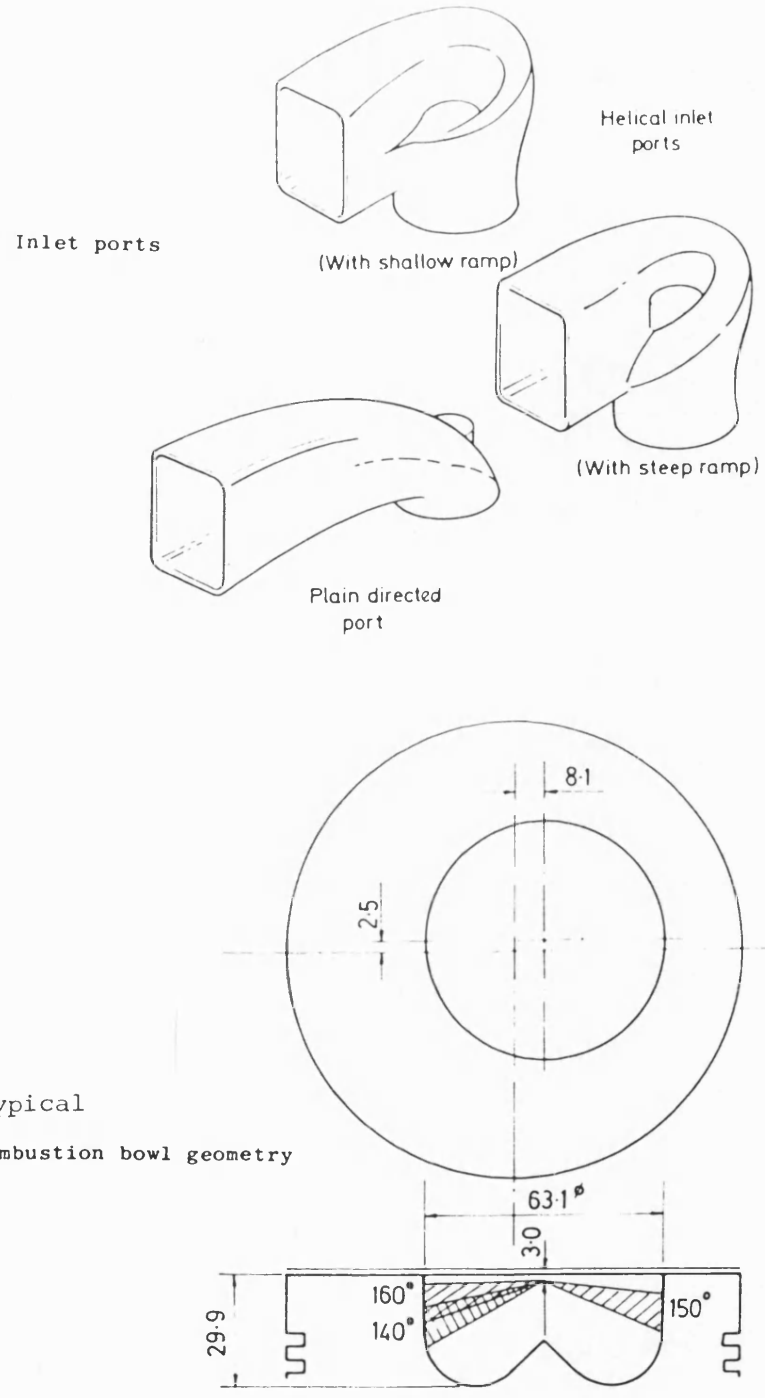

Fig. 4.1a Different types of swirl inducers

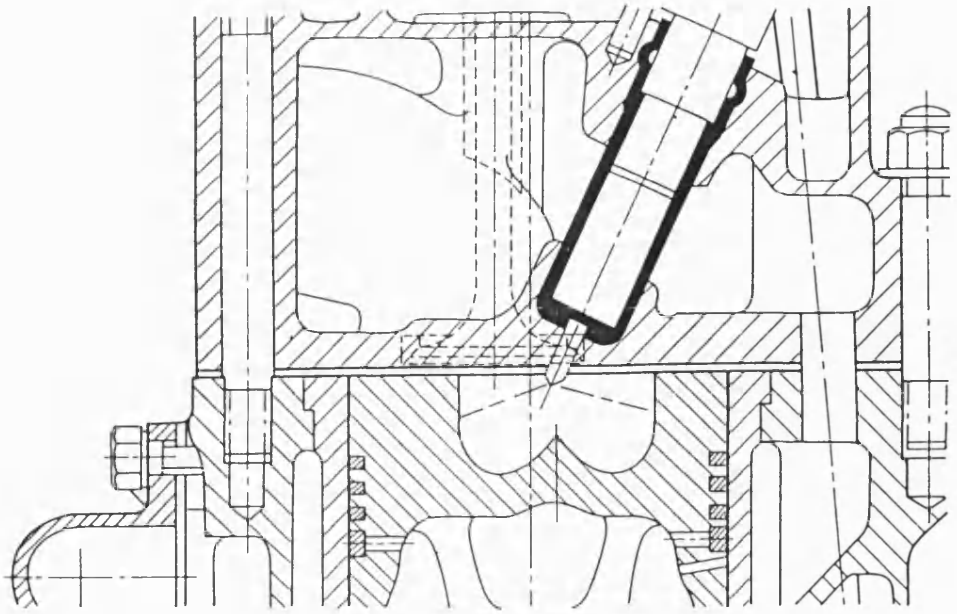

Fig. 4.1b Typical design of medium-swirl open combustion chamber (deep bowl)

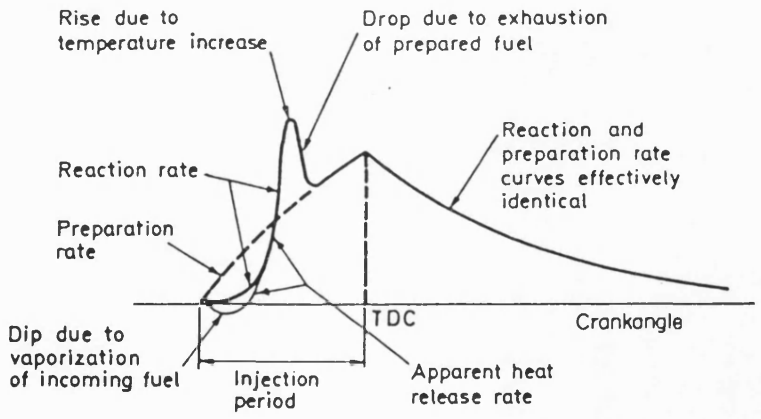

Fig. 4.1c Typical AFBR pattern of swirl type of combustion chamber

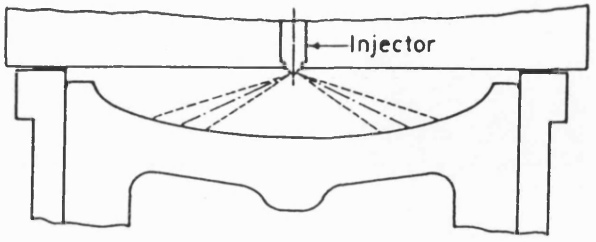

Fig. 4.2a Typical design of quiescent combustion chamber

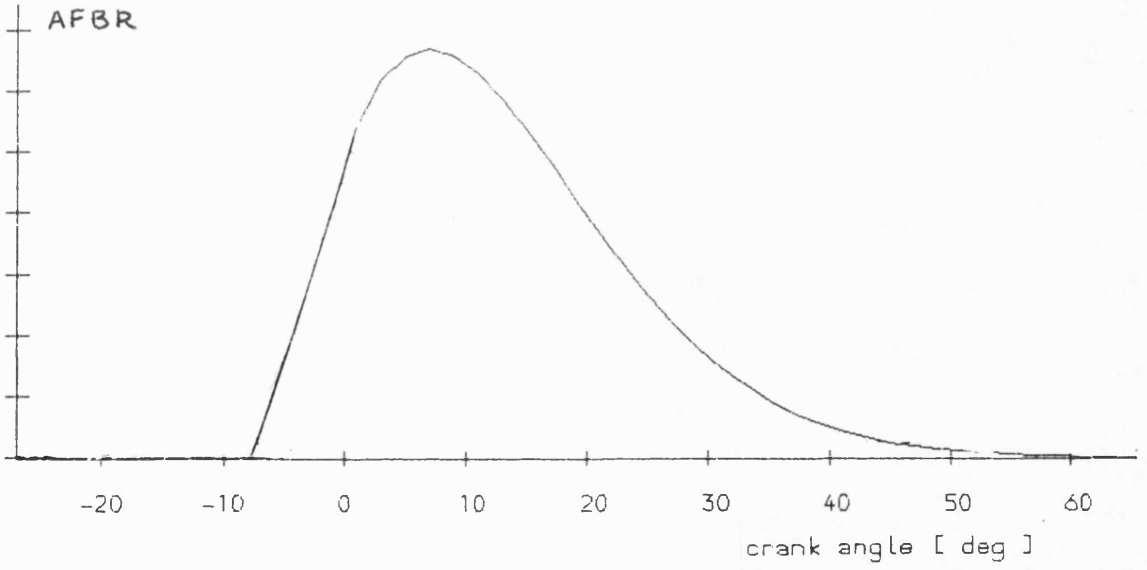

Fig. 4.2b Typical AFBR pattern of quiescent type of combustion chamber

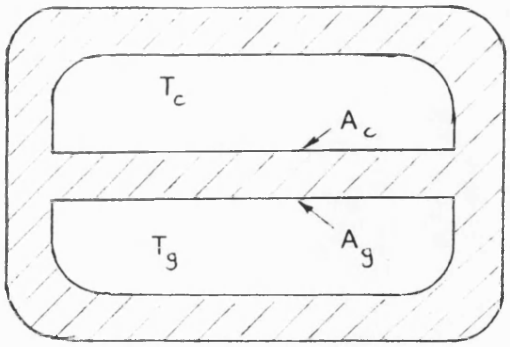

Fig. 4.3 Simple heat exchanger

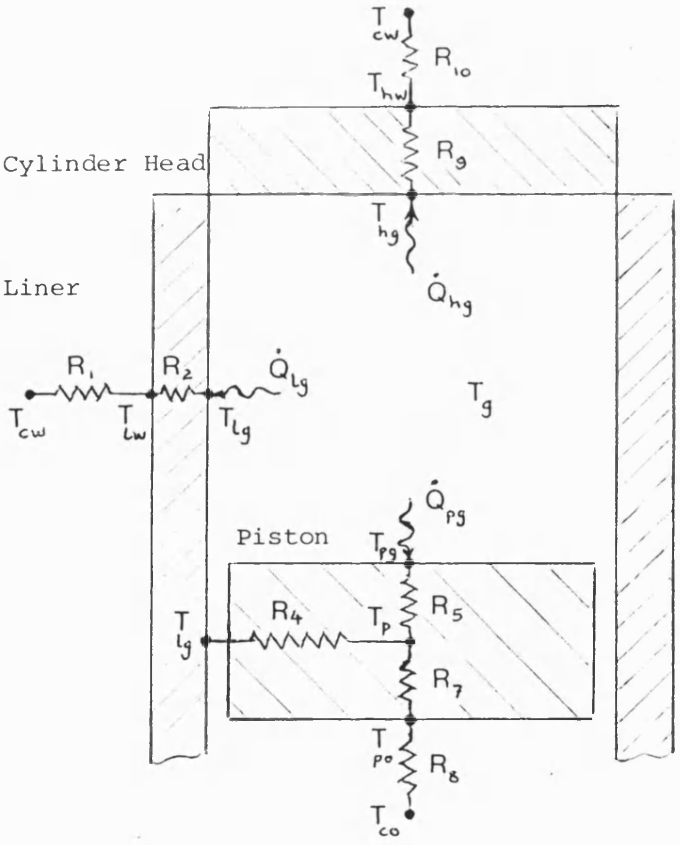

Fig. 4.4a Resistance model for heat transfer used in 'CSP'

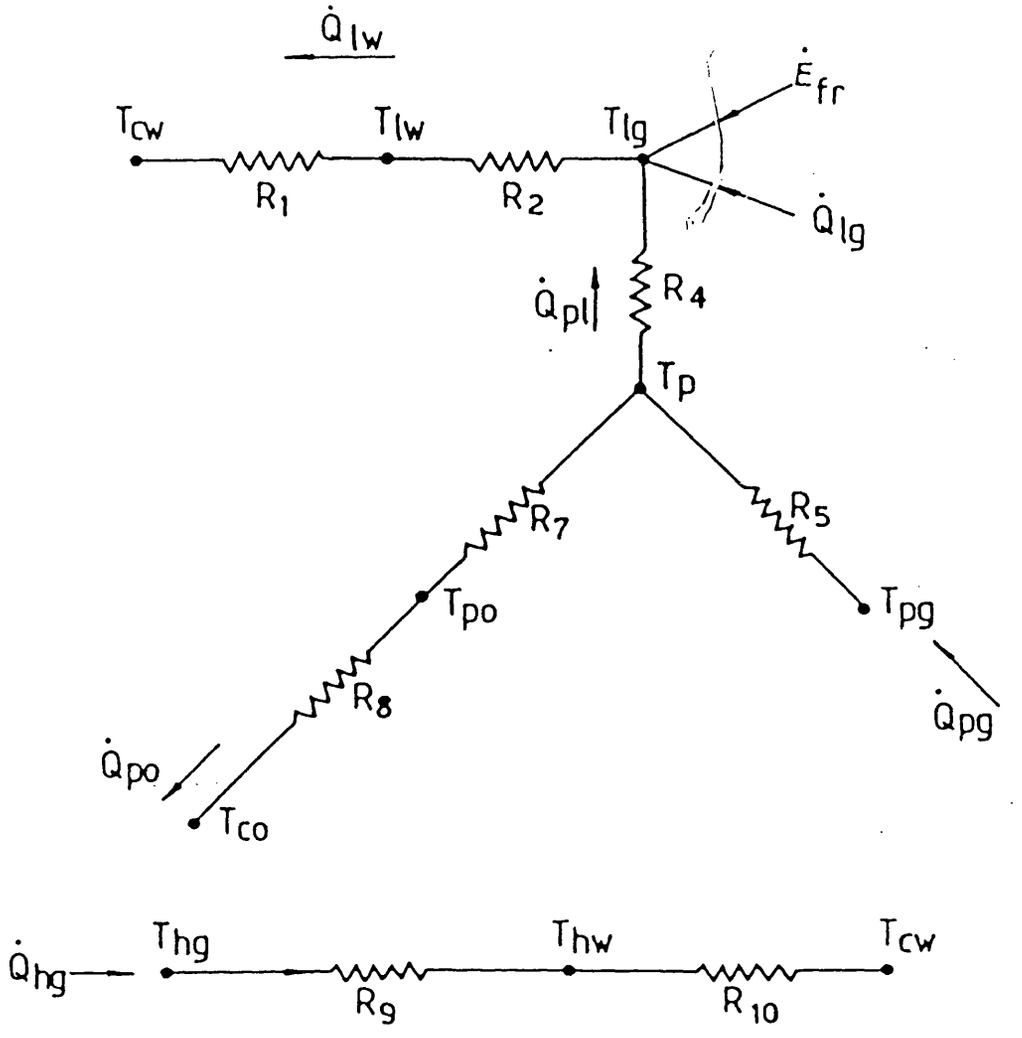

Suffices as used with temperature (T) and heat flow (Q):

co	—	cooling oil
po	—	piston , oil side surface
pg	—	piston , gas side surface
p	—	piston , internal location
lg	—	liner , gas side surface
lw	—	liner, cooling water side surface
cw	—	cooling water
hg	—	cylinder head , gas side surface
hw	—	cylinder head , cooling water side surface

Fig. 4.4b Heat transfer network assumed in 'CSP'

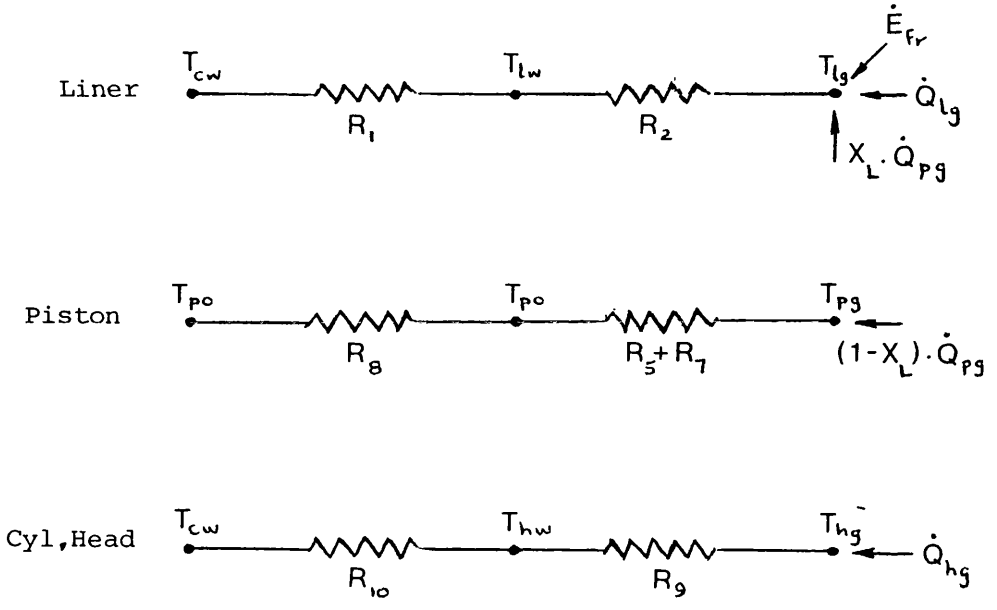

Fig. 4.5 Heat transfer network assumed in 'SPICE'

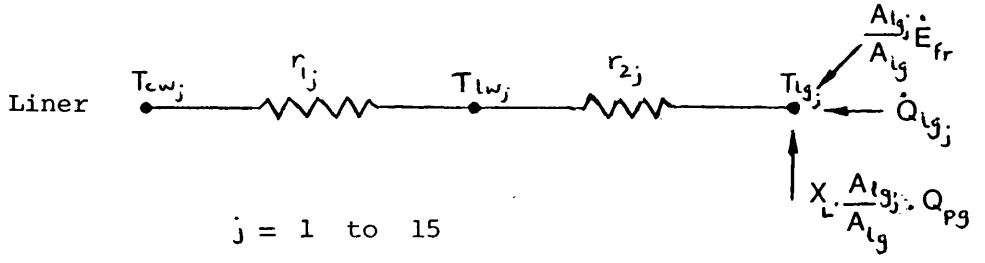

Fig. 4.7 Heat transfer network of the liner zones assumed in 'SPICE'

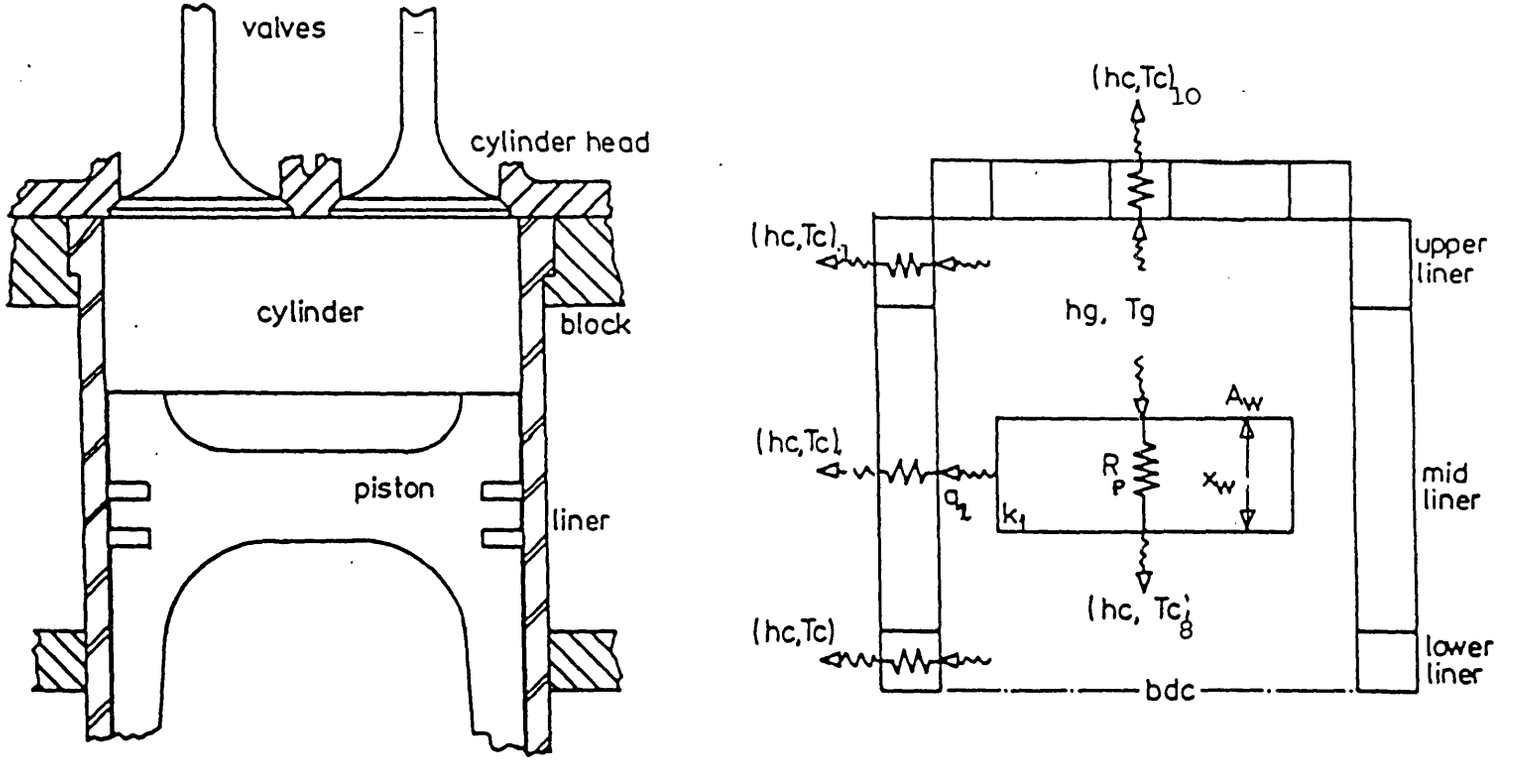

Fig. 4.6 Resistance model used in 'SPICE'

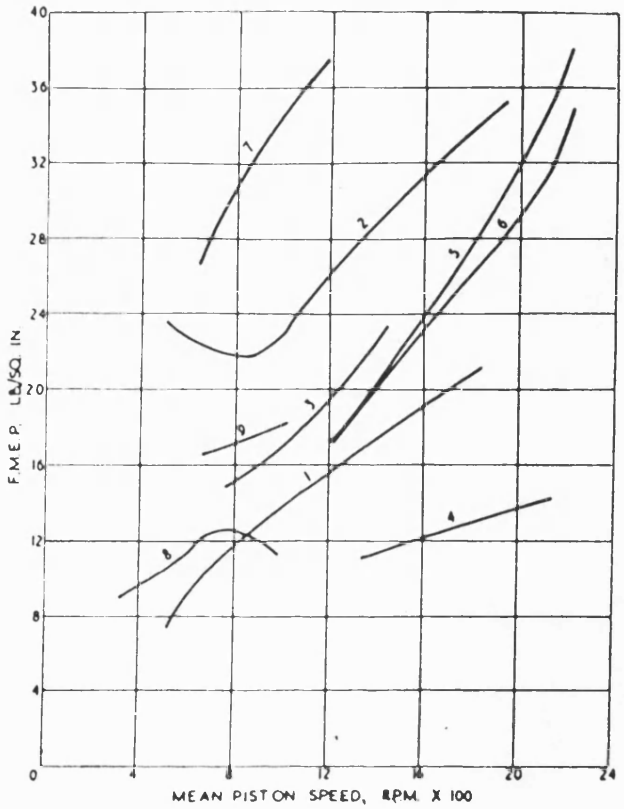

1. "Diesel Engines," by S. A. Green, *The Automobile Engineer*, Vol. 22, 1932: gasoline engine.
2. *Ibid.*, Diesel engine.
3. "Internal Combustion Engine and its Performance," by W. A. Tookey.
4. *The Automobile Engineer*, editorial, Vol. 22, June, 1932, 8 in. × 11 in. oil engine.
5. *N.A.C.A. Report No.* 471, by Schey and Young, 5¼ in. × 6 in. injection engine.
6. *Ibid.*, 5¼ in. × 6 in. gasoline engine.
7. *S.A.E. annual meeting paper*, McLeod, 1937, C.F.R. engine.
8. *Trans. A.S.M.E.*, Vol. 46, 1924, "Large Oil Engines, etc.", by C. E. Lucke, Table 5, No. 3.
9. *Institution of Naval Architects*, July 8, 1930, Hawkes Submarine engine.

Fig. 4.8 Effect of piston speed on FMEP

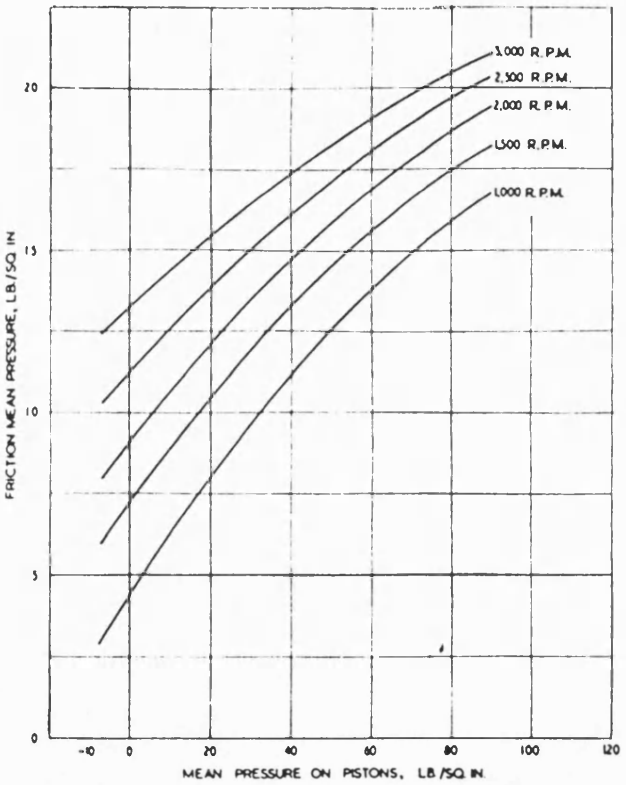

Effect of cylinder mean pressure on FMEP

Fig. 4.9

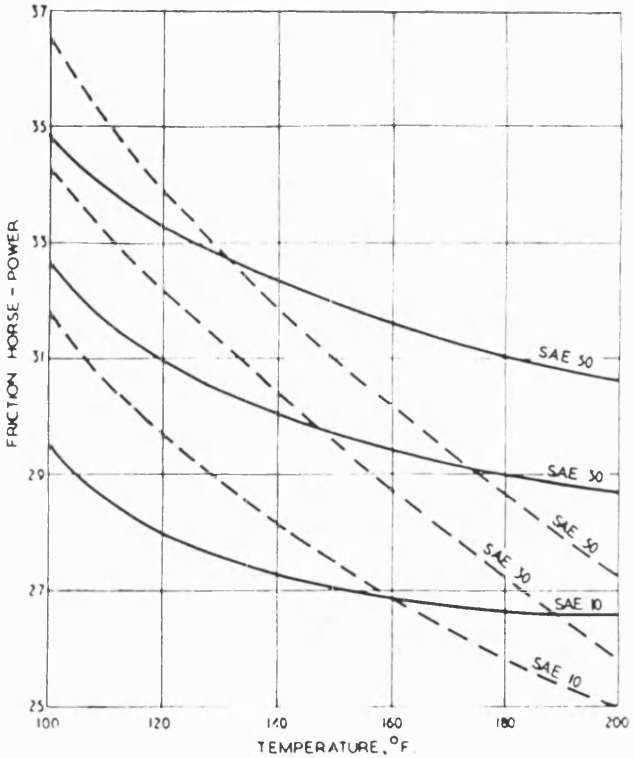

Fig. 20. The effect of oil and water temperature on engine friction (from Ref. 19).

———— Variable oil temperature (water temperature 160–170 F.)
– – – – – – – – – – Variable water temperature (oil temperature 190–210 F.)
Engine capacity: 200 c.u.
Engine speed: 3,100 r.p.m.

Effect of coolant temperatures on FMEP

Fig. 4.10

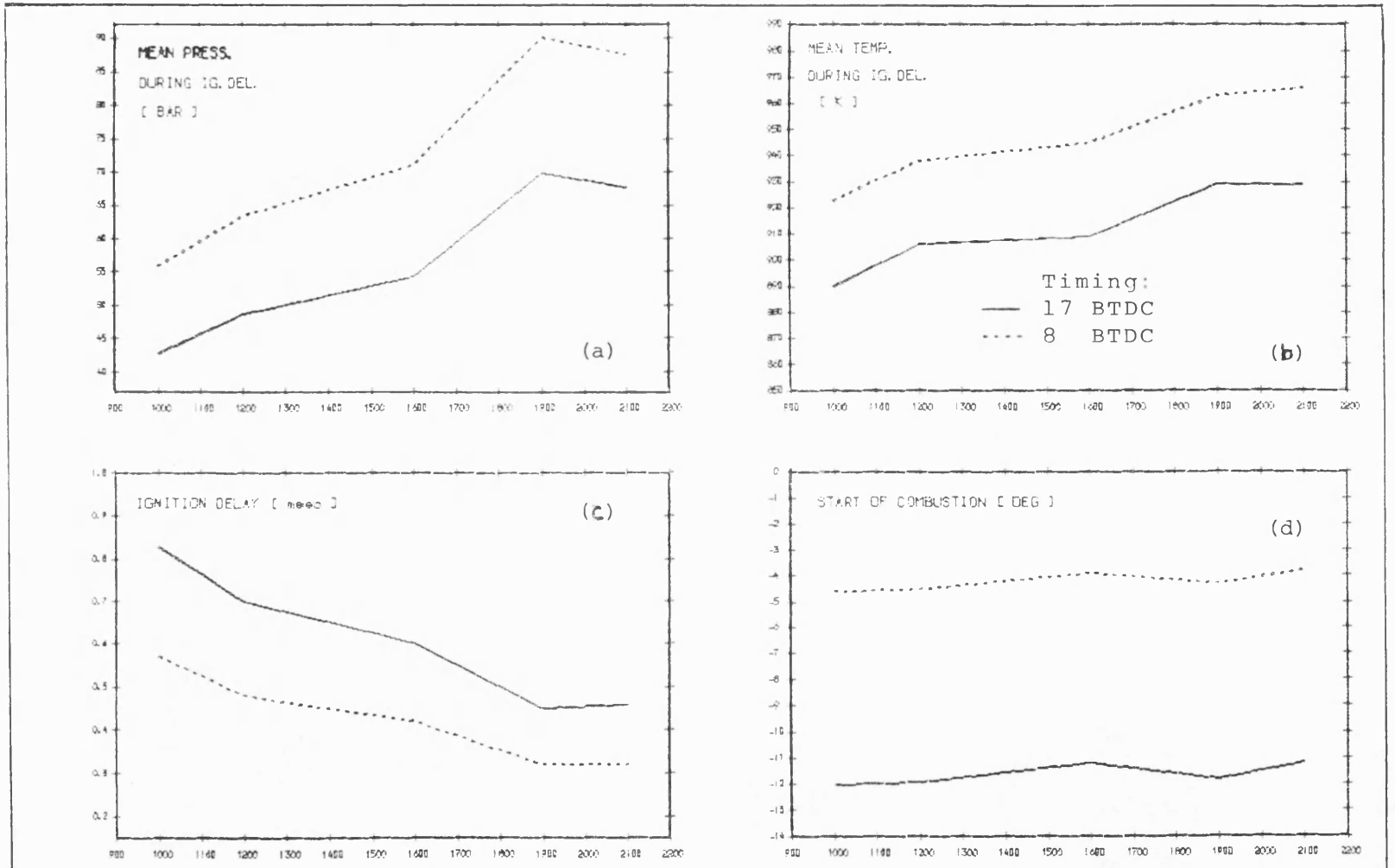

Fig. 4.11 Effect of injection retard on ignition delay and in-cylinder pressure and temperature during ignition lag

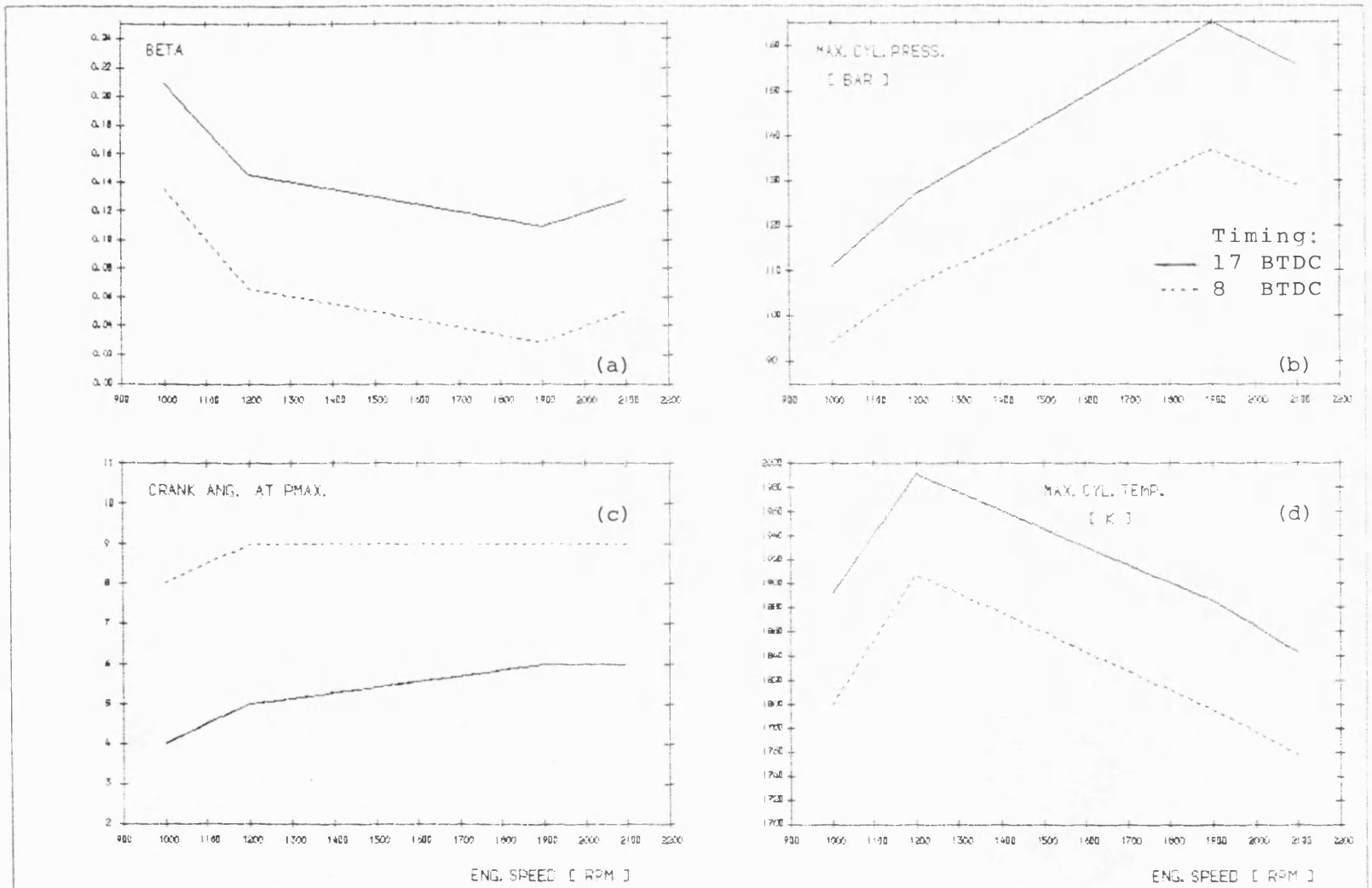

Fig. 4.12 Effect of injection retard on β, P_{max}, T_{max}, CAP_{max}

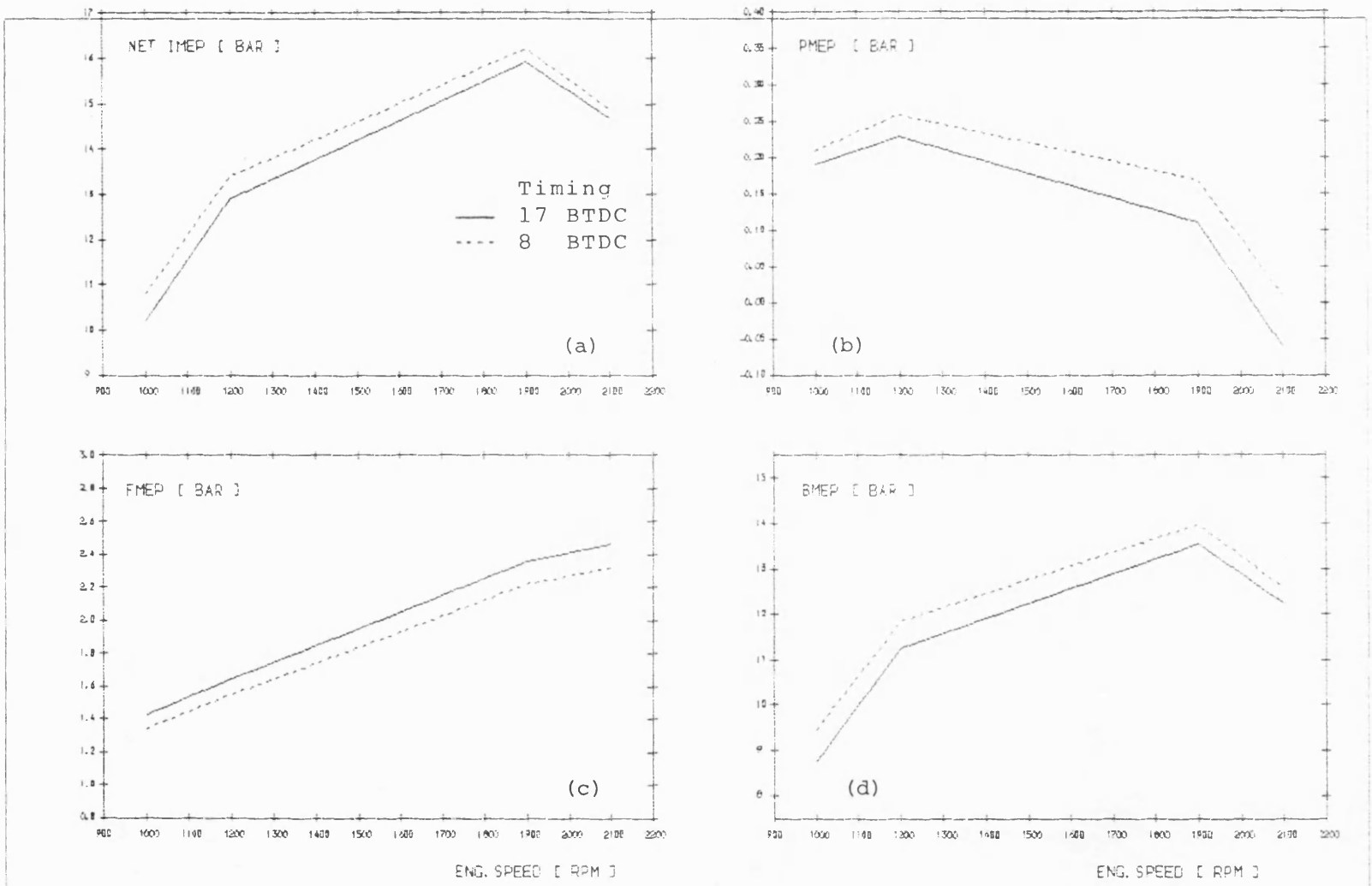

Fig.4.13 Comparison of MEPs based on experimental and simulaion results with two different injection timings

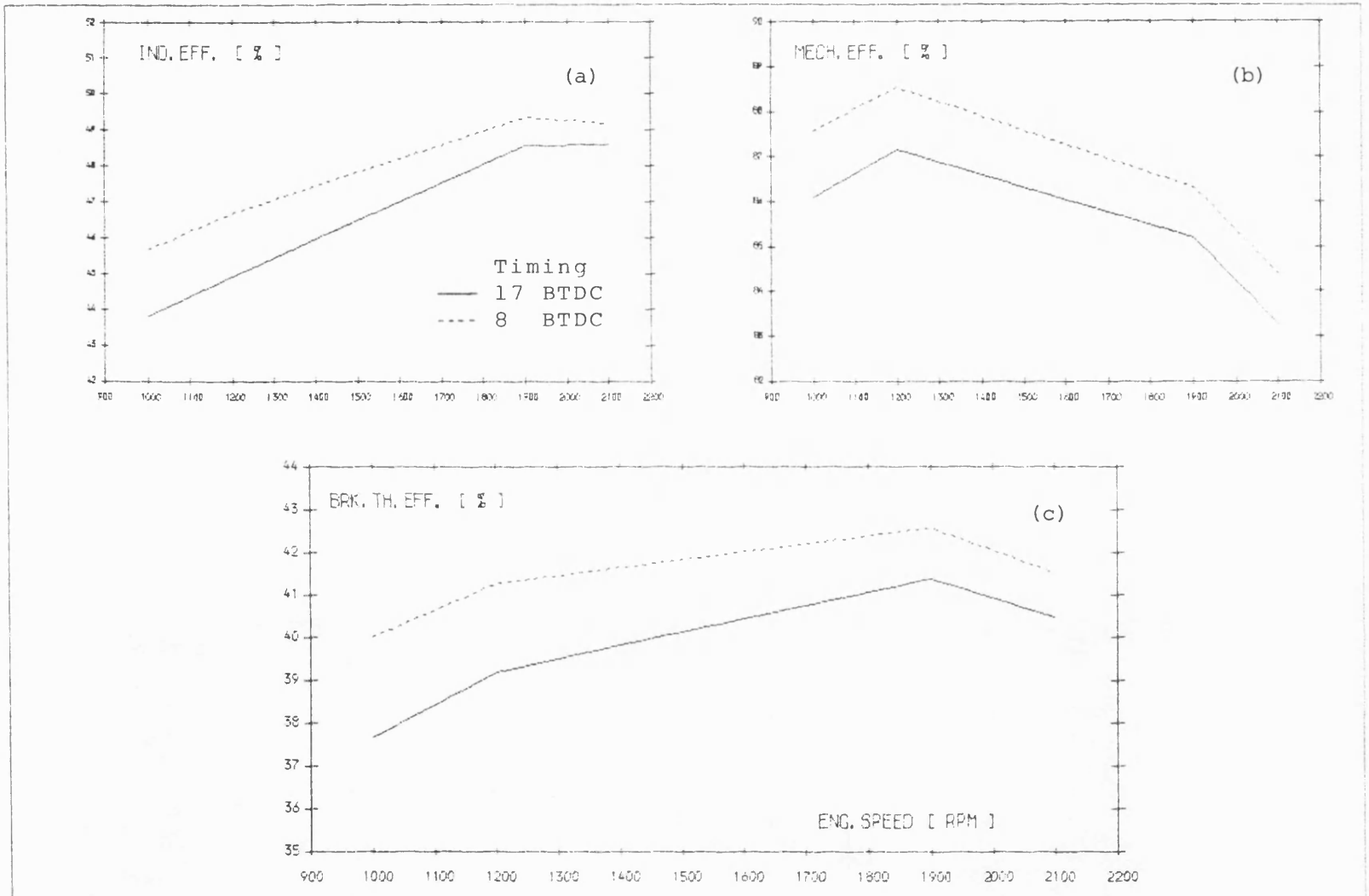

Fig. 4.14 Comparison of brake thermal efficiencies based on experimental and simulation results with two different injection timings

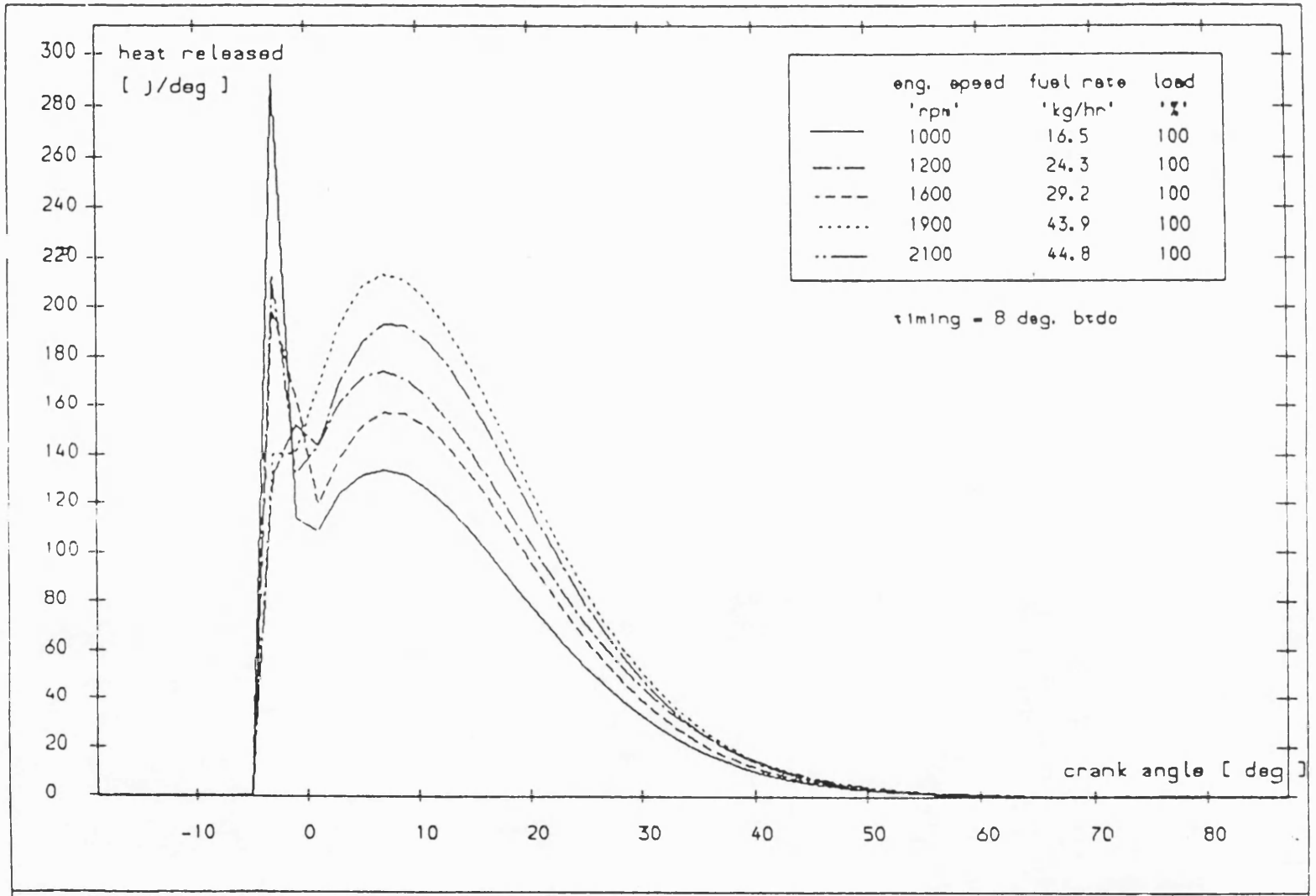

Fig. 4.15 Superimposed heat release diagrams assumed for the Cummins L10-T/C engine at different running conditions near to the LTC

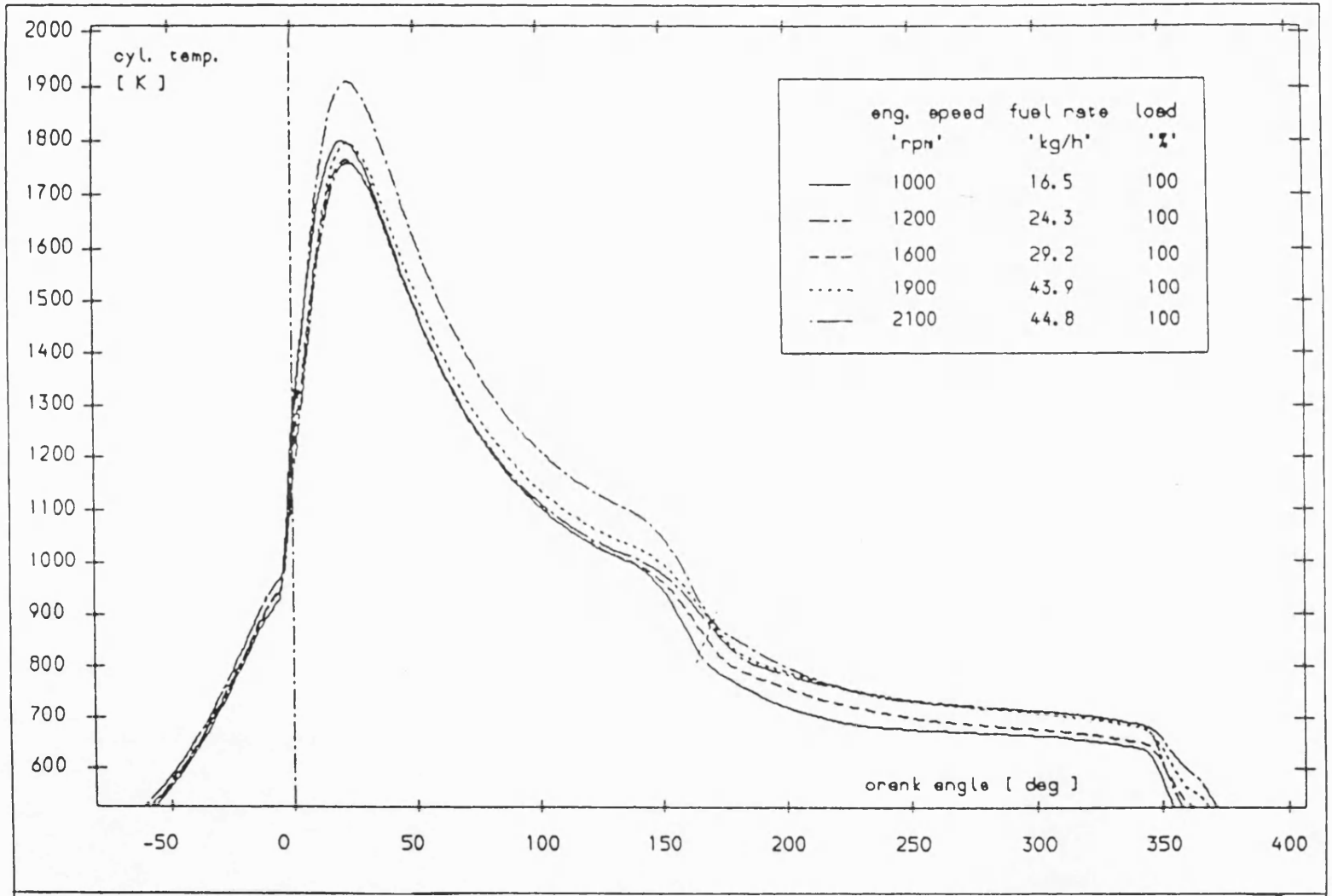

Fig. 4.16 Superimposed in-cylinder gas temperature diagrams resulted from high swirl combustion assumed for the L10-T/C engine at different running conditions near to the LTC

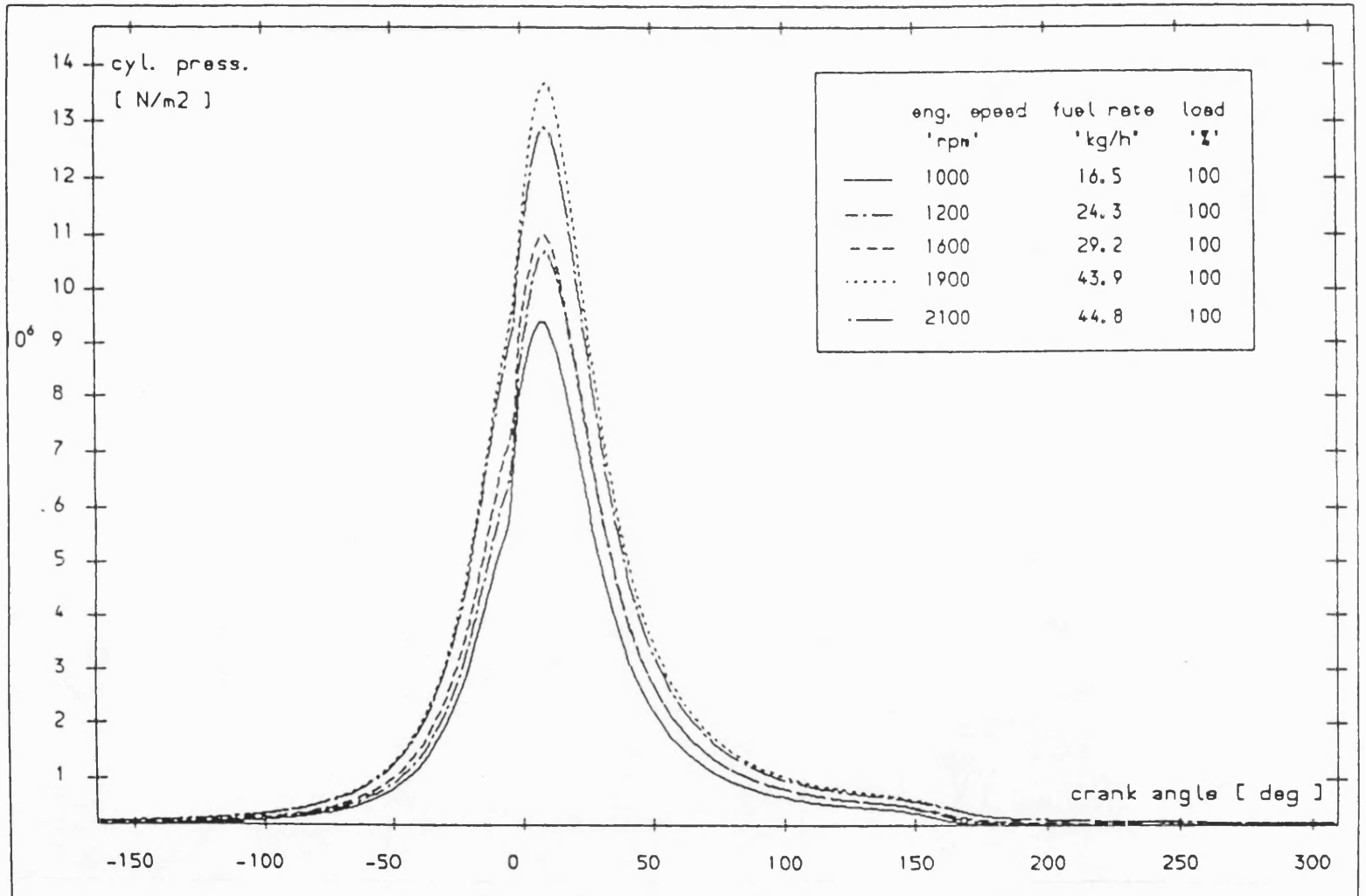

Fig. 4.17 Superimposed cylinder pressure diagrams based on high swirl combustion assumed for the L10-T/C engine at different running conditions near to the LTC

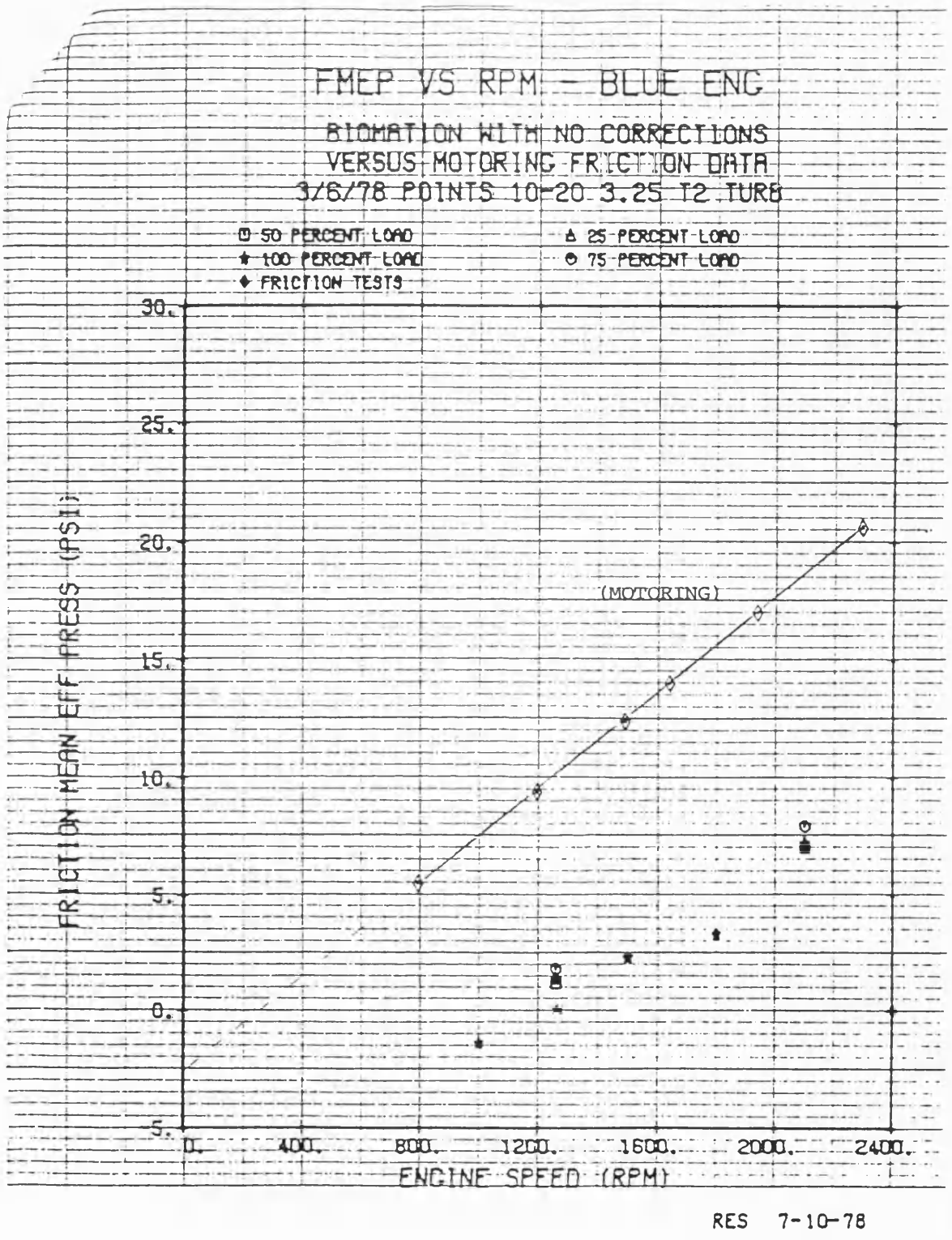

Fig. 4.18 Superimposed FMEPs based on motoring dynamometer tests and unmodified indicator diagrams

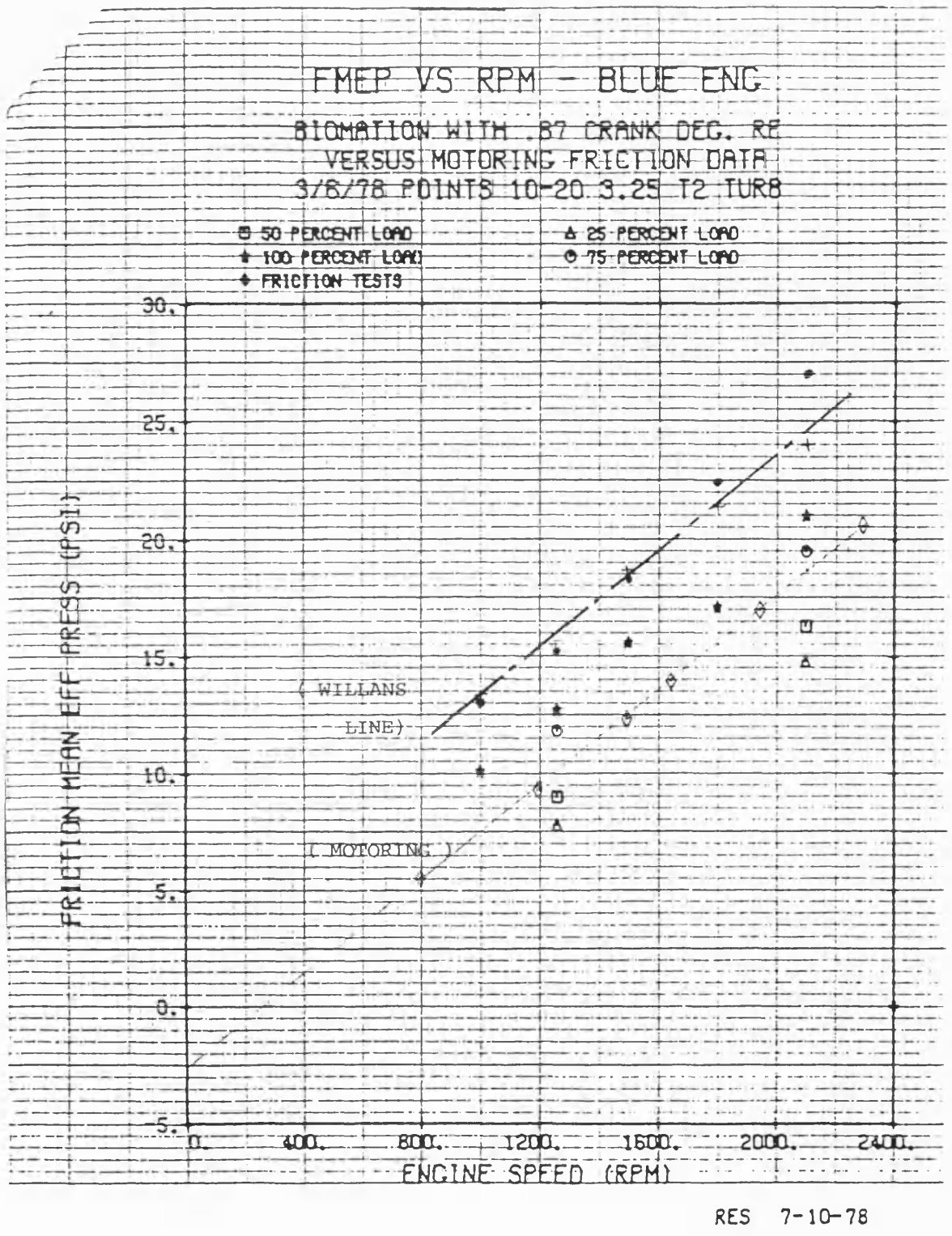

Fig. 4.19 Superimposed FMEPs of the L10 engine based on motoring tests and modified indicator diagrams as well as Willans line method

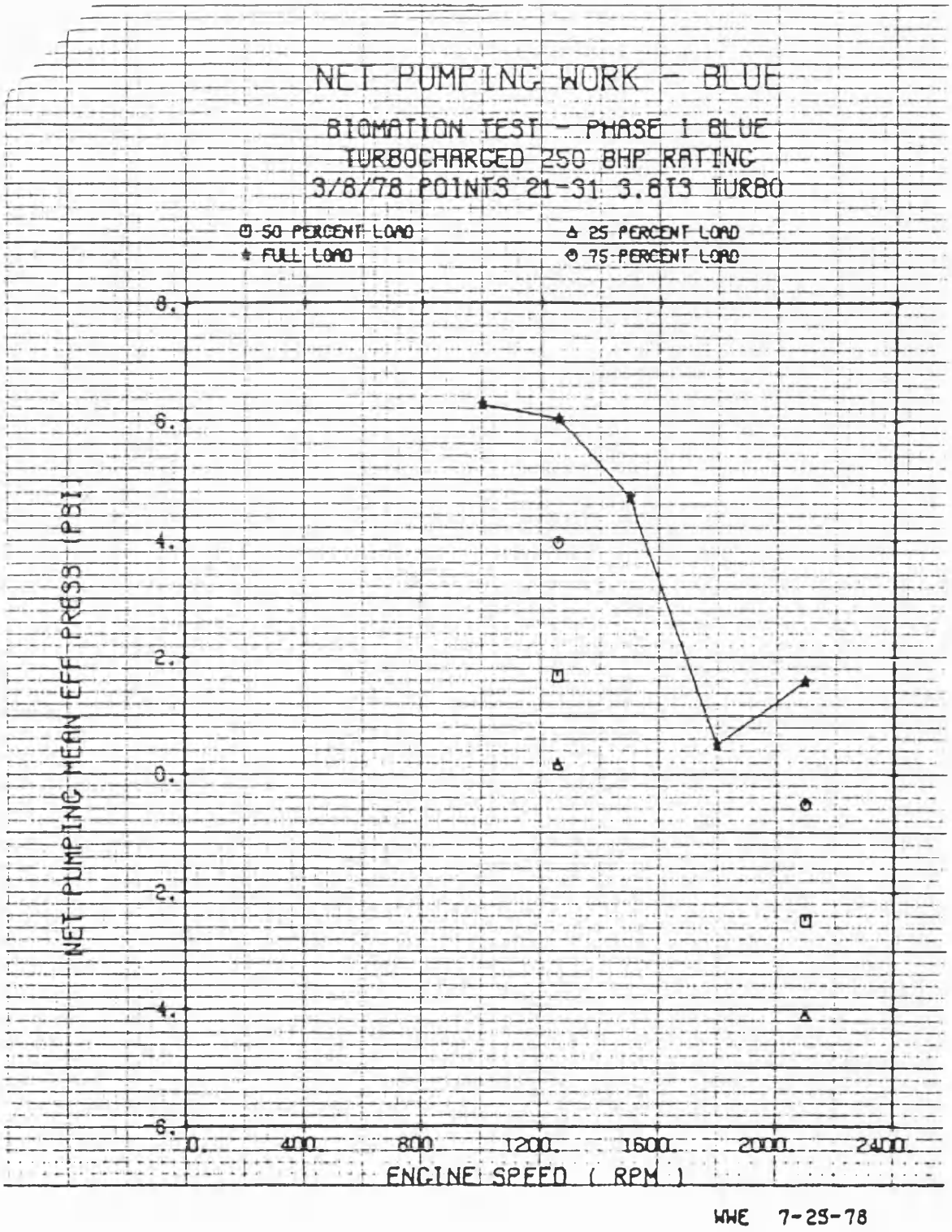

Fig. 4.20 Experimental PMEP of the L10-T/C engine

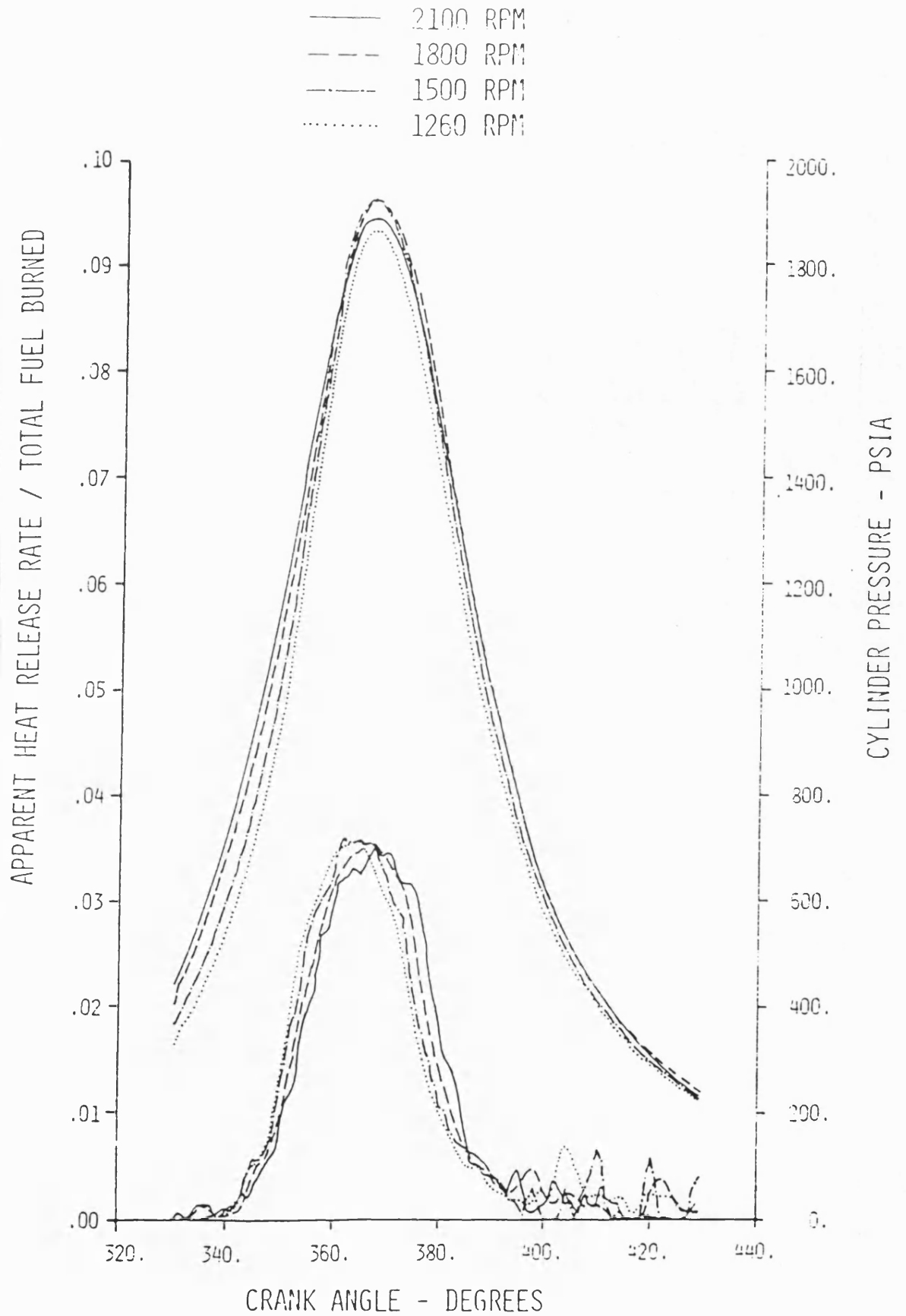

Fig. 4.21 Superimposed experimental heat release diagrams of the L10-T/C engine at different engine speeds at full load

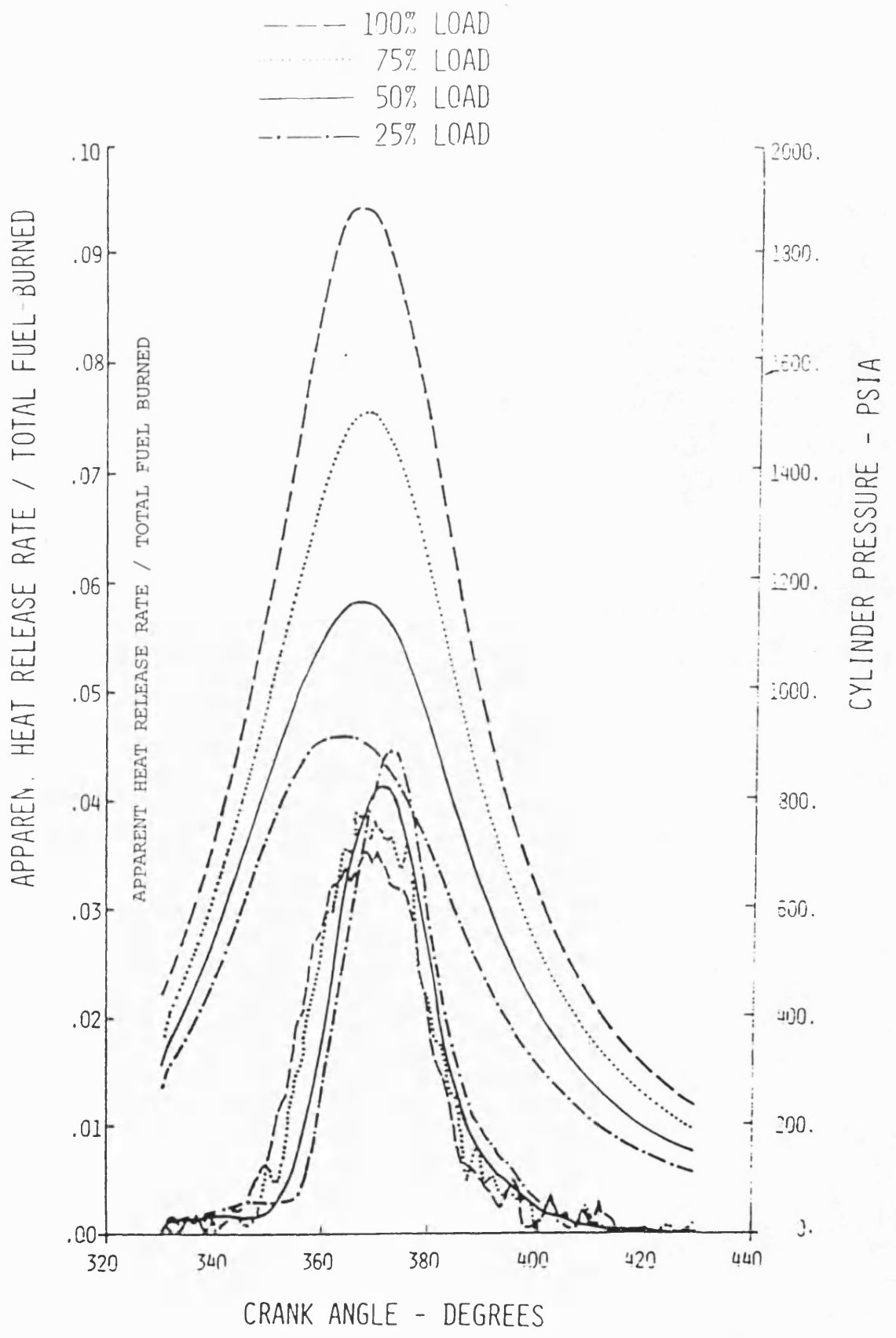

Fig. 4.22 Superimposed experimental heat release diagrams of the L10-T/C engine at different loads at speed of 2100 rpm

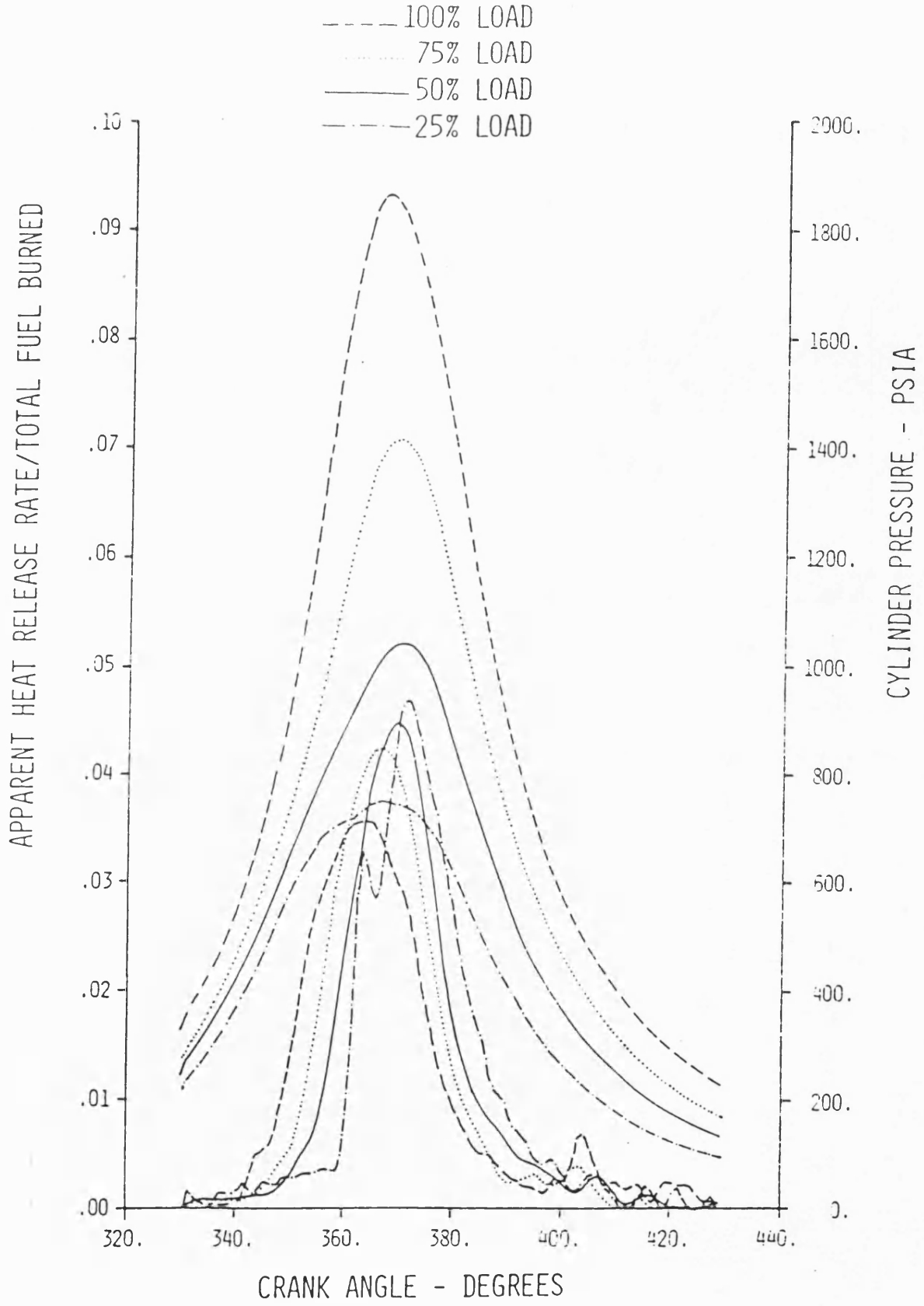

Fig. 4.23 Superimposed experimental heat release diagrams of the L10-T/C engine at different loads at a speed of 1260 rpm

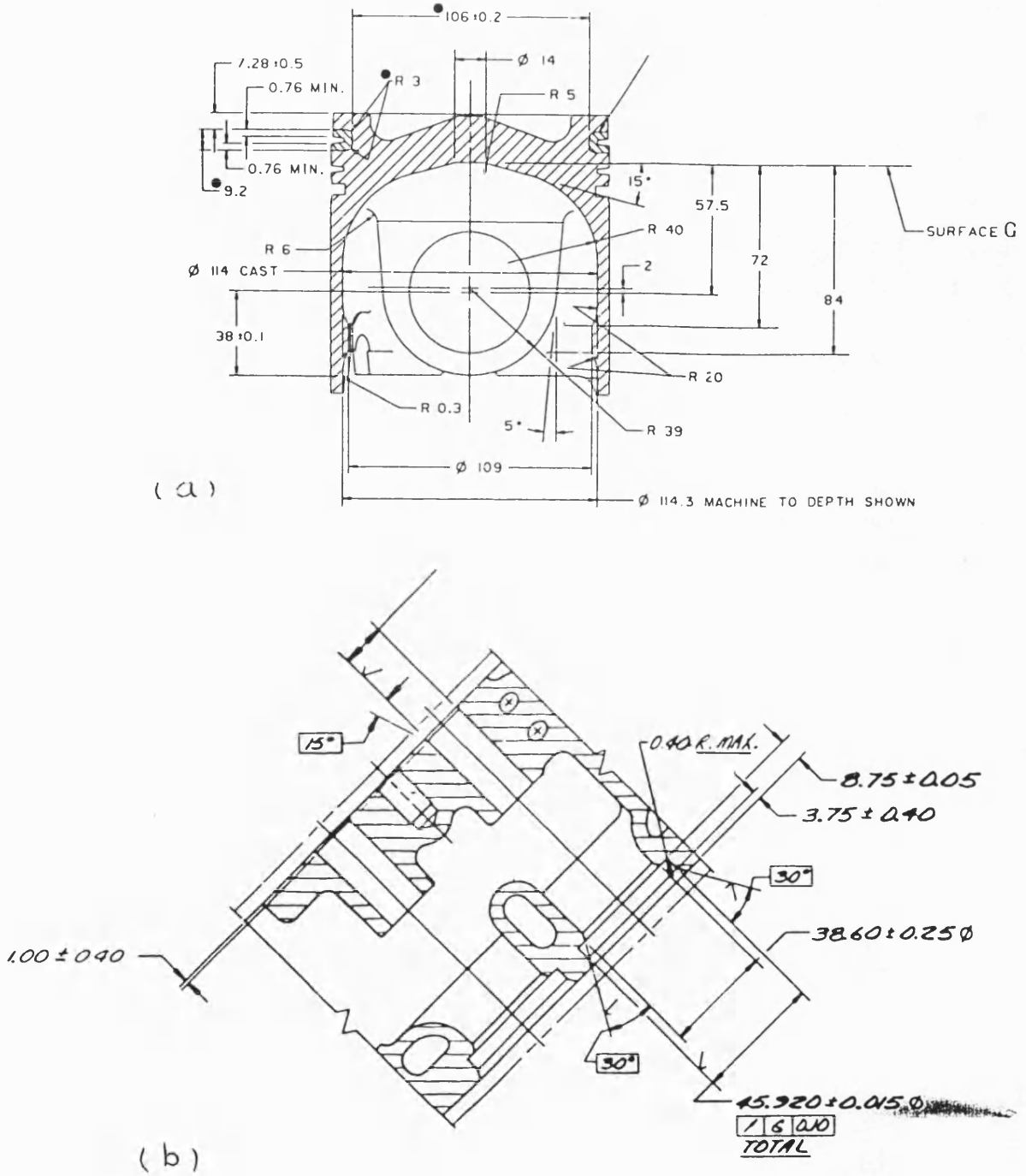

Fig. 4.24 The piston (a) and cylinder head inlet passage ways (b) of the L10 engine

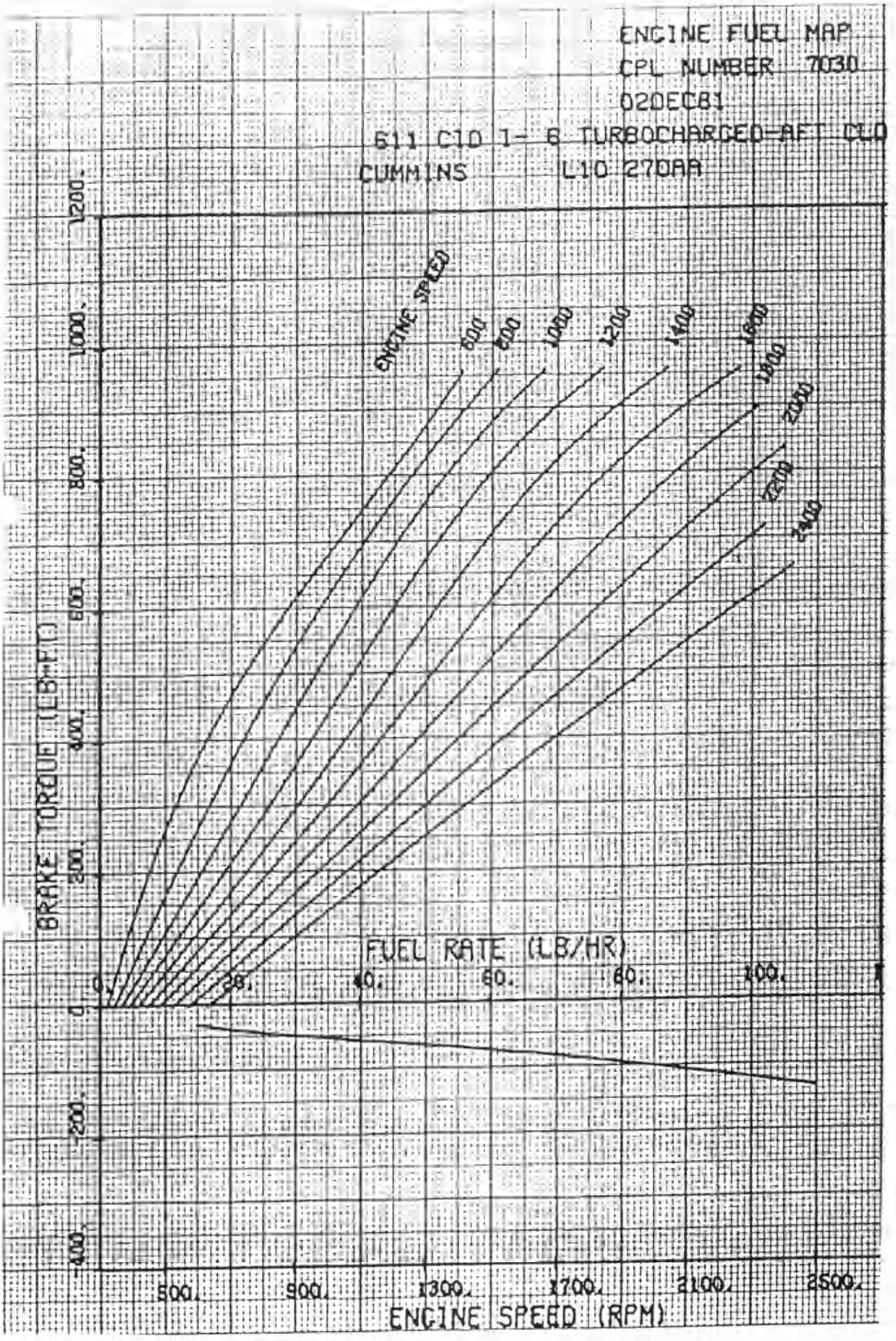

Fig. 4.25 Fuelling map of the L10 engine and resulted Willans line

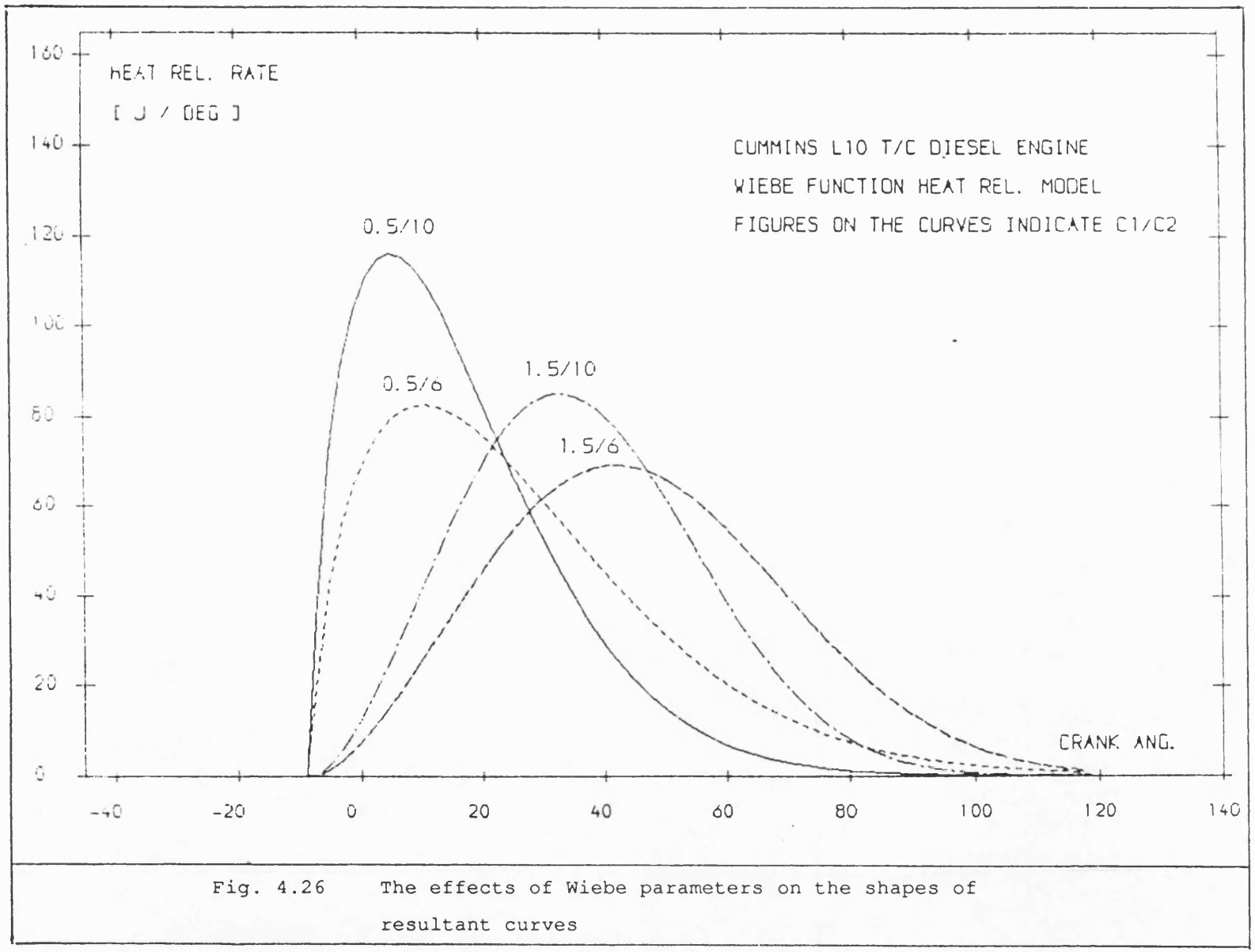

Fig. 4.26 The effects of Wiebe parameters on the shapes of resultant curves

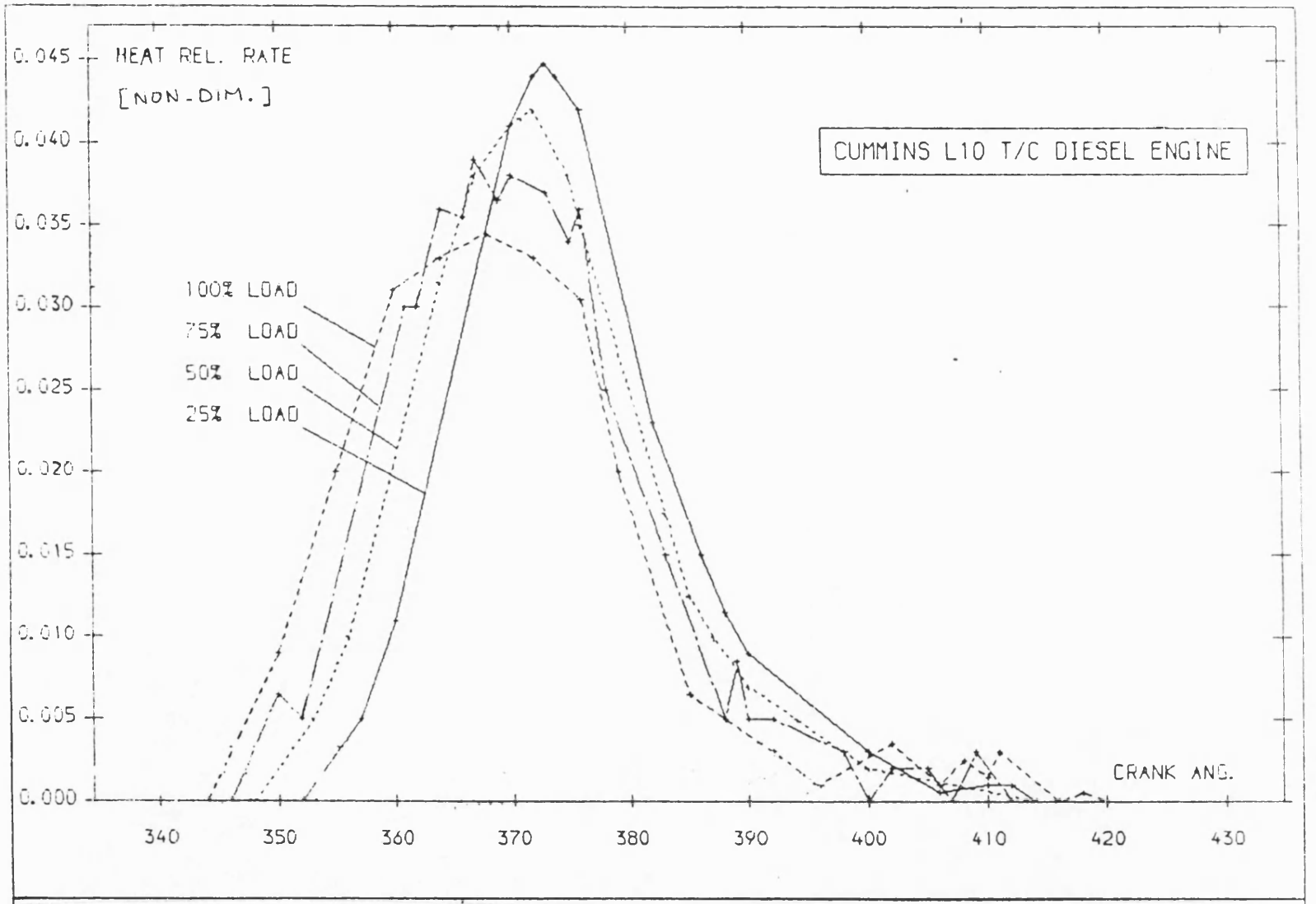

Fig. 4.27 Experimental heat release diagrams of Fig. 4.22 after transfer to the computer files

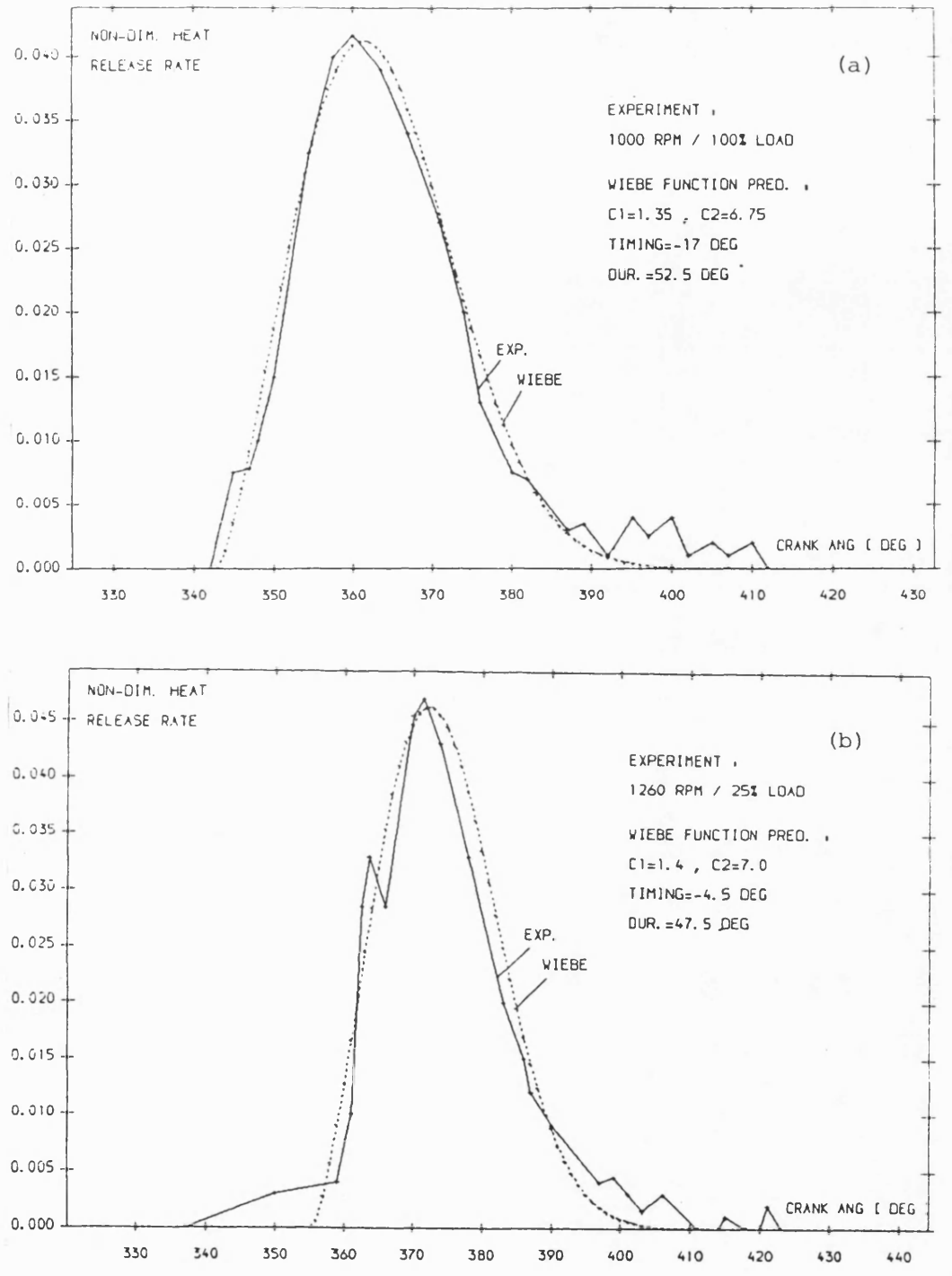

Fig. 4.28 Wiebe curve fitting results on experimental 'AFBR' of the L10-T/C engine

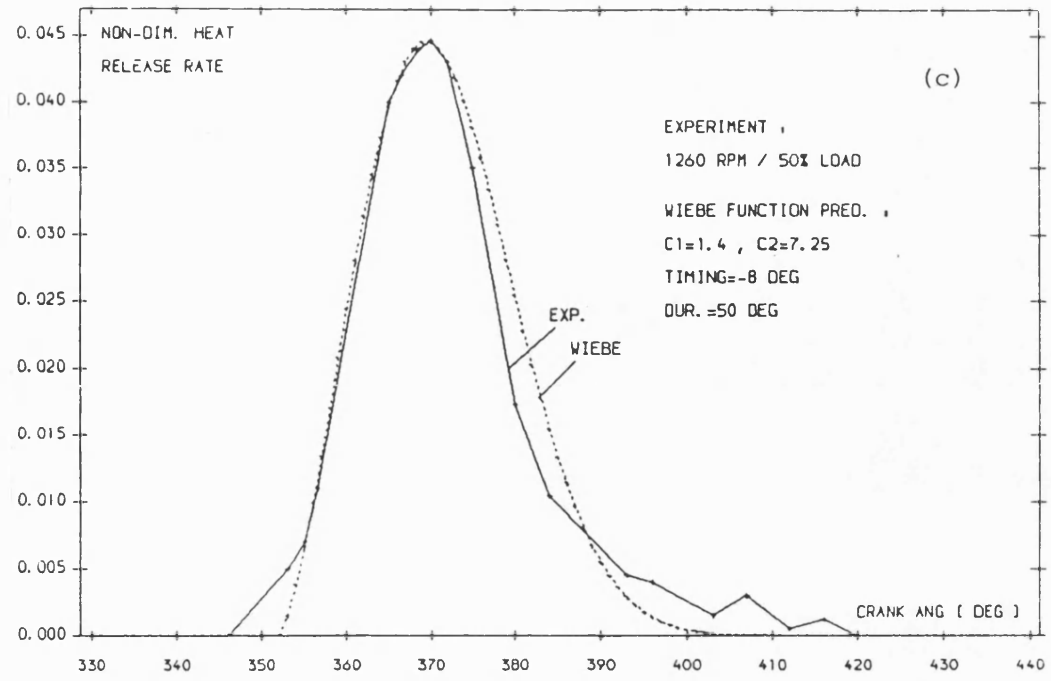

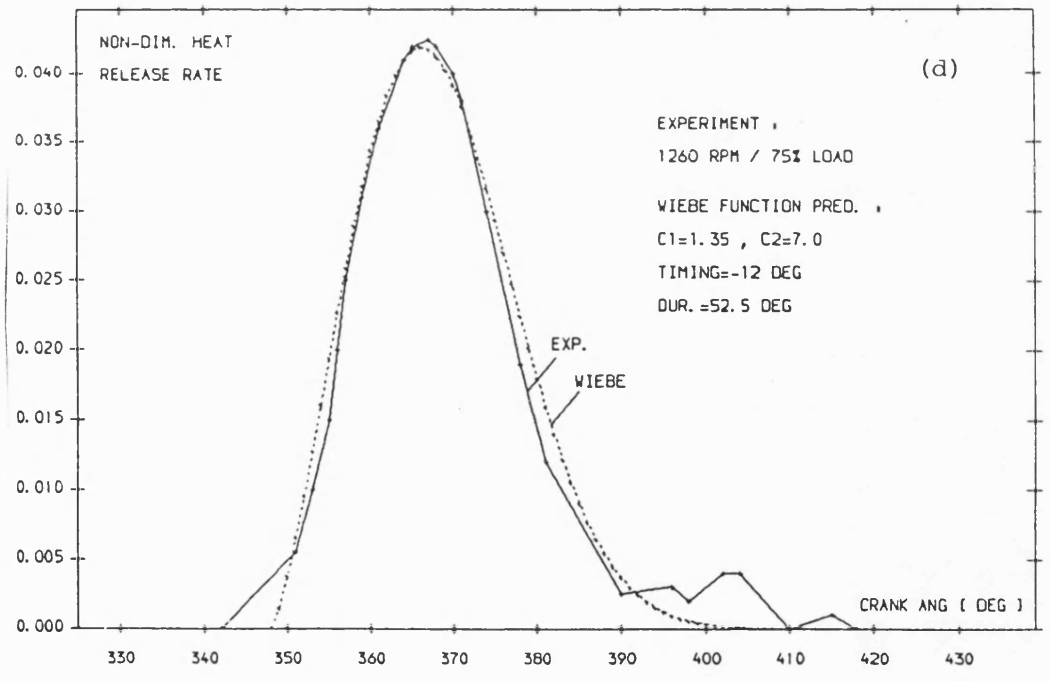

Fig. 4.28 Wiebe curve fitting results on the experimental AFBR of the L1O-T/C engine

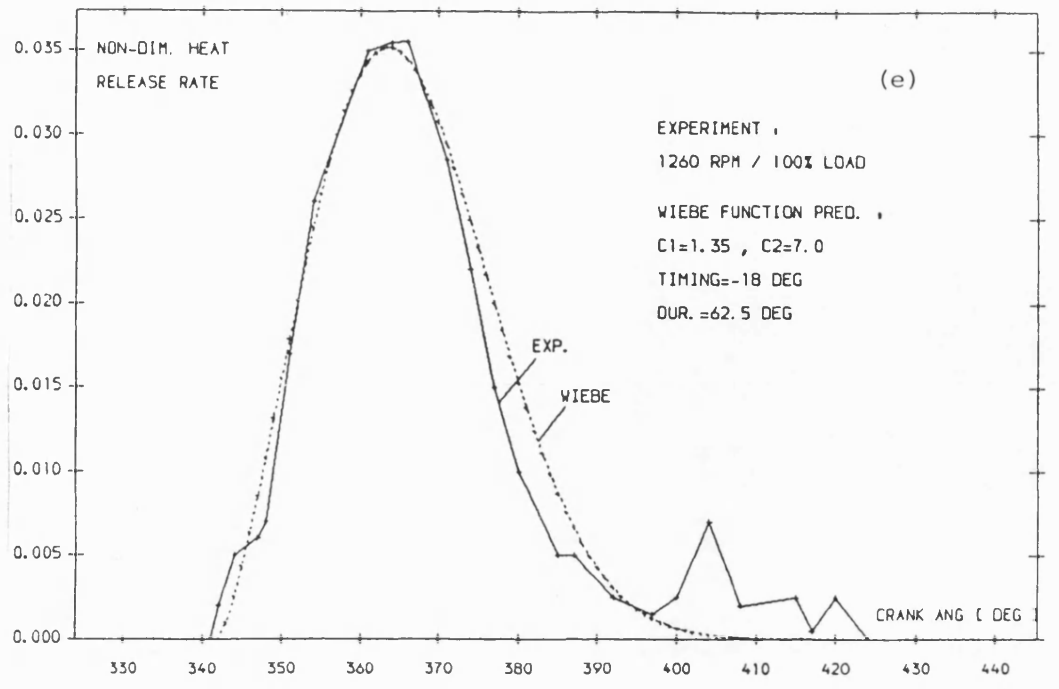

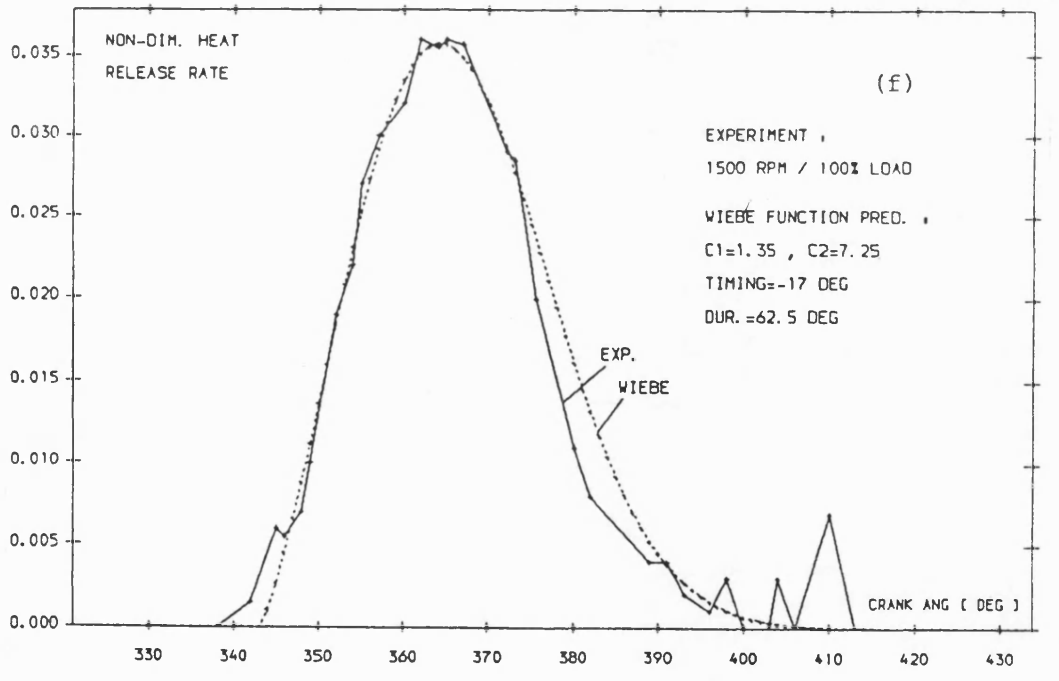

Fig. 4.28 The results of Wiebe curve fitting on the experimental 'AFBR' of the L1O-T/C engine

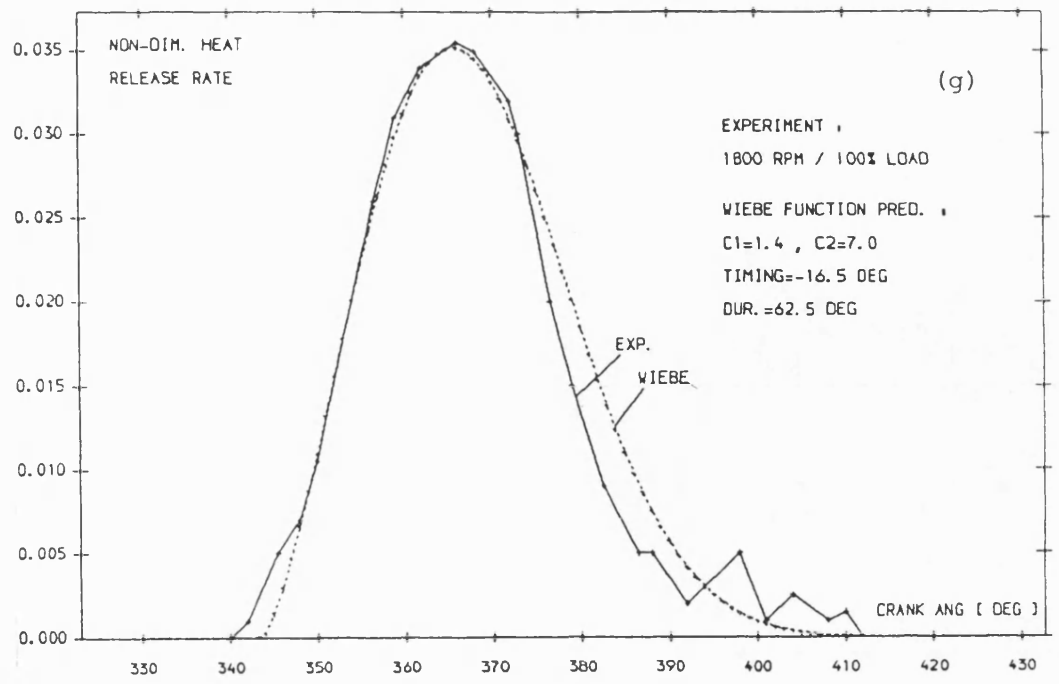

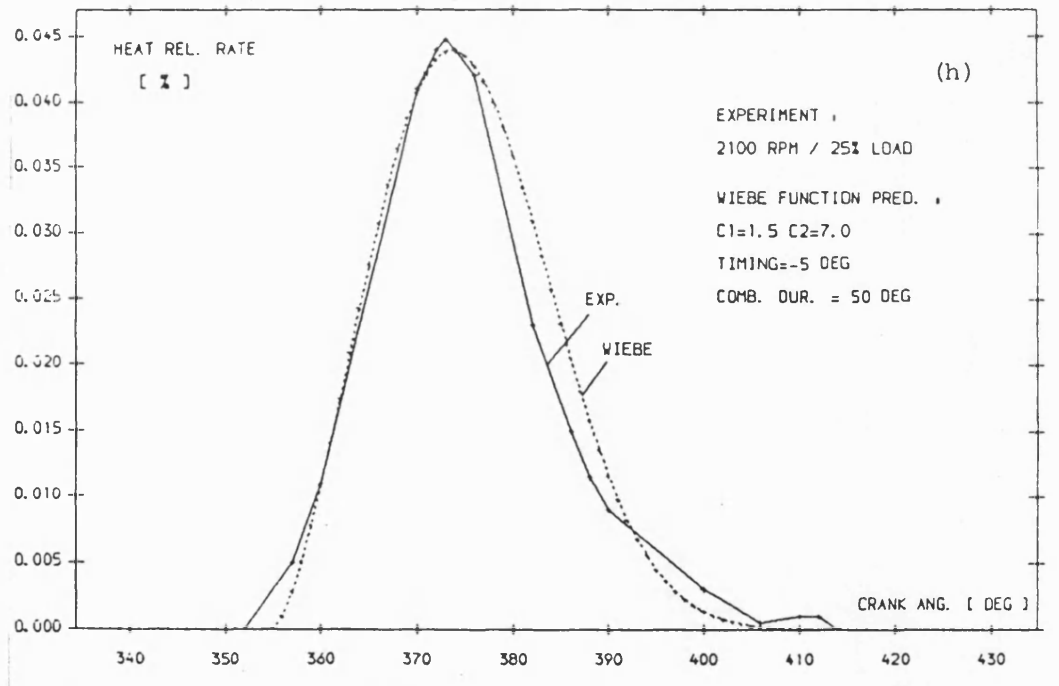

Fig, 4.28 The results of the Wiebe curve fitting on the experimental 'AFBR' of the L1O-T/C engine

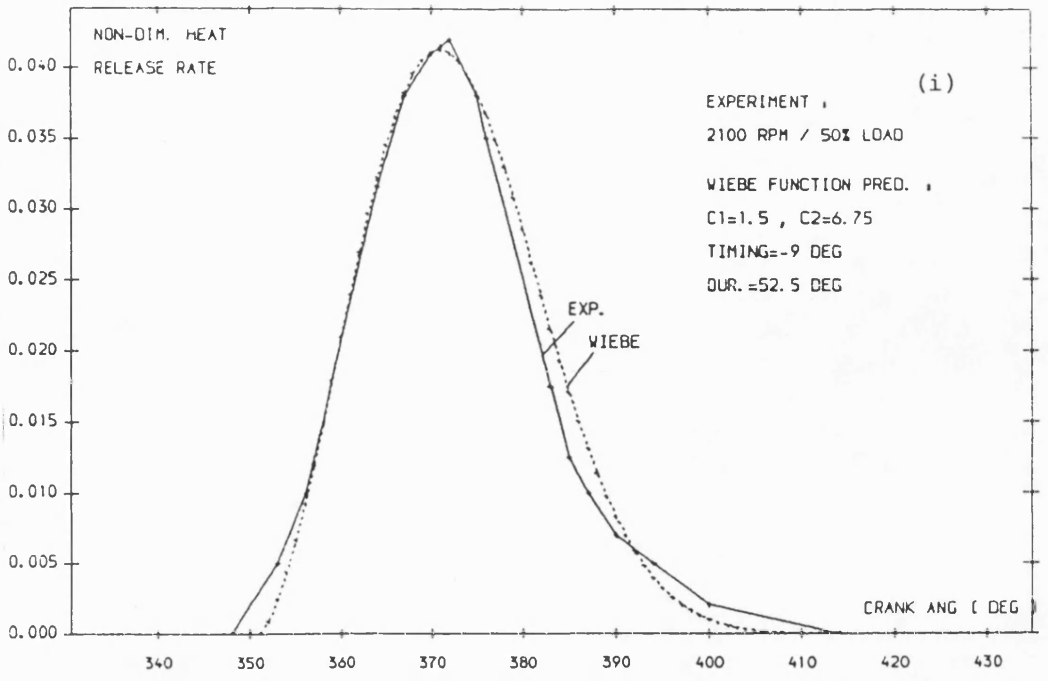

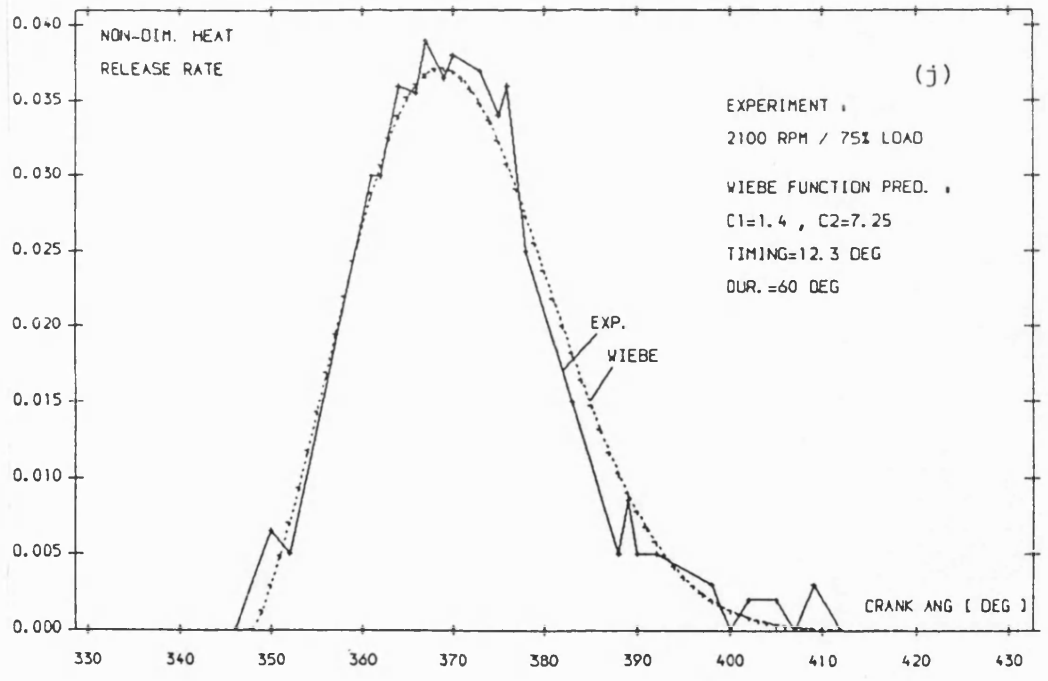

Fig. 4.28 The Wiebe curve fitting on the experimental 'AFBR' of the L1O-T/C engine

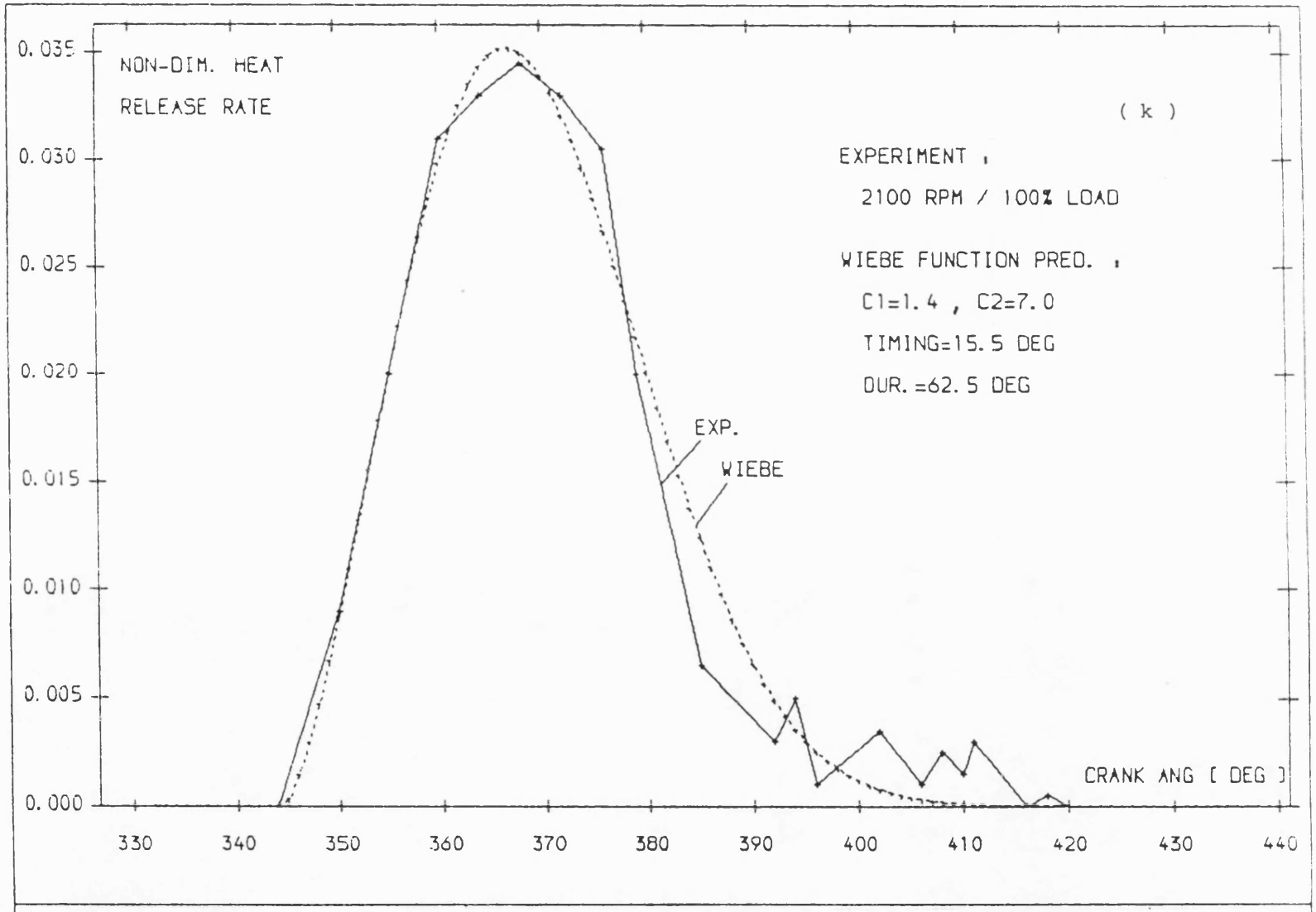

Fig. 4.28 The Wiebe curve fitting on the experimental 'AFBR' of the L10-T/C engine

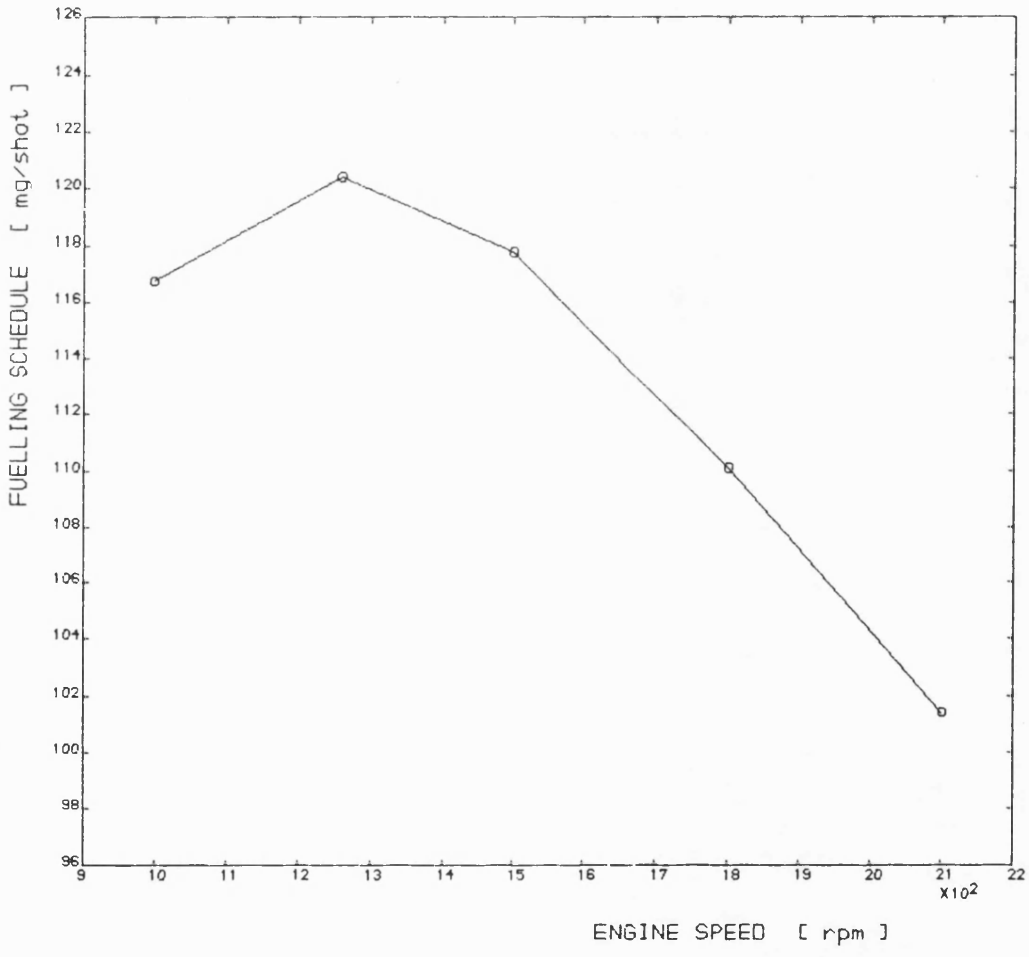

Fig. 4.29 The LTC fuelling schedule of the CUMMINS L10.250-T/C ENGINE

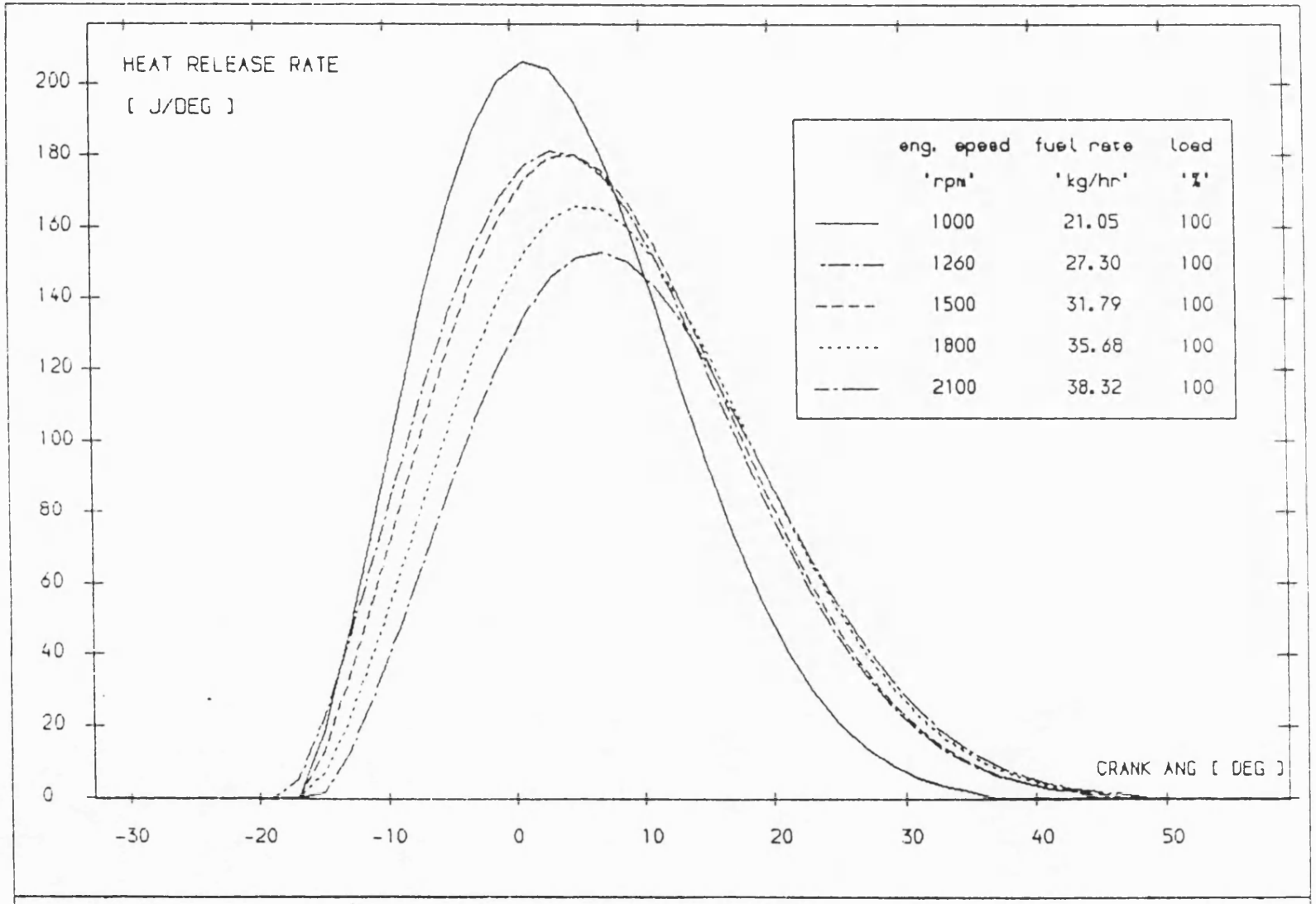

Fig. 4.30 Superimposed heat release rate diagrams of the L10.250-T/C engine at the running conditions along the LTC

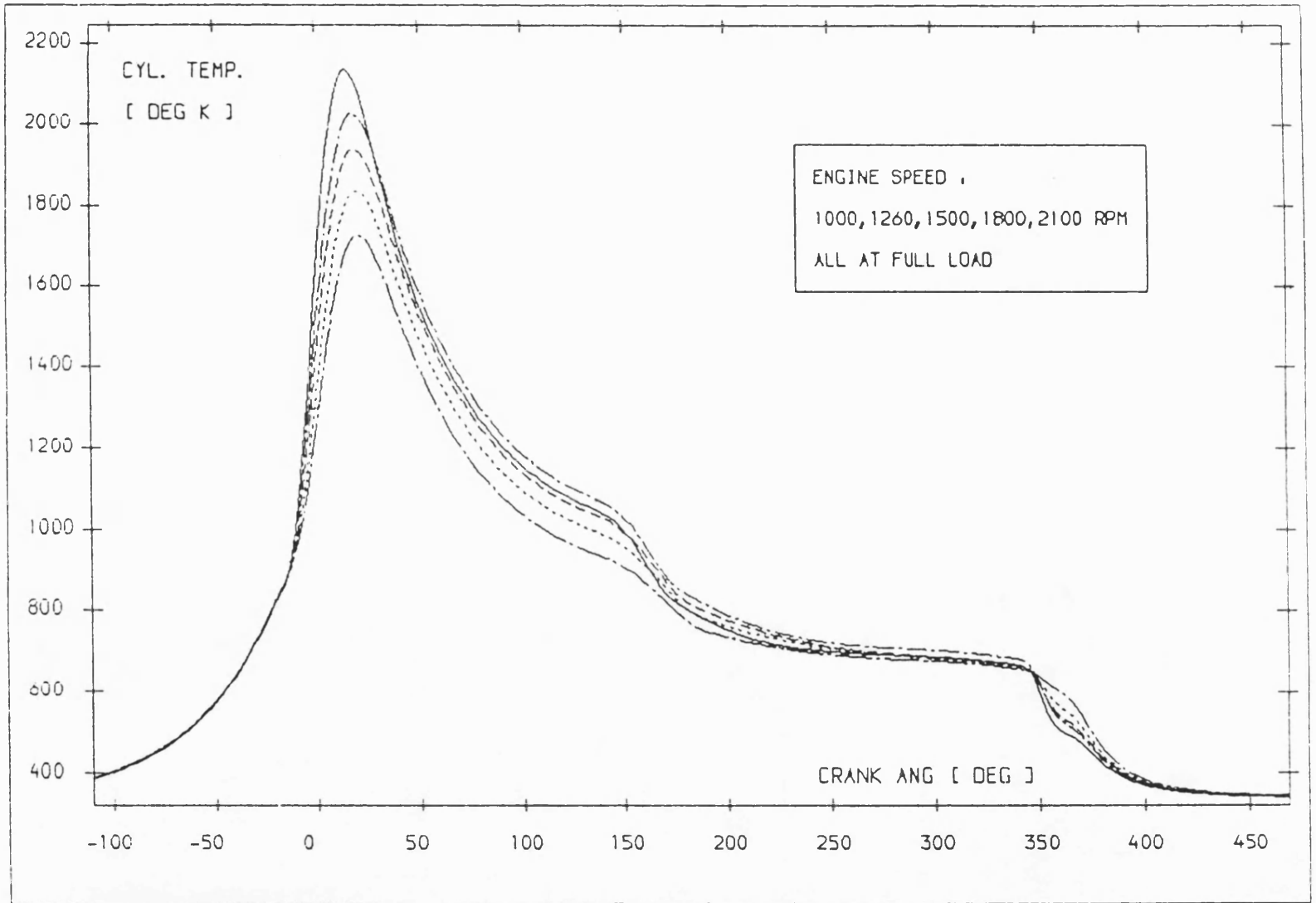

Fig. 4.31 Superimposed in-cylinder gas temperature of the L10.250-T/C engine at the running conditions along the LTC

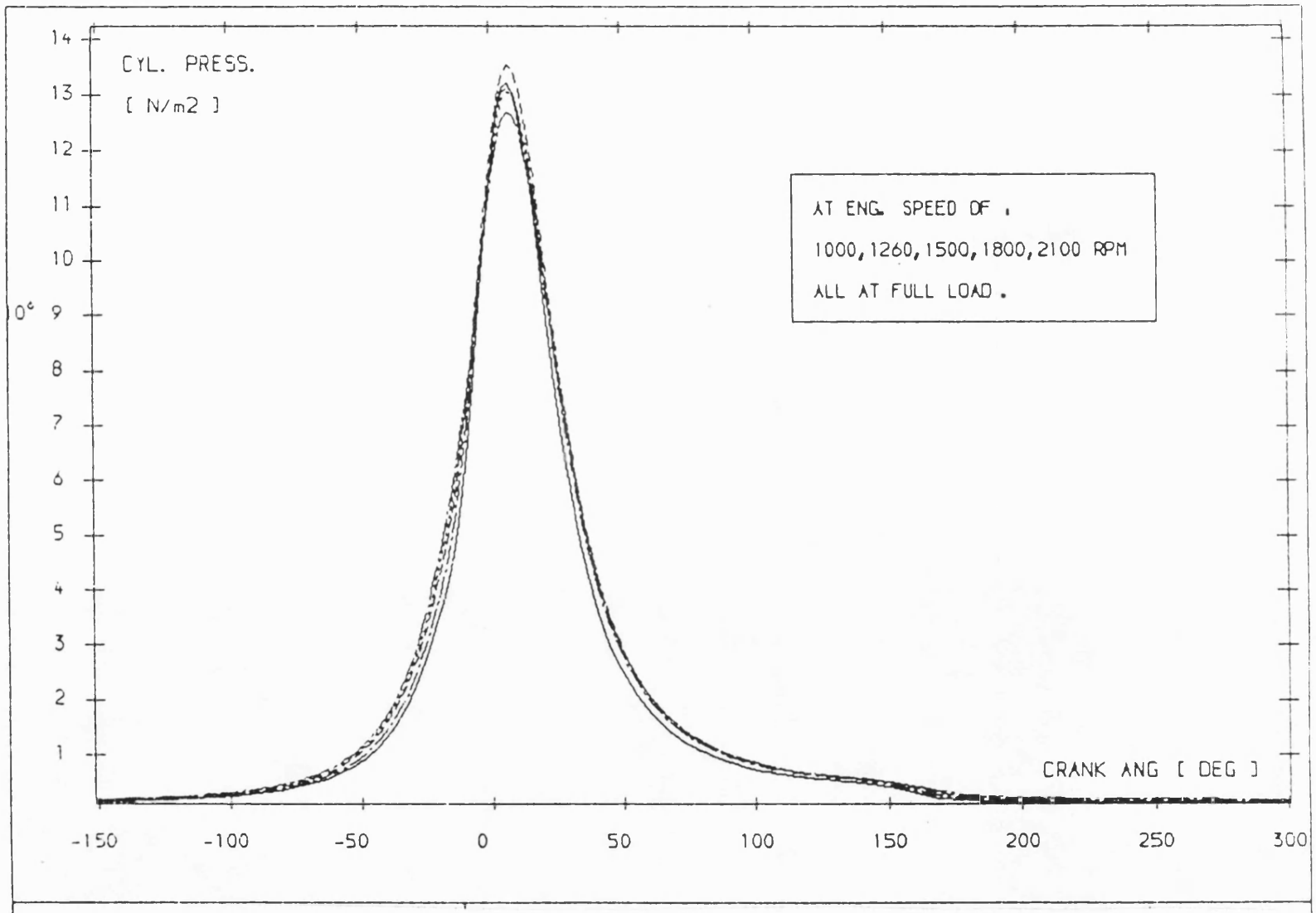

Fig. 4.32 Superimposed cylinder pressure of the L10.25-T/C engine at the running conditions along the LTC

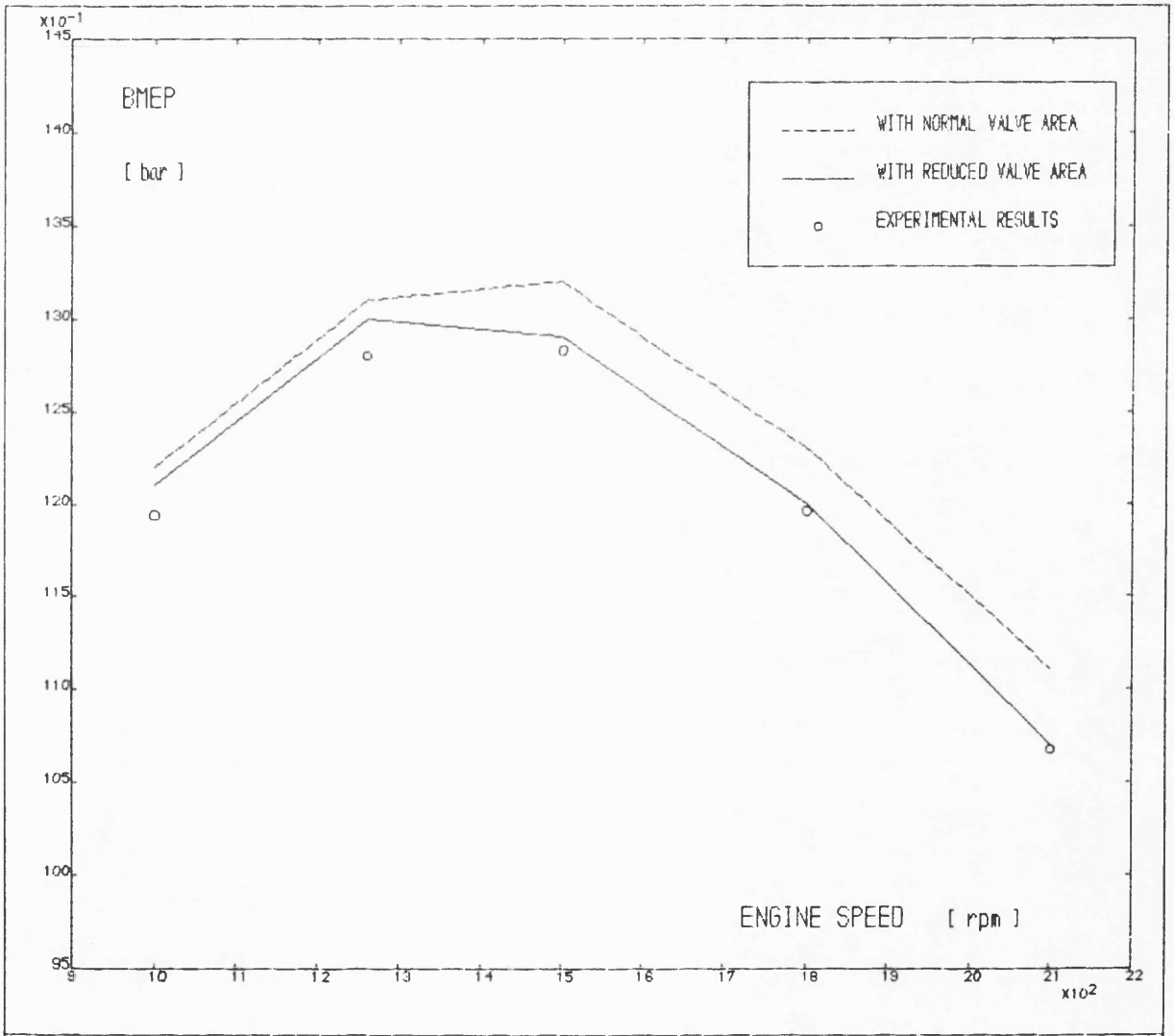

Fig. 4.33 The 'SPICE' predictions for BMEP of the L10.250-T/C engine at full load (LTC) compared with experimental results

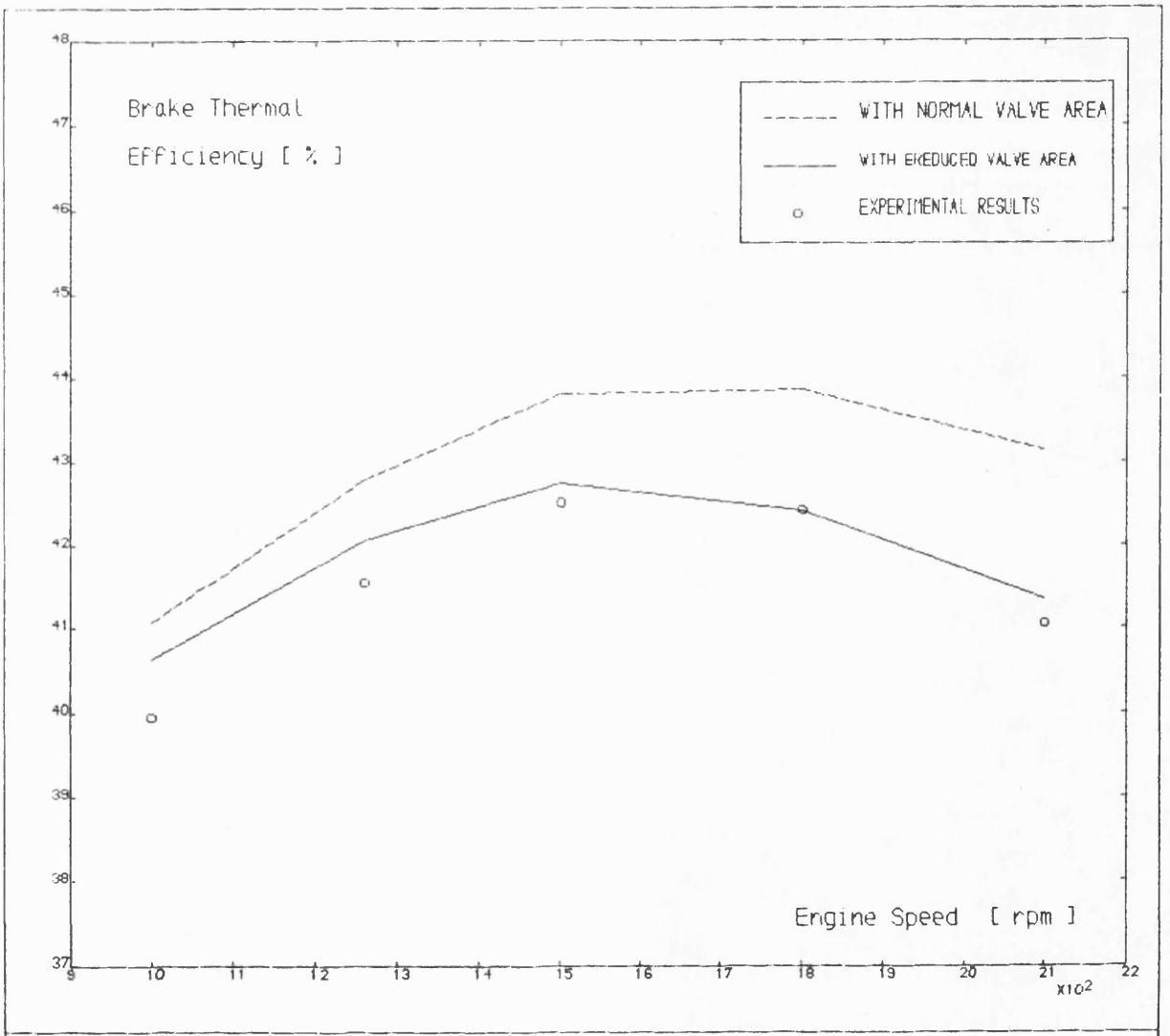

Fig. 4.34 The 'SPICE' predictions for brake thermal efficiency of the L10.250-T/C engine along the LTC compared with experimental results

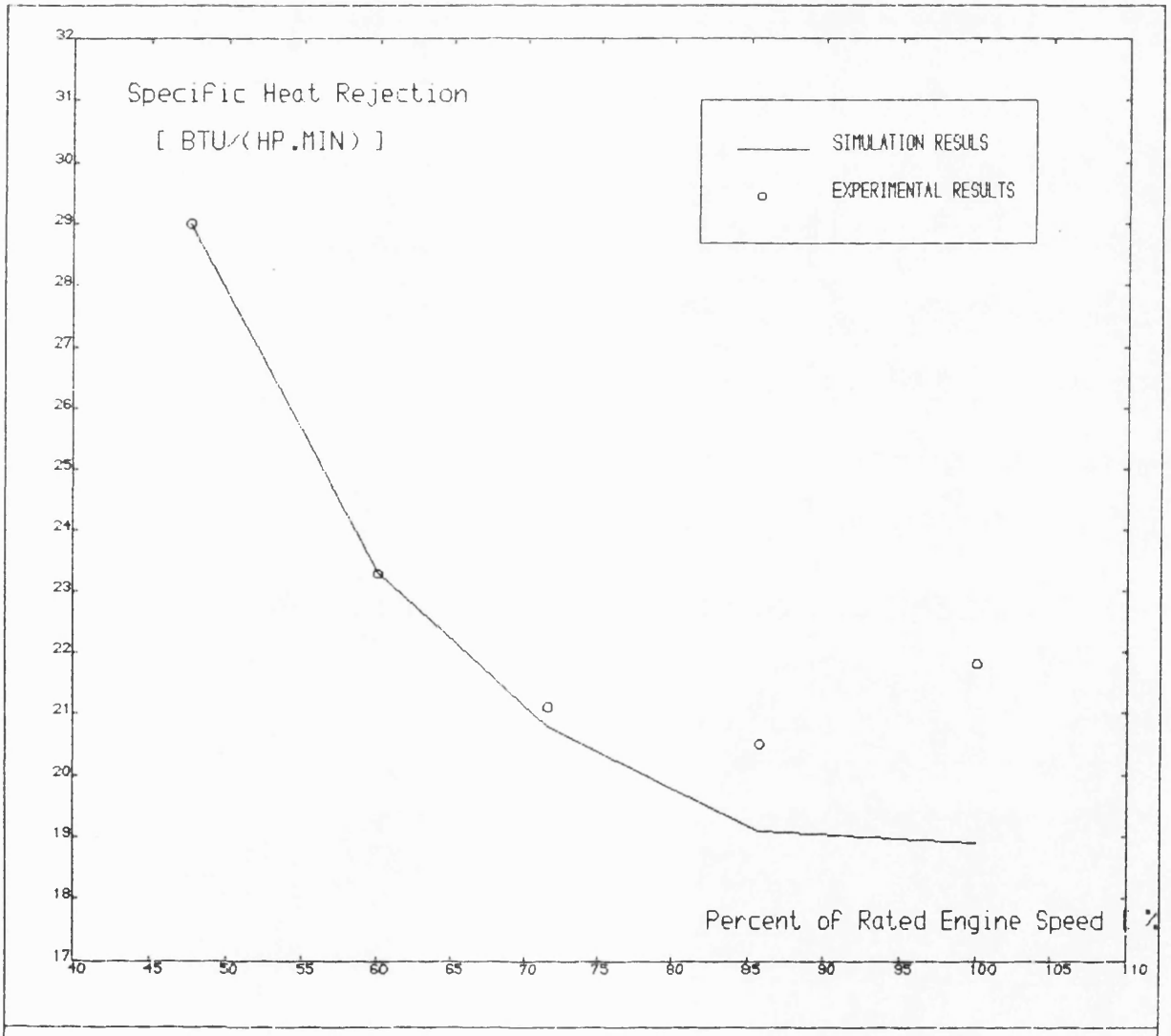

Fig. 4.35 The 'SPICE' predictions for specific heat rejection of the L10.250-T/C engine compared with the corresponding experimental results

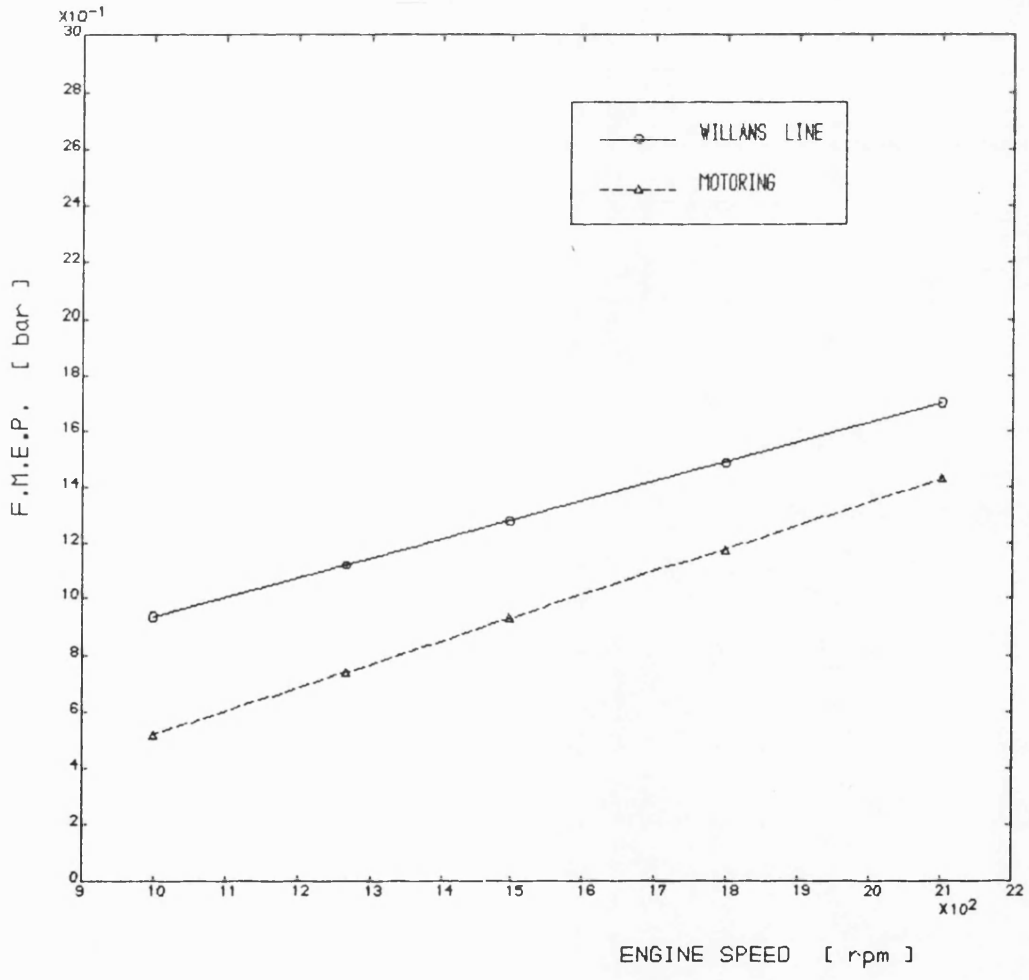

Fig. 4.36 The friction mean effective pressure of the CUMMINS L10 DIESEL ENGINE

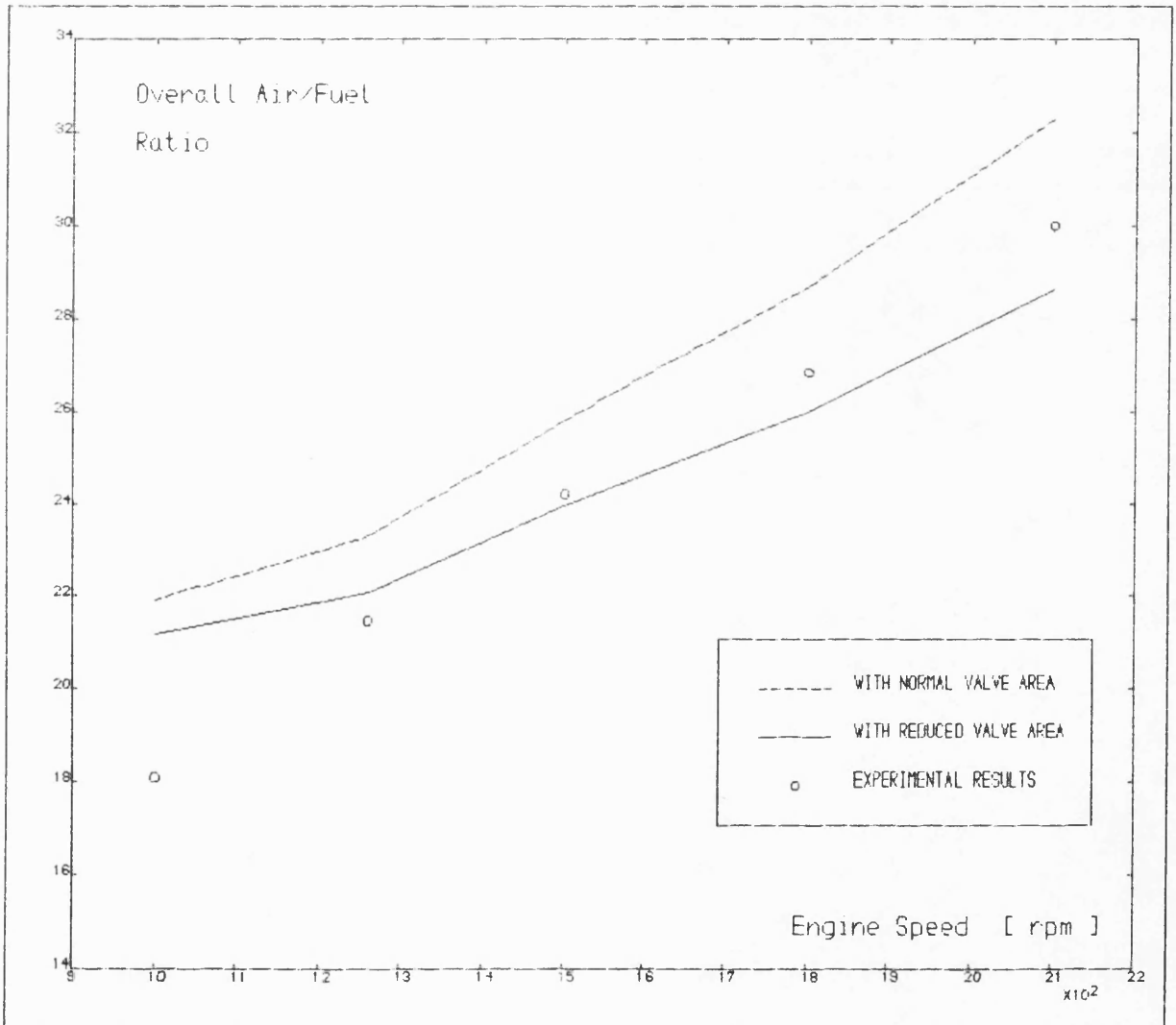

Fig. 4.37 The 'SPICE' predictions for overall air_fuel ratio of the L10.250-T/C engine along its LTC compared with the experimental results

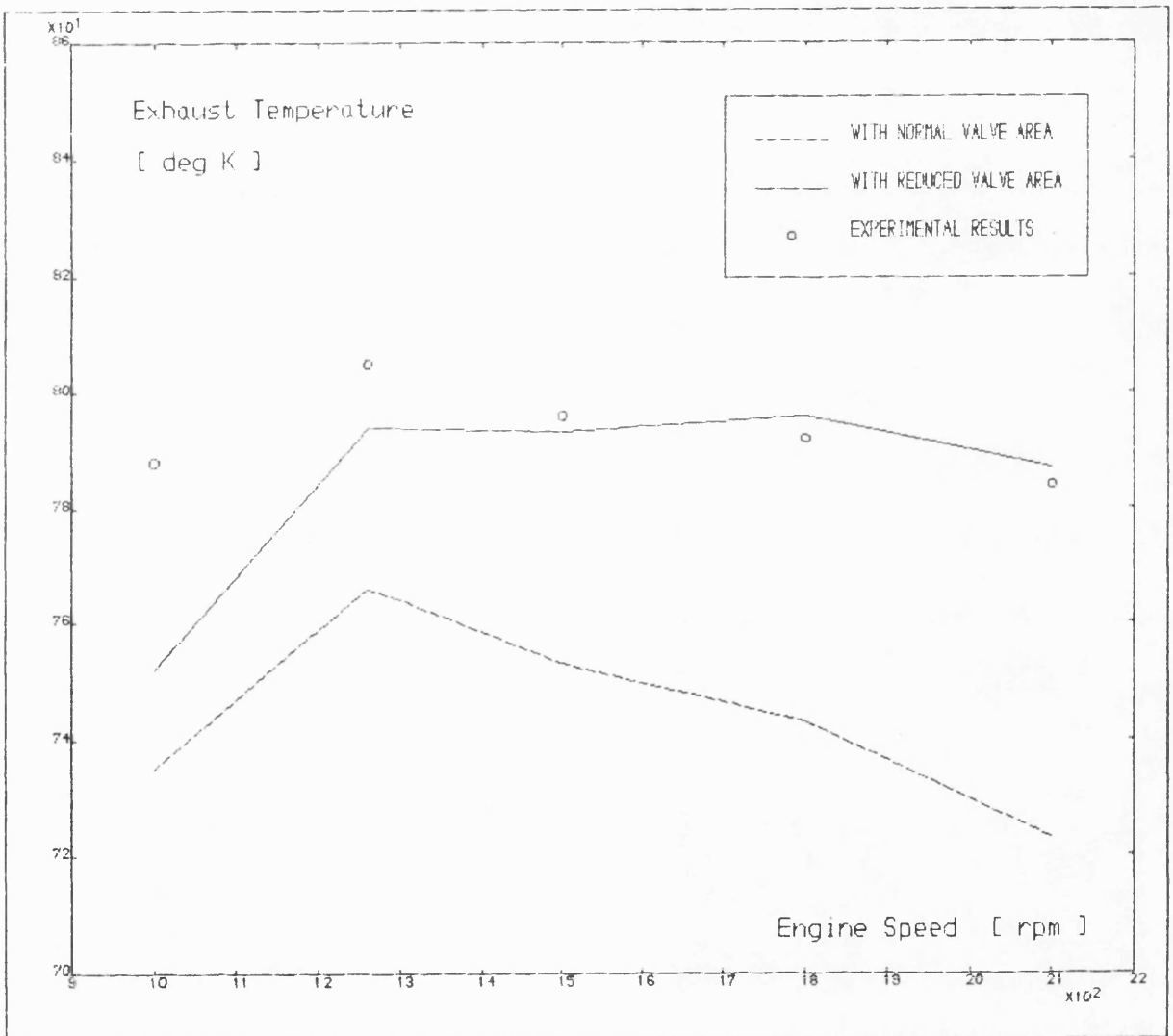

Fig. 4.38 The 'SPICE' predictions for exhaust gas temperature of the L10.250-T/C engine along its LTC compared with the experimental results

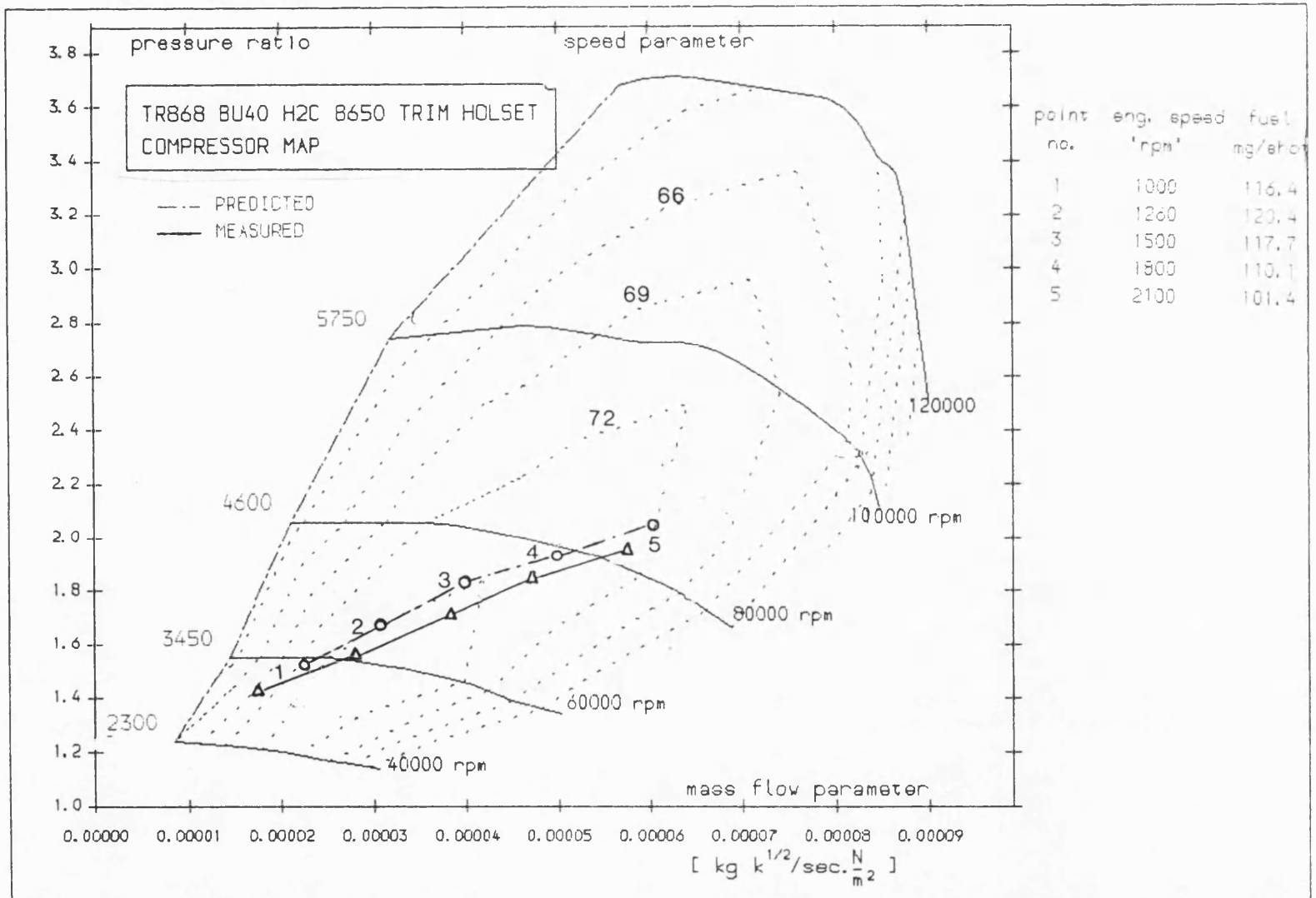

Fig. 4.39 Holset H2C compressor map superimposed with the experimental and predicted operating lines (CUMMINS L10 T/C Engine)

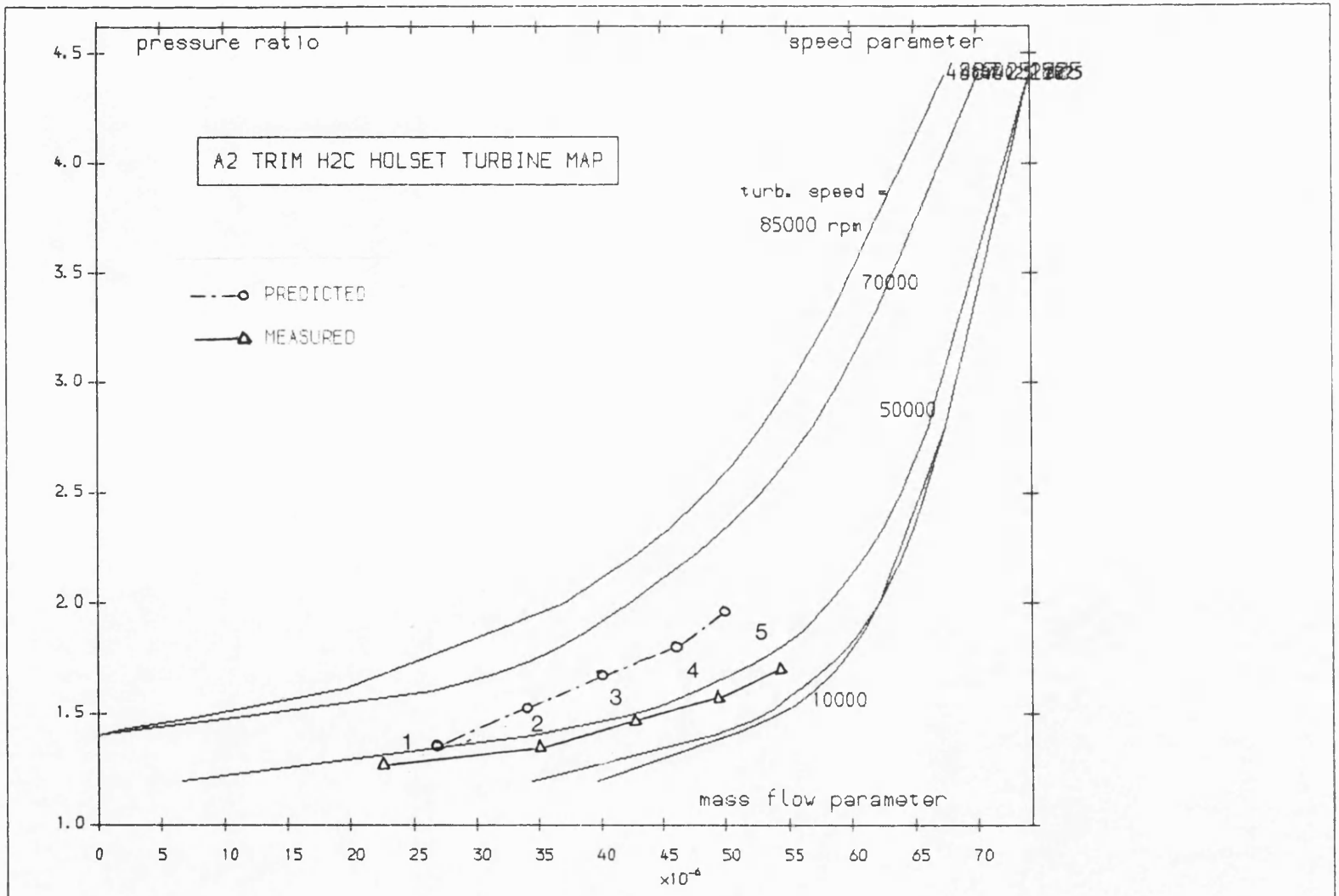

Fig. 4.40 Holset H2C A2 trim turbine map superimposed with the experimental and predicted operating lines (CUMMINS L10 T/C Engine)

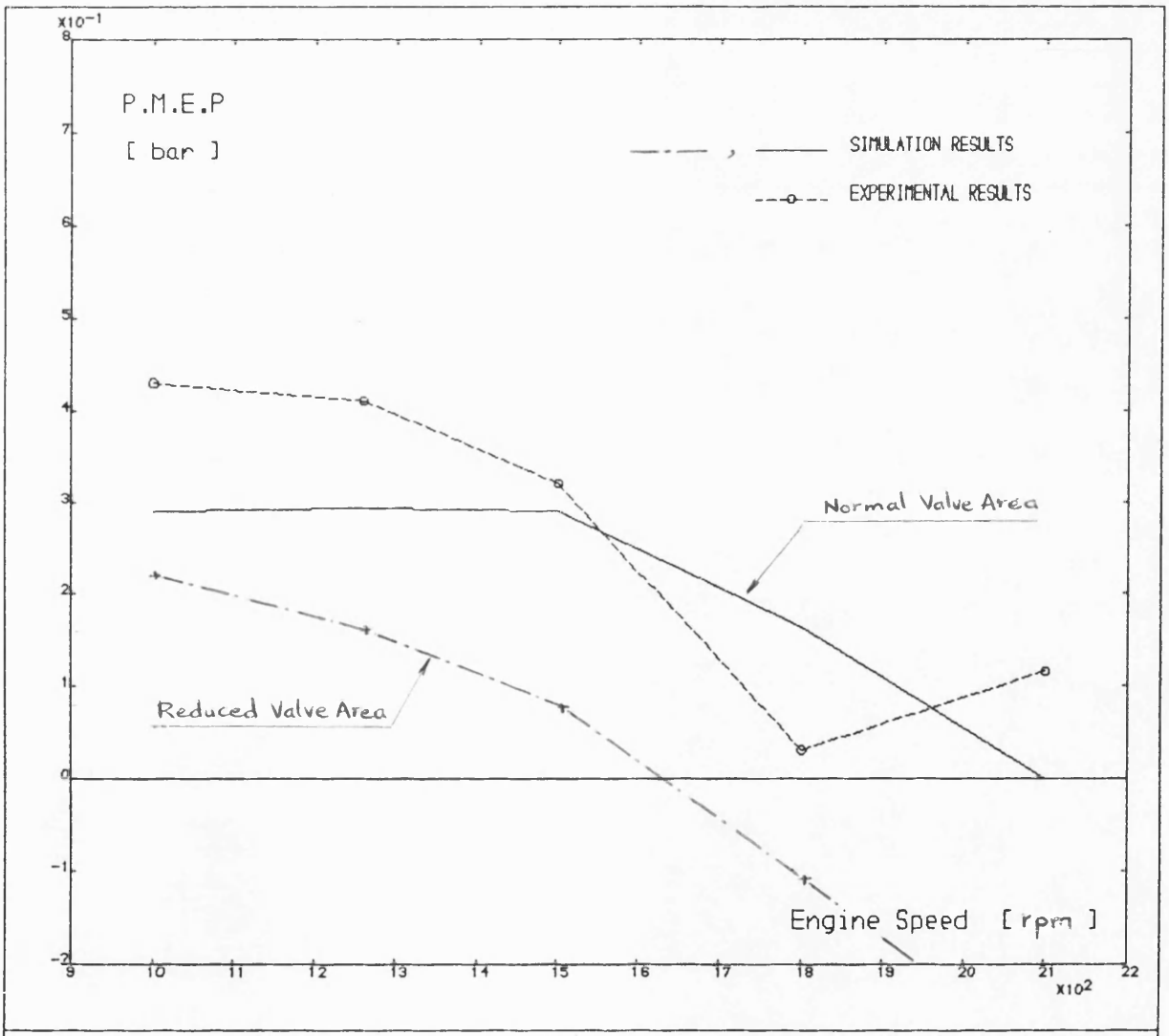

Fig. 4.41 The 'SPICE' predictions for pumping mean effective pressure of the L10.250-T/C engine compared with the corresponding experimental results

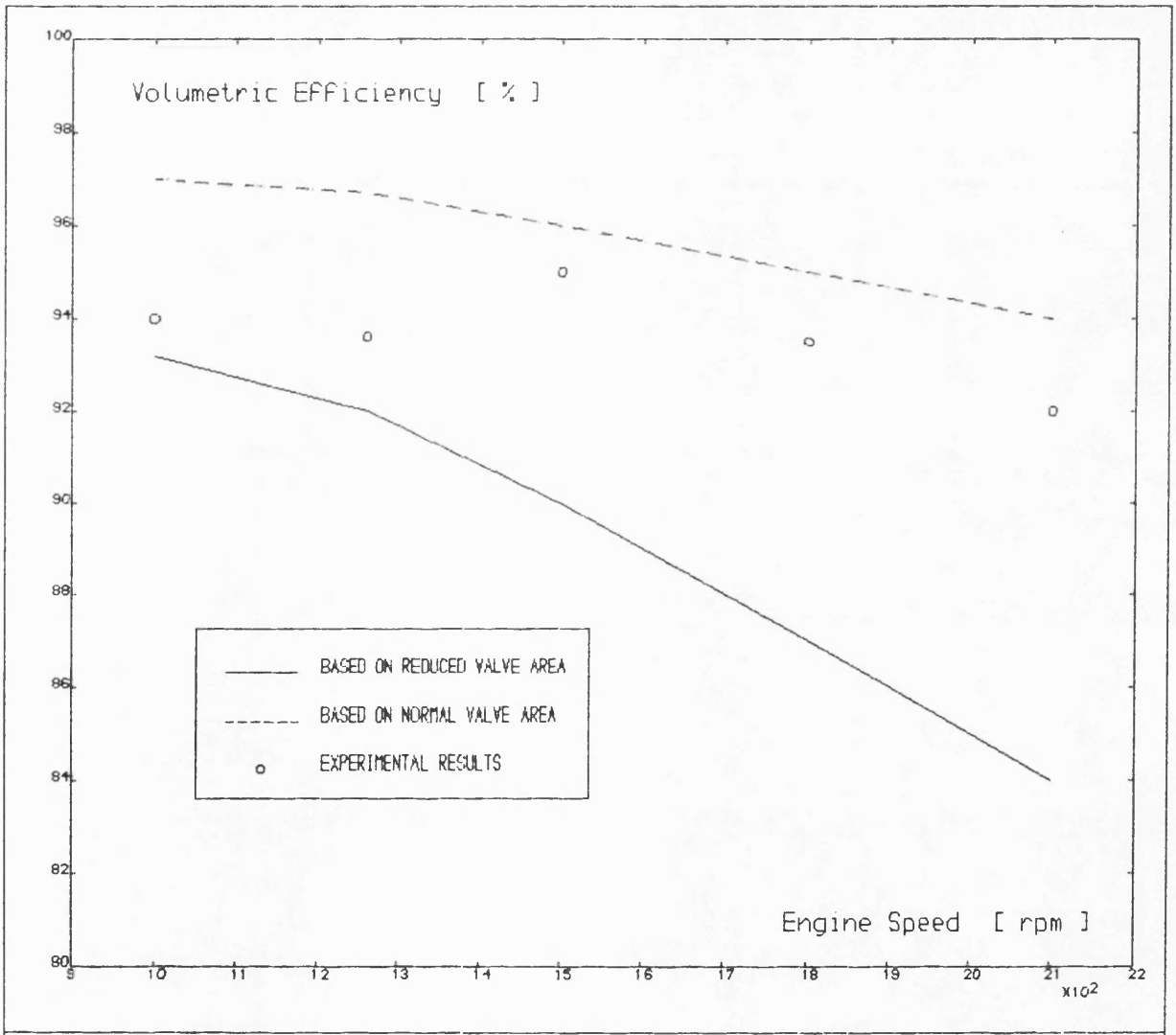

Fig. 4.42 The 'SPICE' predictions for volumetric efficiency of the L10.250-T/C engine compared with the corresponding experimental results

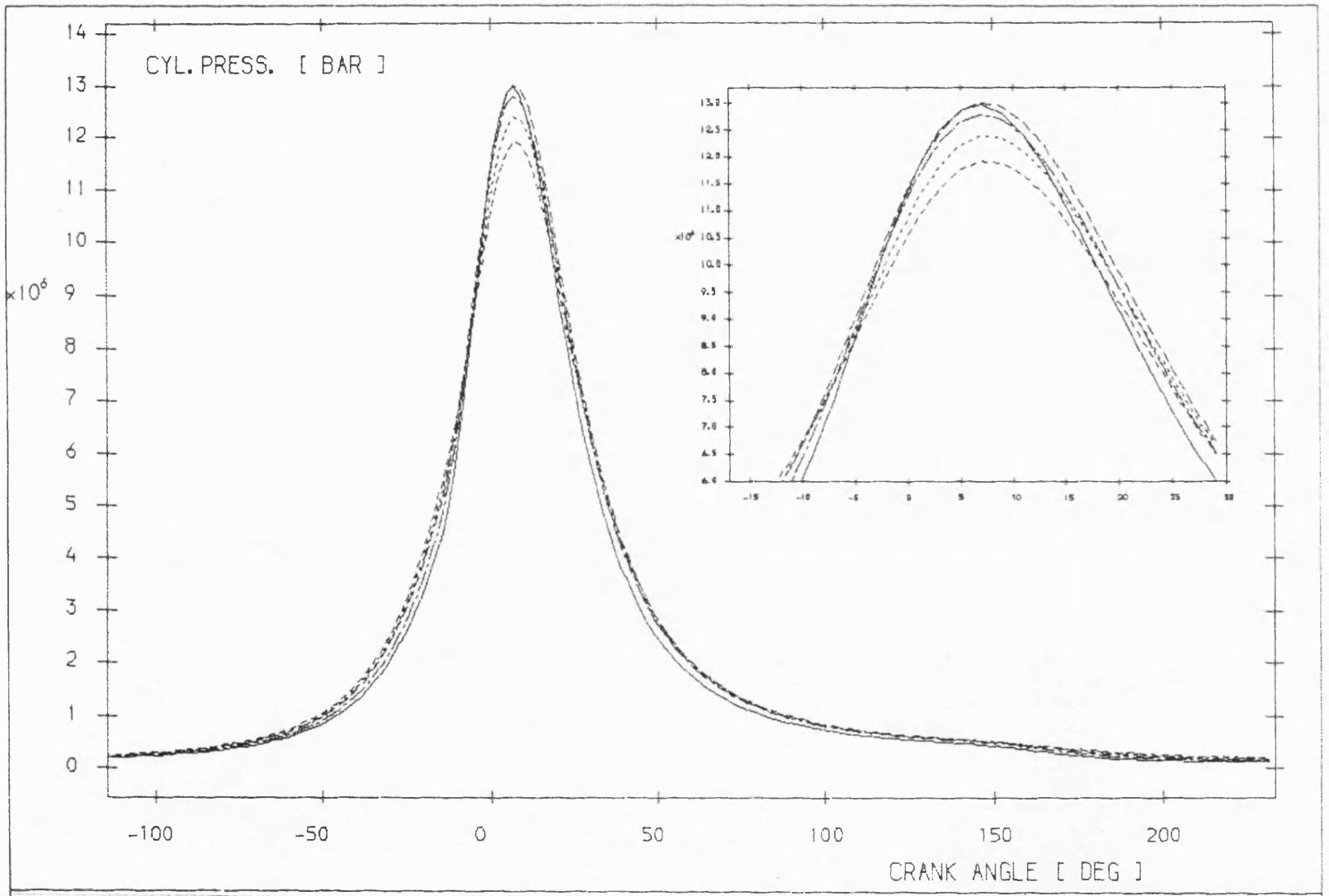

Fig. 4.43 Superimposed cylinder pressure diagrams of the L10.250-T/C engine with reduced valve areas at the running conditions along the LTC

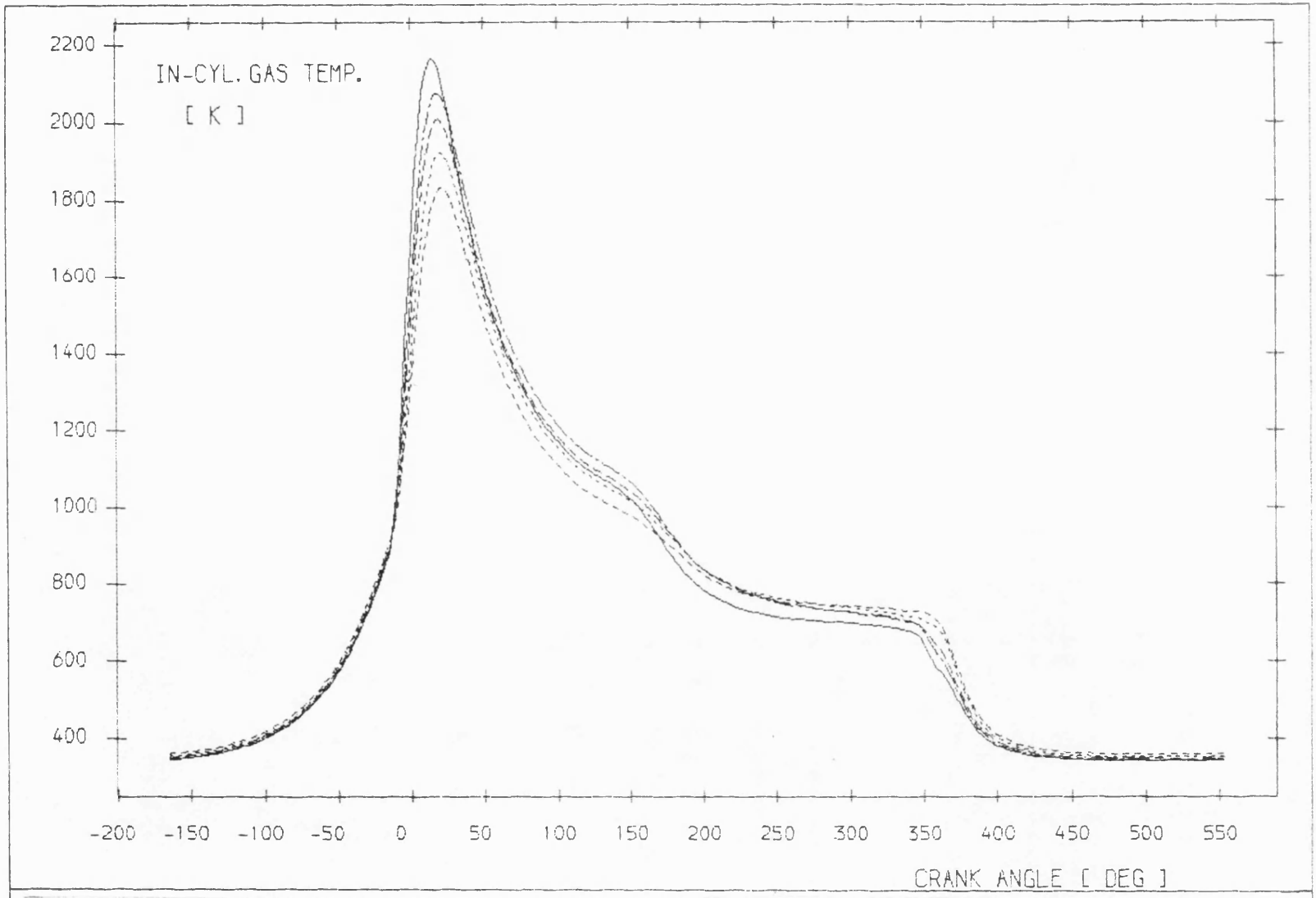

Fig. 4.44 Superimposed in-cylinder gas temperature of the L10.250-T/C engine with reduced valve areas at full load running conditions

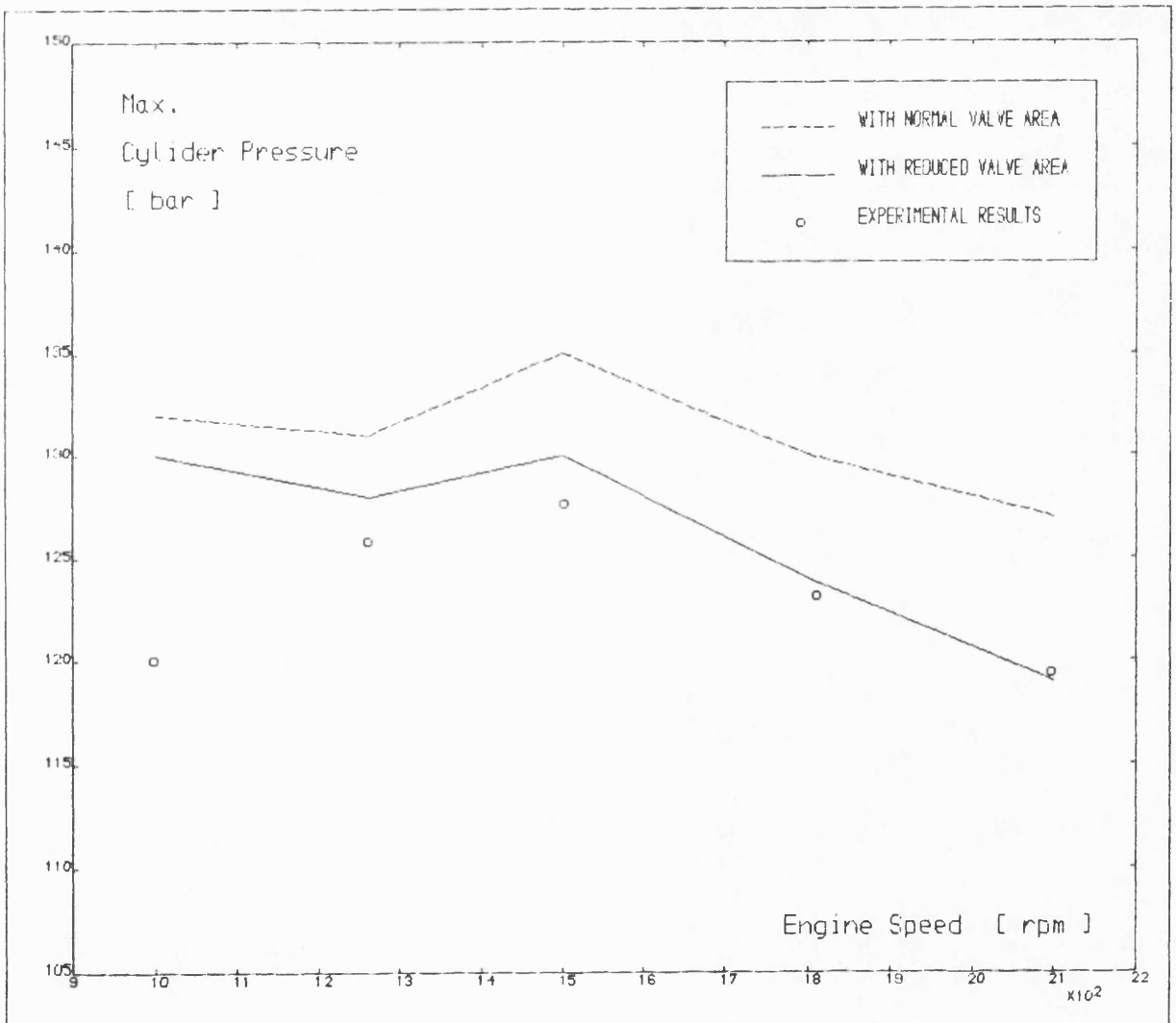

Fig. 4.45 The 'SPICE' predictions for max. cylinder pressure of the L10.250-T/C engine compared with the corresponding experimental results

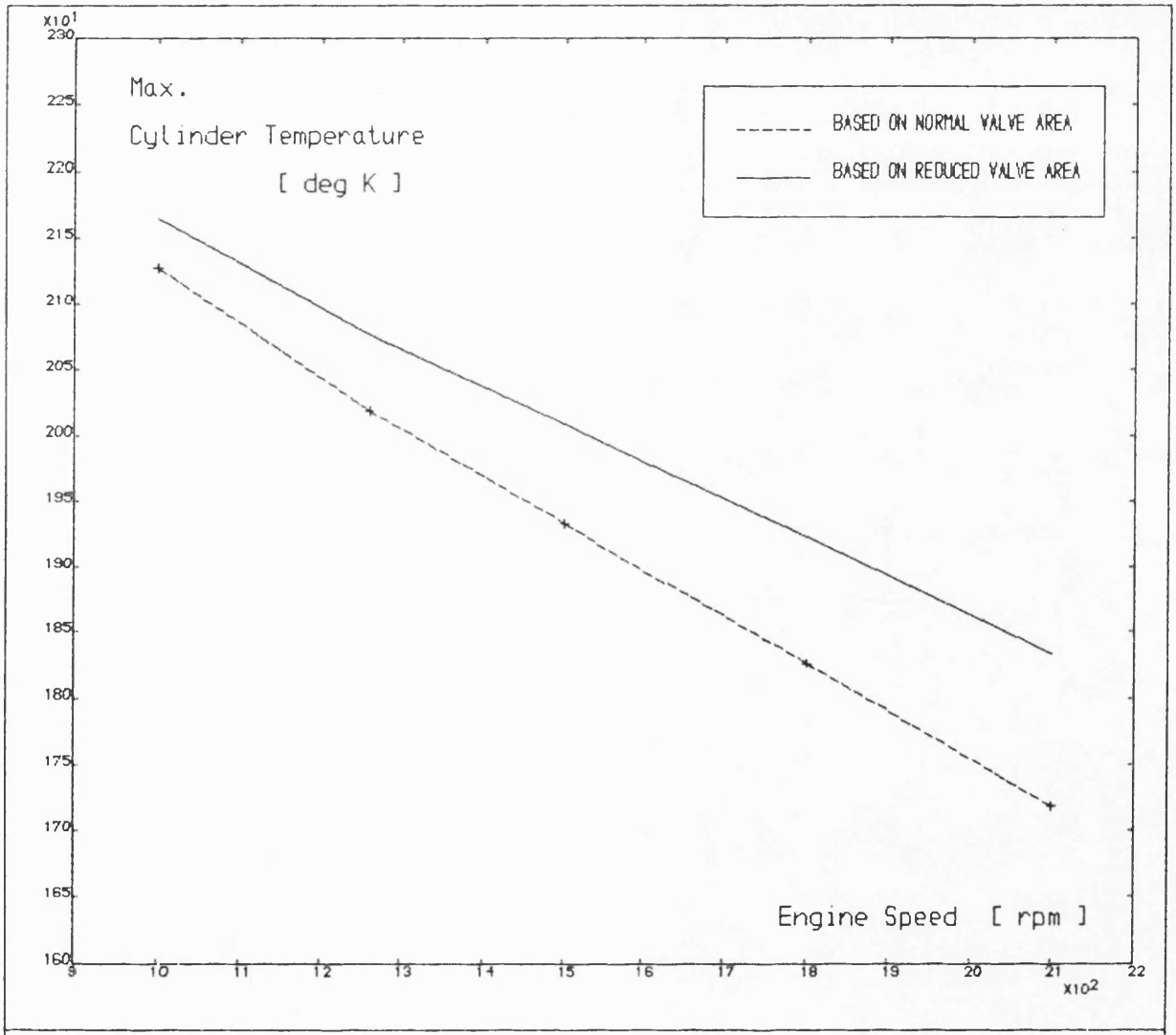

Fig. 4.46 The 'SPICE' predictions for maximum cylinder temperature of the L10.250-T/C engine at the running conditions along the LTC

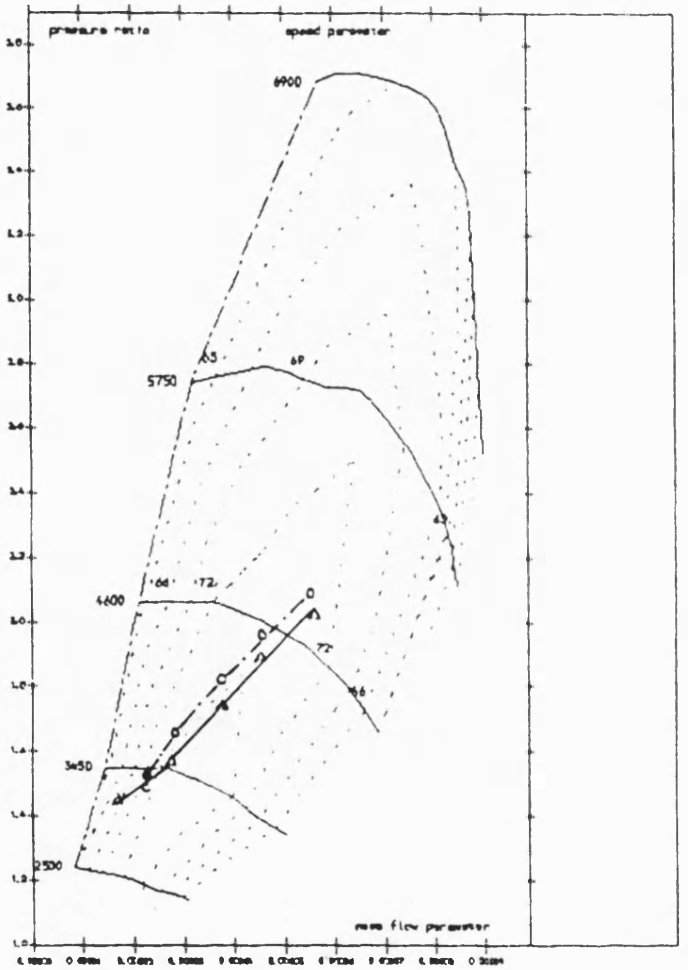

Fig. 4.47

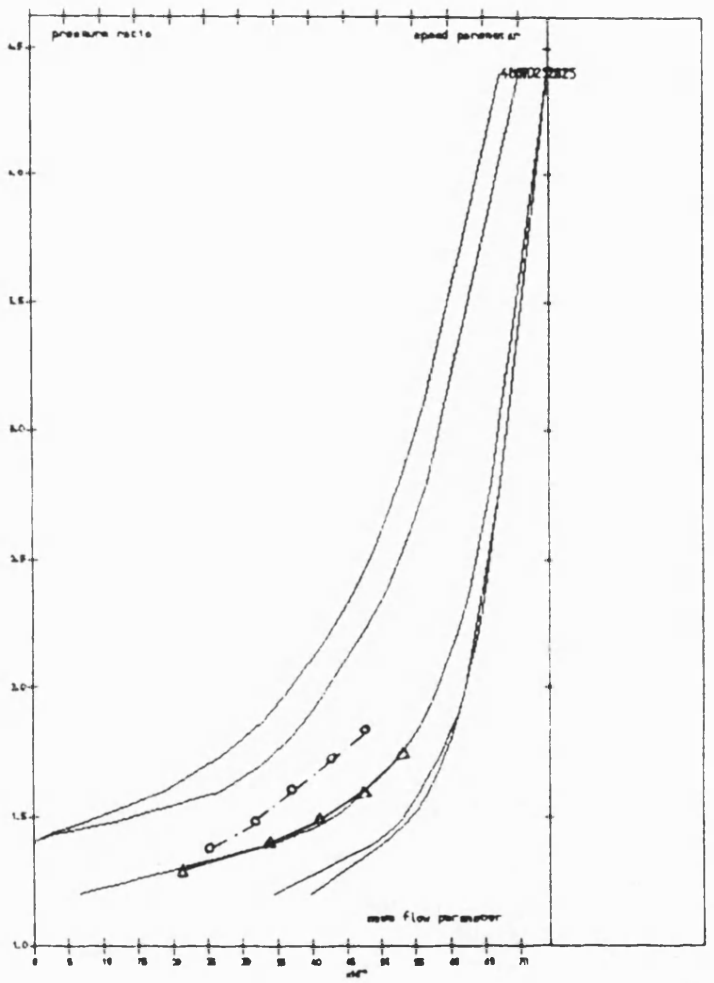

Fig. 4.48

KEY :	TITLE :	FIG : 4.47 & 4.48
—— EXP. – – – PRED.	As per fig. 4.39 and fig. 4.40 but for the L10-T/C engine with reduced valve areas	CUMMINS L10.250-TCE

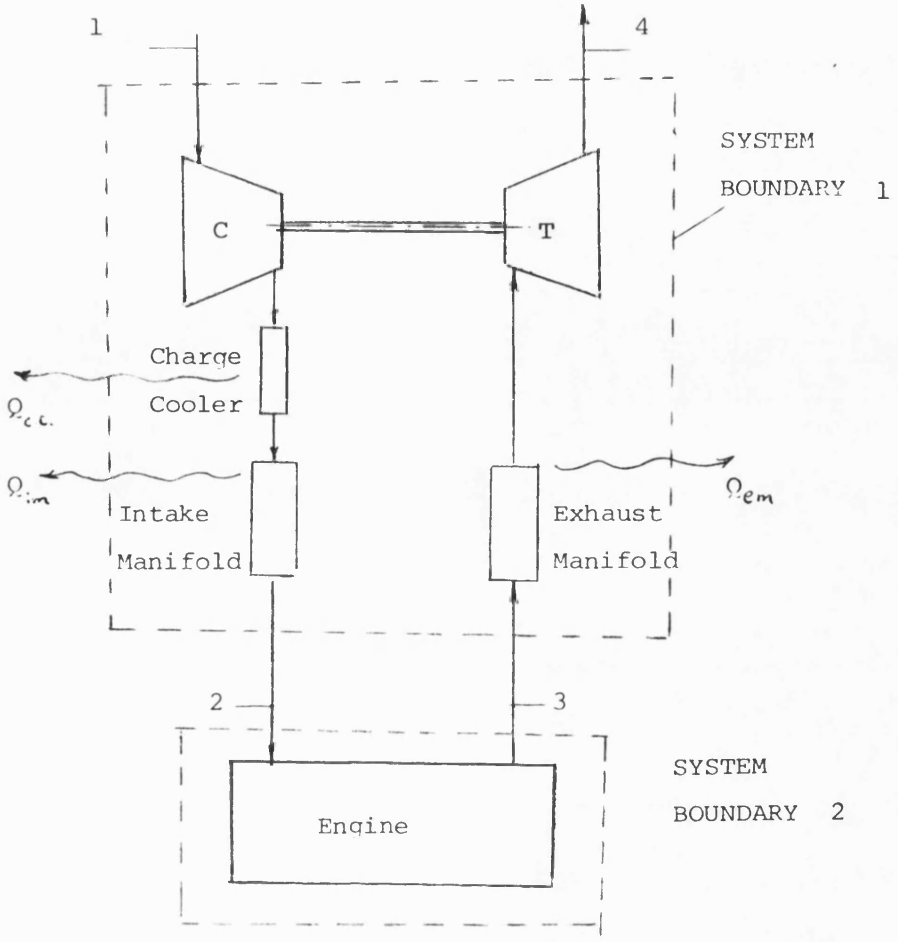

$$\Sigma E = 0$$

$$H_1 + H_3 - H_2 - H_4 - Q_{c.c.} - Q_{im} - Q_{em} = 0$$

$$H_3 - H_2 = H_4 - H_1 + Q_{c.c.} + Q_{im} + Q_{em}$$

CALCULATION OF EXHAUST GAS ENERGY BEFORE ENTERING EXHAUST MANIFOLD

Fig. 4.49 System boundaries applied for calculation of the energy balance of the engine itself

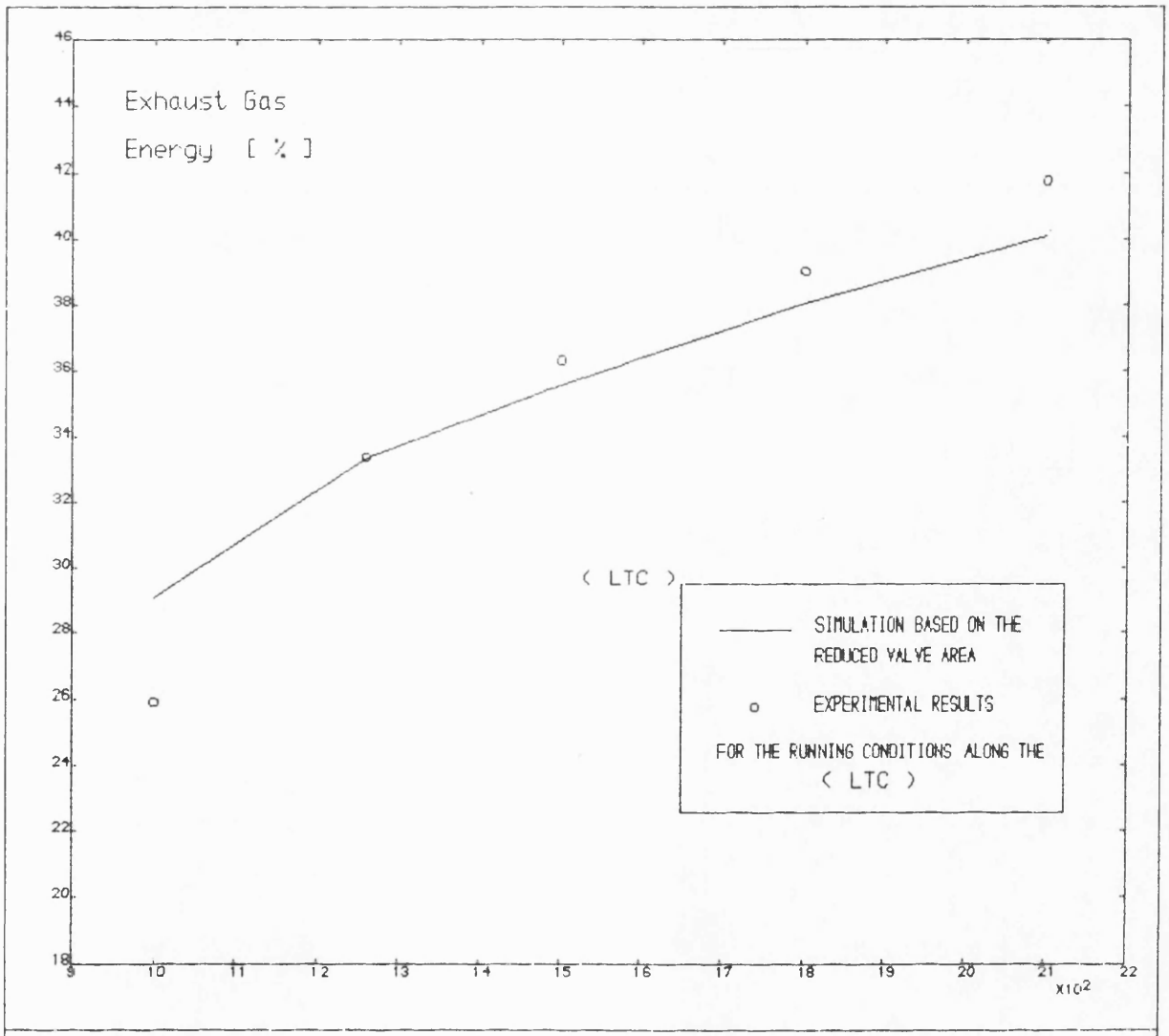

Fig. 4.50 The 'SPICE' predictions for exhaust gas energy of the L10.250-T/C engine compared with the corresponding experimental result

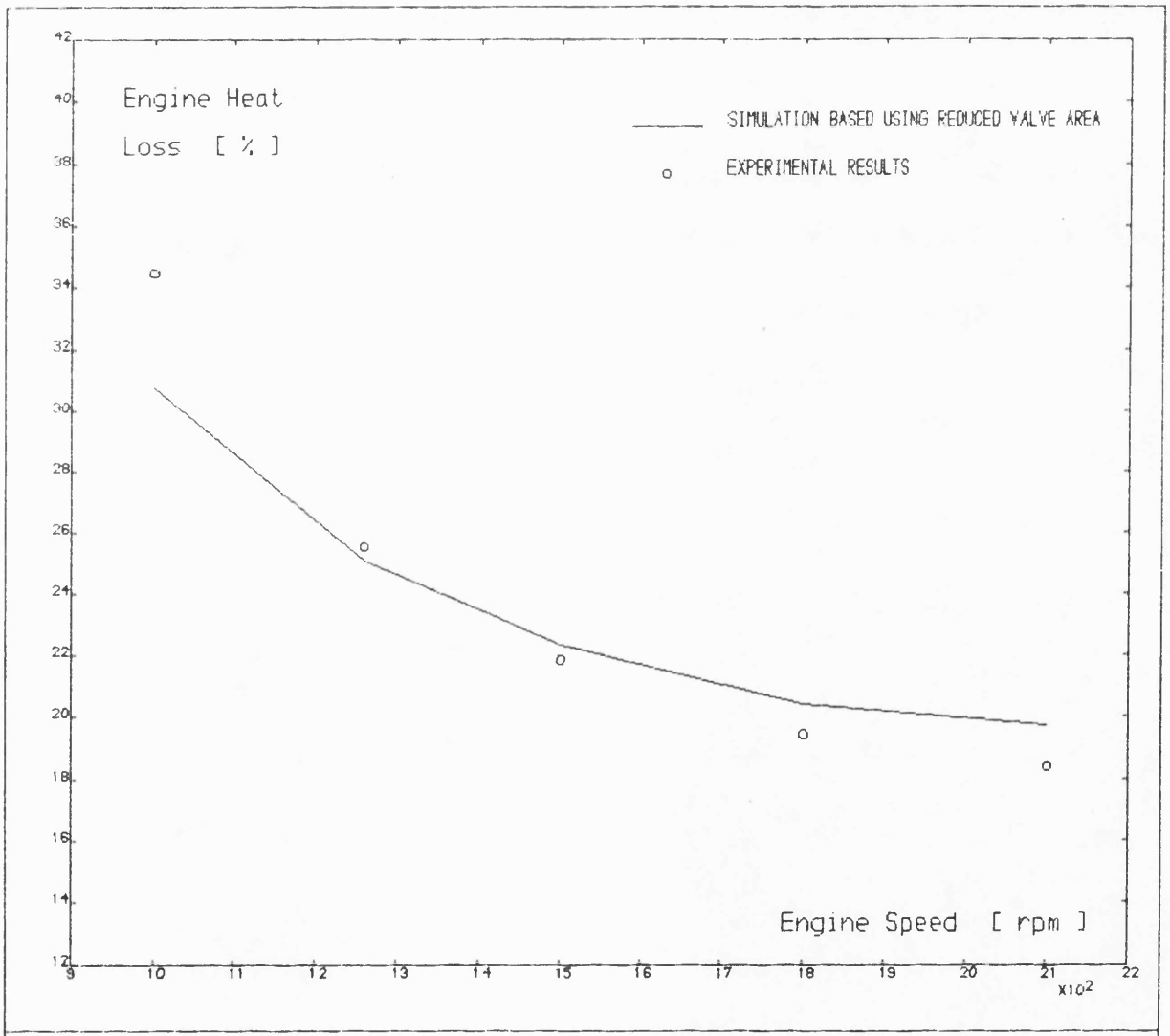

Fig. 4.51 The 'SPICE' predictions for engine heat rejection of the L10.250-T/C engine compred with the experimental results along the conditions along th

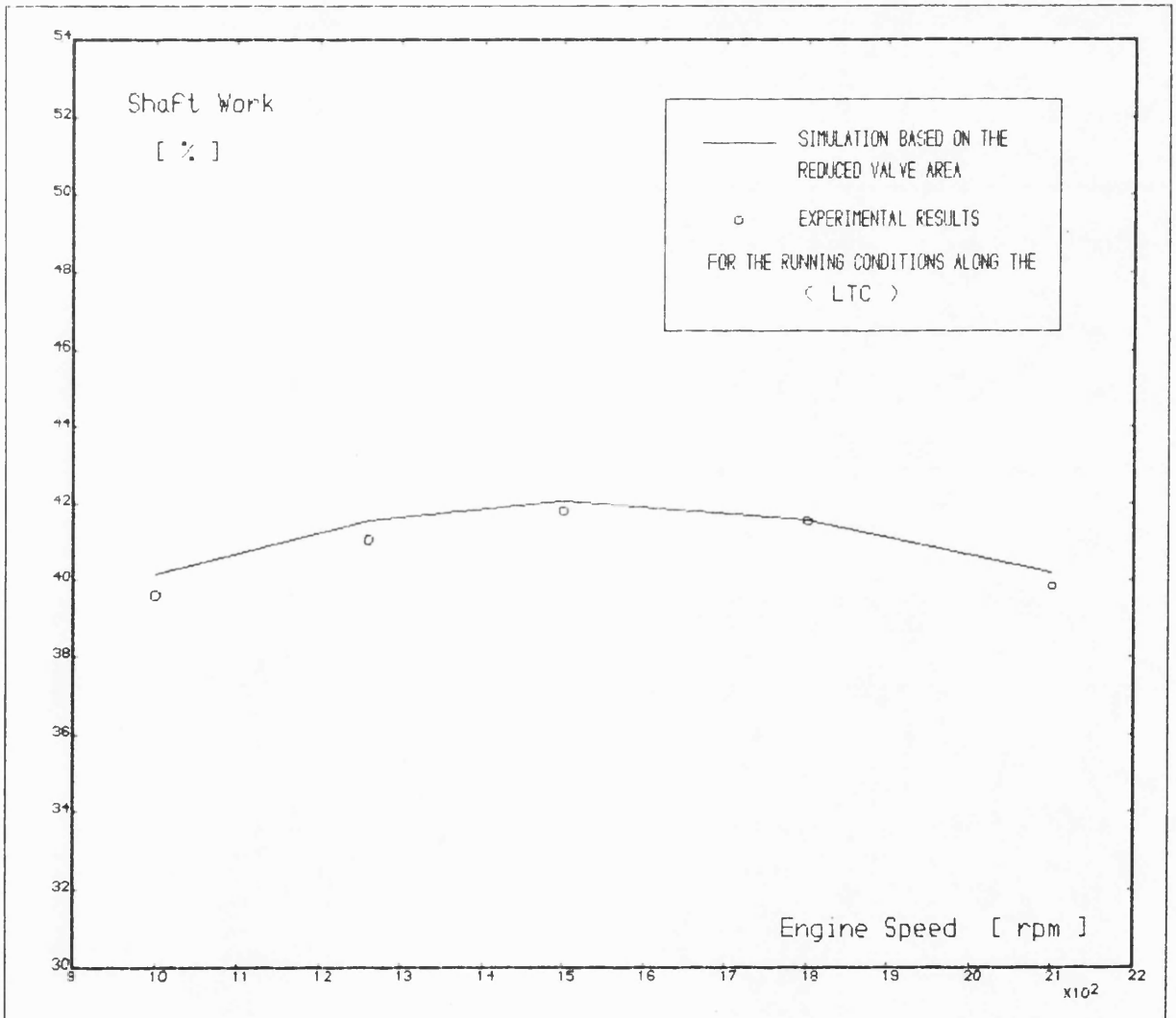

Fig. 4.52 The 'SPICE' predictions for useful shaft work of the L10.250-T/C engine compared with the corresponding experimental results

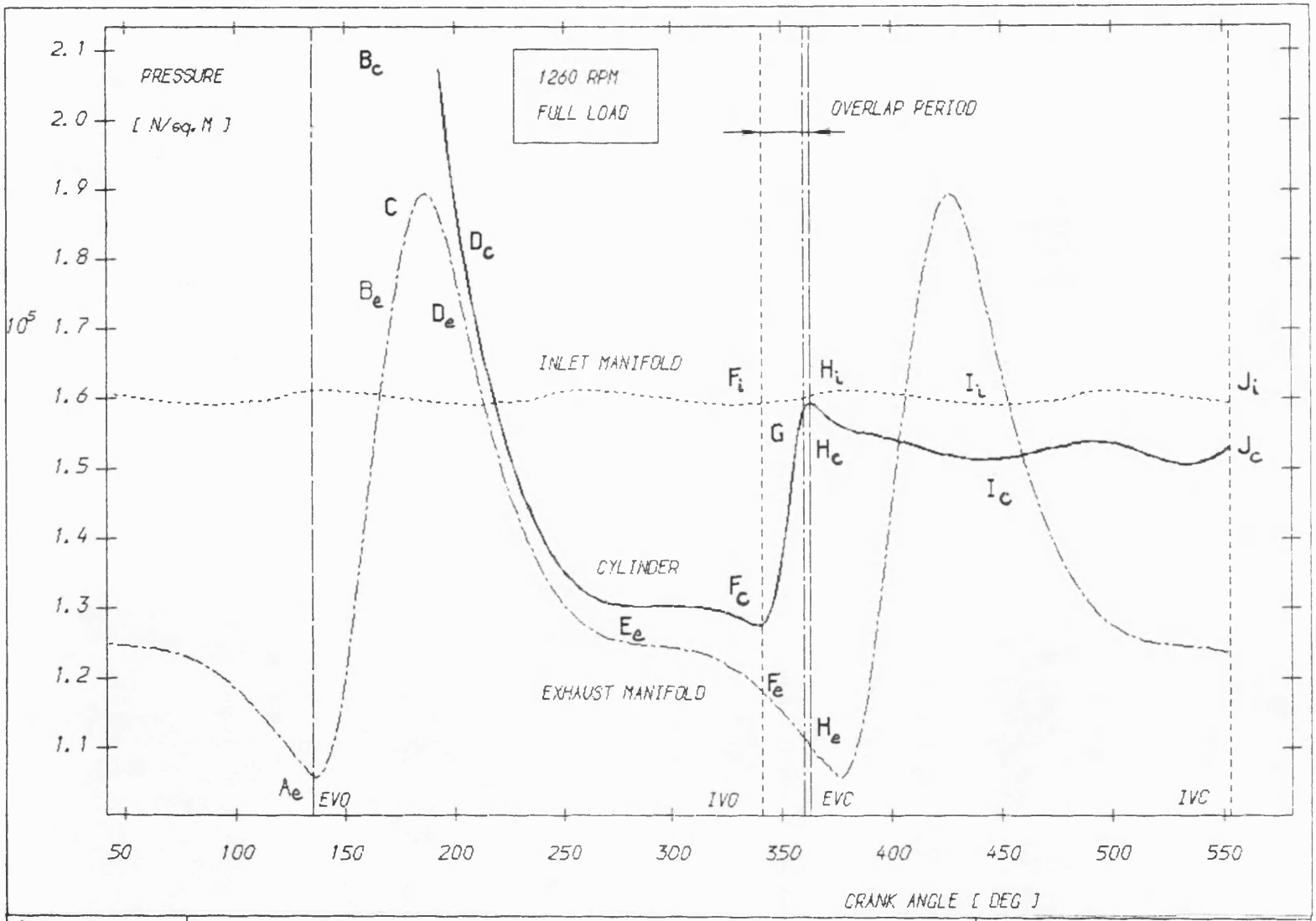

KEY:
—— CYL.
----- INL.
—·— EXH.

TITLE : IN-VOLUME PRESSURE VARIATION DURING OPEN PERIOD AT ENGINE SPEED OF 1260 RPM AT FULL LOAD

FIG : 4.53 , a

CUMMINS L10.250-TCE

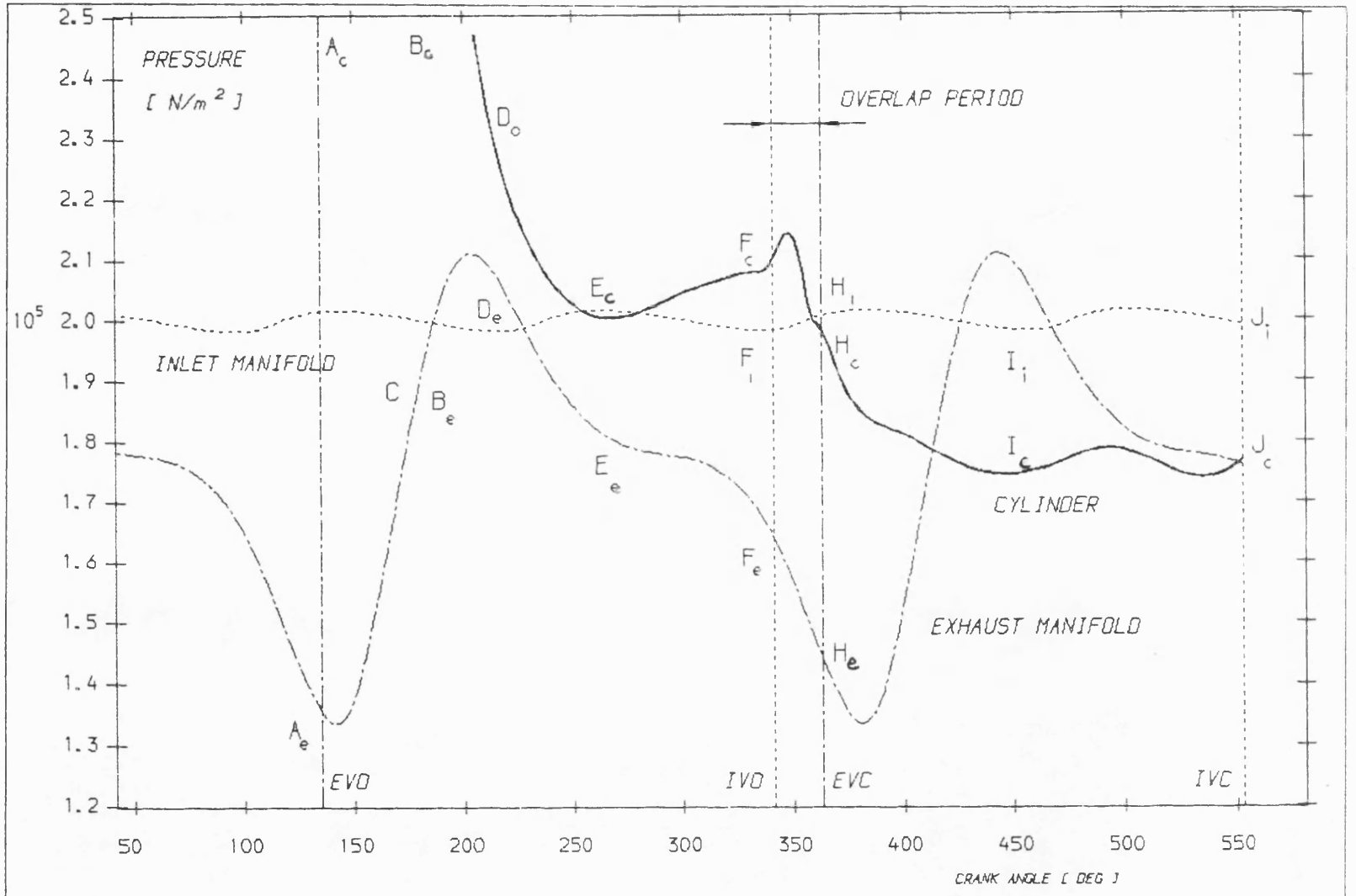

KEY :
CYL
INL
EXH

TITLE : IN-VOLUME PRESSURE VARIATION DURING OPEN PERIOD AT ENGINE SPEED OF 2100 RPM AT FULL LOAD

FIG : 4.53 , b

CUMMINS L10.250-TCE

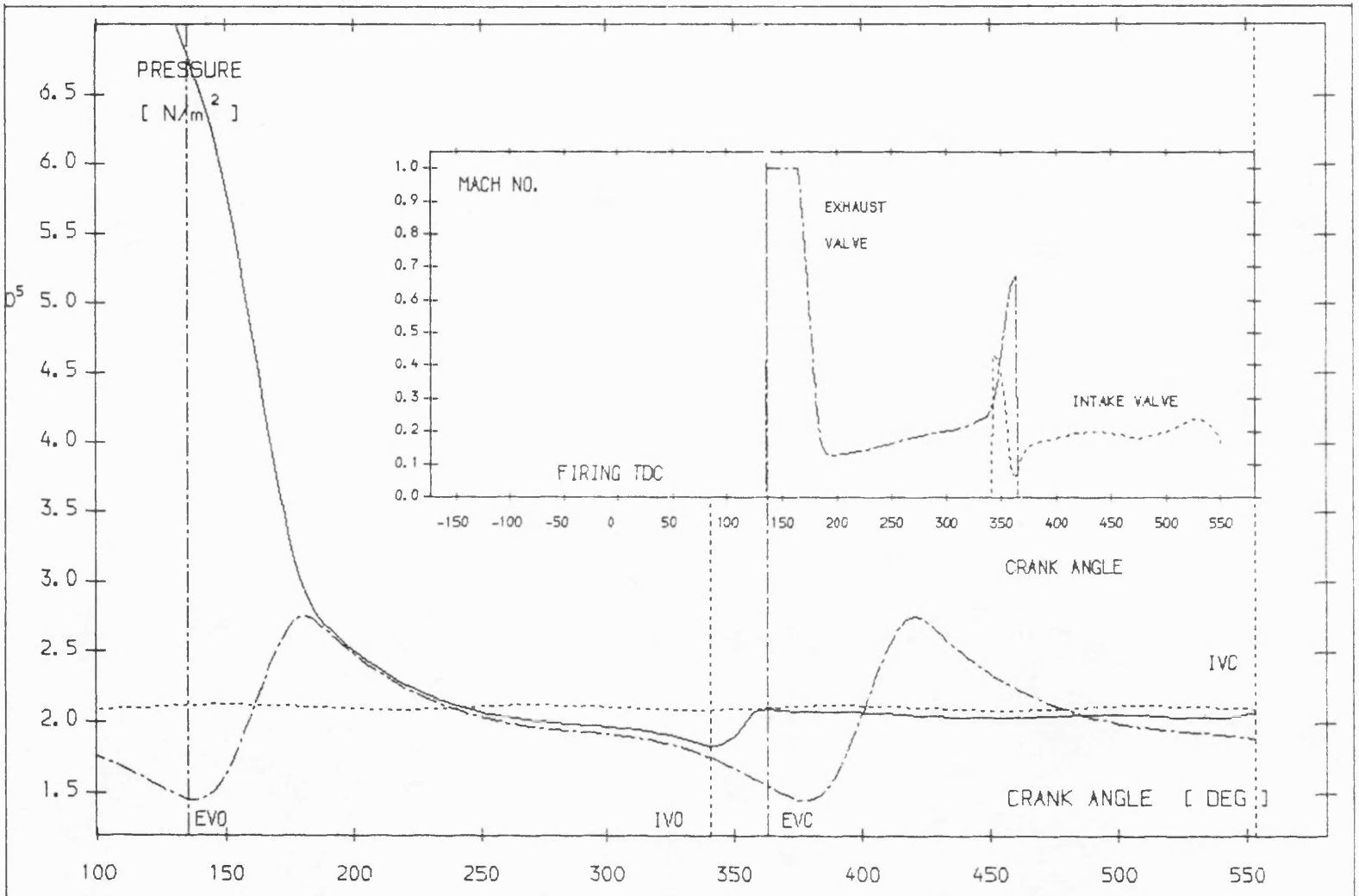

KEY	TITLE : IN-CYLINDER PRESSURE VARIATINS AND VALVE MACH NOs. AT ENGINE SPEED OF 2100 RPM AT FULL LOAD	FIG . 4.53 , C
CYLINDER INTAKE EXHAUST		CUMMINS L10.290-TCE

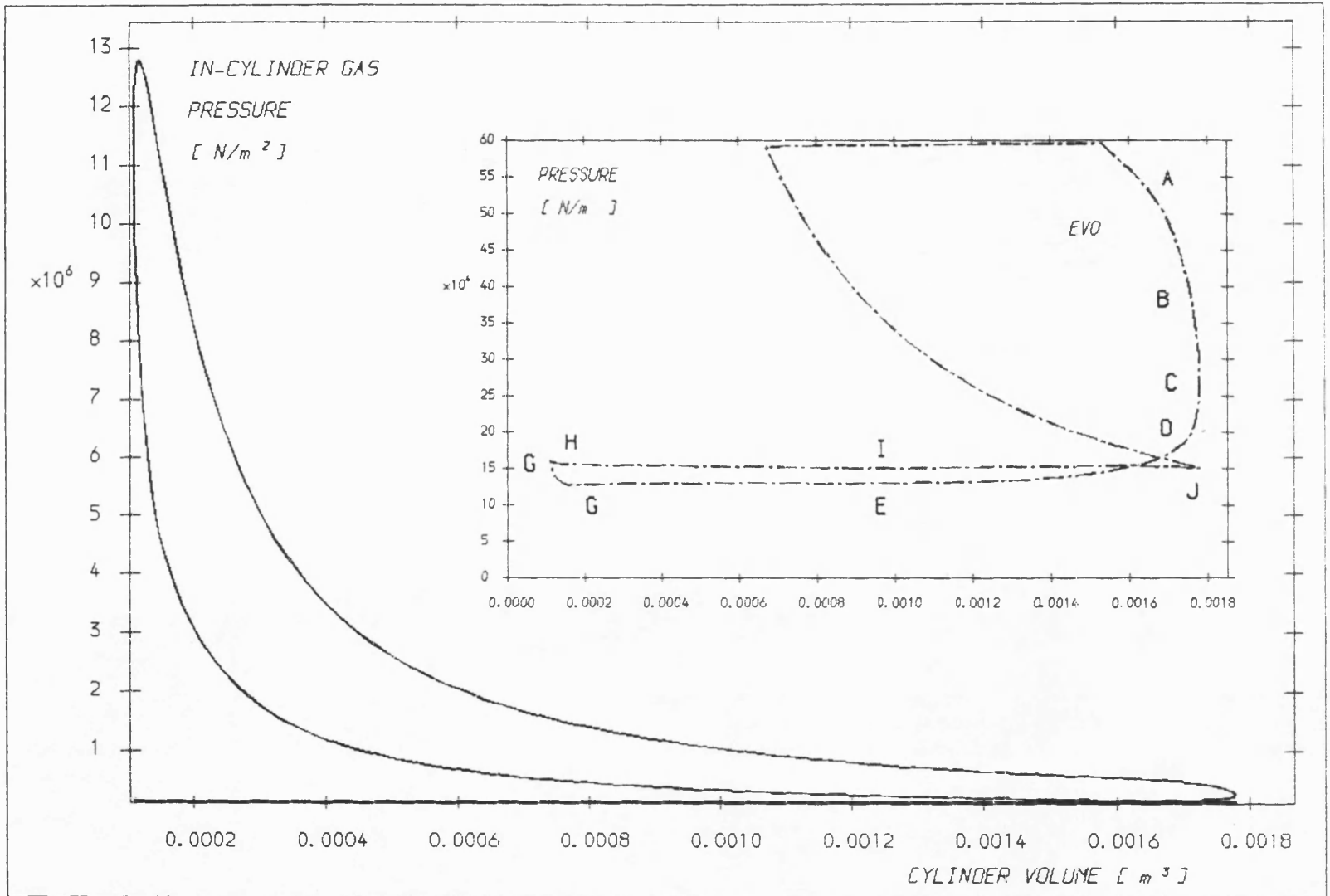

KEY :	TITLE : P-V DIAGRAM AT ENGINE SPEED OF 1260 RPM AT FULL LOAD	FIG : 4.54 , a CUMMINS L10.250-TCE

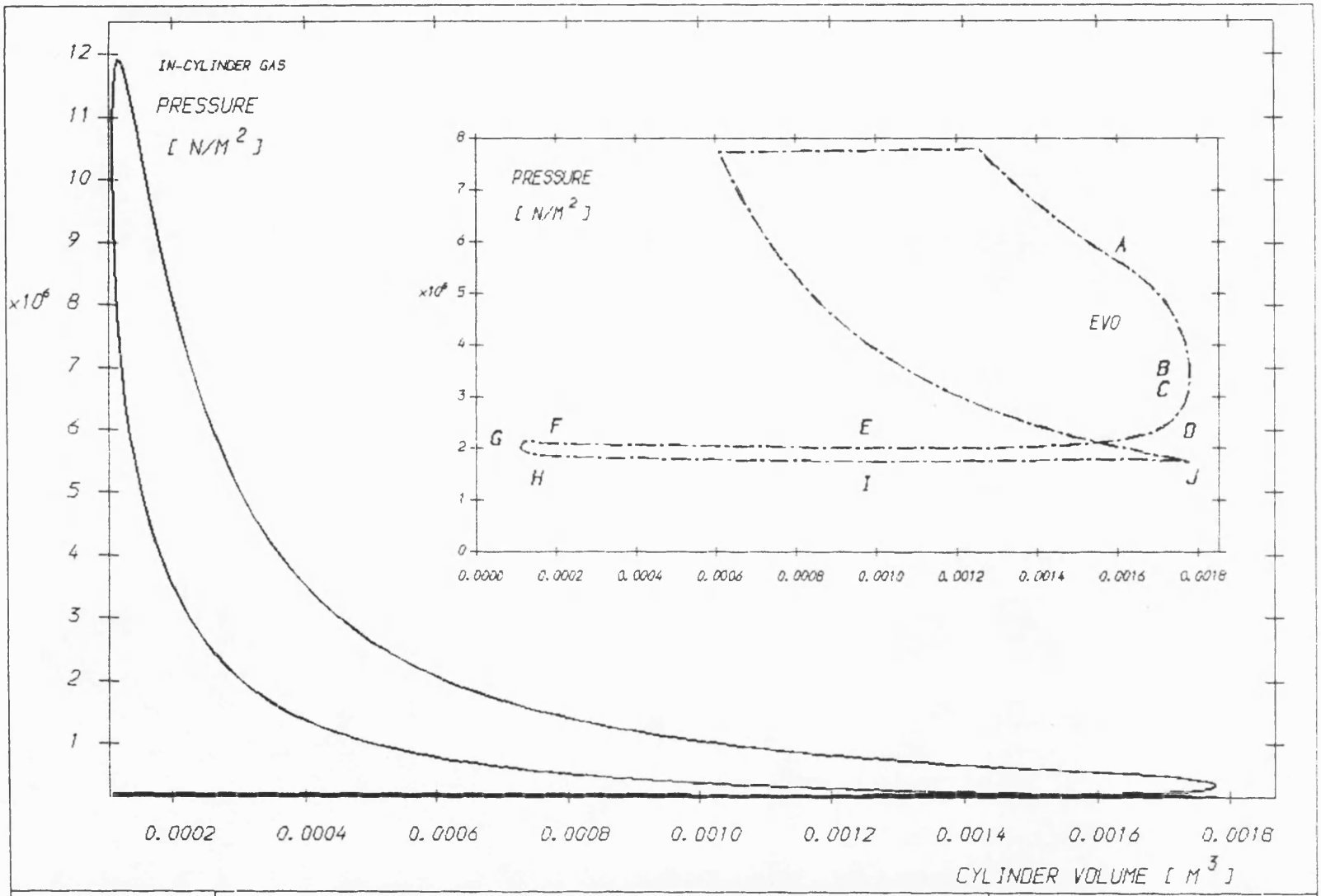

KEY :	TITLE : P-V DIAGRAM AT ENGINE SPEED OF 2100 RPM AT FULL LOAD	FIG : 4.54 , b CUMMINS L10.250-TCE

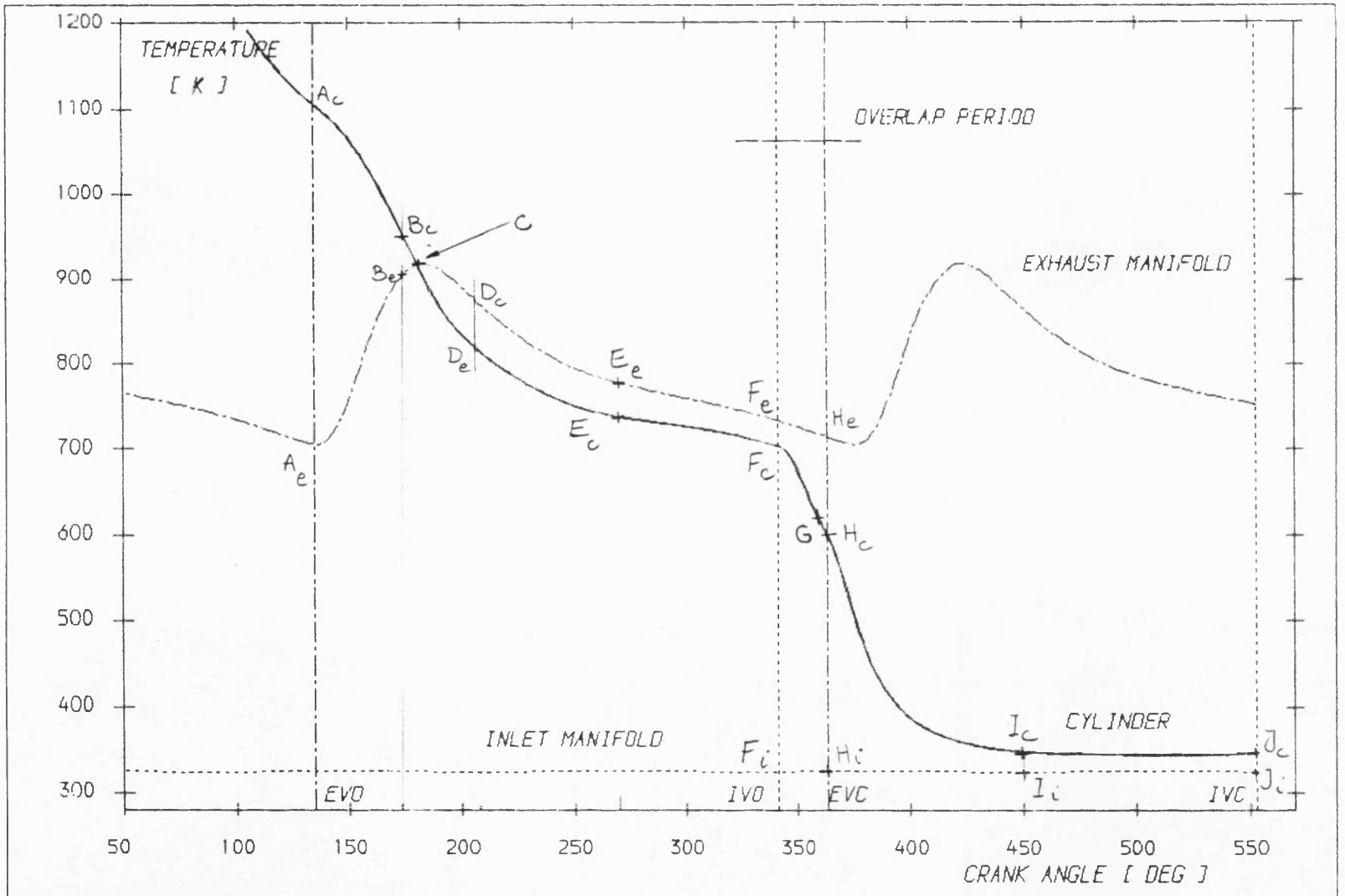

KEY :	TITLE : IN-VOLUME TEMPERATURE VARIATIONS DURING OPEN PERIOD AT ENGINE SPEED OF 1260 RPM AT FULL LOAD	FIG : 4.55, a
		CUMMINS L10.250-TCE

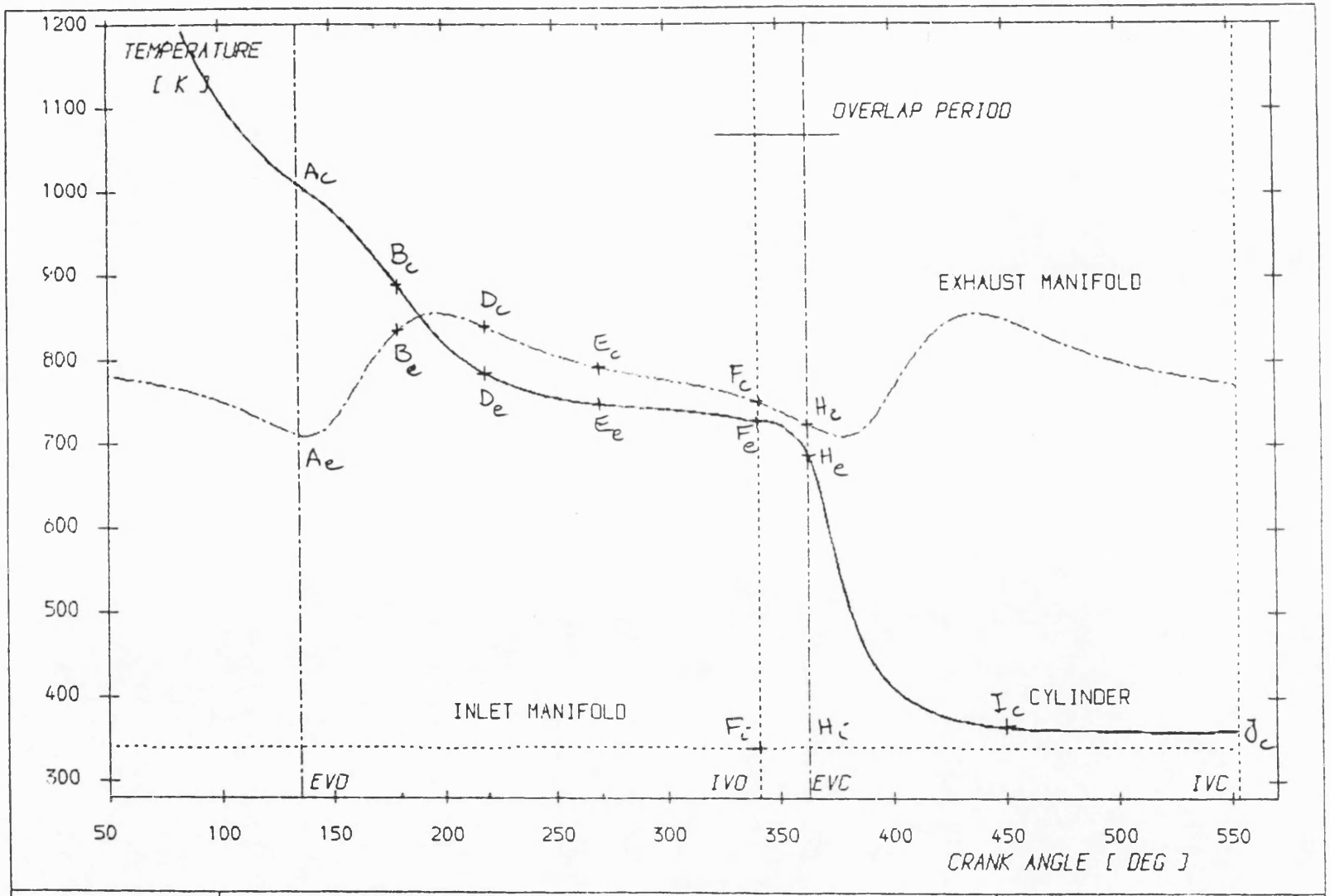

KEY :	TITLE : IN-VOLUME TEMPERATURE VARIATIONS DURING OPEN PERIOD AT ENGINE SPEED OF 1260 RPM AT FULL LOAD	FIG : 4.55 , b
		CUMMINS L10.250-TCE

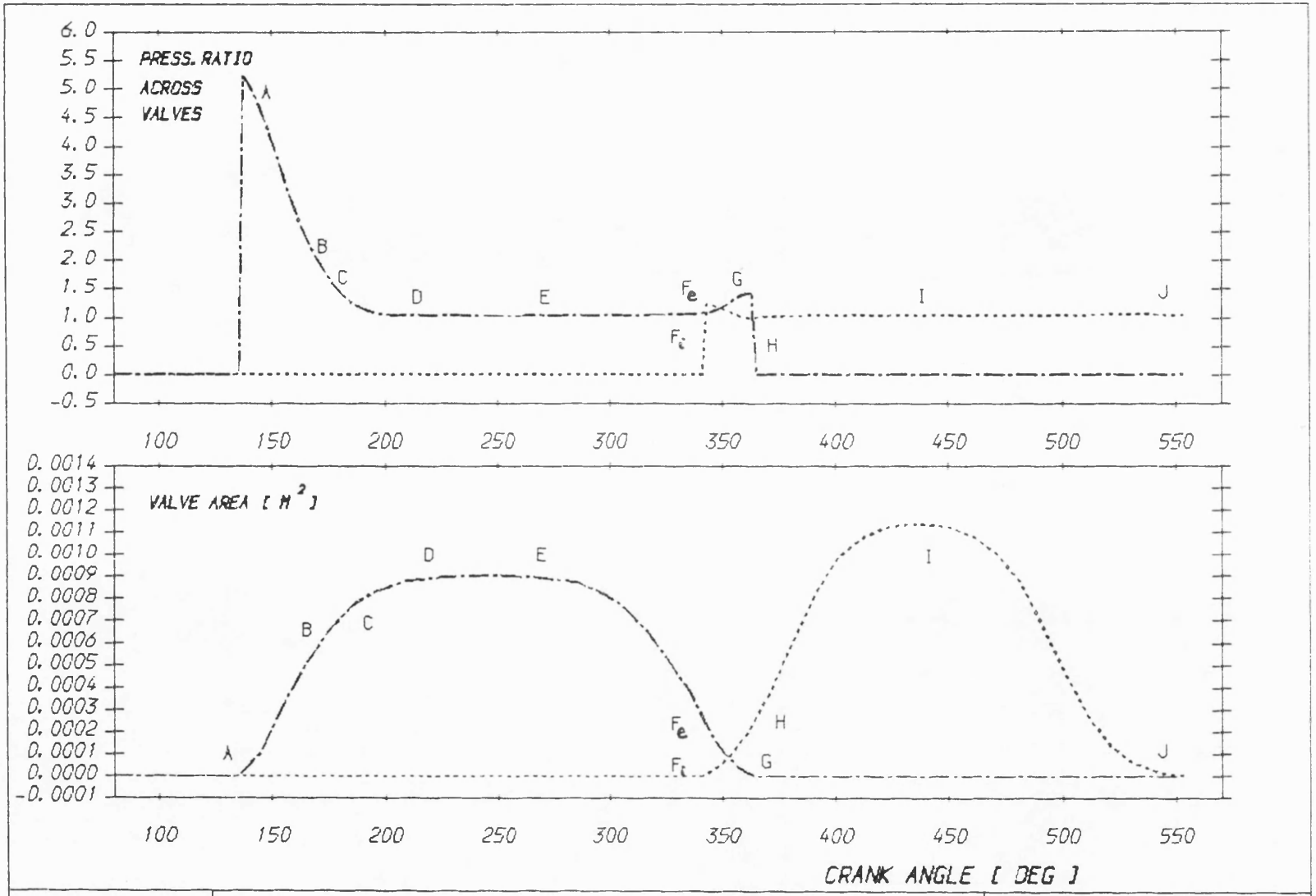

KEY :	TITLE :	FIG :
------- INTAKE -·-·-·- EXHAUST	INTAKE/EXHAUST VALVE FLOW DATA AT ENGINE SPEED OF 1260 RPM AT FULL LOAD	4.56.a CUMMINS L10.250-TCE

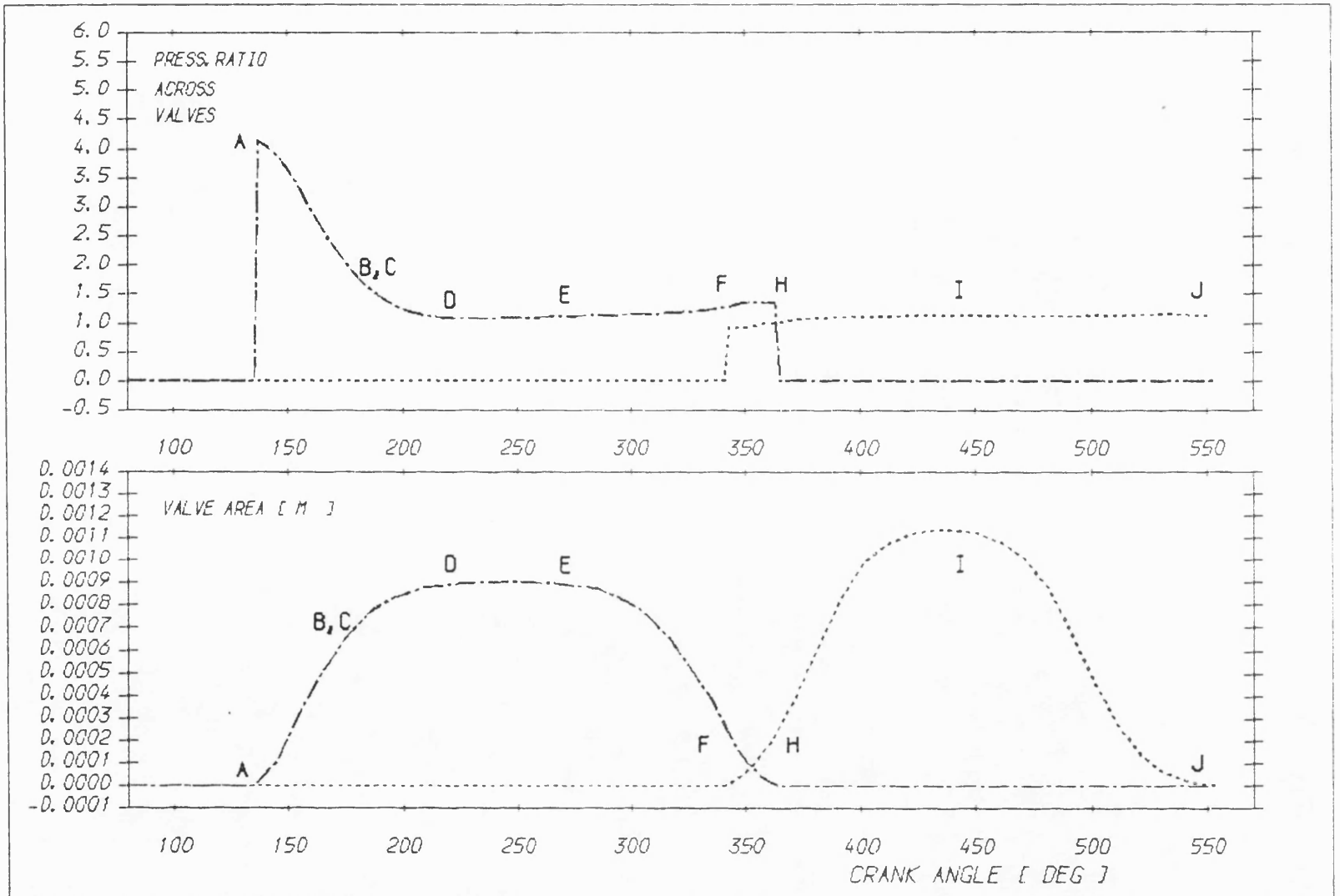

KEY :	TITLE :	FIG : 4.56 , b
..... INTAKE —·—·— EXHAUST	INTAKE/EXHAUST VALVE FLOW DATA AT ENGINE SPEED OF 2100 RPM AT FULL LOAD	CUMMINS L10.250-TCE

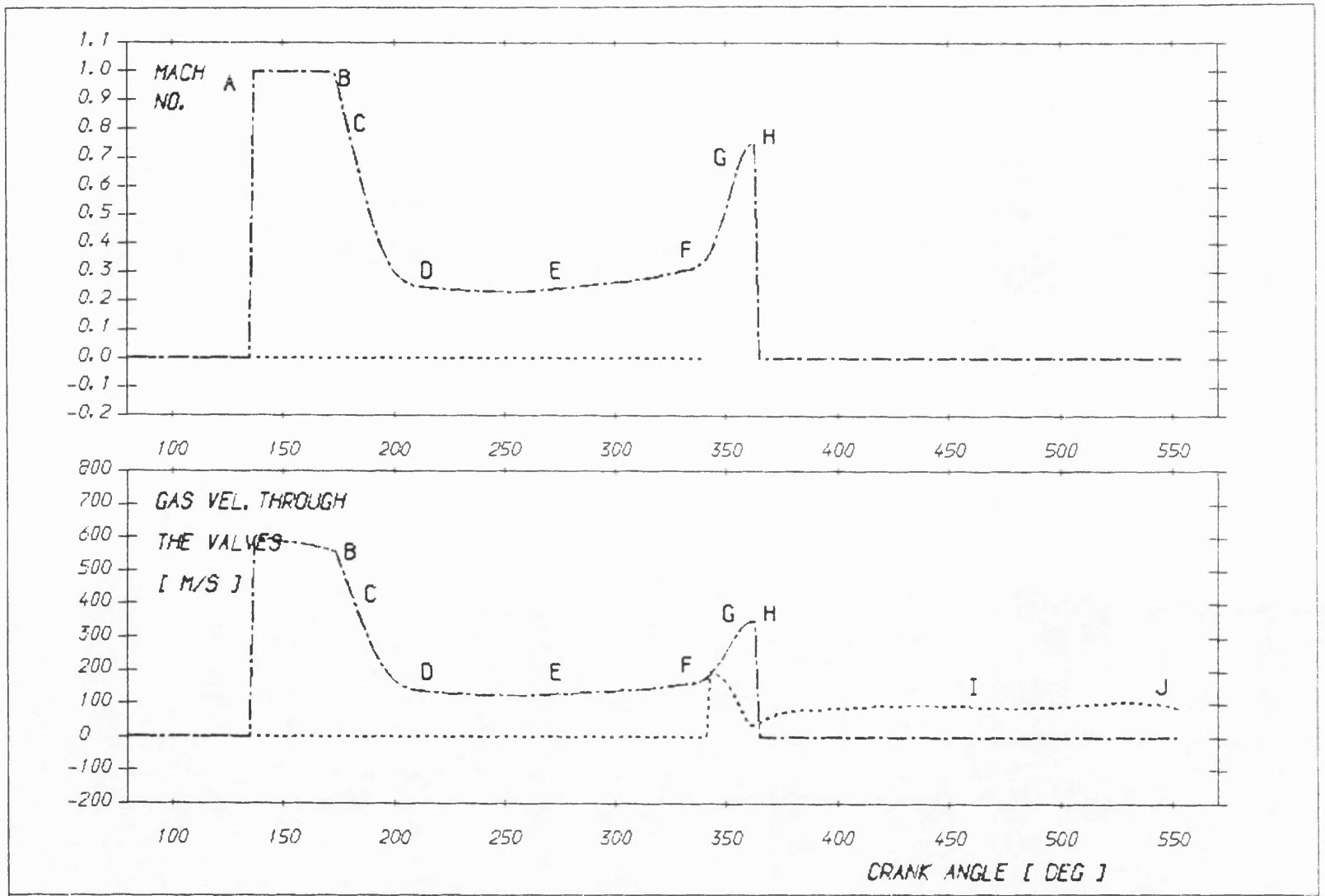

KEY : ..... INTAKE ——— EXHAUST	TITLE : INTAKE/EXHAUST VALVE FLOW DATA AT ENGINE SPEED OF 1260 RPM AT FULL LOAD	FIG : 4.57 , A CUMMINS L10.250-TCE

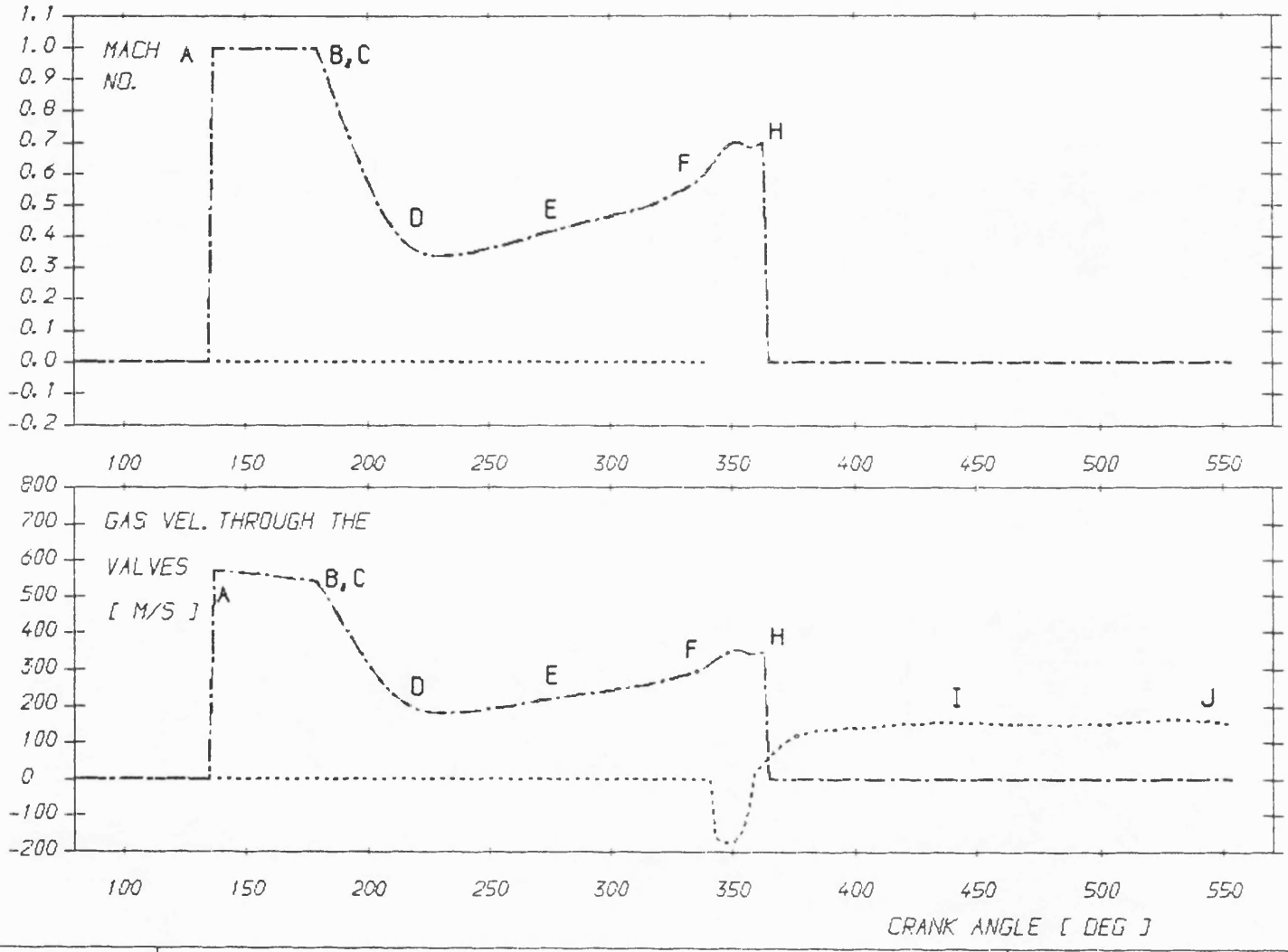

KEY : ..... INTAKE —·—·— EXHAUST	TITLE : INTAKE/EXHAUST VALVE FLOW DATA AT ENGINE SPEED OF 2100 RPM AT FULL LOAD	FIG : 4.57 , b CUMMINS L10.250-TCE

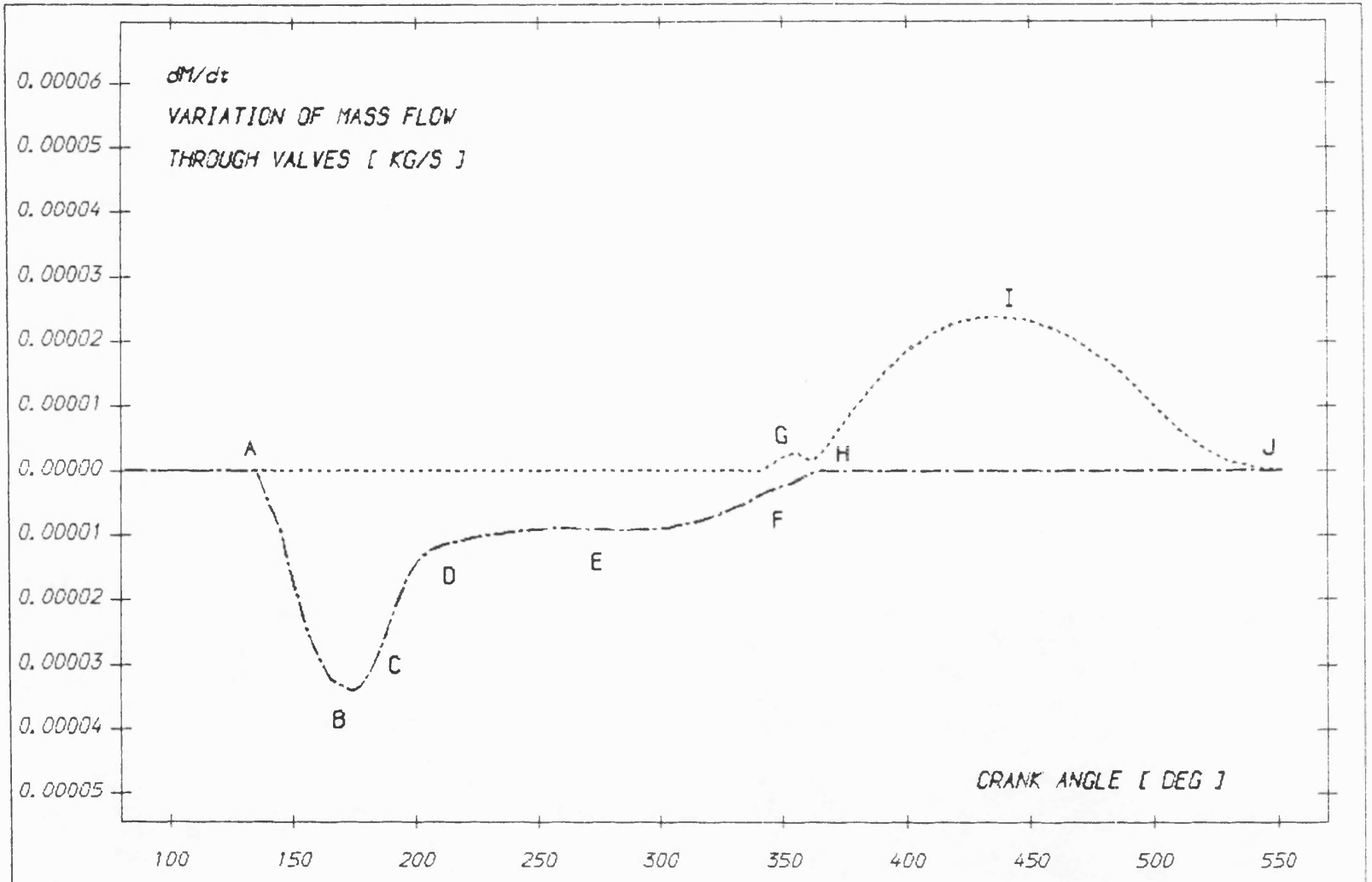

KEY : ------- INTAKE —·—·— EXHAUST	TITLE : INTAKE/EXHAUST VALVE FLOW DATA AT ENGINE SPEED OF 1260 RPM AT FULL LOAD	FIG : 4.58,a
		CUMMINS L10.250-TCE

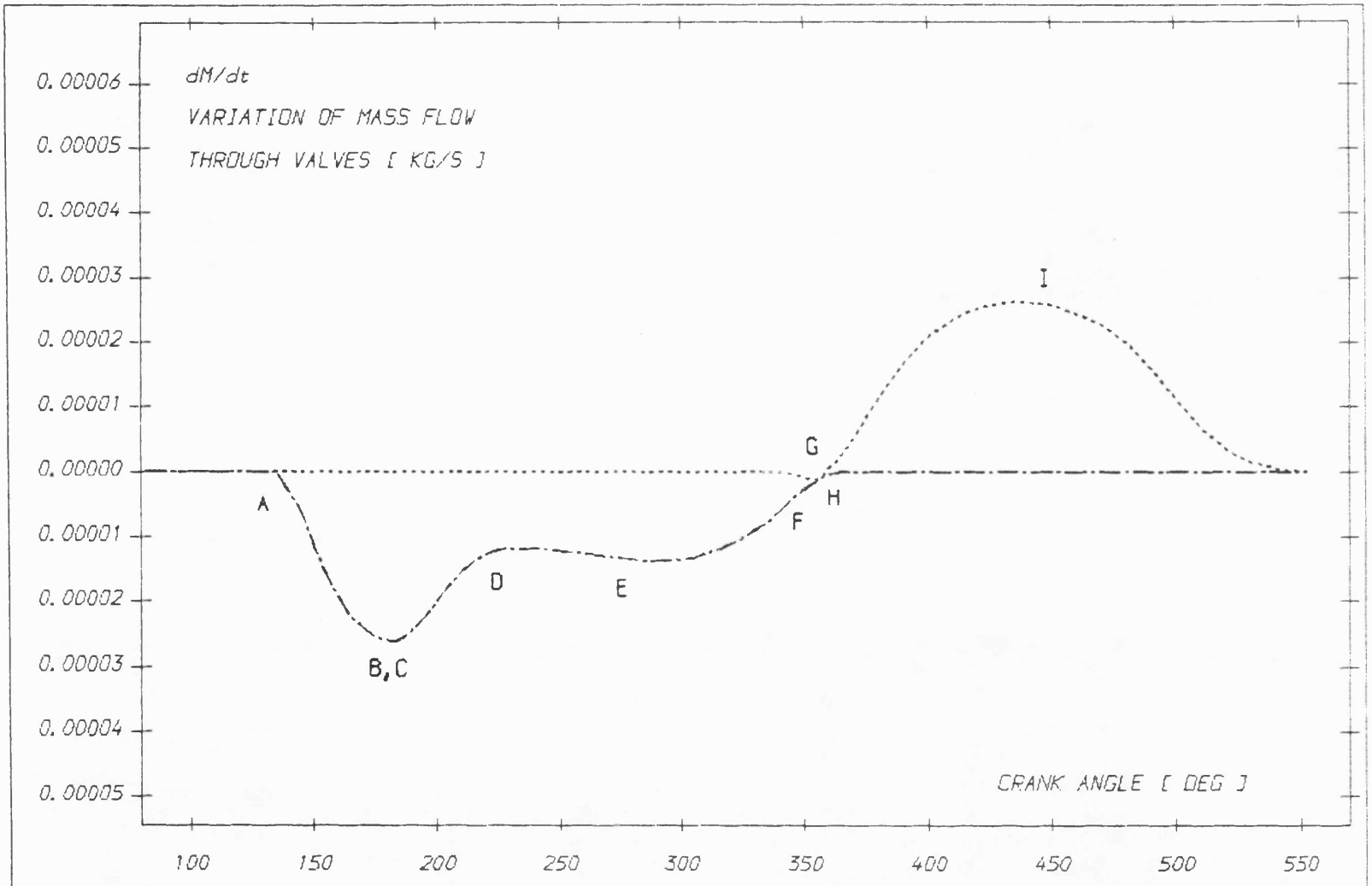

KEY : ..... INTAKE —·—·— EXHAUST	TITLE : INTAKE/EXHAUST VALVE FLOW DATA AT ENGINE SPEED OF 2100 RPM AT FULL LOAD	FIG : 4.58 , b CUMMINS L10.250-TCE

CHAPTER FIVE

SIMPLE STEADY STATE SIMULATION OF THE DCE UNIT BASED ON THE L10 ENGINE USING PROGRAM DCE2

5.1 INTRODUCTION

The present chapter deals with all analytical matching study and optimization in which the uprated Cummins L10 engine (section 7.3) has been substituted for the experimental Leyland 520 engine in the latest DCE configuration as briefly described in Chapter 1. The entire system, including compressor, epicyclic gear step up ratios to the compressor and output shaft, has been completely rematched for optimum rated performance and torque back up. The bulk of the work has been carried out with the rapid matching program 'DCE2' in which the engine subroutine has been calibrated against both turbocharged performance data supplied by the manufacturer, and against runs for the turbocharged build based on the detailed matching program 'SPICE' both described in Chapter 4.

However, to validate the case of the rapid matching program, 'DCE2', use is made of a full set of step-by-step calculations based on the detailed program 'CSPDCE' in the next chapter. As was described in Chapter 2, the latter program essentially has the same features as those of the program 'SPICE'.

5.2 THEORY

5.2.1 Epicyclic Gearset Kinematics and Dynamics

The epicyclic gearset shown in fig. 5.1,a consists of a central sun gear (S) which intermeshes with three or more planetary gears (P). The planets (P) all intermesh at their circumference with a ring gear or annulus (A), and are mounted on bearings attached to the planet carrier (PC). There are three components in the gear set, "A", "PC" and "S", which can be manipulated externally. It is possible to move any two of these entirely independently of the third, and in turn, clamping each member gives the possibility of three fixed gear ratio.

To work out the kinematic relations for the epicyclic gear-set, fig. 5.1,a, let the epicyclic gear ratio, egr, be defined as:

$$egr = \frac{R_A}{R_S} = \frac{\text{number of teeth on annulus}}{\text{number of teeth on sun}} \qquad [5.1]$$

Let, also, clockwise rotation be defined as positive, then at the mesh point 1 (fig. 5.1,b), the velocity diagram gives :

$$\varpi_A R_A = \varpi_{PC} R_A + \varpi_P R_P \qquad [5.2]$$

where ϖ is angular velocity (rad/sec) and R is the pitch radius of a gear. Similarly at the mesh point 2 (fig. 5.1,c):

$$\varpi_S R_S = \varpi_{PC} R_S - \varpi_P R_P \qquad [5.3]$$

Eliminating $\varpi_P R_P$ between equations 5.2 and 5.3:

$$\varpi_A R_A - \varpi_{PC} R_A = \varpi_{PC} R_S - \varpi_S R_S \qquad [5.4]$$

which yields :

$$\varpi_S = (1 + egr)\, \varpi_{PC} - egr\, \varpi_A \qquad [5.5]$$

Fig.5.2shows a complete DCE gearing system. Defining

$$cgr' = \text{sun to compressor step up gear ratio} = \frac{\omega_{COMP}}{\omega_S}$$

$$ogr' = \text{planet carrier to output shaft step up gear ratio} = \frac{\omega_{o/s}}{\omega_{PC}}$$

and

$$cgr = \text{overall compressor gear ratio} = cgr'.\ egr \quad [5.6]$$

$$ogr = \text{overall output-shaft gear ratio} = \frac{egr.ogr'}{(1+egr)} \quad [5.7]$$

and noting the fact that $\varpi_{ENG} = \varpi_A$, equation 5.5 can be written in a new form to correlate the shaft speeds of the DCE components :

$$\omega_{COMP} = [\omega_{ENG} - \frac{(1+egr)}{egr} \frac{\omega_{o/s}}{ogr'}]cgr'.egr \quad [5.8]$$

or

$$\omega_{COMP} = [\omega_{ENG} - \frac{\omega_{o/s}}{ogr}]cgr \quad [5.9]$$

Note that a minus sign has been applied to one side of equations 5.8 and 5.9 to deal with absolute values of angular velocities. It should also be noted that, although 'ogr' in equation 5.7 is defined as overall output shaft gear ratio, it does not refer to the ratio of output shaft speed to engine speed, $\left(\frac{\omega_{o/s}}{\omega_{ENG}}\right)$, unless the sun gear or compressor shaft stops (equation 5.9).

To work out the dynamic relations for the epicyclic gear train, the ratio of engine power to compressor power is studied. Fig. 5.1,d shows the forces acting on the planet. In steady state running condition the same forces act at mesh points 1 and 2. Therefore, the annulus and sun powers can be written as :

$$HP_A = \varpi_A\ \tau_A = \varpi_A.F.R_A \quad [5.10]$$

$$HP_S = \varpi_A\ \tau_S = \varpi_S.F.R_S \quad [5.11]$$

where HP and τ are power and torque and F denotes the force acting at the planet mesh points. Assuming loss free power transmission from the engine to the compressor, (fig. 5.2), the ratio of the engine power to the

compressor power becomes :

$$\frac{HP_{ENG}}{HP_{COMP}} = \frac{HP_A}{HP_s} = \frac{\omega_A \, R_A}{\omega_s \, R_s} \qquad [5.12]$$

Using equations 5.1, 5.5 and 5.7, equation 5.12 can be written in such a form as to correlate the power ratio with the speeds of the DCE components and the system gear ratios :

$$\frac{HP_{ENG}}{HP_{COMP}} = \frac{\omega_{ENG}}{\omega_{ENG} - \frac{\omega_{o/s}}{ogr}, \frac{1+egr}{egr}} \qquad [5.13]$$

$$= \frac{\omega_{ENG}}{\omega_{ENG} \frac{-\omega_{o/s}}{ogr}} \qquad [5.14]$$

The compressor overspeed ratio:

This is defined as follows :

$$r_{overspeed} = \frac{\omega_{COMP} \text{ at rated } \omega_{ENG} \text{ with } \omega_{o/s} = 0}{\omega_{COMP} \text{ at rated } \omega_{ENG} \text{ and } \omega_{o/s}}$$

Applying equation 5.9:

$$r_{overspeed} = \frac{cgr \; \omega_{ENG}}{cgr \; [\omega_{ENG} - \frac{\omega_{o/s}}{ogr}]} \qquad [5.15]$$

which is seen to be identical to equation 5.14. Thus:

$$r_{overspeed} = \left(\frac{HP_{ENG}}{HP_{COMP}} \right)_{rated} \qquad [5.16]$$

5.2.2 General Considerations in the Design of the DCE

Some of the general guidelines as to the overall design of the DCE are as follows :

1. The components of the DCE are first selected through an overall

assessment of the system operation with manual calculations for the two extreme cases of rated and stall running conditions of the output shaft.

2. The steady-state characteristics of the components may be used in the final matching with the aid of program 'DCE2'.

3. For traction purposes, as stated in Chapter 1 (section 1.2.4), in medium severity applications such as trucks, an upper overall transmission ratio of about 55:1 is demanded when a Diesel engine constitutes the prime mover. This together with the back axle ratio range of 3.5 to 4.0 calls for an output torque ratio of over 13:1 for the DCE between stall and rated conditions.

4. As was also stated, the DCE in its vehicular application employs a torque converter after its output shaft. A high torque ratio torque converter can practically provide a system with a torque ratio of about 3.6:1.

To dispense altogether with the normal multi-ratio stepped transmission in such applications, therefore, an output shaft torque ratio between stall and rated conditions of over 3.6 (=13/3.6) is required.

5. With respect to the speed relations of an epicyclic gearset having a typical value of R=3 for the basic epicyclic ratio, the best practical connection of the engine, compressor and turbine to the epicyclic has been examined (Ref. 39) and designed such that the highest epicyclic shaft speed is associated with fastest spinning component, the compressor. This was considered to reduce the complexity and losses of a large step-up ratio to the compressor. The final layout is shown in fig. 5.2.

6. In general, part of the engine power in the DCE is absorbed and converted by the compressor into the total energy of the compressed air. However, this process is thermodynamically irreversible and because of the further flow and mechanical losses involved, it will be a waste of energy to use the engine power to create an airflow or boost pressure greater than that required by the engine at the rated point. At this

point, the compressor speed and hence air flow are at their minimum value along the LTC of the output shaft, while the air flow requirement of the engine may be defined by desirable levels of air-fuel ratio and boost.

7. The engine air flow in the DCE depends on the engine speed and boost and hence it is self-adjusting. On the other hand, for better engine thermal efficiency, air-fuel ratios of the order of 27:1 to 29:1 are recommended. Therefore, the engine rating can directly be controlled by boost level.

Recalling the correlation between B.M.E.P. and other engine variables such as boost pressure ratio and air-fuel ratio :

$$BMEP = \frac{(\eta_{TH} Q_{cal}).(P_{inl} \eta_{vol}).\eta_{mech}}{(R_{air}.T_{inl})(A/F)} \qquad [5.17]$$

where : Q_{cal} = fuel calorific valve (kJ/kg)

η_{TH} = indicated thermal efficiency

η_{vol} = volumetric efficiency

η_{mech} = engine mechanical efficiency

BMEP = brake mean effective pressure

P_{inl} = boost pressure (bar)

R_{air} = air gas constant (kJ/kg.k)

T_{inl} = air temperature at the intake valve (k)

Some typical values are :

Q_{cal} = 43150 kJ/kg η_{TH} = 0.45

R_{air} = 0.287 kJ/kg.k η_{vol} = 0.9

T_{inl} = 320 k η_{mech} = 0.8

This together with A/F = 30 gives in equation 5.17

$$BMEP = 5.0\ P_{inl} \qquad [5.18]$$

Equation 5.18 is valid for any Diesel engine provided that the above assumptions are valid.

As described under 6, above, at the design point, the engine and compressor mass flows are matched, i.e.

$$\dot{m}_{COMP} = \dot{m}_{ENG} \qquad [5.19]$$

With further assumptions with respect to the compressor and intercooler, viz.:

P_{amb} = ambient pressure = 1 bar

compressor pressure ratio = P_{inl}/P_{amb}

compressor isentropic efficiency = 0.75

gamma of air = 1.4

and $T_{inl} = T_{amb}$ where T_{amb} = ambient temperature (k)

and applying equation 5.18, the proportion of engine power consumed by the compressor at the design point becomes (Prince, ref. 39):

$$\left.\frac{HP_{COMP}}{HP_{ENG}}\right|_{des} = 0.84\ (0.63\ BMEP^{0.283} - 1) \qquad [5.20]$$

where HP_{COMP} and HP_{ENG} are the compressor and engine power respectively.

The engine rating at the DCE design point is considered to be as high as possible but leaving an ample margin for increase in BMEP on the limiting torque curve without which the high torque ratio of the system cannot be realised. This calls for BMEP of the order of 15 bar, which in turn, makes the power ratio of the compressor to engine in equation 5.20, equal to 0.3 and the boost ratio equal to 3.0 (equation 5.18).

A correlation for the power ratio of the turbine to engine similar to that represented for the compressor in equation 5.20 was developed in Ref. 39 in which again some assumptions were made as follows :

gamma of engine exhaust gases = 1.33

turbine isentropic efficiency = 0.75

ratio of gas temperatures of engine exhaust to inlet ≃ 3 yielding :

$$\left.\frac{HP_{TURB}}{HP_{ENG}}\right|_{des} = 1.58\ (1-1.495\ BMEP^{-0.25}) \qquad [5.21]$$

With the design point BMEP = 15 bar, this power ratio becomes equal to 0.39. This underlines the power gain associated with having separated compressor and turbine, and will give a power feedback of 9% (0.39 - 0.30) neglecting the gear losses.

8. In an ideal situation, no torque convertor as mentioned in '4' is used while the engine remains at rated torque and speed along the output LTC down to output shaft stall. Thus the compressor also remains at rated torque, i.e.

$$\tau_{S_{stall}} = \tau_{S_{rated}} \qquad (A)$$

where τ is torque.

However, this is not possible due to the high degree of compressor overspeeding at stall (see fig. 1.25 Chapter 1). The compressor overspeed ratio $r_{overspeed}$ is defined as :

$$r_{overspeed} = \frac{N_{S\ stall}}{N_{S\ rated}} \qquad (B)$$

As already shown in Section 5.2.1, equation 5.16, the overspeed ratio $r_{overspeed}$ is also equal to the ratio

$$\left(\frac{HP_{ENG}}{HP_{COMP}}\right)_{rated}$$

which, with the values assumed in 7, above gives

$$r_{overspeed} = \frac{1}{0.3} = 3.33 \qquad [5.22]$$

If the engine were actually run at constant speed, the very large increase in compressor speed at output shaft stall implied by equation 5.22 could not, in practice, be tolerated. Furthermore, when using a rotary positive displacement compressor, this increase in speed would imply a proportional increase in mass flow, with an inevitable large increase in system pressure level. The resultant increase in power demand could not be met by the engine.

9. As described in Chapter 1, a positive displacement compressor is used in the DCE because of :

a) the large area of the operating map and efficiency islands making part-load optimization possible,
b) better control over operating points due to the fact that pressure ratio is independent of speed.

Of the different types of the positive displacement compressor, the screw-type is considered the best in terms of cost, size and efficiency. As already stated the compressor overspeed ratio along the output LTC has to be limited in practice to a value of the order 1.8. This is considerably below that calculated value of 3.3 in equation 5.22. To achieve this lower ratio the following steps are taken :

i) A lower limit is set for output shaft speed, and a torque converter is used over the lower speed range down to output shaft stall.
ii) The engine speed is reduced with reduction of output shaft speed.

10. If the output shaft power is kept constant, the required speed range of the output shaft will be determined by the available torque ratio of approx. 3.6 as described under '4' above. However, with the DCE the difference between turbine power and compressor power obtaining at rated conditions not only decreases gradually with reduction in output shaft speed but becomes negative, reaching its highest negative level at stall.

If engine power is virtually kept constant, the output shaft power will, therefore, decrease with speed, i.e.

$$(\tau.N)_{o/s_{rated}} > (\tau.N)_{o/s_{stall}} \qquad [5.23]$$

$$k = (\tau.N)_{o/s_{rated}} / (\tau.N)_{o/s_{stall}}$$

$$(N_{rated}/N_{stall})_{o/s} = (\tau_{stall}/\tau_{rated})_{o/s}^{\ k}$$

$$(N_{rated}/N_{stall})_{o/s} = 3.6\ k \qquad [5.24]$$

where τ and N denote torque and speed respectively.

To work out a value for K, the power of the turbine and compressor have to be estimated at stall as well as at the design point (step '7').

Referring to the ideal DCE with the engine running at constant power between rated and stall conditions, Prince (Ref. 39) evaluated the turbine power at stall by splitting it into a constant component coming from the engine exhaust and a rising component coming directly from the compressor. Assuming a proportional relation between mass flow and speed for a positive displacement compressor, i.e.

$$\dot{m}_{COMP_{excess}} = (n-1)\ \dot{m}_{COMP_{rated}} = (n-1)\ \dot{m}_{TURB_{rated}} \qquad [5.25]$$

and for the same boost pressure ratio for the stall and design points, the following correlations were developed :

$$HP_{COMP_{stall}} = n.HP_{COMP_{rated}} \cdot \frac{\eta_{c_{rated}}}{\eta_{c_{stall}}} \qquad [5.26]$$

$$HP_{TURB_{stall}} = \frac{\eta_{T_{stall}}}{\eta_{T_{rated}}} \left(1 + (n-1)\ \frac{T_{inl}}{T_{exh_{stall}}}\right) . \ HP_{TURB_{rated}} \qquad [5.27]$$

where

η_C = compressor isentropic efficiency

η_T = turbine isentropic efficiency

n = actual compressor overspeed ratio

T_{inl} = engine inlet air temperature

T_{exh} = engine exhaust gas temperature

Assuming a decrease in the efficiencies of turbine and compressor between stall and design point of the order of 0.9 and using a value of the order of 0.4 for the ratio T_{inl}/T_{exh}, since $HP_{TURB} = 0.39\ HP_{ENG_{des}}$ (step '7') and n = 1.8 (step '9') the values of the power ratios of the turbine and compressor at the stall point become :-

$$\frac{HP_{TURB_{stall}}}{HP_{ENG_{rated}}} = 0.46$$

$$\frac{HP_{COMP_{stall}}}{HP_{ENG_{rated}}} = 0.60$$

Assuming loss free power transmission a value for k in equation 5.23 can now be estimated:

$$HP_{o/s} = HP_{ENG} - HP_{COMP} + HP_{TURB}$$

At the design point:

$$HP_{o/s} = HP_{ENG} - 0.3HP_{ENG} + 0.39HP_{TURB}$$
$$= 1.09\ HP_{ENG}$$

At the stall point:

$$HP_{o/s} = HP_{ENG} - 0.6\ HP_{ENG} + 0.46\ HP_{ENG}$$
$$= 0.86\ HP_{ENG}$$

where HP_{ENG} is assumed to remain constant between rated and stall conditions hence:

$$k = HP_{o/s}\,{}_{rated} / HP_{o/s}\,{}_{stall}$$

$$= 1.09\ HP_{ENG}/0.86\ HP_{ENG}$$

$$= 1.267$$

$$(N_{rated}/N_{stall})_{o/s} = 4.5$$

Equations 5.1 to 5.27 provide approximate guidelines for the assessment of rated and stall conditions for the DCE.

5.3 OUTLINE DESCRIPTION OF THE LABORATORY DCE UNIT AT BATH UNIVERSITY

(see also Chapter 8)

The current DCE unit based on the Leyland 520 engine and rated at 250 hp has been tested since 1986. A detailed description and performance analysis of this unit are given in Ref. 39. The present thesis contains a performance analysis of this unit in Chapter 8 but a brief description is included here for completeness.

In this prototype the output shaft operates over a 1:5 speed range. The engine speed at stall reduces to 65% of its rated value which reduces $r_{overspeed}$ from 3.3 to 1.74. The relevant compressor map with rated and stall point is represented in fig. 5.3. The analytically optimized performance characteristics at two extreme output shaft speeds (design and stall) are reproduced in table 5.1. Boost pressure is allowed to rise along the LTC in order that the engine power may be maintained at an approximately constant level, although it declines to 85% of its rated value.

5.4 ADAPTATION OF THE LATEST DCE DESIGN TO THE L10 ENGINE

Due to similarities in engine rating and output shaft speed range between the current laboratory DCE and those of the DCE based on the L10 engine, the epicyclic gear ratio (egr = 3.074) of the laboratory design was used.

Since the L10-DCE will be applied to the same high duty truck which uses the L10 engine in turbocharged form the output shaft speed of the DCE at the design point was based on the given characteristics of the T/C engined vehicle:

$$N_{o/s} = (v_{veh}/2\pi R_{tyre}) \cdot \frac{1000}{60} \cdot r_b \text{ "rpm"} \qquad [5.28]$$

where v_{veh} = vehicle speed (km/h)

R_{tyre} = driving wheel radius (m)

r_b = back axle ratio

With reference to given Cummins truck data, maximum vehicle speed is 105.6 km/hr, R_{tyre} = 0.5011m and r_b = 3.77, giving

$$N_{o/s_{des}} = (105.6/2\pi \cdot 0.5011) \cdot \frac{1000 \times 3.77}{60}$$

$$= 2107.4 \text{ rpm}$$

Although this speed is almost equal to the rated speed of the L10 engine i.e. 2100 rpm a small degree of overdrive was later adopted to allow optimization of the compressor operating point. This yielded an output shaft speed of 2200 rpm at the design point.

The output shaft step-up ratio, ogr', could be estimated by use of equation 5.14:-

$$\left.\frac{HP_{ENG}}{HP_{COMP}}\right|_{des} = \frac{N_{ENG}}{N_{ENG} - \frac{N_{o/s}}{ogr}}$$

From Section 5.2.2 assuming $\left.\frac{HP_{COMP}}{HP_{ENG}}\right|_{rated} = 0.3$

$$0.7\ N_{ENG}.ogr = N_{o/s} \qquad \text{(see also fig. 5.2)}$$

$$ogr = \frac{2200}{0.7 \times 2100} = 1.496$$

Also, from equation 5.7

$$ogr = \frac{egr}{1 + egr}\ ogr'$$

therefore the planet carrier to output shaft step up gear ratio becomes

$$ogr' = \frac{1+3.074}{3.074} \times 1.496$$

$$= 1.982$$

To size the compressor, with reference to that used with the Leyland 520 (8.8 ℓ engine) a notional mass scale factor of 1.1 based on the swept volume, engine speed and boost levels of the L10 engine was applied.

To determine the compressor step-up ratio, cgr', the stall and design conditions and allowable speed range of the compressor were applied. From the experience in optimization of the existing prototype unit (ref. 39), compressor speeds of 6493 and 11689 rpm at the design and stall points, respectively, were chosen while the corresponding engine speed ratio is 0.65. Hence from equation 5.9:

$$N_{COMP} = [N_{ENG} - \frac{N_{o/s}}{ogr}]cgr$$

At the design point

$$cgr = \frac{6493}{[2100 - \frac{2200}{1.496}]} = 10.31$$

At the stall point

$$cgr = \frac{11689}{[2100 \times 0.65 - \frac{2200}{1.496 \times 5}]} = 10.91$$

The mean value of 10.5 was adopted. Therefore

$$cgr' = \frac{cgr}{egr}$$

$$= \frac{10.5}{3.074} = 3.415$$

However, using the program DCE2 in a later detailed matching study yielded the following step-up gear ratios, ogr' and cgr':

$$ogr' = 1.915$$
$$cgr' = 3.106$$

In this study a margin of 5% to 7% excess compressor air flow over engine demand at the design point was adopted. At the same time the position of the compressor operating point in the compressor map based on the mass scale factor of 1.1, already referred to, was checked for good efficiency. It is noted that the efficiency contours of this original compressor were retained. In fact, scale factor and gear ratio, cgr', are highly interactive and their final choice required many iterations.

So far as fine tuning of the engine subroutine in the program is concerned, the following factors were taken into account:

1) The existing L10 injection system with its fixed end, and variable start of injection timing was taken into consideration.

2) The semi-quiescent combustion process of the L10 engine was modelled with sufficient accuracy by the use of a low combustion rate factor (XK = 0.01 in Section 7.3) so as to result in good agreement between maximum cylinder pressure as calculated by the present engine subroutine on the one hand, and by the detailed program CSPDCE based on careful matching of the WIEBE heat release function against experimental heat release, on the other (Chapter 6).

3) Both engine friction and heat rejection to coolant were matched to give the best possible agreement with CSPDCE.

4) The engine was uprated compared with the after-cooled L10 in turbocharged form (L10-290 T/C) to give 240 kW (322 hp) rather than 216 kW (290 hp) as described in Chapter 7.

5.5 STEADY STATE PERFORMANCE PREDICTIONS FOR THE L10 DCE

As indicated in the introduction of this chapter, the rapid program, DCE2, was used to study the steady state performance characteristics of the L10-DCE. Fig. 2.16 shows the piping model and part of the shaft connections of the system. The input data to the program and the final running conditions are presented in Section 2.5.

The calculations were carried out over the full output shaft speed range from 2200 rpm to 440 rpm and at full, $^3/_4$, $^1/_2$ and $^1/_4$ load (see tables 5.2, 5.3 and 5.4).

The final results were determined through a detailed optimization, using engine speed, turbine gear ratio and turbine nozzle angle as optimizing variables. Before dealing with the discussion of the optimized results, a brief description of the optimization of the DCE is presented in the next section.

5.6 THEORETICAL STEADY STATE OPTIMIZATION OF THE DCE

The steady state optimization of the DCE is achieved by adjustments of the following variables: shaft speeds, turbine nozzle angle and CVT, bypass valve area and injection timing, so as to give maximum system brake thermal efficiency or minimum BSFC at the output shaft.

The optimization procedure is fully described in a number of theses (refs. 39 and 40). However, a brief description of the influences of some of the important variables having first order effect on the overall efficiency is given below.

5.6.1 Effect of Engine Speed and Turbine Nozzle Angle

In general for a selected output shaft torque and speed combination, the optimum operating points are examined for ranges of engine speed. A range of the turbine nozzle angle is covered at each combination of torque and speeds. Investigation has proved that there always exists an optimum engine speed at which the fuel flow rate is at its minimum value.

5.6.2 Effect of Bypass Valve Area and Fuel Injection Timing

The air flow of the Lysholm positive displacement compressor with constant inlet pressure is proportional to compressor speed whereas the engine air flow mainly depends on the engine speed and boost. As was stated, since the percentage decrease of output-shaft speed from the design to the stall point is much higher than that of engine speed, the compressor speed increases substantially. Assuming a constant boost pressure ratio along the output LTC, the compressor air flow increases with decrease in output shaft speed whereas the engine flow decreases. This results in increased bypass mass flow rate in the low output shaft speed range and in turn to dilution of the engine exhaust gas.

The resultant low exhaust gas temperature at the turbine inlet decreases the turbine power markedly, but as will be seen, this can be largely improved by connecting the turbine via a continuously variable transmission (C.V.T) to the output shaft. This implies that the role of

bypass mass flow rate calls for further investigation. The bypass mass flow can be controlled by a bypass valve setting while also affecting boost pressure and hence air-fuel ratio.

The boost pressure ratio increases rapidly with a closed bypass valve resulting in higher demanded engine power, and causing high maximum cylinder pressure beyond the recommended limits.

The cylinder pressure level can be reduced by retarded fuel injection timing, but the resulting deterioration induced in overall efficiency is substantial.

Zero bypassing results in high air-fuel ratios beyond optimum levels for good engine thermal efficiency and counteracts the desirable effect of higher boost pressure ratio. On the other hand, due to the fact that the pressure drop across the engine is very large, the turbine inlet pressure ratio becomes very low leading to a considerable deterioration in developed turbine power.

Consequently, it has been proved that no gain in overall system efficiency is achieved by partially or completely closing the bypass valve under steady state conditions. The best system efficiency is achieved with a wide open bypass even when bypass mass flow is large. However, at certain stages of transient operation it could be advantageous to control the bypass setting to ensure smoke free combustion.

5.6.3 The Effect of a Continuous Variable Turbine Transmission (C.V.T.)

In line with the concept of compounding, the turbine power contribution in the DCE plays an important role in achieving better overall efficiency. Improvement in turbine performance can be gained by the introduction of a C.V.T. to ensure that the turbine always operates at its best efficiency speed. Otherwise, with fixed gearing, the turbine speed is proportional to the output shaft speed and undergoes large variations which usually lead to loss of turbine efficiency.

Fig. 5.4 shows a typical variation of efficiency of a radial inward flow turbine with speed ratio, u/c, where u is peripheral velocity of the turbine rotor tip and c denotes the stage terminal velocity. It has been proved that the turbine efficiency generally peaks at u/c = 0.7.

The value of c is determined by the turbine inlet temperature and expansion ratio whereas, for a given turbine, the value of u only varies with the turbine speed. The turbine C.V.T., therefore, adjusts the turbine speed to cope with the inlet condition so as to give the best turbine efficiency.

Fig. 5.5 from ref. 40, represents the variation of output shaft efficiency, engine efficiency, compressor efficiency and turbine efficiency with output shaft speed, $N_{o/s}$, both with fixed gearing and with a C.V.T. between turbine and output shaft. In the former case, the turbine efficiency decreases considerably with decreasing output shaft speed, whereas in the latter the C.V.T. maintains turbine efficiency and hence output shaft efficiency at high levels.

Fig. 5.6 from the same reference shows the variation of output shaft torque, $\tau_{o/s}$, with output shaft speed, $N_{o/s}$, for these two cases. The large increase in output shaft torque in the low output shaft speed range when using C.V.T. is very noticeable.

5.7 RESULTS AND DISCUSSION

Tables 5.2 to 5.4 summarise the computed results from the lowest output shaft speed $N_{o/s}$ = 440 rpm giving maximum output shaft torque $\tau_{o/s}$ = 4046.9 N.m to the rated conditions, $N_{o/s}$ = 2200 rpm, $\tau_{o/s}$ = 1022.1 N.m. Thus a torque ratio of 3.96 (= 4046.9/1022.1) has been achieved which, together with a torque converter torque ratio of 3.6 provides the drive line with an overall torque ratio of 14.25. It is estimated this would give gradability of between 25 and 30% with a 38 tonne vehicle.

The operating characteristics are presented in graphical form in figs. 5.7 to 5.12 as contours of the various key parameters with output shaft torque and speed respectively as ordinate and abscissa. All operating points have been fully optimized.

The following discussion is based on figs. 5.7 to 5.12 and tables 5.2 to 5.4. In addition, both the design point and the maximum output shaft torque conditions will be discussed in detail.

i) Design point rating (table 5.4)

The engine is operating at its rated speed of 2100 rpm developing 240 kW corresponding to a BMEP of 13.69 bar, and with a trapped air fuel ratio of 30.57 very close to the design value of 30.06 of the L10.290-T/C engine. Brake thermal efficiency is 39.8% compared with the rated value of 41.00% reflecting the effect of the negative pumping loop due to the adverse pressure gradient across the engine, with an exhaust manifold pressure of 2.86 bar compared with a boost pressure of 2.64 bar (corresponding values for the T/C engine are 1.70 bar and 1.96 bar, respectively, i.e. a substantial positive pressure gradient).

Compressor power is 63.94 kW at a total-to-total efficiency of 72.4% as against turbine power of 74.96 kW at an efficiency of 75%, giving a compounding effect of 11.02 kW or 4.68% of the effective shaft power of 235.57 kW.

Bypass flow is very small at 0.128 kg/min or 0.5% of the compressor delivery flow of 25.75 kg/min.

Gear losses are given by (HP denotes power):

$$HP_{GEAR} = HP_{ENG} + HP_{TURB} - HP_{COMP} - HP_{o/s}$$

$$= 240.00 + 74.96 - 63.94 - 235.57$$

$$= 15.45 \text{ kW}$$

or 6.56% of output shaft power, giving an overall gearing efficiency of 93.44% which may be slightly optimistic, yielding an output shaft efficiency of 39.07%

ii) Stall point rating (table 5.2)

The engine has been despeeded to 1350 rpm, and develops slightly above its original power, at 241.77 kW, corresponding to a BMEP of 21.45 bar but retaining a generous trapped air fuel ratio at 32.44. Brake thermal efficiency, as a result of the combination of low speed and high BMEP may have been estimated somewhat optimistically at 44.85%. Boost pressure is high at 3.95 bar which, with an exhaust pressure of 4.12 bar gives an adverse pressure gradient of 0.165 bar, i.e. relatively slight. Maximum cylinder pressure is high at 176.31 bar (2556 psi). Compressor power is 181.77 kW at 67.5% efficiency compared with turbine power of 144.13 kW at 77.4% efficiency, giving a negative compounding effect of 37.64 kW due to substantial bypassing of compressor air (24.63 kg/min or 50.3% of compressor delivery), the bypass air being essentially a torque conversion medium.

Gear losses are 17.58 kW or 9.42% of output shaft power, giving an overall gearing efficiency of 90.58% yielding an output shaft efficiency of 34.61%.

iii) System efficiency contours (fig. 5.7)

These must be regarded as very favourable, with a best efficiency of 39.7% at 1900 rpm on the limiting torque curve, and with the 36% contour covering well over half the total speed-torque map. The nearly hyperbolic

torque-speed envelope is evident.

iv) Boost pressure ratio (fig. 5.8)

These contours substantially follow power demands and generally show a uniform rising trend both with increasing output torque and decreasing output speed. A marked tendency to rise rather more rapidly at low output shaft speeds is apparent. The highest boost pressure ratio is 3.95 at the stall point.

v) Engine BMEP (fig. 5.9)

These contours are virtually identical with those for boost pressure ratio, with the highest value of 21.45 bar (311 psi) at the stall point.

vi) Turbine overall gear ratio (fig. 5.10)

This increases from 22.5 at the design point to 105.7 at the stall condition, giving a ratio range of 4.7 (=105.7/22.5) i.e. well within the range of existing C.V.Ts. Ideally, this range should be extended further into the part load range, as shown in fig. 5.10, down to an effective minimum overall gear ratio of 10:1 covering loads below $^1/_4$ of full load.

vii) Turbine nozzle angle (fig. 5.11)

It has to be pointed out that these predictions are based on an anlytical turbine subroutine which has not been fully tested at very low pressure ratios. It is significant that along the limiting torque curve, the range of nozzle angles is quite small, from 8.886 deg. at rated condition to 9.698 deg. at stall. Only at very low loads, i.e. pressure ratios and low output shaft speeds, are large nozzle angles (approx. 35 deg.) called for, but these values should be treated with caution. It should be pointed out that the program treats the nozzle blades as infinitely thin.

viii) Compressor match (fig. 5.12)

In order to run the positive displacement compressor at moderate speeds, the operating lines have deliberately been shifted to the 'left' giving somewhat lower compressor efficiency, but limiting maximum compressor speed to 10,066 rpm, compared with the somewhat higher value of 11689 rpm applicable to the laboratory prototype.

5.8 CONCLUSION

The optimized steady state performance characteristics of the uprated L10 engine as the power unit for the DCE have been determined and show very satisfactory levels of torque back up and system efficiency, in particular compared with the experimental DCE using the Leyland 520 engine.

The values of the controlling variables such as engine speed, turbine nozzle angle and gear ratios which have been determined through an optimization study, can also be applied to predict and analyse the DCE characteristics in accelerating a vehicle (truck) say from rest. This is performed using the program DCETRAN described in Chapter 7. (This program is similar in structure to the steady state simulation program 'DCE2' but includes the dynamics of the gear train as well as of the various volumes in the system).

The steady state control scheme optimizes turbine nozzle angle and gear ratio in relation to output shaft speed and fuel rack position, which is taken as a measure of torque.

number of cylinders		6.0	bore	(m.m.)	118.11	stroke	(m.m.)	120.47	
conrod length	(m.m.)	218.45	inlet valve closing	(degs)	230.0	compressor scale factor		1.00	
ambient temperature	(deg k)	294.4	ambient pressure	(bar)	0.99				
compression ratio		12.80				turbine flow loss factor		0.00	
engine speed(r.p.m)		1000.00	1200.00	1550.00	1873.00	2250.00	2330.00	2490.00	2660.00
boost pressure ratio		2.006	3.057	3.305	3.793	1.329	1.797	2.319	2.915
delivered air to fuel ratio		23.531	31.226	30.033	27.620	27.634	25.567	25.499	24.710
delivery ratio		0.855	0.858	0.853	0.953	0.852	0.852	0.851	0.850
manifold temp	(deg k)	336.385	318.462	312.912	320.983	298.298	307.259	314.172	320.568
engine power	(k w.)	67.24	120.17	177.86	229.02	65.41	143.95	208.15	265.84
engine torque	(n.m.))	643.79	956.73	1096.23	1304.35	364.44	591.58	799.52	977.53
b.m.e.p	(bar)	9.8210	14.6260	16.7591	19.9932	5.5443	9.0232	12.2089	14.9333
s.f.c.	(kg/kw hr)	0.275	0.224	0.223	0.228	0.309	0.269	0.251	0.242
b.thermal eff.		0.3029	0.3723	0.3733	0.3665	0.2700	0.3096	0.3320	0.3450
fuel / rev	(kg.)	3.086	3.738	4.278	5.192	1.954	2.774	3.501	4.120
max cyl pressure	(bar .)	118.23	149.20	149.37	150.31	86.05	114.28	135.85	148.67
exhaust temperature(deg k)		775.46	737.66	805.82	888.82	804.58	885.02	925.56	932.79
mass flow (kg/min)		7.261	13.993	19.893	23.992	12.150	16.522	22.226	28.609
percentage heat to coolant		39.87	26.42	21.18	19.14	27.84	23.47	19.83	17.21
compressor speed (r.p.m.)		5559.6	7325.5	10416.1	11502.2	3515.6	4222.0	5634.8	6606.1
compressor pressure ratio		2.023	3.120	3.426	3.952	1.408	1.916	2.500	3.171
mass flow (kg/min)		24.145	32.211	47.165	52.186	14.963	17.638	24.282	28.643
compressor power (kw.)		40.79	80.28	131.16	173.16	14.34	28.40	51.51	73.97
compressor torque (n.m)		70.02	104.61	120.20	143.70	38.98	64.21	87.25	106.56
delivery temperature (deg k)		395.50	443.16	460.21	491.83	351.90	390.81	421.17	448.50
compressor efficiency		0.652	0.700	0.748	0.714	0.528	0.626	0.696	0.746
turbine speed (r.p.m)		30000.0	39000.0	42000.0	46500.0	25000.0	37500.0	45000.0	50000.0
turbine pressure ratio		2.023	3.120	3.426	3.952	1.408	1.916	2.500	3.171
mass flow (kg/min)		24.461	32.662	47.836	53.063	15.409	18.288	25.160	29.717
turbine power (kw)		29.30	67.19	114.25	156.40	13.14	33.75	66.43	101.70
turbine torque (n.m)		9.32	16.44	25.97	32.11	5.02	8.59	14.09	19.42
inlet temperature (deg k)		520.99	578.63	615.89	687.33	728.42	857.92	988.39	932.29
turbine nozzle angle		8.262	7.317	10.098	10.276	10.569	8.546	8.837	9.408
turbine efficiency		0.747	0.757	0.771	0.776	0.744	0.745	0.754	0.760
output shaft speed (rpm)		500.00	500.00	500.00	500.00	2500.00	2500.00	2500.00	2500.00
output shaft power (kw)		50.58	97.76	146.88	194.18	75.64	138.00	207.97	274.65
output shaft torque (n./m)		965.64	1866.25	2803.97	3707.05	288.81	526.91	794.07	1048.66
output shaft sfc (kg/kw.hr)		0.366	0.275	0.271	0.269	0.349	0.281	0.251	0.234
output thermal efficiency		0.2279	0.3032	0.3082	0.3108	0.2391	0.2969	0.3317	0.3565
engine fuel flow (kg/min)		0.309	0.448	0.662	0.869	0.440	0.646	0.872	1.071
dynamic injection(degree ca)		329.8	342.1	342.4	345.1	330.1	330.1	330.1	331.4
duration of injection		14.2	18.4	24.7	31.0	19.2	23.8	31.1	37.8
turbine gear ratio		60.0	78.0	84.0	93.0	10.0	15.0	10.0	20.0
		25% load	50% load	75% load	100% load	25% load	50% load	75% load	100% load
		20% speed			STALL	100% speed			RATED

Table 5.1 Analytically optimized steady state performance of laboratoy DCE unit (Ref. 39)

CUMMINS L10 D C E

STALL POINT

45 20 15 26

number of cylinders	6.0	bore (m.m.)	125.03	stroke (m.m.)	136.00		
con-rod length (m.m.)	217.78	inlet valve closing (degs)	193.0	compressor scale factor	1.10		
ambient temperature (deg k)	294.4	ambient pressure (bar)	0.99	cooler effectiveness	0.8104		
compression ratio	16.30	engine diagram factor	0.9874	turbine flow loss factor	0.8000		

engine speed(r.p.m)	1350.00	1250.00	1150.00	1100.00	1400.00	1350.00	1200.00	1100.00
boost pressure ratio	3.950	3.346	2.400	1.337	3.831	3.148	2.329	1.340
delivered air to fuel ratio	32.438	35.505	35.349	35.870	32.089	35.305	35.598	36.069
delivery ratio	0.853	0.853	0.853	0.854	0.853	0.853	0.853	0.854
manifold temp (deg k)	324.959	314.943	306.695	297.590	324.809	314.018	305.326	297.607
engine power (k w.)	241.77	181.62	120.98	60.11	241.98	181.42	120.95	59.94
engine torque (n.m.))	1706.95	1382.92	1002.11	523.83	1646.89	1280.69	960.45	522.25
b.m.e.p (bar)	21.4477	17.4010	12.5990	6.5444	20.6997	16.0937	12.0709	6.5258
s.f.c. (kg/kw hr)	0.186	0.183	0.187	0.204	0.189	0.188	0.188	0.204
b.thermal eff.	0.4485	0.4561	0.4466	0.4093	0.4411	0.4443	0.4427	0.4096
fuel / rev (kg.)	5.550	4.428	3.274	1.856	5.447	4.204	3.165	1.849
max cyl pressure (bar .)	176.31	148.47	107.29	60.13	171.70	140.38	104.11	60.20
exhaust temperature(deg k)	835.89	765.79	737.15	687.70	847.85	777.61	737.04	685.61
mass flow (kg/min)	24.306	19.654	13.310	7.322	24.471	20.038	13.519	7.337
percentage heat to coolant	10.29	11.50	14.30	20.10	10.24	11.34	14.13	20.08
compressor speed (r.p.m.)	9984.5	9029.5	8074.5	7597.0	10065.5	9588.0	8155.5	7200.5
compressor pressure ratio	4.219	3.570	2.573	1.473	4.103	3.378	2.506	1.476
mass flow (kg/min)	48.939	44.257	39.879	38.980	49.469	47.435	40.346	36.775
compressor power (kw.)	181.77	133.09	85.94	41.68	176.74	130.56	83.11	39.38
compressor torque (n.m)	173.77	140.69	101.59	52.36	167.61	129.98	97.27	52.20
delivery temperature (deg k)	515.03	473.54	423.17	358.51	506.75	458.53	417.53	358.61
compressor efficiency	0.675	0.719	0.710	0.540	0.685	0.745	0.719	0.542
turbine speed (r.p.m)	46508.0	41800.0	30800.0	12584.0	45000.0	39300.0	31450.0	12850.0
turbine pressure ratio	4.115	3.466	2.469	1.369	3.999	3.274	2.401	1.372
mass flow (kg/min)	49.696	44.818	40.271	39.116	50.240	48.012	40.746	36.964
turbine power (kw)	144.13	101.99	57.56	8.36	143.47	103.19	56.18	8.22
turbine torque (n.m)	29.58	23.29	17.84	6.35	30.43	25.06	17.05	6.11
inlet temperature (deg k)	683.20	610.48	534.96	425.14	685.12	601.30	531.71	428.80
turbine nozzle angle	9.698	9.901	12.113	36.664	10.123	11.199	12.719	34.230
turbine efficiency	0.774	0.768	0.761	0.718	0.774	0.771	0.765	0.729
output shaft speed (r.p.m)	440.00	440.00	440.00	440.00	500.00	500.00	500.00	500.00
output shaft power (kw)	186.55	137.18	83.91	23.16	190.94	140.43	85.28	25.07
output shaft torque (n./m)	4046.89	2976.00	1820.31	502.39	3645.13	2680.86	1628.07	478.52
output shaft sfc (kg/kw.hr)	0.241	0.242	0.269	0.529	0.240	0.243	0.267	0.487
output thermal efficiency	0.3461	0.3445	0.3098	0.1577	0.3480	0.3439	0.3122	0.1713
engine fuel flow (kg/min)	0.749	0.554	0.377	0.204	0.763	0.568	0.380	0.203
dynamic injection(degree ca)	337.5	340.4	343.3	345.9	337.4	340.5	343.4	345.9
duration of injection	28.7	23.3	17.8	13.4	28.5	22.7	17.6	13.3
turbine gear ratio	105.7	95.0	70.0	28.6	90.0	78.6	62.9	25.7
pressure loss in pipe a (bar)	0.10345	0.10345	0.10345	0.10345	0.10345	0.10345	0.10345	0.10345
pressure loss in pipe b (bar)	0.10345	0.10345	0.10345	0.10345	0.10345	0.10345	0.10345	0.10345
pressure loss in pipe c (bar)	0.10345	0.10345	0.10345	0.10345	0.10345	0.10345	0.10345	0.10345
pressure loss in pipe d (bar)	0.10345	0.10345	0.10345	0.10345	0.10345	0.10345	0.10345	0.10345

Table 5.2 Analytically optimized steady state perfomance characteristics of the L1O-DCE at O/S speed of 440 and 500 rpm under various loads

CUMMINS L10 [illegible] 41 26 20 24

number of cylinders	6.0	bore (m.m.)	125.03	stroke (m.m.)	136.00		
con-rod length (m.m.)	217.78	inlet valve closing (degs)	193.0	compressor scale factor	1.10		
ambient temperature (deg k)	294.4	ambient pressure (bar)	0.99	cooler effectiveness	0.8301		
compression ratio	16.30	engine diagram factor	0.9392	turbine flow loss factor	0.8000		
engine speed(r.p.m)	1500.00	1350.00	1250.00	1100.00	1700.00	1600.00	1460.00	1400.00
boost pressure ratio	3.535	3.113	2.268	1.450	3.167	2.690	1.977	1.277
delivered air to fuel ratio	30.441	34.564	35.776	39.420	29.993	32.846	33.335	40.834
delivery ratio	0.852	0.853	0.853	0.854	0.852	0.852	0.853	0.853
manifold temp (deg k)	325.934	315.835	305.586	298.783	326.065	316.472	306.788	295.031
engine power (k w.)	241.48	181.42	120.95	60.33	241.33	181.09	121.51	60.05
engine torque (n.m.))	1537.48	1281.23	922.49	524.15	1356.61	1081.25	795.18	411.89
b.m.e.p (bar)	19.2797	16.0944	11.5877	6.5684	17.0010	13.5550	9.9676	5.1366
s.f.c. (kg/kw hr)	0.196	0.189	0.190	0.200	0.202	0.203	0.206	0.220
b.thermal eff.	0.4253	0.4424	0.4380	0.4179	0.4128	0.4117	0.4039	0.3799
fuel / rev (kg.)	5.262	4.222	3.071	1.824	4.781	3.822	2.864	1.569
max cyl pressure (bar .)	159.48	139.01	101.61	64.28	142.85	121.20	90.09	57.05
exhaust temperature(deg k)	887.52	788.53	739.43	656.75	906.98	837.49	795.58	669.28
mass flow (kg/min)	24.029	19.703	13.732	7.911	24.375	20.086	13.940	8.972
percentage heat to coolant	10.36	11.50	14.00	19.20	10.27	11.37	13.92	17.63
compressor speed (r.p.m.)	7385.6	5953.1	4998.1	3565.6	5660.6	4705.6	3368.6	2795.6
compressor pressure ratio	3.809	3.342	2.449	1.589	3.454	2.932	2.167	1.429
mass flow (kg/min)	35.126	27.803	23.322	16.430	26.105	21.382	14.596	12.425
compressor power (kw.)	120.94	81.01	48.63	19.55	81.75	53.97	28.36	11.97
compressor torque (n.m)	156.30	129.90	92.86	52.32	137.86	109.49	80.36	40.88
delivery temperature (deg k)	499.15	468.04	419.02	365.70	480.87	445.05	410.59	352.19
compressor efficiency	0.666	0.697	0.690	0.587	0.669	0.703	0.628	0.550
turbine speed (r.p.m)	42000.0	43470.0	32550.0	17115.0	48480.0	43200.0	35680.0	11200.0
turbine pressure ratio	3.705	3.238	2.345	1.485	3.350	2.828	2.063	1.325
mass flow (kg/min)	35.919	28.377	23.712	16.637	26.921	21.996	15.019	12.649
turbine power (kw)	107.30	69.35	35.95	7.19	85.82	55.11	23.66	2.83
turbine torque (n.m)	24.39	15.23	10.54	4.01	16.90	12.18	6.33	2.41
inlet temperature (deg k)	774.91	701.94	615.38	512.11	881.95	816.20	780.06	586.68
turbine nozzle angle	8.355	7.232	8.131	11.673	7.455	7.020	6.995	14.516
turbine efficiency	0.751	0.754	0.747	0.743	0.756	0.748	0.736	0.728
output shaft speed (rpm)	1050.00	1050.00	1050.00	1050.00	1600.00	1600.00	1600.00	1600.00
output shaft power (kw)	212.20	157.74	99.89	43.40	230.46	170.57	108.77	45.80
output shaft torque (n./m)	1929.07	1434.02	908.12	394.52	1374.91	1017.58	648.90	273.22
output shaft sfc (kg/kw.hr)	0.223	0.217	0.231	0.277	0.212	0.215	0.231	0.288
output thermal efficiency	0.3737	0.3847	0.3618	0.3006	0.3942	0.3877	0.3616	0.2898
engine fuel flow (kg/min)	0.789	0.570	0.384	0.201	0.813	0.612	0.418	0.220
dynamic injection(degree ca)	337.4	340.5	343.4	345.9	338.3	340.5	342.7	345.1
duration of injection	28.2	22.8	17.4	13.3	26.8	22.1	17.7	13.1
turbine gear ratio	40.0	41.4	31.0	16.3	30.3	27.0	22.3	7.0
pressure loss in pipe a (bar)	0.10345	0.10345	0.10345	0.10345	0.10345	0.10345	0.10345	0.10345
pressure loss in pipe b (bar)	0.10345	0.10345	0.10345	0.10345	0.10345	0.10345	0.10345	0.10345
pressure loss in pipe c (bar)	0.10345	0.10345	0.10345	0.10345	0.10345	0.10345	0.10345	0.10345
pressure loss in pipe d (bar)	0.10345	0.10345	0.10345	0.10345	0.10345	0.10345	0.10345	0.10345

Table 5.3 As per table 5.2 but at O/S speed of 1050 and 1600 rpm

DESIGN POINT

CUMMINS L10 E C T 42 32 23 23

number of cylinders	6.0	bore (m.m.)	125.03	stroke (m.m.)	136.00			
con-rod length (m.m.)	217.78	inlet valve closing (degs)	193.0	compressor scale factor	1.10			
ambient temperature (deg k)	294.4	ambient pressure (bar)	0.99	cooler effectiveness	0.7853			
compression ratio	16.30	engine diagram factor	0.9000	turbine flow loss factor	0.8000			
engine speed(r.p.m)	1900.00	1775.00	1670.00	1570.00	2100.00	2000.00	1900.00	1800.00
boost pressure ratio	2.932	2.316	1.745	1.225	2.638	2.073	1.548	1.211
delivered air to fuel ratio	31.074	30.478	31.809	41.516	30.575	30.146	31.619	38.363
delivery ratio	0.851	0.852	0.852	0.853	0.851	0.851	0.852	0.852
manifold temp (deg k)	322.578	315.418	306.618	295.463	319.090	312.374	304.462	297.216
engine power (k w.)	240.01	180.88	122.02	59.63	240.00	180.86	120.49	71.47
engine torque (n.m.))	1207.34	974.41	698.91	366.34	1092.77	865.27	607.13	379.90
b.m.e.p (bar)	15.1282	12.2041	8.7500	4.5484	13.6868	10.8300	7.5950	4.7549
s.f.c. (kg/kw hr)	0.205	0.209	0.217	0.234	0.210	0.215	0.225	0.237
b.thermal eff.	0.4069	0.3983	0.3844	0.3569	0.3980	0.3873	0.3715	0.3518
fuel / rev (kg.)	4.315	3.557	2.642	1.479	3.992	3.246	2.373	1.569
max cyl pressure (bar .)	131.14	105.31	79.85	54.71	117.56	93.57	70.46	54.21
exhaust temperature(deg k)	892.53	881.11	831.63	679.34	904.25	892.47	841.16	725.91
mass flow (kg/min)	25.478	19.242	14.037	9.642	25.628	19.571	14.257	10.832
percentage heat to coolant	9.95	11.64	13.86	16.90	9.86	11.46	13.68	15.85
compressor speed (r.p.m.)	5587.9	4394.2	3391.4	2436.4	5515.2	4560.2	3605.2	2650.2
compressor pressure ratio	3.240	2.559	1.941	1.385	2.965	2.331	1.752	1.384
mass flow (kg/min)	25.945	19.917	14.810	10.498	25.756	21.030	16.360	11.687
compressor power (kw.)	71.64	45.22	24.99	9.24	63.94	41.78	22.98	10.44
compressor torque (n.m)	122.38	98.23	70.33	36.20	110.66	87.45	60.85	37.59
delivery temperature (deg k)	459.06	430.02	395.37	347.21	442.58	413.18	378.55	347.98
compressor efficiency	0.713	0.669	0.610	0.546	0.724	0.679	0.610	0.537
turbine speed (r.p.m)	47310.0	41610.0	30970.0	10830.0	49500.0	40700.0	30800.0	11220.0
turbine pressure ratio	3.136	2.455	1.837	1.280	2.861	2.226	1.648	1.280
mass flow (kg/min)	26.768	20.554	15.256	10.732	26.604	21.692	16.821	11.947
turbine power (kw)	81.13	46.97	20.21	1.75	74.96	43.34	16.08	2.08
turbine torque (n.m)	16.37	10.77	6.23	1.54	14.46	10.16	4.98	1.77
inlet temperature (deg k)	885.64	867.62	811.39	654.44	902.24	863.12	787.98	700.76
turbine nozzle angle	7.976	7.990	8.596	17.737	8.886	9.639	12.312	20.740
turbine efficiency	0.756	0.748	0.741	0.752	0.750	0.748	0.725	0.755
output shaft speed (rpm)	1900.00	1900.00	1900.00	1900.00	2200.00	2200.00	2200.00	2200.00
output shaft power (kw)	234.18	170.93	108.82	46.74	235.57	170.57	104.85	56.29
output shaft torque (n./m)	1176.48	858.72	546.71	234.83	1022.10	740.06	454.91	244.21
output shaft sfc (kg/kw.hr)	0.210	0.222	0.243	0.298	0.213	0.228	0.258	0.301
output thermal efficiency	0.3970	0.3764	0.3428	0.2798	0.3907	0.3652	0.3232	0.2771
engine fuel flow (kg/min)	0.820	0.631	0.441	0.232	0.838	0.649	0.451	0.282
dynamic injection(degree ca)	339.7	341.2	342.8	344.7	341.0	342.3	343.6	344.7
duration of injection	25.3	21.5	17.7	13.7	24.6	21.2	17.6	14.7
turbine gear ratio	24.9	21.9	16.3	5.7	22.5	18.5	14.0	5.1
pressure loss in pipe a (bar)	0.10345	0.10345	0.10345	0.10345	0.10345	0.10345	0.10345	0.10345
pressure loss in pipe b (bar)	0.10345	0.10345	0.10345	0.10345	0.10345	0.10345	0.10345	0.10345
pressure loss in pipe c (bar)	0.10345	0.10345	0.10345	0.10345	0.10345	0.10345	0.10345	0.10345
pressure loss in pipe d (bar)	0.10345	0.10345	0.10345	0.10345	0.10345	0.10345	0.10345	0.10345

Table 5.4 As per table 5.2 but at O/S speed of 1900 and 2200 rpm

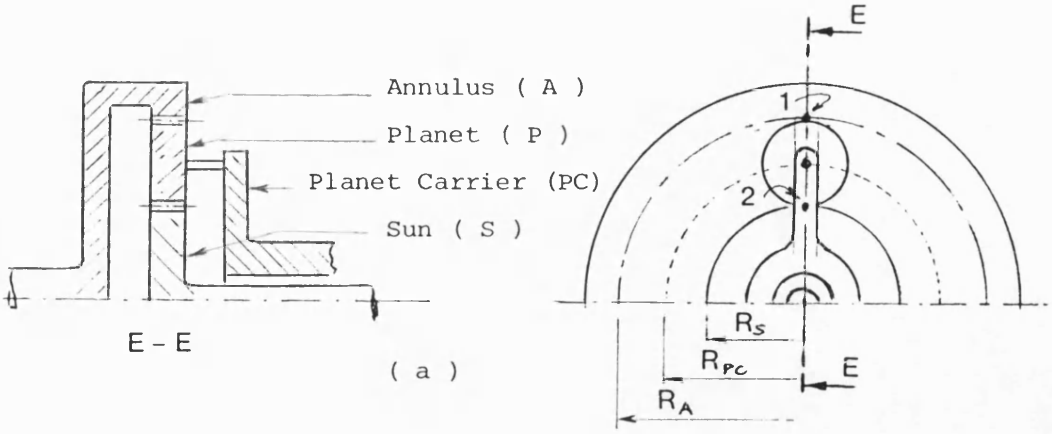

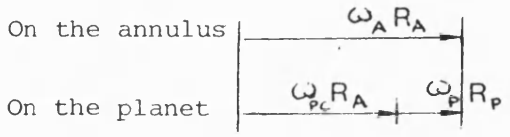

(b) Velocity vectors at mesh point 1

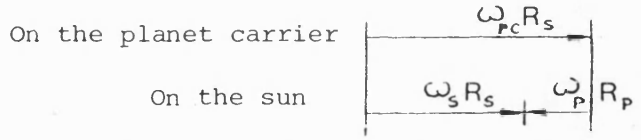

(c) Velocity vectors at mesh point 2

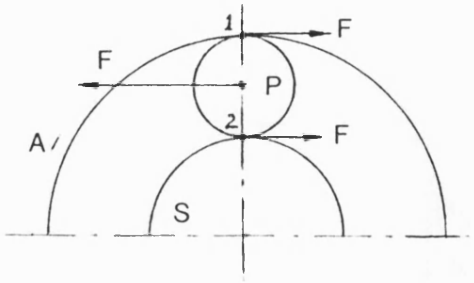

(d) The forces acting on planet

Fig, 5.1

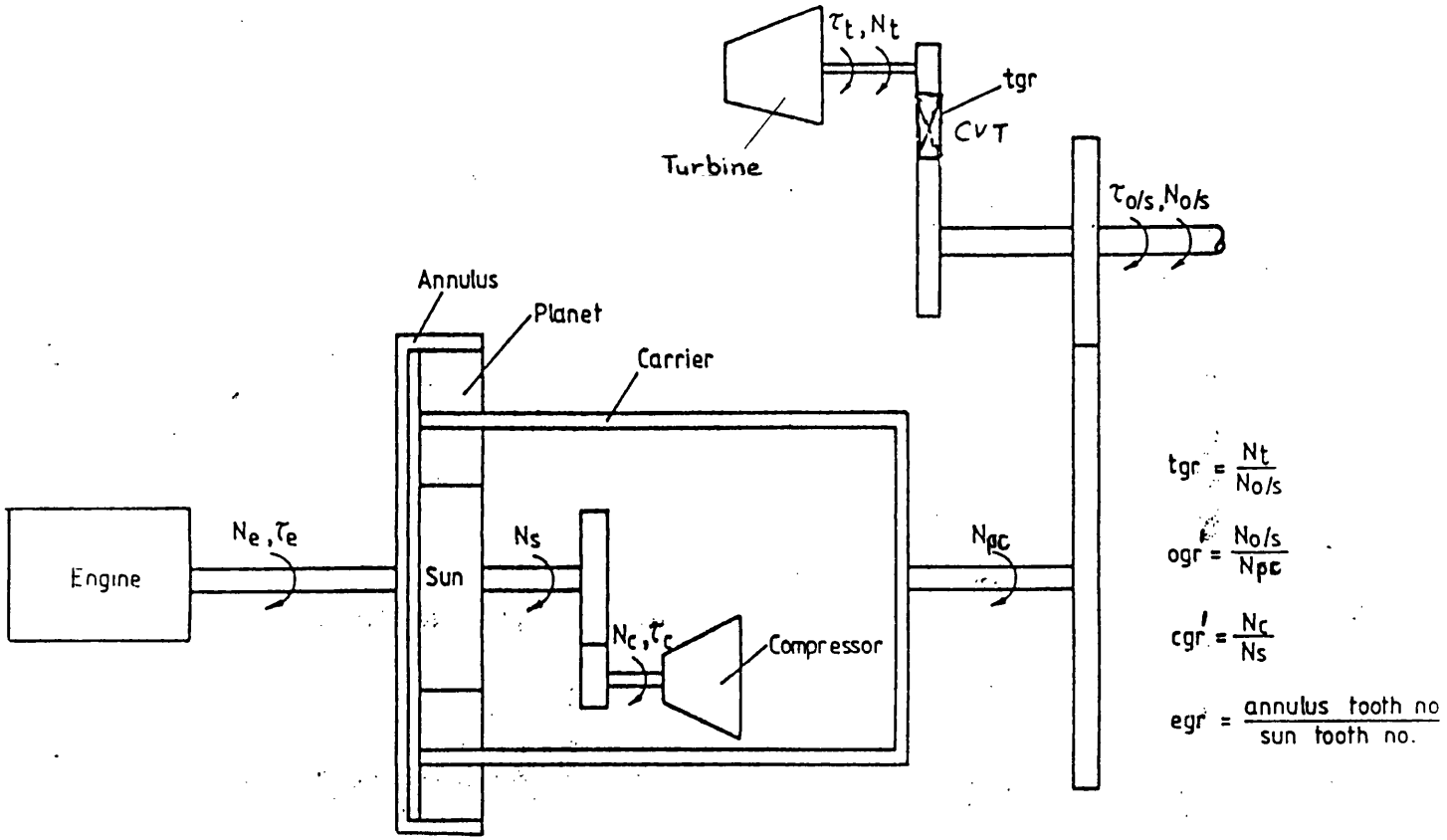

Fig. 5.2 Schematic diagram for gear train of the DCE

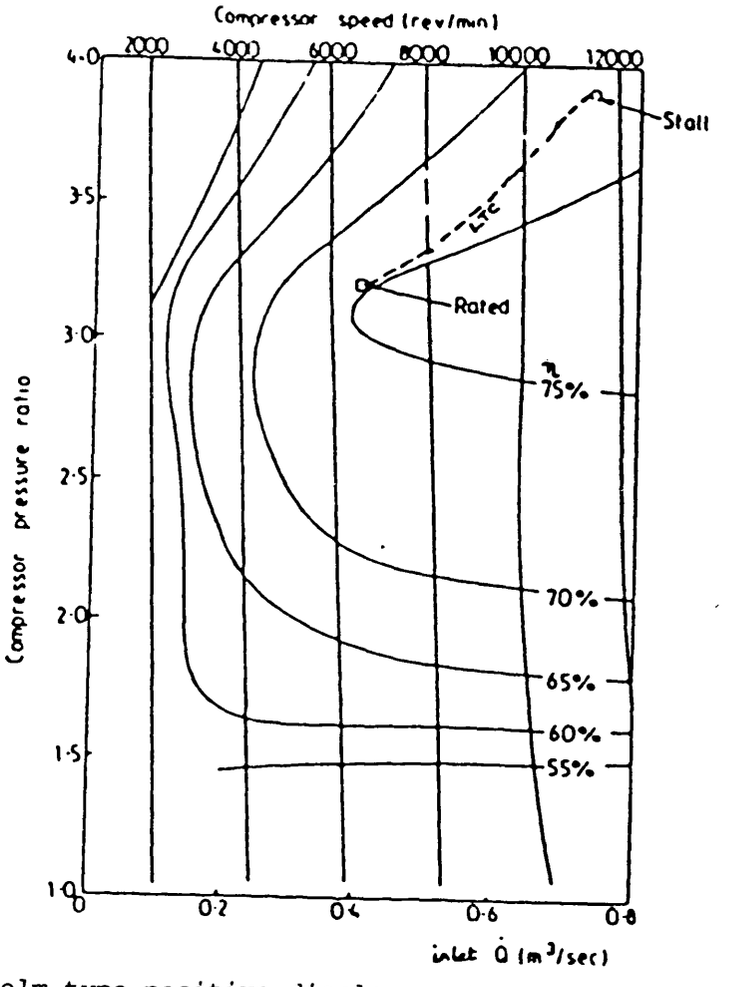

Fig. 5.3 Lysholm type positive displacement compressor map corresponding to the Leyland 520-DCE superimposed with two points of stall and rated running conditions

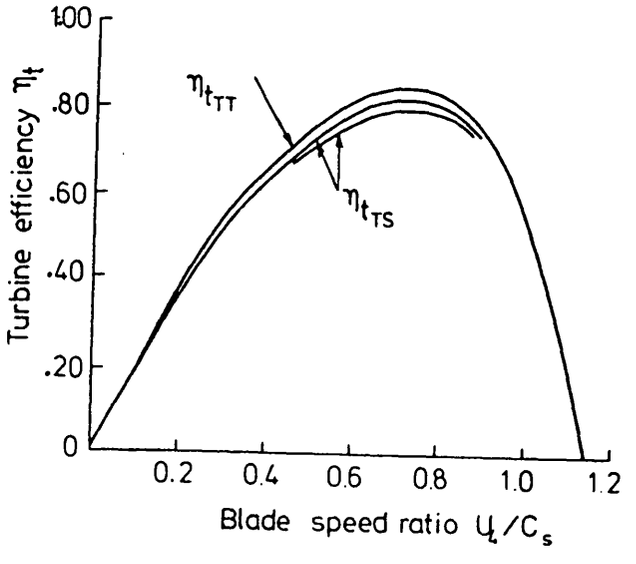

Fig. 5.4 Typical variation of turbine efficiency with blade speed ratio

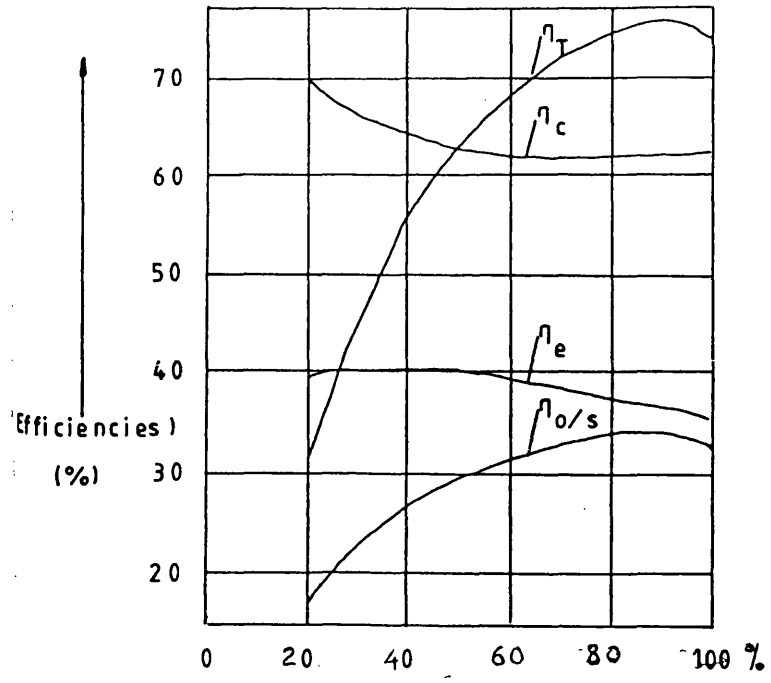

(a) with fixed tgr

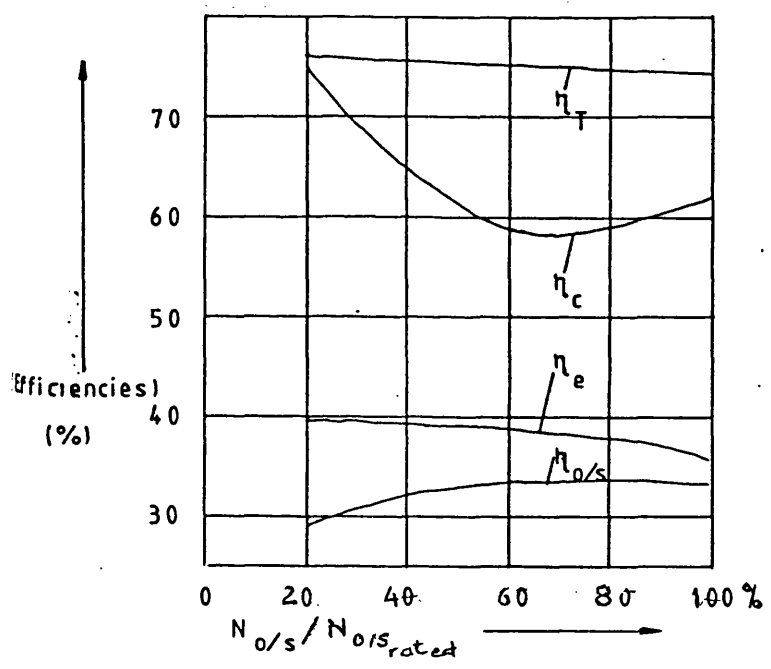

(b) with turbine CVT

Fig. 5.5 Typical effect of a turbine CVT on efficiencies of the DCE components

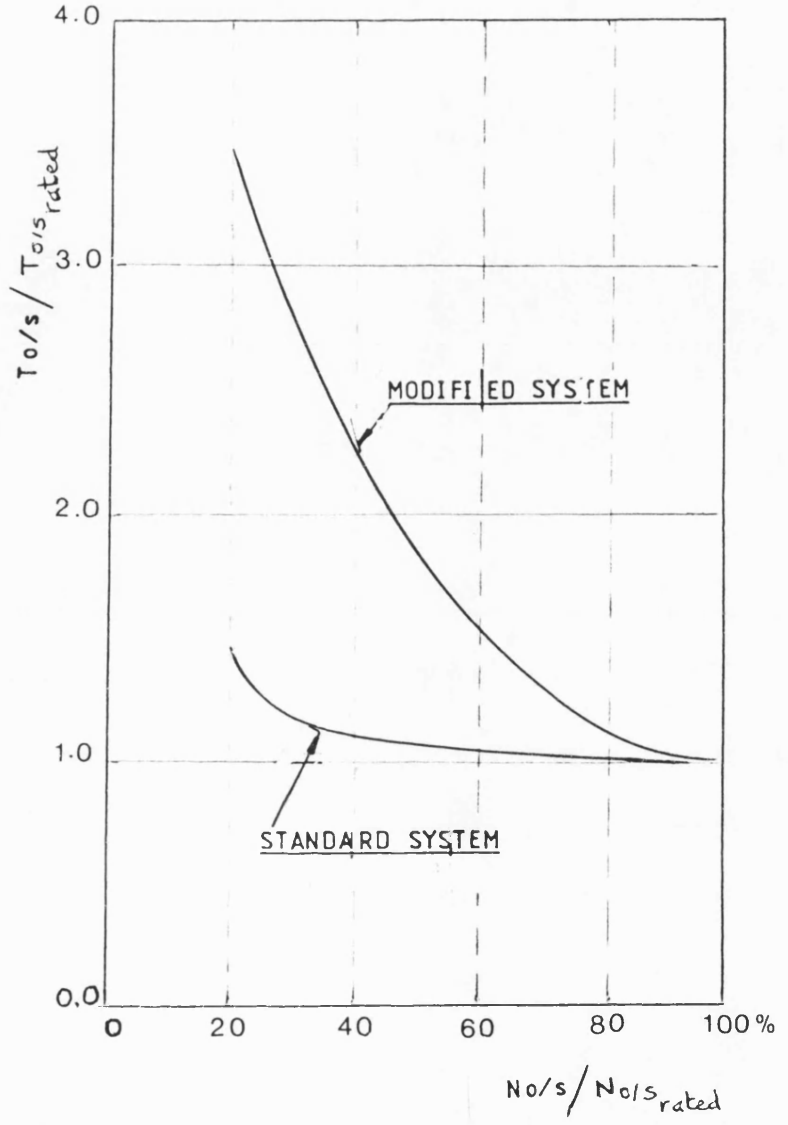

Fig. 5.6 Typical effect of a turbine CVT on torque contribution of turbine incorporated in the DCE

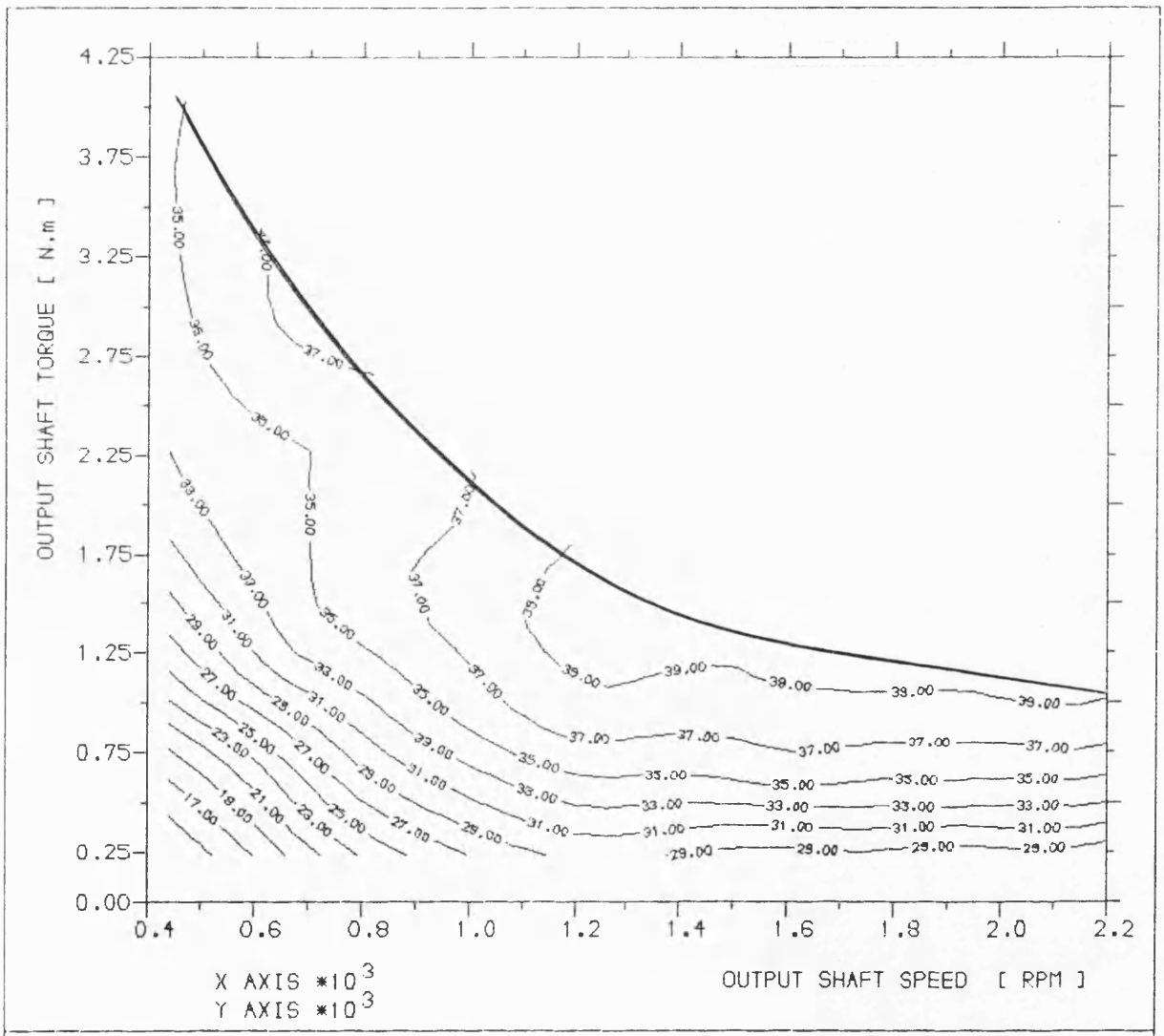

Fig. 5.7 Contours of the predicted output shaft efficiencies for the CUMMINS L10 DIFFERENTIAL COMPOUND ENGINE

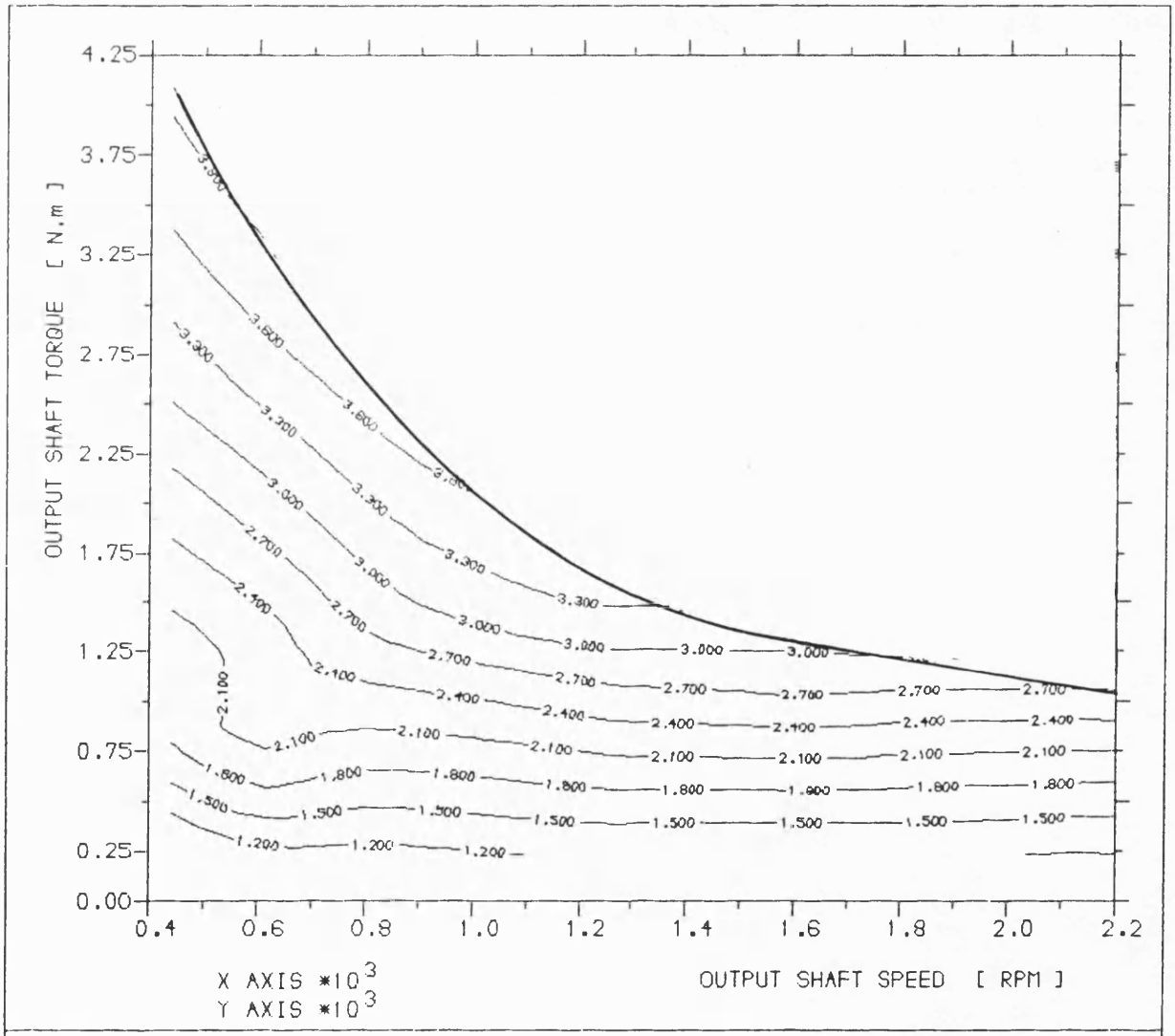

Fig. 5.8 Contours of the predicted boost pressure ratio for the CUMMINS L10 DIFFERENTIAL COMPOUND ENGINE

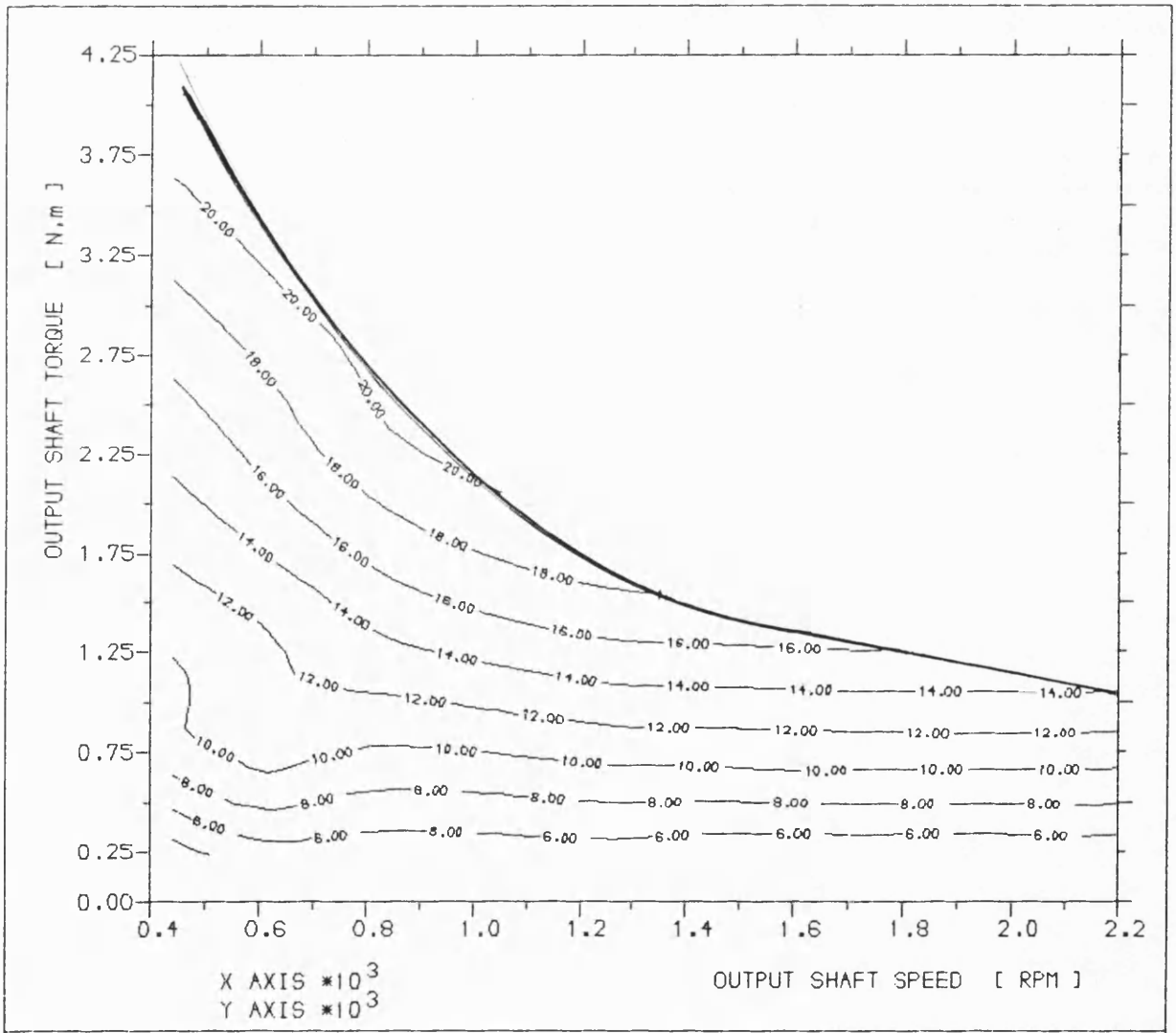

Fig. 5.9 Contours of the predicted brake mean effective pressure for the CUMMINS L10 DIFFERENTIAL COMPOUND ENGINE

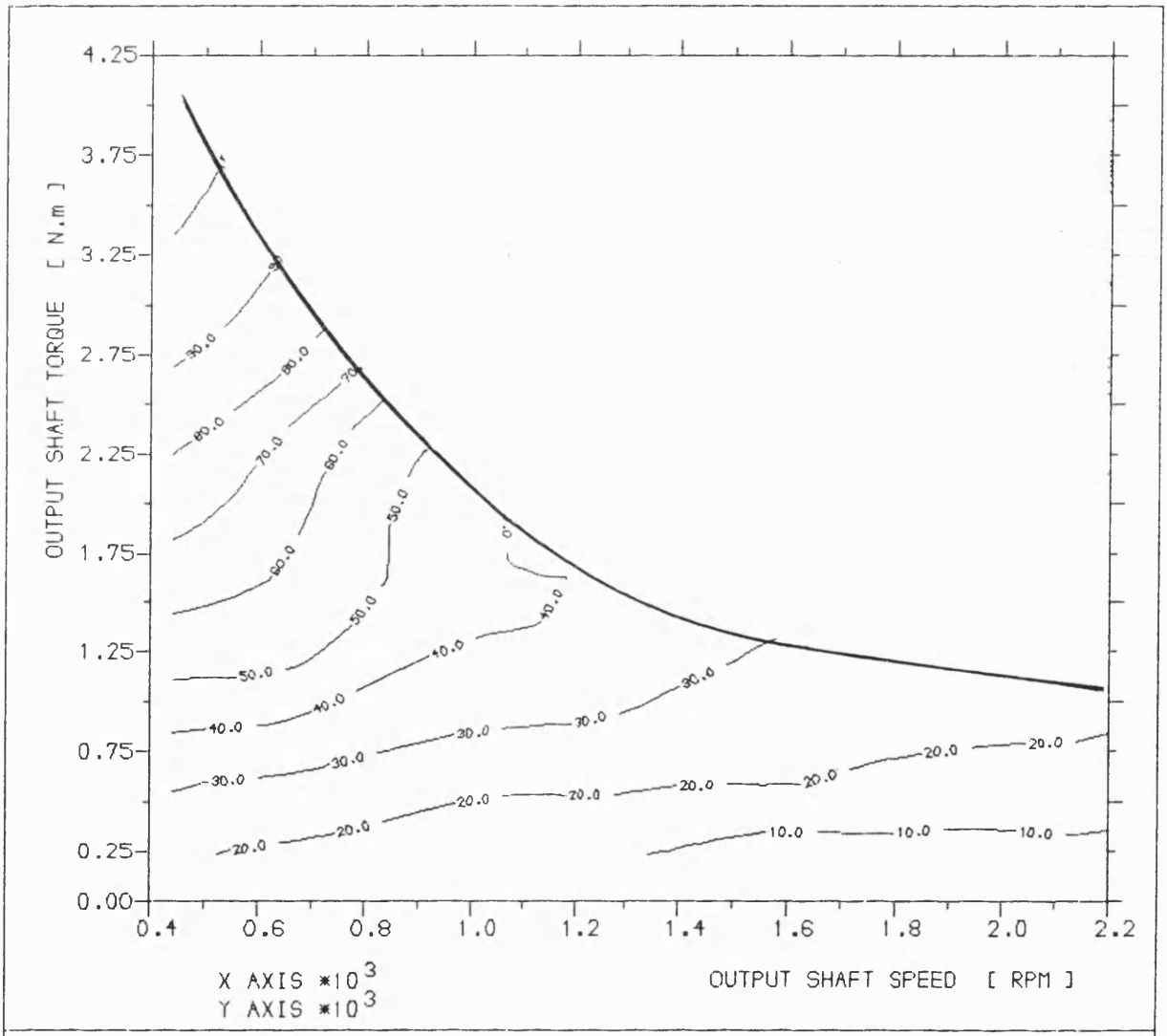

Fig. 5.10 Contours of the predicted turbine gear ratio for the CUMMINS L10 DIFFERENTIAL COMPOUND ENGINE

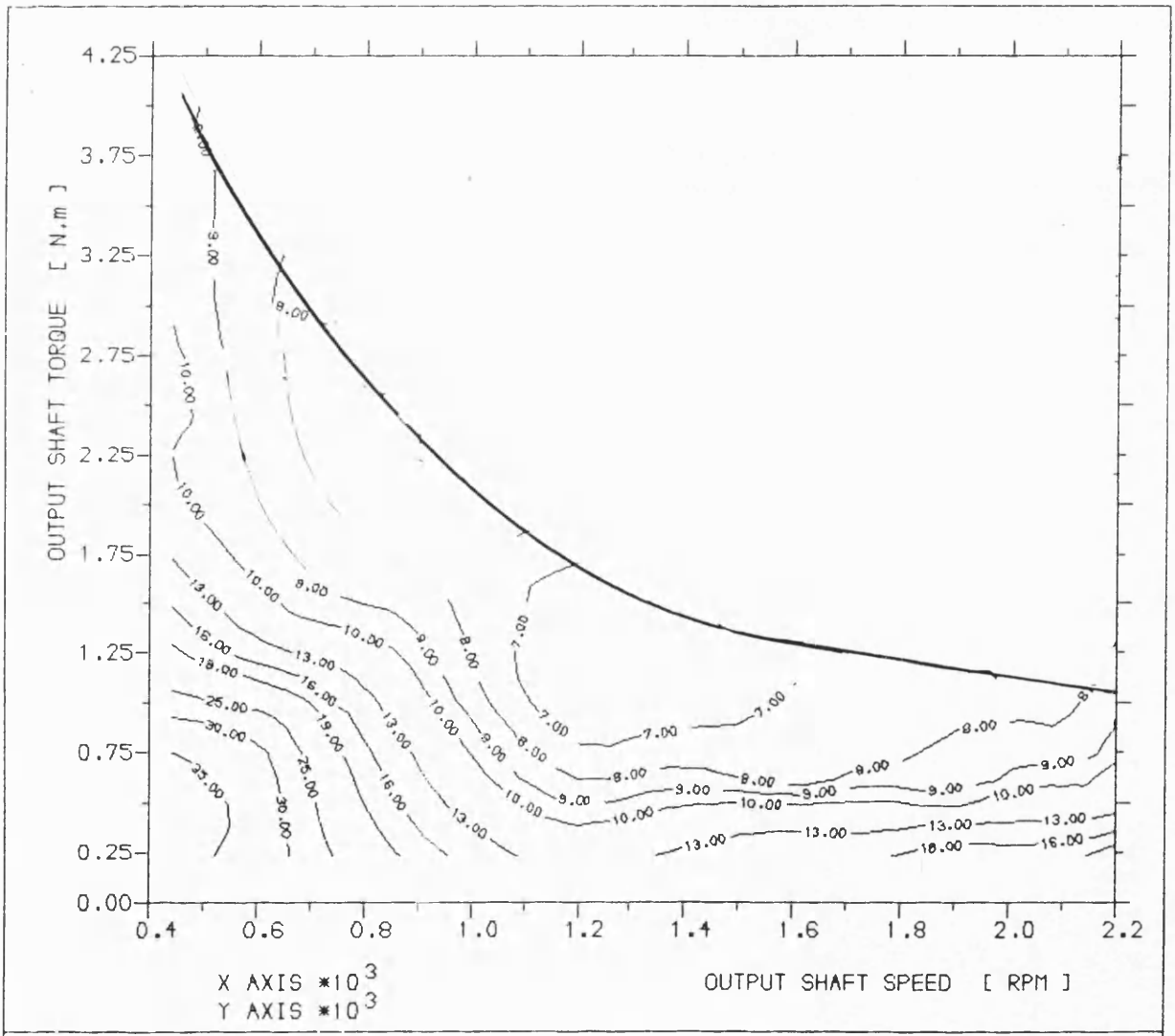

Fig. 5.11 Contours of the predicted turbine nozzle angle for the CUMMINS L10 DIFFERENTIAL COMPOUND ENGINE

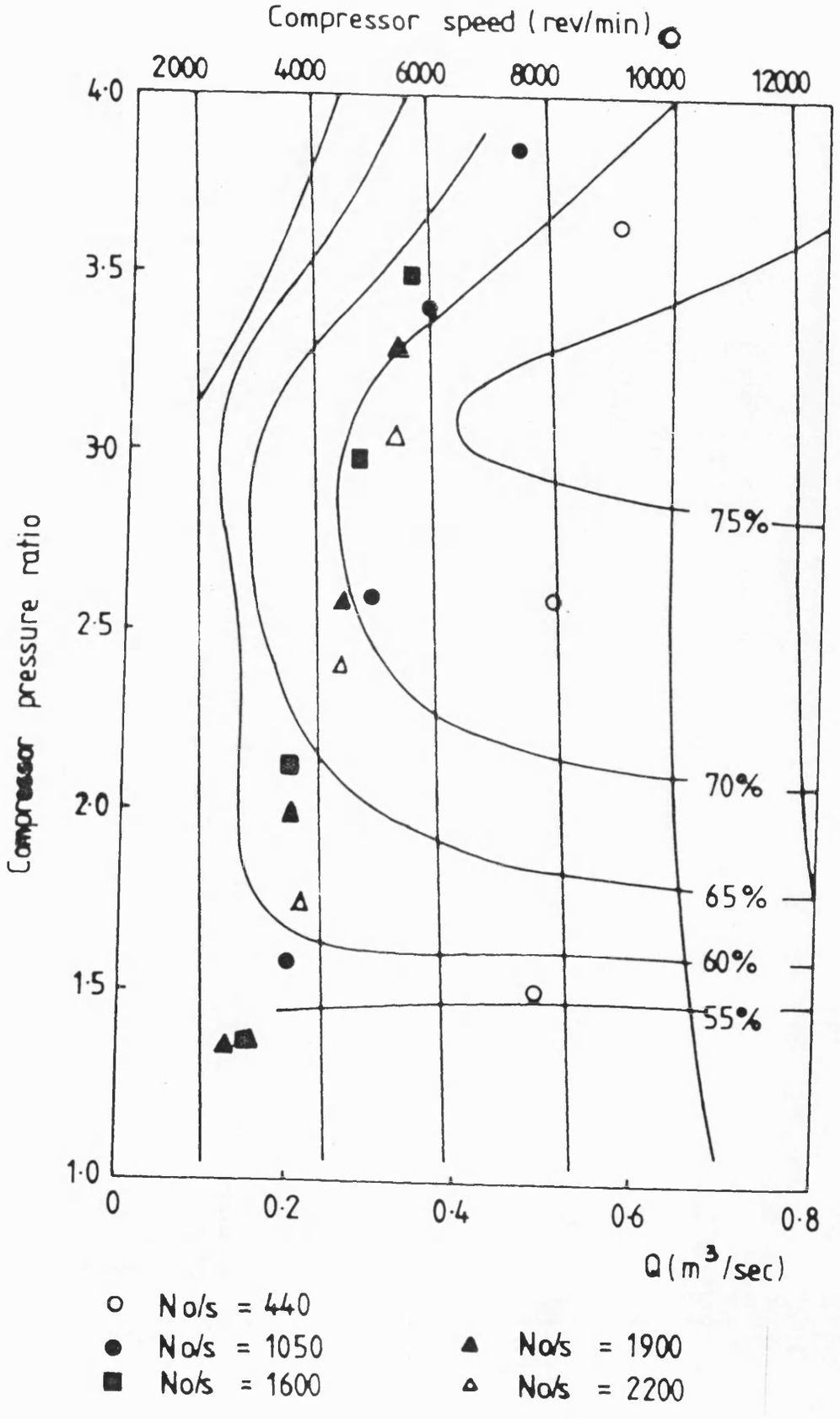

Fig. 5.12 Compressor characteristics of the L10-DCE with operating points of optimized running conditions

CHAPTER SIX

COMPREHENSIVE SIMULATION OF THE L10.DCE USING THE STEP-BY-STEP PROGRAM 'CSPDCE'

6.1 INTRODUCTION

Chapter 5 dealt with the simulation of the L10-DCE under steady state conditions using the simple program DCE2. Based on these results, an optimum control scheme is worked out and applied to the simulation of transient response of the unit described in Chapter 7 where the results are compared with those of its T/C engine counterpart.

In this chapter, the validity of the results of the simple steady state simulation are examined more closely by using the comprehensive step-by-step calculation program 'CSPDCE'. This program uses the same approach as the step-by-step program 'SPICE' used in Chapter 4, i.e. the filling and emptying method, (ref.), as well as essentially the same submodels. Hence the results of the fine tuning performed for the L10 engine with the program 'SPICE' in Chapter 4 can now be used for a more detailed simulation of the DCE.

'CSPDCE' being a dynamic program, has to be run from an assumed initial state, with fixed inputs of fuel flow rate and turbine nozzle angle to calculate a final steady state. Although these two variables could be input at the same values as those resulting from the simple simulation, because of unavoidable differences between the detailed and simplified calculation procedures, different engine powers and shaft speeds inevitably result from the more detailed procedure. Hence to validate the simple program predictions at any desired power and speed, it was required to modify the 'CSPDCE' program altering these two variables in an appropriate manner in the course of the simulation.

To achieve this goal, two alternatives were developed which are presented in this chapter, both involving some modification to the program 'CSPDCE'. 'CSPDCE' was eventually run for four operating conditions along the output shaft LTC of the L10-DCE.

6.2 INTERACTION AND CONTROL OF THE DCE PARAMETERS

It has been well established that there is a degree of flexibility in the DCE concept which makes possible a given output torque and speed combination with a range of conditions for the engine/compressor system. This, as seen in Chapter 5, calls for optimization and careful selection of the controlled parameters.

Amongst the various controlled parameters, the following could be regarded as the most important ones of interest in steady state operation:

1. Output speed and torque.
2. Engine speed and torque/or fuelling.
3. Turbine nozzle angle and C.V.T. ratio.

These parameters are highly interactive in the sense that as a result of the speed and torque relationships governing the fully floating epicyclic gearbox, a wide range of combinations of engine speeds and torques resulting in wide variations of the associated compressor and turbine operating conditions, will produce a given output shaft torque and speed.

The important first order interactions of the various parameters can be summarized as follows :

1. The combination of the engine and output shaft speed determines the compressor speed.
2. The compressor massflow is virtually proportional to the compressor speed, and together with a fixed turbine geometry determines the pressure levels in the system.
3. The compressor torque is virtually proportional to the compressor pressure ratio (boost).
4. Regardless of the epicyclic speeds, the torques acting on the annulus, planet carrier and sun-wheel are always in a fixed ratio to each other.

Hence, the epicyclic torques and boost pressure are related to each other and only one of them can be selected as a control variable. Similarly the

epicyclic speeds and the massflow cannot be controlled independently. These two groups of interactive parameters may be correlated via the turbine geometry which governs the pressure/massflow characteristic of the turbine.

The turbine geometry may be controlled by the nozzle angle, α_N, as described in Chapter 5 and 7, and, through the resultant pressure-mass flow characteristics links the two groups of parameters (i.e. torques/pressure and speeds/mass flow). Consequently, if engine speed and output speed are controlled, then α_N controls boost and hence torques. This in turn demands a matched amount of fuel per stroke. Alternatively, if engine speed and engine torque are controlled, than α_N controls mass flow and the other speeds. This is due to the fact that a demanded torque level corresponds to a certain pressure level. The torque contribution supplied by the turbine through its C.V.T. should also be taken into account.

The turbine C.V.T. ratio as well as some other variables such as fuel injection timing have only a second order effect on the speed-torque-pressure relationships of the system, but they do influence system efficiency.

Thus, it should be noted that not every combination of controls is feasible for the system. To be more exact, a combination of engine fuelling, shaft speeds and turbine geometry contains redundant elements and cannot be set up.

6.3 REVIEW OF DYNAMIC FEATURES OF THE PROGRAM 'CSPDCE'

As described in Section 6.1, the program 'CSPDCE' uses the filling-emptying method in which the engine cycle is divided into a very large number of very small steps. At every step, the flow behaves in the same manner as if the flow were steady. The basis of the model is to consider the multi cylinder engine as a series of thermodynamic control volumes linked by mass or energy transfer. These control volumes are : the inlet manifold, cylinders and exhaust manifolds connected by flow orifices to which the appropriate equations for the conservation of energy, mass and momentum are applied. In general the control volumes are treated as quasi-steady open thermodynamic systems at each time step.

The most basic thermodynamic process involved in filling-emptying consideration is that of mass transfer through the control volumes. In a system like the DCE, inflow to the inlet manifold and outflow from the exhaust manifold are governed respectively by the characteristics of the compressor and turbine which are located at two flow ends of the system. Since a fixed geometry turbine at a given speed acts in a flow sense, like a simple nozzle, any steady flow through the turbine calls for a certain pressure difference across it. Hence considering some fixed turbine back pressure, the exhaust manifold pressure upstream of the turbine will be determined. This in turn implies that in the steady state gas flow, the compressor air delivery together with turbine nozzle area determine the pressure levels throughout the system.

The program 'CSPDCE' in its original form works with fixed turbine nozzle angle, α_N, and fuel flow rate as input. Since the brake thermal efficiency does not undergo major variation, the latter input parameter determines the brake power being supplied by the engine. As long as α_N remains unchanged, regarding the interaction of the DCE parameters the feasibility of the following simulation conditions may be investigated.

1. If all the shaft speeds are fixed at desired levels, the engine torque will be calculated based on fuel flow rate, $\dot{m}_f$, while the

compressor torque is determined based on boost ratio, the latter being a direct result of the combination of compressor air delivery (speed), and α_N. This constitutes an incompatible condition in terms of torque imbalance and hence is not feasible. Fig. 6.1 shows the trend of such an approach.

2. Keeping the speed of only one of the three members of the epicyclic gearset constant, and allowing the others to float always results in speeds other than those intended. Fig. 6.2,a illustrates the case of fixed output shaft speed, $N_{O/S}$, by entering an almost infinite load inertia as input. The remaining speeds then find their own level and there is no correcting loop to deal with speed control.

However, after a few simulation cycles from some initial condition, a final equilibrium condition is found where the steady state speeds under fixed $\dot{m}_f$ and α_N are determined. Fig. 6.2,b shows the graphical representations of some simulation results of the L10 engine using the program 'CSPDCE' in its original form for three cases of a turbine mass scaling factor of 1.1, 0.85 and 0.65 at constant fuelling and output speed. These factors were applied (input) to perform the same duty as different nozzle angles do, although the subsequent corrections needed for the turbine efficiency map were ignored.

Starting from their initial values, the engine speed, boost pressure ratio and bypass mass flow reach their final equilibrium values. Out of balance power is evaluated based on the assumption of a frictionless gearing system. Fig. 6.2,b shows that only when its value is zero, has an equilibrium condition been reached. The power imbalance is the cause of speed variations of both engine and compressor (output shaft speed is kept constant) and is due to the inconsistent torques of the epicyclic gearing members. Equation 5.5 is always retained as the speed correlation whereas the net torques applied on shafts determine the shaft accelerations.

The cause of torque imbalance is, in turn, due to inconsistent initial

input values of engine speed and boost pressure. Considering fig. 6.2,b the following features of the program CSPDCE are apparent.

1. Decreasing the turbine scale factor plays the same role as closing down the turbine nozzles.

2. At constant output shaft speed and engine fuelling, the boost pressure increases when closing down the turbine nozzles in spite of simultaneous decrease in compressor speed and hence air flow.

3. Increase in the boost pressure demands higher compressor torque which in turn calls for higher engine torque, and slows down engine speed.

4. Decrease in bypass mass flow (eventually leading to reverse flow) with progressive decrease in turbine nozzle area results in a turbine plenum pressure greater than that of the compressor plenum. The plenum pressures are governed by mass and energy flow equations.

6.4 MODIFICATIONS APPLIED TO THE PROGRAM 'CSPDCE' TO SIMULATE STEADY STATE CONDITION AT DESIRED SPEEDS

In a detailed review of the comments of the original program documentation, it was found that the integrating calculation for the mean engine air flow was incorrect. The value of this parameter was to be calculated based on integration over the total number of steps in a cycle, as for the compressor, bypass and turbine mass flow. In order to provide consistent values in the 'PRINT OUT' in this respect, the wrong result of integration for the mean engine air flow had to be substituted by a value obtained from the following equation at the end of cycle calculations.

```
emf1 = cmass - bmf                                    [6.1]
emf  = emf1
```

where 'emf(1)', 'cmass' and 'bmf' are the mean mass flow rate for engine, compressor and bypass. It should be noted that any substitution as above would not be needed if 'emf' had already been calculated correctly. The problem put a question mark against the validity of every flow dependent engine parameter (which covers all aspects of the engine performance characteristics).

This problem was found to be due to two missing statements in the integration process of 'emf' and was eventually solved. In a later attempt to solve the problem of running the program to simulate the DCE unit for steady state conditions at given shaft speeds and fuelling, two types of solution were worked out.

In both solutions, the turbine swallowing capacity was changed to provide the system with balanced pressure levels so as to make the boost pressure ratio compatible with the torque balance required in the epicyclic gearset.

6.4.1 Control Strategy with Dynamic Shaft System (First Solution) [Fig. 6.3]

In the first solution the dynamic feature of the program with respect to the shaft system was retained. However, the output shaft speed was kept constant by a very high load inertia whereas the rest of the shaft inertias were reduced to about one-tenth of their real values to speed up the attainment of equilibrium conditions while providing sufficient damping effect.

As shown in fig. 6.3, the sequence of calculations is the same as for the original calculation flow diagram (fig. 6.2,a) but with an extra loop which examines the engine speed for any further adjustment of the turbine mass scale factor, 'tmsf'. This control is performed at the end of every cycle calculation after mean values of the variables have been determined by comparing the mean engine speed in any cycle with that in the one before. This ensures that 'tmsf' is adjusted only after an interim equilibrium condition has been reached.

It should be noted that the loop which changes the nozzle angle is a control loop since a true balance between epicyclic torques at each stage is retained at all times.

Although the engine fuelling is an input, it can optionally be adjusted to keep the engine brake power constant. The control statement in the program is as follows :

$$ffrate = ffrate.\ \{1 + 0.8\ (bhp1-bhp)/bhp1\} \qquad [6.2]$$

where

ffrate = fuel flow rate
bhp1 = intended engine brake power
bhp = updated engine brake power

This control was intended to be used independently of other controls.

6.4.2 Control Strategy with Fixed Speeds (Second Solution)

[Fig. 6.4]

In the second approach, all shaft speeds are kept constant at their input values. Hence no shaft dynamics are taken into consideration. Making the engine brake power constant, the combination sets up the intended steady-state operation by finding a compatible value of the turbine nozzle angle, α_N.

In spite of the use of constant speeds, the program is run fully dynamically in terms of variations of pressures, temperatures and trapped masses in each of the control volumes. Consequently, the torques of compressor and turbine undergo variations governed by the gas conditions in the relevant plenums, resulting in the same torque incompatibility in the epicyclic gearset as discussed earlier in Section 6.3, unless α_N is adjusted.

Thus it should be remembered that use of Lysholm compressor at constant speed provides the system with an almost constant air flow rate which together with a fixed nozzle area of the turbine determines the pressure level of the system.

To solve the problem of torque incompatability, the compressor torque is altered by changing α_N and hence boost pressure so as to reach the balance demanded by the engine torque which has been fixed from the beginning by the combination of constant engine speed and fuel flow rate.

Fig. 6.4 shows the calculation flow diagram based on this alternative. Based on any value of α_N and constant compressor speed, the mean value of boost pressure is calculated in the course of the cycle simulation. This value is compared with a reference boost pressure based on that demanded by the epicyclic gear torque balance. As a result of the comparison the value of α_N is adjusted until agreement between the two values of boost pressure is reached. As in the first solution, this comparison is

performed at the end of a complete cycle calculation using mean values of boost pressure.

It is worth noting that, in this second solution, the loop which changes the turbine nozzle angle is a correcting rather than a control loop. Also, whenever turbine nozzle angle is changed a new set of turbine maps based on application of the analytical turbine subroutine, TURBW, (see Chapter 2) is generated at the beginning of each calculation. The turbine maps are set up as two 2-dimensional arrays of efficiency and N.D. mass flow, each versus expansion ratio and N.D. speed. Therefore, unlike the case when the turbine mass scale factor, tmsf, is used, the true turbine maps are used. To have the turbine map modified repeatedly it was necessary to move the relevant statements into the main loop of the cycle calculations.

For further improvement of the program, some data files generating graphical turbine and compressor maps were created. This made possible the examination of the accuracy of compressor and turbine data supplied to the program. The extra statements required to generate graphical turbine maps are included in the program. To generate graphical compressor maps a subroutine called COMPMAP was written. The maps are generated in response to a value of 1 for the map producing control code, itcmap, in input data.

In checking the compressor maps based on the original compressor arrays (for the Leyland 520-DCE), it was found that more accurate data had to be prepared. Also, in examining the turbine map generated by the analytical turbine subroutine, TURBW4, it was found that some modification of the generated map of mass flow in the choke region was required. The problem was due to having constant mass flow with increasing turbine expansion ratio, which led to numerical iteration problems. Hence some further modification providing a gentle inclination away from constant mass flow in the choke region on the turbine map was applied. Furthermore, in order to handle nozzle angles of less than 8 deg. the turbine subroutine TURBW4 was replaced by TURBW, the subroutine which was being used by the rapid matching program.

6.5 APPLICATION OF SHAFT DYNAMICS TOGETHER WITH TURBINE SCALING CONTROL LOOP

(First solution method - see Section 6.4.1)

The simulation based on consideration of shaft dynamics was carried out for the L10-DCE, synthesizing the design point (table 5.4) with respect to the results presented in Chapter 5. Starting from initial conditions, mean values of all performance parameters vary from cycle to cycle until steady state operation is achieved. Figs. 6.5 and 6.6 give a graphical summary of mean values of some of the important parameters covering :

Fig. 6.5,a - turbine mass scale factor
engine speed
engine torque
engine power
output shaft power
gear friction loss

Fig. 6.5,b - superimposed pressure ratios of compressor and turbine
engine air flow
bypass flow
turbine gas flow
turbine inlet temperature

After ten simulation cycles, all the parameters have converged on an equilibrium condition. However, the engine speed is far from its intended value (2184 c.f 2100 rpm).

The turbine scale factor, tmsf, was altered by application of a control statement in the program as follows :

$$tmsf = tmsf.\ \{1 + xtmf.\ (es1-esm)/es1\} \qquad [6.3]$$

where : xtmf = control factor
es1 = intended mean engine speed (rpm)
esm = updated mean engine speed (rpm)

The value of tmsf in the right hand side of equation 6.3 represents its last value at the end of any cycle which is altered to the extent governed by the control factor, xtmf, and the ratio of engine speeds, i.e. esl and esm. xtmf is an input and selected notionally. As shown in fig. 6.5,a tmsf is varied in progressively smaller steps as the engine speed approaches its intended level. This type of control was applied to avoid any speed overshooting.

The fuel delivery was also adjusted at the same time as the turbine scale factor so as to yield a constant engine brake power. Considering fig. 6.5,a the turbine scale factor is changed only when a new steady state engine speed away from its intended value is reached. With xtmf = 0.5, the desired operating condition is achieved after five steps of turbine scale factor adjustments after passing through four true but unwanted steady state conditions.

Considering fig. 6.5,b the decrease in turbine scale factor causes an increase in the system pressure level. Although the inlet manifold temperature does not change noticeably from one cycle to another (not shown), due to the decreasing trend of engine speed the engine air flow does not increase proportionally with increase in boost pressure. The pressures in the compressor and turbine plenum change in such a way as to cause a decrease in the bypass flow. Therefore, the increase in engine air flow and the simultaneous decrease in bypass flow lead to the observed increase in the turbine inlet temperature (fig. 6.5,b).

Since the output shaft speed is constant, the same trend of decreasing engine speed is followed by the compressor speed (not shown) and hence also air flow. The decreasing trend of compressor air flow can be seen in Fig. 6.5,b in terms of turbine gas flow, as the fuel flow rate remains almost constant. In spite of the increase in the turbine plenum pressure, the decrease in turbine flow is consistent with the decrease in the relevant scale factor.

It should be remembered that in order to accelerate convergence with modified turbine scale factors, all the shaft inertias (except the virtually infinite output shaft inertia) were taken to be one tenth of

their real values. However, with xtmf = 0.5 (see equation 6.3), it took 33 simulation cycles to arrive at the desired operating condition.

Tables 6.1 and 6.2 respectively summarize the results of the tenth and finl cycles, the former being at tmsf = 1.0, and the latter at tmsf = 0.75. The major changes resulting from closing down the turbine nozzle angle can be summarized as follows:

1. The boost pressure ratio increased from 2.5 to 2.7 causing an increase in maximum cylinder pressure from 161 to 170 bar.

2. The brake thermal efficiency improved from 40.8% to 41.4%.

3. The engine air flow increased from 0.412 to 0.43 kg/s.

4. The trapped air-fuel ratio decreased from 29.9 to 28.8 whereas the overall air-fuel ratio increased from 30.2 to 32.0.

5. The compressor air flow decreased from 0.494 to 0.407 kg/s due to a decrease in its speed from 6413 to 5514 rpm.

6. The compressor power absorption decreased from 67.5 to 60.7 kW.

7. The turbine power decreased from 71 to 66.4 kW, despite an increase in inlet temperature from 736 to 752K and an increase in expansion ratio from 2.76 to 2.97. The consistency of these variations is bound up with the decrease in turbine flow from 0.505 to 0.419 kg/s.

8. The output shaft efficiency improved from 39.3 to 40.4%.

Figs. 6.6,a to 6.6,f give a graphical summary of all important cyclically varying parameters covering :

Fig. 6.6,a : in-cylinder gas pressure
in-cylinder gas temperature
in-cylinder trapped mass
in-cylinder equivalence ratio

Fig. 6.6,b : valve areas
cylinder volume
cylinder heat transfer coefficient
apparent rate of burning fuel

Fig. 6.6,c : compressor plenum pressure and temperature
turbine plenum pressure and temperature

Fig. 6.6,d : bypass mass flow

Fig. 6.6,e : engine speed and torque
compressor speed and torque

Fig. 6.6,f : compressor and turbine mass flow
equivalence ratio in compressor and turbine plenum

As indicated in the introduction of this chapter the same models of heat release, heat transfer and friction as set out in Chapter 4 for the L10 engine in its turbocharged form were applied to simulate the engine in its DCE configuration. Since the program is of the degree-by-degree type the results are expected to be highly reliable.

Considering fig. 6.6,a, the cylinder pressure variation follows a very smooth curve, in line with the high boost ratio of 2.69:1. Maximum cylinder pressure is 170 bar which is rather high. This is because of increased fuelling to uprate the engine.

Fig. 6.6,c shows that pressure and temperature in the compressor and turbine plenums oscillate within narrow ranges. These are due to the rather large plenum volumes of 10ℓ. The pressure difference between these two plenums at any calculation step determines the bypass flow.

Fig. 6.6,d shows that the bypass flow oscillates between a negative value of -0.085 and a positive value of 0.138 kg/s resulting in a mean value of -0.014 kg/s over a complete cycle (+ve sign shows flow direction from compressor plenum to exhaust plenum).

Considering Fig. 6.6,e the large speed oscillations of both engine and compressor (in phase and in a fixed ratio to each other) arise because of the artificially reduced input values of shaft system inertias. The compressor speed oscillates between 4700 and 6100 rpm while the engine speed oscillates between 2020 and 2160 rpm. This was considered to yield doubtful results for other speed dependent variables, in particular the gas flows as the most important one. As is shown in Fig. 6.6,f the compressor air delivery oscillates cyclically between 0.35 to 0.45 kg/s which sets up an oscillation amplitude of 25% of the mean compressor air flow.

These oscillations are all far from reality and cast doubt on the result of the results. This called for further development of the program which was intorudced as the second solution method in Section 6.4.2.

6.6 APPLICATION OF CONSTANT SHAFT SPEEDS TOGETHER WITH TURBINE NOZZLE ANGLE CORRECTING LOOP

(Second solution method - see Section 6.4.2)

To simulate a steady state condition at absolutely constant shaft speeds, shaft dynamics have to be eliminated. In view of the fact that the engine power is also required to be under control, the engine torque and consequently other epicyclic gearset torques will be pre-determined. These conditions call for a certain level of boost because of the Lysholm compressor characteristics. On the other hand, pressure level in the system is determined by the compressor air mass flow and the turbine swallowing characteristic. In order to match the boost requirement and pressure level in the system there remains no way but correction of the turbine nozzle angle from its initial (guessed) input value.

First the same design point as before was simulated under this stragegy. Since the results proved to be satisfactory, three other running conditions along the output LTC including stall condition were examined. Again, starting from initial conditions, mean values of all performance parameters except speeds vary from cycle to cycle with any new turbine nozzle angle, until a steady state condition is established. Such conditions would soon be achieved particularly if the manifold volumes could be considered smaller.

The turbine nozzle angle ('a' as denoted in the program) underwent correction by a statement in the program as follows :

$$a = a.\ \{1 - k.xang.(rc1-rcm)/rc1\} \qquad [6.4]$$

where the notations are the same as used in the program :

- a = turbine nozzle angle (deg)
- xang = correction factor
- rc1 = boost pressure ratio demanded by epicyclic torque balance
- rcm = updated mean boost pressure ratio
- k = correction speeding up factor

In this case, 'xang' acts in the same way as 'xtmf' in the previous case and is a notionl input. It is usually set at values of less than 1.0, but higher values can speed-up the required corrections. For this purpose, k is set to 2.0 in the program; however, it is reduced to 1.0 when the intended condition is passed by.

A. Design Point

Table 6.3 contains a summary of results for the overall performance parameters for engine, compressor and output shaft at the design point. Engine output [240 kW at 2100 rpm, BMEP = 13.7 bar] has been matched exactly to that of table 5.4, based on the simple matching program. In general these two sets of results are in good agreement, the main difference being the lower in-cylinder and exhaust temperature levels, resulting inevitably in a lower turbine temperature (772 k cf. 885 k) which in turn leads to a lower turbine power (68.36 kW cf. 74.96 kW).

However, final output shaft power and efficiency are in good agreement (236.4 kW cf. 235.6 kW, 39.55% cf. 39.07%). Additional information not provided by the simple program includes component heat losses and temperatures. In spite of the relatively high rating of 13.7 bar BMEP, the high trapped air-fuel ratio of 28.7:1 ensures that metal temperatures remain modest :

mean piston crow temperature	:	249 C
mean cylinder head temperature	:	202 C
mean liner temperature	:	139 C

Figs. 6.7,a to 6.7,h give a comprehensive graphical summary of all cyclically varying parameters.

Fig. 6.7,a gives the trend of cylinder pressure, rate of burning and cylinder temperature. The rate of burning is a smooth curve, in line with the semi-quiescent combustion model of the L10 engine. Maximum cylinder pressure and temperature are 141.5 bar and 1665 k respectively. These are lower in comparison with those resulting from the first solution method [170 bar and 1750 k shown in Fig. 6.6,a], due to retard in ignition point from 18.5 deg. to 13.5 deg. BTDC (tables 6.2 and 6.3). The relatively high air-fuel ratio of 28.7:1 and rather long burning period of 66.5 deg.

result in a lower peak temperature.

Fig. 6.7,b shows the variations of valve areas, in-cylinder mass, equivalence ratio and heat transfer coefficient, and fig. 6.7,c gives cyclic pressure and temperature versus cylinder volume (i.e. p-V and T-V diagrams). These trends show realistic variations of performance parameters during a cycle.

Fig. 6.7,d shows the trends of engine air flow, ratio of plenum pressures (i.e. compressor to exhaust), and bypass flow. Engine airflow from the inlet manifold is highly cyclical, as expected, fluctuating between 0.32 and 0.48 kg/s. The pressure ratio across the system, i.e. compressor plenum/exhaust plenum, on the other hand, shows only a very small variation between 0.999 and 1.002, due to the fact that the volumes are large and the bypass is wide open, with an area of 30 Cm^2. However, the bypass flow variation is nevertheless quite large, with a swing from -0.08 to +0.16 kg/s (+ve from compressor to exhaust plenum). This proved to be in reasonable agreement with the cyclic variation of bypass flow from -0.085 to 0.138 kg/s (fig. 6.6,d) as experienced with the other control strategy.

Fig. 6.7,e gives the compressor and turbine plenum pressure fluctuations. In view of the wide open bypass, these are substantially in phase and of almost identical amplitude. These also were found to be in line with what was experienced before as shown in fig. 6.6,c.

Considering fig. 6.7,f, the compressor and turbine plenum temperature fluctuations have amplitudes of approdimately ±1.5 and ±1.8 deg.C respectively, i.e. relatively insignificant, again in view of the large plenum volumes and in agreement with fig. 6.6,c.

Three sets of torque fluctuations including compressor, engine and turbine are shown in fig. 6.7,g and have amplitudes of approximately ±2.1 Nm, ±2250 Nm and ±0.5 Nm respectively. The first and last values are related to the much higher rotational speeds and lower power levels handled respectively by the compressor and turbine.

Finally, the compressor air flow and turbine g as flow variation within a cycle are illustrated in fig. 6.7,h. As is expected, due to the cyclic pressure pulsations in the compressor plenum (fig. 6.7,e), the compressor air flow alters cyclicly but within a narrow range of ±0.005 kg/s. This is because the compressor speed is constant while the pressure pulsations in its plenum are confined to a small amplitude of ±0.017 bar. In other words, comparing figs. 6.6,f and 6.7,h the intention (described at the end of section 6.5) of an expected realistic compressor flow was achieved.

The turbine flow pulsates within a wider range partly because of intermittent action of the cylinder exhaust gases carrying the additional mass of injected fuel. The amplitude of pulsation is ±0.013 kg/s.

Comparing the results given in tables 6.3 and 6.2 for mean values of performance parameters, and also all of the cyclically varying parameters except for engine speed, compressor speed and air flow, the results of first solution method based on the shaft dynamics and use of a turbine scaling control loop are justified by this second solution method in which the shaft speeds are kept constant.

B. Stall Point

Table 6.4 summarises the overall performance of the L10-DCE at the stall point. This point refers to the maximum torque condition with an output shaft speed of 440 rpm, giving an output shaft torque of 4047 Nm according to the simplified matching analysis of Chapter 5 (table 5.2).

Engine output [241.8 kW at 1350 rpm, BMEP = 21.46 bar] has again been matched exactly to that of table 5.2. The turbine inlet temperatures are now in much better agreement than at the design point due to the much higher bypass flow (667 k cf. 683 k) so that turbine powers also agree more closely (150 kW cf. 144 kW), the difference being due to the marginally higher pressure ratio across the turbine (4.20 cf. 4.12) in the case of the new calculations. Final output shaft power and efficiency are again in fair agreement (203 kW cf. 187 kW, 34.64% cf. 34.61%). In the case of output shaft efficiency the lower estimated engine efficiency (41.3% cf. 44.85%) is largely offset by the higher turbine output.

With respect to operating temperatures of the main components, the higher engine rating compared with the design point [BMEP = 21.46 bar cf. 13.70 bar] is offset by lower engine speed and higher air-fuel ratio (32.66 cf. 28.7). Consequently the operating temperatures are very similar to those at rated conditions:

mean piston crown temperature : 257 C cf. 249 C
mean cylinder head temperature : 186 C cf. 202 C
mean liner temperature : 139 C cf. 139 C

Figs. 6.8,a to 6.8,g again give a graphical summary of all cyclically varying parameters, as for the rated condition, i.e. figs. 6.7,a to 6.7,g.

Considering fig. 6.8,a the maximum cylinder pressure is high at 195 bar, but would be reduced by still further retarded injection [current ignition point is 13.5 deg. BTDC which is already retarded]. T_{max} is low at 1488 k largely as a result of the generous trapped air-fuel ratio (32.7:1).

Figs. 6.8,b and 6.8,c again show realistic in-cycle variations of performance parameters. The cyclic variation of cylinder pressure and temperature (p-V and T-V diagrams) show very smooth curves and a virtual absence of pumping loop in view of wide open bypass.

Comparing fig. 6.8,d with 6.7,d the pulsations of engine and bypass airflow are considerably larger than for the design point. The engine air flow at stall point fluctuates between 0.32 and 0.55 kg/s whereas the fluctuation at the design point is between 0.32 and 0.48 kg/s. The pressure ratio across the system fluctuates between slightly wider limits than before [0.998 and 1.012 compared with 0.999 and 1.002] due to the larger cyclic fluctuations associated with higher boost [3.96:1 cf. 2.62:1] and lower engine speed [1350 rpm cf. 2100 rpm]. Similarly the bypass flow variation between 0.24 $\frac{kg}{s}$ and 0.54 kg/s is substantially higher than before [-0.08 kg/s and +0.16 kg/s] and shows no reverse flow due to the large net flow through the bypass under stall conditions

[0.372 kg/s cf. 0.01 kg/s].

The top and bottom diagrams in Fig. 6.8,e give the compressor and turbine plenum pressure fluctuations, which are now considerably larger than before [±0.1 bar cf. ±0.015 bar] for the reasons stated above. However, the wide open bypass together with large volumes still maintain pulsations at a relatively low level.

Considering fig. 6.8,f the compressor and turbine plenum temperature fluctuations are again larger than at the design point, at ±1.6C and ±4.75C (cf. ±1.5C and 1.8C).

The 3 sets of torque fluctuations of compressor, engine and turbine shown in Fig. 6.8,g have amplitudes of approximately ±2.25 Nm, ±3600 Nm and ±6 Nm [cf. ±2.1, ±2250 Nm and ±0.5 Nm].

C. Intermediate Results on the Limiting Torque Curve

For completeness 2 other sets of results are presented in the same format as for the design and stall conditions, for output shaft speeds of 1050 and 1600 rpm (table 5.3 of Chapter 5 may be used for comparison).

The tabular and graphical representations [table 6.5 and figs. 6.9,a to 6.9,g for $N_{o/s}$ = 1050 rpm, table 6.6 and figs. 6.10,a to 6.10,g for $N_{o/s}$ = 1600 rpm] follow exactly the same pattern and do not call for detailed comment. Again there is good agreement between the predictions of the present work and that of Chapter 5.

D. Compressor Maps

Figs. 6.11,a to 6.11,c show the compressor maps in the form of contours of efficiency, torque and power based on the application of a mass scale factor of 1.1 as worked out in Chapter 5 to match the original compressor map to the L10-DCE flow requirements. The abscissa and ordinate of these maps are air mass flow and pressure ratio respectively. It should be noted that the map outside the pressure ratio of 4.0 and speed of 12000 rpm is based on extrapolation.

Although the torque contours (fig. 6.11,b) are governed by a constant step (27.7 Nm), the spacing between the torque traces is not regular. This is because of the dependence on the irregular efficiency distribution over the map. A typical trace of constant power is superimposed on the torque map. Also superimposed on these maps are the four operating points of the L10-DCE simulated by the program 'CSPDCE'.

6.7 SUGGESTIONS FOR FURTHER MODIFICATIONS TO THE PROGRAM 'CSPDCE'

1) In calculations of exhaust gas energy an integration method based on incremental gas leaving the engine at varying conditions (of pressure and temperature) during the exhaust stroke is used in the program. However, the results of this integration are not reasonable which is an indication of some problems in the calculation process. The effect of this is confined to itself and does not affect the calculation of any other parameter. On the other hand, taking into account mean values of exhaust temperature and mass flow yields the energy of exhaust gases in conformity with the system energy balance requirement.

Therefore, a modification of the program in this respect is desirable although not vitally important. The problem is guessed to be due to either integration statements or gas property calculations (c_p and c_v), and needs to be examined carefully.

2) In the subroutine modelling the epicyclic gearset, although different friction torques affecting individual gears and shafts are taken into consideration and the friction power loss can be calculated independently of other variables, the difference between mean powers of active and passive components in the system is calculated at the end of each cycle and is regarded as the transmission power loss. The result is valid but only when no shaft acceleration is involved.

Therefore, in the assessment of power utilization in transient conditions, it is vitally important to have a clear picture in this respect, otherwise, the value of gear losses in the print out would be totally misleading. At this stage it is worth referring to fig. 6.2,b where the results appearing as gear losses in the print out were indeed the out of balance power or the power absorbed by shaft inertias in shaft accelerations, since no friction had been assumed in the gearing system at that stage, whereas it appears as gear losses in the print out.

6.8 CONCLUSION

The extensive series of runs undertaken with the detailed program CSPDCE has demonstrated that earlier performance predictions based on the rapid matching (simple) program 'DCE2' are substantially reliable. However, the ability to model cyclic fluctuations of pressures, and temperatures in the various control volumes as well as of the torque of engine, compressor and turbine, and to predict operating temperature levels of piston, head and liner greatly enhances the value of this more detailed simulation.

1

CYCLE SIMULATING PROGRAM

---

cycle10
engine specification:
CUMMINS L10 DCE
number of cylinder 6 cylinder bore (mm) 125.0 piston stroke (mm) 136.0 connecting rod length (mm) 217.8
compression ratio 16.30 firing order 153624 engine displacement (lits) 10.01
exhaust valve open 135. inlet valve open 341. exhaust valve close 363. inlet valve close 553.
thermal resistance:(deg c/kw):r1,r2,r4,r5,r7,r8,r9,r10= 4.1 1.5 34.5 2.7 43.4 21.3 15.0 15.8

---

engine performance:			heat loss analysis:	
engine speed (rev/min)	2194.		energy input (kj)	5.376
boost pressure ratio	2.51		% liner heat loss	7.54
b.m.e.p (kn/m2)	1316.		% piston heat loss	7.49
b.h.p (kw)	240.91		% head heat loss	4.40
b.s.f.c (kg/kw.h)	.2042		% friction loss	6.03
b.s.a.c (kg/kw.h)	6.16		% output shaft energy	40.85
engine air flow (kg/s)	0.4121		% exh max energy	43.33
brake thermal efficiency	0.408		liner temp. (deg k)	422.2
air fuel ratio (trapped)	29.89		piston temp. (deg k)	582.8
air fuel ratio (overall)	30.16		head temp. (deg k)	483.2
volumetric efficiecy	0.866		gas mean h.t.c (w/m2.k)	612.
mechanical efficiency	0.871		gas mean temp. (deg k)	1157.
engine torque (nm)	1051.2		piston max temp (deg k)	
max. cyl. pressure (kn/m2)	16140.			
max. cyl. temperature (deg k)	1802.			
exh. man. pressure (kn/m2)	276.	0.		
exh. man. temperature (deg k)	736.	0.		
inlet man. pressure (kn/m2)	249.			
inlet man. temp. (deg k)	319.			
compressor performance:			combustion parameters:	
compressor speed (rev/min)	6413.		static injection (degree)	
pressure ratio	2.79		dynamic injection (degree)	
torque (nm)	100.50		ignition delay (ms)	
power (kw)	67.54		ignition point (degree)	-18.5
efficiency	0.739		end of burning (degree)	45.0
mass flow (kg/s)	0.494		heat release shape factor:	
turbine performance:			cw1	0.000
turbine speed (rev/min)	49500.		cw2	0.
pressure ratio	2.76		cw3	1.40
torque (nm)	13.71		cw4	7.000
power (kw)	71.06		mode of burning	0.000
efficiency	0.727	0.000	mass of fuel/cyl/cyc (g)	0.12458
mass flow (kg/s)	0.505	0.000	mean temp during delay (degk)	802.
			mean press dur delay (kn/m2)	5369.

---

gear ratio : epicyclic= 3.074 compressor= 3.107 output shaft= 1.915 turbine=22.500
moment of inertia (kg m2): annulus= 0.004 engine= 0.190 compressor=0.0087 carrier= 0.029 planet=.00015
sun= 0.003 turbine=.00044 load=******
output shaft: torque (nm)= 1006. speed (rev/min)=2200. brake power (kw)= 231.7 thermal efficiency=.3928
bypass area (m2)=.00300 bypass mass flow rate (kg/s)=0.079 cooler effectiveness=1.000 nozzle angle = 8.89
turb. mass scale factor = 1.00
fuel flow scale factor = 1.00
gear loss (kw)= 12.77
end of cycle 10

Table 6.1 Summary of the USPDCE performance predictions for the L10-DCE at well established steady state condition at design point with 'tmsf' remaining at its initial value of 1.00

cycle33

engine specification:
CUMMINS L10 DCE
number of cylinder 6 cylinder bore (mm) 125.0 piston stroke (mm) 136.0 connecting rod length (mm) 217.8
compression ratio 16.30 firing order 153624 engine displacement (lits) 10.01
exhaust valve open 135. inlet valve open 341. exhaust valve close 363. inlet valve close 553.
thermal resistance:(deg c/kw):r1,r2,r4,r5,r7,r8,r9,r10= 4.2 1.5 34.5 2.7 43.4 21.3 15.0 16.5

engine performance:			heat loss analysis:	
engine speed (rev/min)	2100.		energy input (kj)	5.517
boost pressure ratio	2.69		% liner heat loss	7.16
b.m.e.p (kn/m2)	1369.		% piston heat loss	7.20
b.h.p (kw)	239.97		% head heat loss	4.21
b.s.f.c (kg/kw.h)	.2014		% friction loss	5.87
b.s.a.c (kg/kw.h)	6.45		% output shaft energy	41.43
engine air flow (kg/s)	0.4302		% exh max energy	41.71
brake thermal efficiency	0.414		liner temp. (deg k)	419.8
air fuel ratio (trapped)	28.84		piston temp. (deg k)	570.8
air fuel ratio (overall)	32.04		head temp. (deg k)	477.8
volumetric efficiecy	0.880		gas mean h.t.c (w/m2.k)	627.
mechanical efficiency	0.876		gas mean temp. (deg k)	1124.
engine torque (nm)	1094.4		piston max temp (deg k)	
max. cyl. pressure (kn/m2)	17063.			
max. cyl. temperature (deg k)	1746.			
exh. man. pressure (kn/m2)	297.	0.		
exh. man. temperature (deg k)	752.	0.		
inlet man. pressure (kn/m2)	267.			
inlet man. temp. (deg k)	319.			
compressor performance:			combustion parameters:	
compressor speed (rev/min)	5514.		static injection (degree)	-19.0
pressure ratio	3.00		dynamic injection (degree)	-18.5
torque (nm)	105.06		ignition delay (ms)	0.00
power (kw)	60.69		ignition point (degree)	-18.5
efficiency	0.731		end of burning (degree)	45.0
mass flow (kg/s)	0.407		heat release shape factor:	
turbine performance:			cw1	0.000
turbine speed (rev/min)	49500.		cw2	0.
pressure ratio	2.97		cw3	1.40
torque (nm)	12.81		cw4	7.000
power (kw)	66.41		mode of burning	0.000
efficiency	0.748	0.000	mass of fuel/cyl/cyc (g)	0.12786
mass flow (kg/s)	0.419	0.000	mean temp during delay (degk)	794.
			mean press dur delay (kn/m2)	5794.

gear ratio : epicyclic= 3.074 compressor= 3.107 output shaft= 1.915 turbine=22.500
moment of inertia (kg m2): annulus= 0.004 engine= 0.190 compressor=0.0087 carrier= 0.029 planet=.00015
sun= 0.003 turbine=.00044 load=******
output shaft: torque (nm)= 1015. speed (rev/min)=2200. brake power (kw)= 233.9 thermal efficiency=.4038
bypass area (m2)=.00300 bypass mass flow rate (kg/s)=-.014 cooler effectiveness=1.000 nozzle angle = 8.89
turb. mass scale factor = 0.75
fuel flow scale factor = 0.98
gear loss (kw)= 11.79
end of cycle 33

Table 6.2 As per table 6.1 but with 'tmsf' changed to 0.75 to adjust for an intended N_{eng}

```
engine specification:
CUMMINS L10 DCE
number of cylinder  6  cylinder bore (mm) 125.0  piston stroke (mm) 136.0   connecting rod length (mm) 217.8
compression ratio  16.30  firing order  153624  engine displacement (lits) 10.01
exhaust valve open 135.  inlet valve open 341.  exhaust valve close 363.  inlet valve close 553.
thermal resistance:(deg c/kw):r1,r2,r4,r5,r7,r8,r9,r10=    5.1    1.5   34.5    2.7   43.4   21.3   15.0   15.1
```

engine performance:		heat loss analysis:	
engine speed (rev/min)	2100.	energy input (kj)	5.692
boost pressure ratio	2.62	% liner heat loss	5.30
b.m.e.p (kn/m2)	1370.	% piston heat loss	5.26
b.h.p (kw)	240.00	% head heat loss	4.15
b.s.f.c (kg/kw.h)	.2078	% friction loss	5.16
b.s.a.c (kg/kw.h)	6.32	% output shaft energy	40.16
engine air flow (kg/s)	0.4216	% exh max energy	39.97
brake thermal efficiency	0.402	liner temp. (deg k)	412.0
air fuel ratio (trapped)	28.67	piston temp. (deg k)	522.3
air fuel ratio (overall)	30.44	head temp. (deg k)	474.5
volumetric efficiecy	0.878	gas mean h.t.c (w/m2.k)	581.
mechanical efficiency	0.886	gas mean temp. (deg k)	1051.
engine torque (nm)	1094.6	piston max temp (deg k)	
max. cyl. pressure (kn/m2)	14148.		
max. cyl. temperature (deg k)	1665.		
exh. man. pressure (kn/m2)	295. 0.		
exh. man. temperature (deg k)	772. 0.		
inlet man. pressure (kn/m2)	295.		
inlet man. temp. (deg k)	319.		
compressor performance:		combustion parameters:	
compressor speed (rev/min)	5515.	static injection (degree)	-14.0
pressure ratio	2.95	dynamic injection (degree)	-13.5
torque (nm)	110.00	ignition delay (ms)	
power (kw)	63.53	ignition point (degree)	-13.5
efficiency	0.727	end of burning (degree)	53.0
mass flow (kg/s)	0.432	heat release shape factor:	
turbine performance:		cw1	0.000
turbine speed (rev/min)	49500.	cw2	0.
pressure ratio	2.95	cw3	1.40
torque (nm)	13.19	cw4	7.000
power (kw)	68.36	mode of burning	0.000
efficiency	0.714 0.000	mass of fuel/cyl/cyc (g)	0.13191
mass flow (kg/s)	0.442 0.000	mean temp during delay (degk)	827.
		mean press dur delay (kn/m2)	6820.

```
gear ratio :  epicyclic= 3.074  compressor= 3.107  output shaft= 1.915  turbine=22.500
moment of inertia  (kg m2):  annulus=******  engine= 1.900  compressor=0.0870  carrier= 0.290  planet=.00020
sun= 0.005  turbine=.00050  load=******
output shaft:        torque (nm)= 1026.  speed (rev/min)=2200.  brake power (kw)= 236.4  thermal efficiency=.3955
bypass area (m2)=.00300  bypass mass flow rate (kg/s)= 0.011  cooler effectiveness= 1.000
 turb. mass scale factor  = 1.00000
 in/out mass flow ratio   = 1.00700
 fuel flow scale factor   = 0.992
 gear loss (kw)=  8.45
 rc     =, 2.957
end of cycle  9
```

Table 6.3 Summary of the CSPDCEperformance predictions for the L1O-DCE at design point with α_N corrected to match the boost with that required by torque balance (2nd solution method)

```
 cycle 9
engine specification:
CUMMINS L10 DCE
number of cylinder  6  cylinder bore (mm) 125.0  piston stroke (mm) 136.0   connecting rod length (mm) 217.8
compression ratio  16.30  firing order  153624  engine displacement (lits) 10.01
exhaust valve open 135.  inlet valve open 341.  exhaust valve close 363.  inlet valve close 553.
thermal resistance:(deg c/kw):r1,r2,r4,r5,r7,r8,r9,r10=    4.8    1.5   34.5    2.7   43.4   21.3   15.0   19.2
```

engine performance:		heat loss analysis:	
engine speed (rev/min)	1350.	energy input (kj)	8.682
boost pressure ratio	3.96	% liner heat loss	6.35
b.m.e.p (kn/m2)	2146.	% piston heat loss	5.67
b.h.p (kw)	241.77	% head heat loss	3.28
b.s.f.c (kg/kw.h)	.2022	% friction loss	2.92
b.s.a.c (kg/kw.h)	6.91	% output shaft energy	41.26
engine air flow (kg/s)	0.4640	% exh max energy	40.53
brake thermal efficiency	0.413	liner temp. (deg k)	412.7
air fuel ratio (trapped)	32.66	piston temp. (deg k)	530.3
air fuel ratio (overall)	34.16	head temp. (deg k)	459.4
volumetric efficiecy	0.956	gas mean h.t.c (w/m2.k)	606.
mechanical efficiency	0.934	gas mean temp. (deg k)	985.
engine torque (nm)	1715.5	piston max temp (deg k)	
max. cyl. pressure (kn/m2)	19482.		
max. cyl. temperature (deg k)	1488.		
exh. man. pressure (kn/m2)	420.	0.	
exh. man. temperature (deg k)	667.	0.	
inlet man. pressure (kn/m2)	422.		
inlet man. temp. (deg k)	325.		
compressor performance:		combustion parameters:	
compressor speed (rev/min)	9984.	static injection (degree)	-14.0
pressure ratio	4.23	dynamic injection (degree)	-13.5
torque (nm)	174.09	ignition delay (ms)	0.00
power (kw)	182.02	ignition point (degree)	-13.5
efficiency	0.692	end of burning (degree)	69.0
mass flow (kg/s)	0.836	heat release shape factor:	
turbine performance:		cw1	0.000
turbine speed (rev/min)	46508.	cw2	0.
pressure ratio	4.20	cw3	1.40
torque (nm)	30.80	cw4	7.000
power (kw)	149.99	mode of burning	0.000
efficiency	0.774 0.000	mass of fuel/cyl/cyc (g)	0.20119
mass flow (kg/s)	0.849 0.000	mean temp during delay (degk)	833.
		mean press dur delay (kn/m2)	11070.

```
gear ratio :  epicyclic= 3.074  compressor= 3.107  output shaft= 1.915  turbine=******
moment of inertia  (kg m2):  annulus=******  engine=******  compressor=0.0180  carrier= 0.268  planet=.00637
sun= 0.010  turbine=.00760  load=******
output shaft:         torque (nm)= 4406.  speed (rev/min)= 440.  brake power (kw)= 203.0  thermal efficiency=.3464
bypass area (m2)=.00300  bypass mass flow rate (kg/s)= 0.407  cooler effectiveness= 1.000   nozzle angle = 9.698
 turb. mass scale factor  = 1.00000
 in/out mass flow ratio   = 1.01961
 fuel flow scale factor   = 1.088
 gear loss (kw)=  6.73
 rc     =, 4.232
end of cycle  9
```

Table 6.4 As per table 6.3 but at O/S stall

cycle 8
engine specification:
CUMMINS L10 DCE
number of cylinder 6 cylinder bore (mm) 125.0 piston stroke (mm) 136.0 connecting rod length (mm) 217.8
compression ratio 16.30 firing order 153624 engine displacement (litts) 10.01
exhaust valve open 135. inlet valve open 341. exhaust valve close 363. inlet valve close 553.
thermal resistance:(deg c/kw):r1,r2,r4,r5,r7,r8,r9,r10= 4.8 1.5 34.5 2.7 43.4 21.3 15.0 19.2

engine performance:		heat loss analysis:	
engine speed (rev/min)	1500.	energy input (kj)	7.929
boost pressure ratio	3.44	% liner heat loss	6.37
b.m.e.p (kn/m2)	1929.	% piston heat loss	5.62
b.h.p (kw)	241.47	% head heat loss	3.23
b.s.f.c (kg/kw.h)	.2055	% friction loss	3.14
b.s.a.c (kg/kw.h)	6.32	% output shaft energy	40.61
engine air flow (kg/s)	0.4241	% exh max energy	41.03
brake thermal efficiency	0.406	liner temp. (deg k)	413.4
air fuel ratio (trapped)	30.00	piston temp. (deg k)	531.4
air fuel ratio (overall)	30.77	head temp. (deg k)	459.4
volumetric efficiecy	0.938	gas mean h.t.c (w/m2.k)	577.
mechanical efficiency	0.928	gas mean temp. (deg k)	1013.
engine torque (nm)	1542.1	piston max temp (deg k)	
max. cyl. pressure (kn/m2)	16932.		
max. cyl. temperature (deg k)	1547.		
exh. man. pressure (kn/m2)	370.	0.	
exh. man. temperature (deg k)	730.	0.	
inlet man. pressure (kn/m2)	370.		
inlet man. temp. (deg k)	326.		
compressor performance:		combustion parameters:	
compressor speed (rev/min)	7385.	static injection (degree)	
pressure ratio	3.71	dynamic injection (degree)	
torque (nm)	147.80	ignition delay (ms)	
power (kw)	114.30	ignition point (degree)	-13.5
efficiency	0.687	end of burning (degree)	69.0
mass flow (kg/s)	0.585	heat release shape factor:	
turbine performance:		cw1	0.000
turbine speed (rev/min)	42000.	cw2	0.
pressure ratio	3.70	cw3	1.40
torque (nm)	23.61	cw4	7.000
power (kw)	103.85	mode of burning	0.000
efficiency	0.732 0.000	mass of fuel/cyl/cyc (g)	0.18375
mass flow (kg/s)	0.600 0.000	mean temp during delay (degk)	839.
		mean press dur delay (kn/m2)	9471.

gear ratio : epicyclic= 3.074 compressor= 3.107 output shaft= 1.915 turbine=40.000
moment of inertia (kg m2): annulus=****** engine=****** compressor=0.0180 carrier= 0.268 planet=.00637
sun= 0.010 turbine=.00760 load=******
output shaft: torque (nm)= 1976. speed (rev/min)=1050. brake power (kw)= 217.3 thermal efficiency=.3654
bypass area (m2)=.00300 bypass mass flow rate (kg/s)= 0.175 cooler effectiveness= 1.000
turb. mass scale factor = 1.00000
in/out mass flow ratio = 0.99834
fuel flow scale factor = 1.048
gear loss (kw)= 13.69
rc =, 3.869
end of cycle 8

Table 6.5 As per table 6.3 but at an intermediate running condition along the system LTC

cycle16
engine specification:
CUMMINS L10 DCE
number of cylinder 6 cylinder bore (mm) 125.0 piston stroke (mm) 136.0 connecting rod length (mm) 217.8
compression ratio 16.30 firing order 153624 engine displacement (lits) 10.01
exhaust valve open 135. inlet valve open 341. exhaust valve close 363. inlet valve close 553.
thermal resistance:(deg c/kw):r1,r2,r4,r5,r7,r8,r9,r10= 4.8 1.5 34.5 2.7 43.4 21.3 15.0 19.5

engine performance:		heat loss analysis:	
engine speed (rev/min)	1700.	energy input (kj)	7.128
boost pressure ratio	3.20	% liner heat loss	6.10
b.m.e.p (kn/m2)	1703.	% piston heat loss	5.49
b.h.p (kw)	241.61	% head heat loss	3.08
b.s.f.c (kg/kw.h)	.2092	% friction loss	3.62
b.s.a.c (kg/kw.h)	6.43	% output shaft energy	39.88
engine air flow (kg/s)	0.4313	% exh max energy	41.83
brake thermal efficiency	0.399	liner temp. (deg k)	414.0
air fuel ratio (trapped)	27.67	piston temp. (deg k)	523.1
air fuel ratio (overall)	30.72	head temp. (deg k)	457.0
volumetric efficiecy	0.923	gas mean h.t.c (w/m2.k)	575.
mechanical efficiency	0.917	gas mean temp. (deg k)	996.
engine torque (nm)	1361.6	piston max temp (deg k)	
max. cyl. pressure (kn/m2)	15333.		
max. cyl. temperature (deg k)	1532.		
exh. man. pressure (kn/m2)	348.	0.	
exh. man. temperature (deg k)	790.	0.	
inlet man. pressure (kn/m2)	347.		
inlet man. temp. (deg k)	326.		
compressor performance:		combustion parameters:	
compressor speed (rev/min)	5660.	static injection (degree)	-14.0
pressure ratio	3.48	dynamic injection (degree)	-13.5
torque (nm)	135.26	ignition delay (ms)	0.00
power (kw)	80.17	ignition point (degree)	-13.5
efficiency	0.667	end of burning (degree)	69.0
mass flow (kg/s)	0.423	heat release shape factor:	
turbine performance:		cw1	0.000
turbine speed (rev/min)	64000.	cw2	0.
pressure ratio	3.48	cw3	1.40
torque (nm)	11.39	cw4	7.000
power (kw)	76.32	mode of burning	0.000
efficiency	0.689 0.000	mass of fuel/cyl/cyc (g)	0.16519
mass flow (kg/s)	0.440 0.000	mean temp during delay (degk)	833.
		mean press dur delay (kn/m2)	8601.

gear ratio : epicyclic= 3.074 compressor= 3.107 output shaft= 1.915 turbine=40.000
moment of inertia (kg m2): annulus=****** engine=****** compressor=0.0180 carrier= 0.268 planet=.00637
sun= 0.010 turbine=.00760 load=******
output shaft: torque (nm)= 1366. speed (rev/min)=1600. brake power (kw)= 228.8 thermal efficiency=.3776
bypass area (m2)=.00300 bypass mass flow rate (kg/s)= 0.006 cooler effectiveness= 1.000 nozzle angle = 7.800
turb. mass scale factor = 1.00000
in/out mass flow ratio = 1.00829
fuel flow scale factor = 1.036
gear loss (kw)= 8.96
rc =, 3.520
end of cycle 16

Table 6.6 As per table 6.3 but at an intermediate running condition along the system LTC

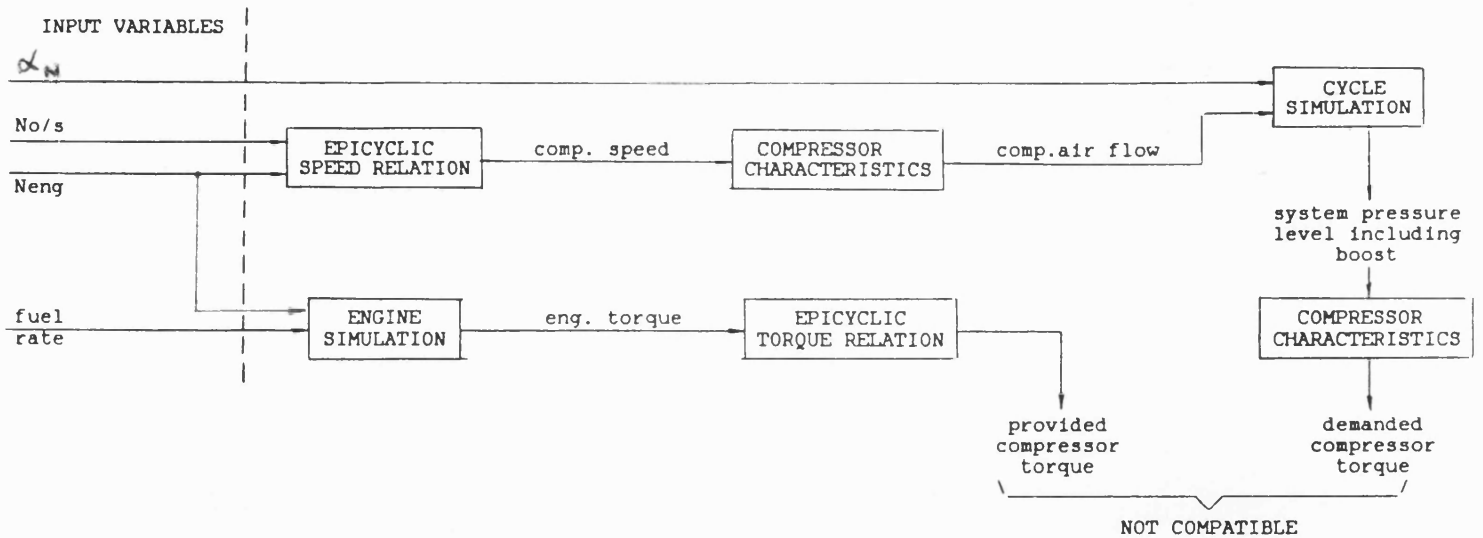

Fig. 6.1 Torque incompatibility resulting from application of the program CSPDCE in its original form simulating constant fuelling and speeds

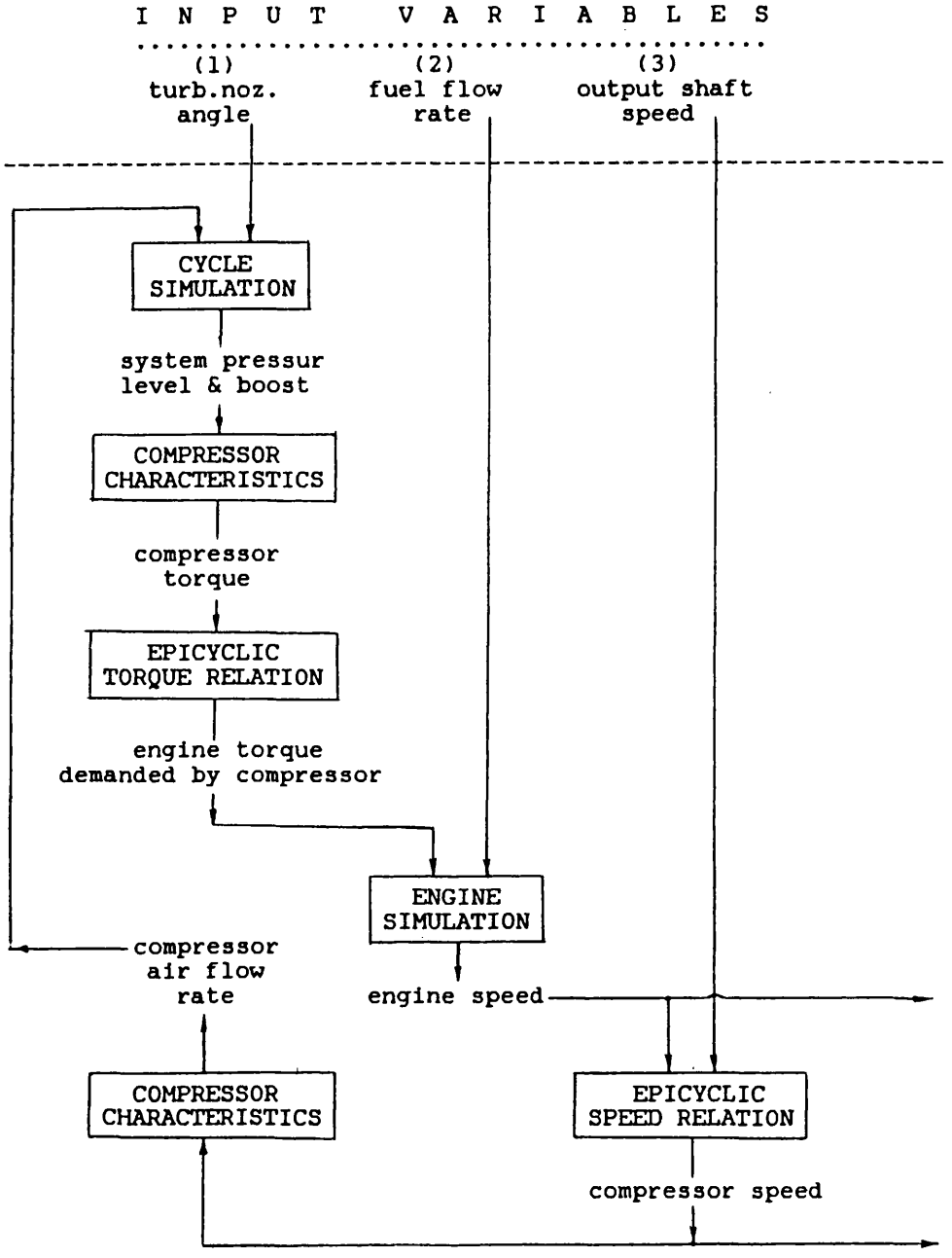

Fig. 6.2,a Logic structure of the program CSPDCE in its original form simulating constant fuelling and output speed having no control over engine speed

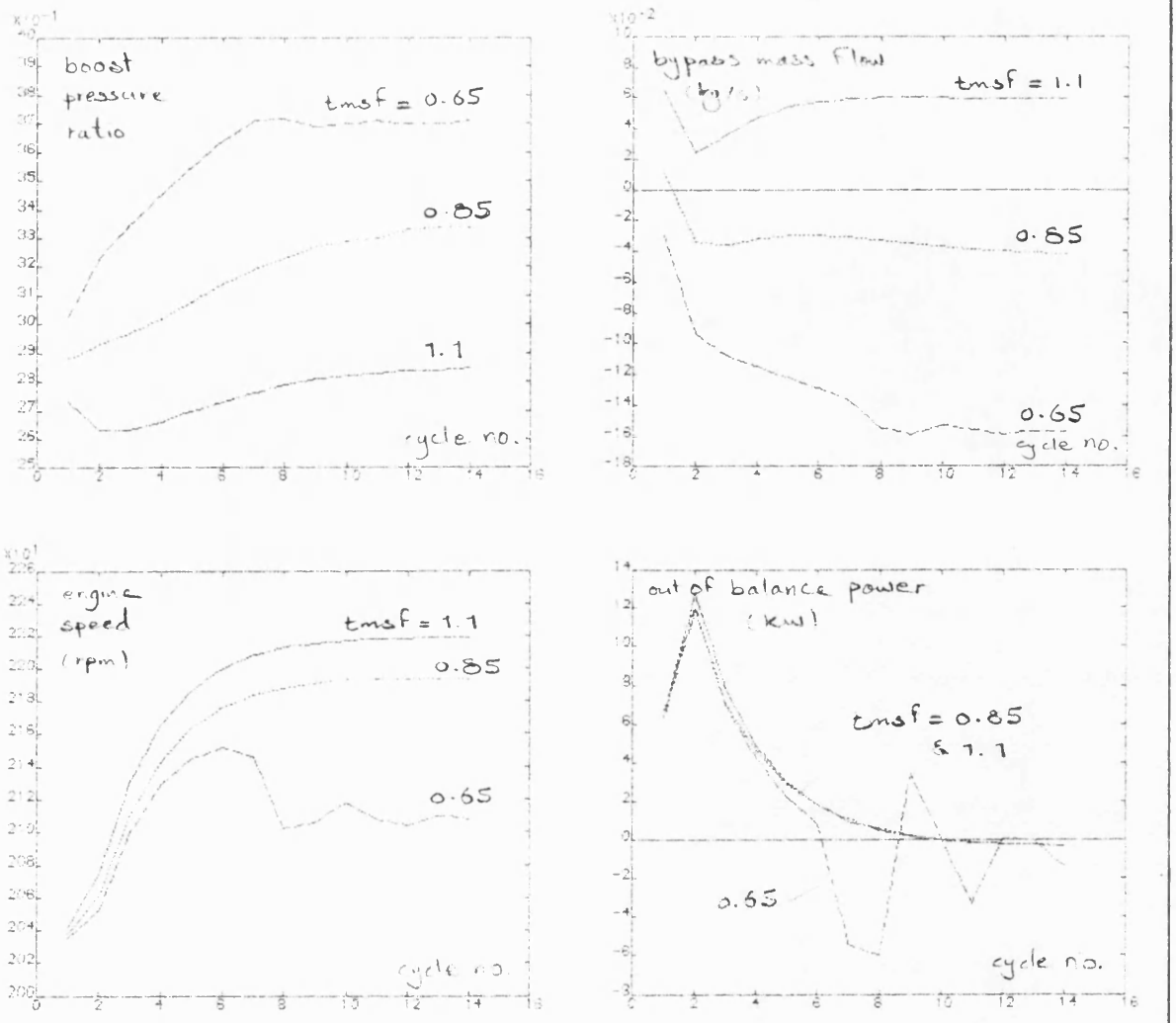

Fig. 6.2,b Effect of turbine swallowing capacity on engine speed at constant fuelling and output speed

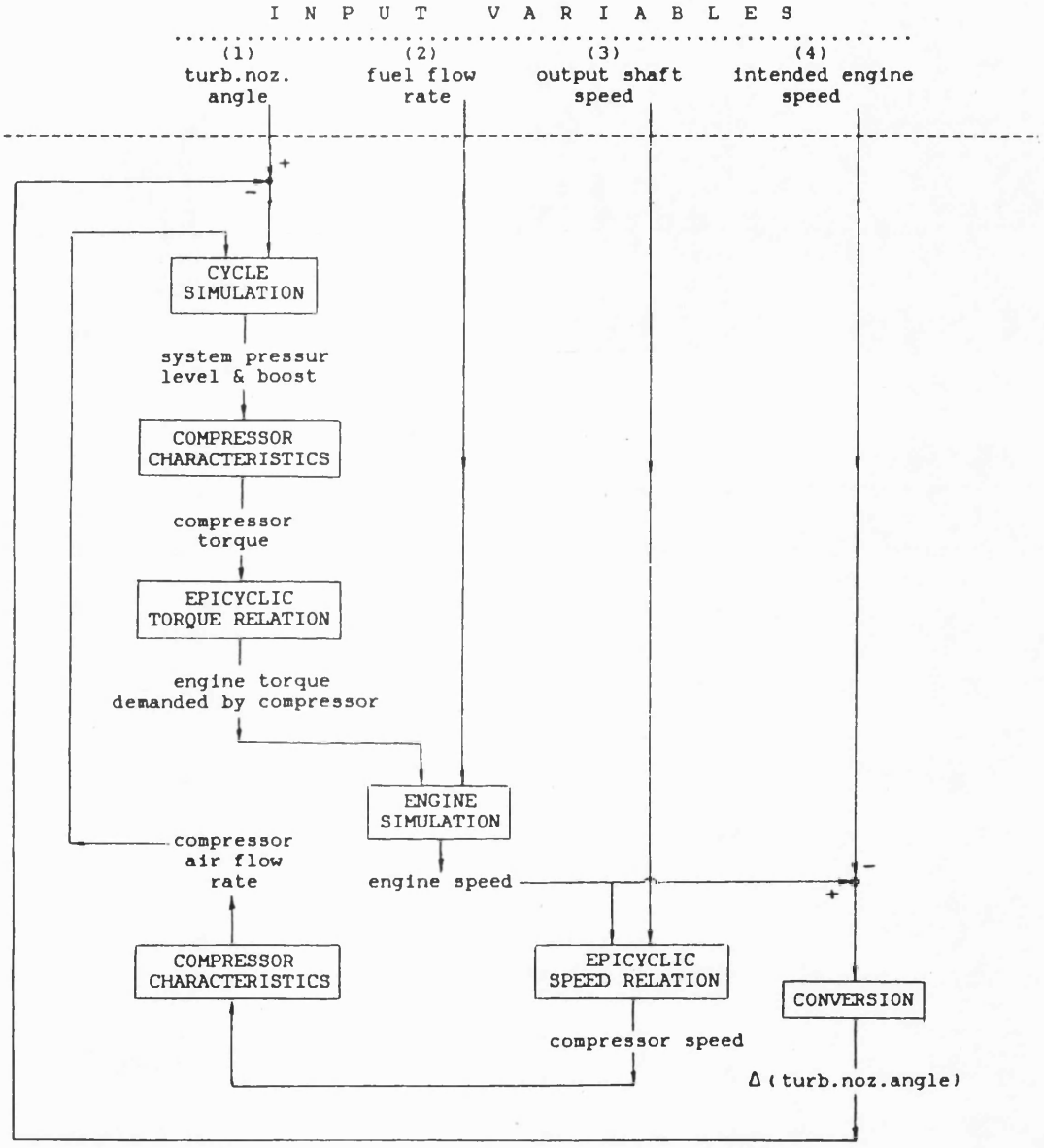

Fig. 6.3 The same as 6.2,a but with control loop to modify turbine swallowing capacity according to intended engine speed

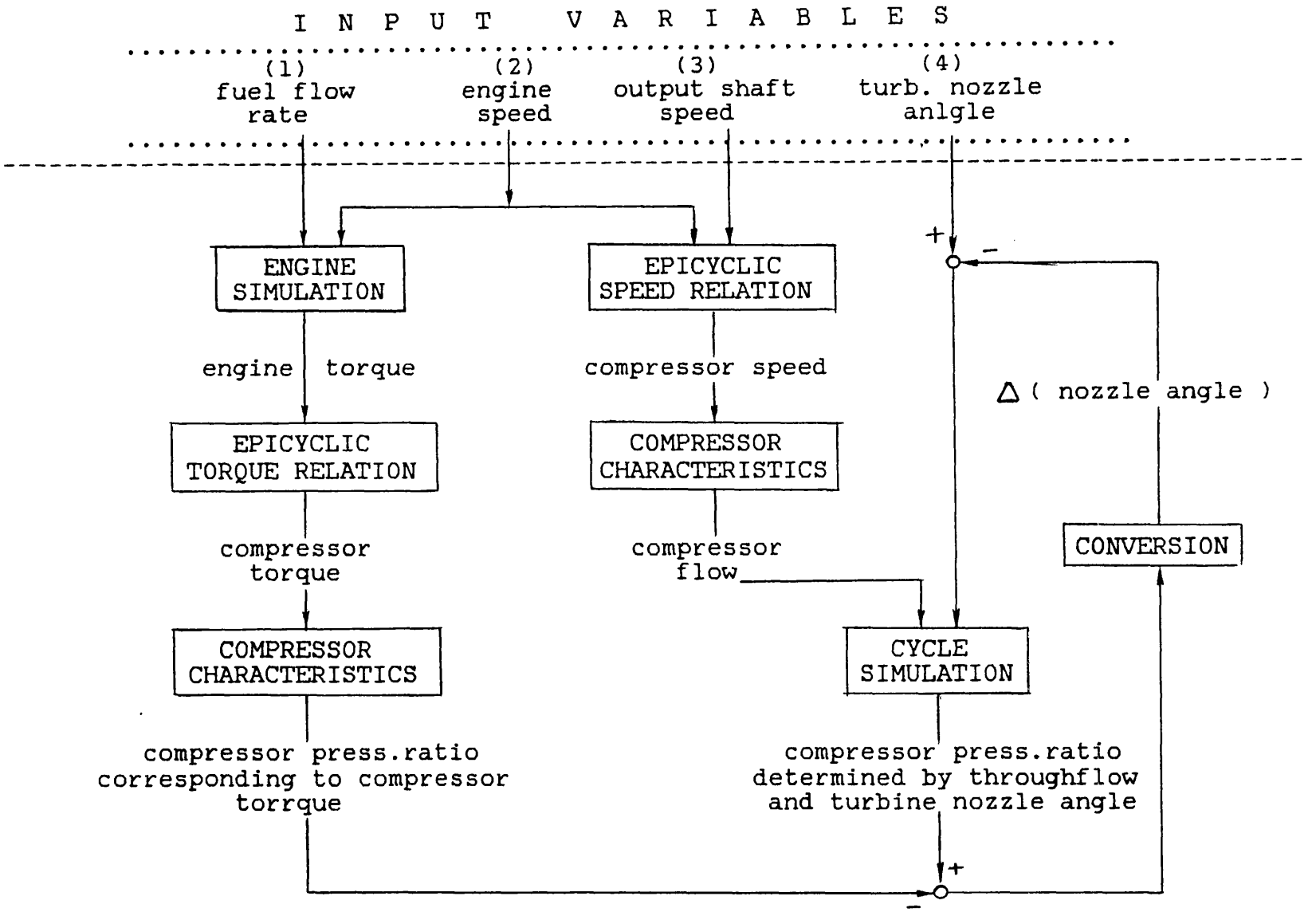

Fig. 6.4 Logic structure of the modified program CSPDCE when simulating the DCE at constant fuelling and speeds

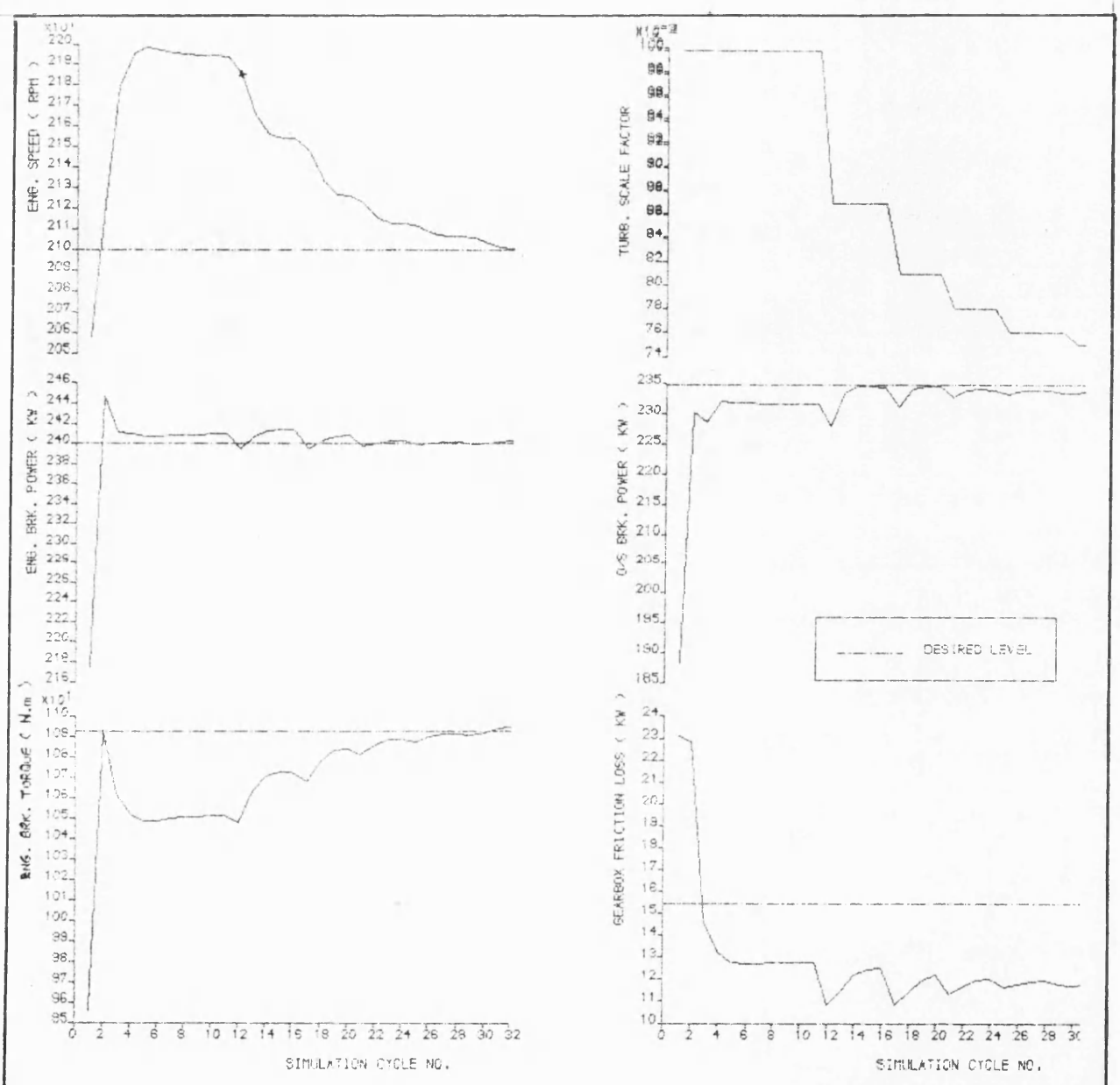

Fig. 6.5,a Cycle-by-cycle variations of performance parameters when simulating the L1O-DCE at design point (shaft dynamics)

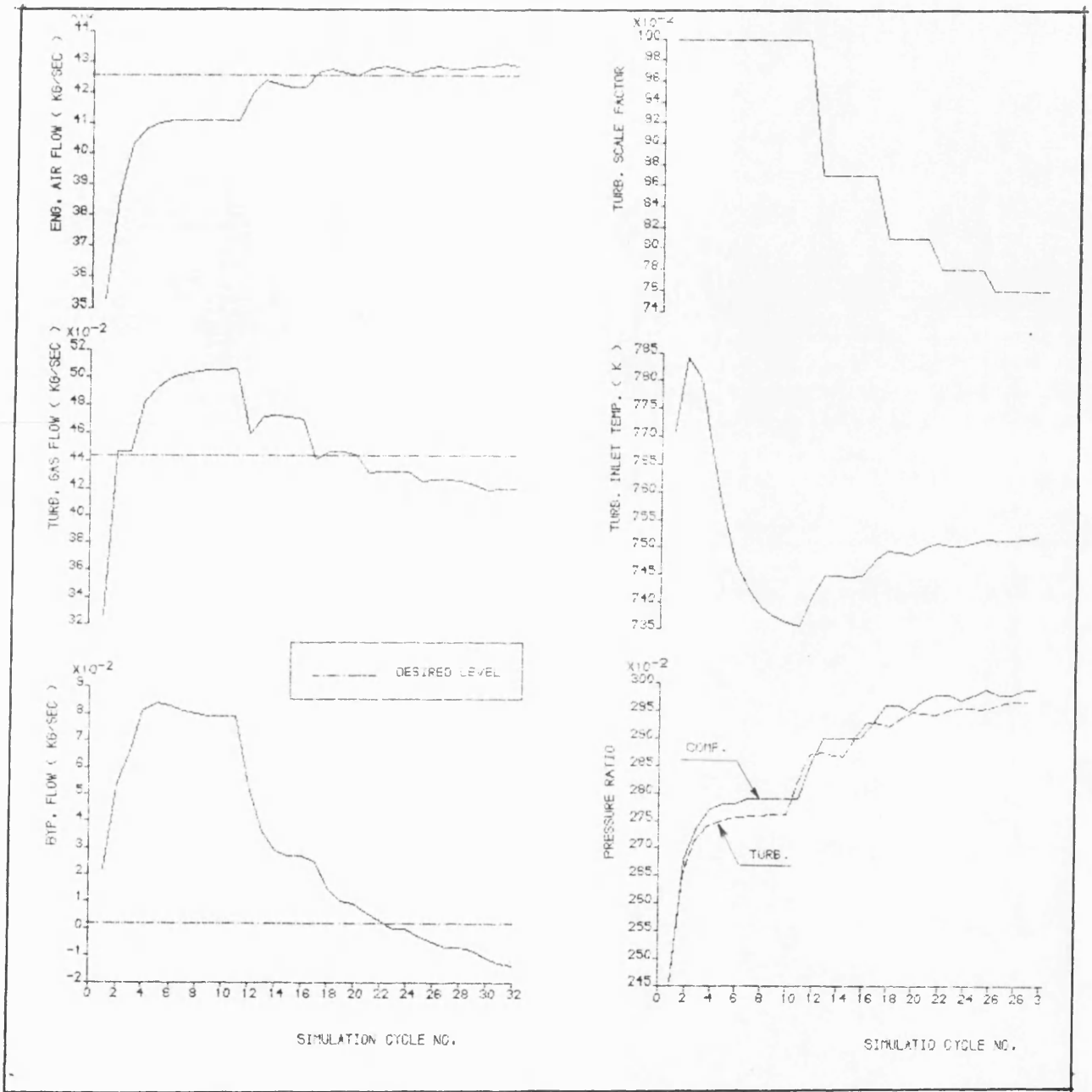

Fig. 6.5,b As per fig. 6.5,a

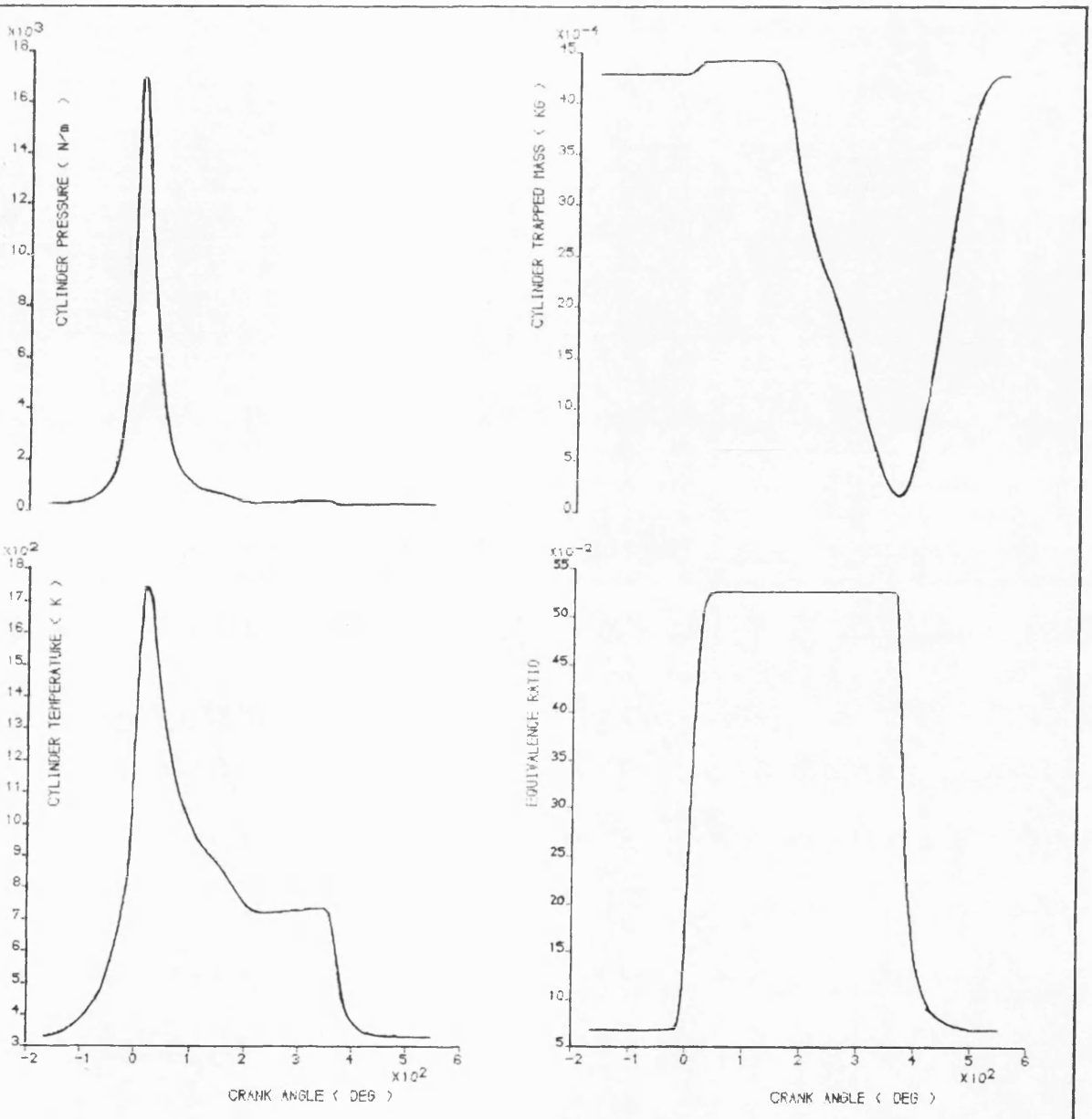

Fig. 6.6.a Cyclically varying parameters of the L10-DCE during a cycle at design point with respect to the engine brake power and shaft speeds relevant to table 7.2

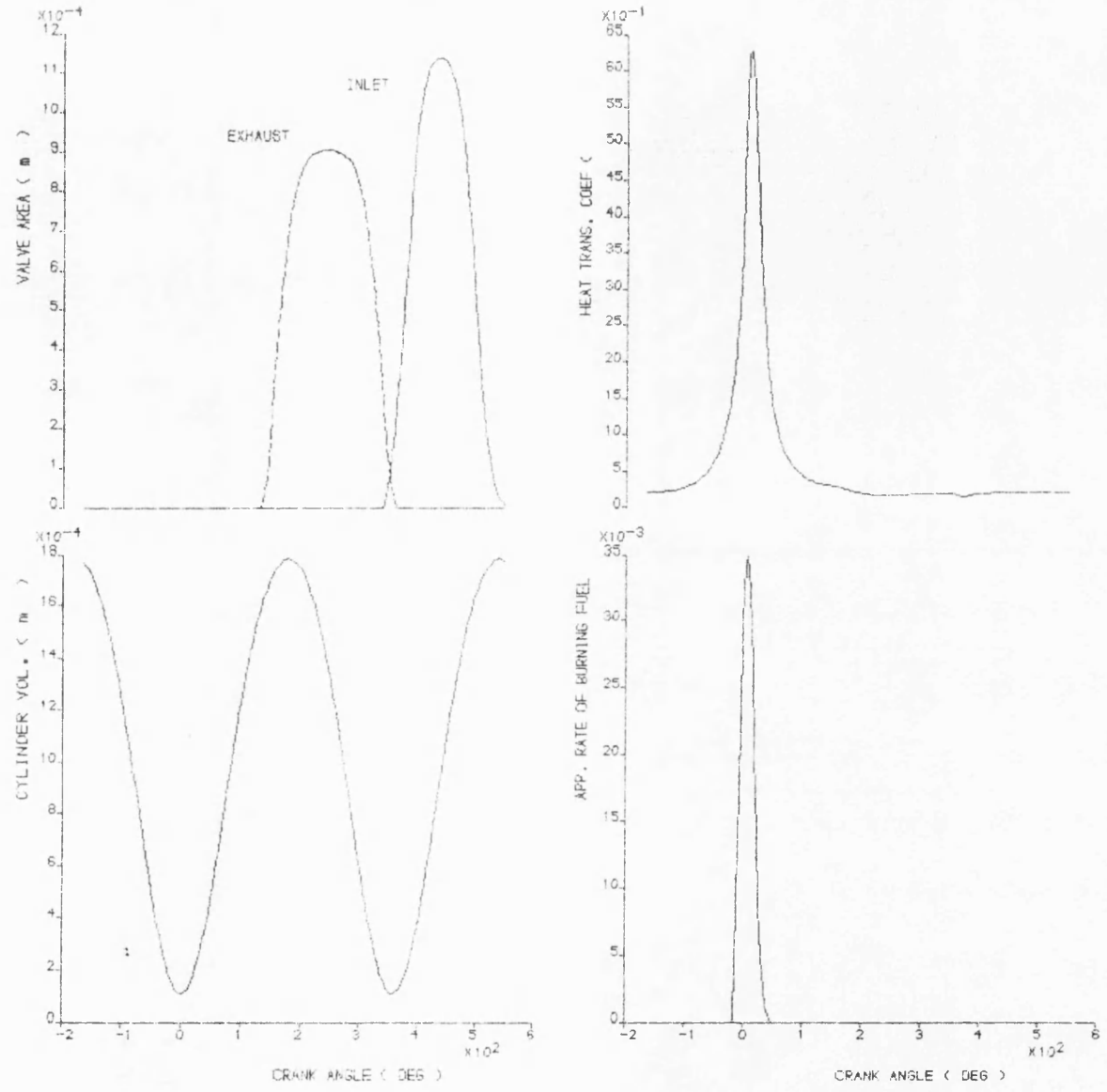

Fig. 6.6,b As per fig.6.6,a

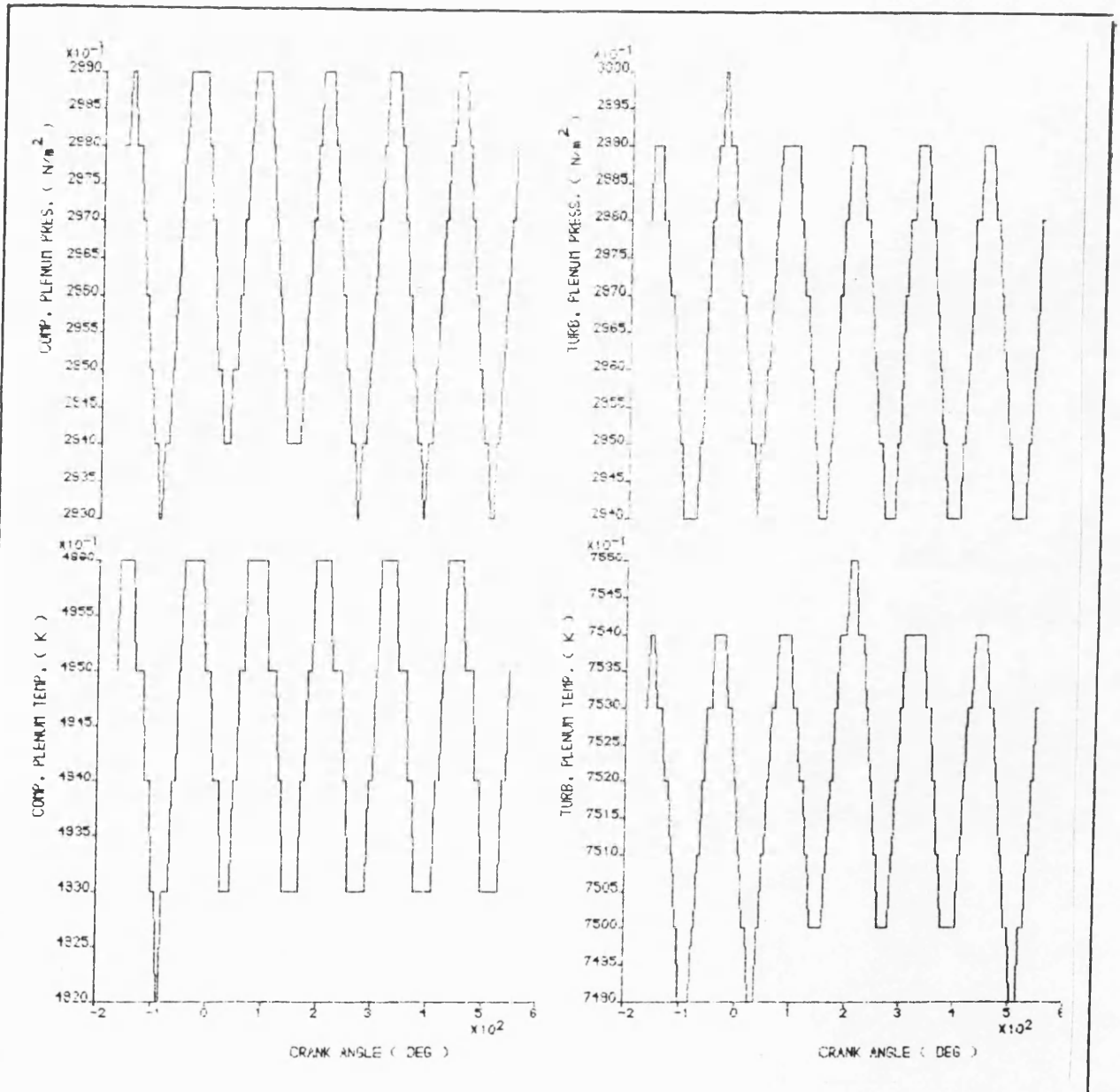

Fig. 6.6,c As per fig.6.6,a

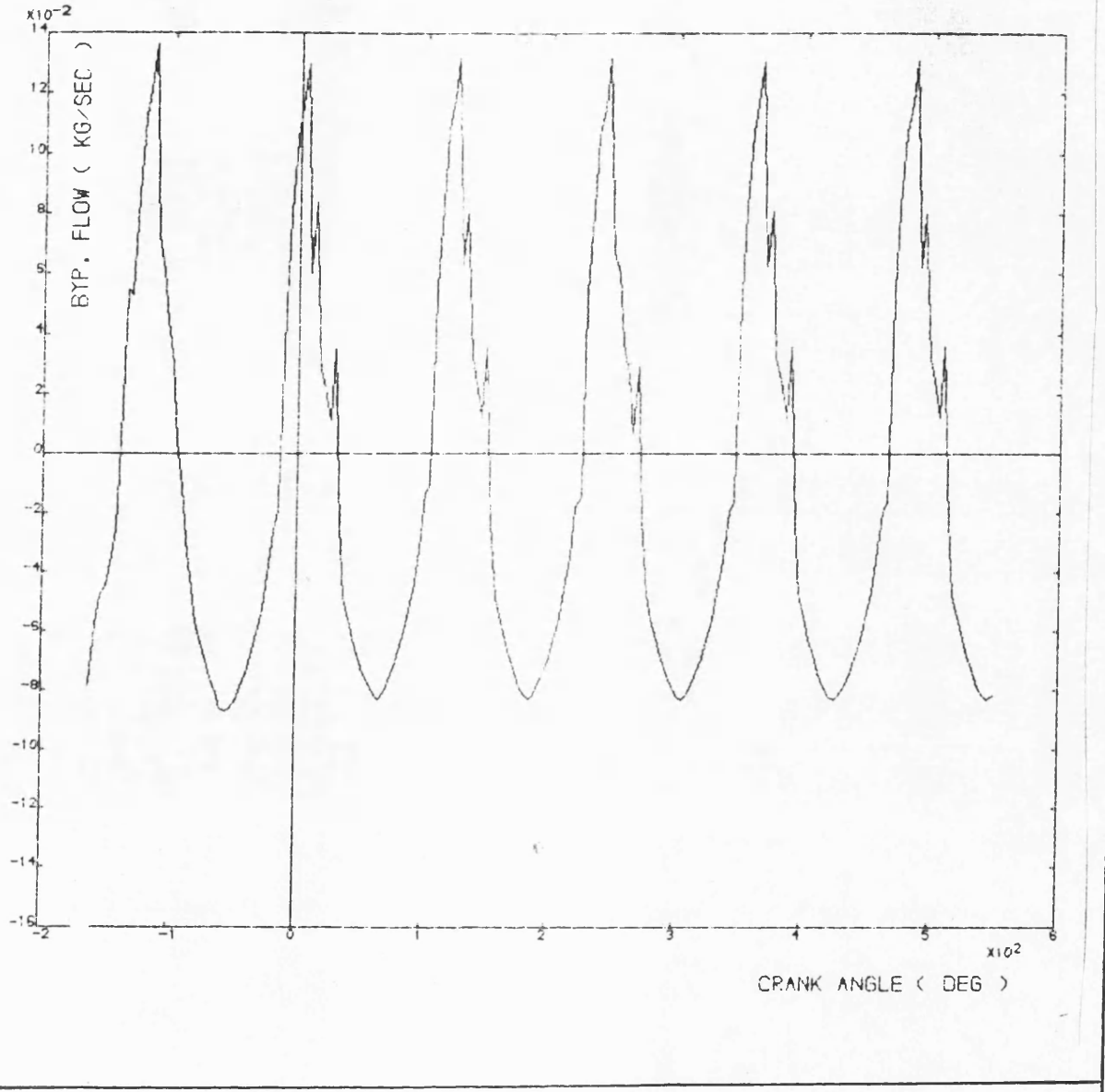

Fig. 6.6,d As per fig.6.6,a

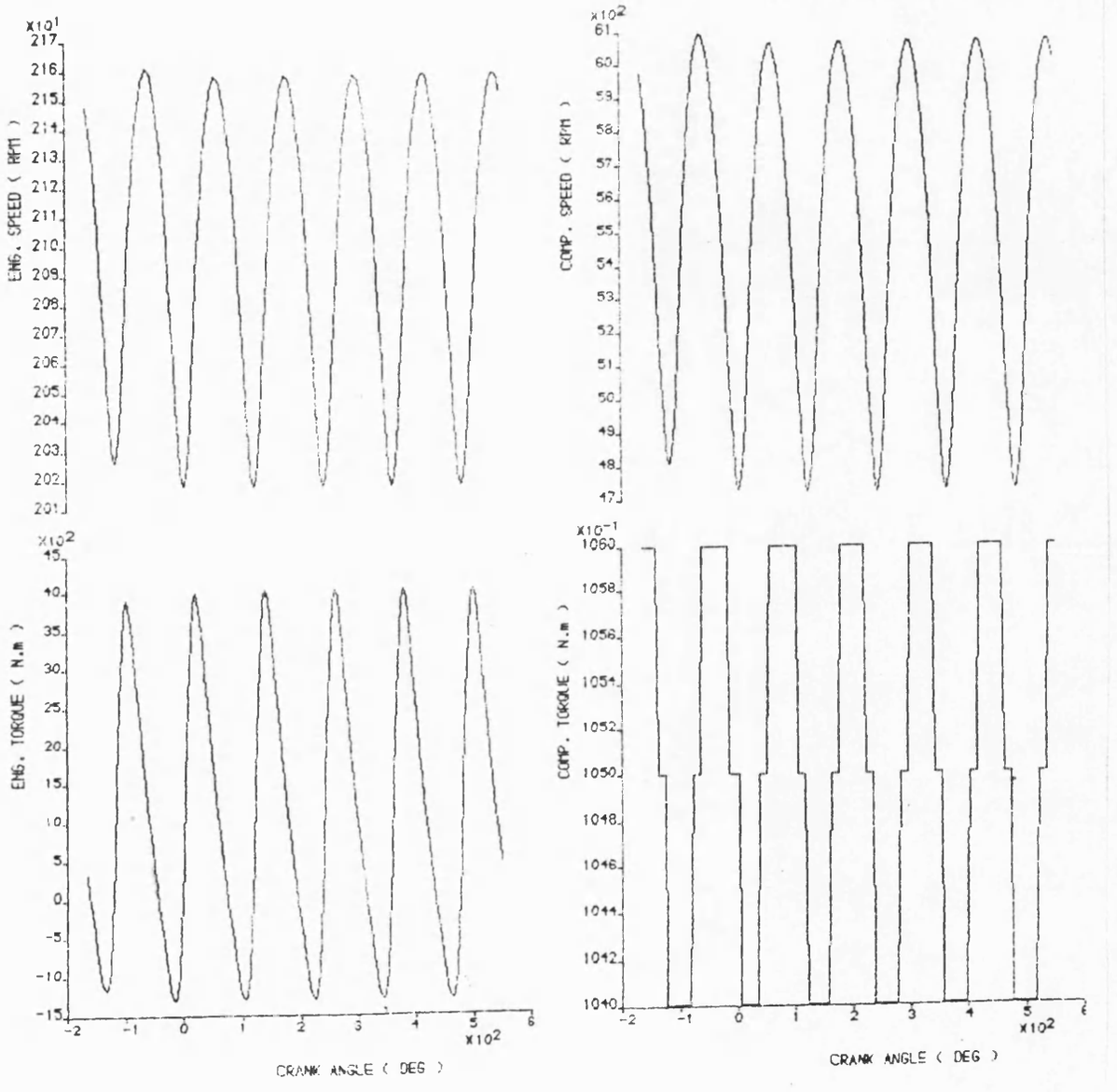

Fig. 6.6,e As per fig.6.6,a

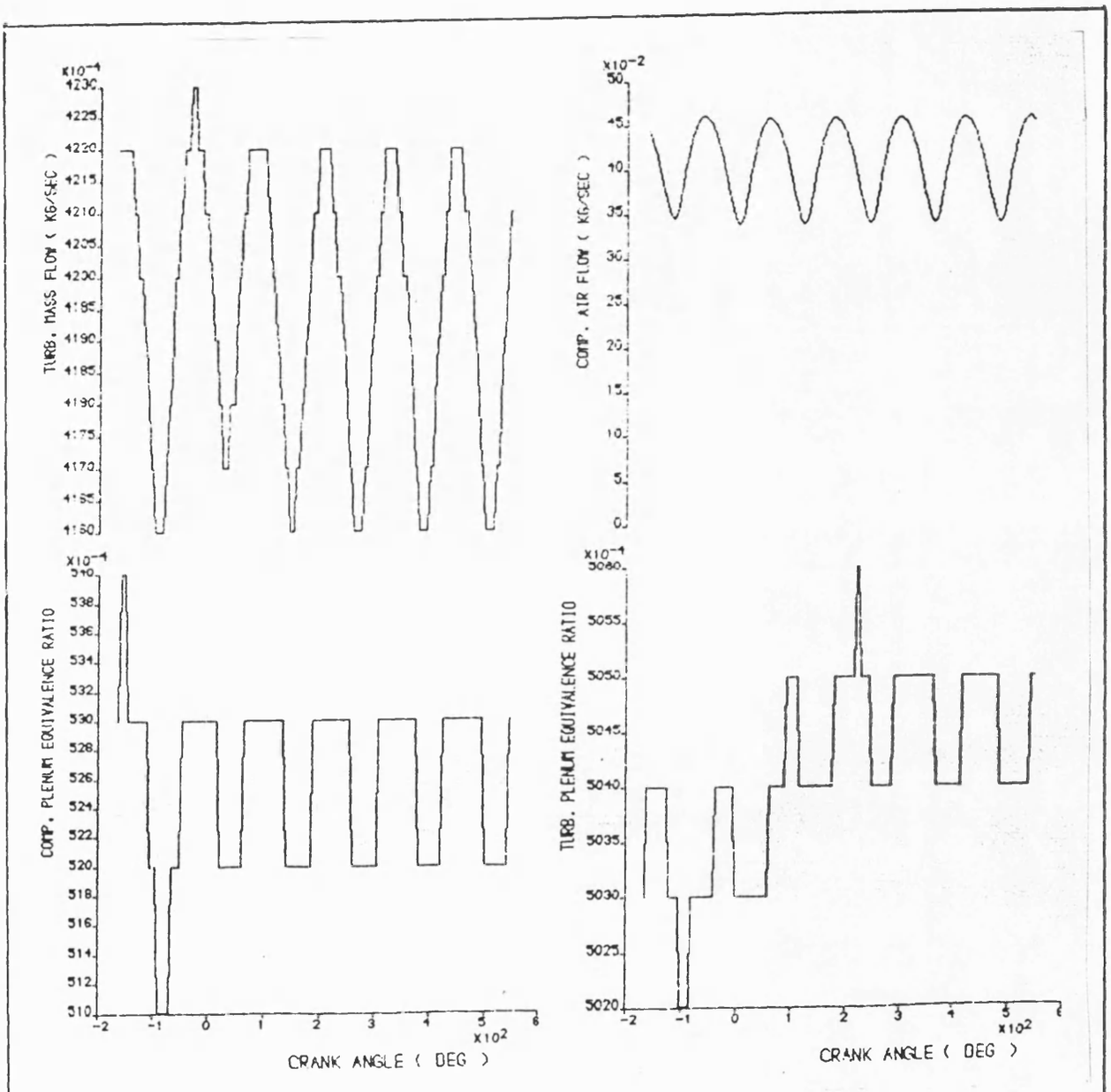

Fig. 6.6,f As per fig.6.6,a

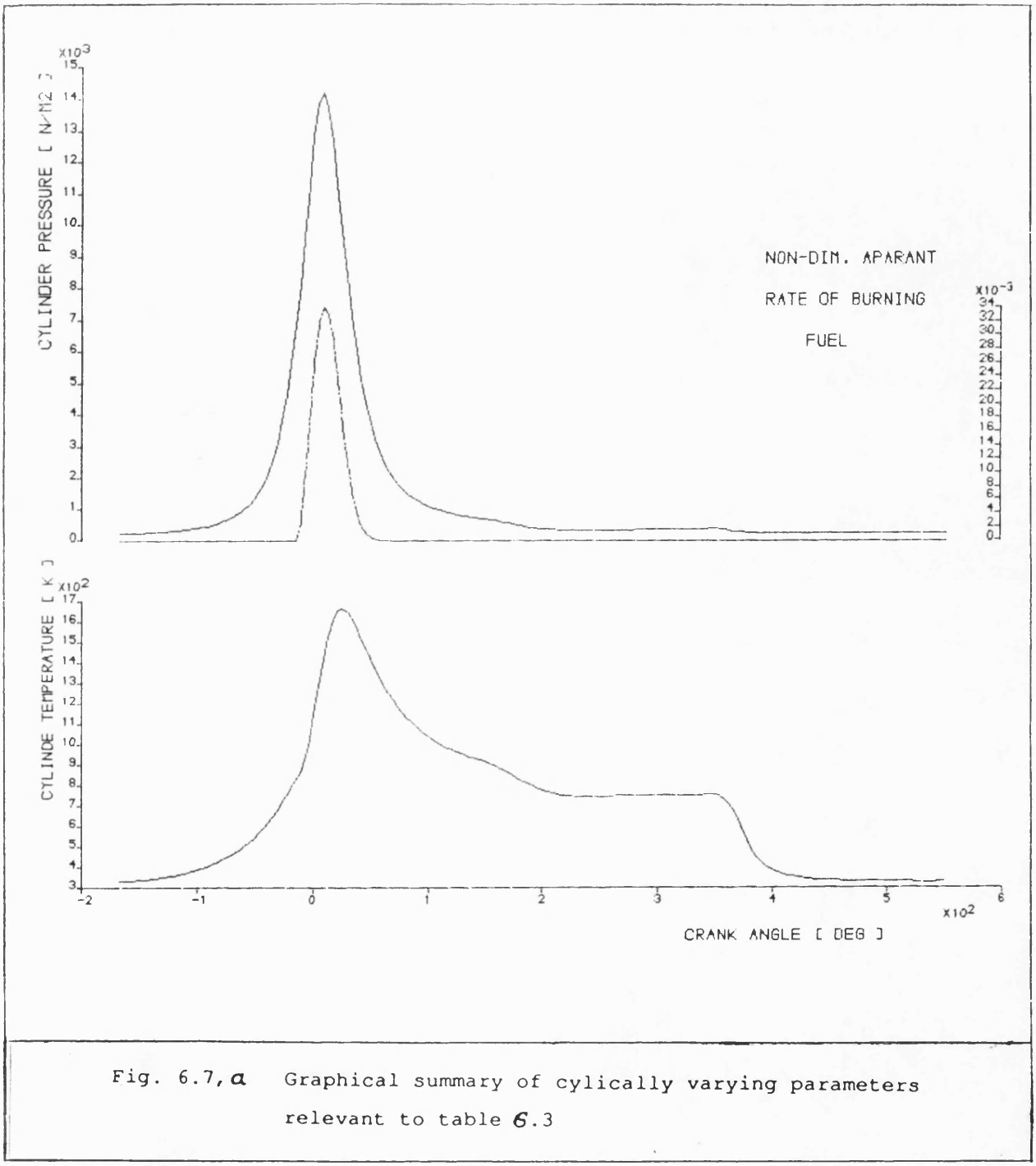

Fig. 6.7, *a* Graphical summary of cylically varying parameters relevant to table *6*.3

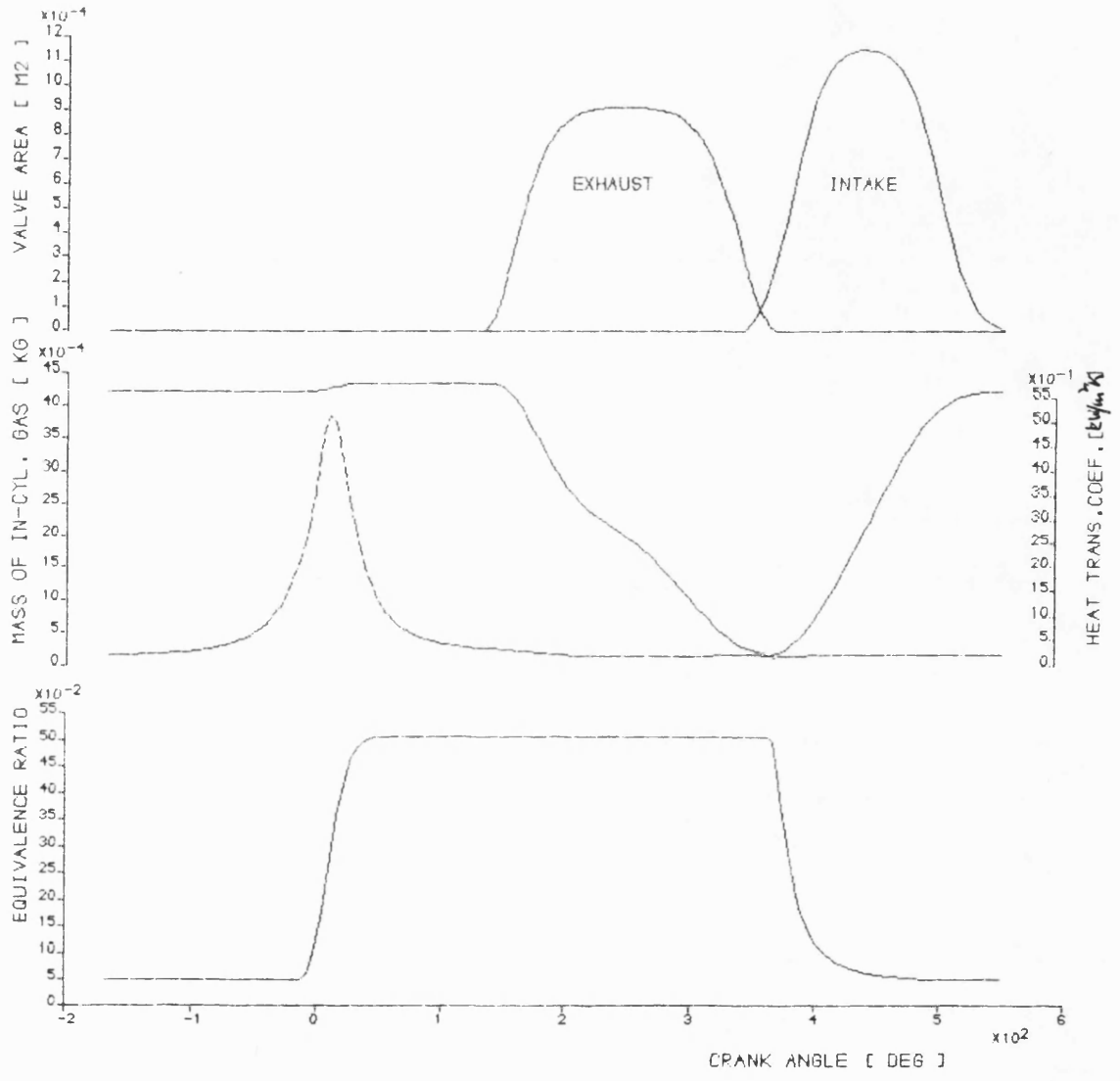

Fig. 6.7, b Graphical summary of cylically varying parameters relevant to table 6.3

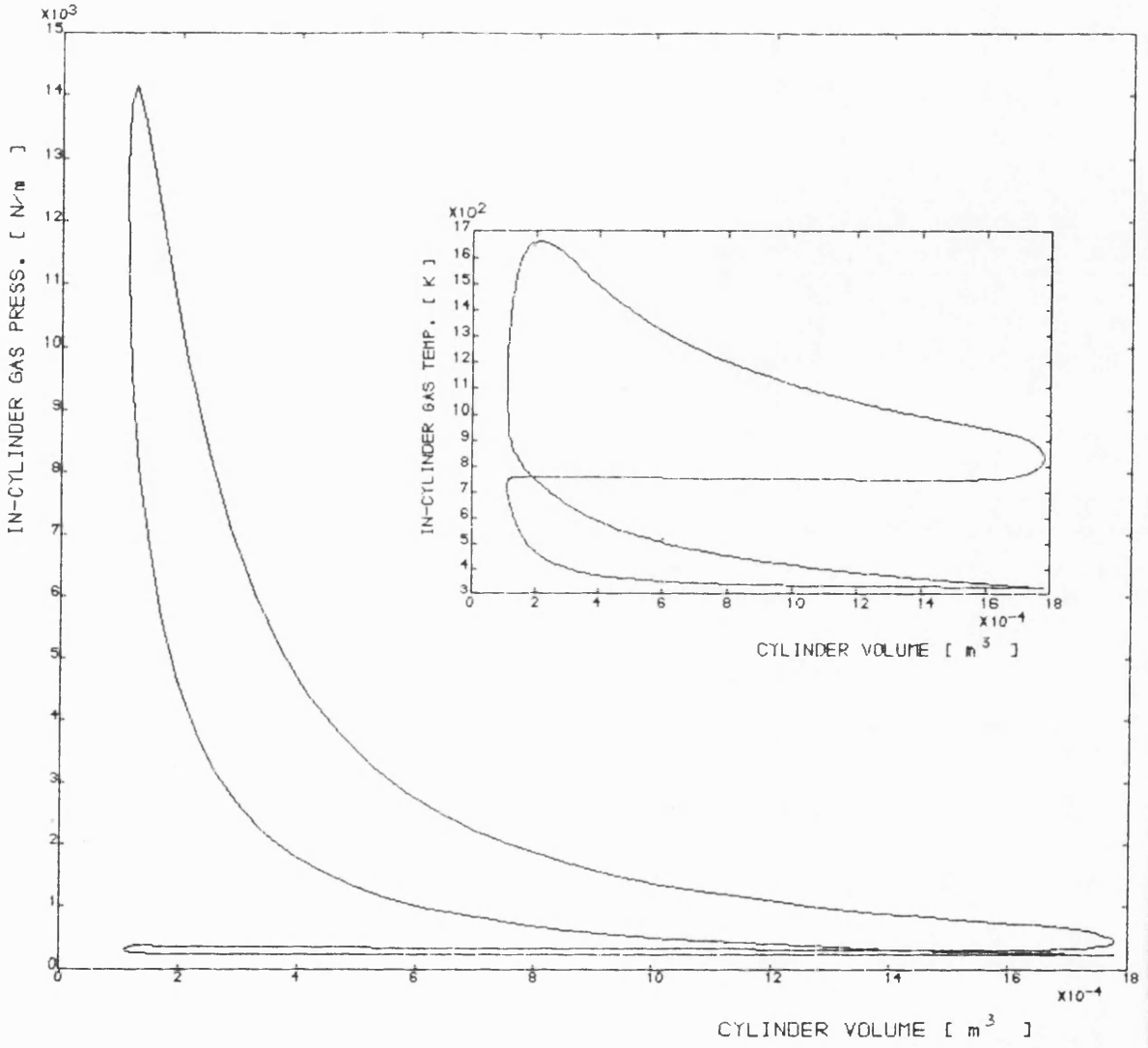

Fig. 6.7, C Graphical summary of cylically varying parameters relevant to table 6.3

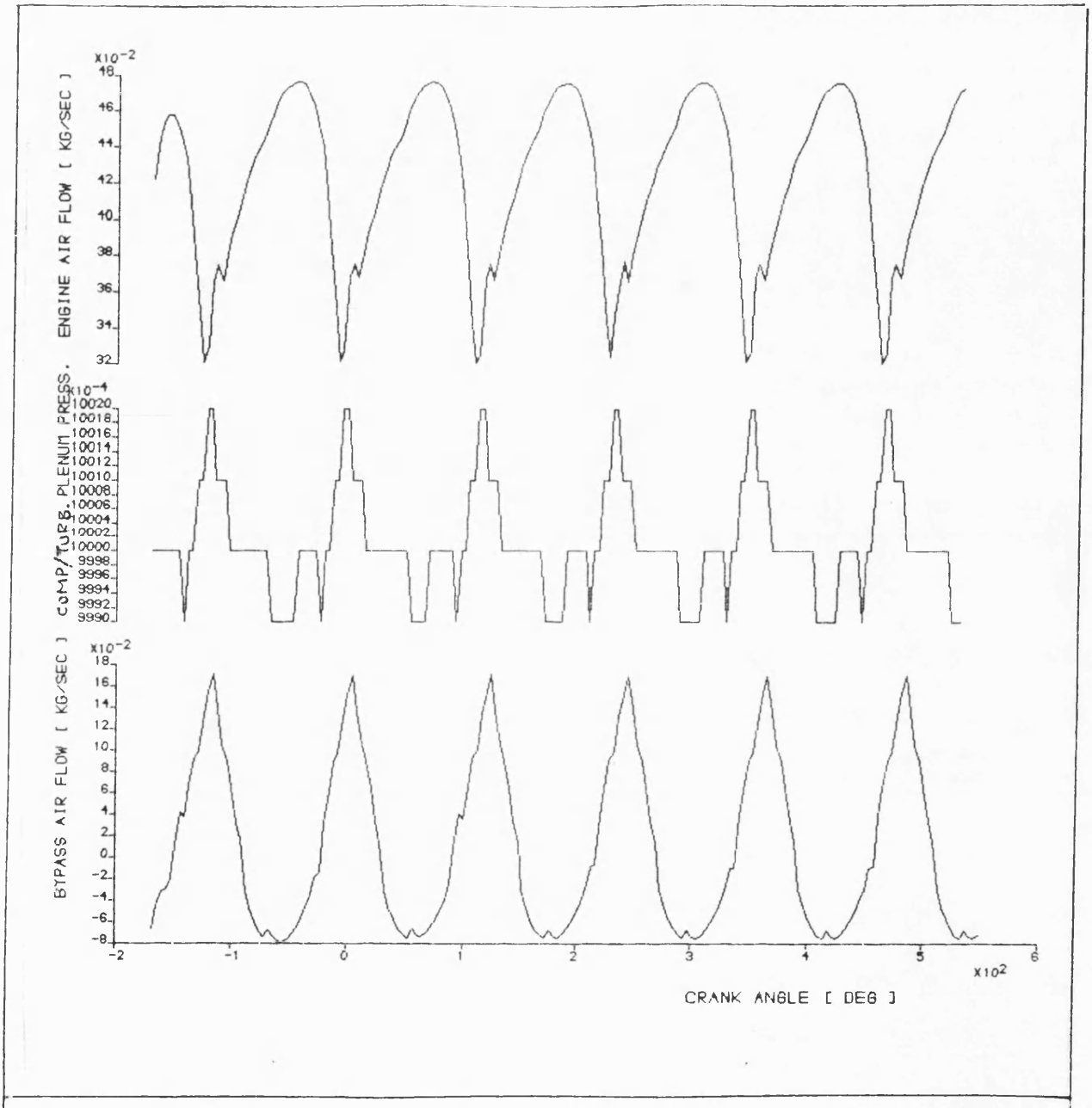

Fig. 6.7, d Graphical summary of cylically varying parameters relevant to table 6.3

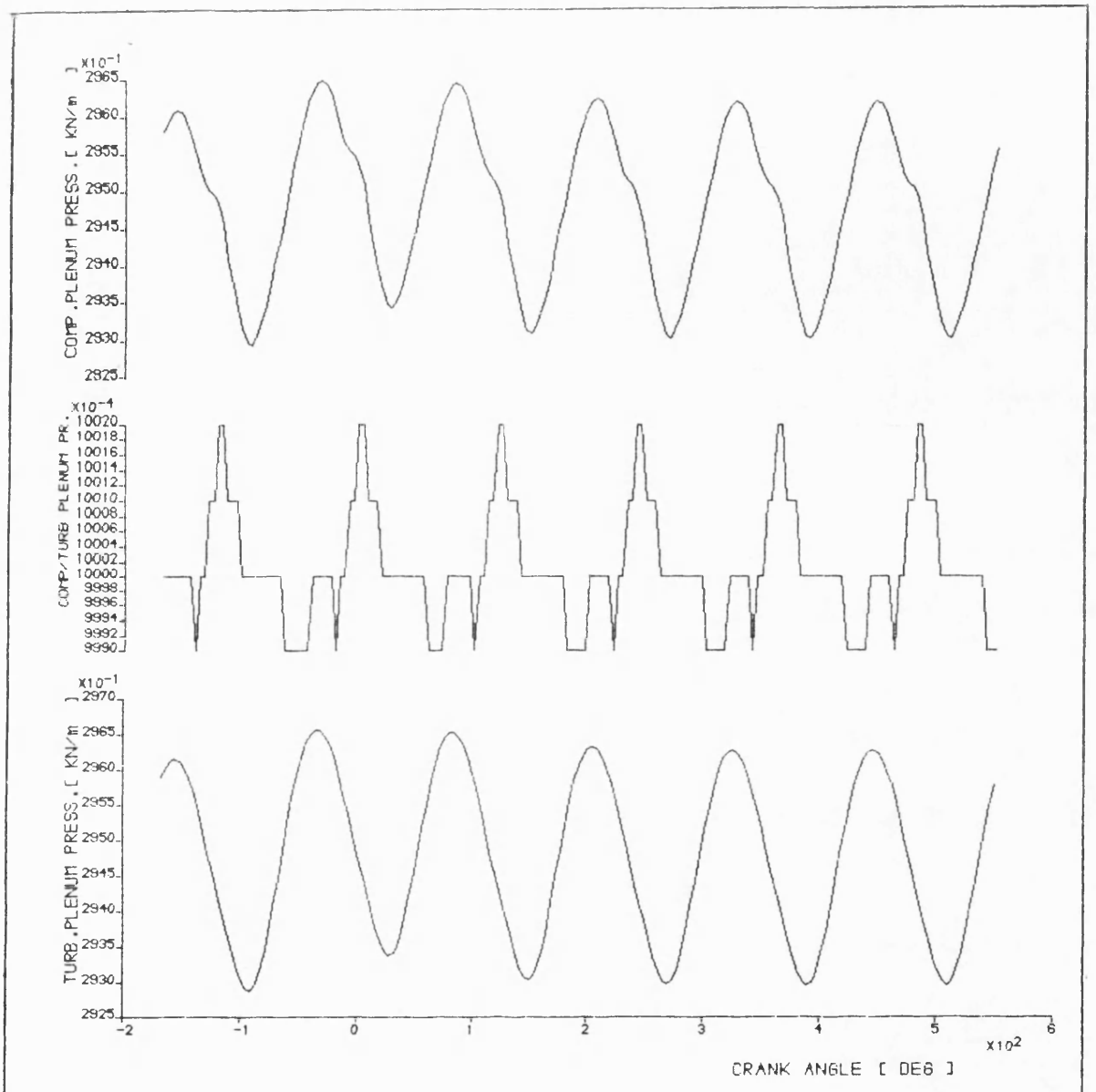

Fig. 6.7,e Graphical summary of cylically varying parameters relevant to table 6.3

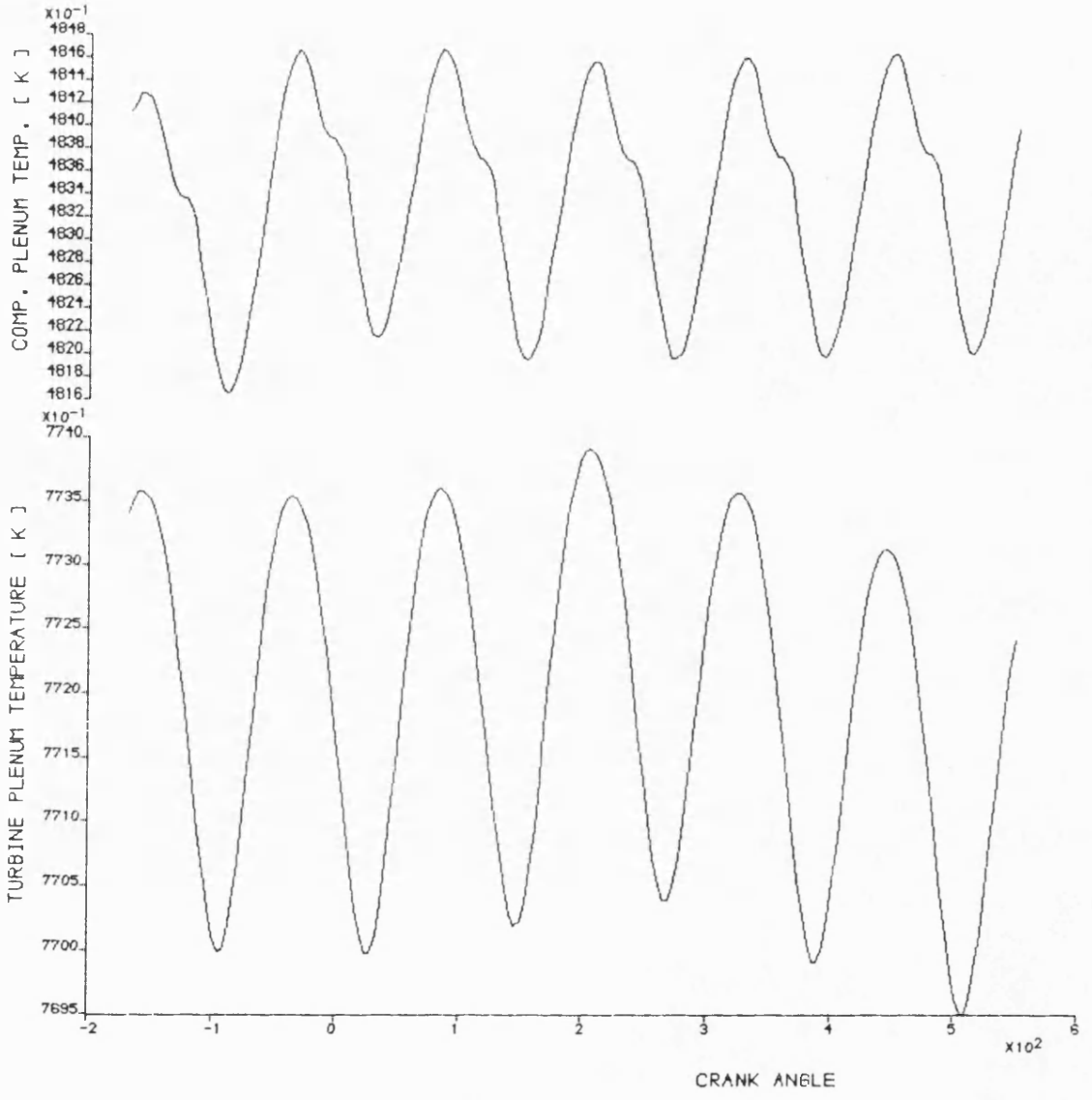

Fig. 6.7, f Graphical summary of cylically varying parameters relevant to table 6.3

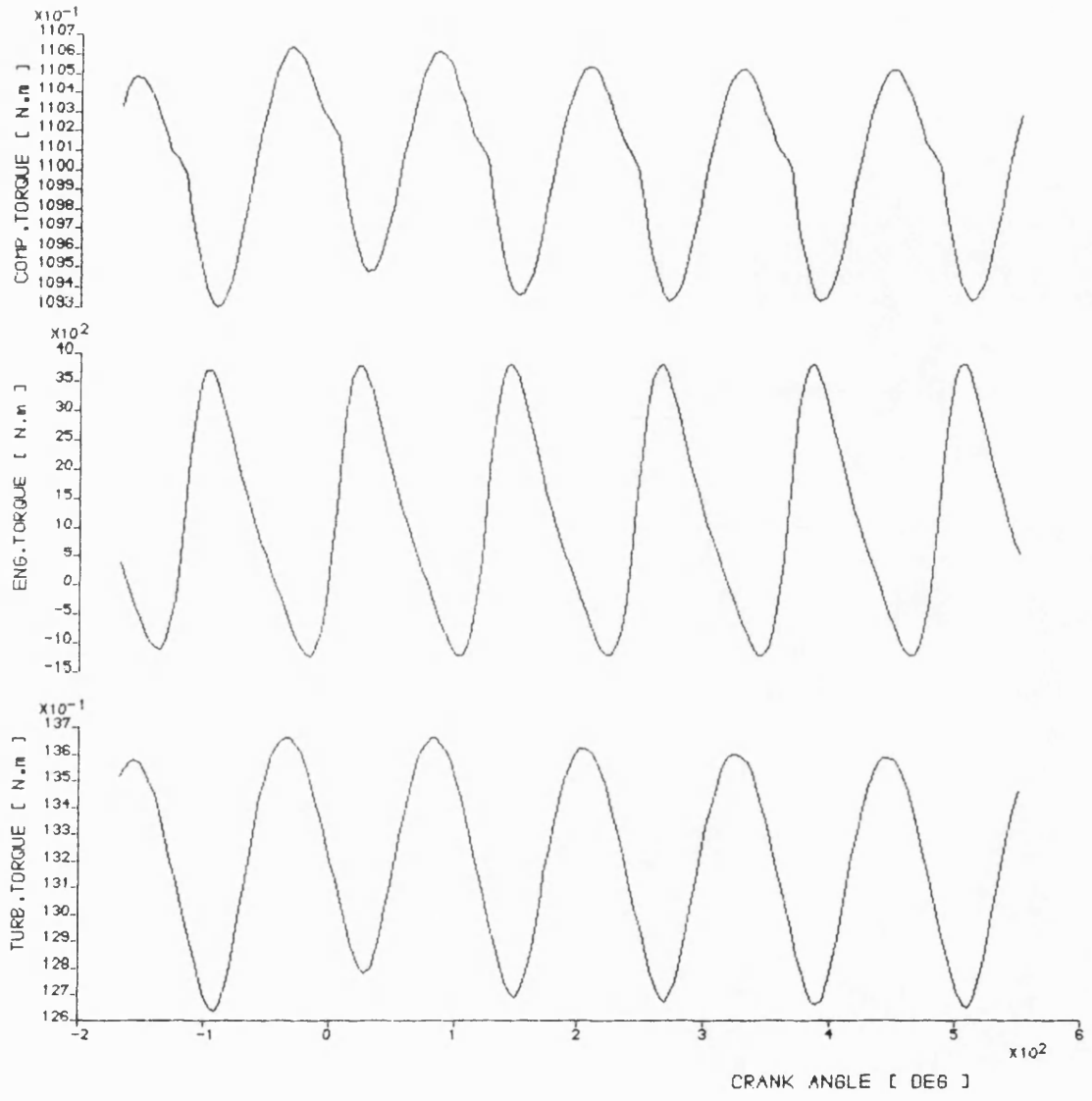

Fig. 6.7,g Graphical summary of cylically varying parameters relevant to table 6.3

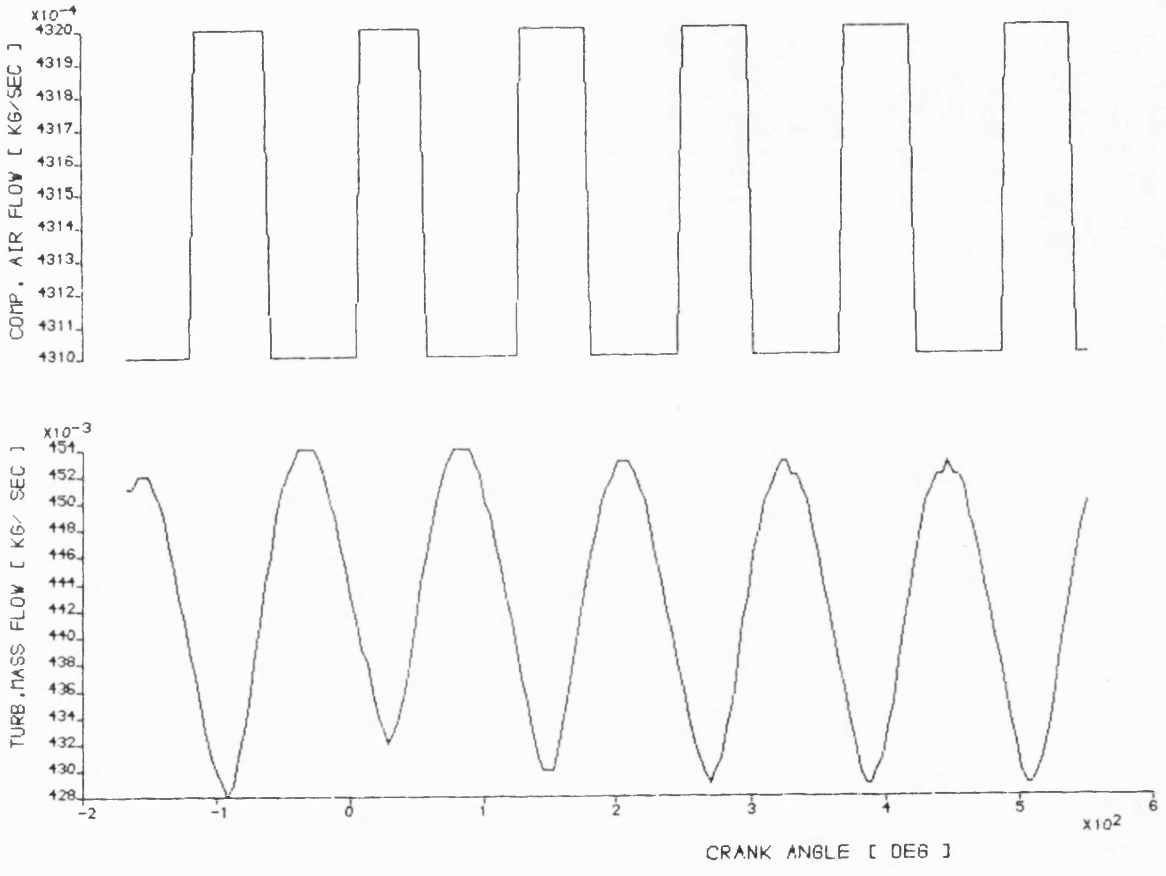

Fig. 6.7, h Graphical summary of cylically varying parameters relevant to table 6.3

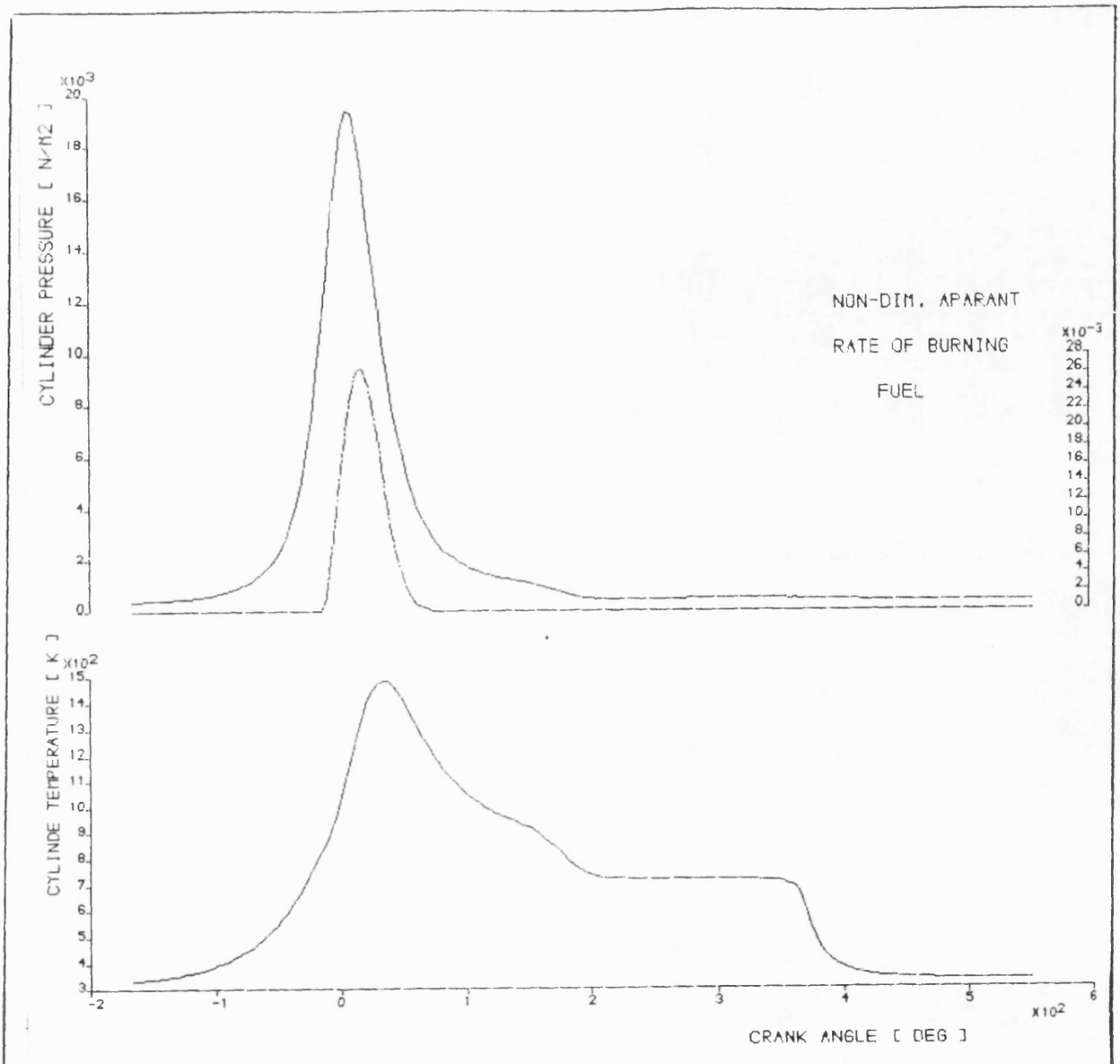

Fig. 6.8,a Graphical summary of cyclically varying parameters relevant to table 6.4

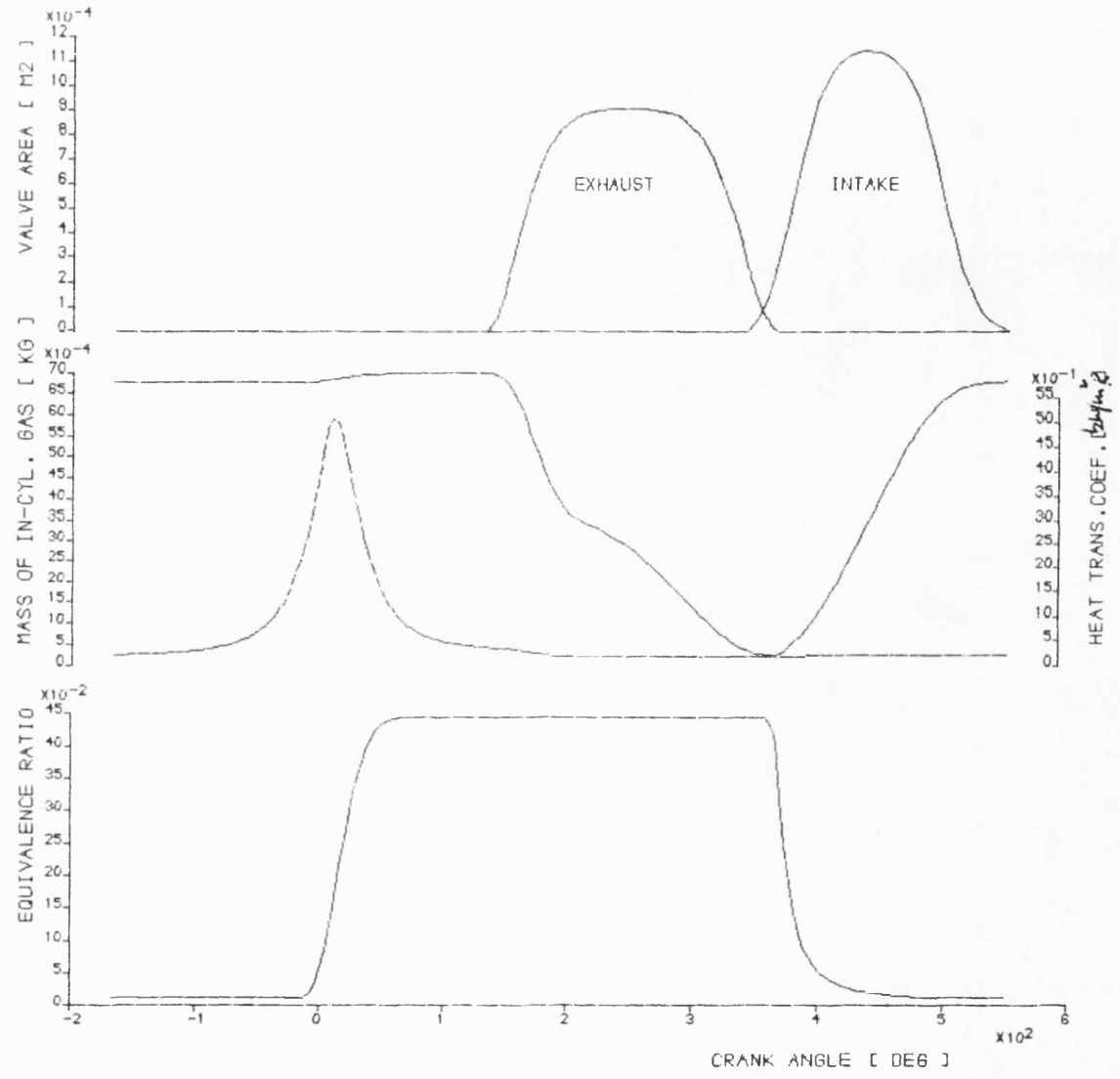

Fig. 6.8,b Graphical summary of cyclically varying parameters relevant to table 6.4

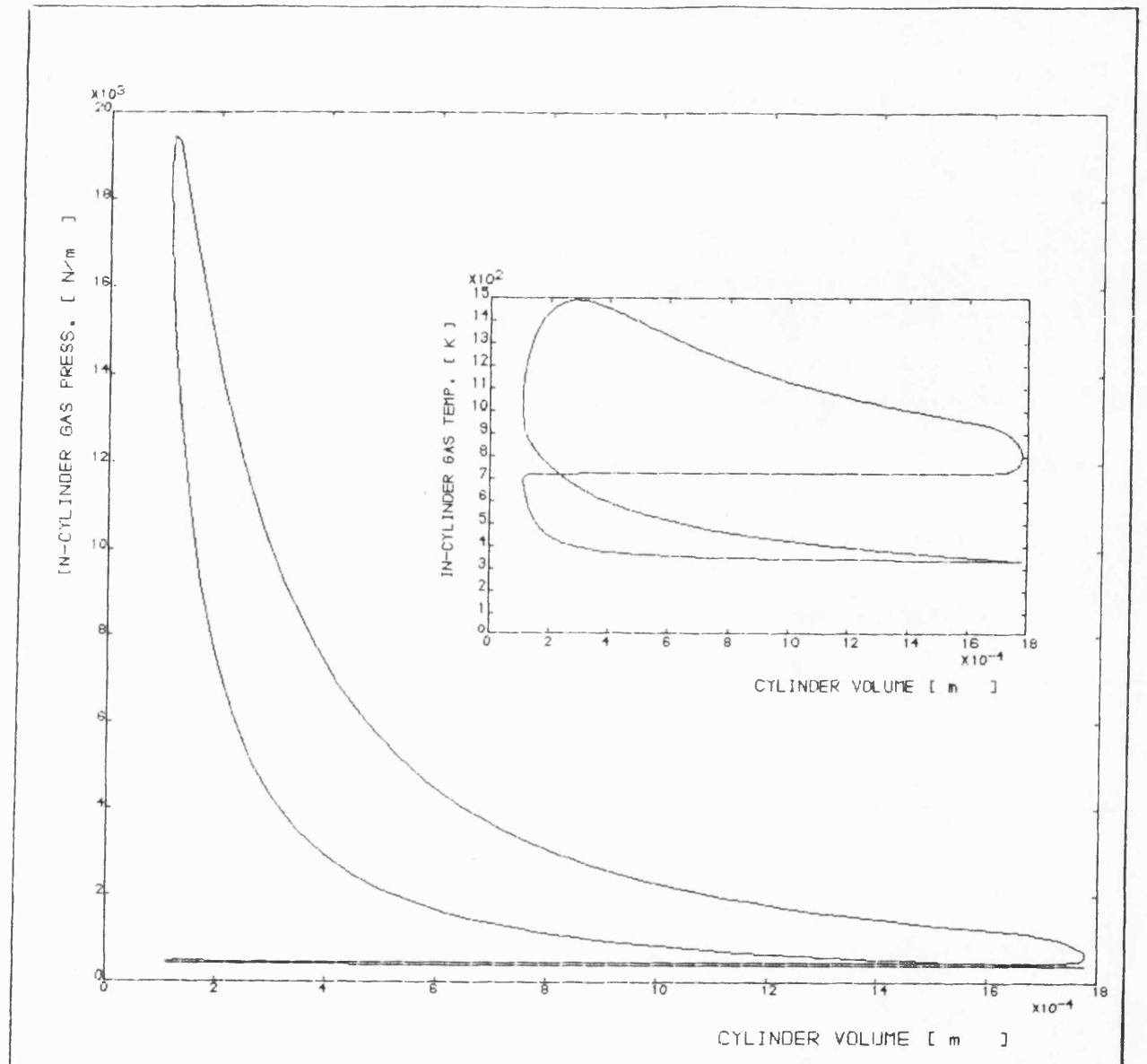

Fig. 6.8,C Graphical summary of cyclically varying parameters relevant to table 6.4

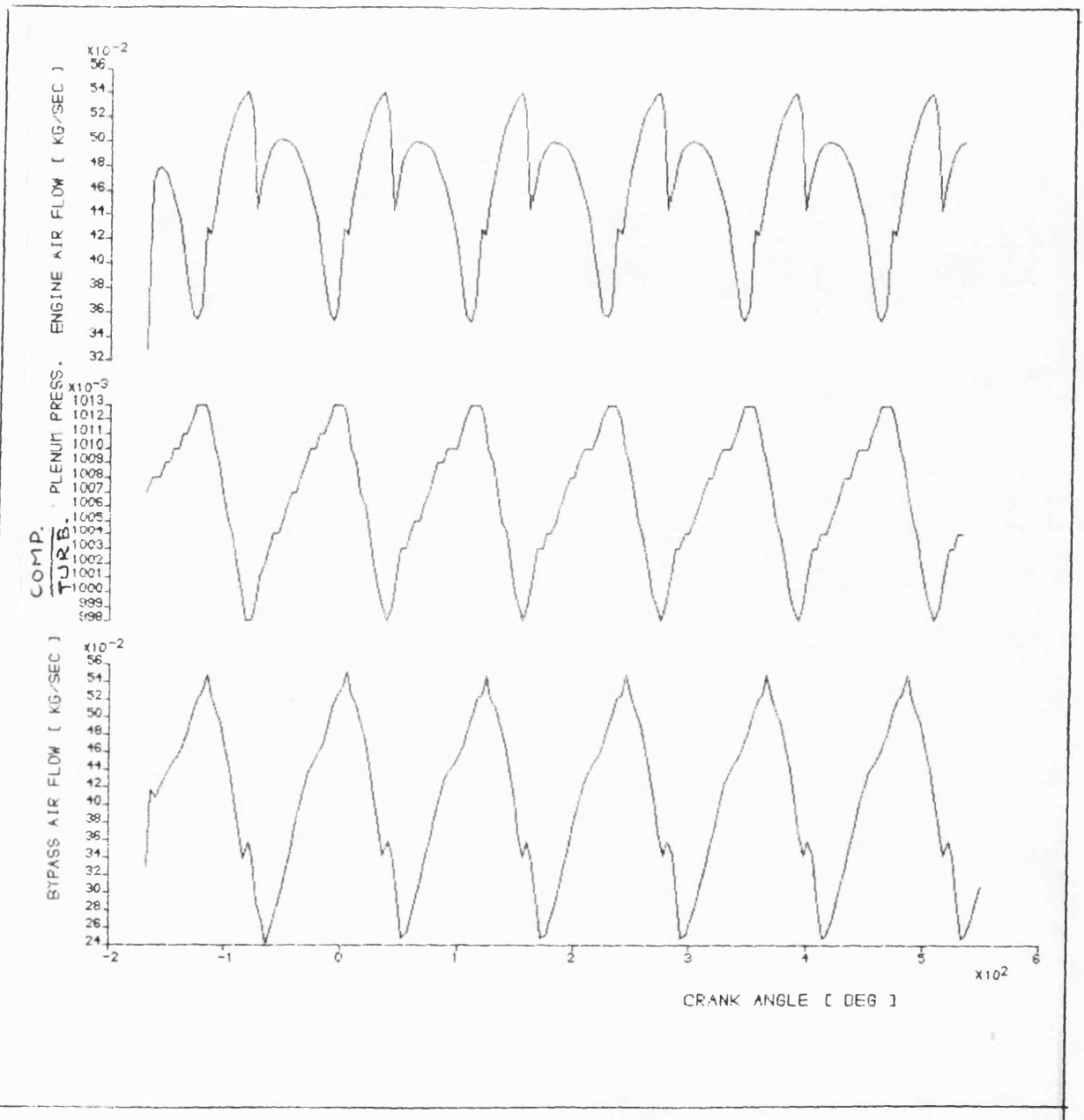

Fig. 6.8,d Graphical summary of cyclically varying parameters relevant to table 6.4

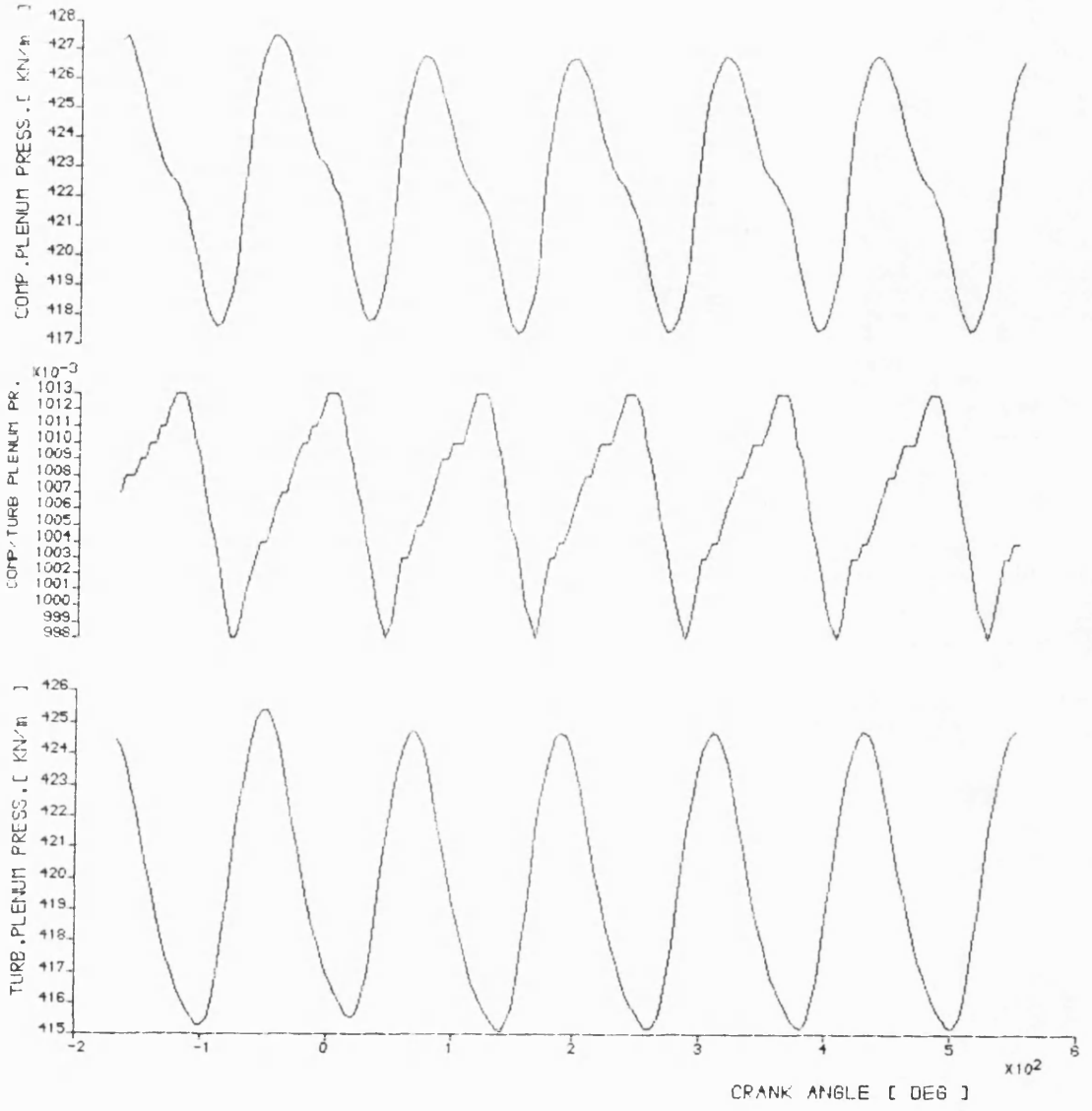

Fig. 6.8,e Graphical summary of cyclically varying parameters relevant to table 6.4

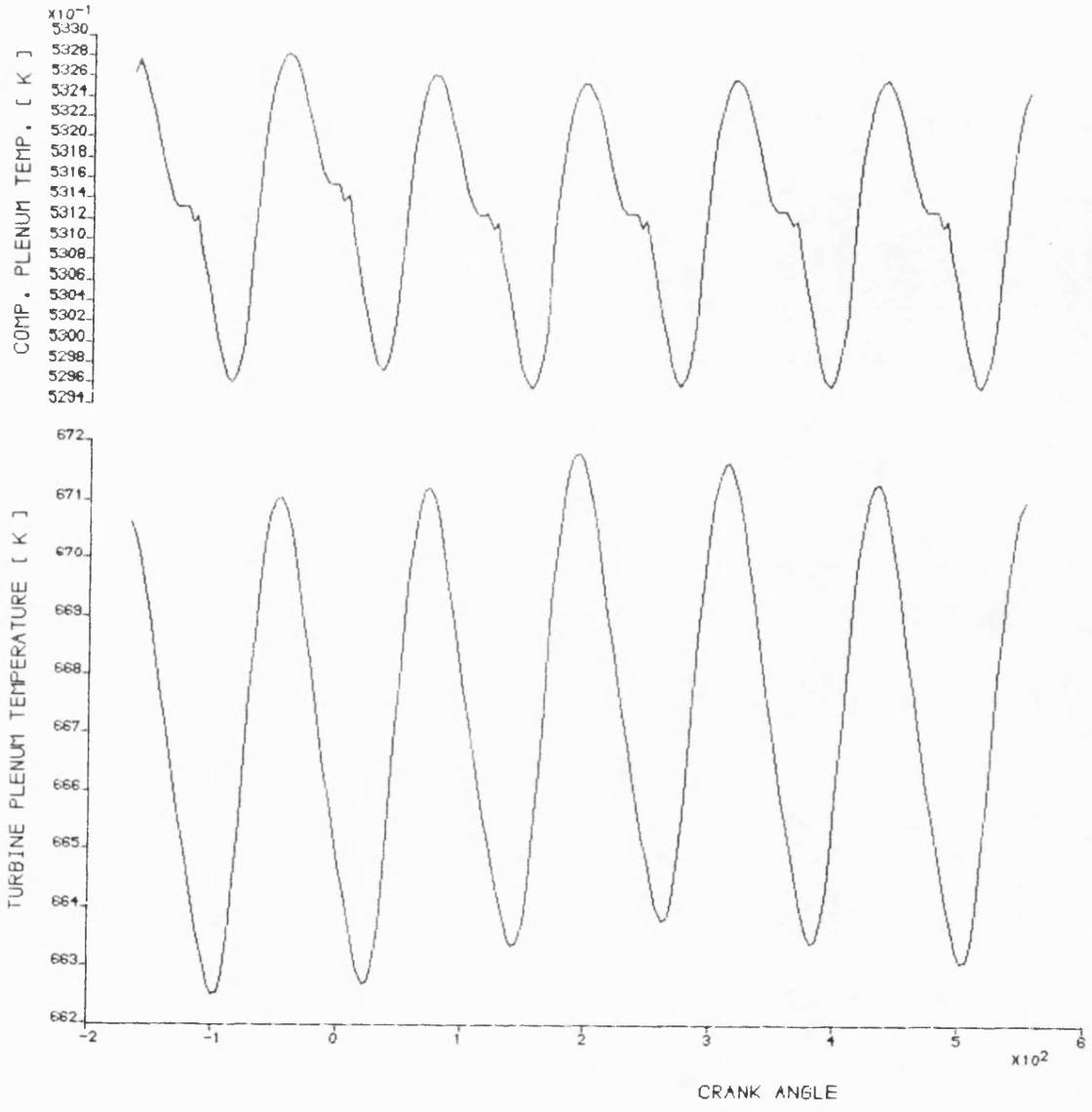

Fig. 6.8, f Graphical summary of cyclically varying parameters relevant to table 6.4

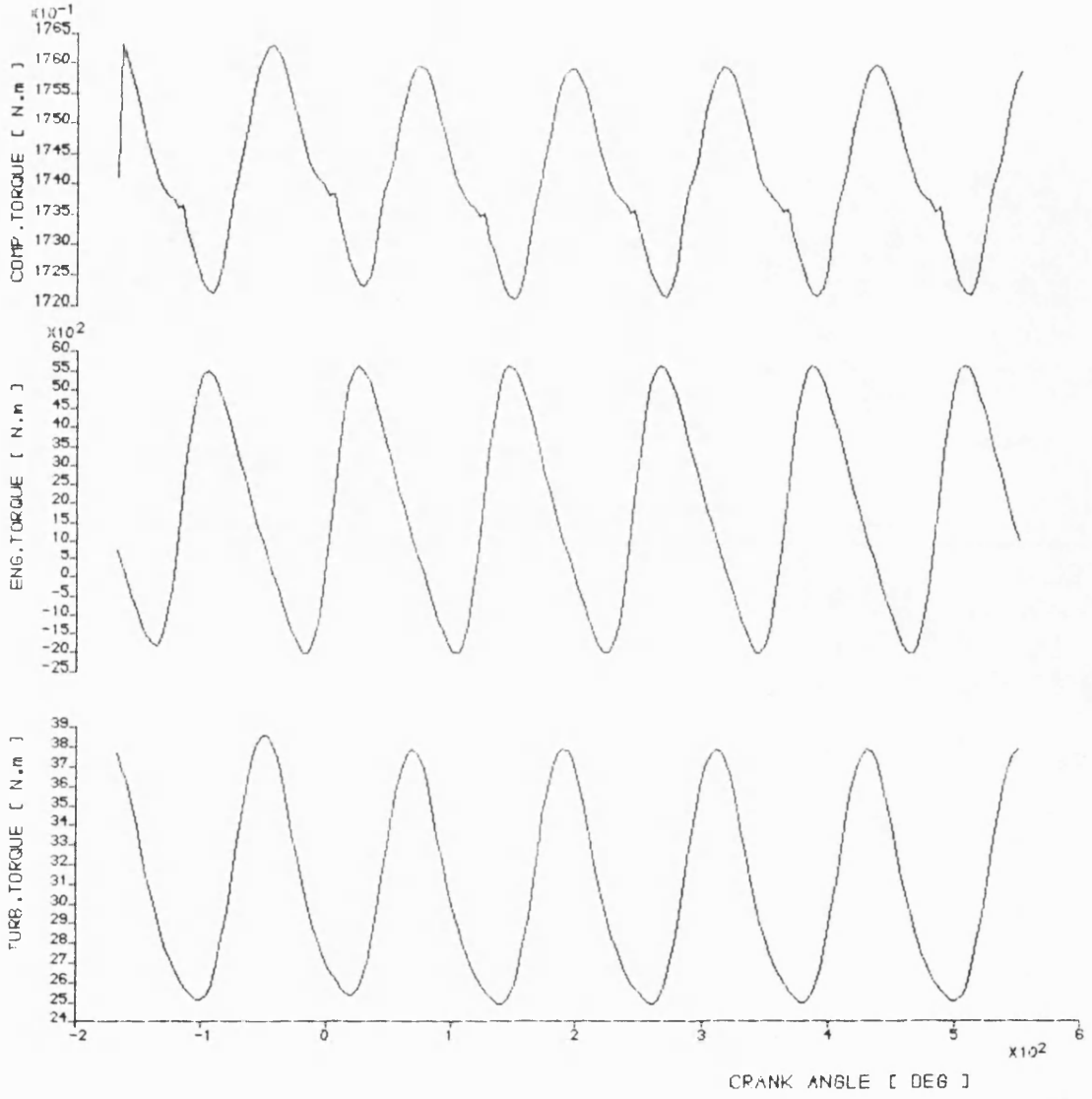

Fig. 6.8,g Graphical summary of cyclically varying parameters relevant to table 6.4

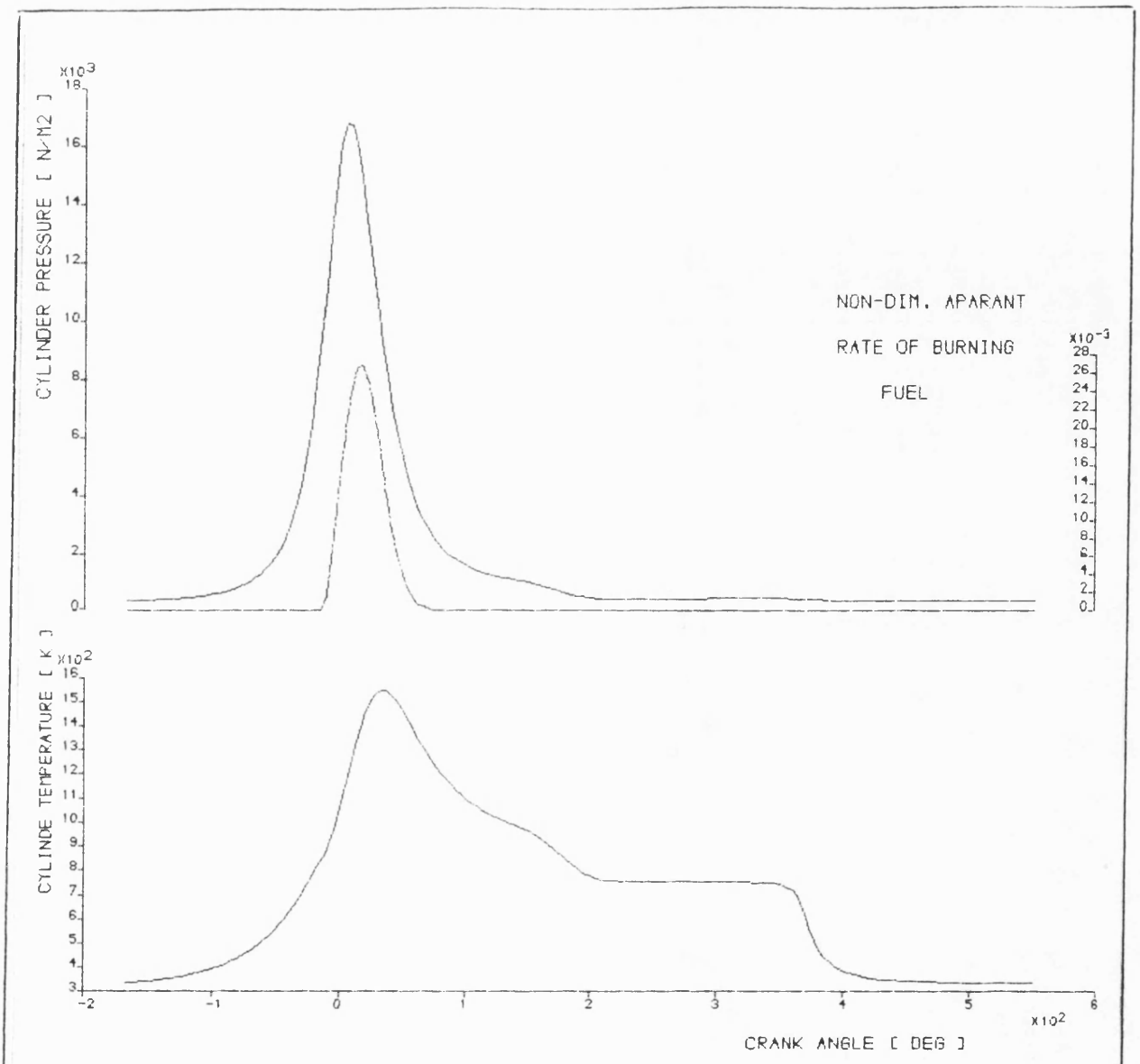

Fig. 6.9,a Graphical summary of cyclically varying parameters relevant to table 6.5

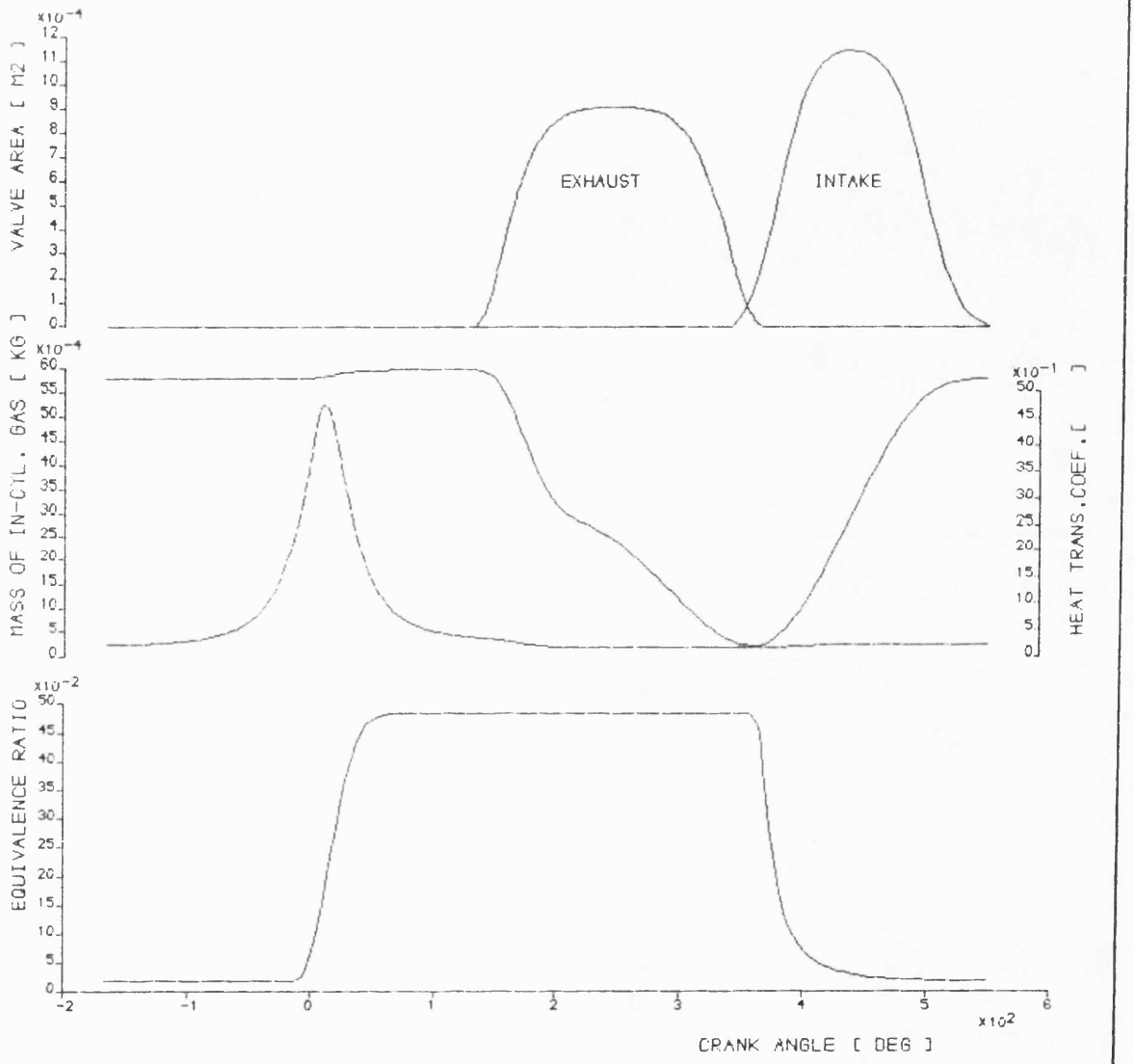

Fig. 6.9, b Graphical summary of cyclically varying parameters relevant to table 6.5

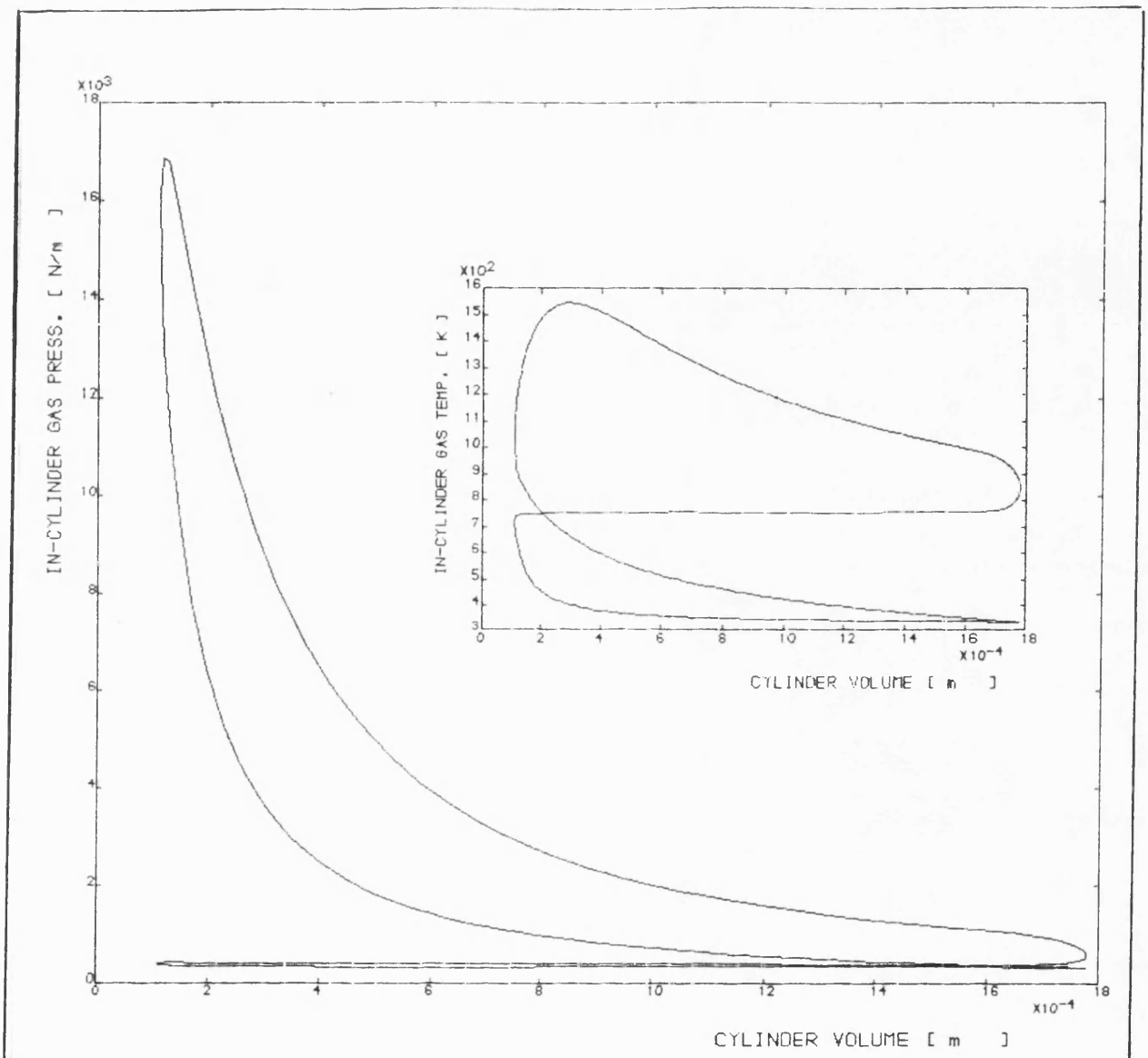

Fig. 6.9,C Graphical summary of cyclically varying parameters relevant to table 6.5

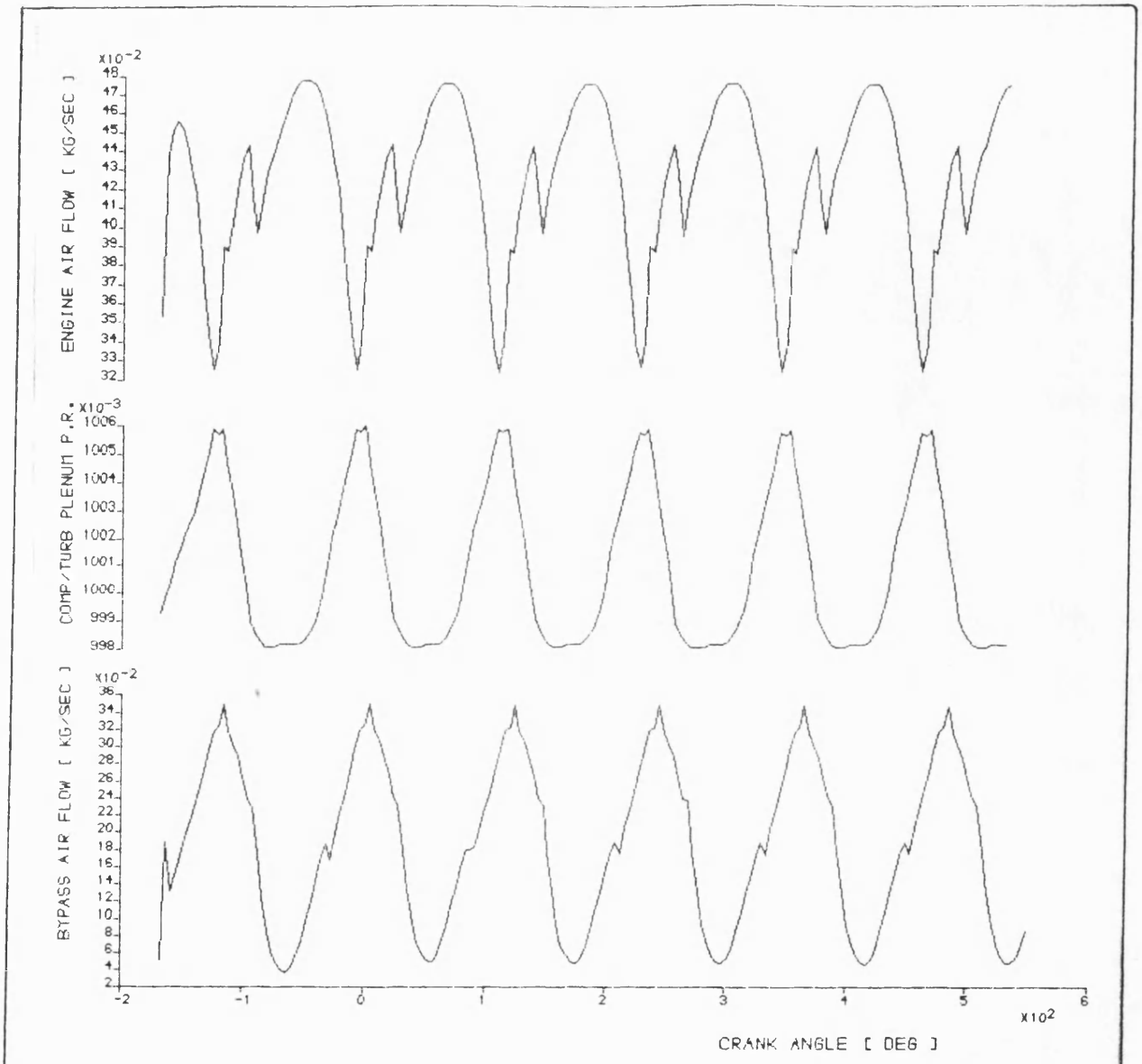

Fig. 6.9,d Graphical summary of cyclically varying parameters relevant to table 6.5

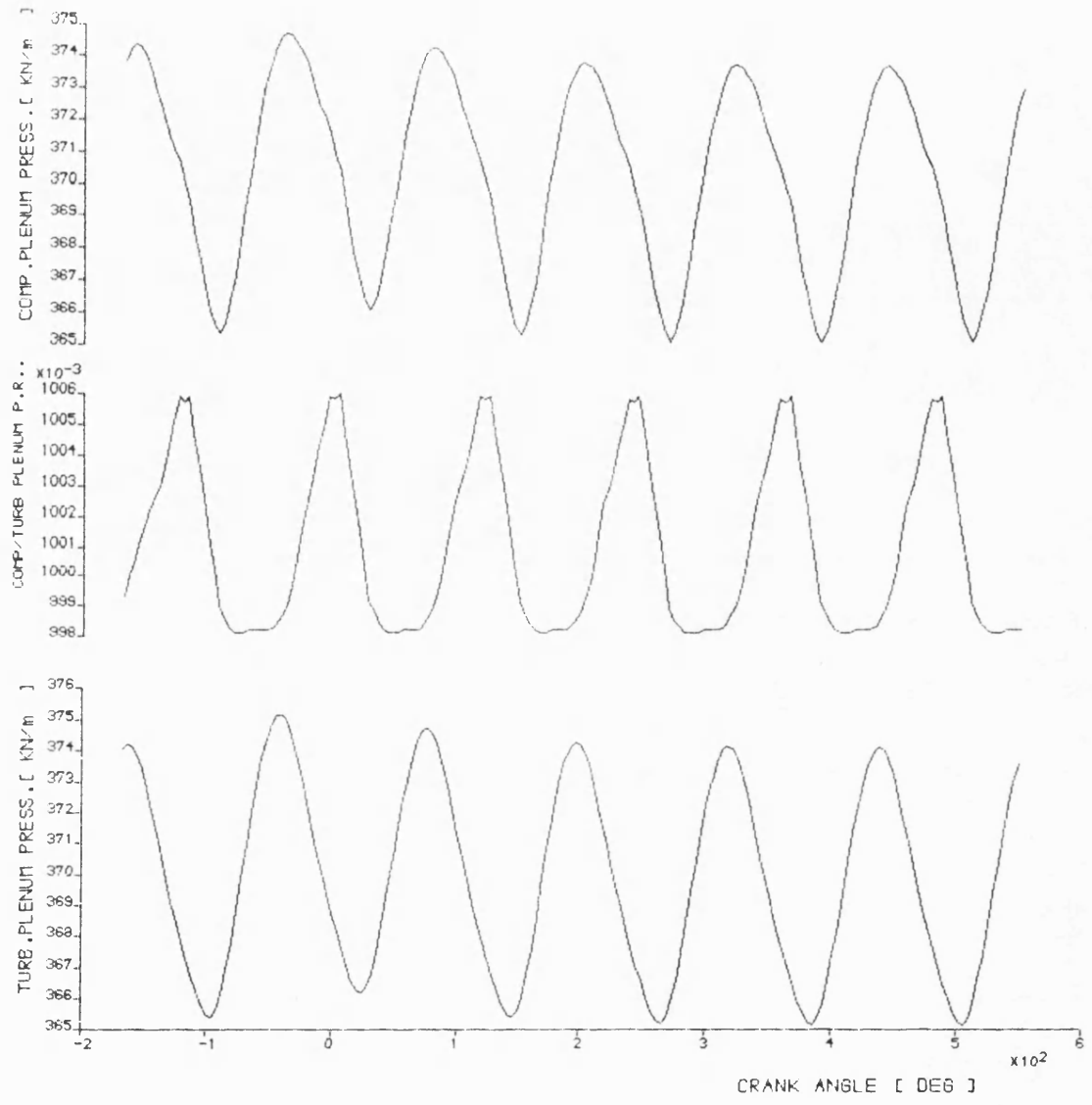

Fig. 6.9, *e* Graphical summary of cyclically varying parameters relevant to table 6.5

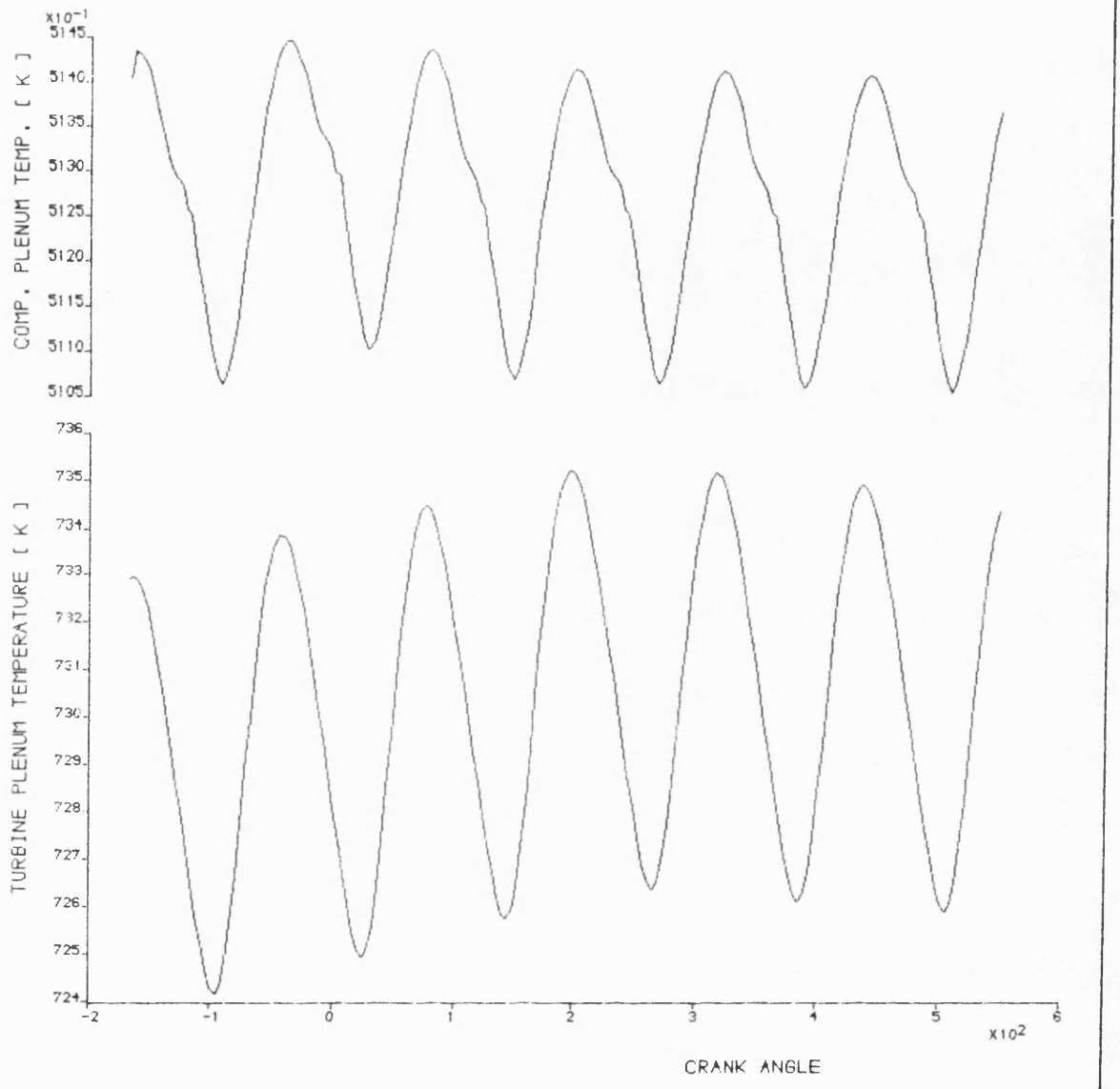

Fig. 6.9,f Graphical summary of cyclically varying parameters relevant to table 6.5

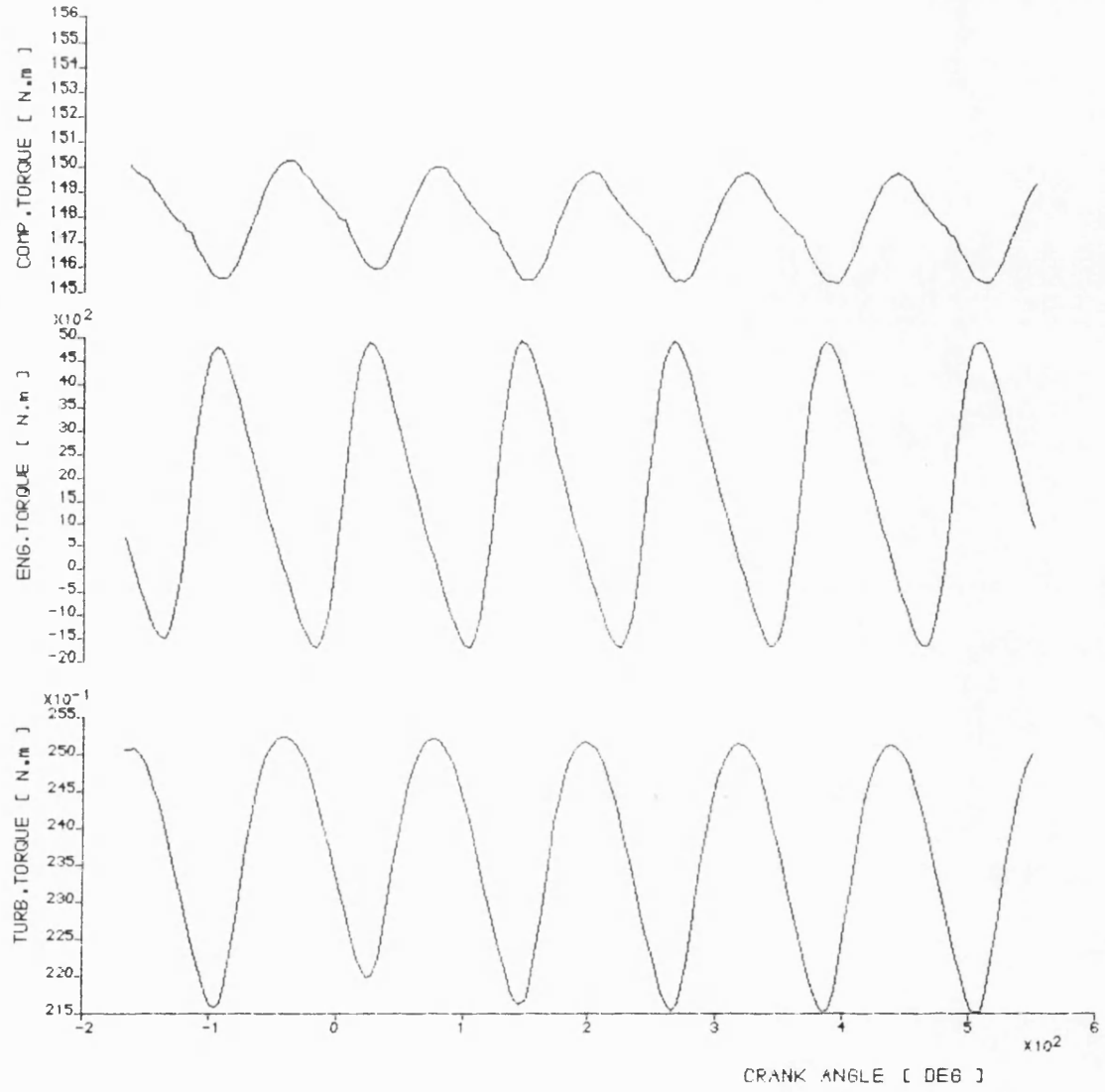

Fig. 6.9,g Graphical summary of cyclically varying parameters relevant to table 6.5

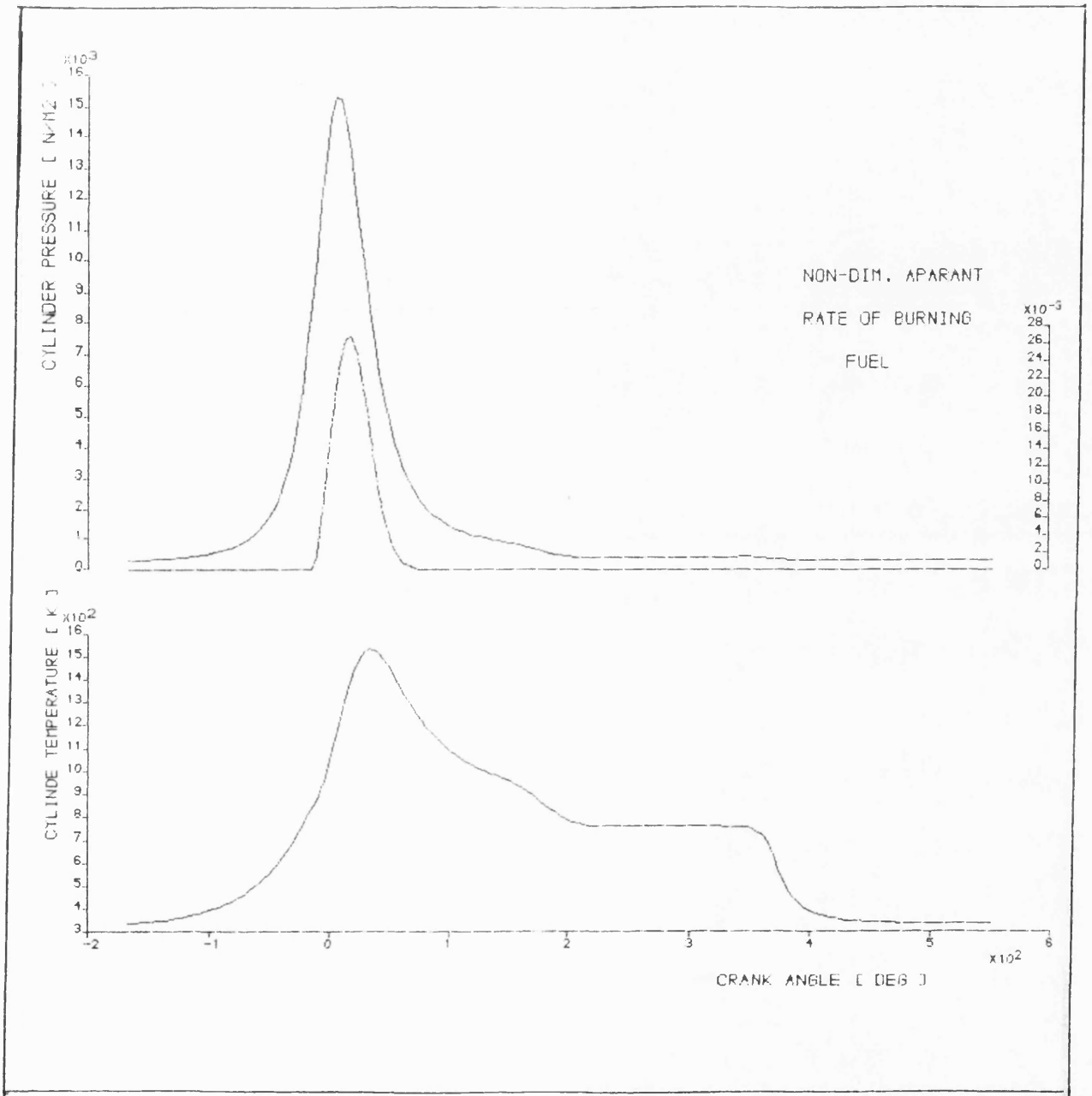

Fig. 6.10,a Graphical summary of cyclically varying parameters relevant to table 6.6

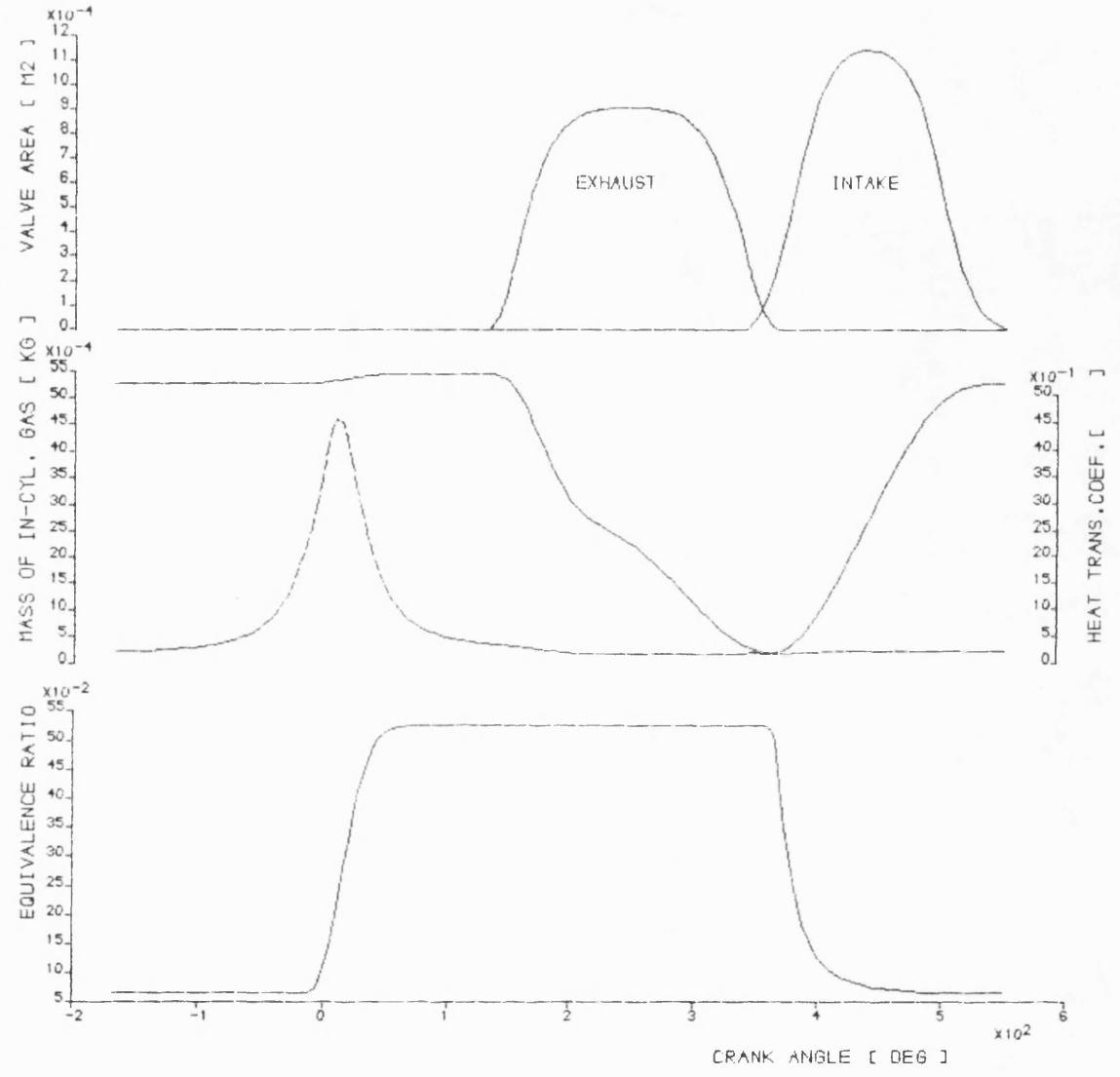

Fig. 6.10, b Graphical summary of cyclically varying parameters relevant to table 6.6

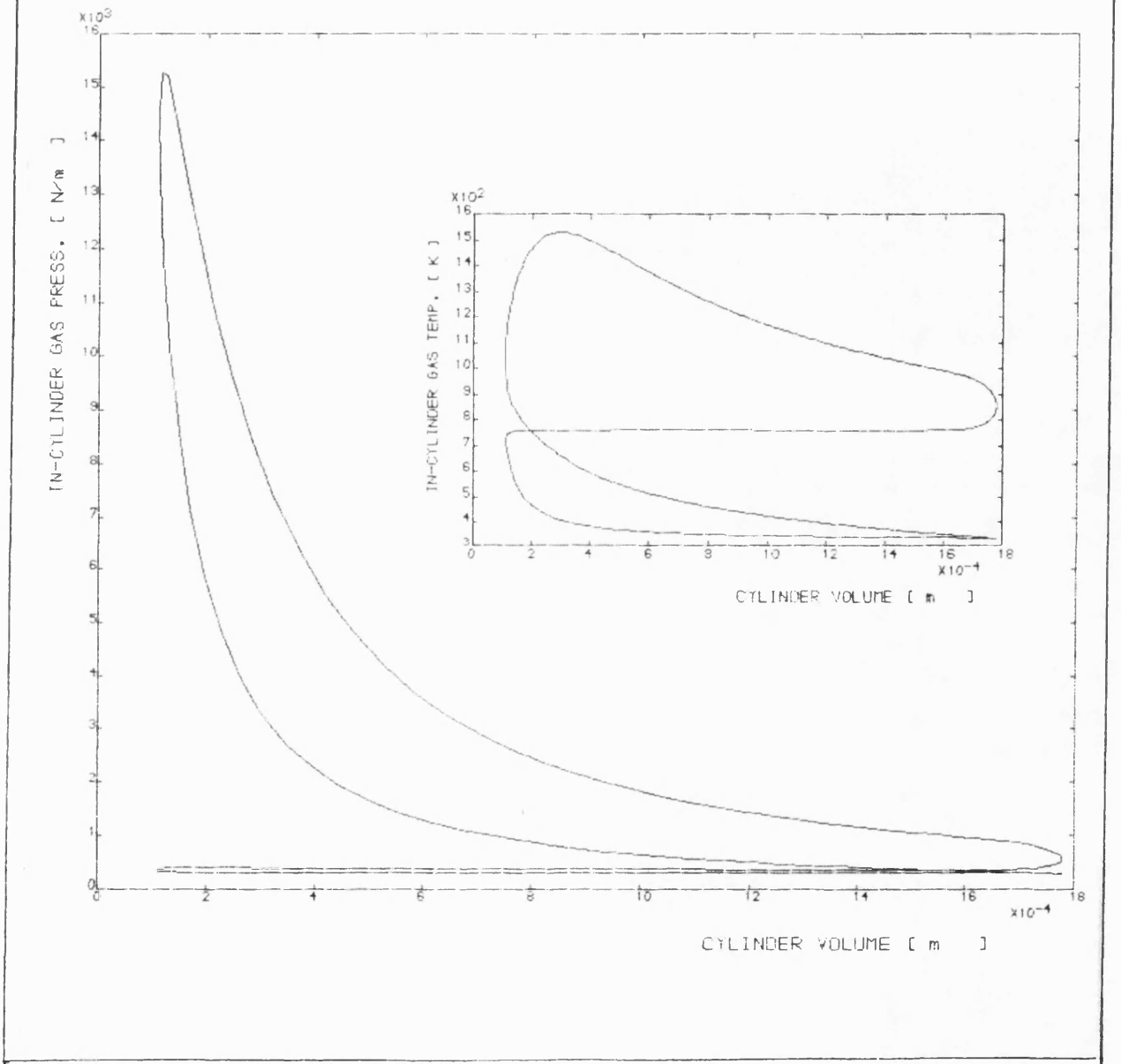

Fig. 6.10,C Graphical summary of cyclically varying parameters relevant to table 6.6

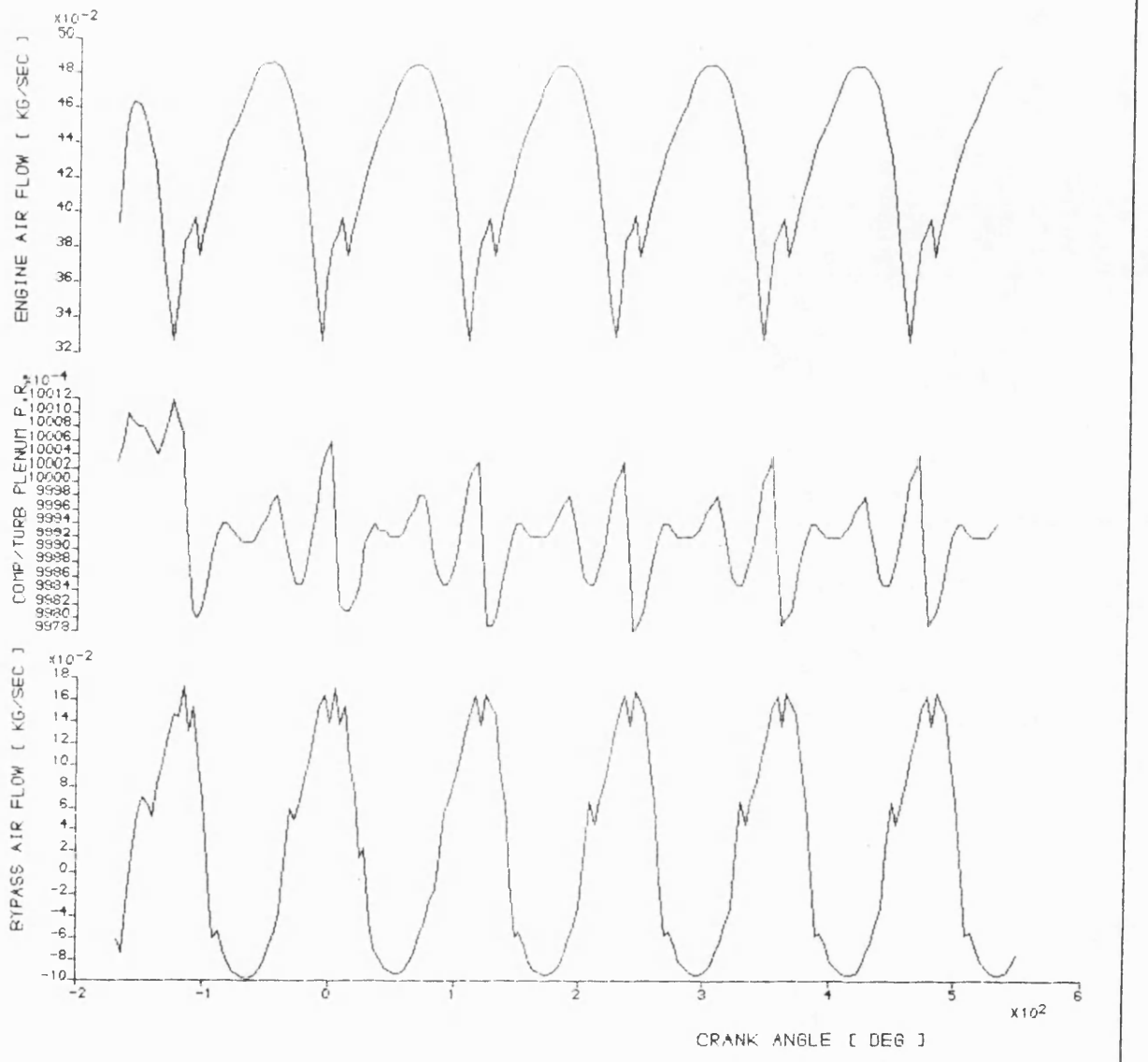

Fig. 6.10, d Graphical summary of cyclically varying parameters relevant to table 6.6

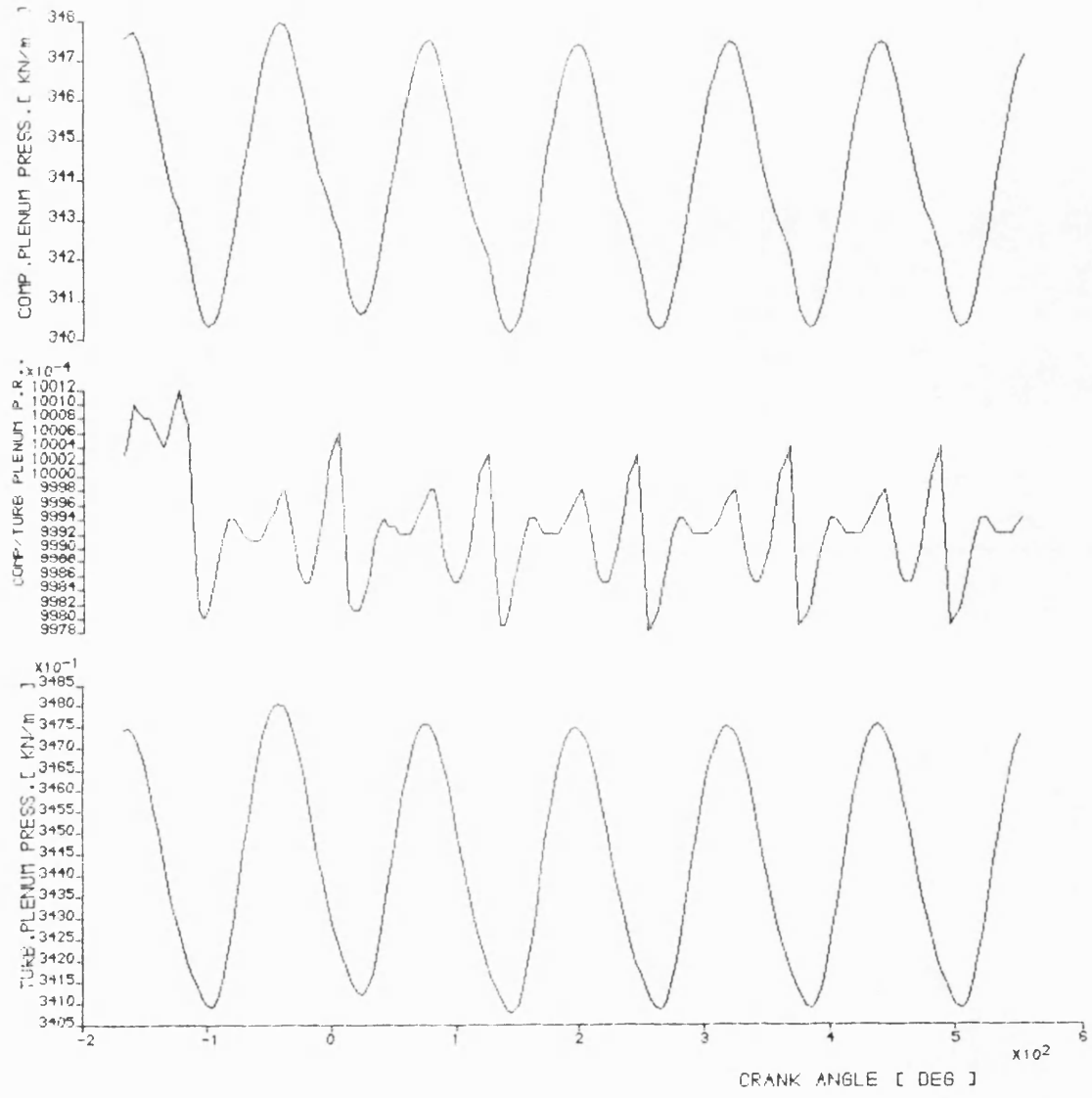

Fig. 6.10,e Graphical summary of cyclically varying parameters relevant to table 6.6

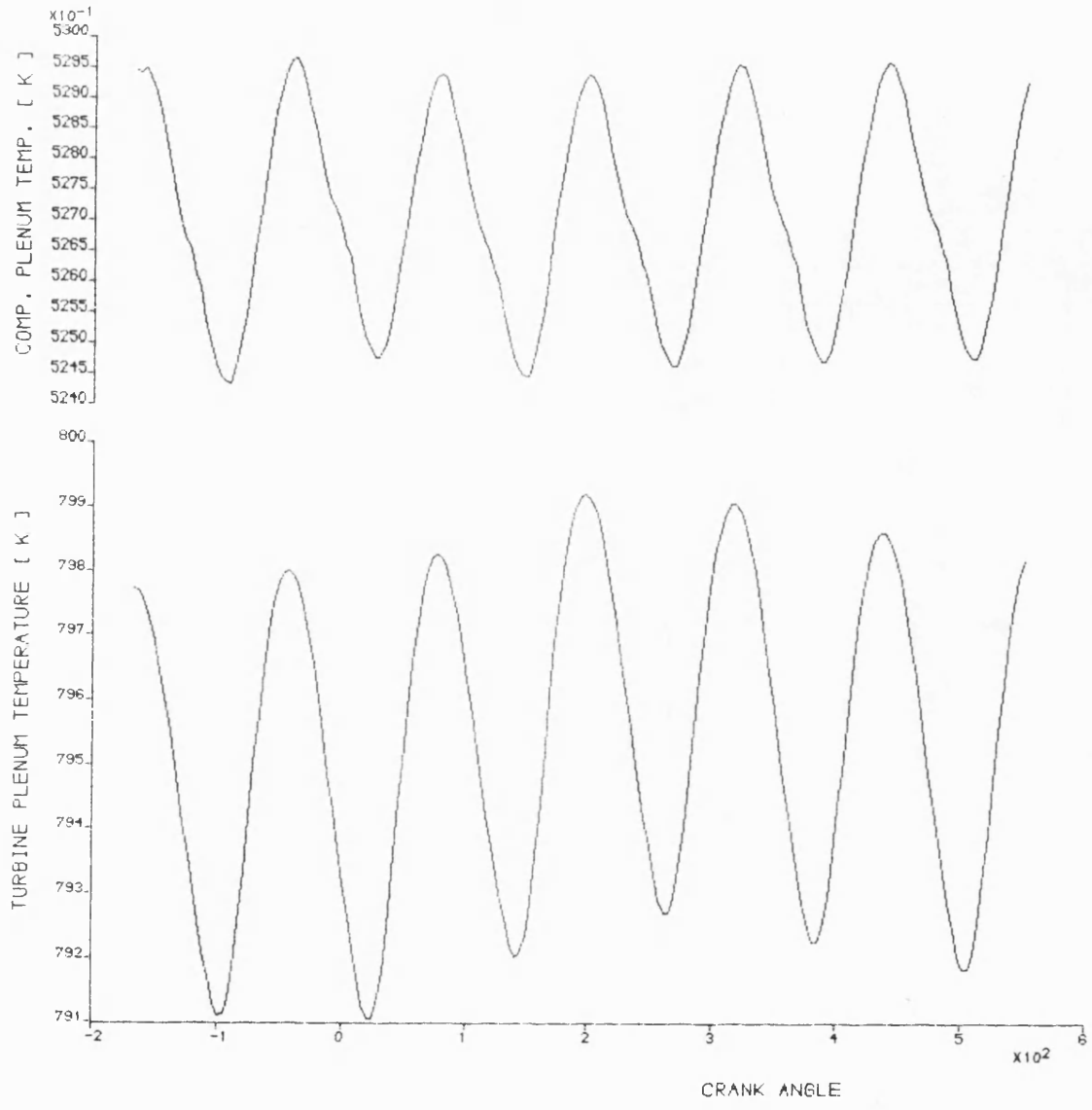

Fig. 6.10,f Graphical summary of cyclically varying parameters relevant to table 6.6

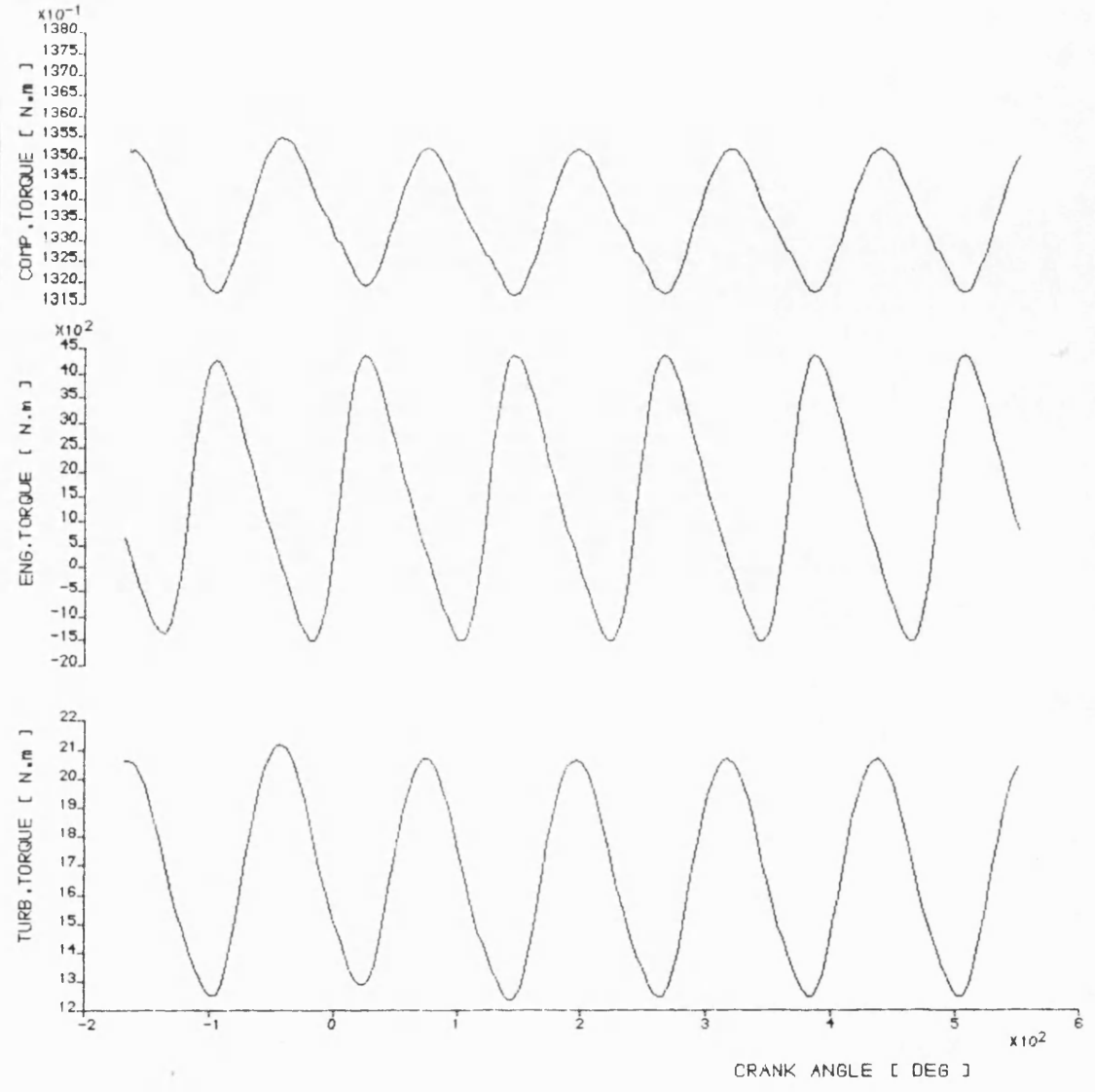

Fig. 6.10,g Graphical summary of cyclically varying parameters relevant to table 6.6

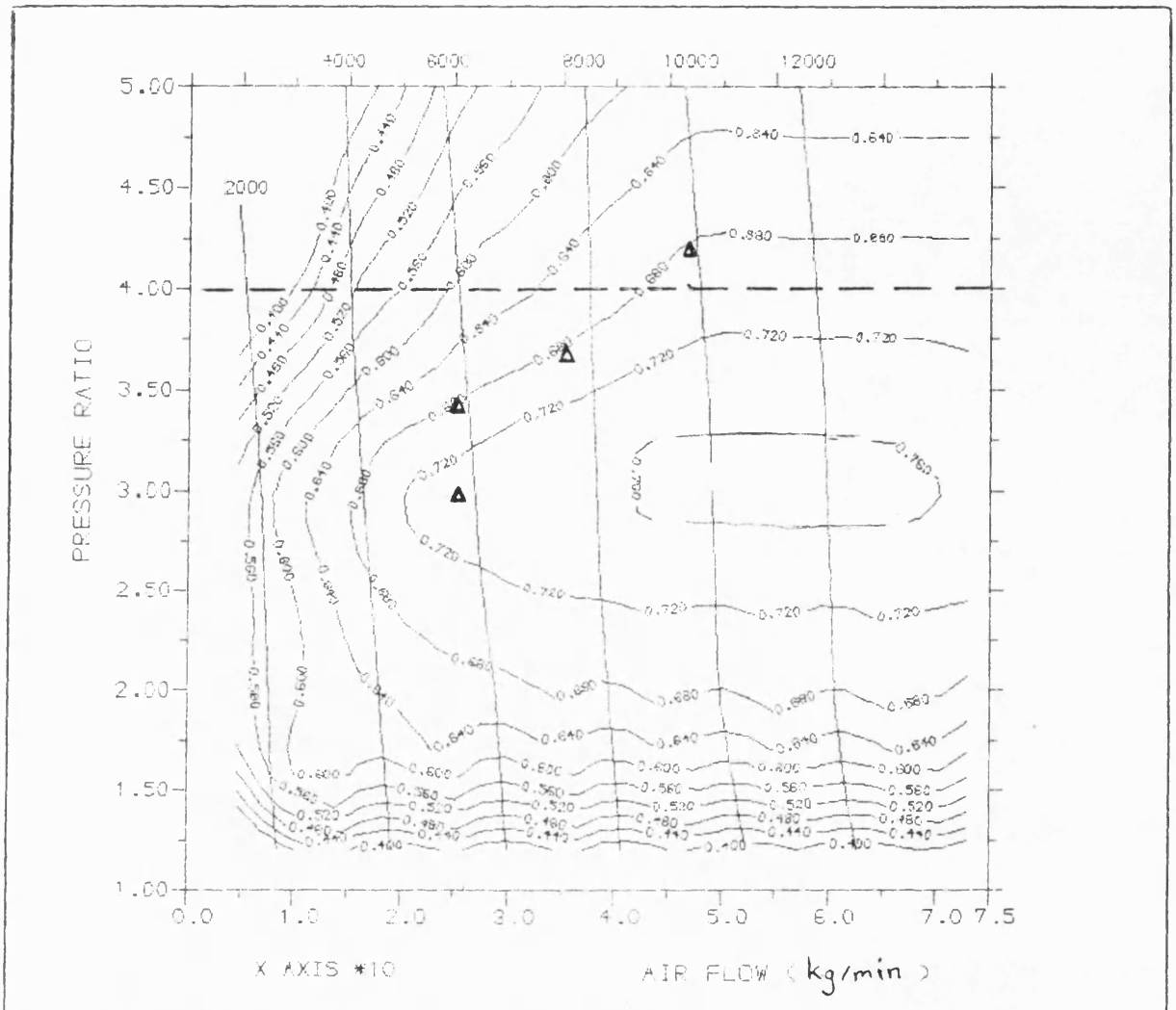

Fig. 6.11,a-c Lysholm compressor characteristics of the L10-DCE with operating points of selected running conditions

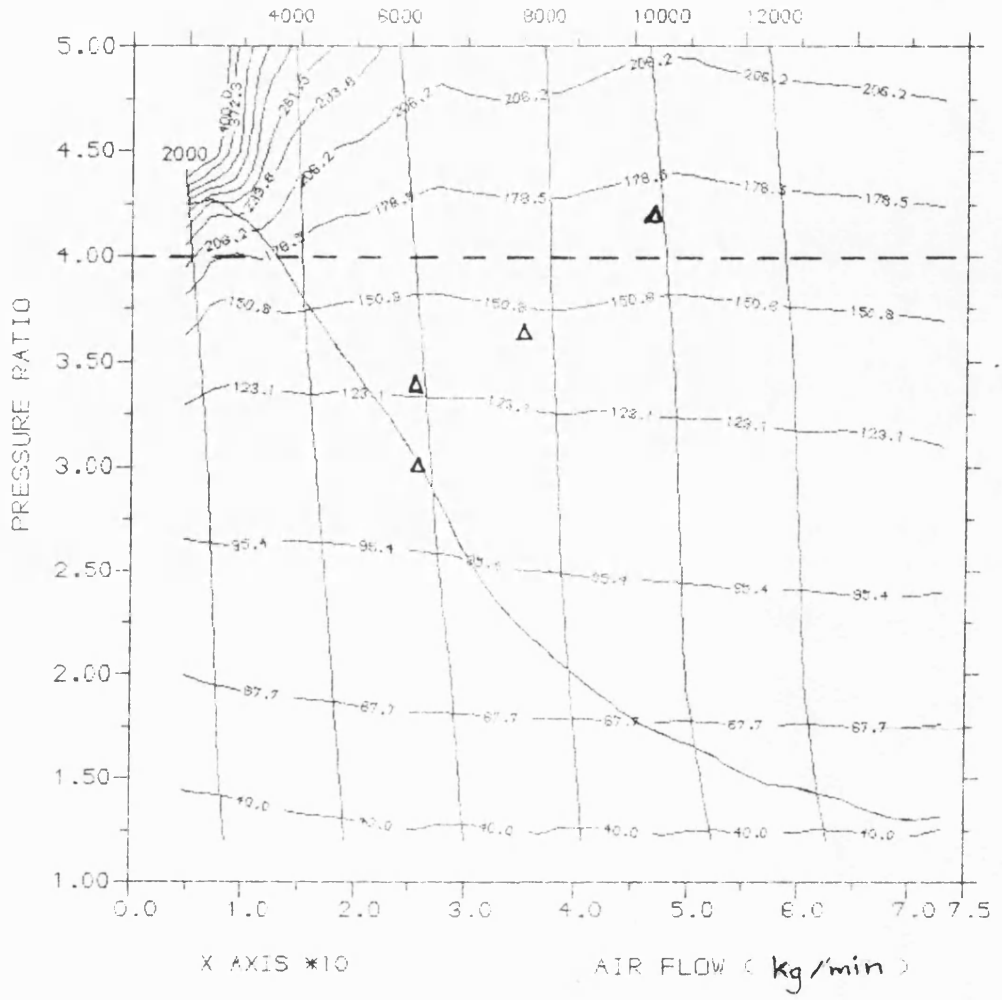

Fig. 6.11,b

LYSHOLM COMPRESSOR TORQUE MAP (S.F.= 1.1)

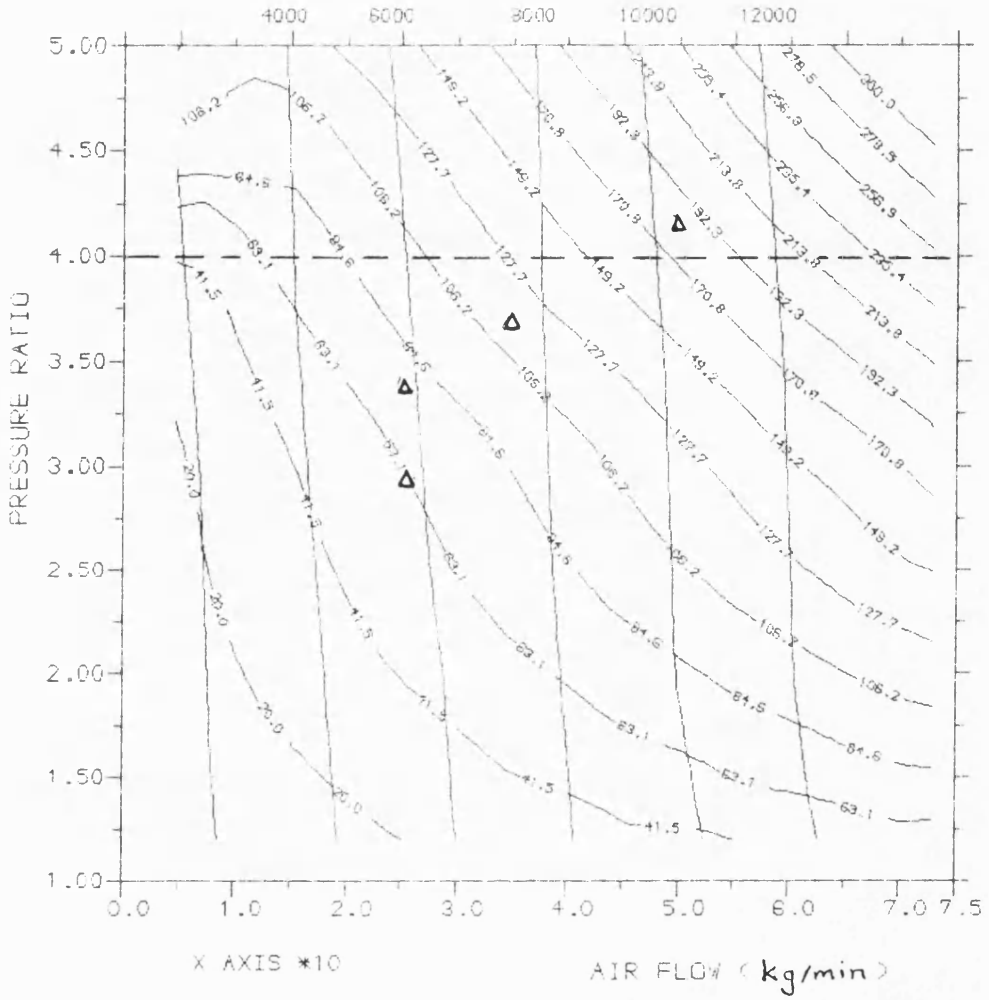

Fig. 6.11,c

LYSHOLM COMPRESSOR POWER MAP (S.F.= 1.1)

CHAPTER SEVEN

SIMULATION OF AN ACCELERATING 650001b TRUCK EQUIPPED WITH THE L10 DIESEL ENGINE IN ITS T/C AND DCE CONFIGURATION USING PROGRAMS 'TRANIC' and 'DCETRAN'

7.1 INTRODUCTION

Chapters 3 and 4 dealt with steady state performance of the L10-T/C engine. This Chapter extends the analysis to the transient performance of this engine in combination with a seven ratio gearbox fitted to a 65000 lb (29,500 kg) truck. The analysis also includes the performance characteristics of its DCE counterpart, under similar running conditions. It is the purpose of the present chapter to compare the very favourable characteristics of the DCE in this respect with those of the T/C engine.

The performance of a T/C Diesel engine under steady or transient conditions is largely governed by engine-turbocharger interaction. When the turbocharger is correctly matched to the engine and the fuel injection system has been optimised, then the compressor will provide sufficient air to maintain good smoke-free combustion during steady running. During a transient, however, the turbocharger is not able to respond to rapid increase in engine power demand and hence air supply to the engine will not be sufficient to ensure complete combustion of the demanded fuel. This deficiency of the turbocharger is called turbocharger lag which is due to either the turbocharger inertia or a delay in required extra exhaust gas energy arriving at the turbine, or a combination of both.

In the case of poor turbocharger acceleration (long lag), the air-fuel ratio becomes excessively rich and black smoke is emitted.

To meet legislation in this respect, Section 1.1.2.E, fuel delivery in T/C Diesel engines during acceleration is usually limited by a device such as boost pressure controlled fuel rack limiter. Although this is an effective technique in solving the problem, it results in a poor engine response.

The DCE, like a naturally aspirated engine, due to its inherently more generous trapped air-fuel ratio, can develop power almost instantaneously in response to sudden power demand free from any type of smoke control requirement. The rapid power development is due to the fact that the inertia of the components directly driven by the engine is greatly reduced. This is because of the interpoisiton of a fully floating epicyclic gearbox between the engine and the load. At the same time, unlike the stepped gearbox usually fitted in trucks powered by T/C Diesel engines, the differential gearing incorporated in the DCE system together with a torque converter interposed between the DCE output shaft and the final drive constitutes a truck drive line with continuously variable speed ratio within the normally required range of about 10:1. This not only prevents any loss of time and energy which accompanies the frequent gear changes required with a stepped gearbox, but also gives the truck better driveability and road performance.

The present analytical investigation of transient behaviour makes use of simple programs based on the application of turbocharger maps and five-point P-V diagram (fig. 2.3) for engine simulation derived from the steady state programs EMAT and DCE2 (see Chapter 2).

7.2 THEORY

7.2.1 Modelling of T/C Engine and Vehicle Dynamics

The analysis and simulation of transient performance of the L10-T/C engine are carried out using the program TRANIC. As described in section 2.4 the mathematical models used are 'quasi-steady' but dynamic parameters are introduced into the simulation to take account of transient phenomena which may be omitted in steady-state models. These mainly include variations of injection parameters (i.e. extent of fuel and timing), shaft speeds and loads and accumulation of gas in mass storage receivers (inlet and exhaust manifolds). The mathematical method for transient response is based on the application of first order differential equations. It should be noted that here integrative techniques rather than iterative ones (as was the case for steady state matching) are employed. The integration is based on the Runge Kutta method, in which different orders can be optionally applied.

Of the major dynamic effects included are speed variations for the engine and turbocharger shafts. The cyclic variations of speed are neglected, and the nominal mean values at each step of calculation are used.

The speed change on both shafts obeys the relation :

$$\tau = I\dot{\omega} \qquad [7.1]$$

where τ = net torque on a shaft (Nm), I = moment of inertia ($kg.m^2$) and $\dot{\omega}$ = angular acceleration $\frac{rad}{s^2}$.

ENGINE DYNAMICS. The net torque acting on the engine crankshaft is the difference between the engine output and that absorbed by the load. The crankshaft dynamics are then represented by the differential equation :

$$\frac{dN_{ENG}}{dt} = \frac{60}{2\pi} (\tau_{ENG}-\tau_L)/(I_{ENG}+I_L) \qquad [7.2]$$

where N_{ENG} = engine speed (rpm), t = time (sec)

τ_{ENG} = engine output torque, I_{ENG} = engine moment of inertia

τ_L = applied load torque, and I_L = load moment of inertia.

This expresses that the crankshaft accelerates subject to the combined inertias of engine and load.

Hence, the speed at the end of a calculation step, N_{ENG_2} is given by :

$$N_{ENG_2} = N_{ENG_1} + \frac{60}{2\pi(I_{ENG}+I_L)} \int_0^{\Delta t} (\tau_{ENG}-\tau_L)dt \qquad [7.3]$$

where N_{ENG_1} = the initial speed and Δt = calculation time step. The calculation step can be freely fixed irrespective of the engine firing interval.

VEHICLE DYNAMICS. In the case of a vehicle such as a truck, the load is created by the various resistances to truck motion, and by acceleration.

Fig. 7.1 shows the drive line arrangement of a truck. The tractive resistance of the truck, F_{tract} is made up of the rolling friction, F_r, aerodynamic drag, F_d, and climbing resistance, F_s, as follows :

$$F_{tract} = F_r + F_d + F_s \qquad [7.4]$$

$$= f_r.W + 0.1389\ \rho\ f_d\ A\ (v+v_o)2 + W \sin \gamma.$$

where : W is the weight of truck (N)

A is the frontal area of truck (m^2)

f_r is coefficient of rolling friction

f_d is coefficient of air drag

ρ is the air density (1.202 kg/m^3)

v and v_o vehicle velocity and head wind velocity (m/sec)

γ is the road slope angle

The tractive torque required from the engine, τ_L, to overcome this resistance is

$$\tau_L = \eta_{tans} \cdot R_{tyre} \cdot F_{tract}/(r_b.r_g) \qquad [7.5]$$

where η_{trans} = efficiency of power transmission

R_{tyre} = the dynamic tyre radius (m)

r_b = back axle gear ratio

r_g = gearbox gear ratio

Another parameter in equation 7.2 which requires determination is the load or the equivalent vehicle moment of inertia, I_L. This is the sum of the drive-train moments of inertia, I_D, and a referred vehicle mass term:

$$I_L = I_D + \frac{W}{g} R^2_{tyre} \ (1/r_b.r_g)^2 \qquad [7.6]$$

The moment of inertia of a multi-cylinder reciprocating engine, I_{ENG}, varies depending on the crank angle position but since this effect as against, I_L, is small, for the purpose of the present work, I_{ENG} is assumed constant.

The vehicle acceleration is directly related to the drive-train angular acceleration by :

$$\frac{dv}{dt} = \frac{2\pi}{60} \cdot \frac{R_{tyre}}{r_b.r_g} \cdot \frac{dN_{ENG}}{dt} \qquad [7.7]$$

TURBOCHARGER DYNAMICS. These are defined by the following differential equation :

$$\frac{dN_{T/C}}{dt} = \frac{60}{2\pi I_{T/C}} \ (\tau_{TURB} - \tau_{COMP} - \tau_F) \qquad [7.8]$$

where $N_{T/C}$ = turbocharger speed (rpm)

I_{TC} = turbocharger moment of inertia (kg.m2)

τ_{TURB}, τ_{COMP}, τ_F = turbine, compressor and bearing friction torque (Nm)

This equation is again integrated over each calculation step.

7.2.2 Modelling of Governor Dynamics

One of the major difficulties encountered in modelling the transient performance of Diesel engines is that of obtaining reliable values for the dynamic response of the engine governor. The problem arises mainly in the assessment of the source of errors in overall engine performance since it is difficult to ascertain whether these are due to the engine or governor models.

The type of governor required depends on the engine application. Vehicular engines are fitted with an all speed governor which is operative over the whole of the speed range and which responds to speed demand signals represented by accelerator pedal position irrespective of load. Maximum speed is determined by maximum rack position (rated condition) together with governor droop. Minimum speed is determined by the minimum rack stop.

SPEED DROOP. A governor is primarily characterized by the slope of the speed droop, σ, which essentially constitutes the control characteristic of its negative feedback system. This is defined as follows :

$$\sigma = \frac{N_{FL} - N_{NL}}{N_{NL}} \cdot 100\% \qquad [7.9]$$

A smaller speed difference between the top no-load speed, N_{NL}, and the top full load speed, N_{FL}, generates a smaller speed droop, and causes the governor to hold a specified speed more precisely.

MECHANICAL GOVERNOR MODEL. The characteristics of the all-speed governor are shown in fig. 7.2 illustrating how the governor operates at idle and when the engine has reached its maximum speed.

Fig. 7.3 represents the assumed response of rack movement against time for a step increase in demand. Mathematically, a time constant T_{gov} is defined by assuming that the rack will travel at a constant velocity equal to the initial slope of :

$$\frac{dr}{dt} = \frac{r_f - r_i}{T_{gov}} \qquad [7.10]$$

where r is the rack position (with arbitrary scale), t is time in sec, T_{gov} is the governor time constant in sec and indexes 'i' and 'f' refer to initial and final position of the rack. This equation expresses that the rack travels to the final position from the initial position in T_{gov} seconds.

If, however, the integration time interval Δt, used in the program is less than T_{gov}, then the new position of the rack after Δt sec is found from

$$r' = r_i + \frac{r_f - r_i}{T_{gov}} . \Delta t \qquad [7.11]$$

At the beginning of the next time interval it is again assumed that the rack will travel at a velocity equal to the new slope given by :

$$\frac{dr}{dt} = \frac{r_f - r'}{T_{gov}} \qquad [7.12]$$

and it will travel to a new position indicated by r" after the next Δt sec as follows :

$$r'' = r' + \frac{r_f - r'}{T_{gov}} . \Delta t \qquad [7.13]$$

This process is repeated for every step until the final position is approached. A shorter integration interval, makes this response follow the originally assumed response.

However, the rack response is also a function of engine speed and consequently the above treatment has to be modified to include this effect.

The steady state behaviour of rack against engine speed is shown in fig. 7.2. The slope of each line is given by :

$$\frac{dr}{dN_{ENG}} = \frac{r_{max} - r_{min}}{\Delta N_{ENG}} = s_d \qquad [7.14]$$

Therefore, for any given governor set point such as N_o and engine speed, N_{ENG}, the rack position is found from

$$r'_{max} = r_{min} + s_d \cdot (N_{ENG} - N_o) \qquad [7.15]$$

During the first integration step, the rack will move with a velocity given by equation 7.10. Hence r_f can be substituted for r'_{max} in equation 7.15 i.e.

$$r_f = r_{min} + s_d \cdot (N_{ENG} - N_o) \qquad [7.16]$$

Assuming that the rack travel is from 0 i.e. r_{min}, then equation 7.10 will change into a final form as follows :

$$\frac{dr}{dt} = \frac{S_d \cdot (N - N_o) - r_i}{T_{gov}} \qquad [7.17]$$

This constitutes a first order differential equation for rack position only when $\Delta t < T_{gov}$.

BOOST CONTROLLED REGIME. In fig. 7.2, in the range between minimum and

maximum speeds, engine torque is determined only by the position of the accelerator. However, in order to improve the smoke emission characteristic of a vehicular T/C engine under transient condition, some complementary device such as a boost compensator (ref. 37) is used. This device makes an appropriate correction to full load fuel delivery.

Mathematically, the behaviour of such a device may be represented by reference to three basic variables as follows :

1) r_{max_1}, the reduced maximum rack position under boost control

2) rb_1, the boost ratio below which r_{max_1} applies.

3) rb_2, the boost ratio above which r_{max} applies.

where r_{max}, as used in equation 7.15 is the maximum rack position at full load. The effect of the boost compensator is to control the rack position, between the boost limits rb_1 and rb_2 according to the following equation :

$$rmx = r_{max_1} + \frac{(rb-rb_1)}{(rb_2-rb_1)} \cdot (r_{max}-r_{max_1}) \qquad [7.18]$$

where rb is instantaneous boost ratio.

During a transient r_{mx} will gradually increase from the initial boost limited position r_{max_1} to its full opening r_{max} thereby ensuring that the engine is never overfuelled.

7.2.3 Quasi-steady Model with Manifold Effects

The program TRANIC combines the inherent simplicity of the quasi-steady approach for predicting the in-cylinder performance as in program EMAT with the improved accuracy of the filling and emptying method for the manifolds simulated as finite volumes. Hence, this technique lies midway between the two approaches.

As was already seen in Section 2.4 the basic data required by this technique are similar to those supplied for quasi-steady models (used in the program EMAT), the empirical constants being obtained from

experiments. However, the transient calculation introduces two effects which are missing from basic quasi-steady formulations, viz. manifold volumes and the associated gas conditions.

Fig. 7.4 shows a manifold with inflow and outflow, and experiencing mass flow storage. It is further assumed that there are no temperature, pressure or composition gradients in the manifold and that the inflow gases mix with the gas in the receiver instantaneously and adiabatically. The governing equations are those of conservation of energy and mass together with the perfect gas equation. Having considered an adiabatic manifold, the differential equation derived from first law of thermodynamics may be written in the form of :

$$\left[\frac{dm}{dt} C_v T + mc_v \frac{dT}{dt}\right]_{manifold} = \left(\frac{dm}{dt}\right)_{out} C_p T - \left(\frac{dm}{dt}\right)_{in} C_p T_{in} \qquad [7.19]$$

where T and m are the mean values of temperature, mass of the gas inside the manifold which are both subject to find at any instant of time (during a time step). To find the solution for these two variables, another equation is needed to establish a set of two simultaneous equations. This extra equation is derived from conservation of mass. The inclusion of mass flow storage with the steady state modelling define the flow between the compressor and engine and that between the engine and turbine to describe the mass flow at any instant during a transient phase as follows :

a) for the inlet manifold

$$\dot{m}_{COMP} = \dot{m}_{ENG} + \dot{m}_{INL.ST} \qquad [7.20]$$

b) for the exhaust manifold

$$\dot{m}_{TURB} = \dot{m}_{ENG} + \dot{m}_f - \dot{m}_{EXH.ST} \qquad [7.21]$$

where '$\dot{m}$' denotes mass flow rate and index 'COMP' stands for compressor, 'ENG' for engine, 'TURB' for turbine, 'f' for fuel, 'INL.ST' for inlet manifold storage and 'EXH.ST' for exhaust manifold storage. Attention is drawn to the fact that '$\dot{m}_{INL.ST}$' amd '$\dot{m}_{EXH.ST}$' are the same $\left(\frac{dm}{dt}\right)$ manifold in general equation presented in equation 7.19. The perfect gas equation is also used to calculate the state of the manifold contents and may be written in its differential form as follows :

$$\left[\frac{1}{P}\frac{dP}{dt} = \frac{1}{m}\cdot\frac{dm}{dt} + \frac{1}{T}\cdot\frac{dT}{dt}\right]_{manifold} \qquad [7.22]$$

It should be noted that thermal delays can be expected in transient conditions for both the compressor and turbine (ref. 38). These have been ignored in the present model for simplicity.

7.2.4 Dynamic Modelling of the DCE

The treatment of the DCE unit for dynamic modelling follows the same approach as is used in the program TRANIC. The steady state characteristics of each component are, therefore, modelled individually and represented by a subroutine. The linking program again covers the transient process on a 'quasi steady' basis, that is, incrementing boost, component speeds, fuel input, etc. and evaluating torques at successive instants. This program is called 'DCETRAN'.

In this model, a dynamic subroutine for the epicyclic gearing as well as an updating routine for the turbine CVT are included. In the epicyclic subroutine, the transient condition is represented by the dynamic equations appropriate to each of the three epicyclic main shafts (fig. 5.2), viz.

1. Annulus A (i.e. epicyclic input directly connected to engine)
2. Planet carrier "PC" (i.e. epicyclic output geared to output shaft)
3. Sunwheel "S" (i.e. output geared to compressor)

As shown in fig. 5.2, turbine is connected to output shaft by a CVT.

The equations for the dynamic model of the gear train are summarized below :

$$\tau_A = (\tau - I.\dot{N})_{ENG} \qquad [7.23]$$

$$\tau_{PC} = \left(\tau_{o/s} + \frac{\tau_{TURB}}{r_{TURB}}\right)\cdot\frac{1}{r_{PC}} + T_{o/s_L} - I_{o/s}\dot{N}_{o/s}r_{PC} \qquad [7.24]$$

$$\tau_S = \frac{\tau_{COMP}}{r_S} + \tau_{L.COMP} - I_{COMP}\dot{N}_{COMP}r_S \qquad [7.25]$$

$$\dot{N}_{ENG} n_A + \dot{N}_{COMP} r_s n_s - \dot{N}_{o/s}\, r_{PC}\, (n_A + n_s) = 0 \qquad [7.26]$$

$$\frac{\tau_A}{n_A} - \frac{\tau_s}{n_s}(n_A - n_s) - I_P \frac{\dot{N}_{ENG} n_A - \dot{N}_{COMP} r_s n_s}{n_p} = 0 \qquad [7.27]$$

$$\tau_A + \tau_s + \tau_{PC} - I_P \frac{(\dot{N}_{ENG} r_A - \dot{N}_{COMP} r_s n_s)}{2\, n_p} = 0 \qquad [7.28]$$

where I = inertia
n = number of teeth
r = gear ratio
τ = torque
N = speed

and subscripts denoted are :

TURB = turbine
COMP = compressor
L = transmission loss
ENG = engine
o/s = output shaft
P = planet
PC = planet carrier
S = sunwheel
A = annulus

These equations establish a set of six simultaneous equations to solve for torques applied on the external shafts of the epicyclic gearset (viz. τ_A, τ_{PC} and τ_s) and for acceleration of the connected shafts (viz. $\dot{N}_{ENG}$, $\dot{N}_{o/s}$ and $\dot{N}_{COMP}$).

7.3 UPRATING THE L10 T/C ENGINE

The normal maximum power of the L10 T/C engine is 215 kW (= 290 hp) at 2100 rpm (Section 4.3). To demonstrate the potential advantages of the L10 engine in its DCE rather than T/C configuration, a hypothetical uprated version of the engine developing 240 kW at 2100 rpm was applied. Furthermore, in order to compare the transient performance of the T/C and DCE versions of the L10 engine, the matching of the uprated engine in its T/C form was arranged to be such as to maintain constant power between 2100 and 1400 rpm.

The program EMAT was used to examine uprating of the L10 engine under steady state conditions. The study was applied at 5 running conditions along the LTC based on the investigation of the uprated L10 engine in DCE form described in Chapter 6, and covering a speed range from 1400 rpm to 2100 rpm. The aim was to achieve substantially constant power of 250 kW. The same engine and turbocharger (Holset H2C 8650 compressor and Holset A2 trim turbine) data and maps as used in chapter 4 for the normally rated engine were applied. The turbine nozzle angle, however, had to be decreased from 26 deg (as in Section 3.1) to 20 deg so as to provide the engine with sufficient boost and air flow particularly at its lower speeds. This value was found after a number of trials.

Table 7.1 gives the results of engine matching based on engine speeds of 1400, 1500, 1700, 1900 and 2100 rpm. Fig. 7.5 illustrates the trends of some of the performance parameters, viz. boost pressure ratio, BMEP, brake thermal efficiency and maximum cylinder pressure. As shown, the boost pressure ratio varies within a range from 2.74 to 2.89, i.e. it is sustained at a high level over the speed range. Fig. 7.6 shows the compressor map on which the LTC operating line is superimposed. As shown in table 7.1, the turbocharger speed increases from 101236 rpm to 108131 rpm with increase in engine speed from 1400 rpm to 2100 rpm. Although the combinations of turbocharger speeds and pressure ratios drive the turbine into a rather poor efficiency region of about 60%, the compressor works in a good efficiency region of approx. 70% and provides the engine with sufficient air flow such that the trapped fuel-air ratio at its minimum level does not go any further below 23:1 (table 7.1).

As shown in fig. 7.5, the trend of BMEP depicts an almost hyperbolic curve as a result of the fuelling schedule corresponding to almost constant power. Although the BMEP reaches as high a level as 21.05 bar, the maximum cylinder pressure was controlled within a limit of 131 bar (fig. 7.5). This was made possible by using a very low value of 0.01 for the combustion rate factor (XK). This low value was based on the detailed investigation, in Chapter 4, of the combustion characteristics of the L10 engine with its virtual absence of premixed burning and its comparatively long combustion period.

In spite of the hypothetical constant power envelope achieved in the uprated engine, the originally specified gear ratios were retained (see table 7.2).

7.4 DATA PREPARATION

To establish a reasonable basis for the comparison between the two truck power plants in the form of the TCE and the DCE, the relevant transient response prediction programs were supplied with the same engine and fuel pump data and maps. Each configuration of the L10 engine, however, has its own turbine-compressor and power transmission system.

The compressor used in the L10-DCE is of the Lysholm positive displacement type, whereas in the L10-TCE, it is of the centrifugal type (table 2.7). The turbine used in the DCE is about twice as big as that used in the TCE counterpart. The turbine nozzle angle in the TCE is fixed at the level determined in the investigation for uprating the L10 engine, whereas in the DCE it is variable and is controlled according to the results of the steady state optimization (Chapter 5).

For the drive-line of the L10-TCE powered truck, the data of the stepped gearbox used in practice is applied. The epicyclic gear ratios and the turbine CVT schedule for the DCE version are based on the results of Chapter 5.

7.4.1 Injection Pump Fuelling Map

The L10 engine is equipped with the 'Cummins PT fuel injection system' which differs from conventional in-line pumps. As described in Ref.37 the metering of fuel in the 'PT system' is based on the rail pressure of the fuel supply, the metering orifice inside the injector unit and the available time for fuel to flow into the injector cup. However, in the absence of detailed information on the governing characteristics of the 'L10 PT fuel injection system' and bearing in mind the need for smoke limited operation, the characteristics outlined in section 7.2.2 for a typical in-line system was adopted in the present investigation.

To provide a comparable basis for the transient performance of a truck equipped with the engine in its turbocharged and DCE configurations, the same fuel map and injection data (the maps of varying injection timing and duration) were used. These are presented in Chapter 2, Section 2.4.4

where the description of the TRANIC input data is given.

7.4.2 Simulation of Gear Change with the Program TRANIC

The program TRANIC in its earlier form was a simulation program for laboratory transients rather than route simulation, and did not include a gear change subroutine. The following method was therefore adopted to represent gear changes :

a) For each gear the engine was run up to its rated speed of 2100 rpm under governor control, using load torque and inertia values appropriate to that gear.

b) On reaching a speed of 2100 rpm in any one gear, the engine was instantaneously declutched and allowed to drop its epeed, under idling fuelling and on minimum governor setting, to the level appropriate for smooth clutch engagement in the next gear. On reaching that speed the clutch was then instantaneously re-engaged. Vehicle speed was assumed to remain constant during the period of the gear change (an optimistic assumption).

c) The procedure (a) and (b) was then repeated for seven successive gears.

d) The program was run in 'segmented' form as described above, for a total period of 75 sec., at the end of which a road speed of 96.23 km/hr (53.6 mph) had been attained by the truck.

It should be noted that the maximum no load speed, N_{NL}, considered in the program runs is 2350 rpm with a speed difference for full rack movement under governor control (ΔN in equation 7.14) of 250 rpm. Therefore, as soon as the negative feedback system starts to control the rack position at the rated speed of 2100 rpm, the engine is declutched.

The gear ratios and back axle ratio were taken directly from the Cummins documents which are given in table 2.8. Applying equation 7.6 the referred inertias of 65000 lb truck at different gears are also given in the same table. In applying equations 7.4 and 7.5 to prepare data arrays of load torque in different gears, a level road and zero power loss in transmission were assumed. These arrays are presented in table 2.8.

Fig. 7.7 gives the variation of resisting force versus vehicle speed.

For stable running of the program, the computation time step had to be reduced to 0.002 sec. which caused the program run time to be very long. The print out time interval was arbitrarily chosen as follows :

0.1 sec. for 1st, 2nd and 3rd gears
0.2 sec. for 4th and 5th gears
0.3 sec. for 6th gear
0.4 sec. for 7th gear
to meet a reasonable computer file space.

7.4.3 Gearing and Load Simulation with the Program DCETRAN

The DCE layout is shown in fig. 1.24 together with the referred inertias attached to each of the shafts, viz.

$I_{annulus} = 3.0474 \text{ kg.m}^2$

$I_{sun} = I_{compressor} \cdot (\text{compressor step-up ratio})^2$
$= 0.294 \text{ kg.m}^2$

$I_{planet\ carrier} = I_{o/s} \cdot (\text{o/s step-up ratio})^2$
$= 0.5 \text{ kg.m}^2$

$I'_{turbine} = I_{turbine} \cdot (\text{turbine gear ratio})^2$
$= 0.015 \times (\text{tgr})^2 \text{ kg.m}^2$

As stated in Chapter 6 the gear ratios incorporated in the system are as follows :

Basic epicyclic ratio	= 3.074
Gear ratio of sun to compressor shaft	= 3.1067
Gear ratio of output shaft to planet carrier	= 1.0903

Gear ratio of output shaft to turbine shaft varies according to the CVT schedule determined by steady state optimization.

This set of data was applied to the 65000 lb truck specified in the Cummins documents, giving a wheel rotational speed of 551.3 rpm at the

specified maximum vehicle speed of 66 mph (106.2 km/h). With the maximum output shaft speed of the DCE of 2200 rpm (see Chapter 5) this gave an axle ratio of 3.991:1 (as against 3.7 for the stepped gearbox) and a referred vehicle inertia of 475.6 $kg.m^2$. The torque converter is operative up to a drive shaft speed of 440 rpm and has the characteristics shown in fig. 7.8 with a stall torque ratio of 3.584.

Rolling resistance are 117.7 N/tonne (see fig. 7.7).

7.5 ANALYTICAL RESULTS FOR TRANSIENT RESPONSE OF THE L10-T/C ENGINE IN ACCELERATING A 65000 lb. TRUCK

The transient behaviour of the uprated L10 T/C engine to accelerate a 65000 lb truck are summarized in figs. 7.9 to 7.2 on a base of elapsed time or vehicle speed. A summary of the results with respect to the different events occurring in the course of total simulation period over seven gear changes (rather than the bulky computer print-outs) are presented in table 7.2.

Since a simulation of the initial engagement of the clutch when moving a vehicle from rest was not available, the starting point of the simulation was considered to be at the engine idling speed of 1000 rpm with a fully engaged clutch in first gear.

Rack position as an indication of fuel per cycle is shown in fig. 7.9 on a base of elapsed time. Idle rack position is taken as 0.5 mm (in arbitrary units) during engine deceleration when declutching. As soon as a new gear is engaged, the accelerator pedal is fully depressed for maximum truck acceleration with rack position under boost control. As in the program the rack is almost instantaneously responsive to what is allowed by controlling boost, so that rack position always undergoes a jump from the idling position to the maximum level allowed by the boost availble at the beginning of each gear engagement. This can clearly be seen in fig. 7.9. However, full engine power of 250 kW is not achieved until full rack position (at 5 mm) is regained.

Fig. 7.10 shows the variation of fuel flow rate which in general follows the trend of rack position. Referring to the fuel map (input data), fuel delivered per cycle decrease with increase in engine speed above 1000 rpm at any given rack position. However, its combination with increasing engine speed yields an increasing trend in fuel flow rate.

Fig. 7.11 shows the development of engine torque during power transmission in successive gears and also the negative engine friction torque applicable during the declutched periods.

In the lower gears, due to the low referred inertia, engine acceleration is rapid. In particular in the first two gears, insufficient time is available for the turbocharger to speed up sufficiently and hence in view of insufficient boost (below a level of 2.2) with the rack operating under boost control, full fuelling cannot occur. In turn, full engine torque cannot be developed.

From third gear on, full fuelling at maximum rack position is possible after the initial acceleration period. The descending trend of engine torque after maximum rack position is regained reflects the trend of fuelling per cycle together with the fact that the brake thermal efficiency remains almost constant over that working range.

This schedule is based on the aim of keeping engine power constant at 250 kW. Therefore, from third gear on, full engine torque becomes available. As also shown in table 7.2, the maximum rack position is regained in the higher gears at lower engine speeds. This gives higher value of fuel per cycle and hence leads to higher maximum torque in the higher gears (increasing from 1351 to 1579 N.m from 3rd to 7th gear).

As expected, because of the larger inertia in successive gears, acceleration time increases progressively. At the same time the wider ratio splits call for a longer engine deceleration time.

Fig. 7.12 shows gearbox output shaft torque versus elapsed time. No losses have been assumed for the gearbox (an optimistic assumption). The torque envelope is therefore essentially that for engine torque multiplied by the appropriate transmission ratios (excluding the back axle ratio) showing the expected nearly hyperbolic shape during periods of maximum rack position (fig. 7.9). The periods of torque shortfall and interruptions along the hyperbolic torque curve are, therefore, due to the operation of the boost control and declutching respectively.

It is worth noting that maximum gearbox output shaft torque under steady state conditions with the fuel map used occurs at a speed of 1000 rpm when full fuelling is applied in first gear. This yields torque of 23760 N.m for an engine power of 250 kW, at a truck speed of 5.04 km/h.

This is the maximum steady torque available for severe hill climbing conditions. However, with the level road resistance assumed in this transient investigation, the highest gearbox output-shaft torque is only 6962 N.m.

Fig. 7.13,a and b show turbocharger speed, first on a base of elapsed time and then on a base of vehicle speed. Obviously the turbocharger speed undergoes very large upward and downward changes while the truck is accelerating through the gears. In 1st gear the range is from 25,000 rpm to 66,000 rpm, while in 6th gear the corresponding speeds are 68,000 rpm and 106,000 rpm respectively. The rather high maximum values of the turbocharger speed are due to the uprating of the L10 engine to 250 kW, already referred to, using the original turbocharger with appropriately adjusted turbine area - see also compressor map, fig. 7.6. The large swings of turbocharger speed imply reduced engine efficiency under accelerating conditions.

Fig. 7.13,a shows that the rate of turbocharger speed change during the periods of fuelling under boost control is almost constant in successive gears. This rate is distinctly higher than during periods of fixed rack position presumably due to the fact that, with the rack gradually opening, fuelling is continuously increasing.

Fig. 7.14 shows the variation of boost pressure ratio versus elapsed time. The pattern shown follows closely that of engine torque (fig. 7.11) during the periods of boost limited rack position in each gear. After full rack position is gained in each gear the trend of boost follows closely that of turbocharger speed (fig. 7.13). It is noticeable that, due to both lower initial engine speeds and longer gear change time intervals in lower gears, starting values of boost ratio rise gradually from 1.002 in first gear to a value 1.71 after the change from 5th to 6th gear, while peak values in each gear rise from 1.637 in first gear to 3.010 in 6th gear. The final value in 7th gear is lower due to the fact that the computer run was terminated before engine speed had attained its full value.

Fig. 7.15 shows the operating lines in the different gears superimposed

on the compressor map. Despite the undesirable swing of turbocharger speed, the operating lines from 3rd gear on lie within the good efficiency region of the map. The amplitude of the swings could be reduced by increasing the turbocharger moment of inertia. However, it should be noted that the overall engine performance is very closely related to turbocharger moment of inertia, reduced moment of inertia resulting in much faster transient response of the engine.

Fig. 7.16 shows the variation of trapped air-fuel ratio versus elapsed time. As shown, this variable moves in a band, from minima between 20:1 and 23:1 at the start of each gear acceleration to maxima between 28:1 and 31:1 in successive gears. Except in 1st and 2nd gear, trapped air-fuel ratio always decreases from a higher level down to its allowable minimum value when moving the rack towards its maximum position in the initial acceleration phase in successive gears. This reveals that turbocharger shaft acceleration lags behind rack movement. To make use of full engine power, it is required to attain maximum rack position as fast as possible once a gear is engaged. However, turbocharger lag imposes unavoidable delays.

Soon after maximum rack position is reached, further turbocharger shaft acceleration leads to further increase in engine extra air supply, hence air-fuel ratio increases in a similar manner as is for turbocharger speed. As the fuel rack is moved instantaneously to the position for engine idling during declutching while the turbocharger continues to run at high speed, the air-fuel ratio shows a sharp increase to high levels of the order of 200.

Trapped air-fuel ratio is a key variable, since it has a major influence on thermal efficiency. Fig. 7.17 shows the trend of brake thermal efficiency through the successive gears. In general, the brake thermal efficiency at the low air-fuel ratio end is some 5 to 6 percentage points worse than at the high end, and remains at lower levels in the lower 3 gears where the engine is provided with richer air-fuel ratios. It should be noted that, as no gear loss in the transmission system is considered, these engine efficiency curves are equivalent to drive shaft efficiencies. However, for purpose of comparison with the DCE

output-shaft efficiency, gear losses have been included in the 2nd curve named 'TCE output shaft', although the latter was not used in the actual computations.

Fig. 7.18,a and b show variation of engine speed on a base of time and vehicle speed. As expected, these illustrate the severity of the transient effects due to wide swings of engine speed between 1200 rpm and 2100 rpm in the 3 lower gears and between 1500 rpm and 2100 rpm in the higher gears. These, of course, are due to the gear split originally chosen for the standard L10 engine with 20% torque back up. With the fuel map applied in the simulation, the engine torque curve itself approaches a perfect hyperbola over the range 1400-1800 rpm under steady state running condition (see fig. 7.5). This could result in a reduced number of gear ratios. However, under transient conditions and boost control fuelling, such a fuel map cannot be fully utilized but, as shown in figs. 7.11 and 7.12, a large deficit in developed torque is always encountered upon the engagement of successive gears. This was assumed to be in line with what happens in practice (at least in the boost control part of successive gears), although, the assumption of nearly constant power for the max. rack position is probably optimistic. Acceleration times in successive gears increase progressively as the referred vehicle inertia increases.

Fig. 7.19 shows the engine power envelope illustrating the marked shortfall in power in bottom gear due to the boost limited governor action. However, in the higher gears the calculated maximum engine power slightly exceeds the steady state value of 250 kW due to the fuel pump rack stop setting being somewhat in excess of that implied by the steady state rating. This obviously has a favourable effect on transient response which in spite of the absence of gear losses in the transmission line still remains greatly inferior to that of the DCE powered truck, particularly in the lower gears.

Fig. 7.19 also illustrates the negative power obtaining during clutch disengagement periods, and the highly intermittent nature of power availability.

7.6 THE ANALYTICAL RESULTS FOR TRANSIENT RESPONSE OF THE L10-DCE AND COMPARISON WITH THE L10-T/C ENGINE

Table 7.3 gives a summary of the results of the analytical transient characteristics of the uprated L10-DCE in accelerating the 65000 lb truck from rest. A transmission torque converter locks up above an output shaft speed of 440 rpm, this being the speed level specified in chapter 5 below which the steep torque rise of the DCE is continued down to drive shaft stall (vehicle at rest) via the torque converter.

Fig. 7.9 shows the DCE fuel rack position. In order to develop full engine power from the very beginning of the truck acceleration a step input to the rack position to its ultimate level was applied. This was made possible due to sufficient air being available over the entire period of acceleration as no engine declutching was involved. As shown in fig. 7.10 fuel delivery rate in the DCE follows a continuous trend increasing sharply from an engine idling level.

Fig. 7.18,a shows the engine and output shaft speed of the L10-DCE versus elapsed time. The characteristic feature of the DCE is the independent behaviour of engine and output shafts due to the fully floaing epicyclic gearbox. The relatively low inertia of 1.83 kg.m^2 coupled to the engine, together with the possibility of stepping instantaneously to full power fuel delivery, make engine speed rise rapidly in the early stages, reaching 1450 rpm from 1000 rpm after approx. 1 sec. The DCE output shaft speed is governed to remain at 440 rpm while the torque converter is operative, but then rises relatively slowly due to the attached high referred inertia of 475.6 kg.m^2.

Fig. 7.18,b shows engine speed versus vehicle speed. Before the torque converter is locked up after 2.3 sec. at a vehicle speed of about 20 km/h the engine speed rises rapidly starting with a slope equivalent to that of the 2nd gear in the stepped gearbox. The slope subsequently decreases substantially and soon after the torque converter is locked up, engine speed accelerates more slowly than the T/C engine even in top gear. However, the speed increase is continuous and smooth.

Figs. 7.18,a and b give a clear picture of the better driveability of the vehicular DCE over its TCE counterpart for the following reasons :-

1- Total engine revolutions over a given acceleration period with the DCE are lower.
2- There is no need for engine declutching and gear changing with the DCE resulting in less driver fatigue.
3- The average ratio of the engine speed to the vehicle speed with the DCE is lower which yields lower noise and vibration.
4- The overall drive-train ratio coverage required by a truck is not only satisfied but is also continuous and self-adjusting.

The driving comfort is, therefore, in line with what has practically been experienced with a DDE powered truck described in Chapter 1.

The combination of output shaft speed and engine running conditions throughout the transient operation determines the best schedules for the variable nozzle angle and CVT of the turbine. These schedules are given in fig. 7.20. The turbine gear ratio (fig. 7.20,b) decreases from a maximum of 88.8 to a value of 25.0 with increase in output shaft speed from its minimum of 440 rpm to 1770 rpm. As a result the turbine operates between a minimum speed of 35430 rpm at the time of torque converter lock-up, increasing to a maximum speed of 50290 rpm after 24.6 sec. elapsed time, then decreasing smoothly to a speed of 44268 rpm at the end of the simulation. The trend of the turbine speed is given in fig. 7.13.

The turbine nozzle angle (fig. 7.20,a) starts from a low level of 10.75 deg. at 0.2 sec. elapsed time to provide the system with rapidly increasing boost, then after reaching a maximum of 13.0 deg at torque converter lock up (2.3 sec. elapsed time), it decreases smoothly to a level of 9.04 deg at the end of the simulation.

Fig. 7.11 shows that the engine torque response is very rapid indeed following the sudden opening of the fuel rack (fig. 7.9). Engine torque reaches a peak value of 1737 N.m immediately following application of the step input to the fuel rack, and then decreases slowly as speed increases in line with the fuelling schedule described in Section 7.5.

Fig. 7.14 shows the trend of boost pressure ratio, with extremely rapid rise over the first 2 secs. to a maximum value of approx. 3.5 and then decreasing slowly as the output shaft speeds up with resultant reduction in compressor speed (fig. 7.13) and air mass flow.

The tendency of the compressor to overspeed (fig. 7.13,a) during the initial phase of acceleration which in turn causes the tendency to overboost is the very feature of the DCE that makes possible the initial step change to full fuelling. As demonstrated for the T/C engine (Section 7.5, fig. 7.14) this is in marked contrast to what occurs in that case due to turbocharger lag.

Fig. 7.19 shows the division of power between the different components of the DCE system. As a result of virtually instantaneous response, virtually full engine brake power of 236 kW is developed from idling within 0.6 secs. The output-shaft power, however, is less than engine brake power for the following reasons:

1. As long as the torque converter is operative, it imposes hydrodynamic losses, in line with the efficiency curve shown in fig. 7.8. The maximum power loss of approx. 50.0 kW occurs after 0.2 sec. elapsed time, decreasing to zero when the torque converter is locked up after 2.3 secs. (fig. 7.19).

2. Since the compressor and turbine incorporated in the DCE work separately, the power difference between them may act on the system either as a positive or a negative power contribution. The latter occurs in practice, as power absorption increasing from 14 kW to a maximum of 43 kW within the first 2.4 secs., then decreasing to 1.3 kW at the end of the simulation after 60.0 secs. (fig. 7.19).

3. The remaining power loss is caused by the gears (fig. 7.19). The gear losses decrease from 22 kW to 17 kW with moderate increases in engine and output shaft speeds (i.e. decrease in the torque levels), but rapid decrease in compressor speed (fig. 7.13). The gear loss model takes account of viscous effects as well as transmitted torque.

Fig. 7.19 shows that, as soon as the torque converter is locked up, the rate of increase in output shaft power is at approximately the same rate as the decrease in the difference between compressor and turbine powers. This is due to small variations of the engine power and the gear losses. It should be noted that both the compressor and turbine efficiencies are being sustained above 72%. Although output shaft power is less than engine power, it is still superior to the intermittent power delivered by the turbocharged engine, in particular over the first 25 secs. Attention is drawn to the fact that no gear losses were taken into account in the simulation of the driveline of the turbocharged engined truck.

The trend of output shaft torque after torque converter lock up is shown in fig. 7.12. This shows an almost instantaneous rise to a peak level of 5800 N.m after 0.2 sec. This is achieved at an output shaft torque (before the torque converter) of 2600 N.m, i.e. a torque ratio of 2.23, but at the expense of 30% power loss.

The output shaft torque rises to a peak value of 3905 N.m after 2.0 secs. which almost coincides with torque converter lockup. After the initial peak, output torque falls with increasing output speed, in line with the steady state characteristics of the DCE on maximum fuelling as shown in chapter 5.

[Again the torque deficit of output shaft of the DCE to that of the TCE together with stepped gearbox is only due to the difference between the relevant powers demonstrated in fig. 7.19].

Fig. 7.17 shows the trend of the DCE brake thermal efficiencies with respect to both crankshaft and output shaft. The engine brake thermal efficiency is well sustained above a level of 40% due to the favourable air-fuel ratio throughout the transient operation (fig. 7.16). It is distinctly superior to that of the TCE particularly in the early stage of truck acceleration from rest. However, the output shaft efficiency stays at much lower levels compared to that of the engaged TCE through the gears over the simulation period. The torque converter induces a considerable power loss during its operation and causes low output shaft efficiencies of below 32%. After torque converter lock up, the output

shaft efficiency increases steadily to a final level of 37.4%.

It should be noted that the efficiency of the turbocharged engine becomes negative during declutching. A notional stepped gearbox efficiency of 85% will bring the TCE output shaft efficiency into line with that of the DCE, although this was not applied in the present investigation.

7.7 TRUCK PERFORMANCE COMPARISON

Fig. 7.21 gives a comparison of the vehicle speed-time relationship for the two systems. For the T/C engine and stepped gearbox system, vehicle speed is optimistically assumed to remain constant during gear changes (as already stated). The ultimate vehicle speed (on termination of the computer run) is 86.23 km/hr (56.3 mph) after a total elapsed time of 76.65 secs. For direct comparison with the DCE, which reaches 77.8 km/hr (48.4 mph) after 50 sec., the T/C engined truck only reaches 68.8 km/hr (42.8 mph) after the same elapsed time.

What is even more striking is the very much more sluggish acceleration of the T/C engined truck over the first 10.6 secs., reaching only 17.9 km/hr (11.13 mph) during the gear change from 2nd to 3rd, as against the DCE's 40 km/hr (24.86 mph).

Furthermore, the improved transient response of the DCE powered truck is obtained with the engine operating at all times at or near best efficiency, as against the violent transient swings of the T/C engine with inevitable fuel consumption penalties. These adverse effects would be even more pronounced during down-changes as opposed to up-changes.

Fig. 7.22 shows cumulative fuel consumption for the T/C engine and the DCE powered truck, based on integration of instantaneous fuel consumption rates for both power plants as given by the computer print out over the time interval required to reach any particular speed. Fuel continues to be consumed during the periods of gear shift in line with the minimum rack position of 0.5 mm during clutch disengagement.

The superior consumption characteristics of the DCE under transient conditions become very apparent. Thus to reach a road speed of 20 km/h, the DCE consumes approx. 25 gr fuel as against approx. 40 gr for the T/C engine powered truck. The advantage is again particularly marked in the early stages of acceleration.

7.8 DEVELOPMENT OF THE PROGRAM TRANIC TO PERFORM A CONTINUOUS RUN IN SUCCESSIVE GEARS FOR VEHICLE SIMULATION.

The program TRANIC in its basic version can simulate an engine under a fixed load inertia together with a single load array against engine speed. In the simulation of the complete vehicle, however, load inertia and load array depend upon overall speed ratio between crankshaft and drive axle. Therefore, in the case of a vehicle equipped with a multi-ratio gearbox the program has to be run separately in successive gears with due allowance for gear changes. The end results of each stage are considered as input to the next one. Although this procedure is possible and was indeed used in the simulation of the L10 engine, it is neither very accurate nor economical.

It was therefore decided to develop an integrated program to handle the complete vehicle simulation including gear changes. The modifications applied to the program are as follows:

1) The program was modified to include successive gear ratios of stepped gearbox and back axle, vehicle particulars (viz. weight, frontal area and driving wheel radius) and road data (viz. slope, wind velocity and coefficients of rolling friction and air drag).

2) In successive gears, the engine is assumed to be accelerating under the action of boost controlled rack position and vehicular load. The latter is made up of referred values of vehicle inertia and road load torque and is calculated based on the overall transmission ratio, vehicle particulars and road data in the subroutine ROAD. The load torque is updated at every calculation time step in any one gear.

3) The program stops calculations of engine acceleration immediately after rated engine speed (defined in input data) is reached and the results are written into output files regardless of the print out time step which is usually a multiple of the calculation time step.

4) At the end of engine acceleration in each gear the engine is declutched by performing the step "3". During the declutched period,

the engine is decelerated under instantaneous application of idle rack position (defined in the program) and under the action of its own friction and inertia. At the same time, the vehicle decelerates since no power is supplied while road resistance forces are being applied on it.

5) The print out time step does not change and the elapsed simulation time increases continuously without being reset to zero.

6) Deceleration of the engine is continued down to a speed level determined by the rated engine speed, the split of the adjacent gear ratios, and the ratio of updated vehicle speed and its value at the beginning of the declutching period.

7) Again, regardless of the printout time step, deceleration end results are written into output files.

8) The above steps "1 to 7" are carried out for all gears until the total simulation time defined in input data has been reached.

9) It should be noted that, in the case of severe road conditions in terms of high road slope and wind velocity, the vehicle speed may reach its ultimate value well before the end of simulation time, thereafter the engine speed remains constant.

10) At any calculation time step, elapsed time is checked against total simulation time. The same control is applied when ultimate vehicle speed based on the rated engine speed in top gear is reached. In either case the program is stopped.

11) To show the end of each stage of acceleration or deceleration more clearly in the output file, the results of each new stage start on a new page.

A flowchart representation of the modifications described above is given in fig. 7.23.

7.9 TYPICAL RESULTS OF THE PROGRAM 'TRANIC' AFTER MODIFICATION

A typical set of results of the modified program for road simulation of a truck equipped with a multi-ratio gearbox is given in table 7.4. The simulation starts with a declutched engine idling at a speed of 1000 rpm. The calculation time step is 0.002 sec. and the print out time step is 0.2 sec. The total simulation time considered is 8.0 sec.

As far as the input data for this program run is concerned the same engine and turbocharger data as in Section 7.4 (of this chapter) was used. However, for better demonstration and having more gear changes within 8 sec. simulation time, the acceleration behaviour of an unladen truck (32,500 lb) was simulated. Furthermore, the rack set point during declutching period was reduced to a very low level.

Table 7.4,a gives the results of the engine and vehicle acceleration in 1st gear. As soon as a rated engine speed of 2100 rpm is reached, the relevant results with a print out time increment of 0.196 sec. are printed (regardless of normal value of 0.2 sec.); thereafter the deceleration period starts. Table 7.4,b gives the results of the engine deceleration down to a speed of 1241.64 rpm determined for a smooth 2nd gear engagement. As shown, elapsed time accumulates without being reset to zero, while the print out time step retains its initial value of 0.2 sec. Again, the results at the end of deceleration are printed with a freely found print out time step of 0.15 sec., the total deceleration time increment being 1.55 sec. The results of engine and vehicle acceleration in 2nd gear are given in table 7.4,c. The calculations continue until the end of the simulation time is reached, when the engine is accelerating in 3rd gear. The total acceleration period in 2nd gear (table 7.4,c) is 1.294 sec., followed by a further gear change period (table 7.4,d) of 1.216 sec. and a final acceleration period in 3rd gear (table 7.4,e) terminating after 8.056 secs. of elapsed time. Although not shown on these tables, some of the road performance characteristics such as cumulative fuel consumption are also calculated. This value, for example, in the present simulation is 36.0 gr.

7.10 CONCLUSION

In an analytical investigation the transient response of a T/C engine powered truck was compared with that of its DCE counterpart. The uprated L10 engine with a rated output of 250 kW (335 hp) applied to a 65,000 lb. truck gave a favourable power/weight ratio of approx. 11.5 hp/ton.

The DCE constitutes an integrated engine-transmission system which together with a torque converter can be regarded as a stepless replacement for the conventional T/C engine with a multi-ratio gearbox.

The greatly superior performance of the DCE in terms of transient response has been conclusively demonstrated, particularly in the early stages of acceleration.

The total elimination of gear changes under all route conditions is demonstrably a major advantage in a number of ways as follows :

1- Driverfatigue is greatly reduced.

2- In the absence of gear changes with their substantial demands for additional time and fuel - particularly in the lower gears - there is every expectation that the DCE would achieve not only savings in time, but also in fuel, even if steady state efficiencies are marginally worse.

3- The total number of engine revolutions in a journey is substantially reduced resulting in a longer engine life.

The DCE, like a naturally aspirated engine, does not have any difficulty in suddenly accepting its full rated load. In accelerating a fully laden truck, therefore, it can respond to full engine power requirements almost instantaneously since sufficient air for complete combustion is available almost immediately.

CUMMINS L10 DIESEL ENGINE, HOLSET H2C TURBOCHARGER 116 115 575

number of cylinders	6.0	bore (m)	0.12500	stroke (m)	0.13600			
con-rod length (m)	0.21790	inlet valve closing (degs)	193.0	compressor scaling factor	1.000			
ambient temperature (deg k)	294.5	max. pressure limit (bar)	0.0000	ambient pressure (bar)	0.98000			
compression ratio	16.30	exhaust valve opening (degs)	495.0	turbine flow loss factor	0.8000			
engine speed(r.p.m)	1400.00	1500.00	1700.00	1900.00	2100.00	0.00	0.00	0.00
boost pressure ratio	2.739	2.839	2.890	2.850	2.797	0.000	0.000	0.000
trapped a/f ratio	23.441	25.010	27.833	30.185	31.651	0.000	0.000	0.000
delivery ratio	0.852	0.854	0.858	0.862	0.861	0.000	0.000	0.000
manifold temp (deg k)	312.415	314.974	318.831	321.937	325.295	0.000	0.000	0.000
engine power (k w.)	246.01	249.62	251.32	249.78	249.65	0.00	0.00	0.00
engine torque (n.m.))	1678.01	1589.14	1411.71	1255.40	1135.23	0.00	0.00	0.00
b.m.e.p (bar)	21.0574	19.9422	17.7156	15.7540	14.2461	0.0000	0.0000	0.0000
s.f.c. (kgs/kw hr)	0.186	0.190	0.194	0.197	0.202	0.000	0.000	0.000
b.thermal eff.	0.4483	0.4399	0.4300	0.4232	0.4133	0.0000	0.0000	0.0000
fuel / rev (kg.)	5.450	5.260	4.780	4.320	4.000	0.000	0.000	0.000
max cyl pressure (bar .)	127.74	131.06	128.19	127.31	124.79	0.00	0.00	0.00
max cyl temperature(deg k)	1944.08	1890.10	1797.75	1741.12	1711.96	0.00	0.00	0.00
exhaust temperature(deg k)	962.26	946.63	913.77	885.95	876.65	0.00	0.00	0.00
percentage heat to coolant	12.09	11.44	10.61	10.10	9.75	0.00	0.00	0.00
compressor pressure ratio	2.8378	2.9483	3.0219	3.0040	2.9735	0.0000	0.0000	0.0000
delivery temperature(deg k)	445.58	448.43	448.21	446.72	448.65	0.00	0.00	0.00
delivery pressure (bar)	2.786	2.899	2.957	2.940	2.945	0.000	0.000	0.000
compressor speed (r.p.m.)	101236.8	103846.5	106170.3	106979.9	108131.1	0.0	0.0	0.0
volume flow (cu m / min)	15.43	17.02	19.51	21.37	22.93	0.00	0.00	0.00
compressor power (kw.)	45.123	50.721	58.048	62.973	68.432	0.000	0.000	0.000
compressor efficiency	0.681	0.697	0.717	0.719	0.703	0.000	0.000	0.000
turbine speed (r.p.m)	101236.8	103846.5	106170.3	106979.9	108131.1	0.0	0.0	0.0
turbine power (kw)	45.538	51.074	58.562	63.487	68.954	0.000	0.000	0.000
effective turbine efficiency.	0.642	0.631	0.617	0.607	0.599	0.000	0.000	0.000
fract of flow thro turbine.	1.000	1.000	1.000	1.000	1.000	0.000	0.000	0.000
first step press. ratio(entry 1)	2.687	2.861	3.090	3.250	3.409	0.000	0.000	0.000
press. ratio(entry 2)	0.000	0.000	0.000	0.000	0.000	0.000	0.000	0.000
n.d. torque	2.2287	2.1937	2.1298	2.0888	2.0699	0.0000	0.0000	0.0000
n.d. mass flow.	266.2939	265.1605	262.7556	261.1585	259.8494	0.0000	0.0000	0.0000
n.d.speed	3151.6214	3296.7428	3469.9639	3577.1415	3651.1975	0.0000	0.0000	0.0000
efficiency.	0.653	0.640	0.622	0.611	0.601	0.000	0.000	0.000
final step press. ratio(entry 1)	2.054	2.255	2.551	2.783	2.999	0.000	0.000	0.000
press. ratio(entry 2)	0.000	0.000	0.000	0.000	0.000	0.000	0.000	0.000
n.d. torque	1.3040	1.4457	1.6029	1.7004	1.7836	0.0000	0.0000	0.0000
n.d. mass flow.	232.6531	239.9661	246.7615	250.1699	252.5691	0.0000	0.0000	0.0000
n.d.speed	3253.4642	3391.6026	3551.3551	3645.5085	3708.9982	0.0000	0.0000	0.0000
efficiency.	0.601	0.604	0.602	0.598	0.595	0.000	0.000	0.000
compressor mass flow(kg/min).	17.89	19.73	22.62	24.78	26.59	0.00	0.00	0.00
delevered air to fuel ratio	23.44	25.01	27.83	30.19	31.65	0.00	0.00	0.00
v.g. nozzle width (m.m.)	13.5000	13.5000	13.5000	13.5000	13.5000	0.0000	0.0000	0.0000
cooler effectiveness	0.8397	0.8267	0.8026	0.7813	0.7631	0.0000	0.0000	0.0000
engine diagram factor	0.9392	0.9200	0.9043	0.8963	0.8921	0.0000	0.0000	0.0000
turbine nozzle angle (degs)	20.0000	20.0000	20.0000	20.0000	20.0000	0.0000	0.0000	0.0000

Table 7.1 Summary of the performance predictions for the uprated L10-T/C engine implementing L10-290 turbocharger

Gear Mesh No.	Ov.Gear Ratio --	Refferd Inertia kg.m	*	Elapsed Time sec	Rack Positn mm	Fuel/ Shot	Eng. Speed rpm	Eng. Power kw	B.Th. Eff. %	Eng. Torque N.m	Axle Torque N.m	Road Res.Toq N.m	T/C Speed rpm	Boost Ratio --	A/F Ratio --	Vehicle Speed km/h
1st Gear	37.48	7.2	B	0.0	1.60	35.0	1000.	59.0	36.7	532.0	19940.	1752.	24738.	1.00	23.9	5.04
			E	1.59	3.36	44.6	2100.	151.2	37.4	687.3	25760.	1770.	65728.	1.64	28.4	10.59
2nd Gear	22.16	17.2	B	5.59	1.96	38.5	1241.	80.0	38.5	617.	13672.	1770.	33400.	1.13	23.9	10.59
			E	7.87	5.00	68.0	2100.	250.4	40.6	1138.	25225.	1813.	90317.	2.36	25.3	17.90
3rd Gear	13.17	45.3	B	11.87	2.13	42.3	1248.	90.2	39.5	689.	9080.	1813.	37550.	1.19	23.3	17.90
			M	15.12	5.00	76.7	1762.	249.8	42.7	1351.	17793.	1873.	86407.	2.23	21.8	25.29
			E	16.55	5.00	68.0	2100.	257.4	41.7	1170.	15413.	1929.	104953.	2.96	30.6	30.12
4th Gear	9.51	85.3	B	18.10	2.49	41.5	1516.	102.5	37.7	645.	6133.	1929.	46660.	1.32	25.8	30.12
			M	20.30	5.00	78.2	1704.	248.5	43.2	1392.	13239.	1986.	87844.	2.28	21.9	33.85
			E	23.60	5.00	68.0	2100.	257.7	41.8	1172.	11142.	2110.	105760.	2.99	30.9	41.72
5th Gear	6.81	164.8	B	25.22	3.50	59.0	1504.	160.0	41.4	1015.	6909.	2110.	67200.	1.68	22.4	41.72
			M	26.90	5.00	80.9	1594.	244.7	43.9	1666.	11348.	2155.	85500.	2.20	20.7	44.23
			E	35.80	5.00	68.0	2100.	257.8	41.8	1172.	7982.	2455.	106016.	3.00	31.0	58.26
6th Gear	4.92	313.7	B	37.35	3.59	60.3	1517.	163.9	41.6	1033.	5083.	2455.	68300.	1.71	22.4	58.26
			M	38.85	5.00	81.8	1550.	242.0	44.1	1488.	7323.	2484.	85480.	2.20	20.5	59.51
			E	62.78	5.00	68.0	2100.	257.8	41.8	1172.	5767.	3100.	106130.	3.01	31.0	80.63
7th Gear	3.70	553.4	B	64.10	5.00	81.3	1579.	245.6	44.3	1484.	5492.	3102.	69752.	2.43	22.4	80.63
			T	74.90	5.00	78.6	1689.	250.9	43.8	1419.	5250.	3295.	95215.	2.56	24.2	86.23

* B = Beginning of truck acceleration in a gear M = Beginning of maximum rack position in a gear
E = End of truck acceleration in a gear T = Termination of program run

Table 7.2 The result summary for transient response of the uprated L10-TCE together with a multi-ratio gearbox in accelerating a 65000 lb truck

Time (sec)	0.0	0.4	0.8	1.2	1.6	2.0	2.4	3.0	4.0
Fuel / Rev (mg)	194.6	544.5	528.5	517.7	511.8	508.7	506.4	502.9	499.1
Eng.Speed (rpm)	1000.0	1265.0	1425.0	1500.0	1537.0	1558.0	1572.0	1595.0	1620.0
Eng.Power (kw)	58.8	225.8	239.3	242.6	244.8	245.9	246.8	247.8	248.9
Eng.Torque (N.m)	561.3	1704.7	1602.9	1544.3	1519.9	1507.7	1498.7	1483.0	1466.0
Boost Press. Ratio	1.45	3.08	3.34	3.46	3.52	3.55	3.56	3.56	3.53
Eng.Air Flow (kg/s)	0.118	0.29	0.353	0.384	0.400	0.408	0.413	0.418	0.422
Air / Fuel Ratio	36.25	25.24	28.10	29.64	30.46	30.87	31.12	31.29	31.34
Brk. Th. Eff. (%)	42.00	45.60	44.20	43.40	43.20	43.10	43.10	42.90	42.80
Comp.Speed (rpm)	6642.0	9173.0	10702.0	11420.0	11777.0	11966.0	12042.0	11995.0	11829.0
Comp.Power (kw)	38.3	116.9	153.5	170.8	179.6	184.1	186.2	185.1	181.2
Comp.Air Flow (kg/s)	0.559	0.755	0.890	0.953	0.985	1.001	1.008	1.004	0.989
Turb.Gear Ratio	26.0	88.8	87.6	86.2	84.5	81.8	78.7	75.0	72.2
Turb.Speed (rpm)	11440.0	39058.0	38542.0	37962.0	37219.0	36049.0	35432.0	36780.0	39847.0
Turb.Noz.Ang. (deg)	34.00	10.75	12.02	12.56	12.82	12.95	13.00	12.96	12.82
Turb.Power (kw)	5.9	97.5	123.9	135.8	141.0	142.7	143.3	144.9	146.0
O/S Speed (rpm)	440.0	440.0	440.0	440.0	440.4	440.6	450.4	490.4	551.9
O/S Power (kw)	22.4	137.8	162.8	173.7	178.5	180.2	180.6	185.9	192.5
O/S Torque (N.m)	485.0	2990.0	3531.0	3767.0	3871.0	3905.0	3829.0	3620.0	3330.0
O/S Th. Eff. (%)	16.0	27.8	30.0	31.1	31.5	31.6	31.6	32.2	33.1
Torq.Conv.Speed (rpm)	0.0	187.0	248.3	309.1	362.2	411.5	450.4	490.4	551.9
" " Torq. (N.m)	0.0	5657.0	5430.0	4796.0	4250.0	3877.0	3830.0	3620.0	3330.0
" " " * 3.99/3.7	0.0	6102.0	5857.0	5174.0	4584.0	4182.0	4132.0	3905.0	3592.0
Vehicle Speed (km/h)	0.0	8.86	11.75	14.63	17.15	19.48	21.30	23.2	26.1

Time (sec)	6.0	10.0	15.0	20.0	25.0	30.0	40.0	50.0	60.0
Fuel / Rev (mg)	493.6	485.3	477.6	471.6	466.5	461.3	453.9	447.6	442.2
Eng.Speed (rpm)	1656.0	1709.0	1760.0	1800.0	1835.0	1874.0	1928.0	1972.0	2005.0
Eng.Power (kw)	250.1	251.8	253.2	253.8	256.9	257.6	257.9	257.8	257.3
Eng.Torque (N.m)	1442.0	1406.0	1374.0	1347.0	1336.0	1313.0	1277.0	1248.6	1224.7
Boost Press. Ratio	3.48	3.41	3.34	3.28	3.29	3.26	3.19	3.14	3.10
Eng.Air Flow (kg/s)	.426	.431	.435	.438	.442	.447	.449	.450	.451
Air / Fuel Ratio	31.27	31.14	31.08	30.96	30.98	31.00	30.75	30.60	30.48
Brk. Th. Eff. (%)	42.5	42.2	41.9	41.8	41.7	41.4	41.0	40.6	40.3
Comp.Speed (rpm)	11463.0	10848.0	10215.0	9684.0	9250.0	8951.0	8350.0	7864.0	7451.0
Comp.Power (kw)	172.8	159.3	146.6	136.1	130.6	124.9	113.3	103.9	96.3
Comp.Air Flow (kg/s)	.957	.902	.846	.798	.759	.733	.680	.636	.600
Turb.Gear Ratio	67.5	57.2	49.2	44.0	40.1	37.0	32.4	28.7	25.0
Turb.Speed (rpm)	44463.0	47432.0	49070.0	49966.0	50277.0	50077.0	49295.0	47600.0	44268.0
Turb.Noz.Ang. (deg)	12.53	12.03	11.50	11.07	10.91	10.58	9.96	9.46	9.04
Turb.Power (kw)	142.5	134.1	126.0	120.5	106.0	104.5	100.7	97.9	95.0
Gear Losses (kw)	21.3	21.1	20.8	20.6	19.5	16.8	16.9	17.3	17.5
O/S Speed (rpm)	659.7	829.2	997.6	1135.0	1253.0	1353.0	1523.0	1659.0	1770.0
O/S Power (kw)	198.5	205.5	211.9	217.6	214.4	220.4	228.4	234.5	238.5
O/S Torque (N.m)	2878.0	2366.0	2029.0	1830.0	1634.0	1555.0	1433.0	1350.0	1286.0
" " * 3.99/3.7	3105.0	2552.0	2189.0	1974.0	1763.0	1677.0	1545.0	1456.0	1387.0
O/S Th. Eff. (%)	33.7	34.4	35.1	35.6	34.8	35.5	36.3	36.9	37.4
Vehicle Speed (km/h)	31.2	39.3	47.3	53.8	59.4	64.1	72.1	78.6	83.8

Table 7.3 The result summary for transient response of the uprated L10-DCE in accelerating a 65000 lb truck

time	0.200	0.400	0.600	0.800	1.000	1.200	1.400	1.600	1.800	1.996	sec
engine											
speed	1129.79	1250.24	1362.83	1467.87	1568.42	1669.77	1774.39	1882.05	1991.15	2100.56	rpm
load torq	23.48	23.52	23.56	23.61	23.65	23.69	23.75	23.80	23.86	23.92	n.m
eng torque	400.47	361.90	349.69	325.97	322.83	329.60	340.73	347.11	351.20	364.90	n.m
eng power	47.38	47.38	49.91	50.11	53.02	57.63	63.31	68.41	73.23	80.27	kw
b.m.e.p.	5.03	4.54	4.39	4.09	4.05	4.14	4.28	4.36	4.41	4.58	bar
s.f.c.	0.247	0.252	0.264	0.284	0.293	0.295	0.296	0.301	0.312	0.320	kg/kw.hr
th.effy	0.338	0.330	0.316	0.294	0.285	0.283	0.282	0.277	0.267	0.261	
boost rat	0.992	1.023	1.058	1.100	1.149	1.203	1.264	1.327	1.404	1.517	total
inlet temp	293.94	296.21	297.18	298.11	299.23	300.58	302.12	303.97	306.70	311.23	k
del rat	0.841	0.840	0.839	0.837	0.835	0.834	0.832	0.831	0.829	0.828	
tr af rat	28.50	31.52	32.07	33.11	33.66	34.06	34.26	34.42	34.42	34.35	
fuel/rev	172.37	159.46	161.33	161.62	165.05	169.81	176.02	182.53	191.18	203.62	kg*10e6
inl m.flow	5.55	6.28	7.05	7.85	8.71	9.66	10.70	11.82	13.10	14.69	kg/min
exh m.flow	5.75	6.48	7.27	8.09	8.97	9.94	11.01	12.17	13.48	15.12	kg/min
fuel flow	0.195	0.199	0.220	0.237	0.259	0.284	0.312	0.344	0.381	0.428	kg/min
max.press.	79.44	79.36	82.57	85.60	89.59	94.20	99.44	104.44	109.11	115.66	bar
max.temp.	1880.77	1830.37	1841.43	1836.54	1845.52	1859.54	1878.50	1873.99	1858.13	1853.58	k
exh.temp.	627.10	623.32	648.52	669.09	686.58	701.90	718.12	736.52	762.41	789.90	k
cool heat	35.57	33.05	30.89	28.97	27.27	25.69	24.23	22.89	21.63	20.36	%
fuel pump											
f.pump spd	564.90	625.12	681.42	733.94	784.21	834.89	887.20	941.03	995.57	1050.28	rpm
gov set pt	2350.00	2350.00	2350.00	2350.00	2350.00	2350.00	2350.00	2350.00	2350.00	2350.00	engine rpm
rack posn	1.60	1.60	1.75	1.87	2.01	2.16	2.32	2.50	2.72	3.03	usually mm
fuel/strk	33.80	31.27	31.63	31.69	32.36	33.30	34.51	35.79	37.49	39.93	kg*10e6
inj start	345.06	344.87	344.33	343.75	343.48	343.42	343.40	343.36	343.35	343.35	deg atdco
duration	8.01	8.21	8.78	9.39	10.15	11.02	12.00	13.02	14.13	15.41	deg ca
compressor											
speed	23960.2	26131.1	28580.5	31444.0	34731.8	38448.9	42619.7	47375.7	53009.9	59702.4	rpm
press rat	0.967	0.992	1.020	1.054	1.093	1.138	1.192	1.257	1.338	1.441	total
out temp	288.57	291.69	295.29	299.58	304.46	309.72	315.13	320.47	326.89	337.04	k
mass flow	5.61	6.38	7.17	8.00	8.87	9.83	10.88	12.02	13.35	15.07	kg/min
torque	-0.126	-0.032	0.083	0.229	0.411	0.639	0.907	1.163	1.393	1.726	n.m
power	-0.32	-0.09	0.25	0.76	1.49	2.57	4.05	5.77	7.73	10.79	kw
effic	0.829	0.834	0.824	0.796	0.755	0.711	0.684	0.693	0.739	0.759	
cooler											
out p rat	0.989	1.020	1.054	1.096	1.143	1.197	1.256	1.318	1.394	1.504	static
out temp	294.64	295.09	295.71	296.55	297.63	298.97	300.56	302.52	305.23	309.65	k
effectvns	1.041	1.254	-0.473	0.585	0.679	0.702	0.703	0.689	0.667	0.642	
turbine											
p rat max	1.419	1.484	1.618	1.777	1.959	2.180	2.438	2.723	3.060	3.466	total
p rat min	1.399	1.466	1.601	1.761	1.944	2.166	2.425	2.712	3.051	3.459	total
inl temp	594.79	625.63	646.63	667.57	686.85	703.24	719.56	736.46	761.49	788.75	k
mass flow	6.02	6.35	7.13	7.91	8.75	9.65	10.70	11.84	13.13	14.66	kg/min
torque	1.23	1.41	1.78	2.20	2.64	3.15	3.73	4.44	5.34	6.51	n.m
power	3.10	3.87	5.34	7.23	9.61	12.69	16.66	22.01	29.64	40.73	kw
effic	0.532	0.534	0.527	0.527	0.534	0.544	0.559	0.581	0.607	0.641	
vehicle											
speed	5.69	6.30	6.87	7.40	7.91	8.42	8.94	9.49	10.04	10.59	km/h
accelratn.	0.887	0.796	0.767	0.711	0.703	0.719	0.745	0.760	0.769	0.801	m/s/s

Table 7.4,a Example of automatic simulation termination in the 1st gear at rated engine speed to be followed continuously by next simulation sequence (declutching)

time	2.196	2.396	2.596	2.796	2.996	3.196	3.396	3.596	3.746	0.000	sec
engine											
speed	2099.79	1961.50	1832.79	1710.15	1593.98	1485.29	1387.21	1300.79	1241.64	0.00	rpm
load torq	0.00	0.00	0.00	0.00	0.00	0.00	0.00	0.00	0.00	0.00	n.m
eng torque	-295.72	-204.73	-197.92	-187.46	-177.11	-163.33	-144.30	-128.12	-119.83	0.00	n.m
eng power	-65.03	-42.05	-37.99	-33.57	-29.56	-25.41	-20.96	-17.45	-15.58	0.00	kw
b.m.e.p.	-3.71	-2.57	-2.48	-2.35	-2.22	-2.05	-1.81	-1.61	-1.50	0.00	bar
s.f.c.	1000.000	1000.000	1000.000	1000.000	1000.000	1000.000	1000.000	1000.000	1000.000	0.000	kg/kw.hr
th.effy	-13.381	-8.825	-8.138	-7.327	-6.557	-5.704	-4.761	-4.008	-3.611	0.000	
boost rat	1.520	1.539	1.538	1.535	1.528	1.518	1.505	1.490	1.479	0.000	total
inlet temp	311.35	310.39	309.47	308.72	307.98	307.23	306.48	305.75	305.22	0.00	k
del rat	0.829	0.840	0.840	0.841	0.842	0.844	0.845	0.846	0.847	0.000	
tr af rat	200.00	200.00	200.00	200.00	200.00	200.00	200.00	200.00	200.00	0.00	
fuel/rev	3.22	3.38	3.54	3.73	3.93	4.17	4.41	4.65	4.83	0.00	kg*10e6
inl m.flow	14.72	14.15	13.26	12.39	11.54	10.72	9.97	9.29	8.83	0.00	kg/min
exh m.flow	14.73	14.16	13.26	12.39	11.55	10.73	9.98	9.30	8.83	0.00	kg/min
fuel flow	0.007	0.007	0.006	0.006	0.006	0.006	0.006	0.006	0.006	0.000	kg/min
max.press.	59.39	57.57	57.57	57.32	56.92	56.41	55.82	55.20	54.73	0.00	bar
max.temp.	857.03	852.94	850.60	848.43	846.28	844.27	842.42	840.67	839.38	0.00	k
exh.temp.	318.28	317.59	317.10	316.84	316.65	316.53	316.44	316.37	316.33	0.00	k
cool heat	223.27	222.13	218.89	215.43	211.23	206.09	200.87	196.01	192.66	0.00	%
fuel pump											
f.pump spd	1049.89	980.75	916.40	855.08	796.99	742.65	693.60	650.39	620.82	0.00	rpm
gov set pt	2350.00	2350.00	2350.00	2350.00	2350.00	2350.00	2350.00	2350.00	2350.00	0.00	engine rpm
rack posn	0.05	0.05	0.05	0.05	0.05	0.05	0.05	0.05	0.05	0.00	usually mm
fuel/strk	0.63	0.66	0.69	0.73	0.77	0.82	0.87	0.91	0.95	0.00	kg*10e6
inj start	345.52	345.91	346.22	346.28	346.18	346.31	346.79	347.25	347.48	0.00	deg atdco
duration	7.68	7.11	6.59	6.06	5.55	5.19	5.06	4.99	4.94	0.00	deg ca
compressor											
speed	59850.7	60674.6	60532.1	60270.9	59827.4	59204.5	58426.4	57543.7	56838.2	0.0	rpm
press rat	1.444	1.489	1.504	1.513	1.514	1.510	1.501	1.489	1.479	0.000	total
out temp	337.32	339.73	340.58	341.59	342.47	343.10	343.37	343.25	342.97	0.00	k
mass flow	15.11	14.17	13.27	12.39	11.52	10.70	9.94	9.26	8.79	0.00	kg/min
torque	1.735	1.688	1.613	1.545	1.477	1.406	1.334	1.260	1.204	0.000	n.m
power	10.87	10.72	10.22	9.75	9.25	8.72	8.16	7.59	7.17	0.00	kw
effic	0.758	0.786	0.792	0.787	0.773	0.756	0.739	0.725	0.716	0.000	
cooler											
out p rat	1.507	1.527	1.528	1.526	1.521	1.511	1.499	1.486	1.475	0.000	static
out temp	309.76	309.34	308.64	308.04	307.44	306.83	306.19	305.55	305.07	0.00	k
effectvns	0.642	0.670	0.692	0.711	0.729	0.745	0.759	0.772	0.780	0.000	
turbine											
p rat max	3.343	2.185	2.200	2.132	2.047	1.957	1.871	1.796	1.745	0.000	total
p rat min	3.375	2.199	2.214	2.145	2.058	1.967	1.880	1.804	1.752	0.000	total
inl temp	768.52	342.69	320.62	316.09	314.79	314.22	314.04	314.05	314.07	0.00	k
mass flow	14.42	12.88	13.23	12.61	11.82	11.02	10.24	9.54	9.06	0.00	kg/min
torque	6.05	1.65	1.56	1.38	1.20	1.02	0.86	0.74	0.66	0.00	n.m
power	37.93	10.49	9.89	8.74	7.52	6.33	5.29	4.45	3.92	0.00	kw
effic	0.652	0.688	0.667	0.647	0.628	0.614	0.605	0.600	0.598	0.000	
vehicle											
speed	10.59	10.59	10.59	10.59	10.59	10.59	10.59	10.59	10.59	0.00	km/h
accelratn.	0.000	0.000	0.000	0.000	0.000	0.000	0.000	0.000	0.000	0.000	m/s/s

Table 7.4,b Example of integrated simulation for declutching period (between 1st and 2nd gear)

time	3.946	4.146	4.346	4.546	4.746	4.946	5.146	5.240	0.000	0.000	sec
engine											
speed	1273.24	1400.08	1520.73	1638.37	1761.69	1894.43	2037.22	2100.20	0.00	0.00	rpm
load torq	40.51	40.74	40.99	41.24	41.53	41.86	42.24	42.42	0.00	0.00	n.m
eng torque	768.54	737.32	698.42	711.00	752.51	827.18	811.17	772.28	0.00	0.00	n.m
eng power	102.47	108.10	111.22	121.99	138.82	164.10	173.05	169.85	0.00	0.00	kw
b.m.e.p.	9.64	9.25	8.76	8.92	9.44	10.38	10.18	9.69	0.00	0.00	bar
s.f.c.	0.219	0.226	0.235	0.237	0.240	0.243	0.252	0.257	0.000	0.000	kg/kw.hr
th.effy	0.380	0.370	0.356	0.353	0.348	0.343	0.331	0.324	0.000	0.000	
boost rat	1.484	1.548	1.624	1.725	1.870	2.103	2.504	2.753	0.000	0.000	total
inlet temp	305.56	308.39	310.81	314.07	318.93	326.30	337.96	344.02	0.00	0.00	k
del rat	0.836	0.836	0.835	0.834	0.832	0.830	0.830	0.831	0.000	0.000	
tr af rat	23.91	25.04	26.43	27.01	26.86	26.38	29.87	33.19	0.00	0.00	
fuel/rev	294.29	290.51	286.02	293.62	314.60	351.39	356.72	346.93	0.00	0.00	kg*10e6
inl m.flow	8.96	10.18	11.49	12.99	14.89	17.56	21.71	24.18	0.00	0.00	kg/min
exh m.flow	9.33	10.59	11.93	13.47	15.44	18.23	22.43	24.91	0.00	0.00	kg/min
fuel flow	0.375	0.407	0.435	0.481	0.554	0.666	0.727	0.729	0.000	0.000	kg/min
max.press.	133.89	137.53	141.42	149.31	159.76	175.02	187.05	192.27	0.00	0.00	bar
max.temp.	2174.62	2158.50	2132.34	2142.06	2126.55	2132.56	2008.32	1917.53	0.00	0.00	k
exh.temp.	786.83	799.50	808.45	823.75	859.17	908.69	892.49	861.79	0.00	0.00	k
cool heat	27.20	25.28	23.58	22.01	20.43	18.68	16.80	15.98	0.00	0.00	%
fuel pump											
f.pump spd	636.62	700.04	760.37	819.19	880.84	947.22	1018.61	1050.10	0.00	0.00	rpm
gov set pt	2350.00	2350.00	2350.00	2350.00	2350.00	2350.00	2350.00	2350.00	0.00	0.00	engine rpm
rack posn	2.96	3.14	3.35	3.63	4.03	4.68	5.00	5.00	0.00	0.00	usually mm
fuel/strk	57.70	56.96	56.08	57.57	61.69	68.90	69.94	68.02	0.00	0.00	kg*10e6
inj start	342.58	341.99	341.57	341.33	341.04	340.64	341.10	341.54	0.00	0.00	deg atdco
duration	11.18	12.16	13.17	14.53	16.43	19.13	20.99	21.24	0.00	0.00	deg ca
compressor											
speed	57162.3	60672.3	64348.4	68851.2	74618.3	82508.7	93805.0	100049.5	0.0	0.0	rpm
press rat	1.483	1.547	1.621	1.723	1.872	2.095	2.461	2.700	0.000	0.000	total
out temp	342.94	347.03	351.88	359.01	370.00	386.69	410.80	425.12	0.00	0.00	k
mass flow	9.07	10.37	11.73	13.31	15.35	18.33	22.92	25.55	0.00	0.00	kg/min
torque	1.235	1.429	1.645	1.967	2.504	3.254	4.580	5.337	0.000	0.000	n.m
power	7.39	9.08	11.08	14.18	19.56	28.12	44.99	55.91	0.00	0.00	kw
effic	0.721	0.748	0.773	0.779	0.759	0.757	0.738	0.740	0.000	0.000	
cooler											
out p rat	1.479	1.543	1.616	1.716	1.859	2.088	2.484	2.730	0.000	0.000	static
out temp	305.33	307.26	309.50	312.62	317.27	324.22	335.00	341.18	0.00	0.00	k
effectvns	0.775	0.756	0.737	0.718	0.698	0.677	0.651	0.642	0.000	0.000	
turbine											
p rat max	2.465	2.568	2.798	3.157	3.662	4.389	5.271	5.677	0.000	0.000	total
p rat min	2.431	2.534	2.766	3.127	3.633	4.361	5.248	5.658	0.000	0.000	total
inl temp	494.03	775.64	811.19	825.85	857.30	905.54	915.62	887.94	0.00	0.00	k
mass flow	12.93	10.82	11.59	13.04	14.93	17.51	21.15	23.37	0.00	0.00	kg/min
torque	3.08	3.66	4.24	5.21	6.75	9.29	12.65	14.19	0.00	0.00	n.m
power	18.41	23.23	28.57	37.57	52.73	80.27	124.30	148.63	0.00	0.00	kw
effic	0.729	0.677	0.681	0.694	0.713	0.745	0.811	0.853	0.000	0.000	
vehicle											
speed	10.85	11.93	12.96	13.96	15.02	16.15	17.36	17.90	0.00	0.00	km/h
accelratn.	1.543	1.474	1.391	1.416	1.503	1.659	1.628	1.546	0.000	0.000	m/s/s

Table 7.4,c Example of integrated simulation in the 2nd gear terminated at rated engine speed to be followed continuously by next simulation sequence (declutching)

time	5.440	5.640	5.840	6.040	6.240	6.440	6.640	6.656	0.000	0.000	sec
engine											
speed	2013.34	1862.19	1716.01	1580.10	1456.29	1348.22	1254.79	1247.80	0.00	0.00	rpm
load torq	0.00	0.00	0.00	0.00	0.00	0.00	0.00	0.00	0.00	0.00	n.m
eng torque	-232.28	-236.73	-221.70	-204.66	-182.82	-156.86	-137.80	-136.55	0.00	0.00	n.m
eng power	-48.97	-46.16	-39.84	-33.87	-27.88	-22.15	-18.11	-17.84	0.00	0.00	kw
b.m.e.p.	-2.91	-2.97	-2.78	-2.57	-2.29	-1.97	-1.73	-1.71	0.00	0.00	bar
s.f.c.	1000.000	1000.000	1000.000	1000.000	1000.000	1000.000	1000.000	1000.000	0.000	0.000	kg/kw.hr
th.effy	-10.200	-9.844	-8.687	-7.523	-6.281	-5.054	-4.188	-4.131	0.000	0.000	
boost rat	2.759	2.588	2.442	2.313	2.199	2.098	2.010	2.003	0.000	0.000	total
inlet temp	340.96	334.43	329.88	325.59	321.74	318.35	315.52	315.32	0.00	0.00	k
del rat	0.844	0.841	0.842	0.843	0.844	0.845	0.847	0.847	0.000	0.000	
tr af rat	200.00	200.00	200.00	200.00	200.00	200.00	200.00	200.00	0.00	0.00	
fuel/rev	3.32	3.50	3.72	3.96	4.24	4.52	4.79	4.81	0.00	0.00	kg*10e6
inl m.flow	23.82	21.00	18.52	16.39	14.55	13.01	11.72	11.63	0.00	0.00	kg/min
exh m.flow	23.83	21.01	18.53	16.39	14.56	13.02	11.73	11.63	0.00	0.00	kg/min
fuel flow	0.007	0.007	0.006	0.006	0.006	0.006	0.006	0.006	0.000	0.000	kg/min
max.press.	100.44	94.98	89.70	84.97	80.76	77.02	73.72	73.48	0.00	0.00	bar
max.temp.	915.95	901.80	891.27	881.36	872.62	865.06	858.73	858.28	0.00	0.00	k
exh.temp.	344.97	339.05	335.16	331.57	328.49	325.88	323.84	323.70	0.00	0.00	k
cool heat	360.72	332.92	311.37	290.76	271.35	254.45	240.52	239.53	0.00	0.00	%
fuel pump											
f.pump spd	1006.67	931.10	858.01	790.05	728.14	674.11	627.40	623.90	0.00	0.00	rpm
gov set pt	2350.00	2350.00	2350.00	2350.00	2350.00	2350.00	2350.00	2350.00	0.00	0.00	engine rpm
rack posn	0.05	0.05	0.05	0.05	0.05	0.05	0.05	0.05	0.00	0.00	usually mm
fuel/strk	0.65	0.69	0.73	0.78	0.83	0.89	0.94	0.94	0.00	0.00	kg*10e6
inj start	345.76	346.17	346.28	346.18	346.42	347.02	347.43	347.46	0.00	0.00	deg atdco
duration	7.33	6.71	6.08	5.49	5.13	5.03	4.95	4.95	0.00	0.00	deg ca
compressor											
speed	100086.7	95781.1	91922.9	88373.1	85054.3	81942.0	79034.3	78810.5	0.0	0.0	rpm
press rat	2.750	2.589	2.457	2.344	2.230	2.129	2.037	2.030	0.000	0.000	total
out temp	429.73	422.89	416.38	409.50	402.79	396.51	391.11	390.71	0.00	0.00	k
mass flow	23.52	20.64	18.20	16.10	14.29	12.78	11.51	11.41	0.00	0.00	kg/min
torque	5.078	4.432	3.830	3.309	2.891	2.539	2.247	2.226	0.000	0.000	n.m
power	53.23	44.45	36.87	30.62	25.75	21.78	18.60	18.37	0.00	0.00	kw
effic	0.731	0.716	0.713	0.715	0.705	0.697	0.688	0.687	0.000	0.000	
cooler											
out p rat	2.740	2.573	2.429	2.303	2.191	2.092	2.004	1.998	0.000	0.000	static
out temp	339.17	334.24	329.79	325.55	321.85	318.58	315.95	315.76	0.00	0.00	k
effectvns	0.669	0.690	0.710	0.729	0.747	0.763	0.777	0.778	0.000	0.000	
turbine											
p rat max	3.499	3.564	3.332	3.065	2.811	2.585	2.387	2.372	0.000	0.000	total
p rat min	3.516	3.585	3.352	3.081	2.826	2.597	2.397	2.382	0.000	0.000	total
inl temp	418.71	348.70	335.18	329.40	325.56	322.64	320.39	320.23	0.00	0.00	k
mass flow	19.27	20.78	19.12	17.10	15.24	13.64	12.29	12.19	0.00	0.00	kg/min
torque	2.37	1.99	1.60	1.25	0.96	0.73	0.56	0.55	0.00	0.00	n.m
power	24.85	19.98	15.43	11.54	8.51	6.27	4.66	4.56	0.00	0.00	kw
effic	0.522	0.442	0.420	0.408	0.405	0.407	0.415	0.416	0.000	0.000	
vehicle											
speed	17.90	17.90	17.90	17.90	17.90	17.90	17.90	17.90	0.00	0.00	km/h
accelratn.	0.000	0.000	0.000	0.000	0.000	0.000	0.000	0.000	0.000	0.000	m/s/s

Table 7.4,,d Example of integrated simulation for declutching period (between 2nd and 3rd gear)

time	6.856	7.056	7.256	7.456	7.656	7.856	8.056	0.000	0.000	0.000	sec
engine											
speed	1323.53	1412.49	1499.61	1582.19	1660.85	1736.37	1808.96	0.00	0.00	0.00	rpm
load torq	72.00	72.79	73.62	74.45	75.28	76.11	76.95	0.00	0.00	0.00	n.m
eng torque	1195.29	1229.69	1174.67	1117.10	1073.72	1036.19	998.79	0.00	0.00	0.00	n.m
eng power	165.67	181.89	184.47	185.09	186.74	188.41	189.20	0.00	0.00	0.00	kw
b.m.e.p.	15.00	15.43	14.74	14.02	13.47	13.00	12.53	0.00	0.00	0.00	bar
s.f.c.	0.202	0.203	0.208	0.213	0.216	0.218	0.221	0.000	0.000	0.000	kg/kw.hr
th.effy	0.413	0.410	0.402	0.393	0.387	0.382	0.377	0.000	0.000	0.000	
boost rat	2.103	2.249	2.430	2.656	2.938	3.287	3.665	0.000	0.000	0.000	total
inlet temp	319.91	324.32	329.39	335.34	342.08	350.44	360.65	0.00	0.00	0.00	k
del rat	0.837	0.838	0.837	0.837	0.837	0.837	0.837	0.000	0.000	0.000	
tr af rat	22.62	23.06	25.13	27.70	30.78	34.46	38.25	0.00	0.00	0.00	
fuel/rev	421.41	436.31	425.62	414.39	404.29	394.62	385.47	0.00	0.00	0.00	kg*10e6
inl m.flow	12.62	14.21	16.04	18.16	20.67	23.61	26.67	0.00	0.00	0.00	kg/min
exh m.flow	13.17	14.83	16.68	18.82	21.34	24.30	27.37	0.00	0.00	0.00	kg/min
fuel flow	0.558	0.616	0.638	0.656	0.671	0.685	0.697	0.000	0.000	0.000	kg/min
max.press.	194.85	206.31	212.86	218.32	225.82	235.29	245.01	0.00	0.00	0.00	bar
max.temp.	2316.44	2325.09	2250.55	2141.22	2042.37	1948.79	1873.47	0.00	0.00	0.00	k
exh.temp.	860.43	875.50	863.69	848.79	826.54	800.80	779.39	0.00	0.00	0.00	k
cool heat	22.55	21.11	19.79	18.58	17.44	16.44	15.69	0.00	0.00	0.00	%
fuel pump											
f.pump spd	661.77	706.25	749.80	791.09	830.42	868.19	904.48	0.00	0.00	0.00	rpm
gov set pt	2350.00	2350.00	2350.00	2350.00	2350.00	2350.00	2350.00	0.00	0.00	0.00	engine rpm
rack posn	4.71	5.00	5.00	5.00	5.00	5.00	5.00	0.00	0.00	0.00	usually mm
fuel/strk	82.63	85.55	83.45	81.25	79.27	77.38	75.58	0.00	0.00	0.00	kg*10e6
inj start	339.74	338.90	338.75	338.87	339.07	339.35	339.66	0.00	0.00	0.00	deg atdco
duration	15.15	16.91	17.74	18.19	18.56	18.95	19.42	0.00	0.00	0.00	deg ca
compressor											
speed	82095.9	86477.3	91503.9	97340.1	104056.7	111622.8	119658.7	0.0	0.0	0.0	rpm
press rat	2.134	2.280	2.459	2.674	2.961	3.309	3.678	0.000	0.000	0.000	total
out temp	396.48	406.75	419.09	433.68	450.92	474.57	502.24	0.00	0.00	0.00	k
mass flow	12.97	14.62	16.55	18.78	21.44	24.45	27.43	0.00	0.00	0.00	kg/min
torque	2.572	3.009	3.567	4.294	5.108	6.205	7.614	0.000	0.000	0.000	n.m
power	22.11	27.25	34.18	43.77	55.66	72.53	95.40	0.00	0.00	0.00	kw
effic	0.700	0.703	0.700	0.687	0.691	0.678	0.640	0.000	0.000	0.000	
cooler											
out p rat	2.096	2.240	2.420	2.644	2.923	3.269	3.645	0.000	0.000	0.000	static
out temp	318.86	322.99	327.89	333.68	340.26	349.11	360.07	0.00	0.00	0.00	k
effectvns	0.760	0.746	0.731	0.718	0.707	0.696	0.684	0.000	0.000	0.000	
turbine											
p rat max	3.403	3.582	3.938	4.355	4.805	5.295	5.788	0.000	0.000	0.000	total
p rat min	3.349	3.524	3.884	4.306	4.759	5.253	5.750	0.000	0.000	0.000	total
inl temp	791.57	876.22	872.86	859.47	838.85	813.33	789.70	0.00	0.00	0.00	k
mass flow	14.47	14.52	16.14	18.19	20.59	23.44	26.54	0.00	0.00	0.00	kg/min
torque	5.44	6.02	7.06	8.33	9.72	11.27	12.84	0.00	0.00	0.00	n.m
power	46.74	54.54	67.65	84.88	105.95	131.77	160.93	0.00	0.00	0.00	kw
effic	0.755	0.758	0.779	0.807	0.839	0.872	0.902	0.000	0.000	0.000	
vehicle											
speed	18.98	20.26	21.51	22.69	23.82	24.90	25.94	0.00	0.00	0.00	km/h
accelratn.	1.724	1.778	1.693	1.603	1.534	1.475	1.417	0.000	0.000	0.000	m/s/s

Table 7.4,e As per table 7.4,c but for the 3rd gear terminated by total simulation time (8 sec)

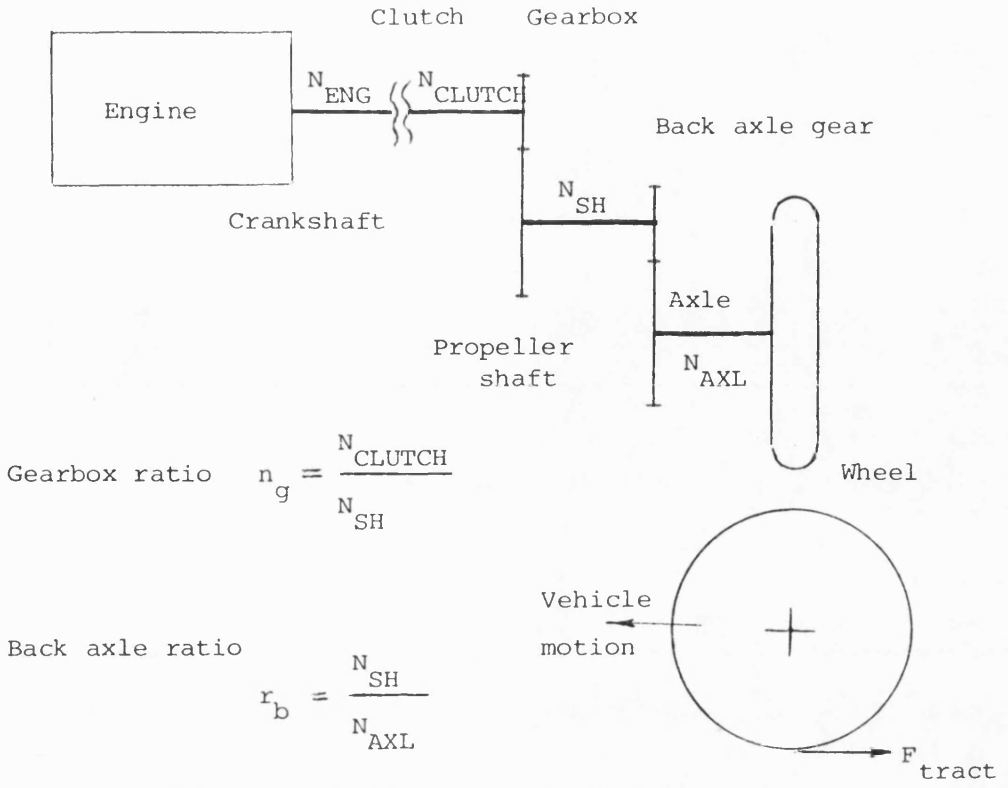

Fig, 7.1 Schematic diagram for a truck driveline

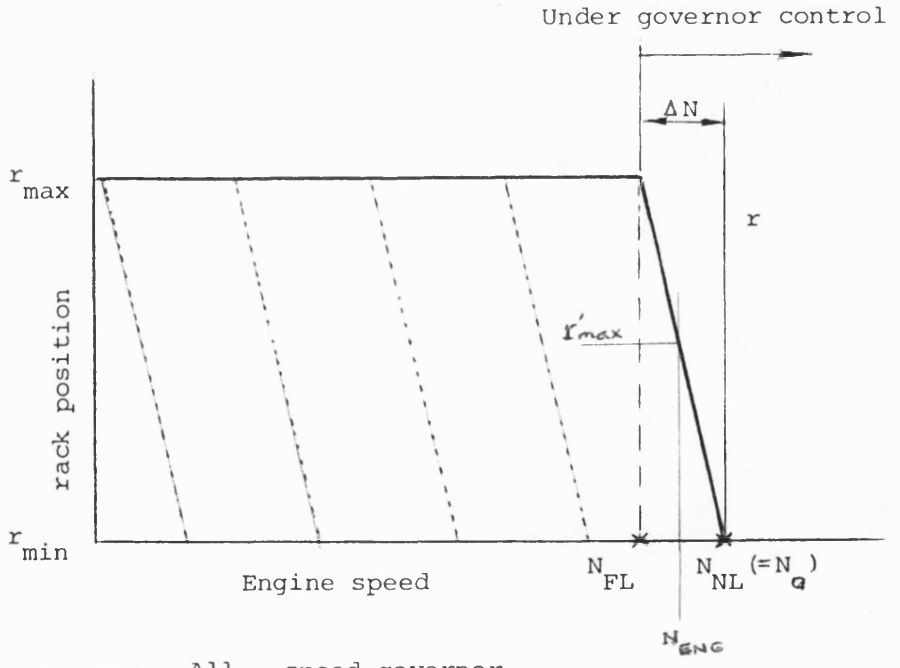

Fig. 7.2 All - speed governor

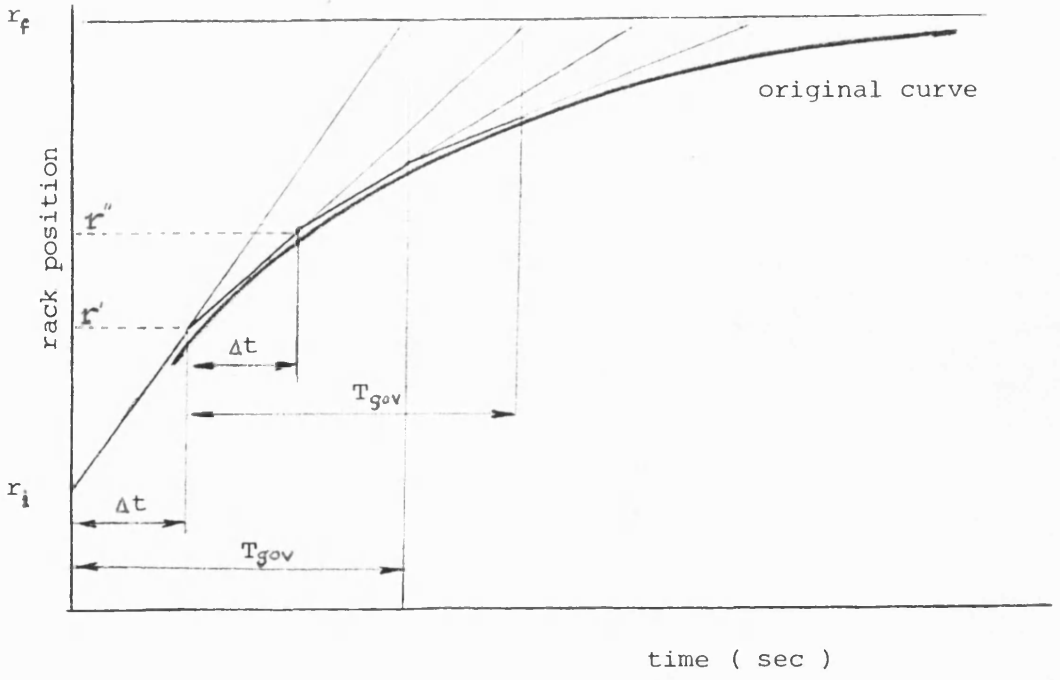

Fig. 7.3 Assumed governor dynamic response

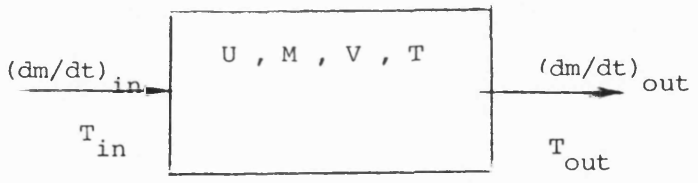

Fig. 7.4 Inflow and outflow of a manifold

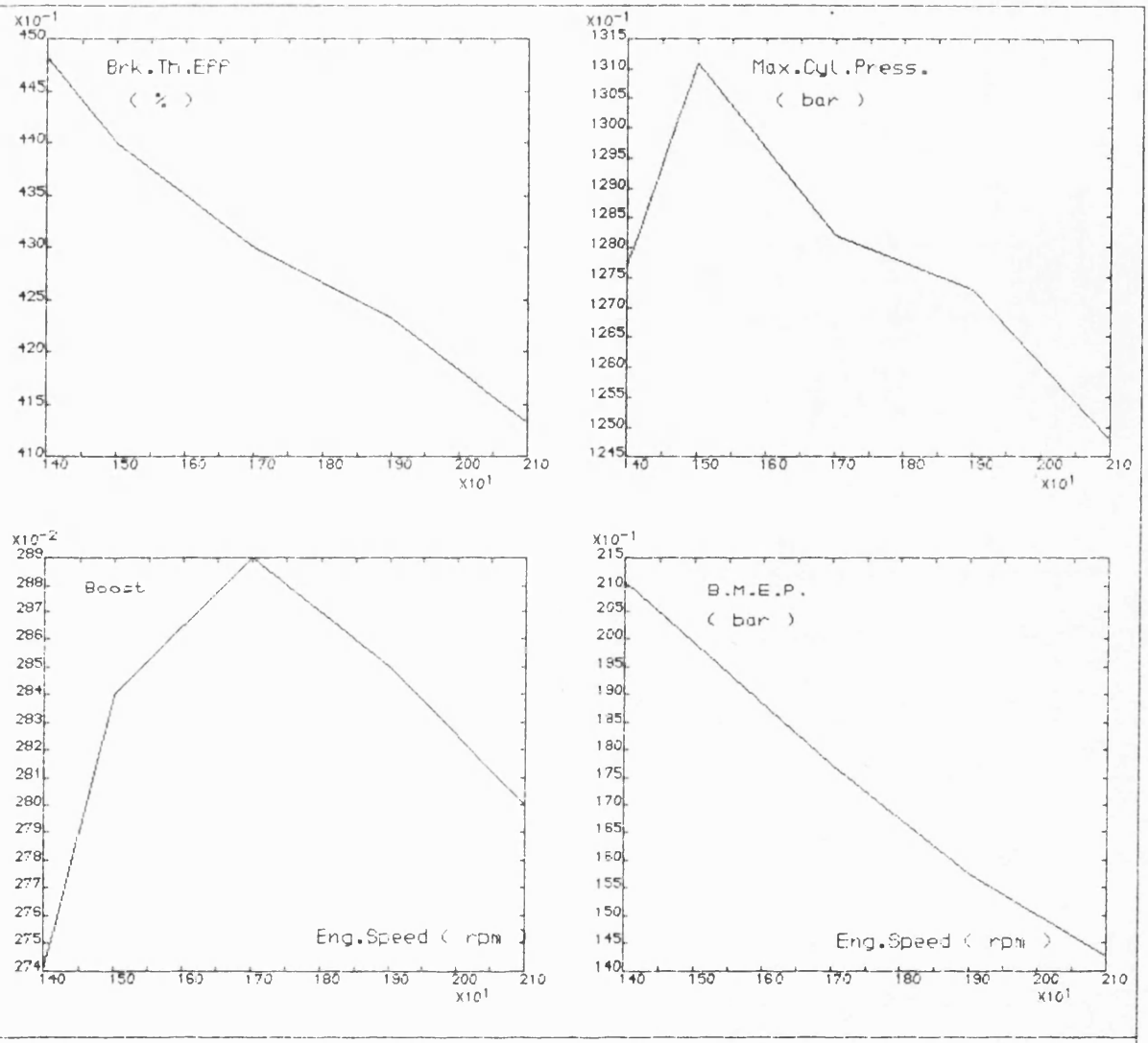

Fig. 7.5 Trends of some of the performance parameters of the uprated L10-T/C engine along the LTC

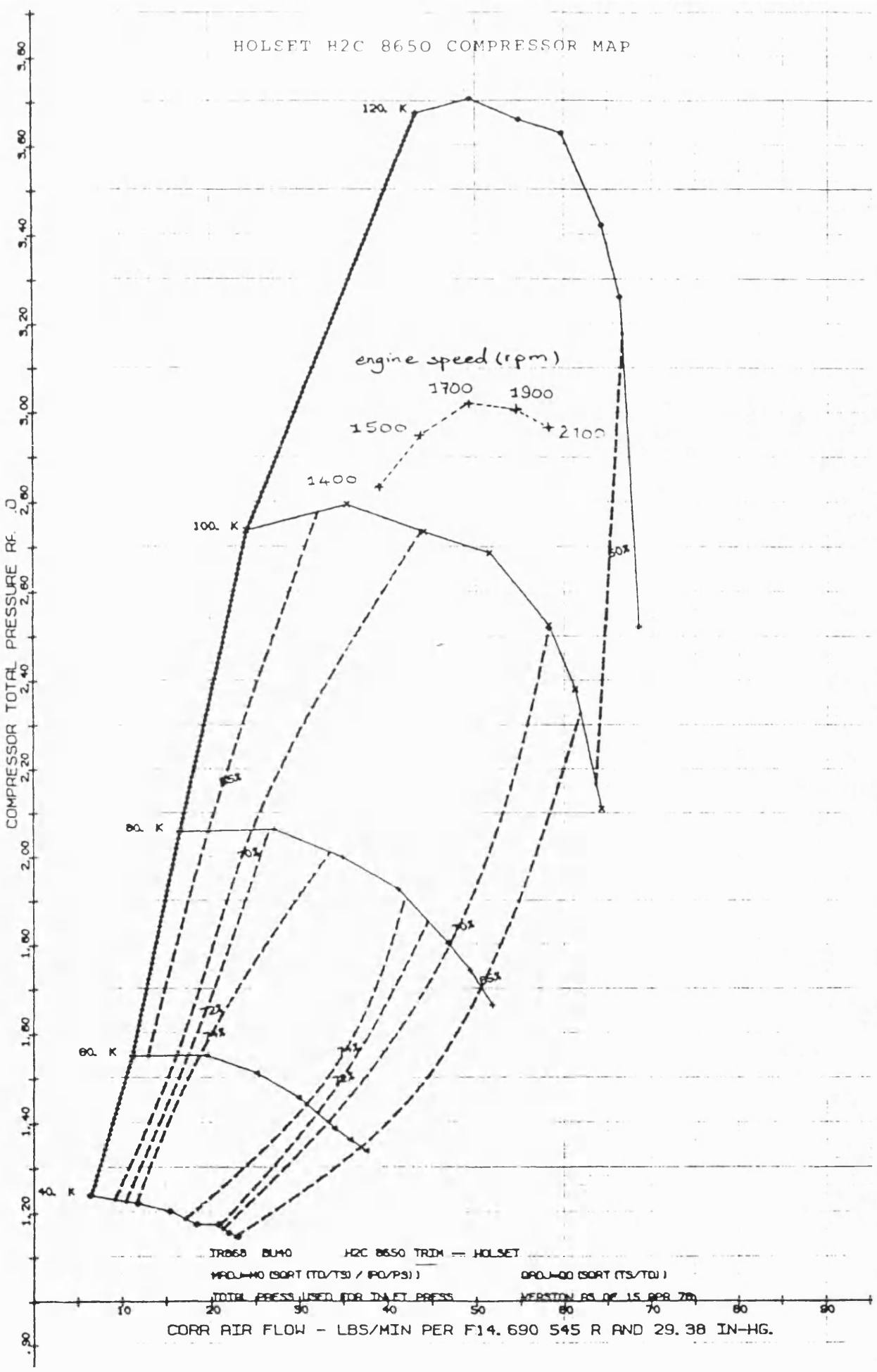

Fig. 7.6 Holset H2C 8650 compressor map superimposed with the LTC operating line of the uprated L10-T/C engine

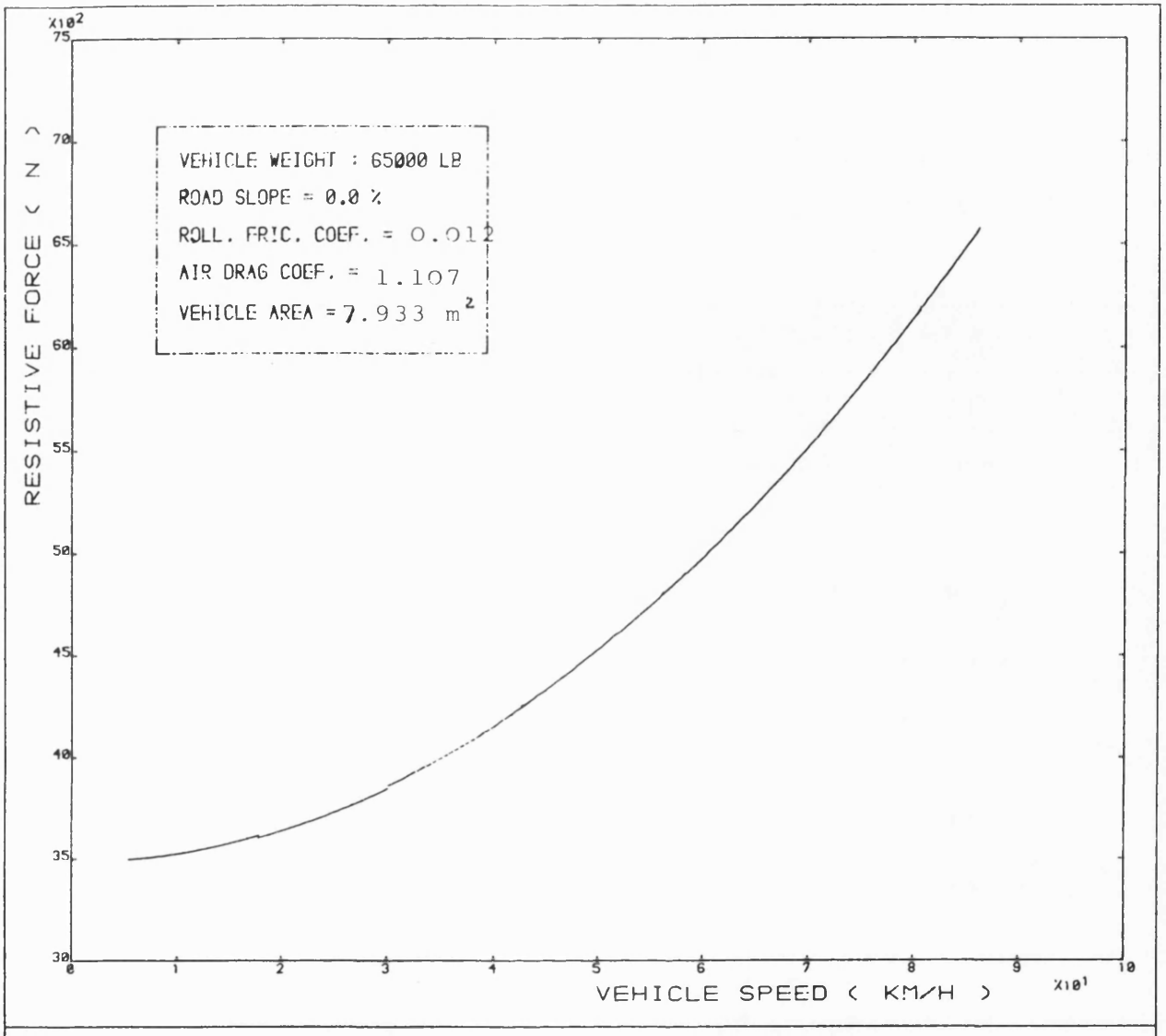

Fig. 7.7 The road resisting force

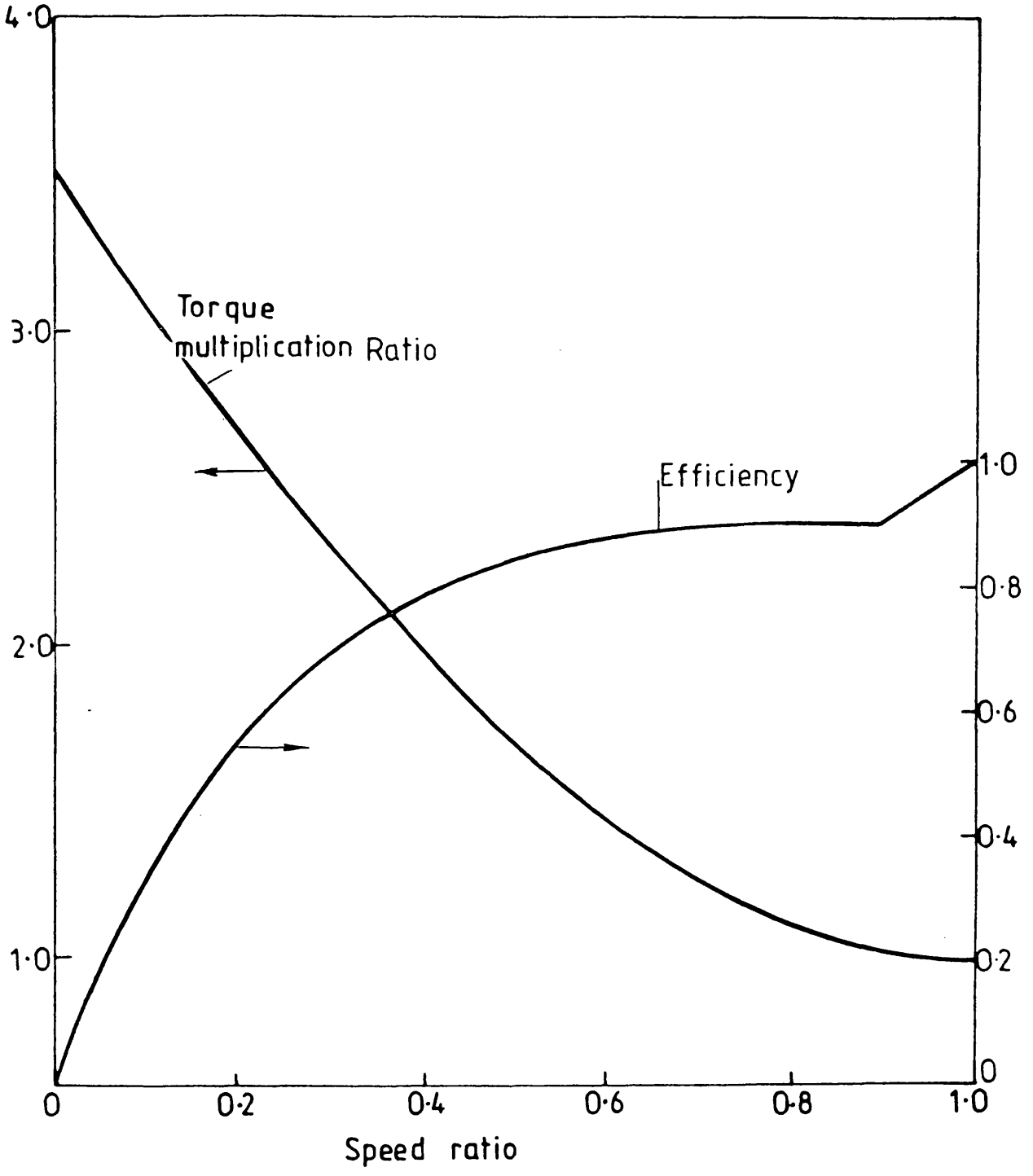

Fig. 7.8 The torque converter characteristics

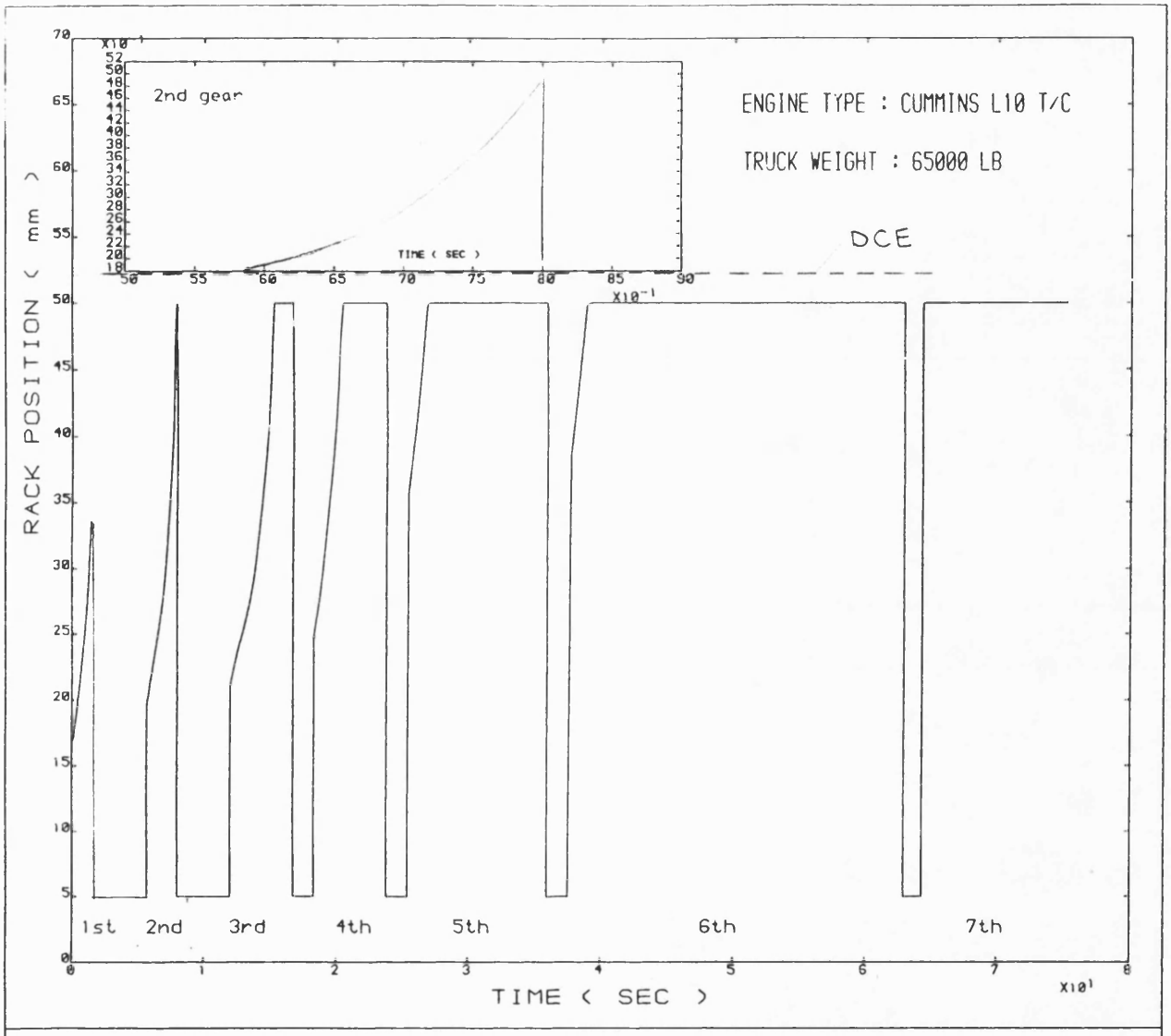

Fig. 7.9 Variation of rack position vs-time

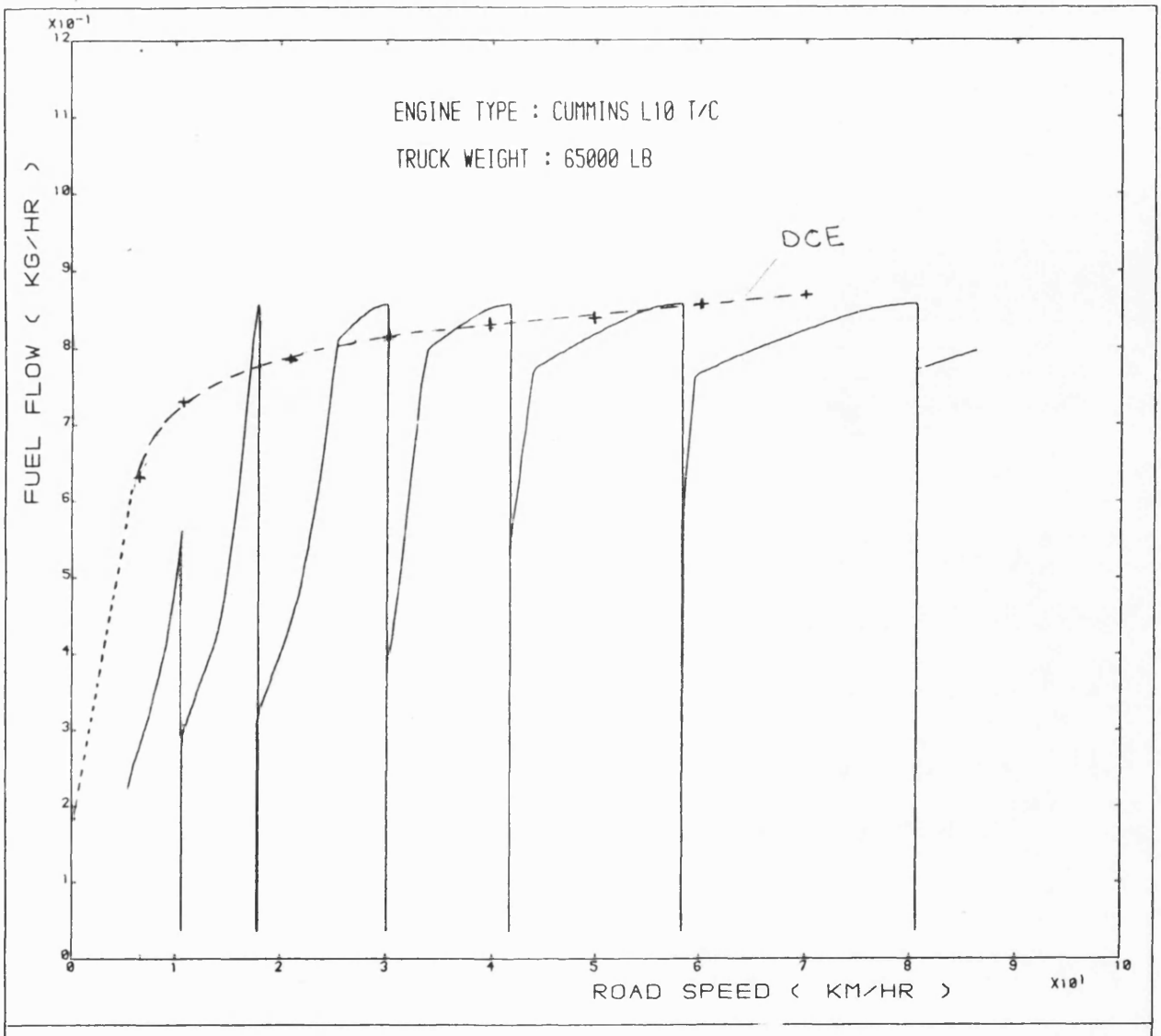

Fig. 7.10 Variation of fuel flow rate vs vehicle speed

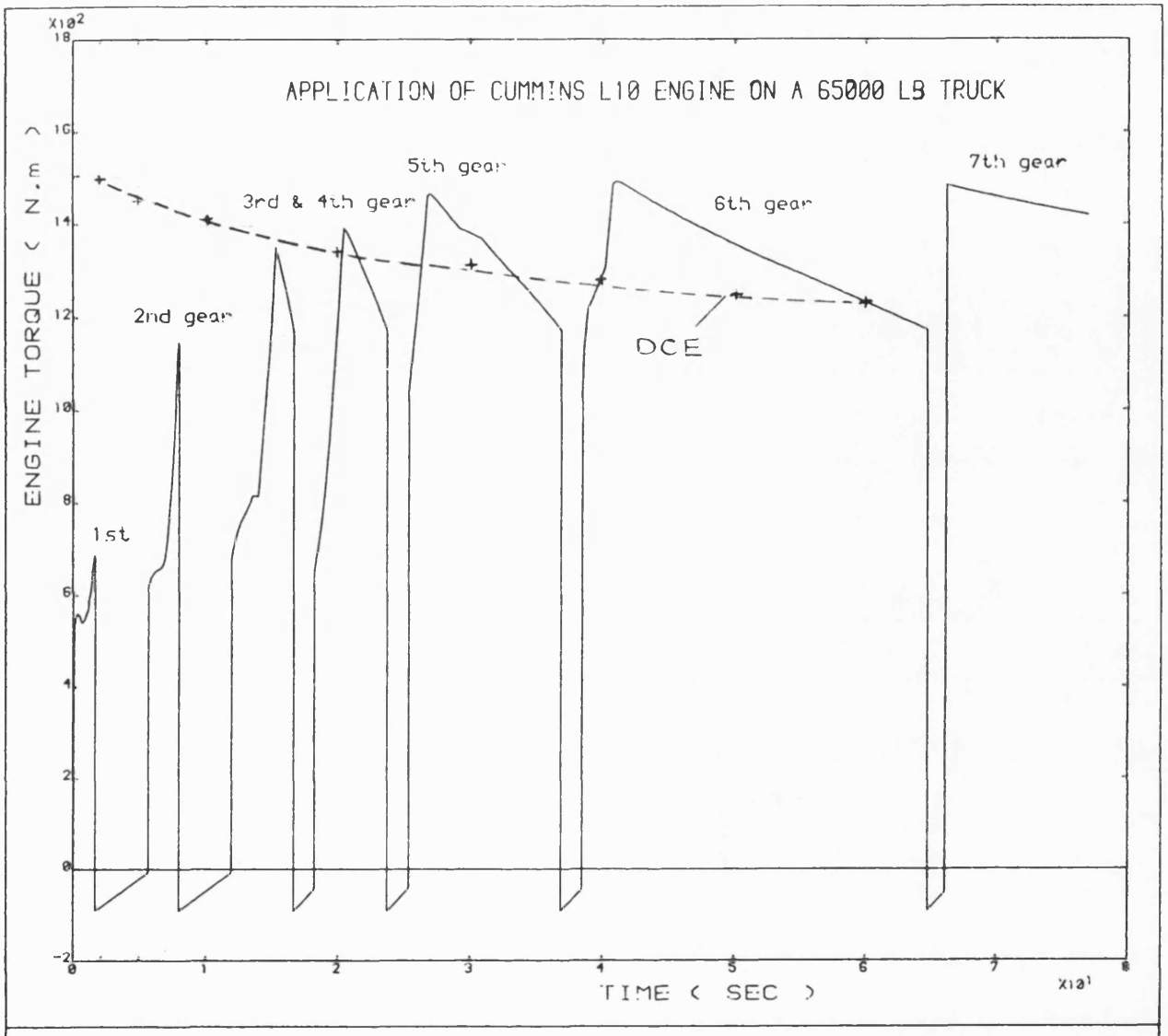

Fig. 7.11 Development of the engine torque vs time

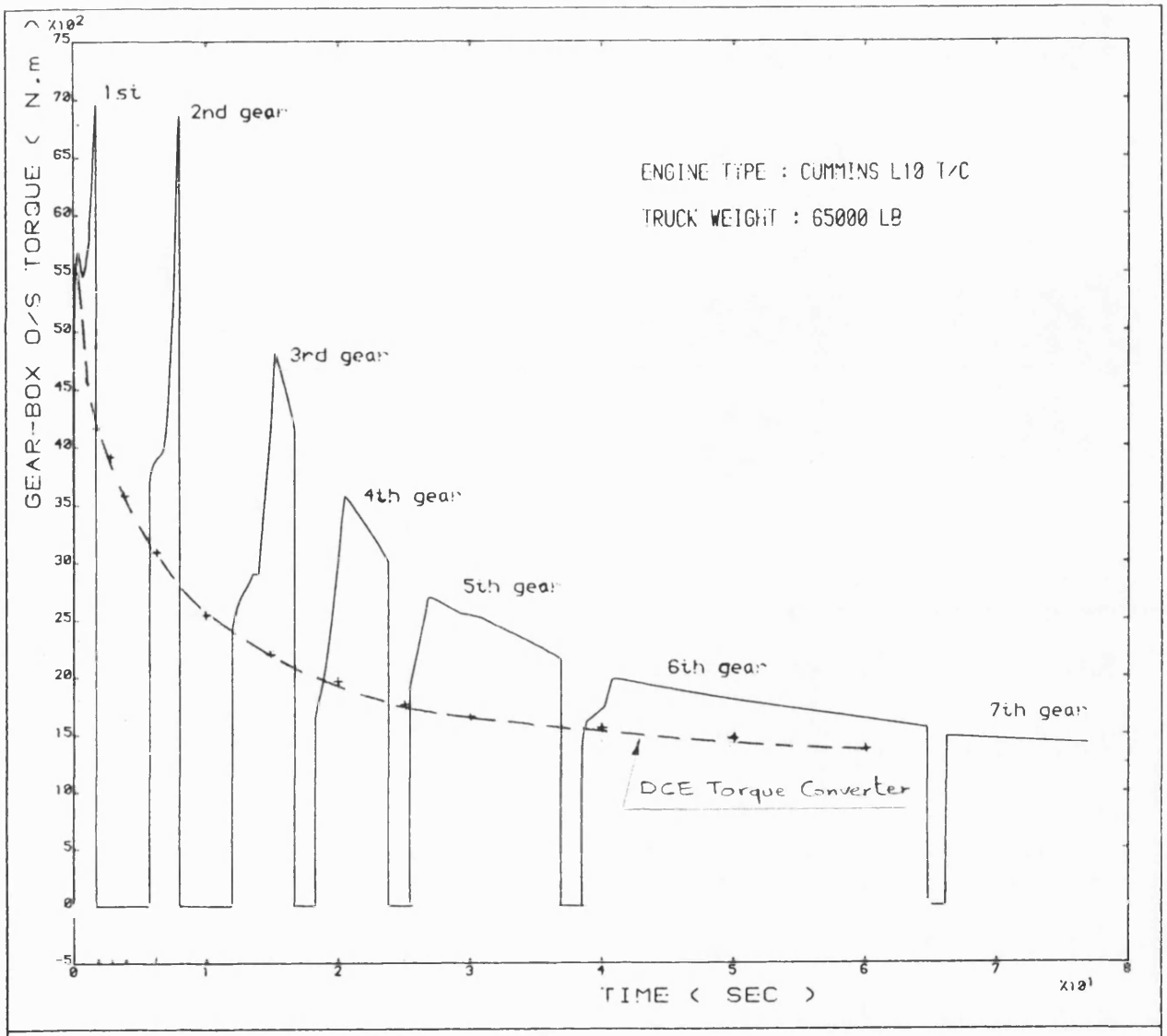

Fig. 7.12 Development of the gearbox output shaft torque vs time

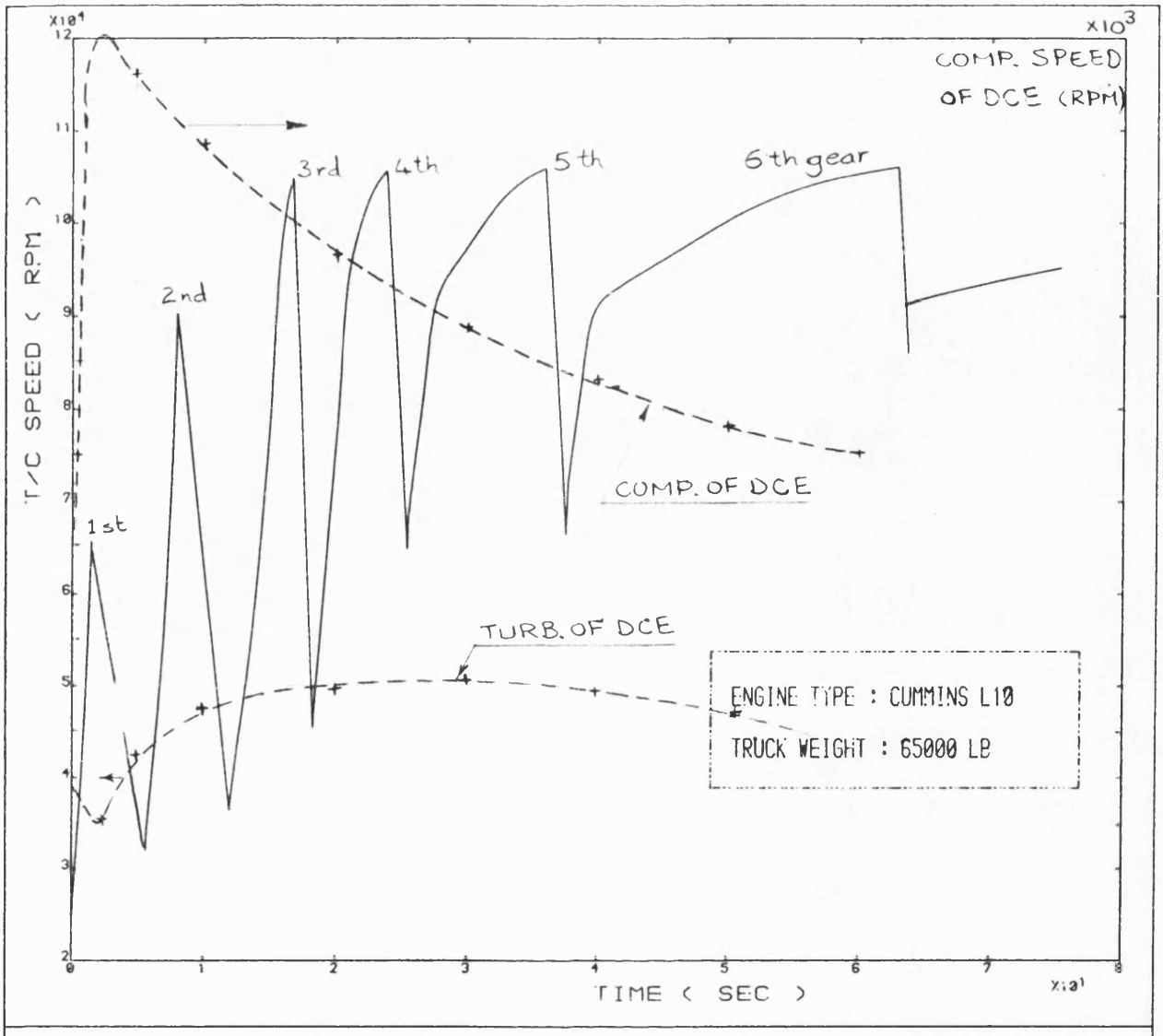

Fig. 7.13,a Variation of the T/C speed vs time

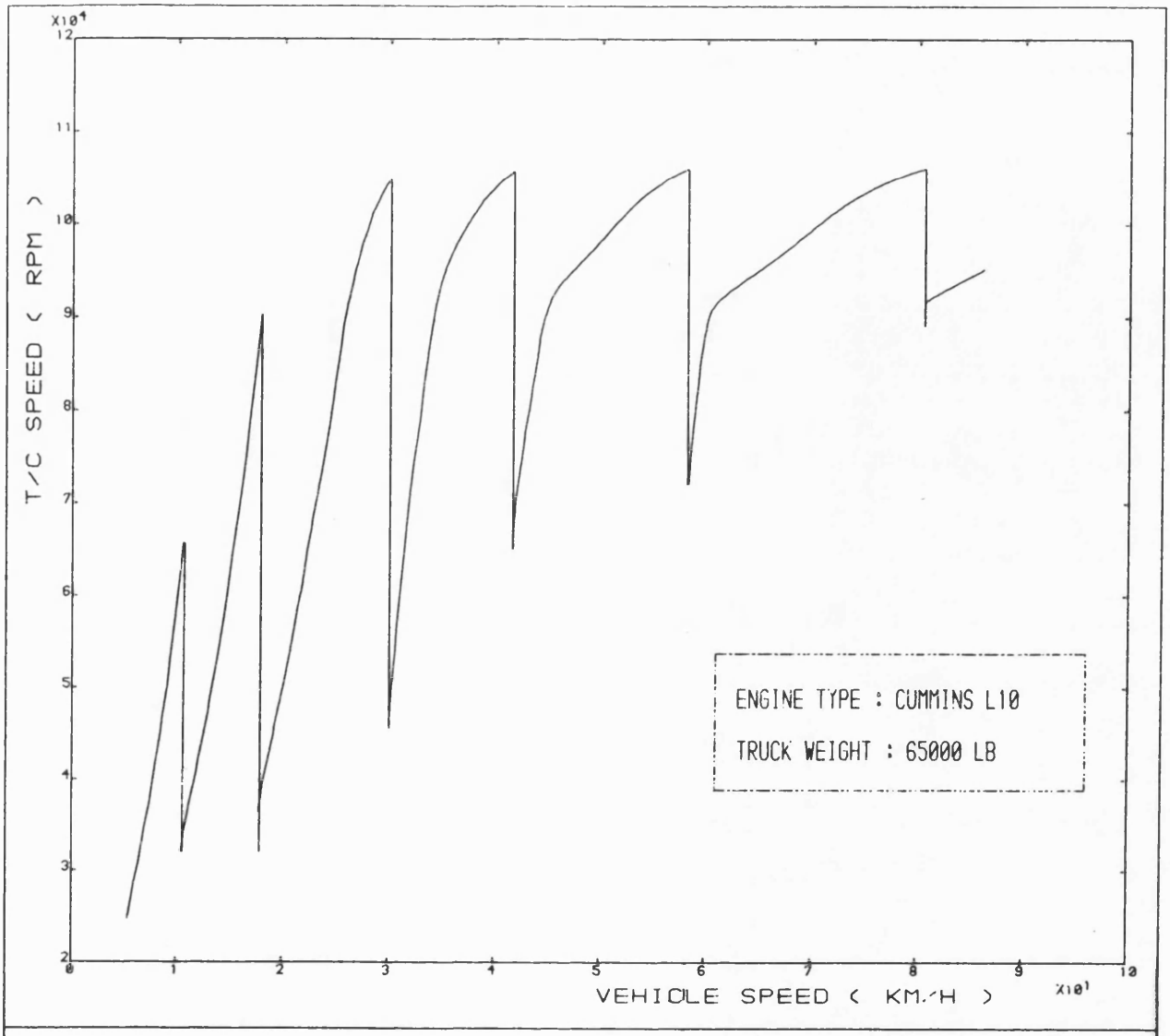

Fig. 7.13, b Variation of the T/C speed vs vehicle speed

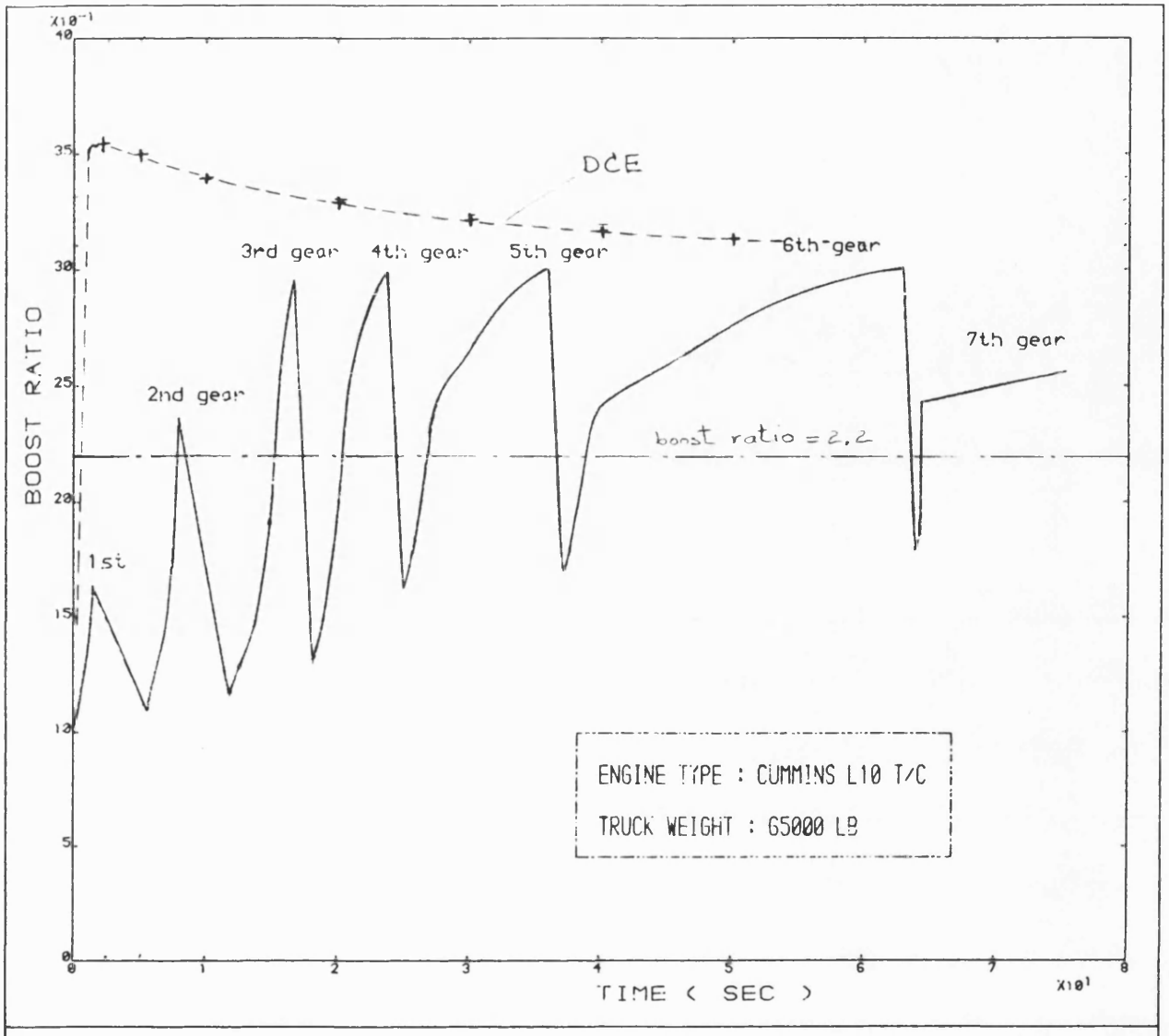

Fig. 7.14 Trend of boost pressure ratio

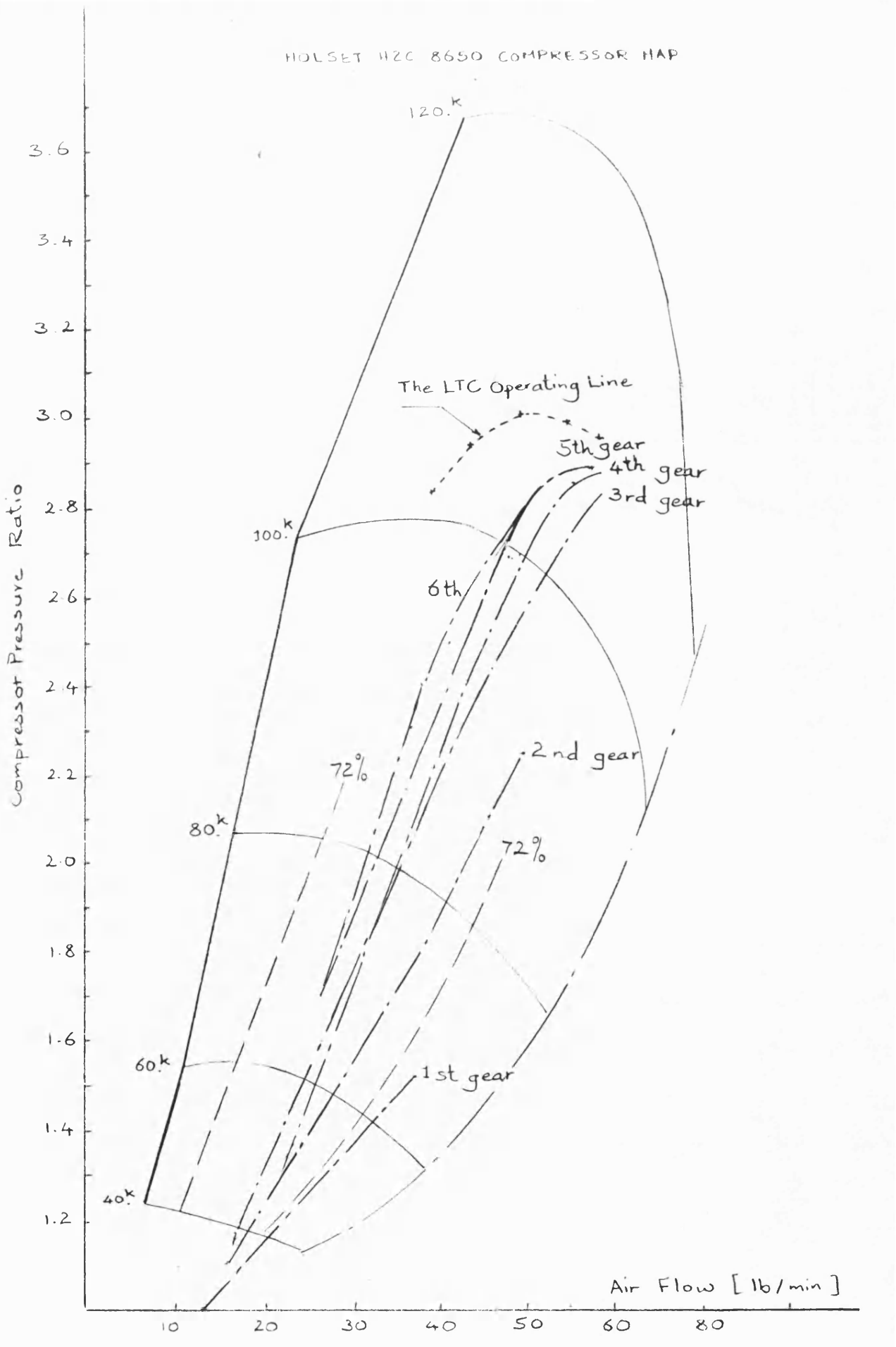

Fig. 7.15 Holset H2C 8650 compressor map superimposed with the operating lines in different gears

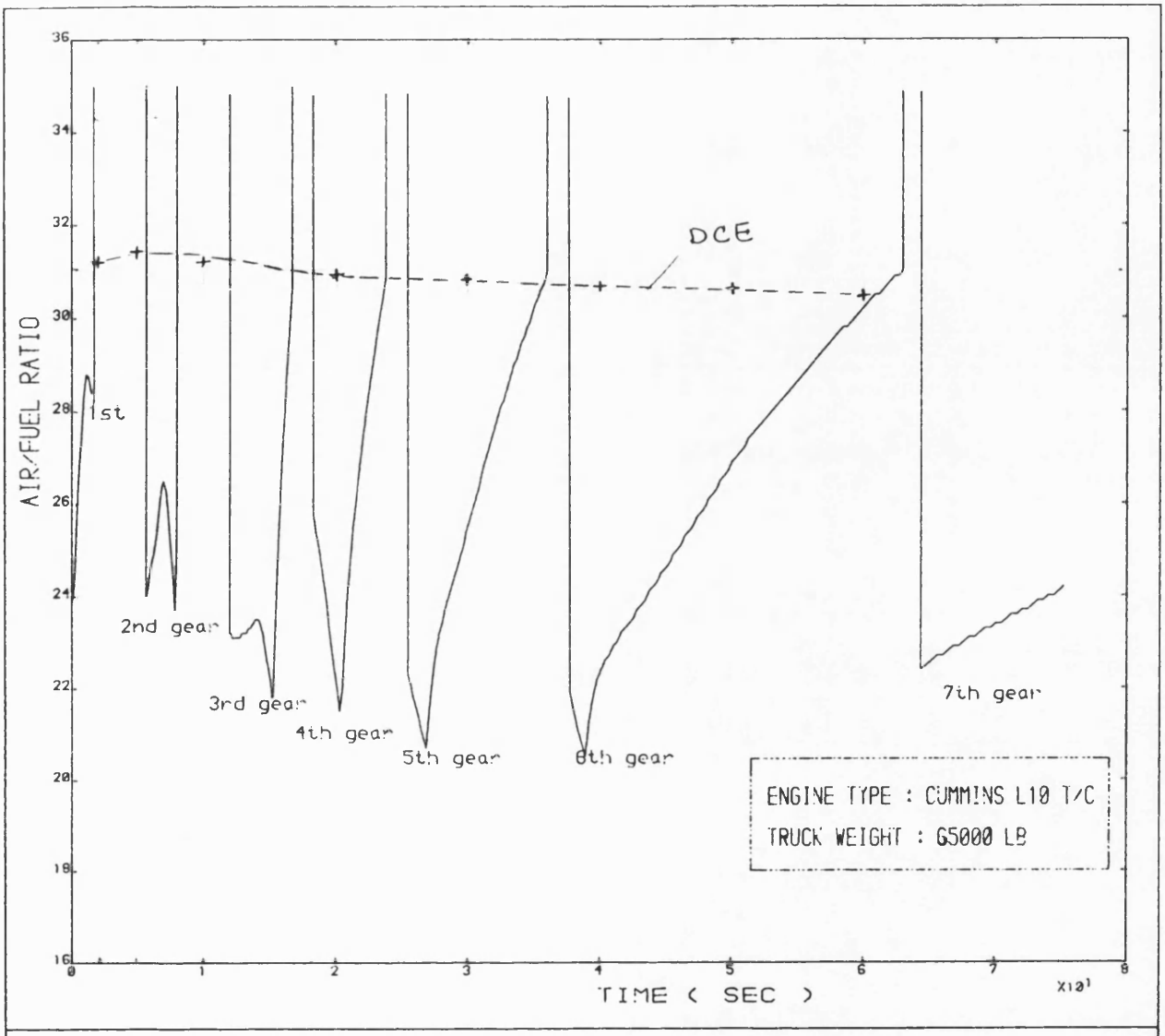

Fig. 7.16 Variation of air/fuel ratio vs time

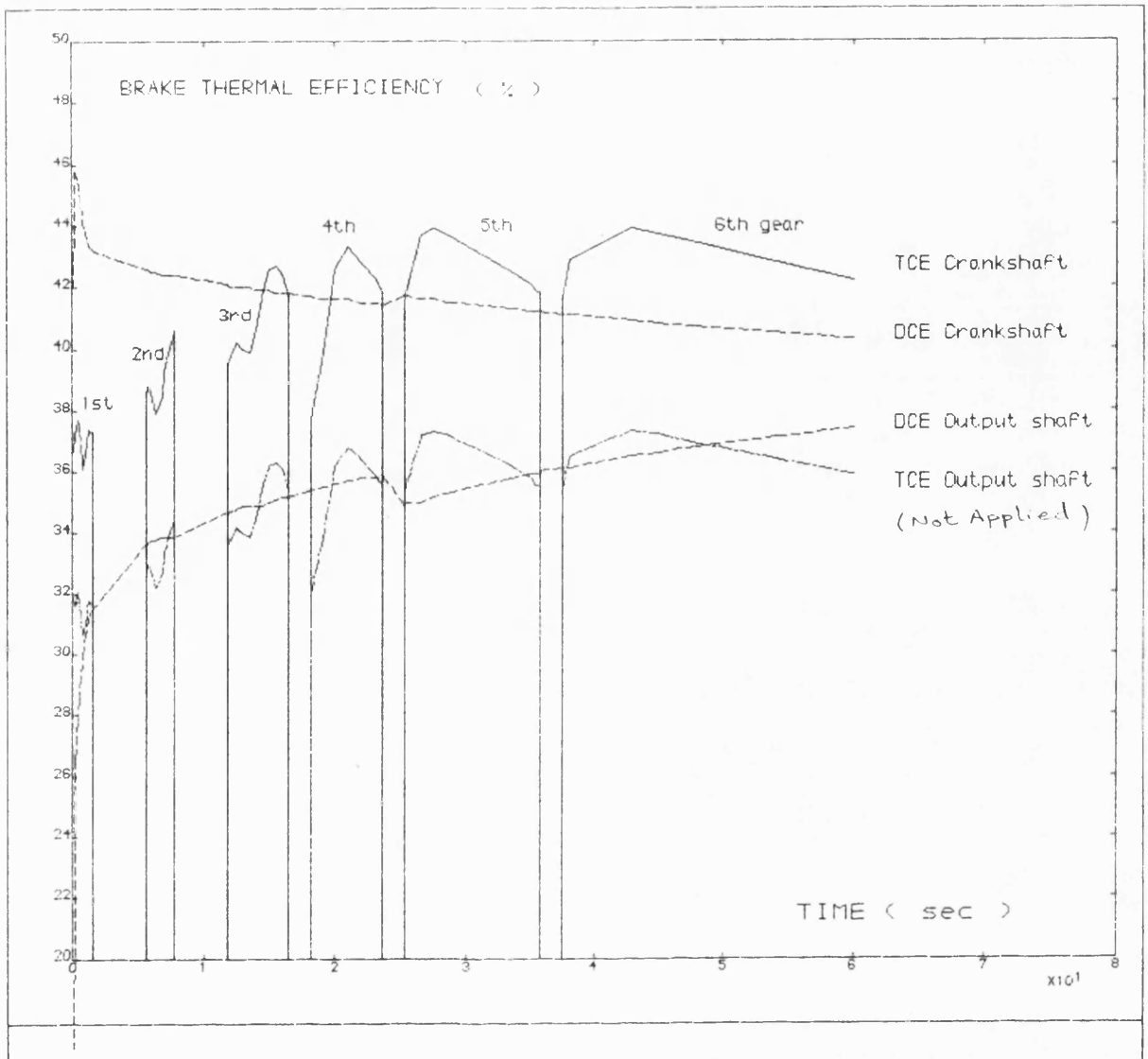

Fig. 7.17 Variation of overall and brake thermal efficiencies vs time

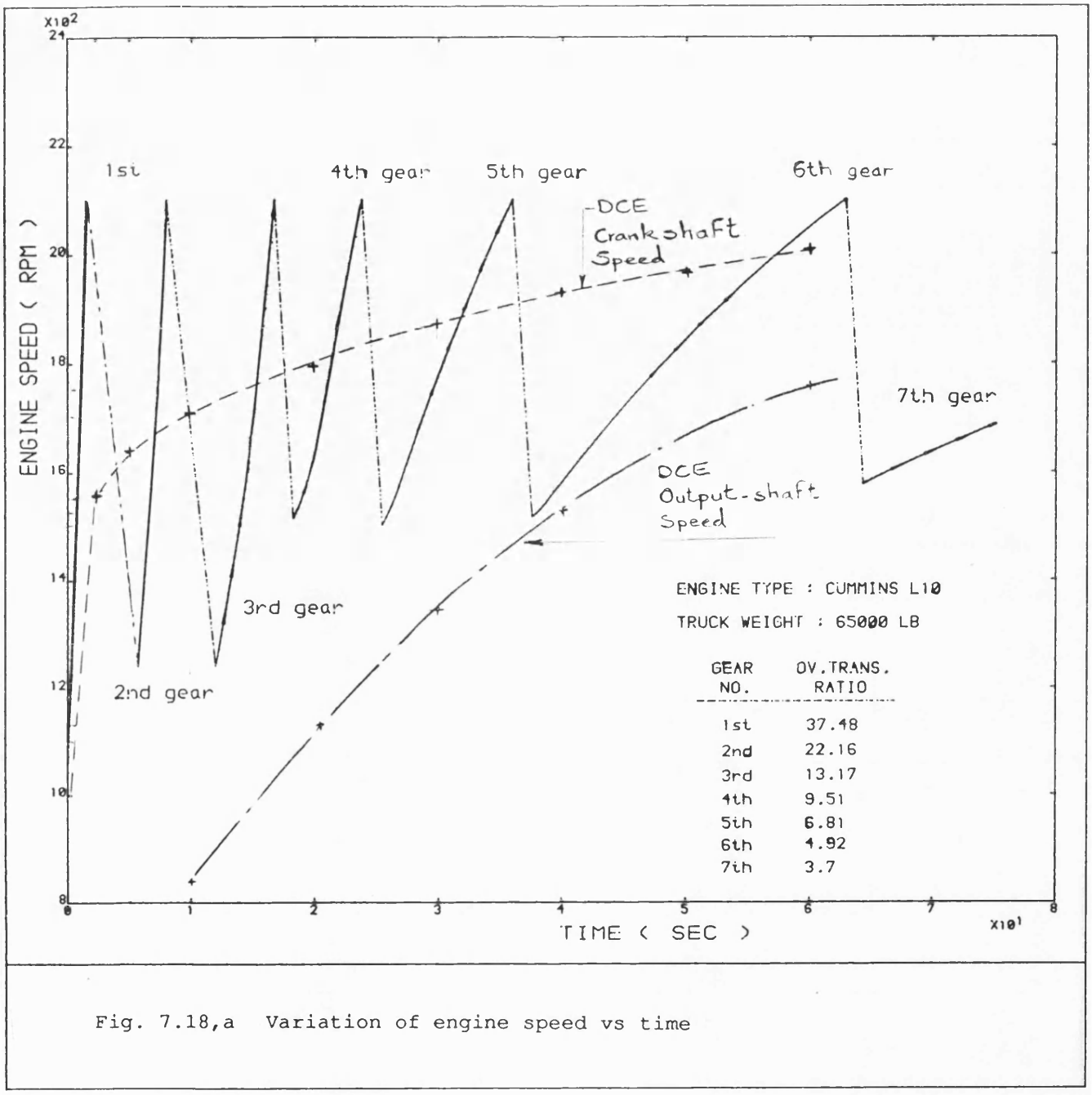

Fig. 7.18,a Variation of engine speed vs time

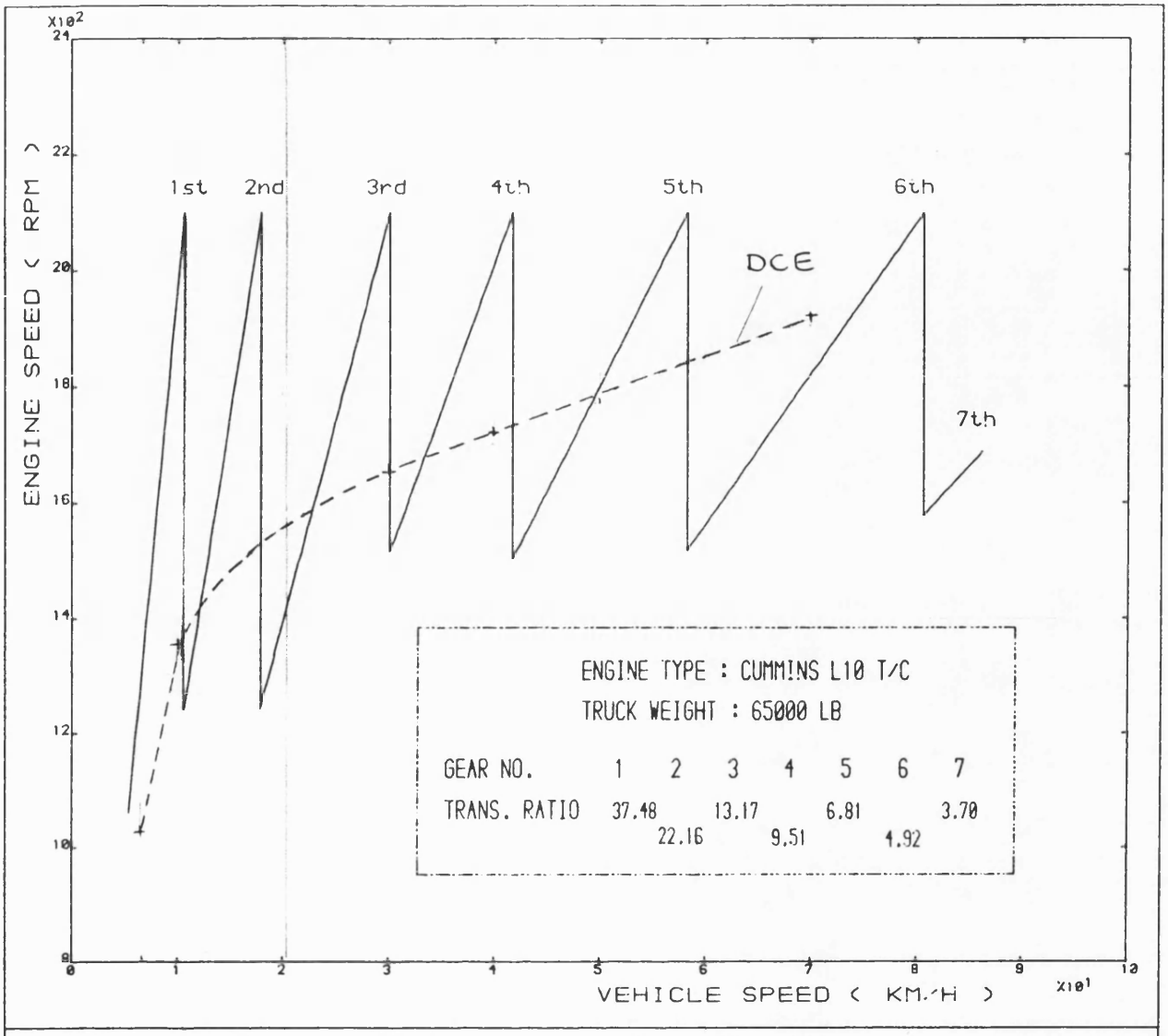

Fig. 7.18, b Variation of engine speed vs vehicle speed

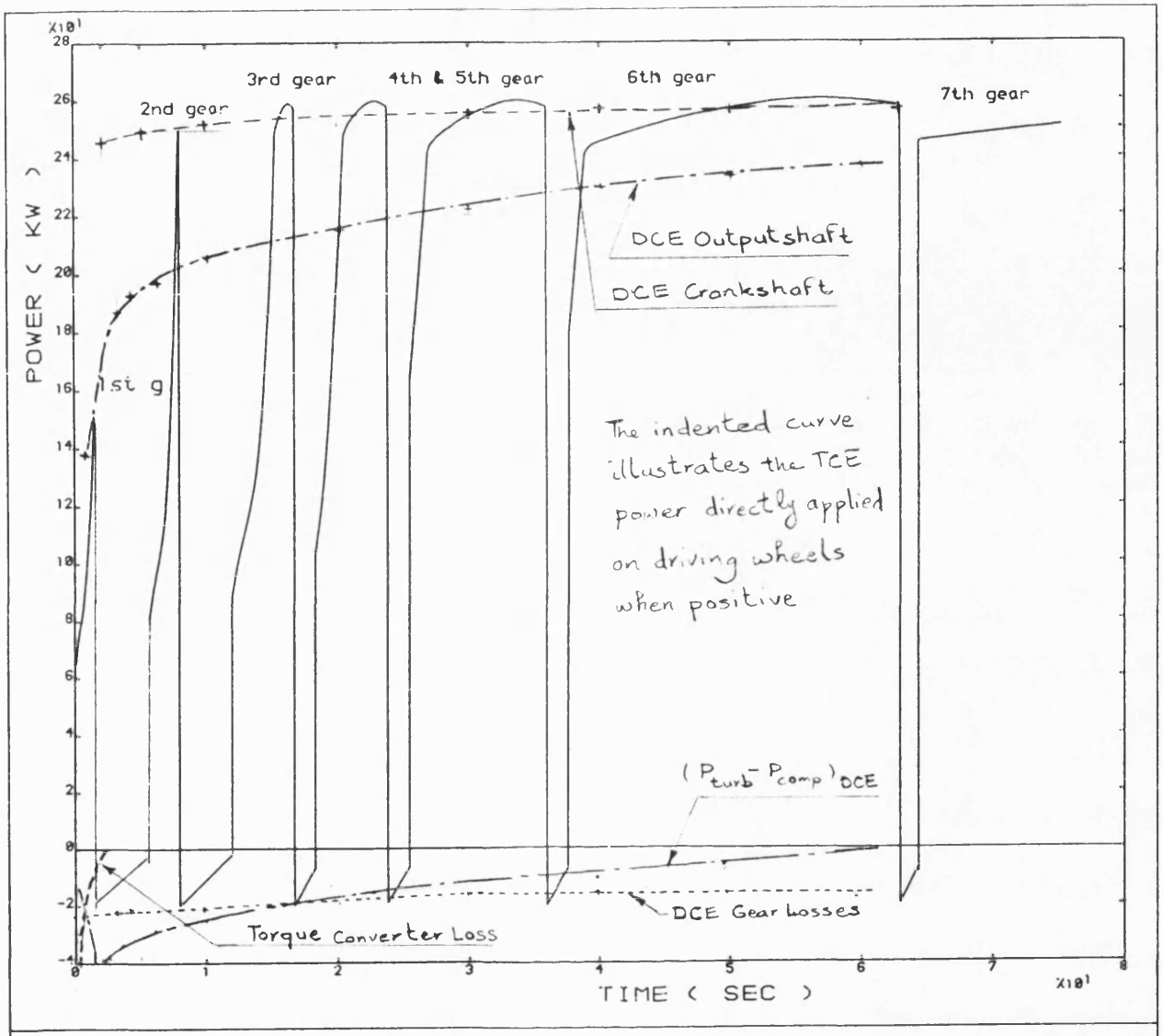

Fig. 7.19 Variation of transmitted power vs time

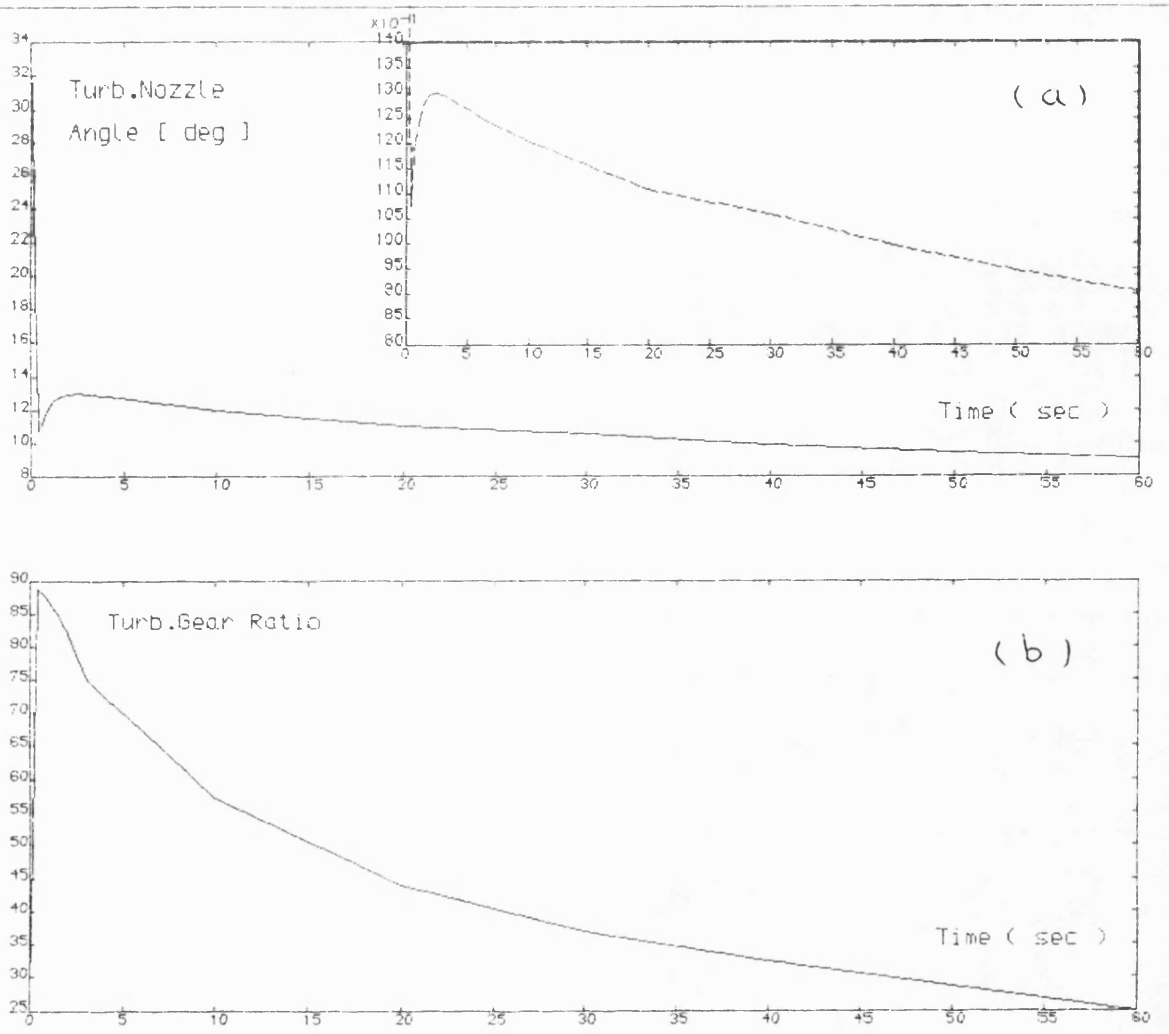

Fig. 7.20 Schedule of the turbine V.G and C.V.T for transient running conditions of the uprated L10-DCE (based on optimized steady-state running conditions) vs time

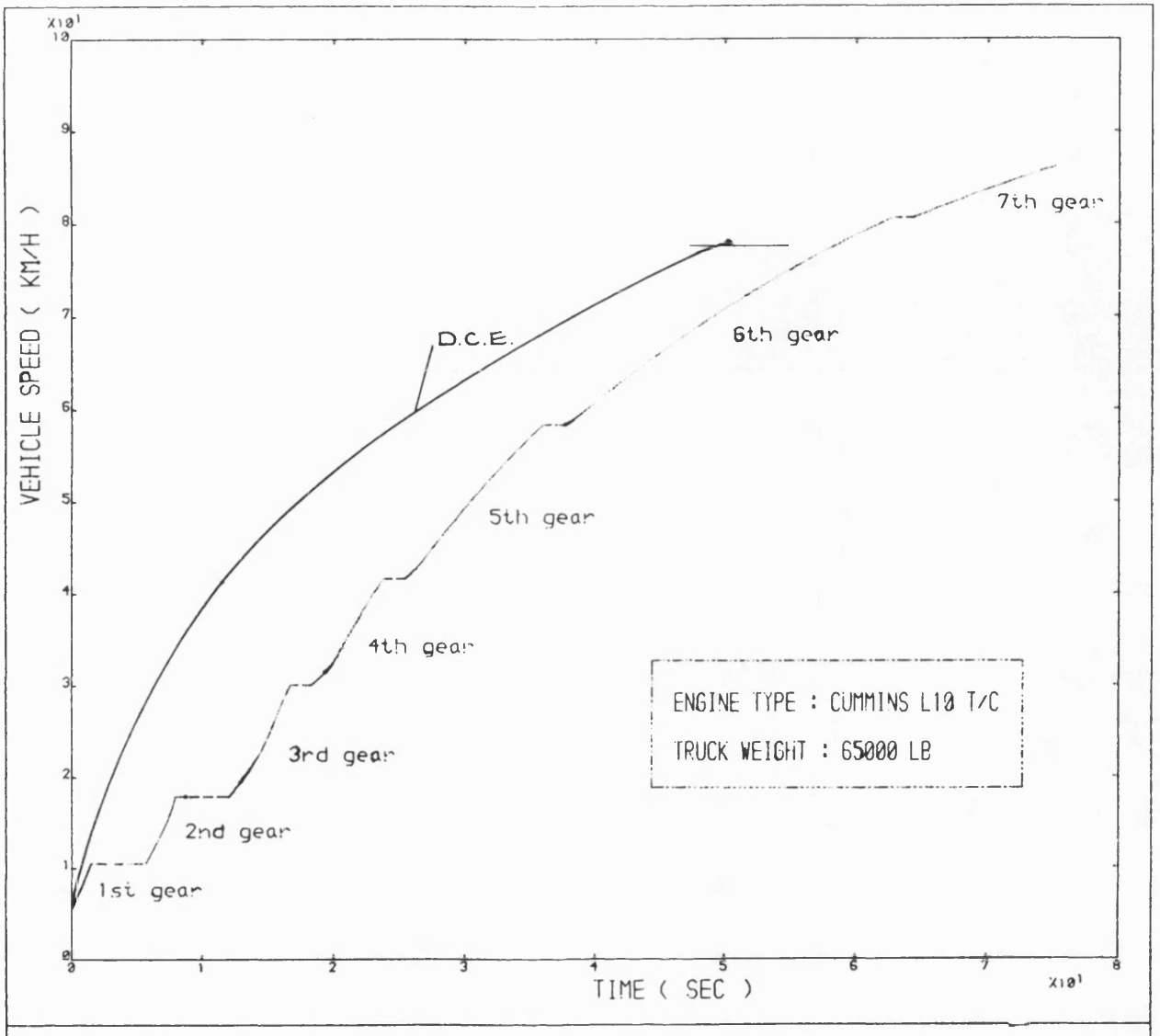

Fig. 7.21 Trend of road speed vs time for a 65000 lb truck equipped with the uprated L10 engine in its T/C or DCE configurations

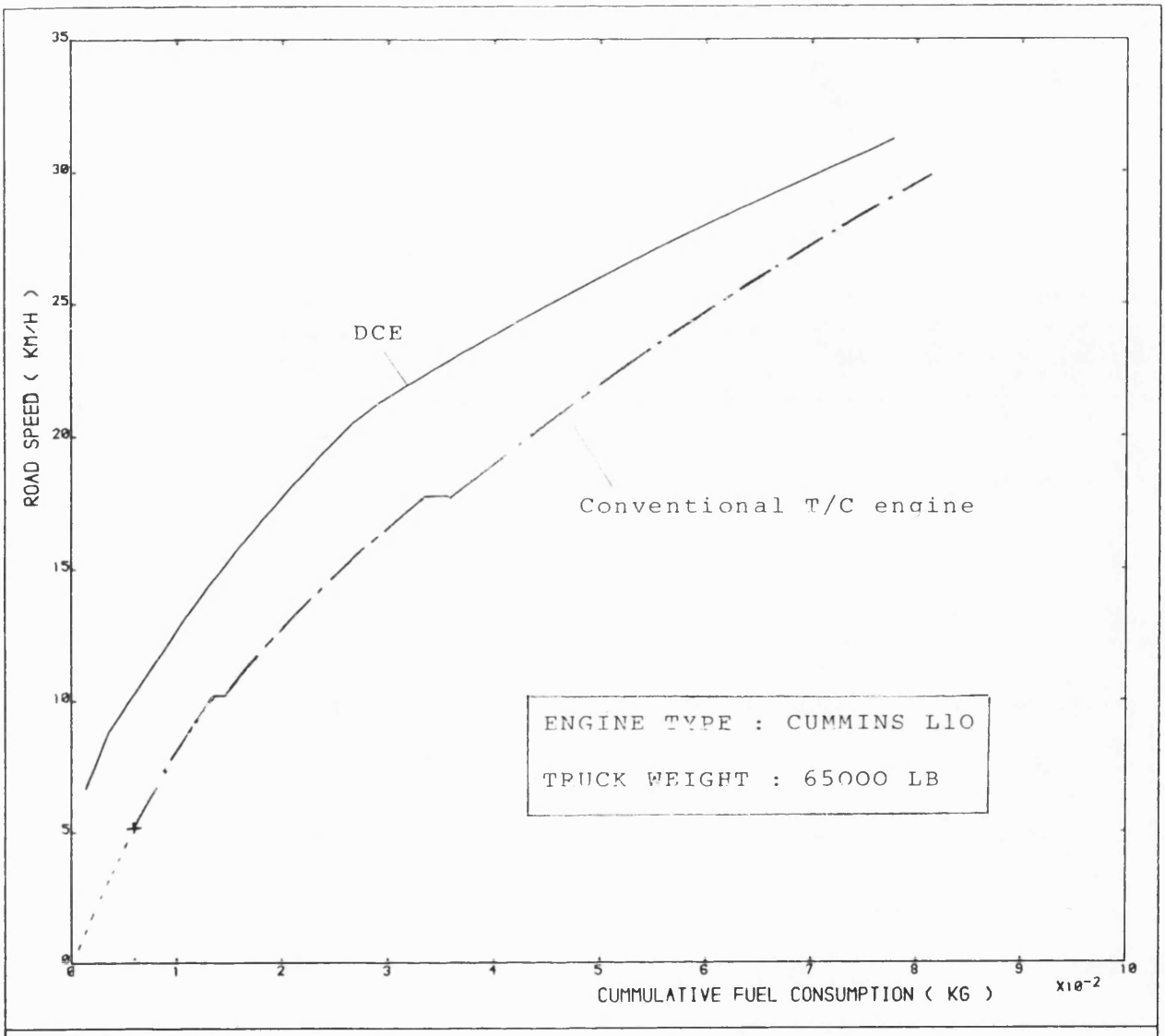

Fig. 7.22 Cumulative fuel consumption to reach any specified road speed for a 65000 lb truck equipped with the uprated L10 engine in T/C and DCE configurations

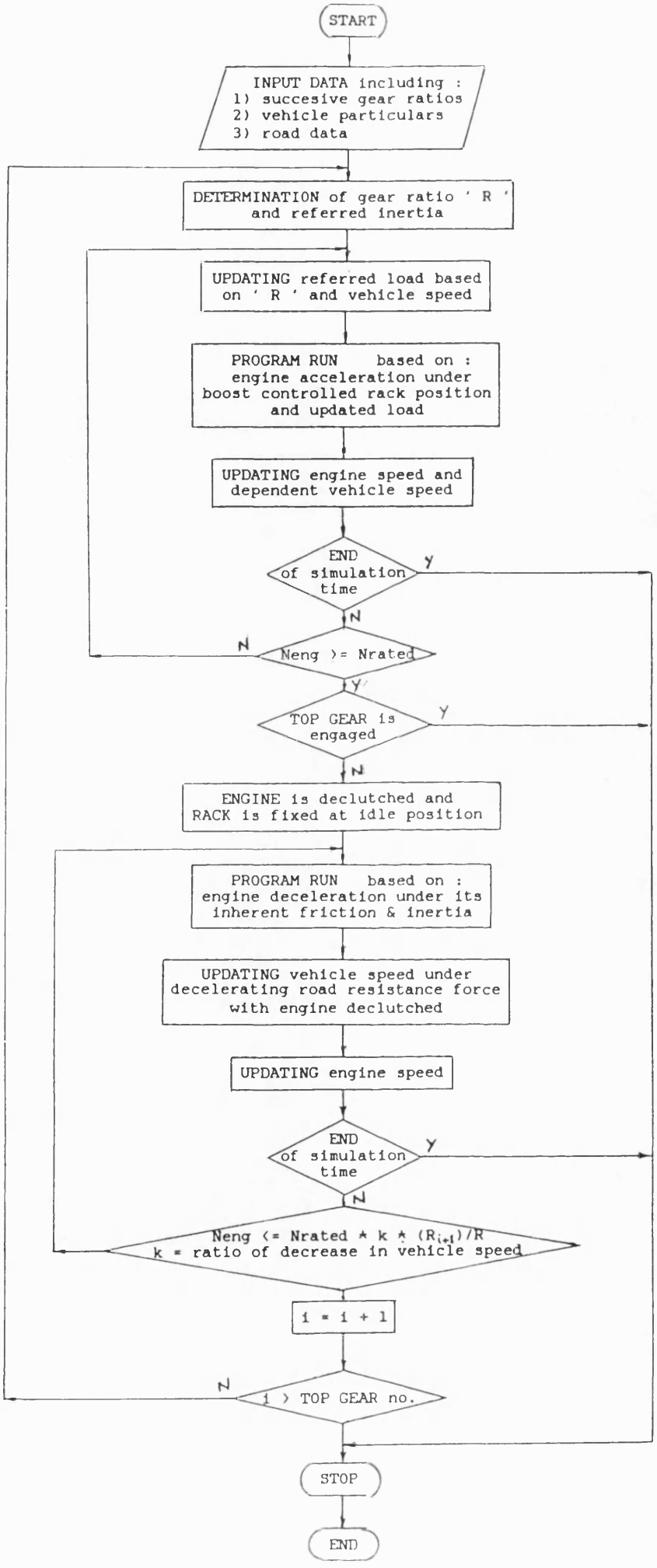

Fig. 7.23 The flow diagram of the modifications applied to the program TRANIC to simulate road and truck gear change

CHAPTER EIGHT

EXPERIMENTAL RESULTS OF THE LEYLAND 520-DCE AND VALIDATION OF THE PROGRAM 'DCE2' PREDICTIONS

8.1 INTRODUCTION

To demonstrate the degree of reliability of performance predictions made by different versions of the program 'EMAT' for the L10 engine in its DCE configuration under steady-state and transient operating conditions, this chapter compares the available steady-state experimental results of the Leyland 520-DCE with the program DCE2 calculations based on synthesizing the same test conditions.

A brief description of the test bed is given. This, together with the description of test procedures illustrates the possibility and practicability of the system optimization. In order to simulate the prototype at exactly the same tested running conditions, it was required to modify the program DCE2 so as to make it possible to input the exact piping pressure drops as part of running data while the input data with respect to the gear losses had to be calibrated.

The results of the simulation as compared with those obtained from experiments not only demonstrated the degree of accuracy of the program predictions but also determined some of the performance parameters which were not available experimentally.

In a second series of simulations the same piping pressure drops and gear losses were used as in the simulation of the L10 engine. Comparison of these two simulation results for the experimental Leyland 520-DCE not only showed the extent of improvements achievable by reducing the above losses, but also qualitatively evaluated the degree of accuracy of the performance predictions for the L10-DCE presented in Chapters 5 and 6.

8.2 DESIGN AND BUILD

The detailed description and specification of the latest form of the laboratory DCE based on the Leyland 520 engine is fully presented in ref. 39. From this reference a summary of the mechanical specification and arrangement, as well as of the instrumention is presented in this chapter for completeness.

Design of the unit was carried out by Prince (ref. 39) with respect to the past experiments (ref. 40) based on the Perkins 6.354 DCE. The matching calculations were carried out by using the rapid matching program DCE2.

The overall silhouette of the prototype is represented in fig. 8.1 and the design figures are shown in table 8.1. The pipework arrangement is shown in fig. 8.2.

8.2.1 Engine

The Leyland 520 engine incorporated in the system is fitted with low compression pistons and an uprated fuel system. The specification of the engine is given in table 8.2. The engine is also fitted with uprated oil and water coolers of 30 kW and 135 kW heat dissipation capacities respectively.

Fuel supply to the engine may be switched between a tank supply and a beaker. The latter is used for accurate measurement of steady-state fuel flowrate. The fuel sysem uses an in line pump with max. delivery of 0.28 cc/shot per cylinder. The injector overflow is mixed with incoming fuel after the beaker rather than returned to the tank, in order to make fuel flow measurement possible. Fuel temperature at inlet to the in line pump is held constant.

The mechanical governor has been replaced by a hydraulic actuator which together with a servo-valve and a LVDT constitutes a control system. The mode of governing is implemented electrically e.g. speed governing with droop.

The standard injection timing is 28 deg BTDC. However, a variable timing device is fitted. This is based on the same design as was applied in ref. 41 using a helically splined shaft and matching collar. As the collar is moved up the shaft, it produces an angular displacement between collar and shaft to retard the injection pump. The collar is moved by a yoke and arm which in turn is moved by a jack. Finally, the jack is controlled by a hydraulic actuator. If the servo fails the timing device goes to full retard. This was considered to protect the engine from possible conditions of dangerously high cylinder pressures.

A needle-lift transducer is fitted into the injector of no.1 cylinder. The electric signal of this together with that of an electromagnetic TDC marker of the same cylinder are detected by an oscilloscope to yield injection timing and duration.

8.2.2 Compressor

The compressor is of the rotary positive displacement screw type supplied by CompAir Industrial Ltd. Some of the important performance characteristics are given in table 8.2.

8.2.3 Turbine

The turbine is of the twin entry radial inflow type supplied by Napier. The original unit is of the fixed nozzle type (CO-45B) with a throat area range between 3.23 and 8.98 sq.in, capable of handling an expansion ratio of 2:1. However, the unit was adapted for variable throat area between 0 and 5 sq.in and pressure ratio of 4:1. Some of the important performance characteristics of the unit are given in table 8.2.

There are 16 nozzle blades each attached to a rod rotating in a bush in the housing. The nozzle blades are equally turned by a rotating ring via arms each as an outer extension of a nozzle blade rod. An arm is attached to the rotating ring of the nozzle mechanism and this is actuated by a hydraulic jack. This is, in turn, driven by a servo-valve, and its position feedback is given by LVDT. The nozzle movement is confined to a range between 0 and 12 degrees.

8.2.4 Piping System (fig. 8.2)

The piping system is designed for the lowest pressure losses possible. Starting from the compressor inlet, is a 7 in diameter flexible tube. This permits having a free-standing inlet unit moveable to wherever appropriate to take in a mixture of air from outside and inside of the test cell to adjust inlet temperature. A panel air-filter is adapted to meet the high air flowrate of the screw compressor. A butterfly valve just before the filter is used to control the inlet depression.

A plenum of 10 ℓ capacity is fitted to damp out the compressor delivery pulses. The bypass and engine intake pipes are connected to this plenum (fig. 8.2). In fact the bypass and intake pipe effectively make this volume much bigger since the largest practical diameters are used for minimum pressure loss, although this is disadvantageous for transient performance.

Both the intake and the exhaust pipe are of 4 in diameter giving a total pressure loss of the order of 0.02 bar at rated conditions. The intercooler pressure drop is of the order of 0.1 bar at these conditions and is thus the major pressure loss in the pipework.

The intercooler is an air/water cooler and has a max. heat dissipation capacity of 70 kW. This can lower the air temperature from 220°C to 50°C at an air flowrate of 28.6 kg/min.

To prevent the engine from overfuelling and overspeeding, the air supply is cut off by an inlet air shut-off valve as an ultimate safety measure. This technique avoids any complication with electronic fuel shut-off by using a simple butterfly valve on the inlet side of the intercooler. An air pressure-reducing valve is also provided immediately before the shut-off valve, designed to release over-boost pressure and thus prevent the compressor from overloading.

The original pulse type exhaust manifold was replaced by a cylindrical exhaust plenum sufficiently large to provide an almost constant pressure manifold. A 3 in. diameter pipe connects the compressor and turbine

plenums by the shortest route. At its mid point, it has a manually operated butterfly valve which is normally left open controlling bypass flow.

The constant pressure exhaust plenum makes it possible to drive the bypass flow by the mean pressure drop across the engine after which it mixes with the exhaust gases before the turbine.

The turbine thus operates under steady state conditions giving higher turbine efficiencies. It should be noted that the pulse characteristics of the original manifold are unnecessary with the DCE. However, the large exhaust manifold is detrimental to the scavenge process, while the mixing process causes additional losses. The total capacity of the manifold is 20 ℓ, made up of 8 ℓ of the exhaust manifold itself, 8 ℓ of the turbine plenum for mixing exhaust gases and bypass flow and 4 ℓ in the connecting pipework.

The exhaust gases leave the system after the turbine through a 6 in. pipe leading to the smoke stack in the cell roof. Again a butterfly valve in this pipe is used to control the system back pressure. The wide open valve creates a back pressure of about 0.1 bar.

8.2.5 Services

Services include all facilities required to provide controlled running conditions for the test bed and cover :-

1- Fuel supply provision
2- Lubricating oil recirculating systems
3- Cooling water recirculation systems
4- Hydraulic oil recirculation system
5- Electric and electronic control circuits

8.2.6 Shaft Connections

As described in Chapter 1, Section 1.3, an epicyclic gearset interposed between the DCE components provides the characteristic features of the system. The gearbox used on the test bed for this purpose was originally supplied by Allen Gears, Ltd. but is of marine rather than automotive design. Although some adaptations were carried out, the losses and inertias are still unrepresentatively large. The gear arrangement is shown in fig. 8.3 with the rated and stall rotation speeds of all elements including the shafts, external to the epicyclic gearbox.

ENGINE. Due to complexity of the interconnecting shafts and inertias as well as having included unusually long shafts, torsional vibration had to be carefully checked for resonance. To tackle the problem a soft coupling (torsional damper) was fitted in the engine driveline being bolted directly onto the engine's flywheel.

The flexibly mounted engine is coupled to the rigidly mounted epicyclic gearbox via a propshaft, part of which is a torquemeter. To remove any extra strain on either side of the shaft, special couplings were used so as to provide an angular tolerance of 0.6° at the engine end and of 1° at the epicyclic end.

COMPRESSOR. The coupling arrangement of the compressor incorporates a brake disc at the epicyclic shaft end. The brake disc acts as a part of the shut-down system's operation and prevents compressor reversal.

TURBINE. Although it is quite important that the DCE should ideally incorporate a turbine CVT, a fixed gear ratio is used in the experimental unit.

DYNAMOMETER. A twin hydraulic pump arrangement is used to act as the dynamometer for the system. The unit is driven through a fixed-ratio splitter gearbox (i.e. the DCE output shaft as the single gearbox input and two outputs for the dynamometer) supplied by Waring-Rigby Transmission. The splitter gearbox is coupled to the epicyclic box via a long shaft incorporating a second torquemeter. Gear couplings are used at

either end of the shaft to provide adequate misalignment capability.

8.2.7 Instrumentation

SPEEDS. Shaft speeds are measured for engine, compressor and output shaft by toothed wheels and magnetic pick-ups. Compressor speed is also calculated by an analogue calculating card using the epicyclic speed relation. Turbine speed is not measured as it is in a fixed ratio to the output speed.

TORQUES. Engine and output torques are measured directly by strain-gauge type transducers. Compressor and turbine torques are not measured directly because of lack of space and practical difficulties. However, compressor torque is estimated using pressure ratio, speed and experimental performance data. In the case of the turbine, thermodynamic work and isentropic efficiency are calculated from the temperature drop, mass flow and pressure ratio using average values for C_p and γ for the exhaust gases. This inevitably allows only approximate estimation of gear losses.

GAS PRESSURES. Gas pressures are all measured by manometers filled with mercury or water as appropriate, except for boost pressure which is measured by a transducer. Pressures are all static, although in the plenums they should be regarded as stagnation values. The gas pressure measurements are as follows :

1- Compressor inlet depression with reference to ambient.
2- Compressor plenum damped pressure.
3- Pressure drop between compressor plenum and inlet manifold.
4- Pressure drop between exhaust manifold and turbine plenum.
5- Pressure drop across bypass valve (between compressor and turbine plenums).
6- Turbine back pressure with reference to ambient.
7- Cylinder pressure is measured by a Kistler 6502 pressure transducer.

GAS TEMPERATURES. These are all measured by K-type Cr/Al thermocouple probes. Although the measured values are static temperatures, they should be regarded as stagnation temperatures since the dynamic effect ($u^2/2Cp$)

does not exceed 0.5 k. The gas temperature measurements are as follows :

1- Compressor inlet orifice place temperature.

2- Compressor inlet air temperature.

3- Compressor outlet air temperature.

4- Inlet manifold temperature.

5- Exhaust manifold temperature.

6- Turbine inlet temperature.

7- Turbine outlet temperature.

GAS FLOWS. Flow is measured at inlet to compressor and engine by using orifice plates. The lengths of pipes to the manometers lead to inaccuracies in measurements. Hence bypass flow (the difference between the two flows) may be very inaccurate where it is small.

CONTROLS. All controls implemented are automated by electro-hydraulic actuators and feedback control circuits. The only exception is the bypass valve which is adjusted manually. The controlled parameters are : output speed, output torque, engine speed, fuel/shot (rack positon), flowrate, nozzle position, timing position, bypass opening. As fully described in Chapter 7, not all of these parameters can be controlled independently.

SMOKE. Smoke measurement is carried out by Bosch smokemeter under steady-state running conditions and by a Celesco type meter under transient conditions.

SERVICES. Table 8.3 shows temperatures and pressures of all services.

SAFETY. System safety is provided by an automated shutdown system in which the engine inlet air pipe is closed off under the action of a gravity operated shut-off valve. A number of different signals can actuate shutdown and can be individually identified. These signals are listed in table 8.4. All mechanical services may be switched off from outside the cell. All shafts are surrounded by metal cages. Part of the shutdown system's operation is to prevent compressor reversal by activating a disc brake if compressor under-speed is detected.

8.3 OPTIMISATION OF THE DCE BY ADJUSTING THE TURBINE NOZZLE ANGLE AND INJECTION TIMING

The purpose of the experimental work is to find the best settings for the DCE control variables, viz. the turbine nozzle angle and injection timing so as to yield the highest output shaft thermal efficiency at any particular running condition. Due to practical difficulties in fitting a proper turbine CVT, these optimization tests were carried out with a fixed turbine gear ratio. The tests were intended to cover the whole output shaft torque-speed map with 24 points at 25%, 50%, 75% and 100% engine power levels and 6 equally spaced output shaft speeds from 682 to 3410 rpm. The possible control modes available on the test bed are :

i) constant output shaft torque mode.
ii) three optional control modes using the electronic governor:
    a) engine speed demand (along a droop line)
    b) fixed rack position demand (constant fuel/shot) and
    c) constant fuel flow rate demand (constant engine power)
iii) variable injection timing to maximize the output shaft efficiency and control the maximum cylinder pressure
iv) variable turbine nozzle angle mainly to control pressure levels in the system to maximize the output shaft efficiency.
v) extendable shutdown limits to give reasonable headroom for optimization.

Up to the present, three different optimization test procedures have been realized and can be applied optionally with respect to their advantages and disadvantages.

8.3.1 Fixed Output Shaft Torque and Engine Fuelling

This test procedure was used by Prince (Ref.39) in which the load was controlled in the torque mode and the engine governor in the speed mode. From this base condition, optimization was carried out by switching the governor to the fuel flow mode and then adjusting the turbine nozzle and injection timing positions in order to maximise output speed. As reported in Ref.39, the fuel flow control mode is not suitable for taking results

because of the lack of tight control on speeds. Therefore, having found and recorded the optimized settings, the governor is switched back to the speed mode for taking results. The speed demand mode will need further adjustments to recover the optimized engine speed. This optimized condition is then recorded.

Although this procedure uses the simple concept of optimization by having a constant rate of input energy (fuel flow rate) and achieving maximum rate of output energy (the highest output shaft speed at constant output shaft torque), it has the following practical disadvantages :

i) the engine control is loose which makes the repeatability of the tests very difficult and requires a long settling time due to switching the engine governor from the speed demand mode to the fuel flow rate mode and back to the former to take results. Each such test usually takes half a day.

ii) the location of the operating point on the output shaft torque-speed map is indeterminate since the highest output shaft speed is being sought, and is not known in advance.

8.3.2 Fixed Output Shaft Torque and Adjusted Engine Speed

In this optimization test procedure the load is controlled in the torque mode and the engine governor in the speed mode. The fuel flow rate is adjusted to give a desired engine speed. At different turbine nozzle angles this adjustment is repeated, and each time the accurate fuel flow rate and output shaft power is measured to yield the output shaft SFC. The point of minimum SFC reveals the optimum nozzle angle.

To set up the optimum adjustment with respect to injection timing, the same measurements are repeated at different timings while the turbine nozzles are kept fixed in their previous optimum position. Again a point of minimum output shaft SFC is found which will be found, in this case with respect to both nozzle angle and timing. To make sure and double-check that the final optimum result still holds true for the former, the procedure may be repeated for nozzle angle, but experiment

has shown that it is not actually needed. This test procedure has proved to be successful but the location of the operating point is again somewhat indeterminate on the output shaft torque-speed map. Although a number of accurate fuel flow measurements are required in each test, the procedure is straightforward.

8.3.3 Fixed Output Shaft Torque and Adjusted Output Shaft Speed

For further improvement of the test procedure, the load is controlled in torque mode and the engine governor in speed demand mode, but the fuel delivery is adjusted to give a targeted output shaft speed.

Again, first at different turbine nozzle angles and then at different injection timings, the fuel flow rate is adjusted and read from fuel flow meter on the panel. The optimum adjustments of nozzle position and timing are given by the minimum value read from the fuel meter.

This procedure not only arrives at the targeted operating point on the output shaft torque-speed map but also involves only one accurate fuel flow measurement. The procedure also proved to be successful although adjustment of output shaft speed by control of fuel flow takes rather more time than that of engine speed.

8.4 EXPERIMENTAL RESULTS

Table 8.5, a to f, [first column of each entry] give the experimental results. These results are all fully optimized based on which some of the performance characteristics are summarized in figs. 8.4,a to f, in the form of contours each with output shaft torque as ordinate and output shaft speed as abscissa. Due to practical difficulties, the points on the notional output shaft limiting torque curve were not tested and hence only approximate lines for it are shown on these figures. It is evident that the torque rises continuously and rather steeply over the range of output shaft speed. This does not quite achieve the desired constant horsepower characteristic, but since it is achieved steplessly, system flexibility will nevertheless be superior to that of a conventional T/C engine coupled to a multi speed gearbox.

Fig. 8.4,a gives contours of overall, i.e. output shaft efficiencies which considering the unduly high gear losses (dealt with later) must be considered quite satisfactory, with the 30% contour covering rather a wide operating field. As will be seen in Section 8.6, although due to high gear losses, the actual turbine power contribution never exceeds the actual power absorbed by the compressor when transmission power losses are included, the compounding conditions (i.e. excess of turbine 'wheel power' over compressor power) are achieved over approximately the same region of high overall efficiencies.

However, overall efficiency is depressed somewhat by the relatively low engine brake thermal efficiencies associated with the low compression ratio (LCR) pistons (12.8:1) designed to allow high boost operation (up to 3.8:1) without exceeding a max. cylinder pressure of 150 bar.

Fig. 8.4,b shows contours of engine brake thermal efficiencies. As shown the efficiency decreases with both decrease in output shaft torque and increase in output shaft speed. However, despite this fact, the overall efficiencies (fig. 8.4,a) deteriorate in the region of higher torques and lower speeds of output shaft because of excess of compressor over turbine power.

Fig. 8.4,c shows contours of engine speed for optimum running conditions. From an output shaft speed of about 2500 rpm onwards, at any constant output shaft speed, the difference in engine speed remains within a range of approx. 300 rpm in response to power demand from low to full levels. This can efficiently be covered by the engine governor droop. However, in the region of lower output shaft speeds, variation of power demand calls for considerable greater changes in engine speed.

It is also worth noting that at any particular demanded output shaft torque, output shaft speed varies proportionally with engine speed.

Fig. 8.4,d gives contours of BMEP. Like the engine speed contours, these also show a regular pattern. The increase in BMEP at any output shaft speed, as shown, is associated with an almost proportional increase in output torque taking account of a multiplying factor of approx. 1.18. This factor has to be applied because of the droop of the engine speed contours (fig. 8.4,c).

It may be noted that BMEP values remain at almost the same levels while output shaft torque is constant. However, this pattern changes in the range of output shaft speeds lower than approx. 2500 rpm at output shaft torques higher than 750 Nm.

Fig. 8.4,e gives boost pressure ratio contours showing that on the limiting torque curve (LTC) this varies from approx. 2.46 under rated conditions to 3.8 at the extreme corner of the high output shaft torque envelope. However, in spite of the very high boost under these latter conditions, max. cylinder pressure does not exceed 150 bar due to a combination of low compression ratio pistons and retarded injection. Below the LTC, boost pressure ratio is approximately proportional to BMEP level (fig. 8.4,d) and is mainly affected by compressor speed and turbine nozzle angle.

Finally, fig.8.4,f shows contours of dynamic injection timing showing that this is retarded progressively from 20.7 to 9.7 deg BTDC. This overall range of 11 deg. is by no means excessive and can easily be provided.

8.5 ASSESSMENT OF THE EXPERIMENTAL PERFORMANCE RESULTS

8.5.1 Turbine Power

The turbine in use is of the radial inflow type consisting of a scroll or inlet casing (fig. 8.5,a) a set of inlet nozzles followed by a short vaneless space and the turbine wheel itself.

Fig. 8.5,b shows the flow process through the turbine plotted on a temperature or enthalpy/entropy diagram. Station 03 refers to stagnation conditions at the entry to the casing. Energy transfer occurs in the rotor between stations 5 and 4 down to the exit pressure (P_4). The stagnation pressure (P_{04}) will be higher than P_4 because of significant exit velocity.

The steady flow energy equation for the process from state 3 to 4 can be written as :

$$\dot{Q} - \dot{W} = \dot{m}(h_{04} - h_{03}) \qquad [8.1]$$

where $\dot{Q}$ = heat rejection (kW)
$\dot{W}$ = work transfer to the turbine rotor kW)
$\dot{m}$ = gas flow rate (kg/sec)
h_{03} and h_{04} = stagnation enthalpy at inlet and exit of the turbine.

Applying the following simplifying assumptions :
i) absence of external friction in the bearings, etc.,
ii) considering the working fluid as a perfect gas,
iii) ignoring the gas kinetic energy at the rotor exit,
iv) absence of heat transfer throughout the process,
equation 8.1 may be written as follows :

$$\dot{W} = \dot{m}\, C_p\, (T_{03} - T_4) \qquad [8.2]$$

where C_p = constant pressure specific heat (kj/kg.k)
T_{03} = gas stagnation temperature at the turbine inlet
T_4 = gas static temperature at the rotor exit

and $\dot{W}$ will yield the turbine power output.

Equation 8.2 is used in estimating experimental values of turbine power based on measured T_{03} and T_4 and an assumed value for

$$C_p = 1.18 \quad \frac{kJ}{kg.K}$$ (i.e. for gas mixture at air-fuel ratio

of 33 at temperature of 900 k).

Having assumed the above conditions, the estimated turbine outputs reported in the experimental results are highly optimistic far from their real values and sometimes even result in invalid isentropic efficiencies higher than 100%. On the other hand, as turbine mass flow is an inaccurate value, it is another source of error in turbine power estimation.

8.5.2 Air Massflow and Compressor Performance

Two values for compressor air massflow are given in the test results; one being interpolated from the compressor manufacturer's performance map, and the other being derived from measurements. As shown in tables 8.5, a to f, the manufacturer's figures are always higher than those measured. This affects the calculation of compressor performance as well as of bypass flow.

The overestimation of air massflow based on the map can be explained by the level of compressor inlet pressure as the manufacturer's figures quote volume flow without any inlet depression. Since the measured value is more reliable, it is used in all calculations (except for compressor performance) despite the difficulty in the accurate measurement.

Using the compressor manufacturer's data (map) based on ignoring the inlet depression makes the calculation of compressor power and efficiency inaccurate. Fig. 8.6 shows the experimental results for the compressor torque (based on the map) as a function of the engine torque for different running conditions taken from tables 8.5,a to f. The location of these points compared with the proportionality line of compressor

torque against engine torque in a frictionless epicyclic and step up gearing (fig. 8.6) shows the degree of accuracy for compressor torques used in experimental data.

Assuming a power transmission efficiency of 96% produces the chain line in the same figure and shows that the experimental compressor torque and hence power is usually over-estimated, which explains why the figures for compressor efficiencies are rather poor. Furthermore, it should be noted that this compressor torque is too far from the torque compatibility condition required by the gearing system and hence should not be used as a reference value.

8.5.3 Gear Losses

The combination of uncertainties in compressor and turbine performance are cumulative in the calculation of gearbox losses. However, the over-estimation of compressor power and that of turbine power counteract the effect of each other on gear loss calculations. Nevertheless their accurate quantitative values are still not known unless either extra relevant measurements are carried out or a realistic simulation is performed.

Although the experimental values of gear losses, $\dot{W}_{L_{tot}}$, calculated from the energy balance :

$$\dot{W}_{L\,tot} = \dot{W}_{ENG} + \dot{W}_{TURB} - \dot{W}_{COMP} - \dot{W}_{o/s}$$

are very high as compared with typical toothed transmission systems, and are likely to be an overestimate, there is excessive windage losses of the excessive size of the epicyclic gearset employed in the prototype.

8.6 SIMULATION OF THE LABORATORY LEYLAND 520-DCE USING MODIFIED VERSION OF PROGRAM DCE2

To examine the actual gear losses as well as compressor and turbine performance characteristics at the tested running conditions, the program DCE2 was modified so as to simulate the prototype with all mechanical and flow losses as close as possible to those existing in practice. The following subsections give some details about these modifications as well as the simulation results.

8.6.1 Adjustments for pressure drops

Considering Fig. 2.16 the flow losses occur in :

i) the compressor inlet ducting
ii) the pipes designated by 'a', 'b', 'c' and 'd'
iii) the charge cooler
iv) the turbine exhaust ducting

'i' results in a compressor inlet depression and 'iv' in turbine back pressure. These, together with pressure drops in the piping system and across the charge cooler determine the air or gas conditions at inlet and outlet of the compressor, engine and turbine and play an important role in their performance characteristics. All of the flow losses can now be input to the modified version of the program in the form of pressure drops and the relevant experimental data may be applied where appropriate while pressure drops in the pipe, and across the cooler can still be calculated optionally using the subroutines 'PIPE' and 'COOL' respectively, as in the original form of the program, but using modified coefficients.

The charge cooler pressure drop in the routine 'COOL' is calculated by the following formula :

$$dp = f_c\,[0.4(enf/15) + 1.2(enf/15)^2 - 0.1(enf/15)^3] \qquad [8.3]$$

where dp = pressure drop across cooler

enf = air flow through cooler

f_c = cooler pressure drop coefficient

The coefficient f_c was adjusted to the value 1.0 to result in a higher pressure drop as actually experienced. This increase will adjust the inlet manifold pressure to the experimental values at corresponding running conditions.

The pressure losses in the pipes modelled by the routine 'PIPE' is based on the following formula:

$$\Delta p = 2 f_p . \ell . \rho \, u^2/d \qquad [8.4]$$

where Δp = pipe pressure loss

d = pipe diameter

ℓ = pipe length

ρ = air density

u = air flow mean velocity

f_p = pressure drop coefficient

The value of 'f_p' is in turn calculated by the following formula :

$$f_p = .001375 \left[1 + 20000 \frac{k}{d} + \left(\frac{10^6}{Re}\right)^{\frac{1}{3}}\right] \qquad [8.5]$$

where Re = Reynolds number

$\frac{k}{d}$ = relative roughness

The relative roughness could therefore be taken as the variable to adjust the pressure losses in the different pipes to their experimental values at corresponding running conditions.

However, the pressure drops in pipes b and c were directly input since the measured data were available. The pressure drop in pipe c is considerably higher than in the other pipes because of the bypass valve and three elbows as well as energy dissipation at the junction of the pipe and the turbine plenum.

The pressure drops in pipes a and d were calculated based on equation 8.4 and using a pipe diameter of 0.127 and 0.12 m and pipe length of 0.3 and 0.35 m respectively. A common relative roughness of 0.03 was assumed. This combination of data yielded rather low pressure drops along pipes a and d, although their measured values were not available.

8.6.2 Adjustment of Gearing System Efficiencies

In general terms, the total power losses, $\dot{W}_{L_{tot}}$, in the system of mechanical connections is the difference between the powers of active (engine and turbine) and passive (compressor and load) elements, i.e.

$$\dot{W}_{L_{tot}} = \dot{W}_{ENG} + \dot{W}_{TURB} - \dot{W}_{COMP} - \dot{W}_{o/s} \qquad [8.6]$$

$\dot{W}_{L_{TOT}}$ can also be written in terms of its components :

$$\dot{W}_{L_{TOT}} = \dot{W}_{L_{TURB}} + \dot{W}_{L_{COMP}} + \dot{W}_{L_{o/s}} \qquad [8.7]$$

These power loss components are calculated based on attributable constant friction torques and transmission efficiencies in the input to program 'DCE2'. These values have to be adjusted by making the resultant power loss calculations against experimental data. These elements of friction losses cannot readily be isolated in practice. However, as a more convenient and very effective step, the sum of $\dot{W}_{L_{COMP}}$ and $\dot{W}_{L_{o/s}}$ was measured with sufficient accuracy by finding the actual turbine power contribution ($\dot{W}_{TURB} - \dot{W}_{L_{TURB}}$) at a number of running conditions.

This was achieved by removing the turbine rotor, but otherwise retaining the original operating conditions i.e. engine fuelling, boost pressure and shaft speeds. Having kept the engine fuelling constant, the shaft speeds may be retained by some adjustment of the dynamometer torque level. Also to keep the boost pressure at the same level, suitable adjustment of the turbine nozzles in the retained turbine stator housing are called for.

These two adjustments of output shaft torque and nozzle angle thus

allowed the original engine and compressor running conditions to be maintained so that the difference in output shaft power with and without the turbine rotor yielded the actual (net) turbine power contribution (i.e. $\dot{W}_{TURB} - \dot{W}_{L_{TURB}}$) to the output shaft.

From equations 8.6 and 8.7 the following equation may be deduced :

$$\dot{W}_{L_{COMP}} + \dot{W}_{L_{o/s}} = \dot{W}_{ENG} + (\dot{W}_{TURB} - \dot{W}_{L_{TURB}}) - \dot{W}_{o/s} - \dot{W}_{COMP} \qquad [8.8]$$

In this equation, $\dot{W}_{ENG}$, $(\dot{W}_{TURB} - \dot{W}_{L_{TURB}})$ and $\dot{W}_{o/s}$ all are known from direct measurements, for any running condition. To determine the right-hand side of equation 8.8, $\dot{W}_{COMP}$ has to be determined first and may be obtained by synthesizing the experimental running conditions with respect to compressor air flow and pressure ratio. This procedure was applied for a range of operating conditions and sufficient data was obtained to evaluate the friction torques and transmission efficiences (used in the DCE input data) from the engine (annulus) up to the compressor and to the output shaft separately while satisfying the expected total value of $(\dot{W}_{L_{COMP}} + \dot{W}_{L_{o/s}})$. Having thus obtained $(\dot{W}_{L_{COMP}} + \dot{W}_{L_{o/s}})$, the turbine gear loss $\dot{W}_{L_{TURB}}$ was evaluated by overall system simulation at the same running conditions so as to yield an acceptable match between calculated and measured output shaft power. The following is the result of this gear loss investigation :

TABLE 8.6

	constant efficiency (%)	constant friction torque (Nm)
output shaft	95	20
turbine	61	20
compressor	99	2

Low compressor gearing losses are considered to yield an acceptable match between simulation and experimental results for boost pressure ratio, except at the highest pressure ratios.

The turbine gearing losses, on the other hand, are rather high. This may be partly justified by the high gear ratio of 14.67 between turbine and output shaft. In order to show how the two elements of transmission efficiency and constant friction torque in the gearing system in the program affect overall efficiency, turbine and output gearing is taken into consideration as follows :

(The notations are with reference to the program DCE2 variable listing)

$$tge' = [(tgr.tt-tgft).tge]/(tgr.tt)$$

$$tge' = [1 - tgft/(tgr.tt)]tge \qquad [8.9,a]$$

and

$$oge' = [(et-ogft).oge/ogr]/(et/ogr)$$

$$= (1-ogft/et).oge \qquad [8.9,b]$$

where :

tge/oge = turbine/output shaft constant gear efficiency
tge'/ogr' = " " overall gear efficiency
tgr/ogr = " " gear ratio
tgft/ogft = " " static friction torque (Nm)
tt/et = " /engine torque (Nm)

Substituting the tabulated values of efficiency into equations 8.9,a and 8.9,b and friction torque into equations 8.9,a and 8.9,b yields :- (see table 8.6)

$$tge' = .61\ (1-1.363/tt) \qquad [8.10,a]$$

$$oge' = .95\ (1-20/et) \qquad [8.10,b]$$

Therefore, this approach suggests a torque dependent transmission efficiency. The lower parts of figs. 8.7,a and 8.7,b give a graphical representation of equations 8.10,a and 8.10,b and show the importance of static friction torque in the lower range of transmitted torque.

8.6.3 Modified Simulation Results

Having adjusted all of the gear losses input to the program DCE2 against

experimental data, the program was run for 17 optimized tested running conditions. As indicated in Section 8.6.1, the compressor inlet depression, turbine back pressure, as well as pressure drop across the charge cooler and along the pipes 'b' and 'c' (fig. 2.16) were taken from experimental data and used as part of running condition. Actually, the name 'modified simulation' stands for adoption of such extra input data although this includes the application of adjusted gear losses.

Table 8.5,a to f (2nd column) give the adjusted predictions against experimental results. As described, the main objective of the manifold simulations is to obtain the best approximation to the gear losses for a number of test conditions. To provide adjusted performance predictions, it was essential to match output shaft efficiencies, as being the first order importance. Figs. 8.8,a and 8.8,b are prepared based on both the experimental and adjusted prediction values of the output shaft torque and overall thermal efficiency given in tables 8.5,a to f. The broken line depicts the conditions for a perfect match between the predicted and experimental values. The square symbols represent the actual comparisons i.e. the closer the symbols are to the line, the better the match. Since the input data with respect to the gear losses had to be kept constant for all of the running conditions, the concentration of the squares around the perfect match line proves that the loss data of table 8.6 leads to acceptable results.

Having accepted the accuracy of the modified simulation predictions as against the experimental results with respect to all of the important performance characteristics, new performance maps can be prepared. Since a perfect match between experimental and predicted output shaft efficiency was still not achieved, the predicted efficiency contours are presented in fig. 8.9,a. Comparing figs. 8.9,a and 8.4,a, the major difference appears to be in the region of low output shaft torques and speeds. The predicted values are generally approx. 0.5 per-cent point lower than the measured values.

The contours of the difference between compressor and turbine wheel powers (compounding effect) are shown in fig. 8.9,b. This figure was prepared to show whether a regular pattern exists, and demonstrates a

positive compounding effect in the region above 70% rated output shaft speed, which amounts to about +13.7 kW near the design point. The negative compounding effect increases with decrease in output shaft speed below 70% of rated speed. This trend accelerates below a speed of about 45% rated speed at higher output shaft torques and reaches a level of about -95 kW in the region of full load near the stall point, due to a combination of poor turbine efficiency and high bypass flow.

Fig. 8.9,c shows the turbine efficiency contours which, as already stated, influence the pattern of the compounding effect contours. As shown, the turbine efficiency is good in the region above 60% rated output shaft speed, but falls progressively as the output shaft speed decreases below this level and with increase in load, reaching a level of about 32% in the region of full load near stall. This trend of turbine efficiency is mainly because of the fixed gear ratio interposed between turbine and output shaft. There is every expectation of improving the situation with the application of a turbine CVT.

Another set of contours of interest is that of bypass mass flow. These are shown in fig. 8.9,d. Again, the bypass flow is at its minimum (approx. zero) at about design point and increases with decrease in output shaft speed. The maximum value occurs in the region of full load at stall point, and is about 55% of the total compressor air delivery.

Finally, the contours of total gear losses are given in fig. 8.9,e. The pattern is quite regular and follows almost the pattern of constant output shaft power. The overall power transmission efficiency is about 80% on an average basis using the following formula :

$$\text{overall trans. eff.} = \frac{\text{o/s power}}{\text{o/s power+total loss}} \qquad [8.11]$$

Although this definition may hold true in conventional systems to predict the output shaft power for any set of conditions, it is not directly applicable to the DCE because of its highly interactive components. For example, if gear losses between engine and compressor decrease, the compressor will experience a higher input torque provided that all

speeds, as well as engine torque are assumed constant. This new condition calls for higher boost pressure level which, in turn, will supply the turbine with more gas energy. Hence the turbine power contribution to the output shaft increases, due to the reduction in gear losses. These two effects reinforce the output shaft power in an inherently complex way. On the other hand, the compressor absorbs more power, thus tending to reduce output shaft power. These interactions make the exact prediction of new performance parameters (without resorting to simulation) very difficult.

It should be noted that the compressor gear losses were set (see table 8.5) at an optimistically low level (trans. eff. = 99% and constant friction torque = 2 N.m).

8.7 SIMULATION OF THE LEYLAND 520-DCE USING ORIGINAL VERSION OF 'DCE2'

To examine simulation results for the Leyland 520-DCE based on gear losses approximating to those to be expected in a purpose built automotive epicyclic gearset, the same gear loss data as used for the L10-DCE (Chapters 5 and 6) were applied. At the same time, in order to reflect the effect of pressure drops lower than those of the piping system of the current prototype, the same pressure drop data as used for the L10-DCE were applied.

Referring to the corresponding data from table 2.9,a given in Chapter 2, the gear loss data is as follows :

TABLE 8.7.

	constant efficiency (%)	constant friction torque (Nm)
output shaft	98	10
turbine	93	10
compressor	98	10

The turbine efficiency has been set at a lower level than the other two to reflect the high turbine gear ratio of 14.67. Substituting these values for the corresponding variables in equations 8.9,a and 8.9,b yields:

$$tge' = 0.93\ (1-0.6815\ tt) \qquad [8.12,a]$$

$$oge' = 0.98\ (1-10/et) \qquad [8.12,b]$$

The upper parts of figs. 8.7,a and 8.7,b give the graphical representation of these two equations. From these figures the differences in component efficiences of the gearset of the prototype (lower parts of figs. 8.7,a and 8.7,b) and those of a probable commercial one, become very apparent.

8.7.1 Simulation Results based on the Application of Reduced Gear Losses

Tables 8.5,a to f (3rd column) contain the simulation results based on these reduced gear losses as against the experimental and adjusted simulation results of the prototype.

Figs. 8.10,a to c show the contours of some of the performance characteristics which are of major interest. These include odutput shaft efficiency, compounding effect (difference of wheel powers of turbine and compressor) and gear losses.

Fig. 8.10,a gives contours of output shaft efficiency while differing substantially from those presented in fig. 8.4,a for the prototype. A large region of the map, including that of moderate output shaft speeds and torques is covered by the contour islands higher than 34%, reaching a maximum value of 38.06 ~~36.31~~ %. This is quite promising as in truck applications the power plant is used predominantly at vehicle speeds and power demands of between 40% to 80%.

Fig. 8.10,b, compared with fig. 8.9,b, depicts approximately the same trends for the compounding effect. The values are about the same in the region of the map above output shaft speeds of 45%. However, the maximum negative values reach about -75 kW in the region near to stall as against -95 kW for the prototype (fig. 8.9,b).

Finally, the contours presented in fig. 8.10,c are concerned with total gear losses. Although the pattern is similar to that presented before (fig. 8.9,c), the values are much lower. This, of course, does not hold true in the region below the output shaft speed of 1250 rpm, particularly that in low loads. But, as soon as output shaft speed and load increase, the total gear losses (as in fig. 8.10,c) become increasingly less than those of the prototype. Having applied equation 8.11 to the existing results, an average value for the overall transmission efficiency of about 92% may be deduced.

8.7.2 Direct Comparison of Simulation Results based on Reduced (Tentative) Gear Losses with those for the Prototype

The comparison includes some of the important performance parameters, viz. output shaft torque and efficiency, compounding effect and gear losses. The method of comparison is the same as that used to compare the experimental with adjusted simulation results (figs. 8.8,a and b) but with the difference that the line of perfect match is replaced by a line which can be referred to as a datum for comparison.

Fig. 8.11,a shows the comparison for output shaft torques. The distance away from the broken line indicates the output gain provided by the effects of lower gear losses.

Fig. 8.11,b shows the comparison for output shaft efficiencies. On an average basis, an improvement of approx. 3 per-cent point may be realised in the region above 28% for the prototype output shaft efficiencies. Returning to fig. 8.4,a which shows the corresponding map for the prototype, such region covers about half of the map.

In order to investigate whether the output shaft efficiency improvements are brought about by compounding effect or lower gear losses themselves, fig. 8.11,c and d show the corresponding trends. As shown in fig. 8.11,c the compounding effects for both simulations seem to be approximately in good agreement as most of the comparator symbols are quite concentrated around the datum line. This makes it clear that small change in compressor gear efficiency from 99% to 98% and in the corresponding constant friction torque from 2 to 10 Nm do not make any major difference in compounding effect.

As is shown in fig. 8.11,d the total gear losses in tentative simulation runs are considerably lower than that in the simulation of the prototype. The absolute difference becomes greater as the DCE operates under heavier loads. For the existing tentative simulation results the differences in gear losses are the only major difference in output shaft performance characteristics.

a) ENGINE :		
.....		
Rated speed	2600	rpm
Rated torque	980	Nm
Stall torque	1310	Nm
Max. cylinder pressure	150	bar
Max. exhaust temperature	650	C
Max. heat to coolant	135	kW
Max. intercooler heat transfer	70	kW
Max. air flow	29	kg/m
b) COMPRESSOR :		
.....		
Stall speed	11500	rpm
Stall torque	144	Nm
Stall pressure ratio	4	-
Stall mass-flow	52	kg/m
Max delivery temperature	220	C
c) TURBINE :		
.....		
Max. speed	50000	rpm
Stall power	156	kW
Max. inlet temperature	650	C
Stall mass-flow	53	kg/m
d) OUTPUT :		
.....		
Rated speed	3410	rpm
Rated torque	1050	Nm
Stall torque	3710	Nm

Table 8.1 Design figures fo the Leyland 520-DCE

a) ENGINE :		
.....		
Type	Leyland 520	
Firing order	153624	
Number of cylinders	6	
Bore	118	mm
Stroke	125	mm
Capacity	8.2	l
Connecting rod length	218.5	mm
Compression ratio	12.8	
Valve timing IVO	10.0	deg
(BTDC) IVC	50.0	deg
EVO	46.0	deg
EVC	14.0	deg
Valve lift	13.1	mm
Inlet valve head dia.	53.0	mm
Exhaust " "" "	46.0	mm
Type of fuel pump	In-line Sigma RMSP	
Max. power	265.8	kW
Max. torque	1308.0	Nm
Max. cyl. pressure	150.0	bar
b) COMPRESSOR :		
.....		
Type	CompAir	
Max. speed	115000	rpm
Max. pressure ratio	4	-
Max. flow	52.2	kg/m
(@ max.speed & press.ratio)		
Max. delivery temp.	220	C
Best efficiency	77	%
c) TURBINE :		
.....		
Type	Napier CO-45B	
Max. inlet temp.	650	C
Max. speed	50000	rpm
Max. press. ratio	4	-

Table 8.2 Specification of the components of the laboratory DCE unit

ENGINE oil pressure (@ idel)	10	psi
(@ normal)	55/65	psi
" " temperature (max)	110	C
" water pressure	60 ft	H_2O
" " temperature (max)	93	C
COMPRESSOR oil pressure	30	psi
" tank temperature	60	C
GEARBOX oil pressure	30	psi
" sump temperature	60	C
DYNAMOMETER load pressure (max)	350	bar
(intermittent)	420	bar
" boost "	14-20	bar
" water "	30	psi
" loop temperature (max)	80	C
" tank " (")	80	C
Boost pump vaccume	1-2 ft	H_2O
SERVO oil pressure	1200	psi
" return temperature (max)	60	C
FUEL pressure	2	bar
" temperature	40(+/-3)	C
AIR inlet temperature	20-25	C

Table 8.3 Service Pressures and temperatures of the laboratory DCE unit

PARAMETER	SIGNAL GENERATOR	TRIP LEVEL SETTING	TRIP No.	ACTION
COMP. speed reference	60 T F-V CARD	REFERENCE		FUEL & BRAKE
" " reversal	Calculating CARD	SD : < 600 RPM	13	" "
		W : < 1200 RPM	5	WARNING
" overspeed	" CARD	SD : > 12000 RPM	9	FUEL & AIR
		W : > 10000 RPM	1	WARNING
ENGINE overspeed	120 T F-V CARD	SD : > 2800 RPM	10	FUEL & AIR
		W : > 2430 RPM	2	WARNING
OUTPUT overspeed	120 T F-V CARD	SD : > 3500 RPM	11	FUEL & AIR
		W : > 3000 RPM	3	WARNING
OVERBOOST	PR TRANSD. CARD	SD : > 4.0 BAR	12	FUEL & AIR
		W : > 3.8 BAR	4	WARNING
OIL PRESSURES :	Measured by gauges			
Engine	SMITH (NON-ADJ)		35	FUEL
Gearbox	MURPHY "	< 15 PSI	18	"
Compressor	" "	< 8 PSI	19	"
Dynamometer	" "	< 10 PSI	17	"
Servo	" "	< 600 PSI	31	"
OIL TEMPERATURES :	Measured by gauges			
Engine	MURPHY (ADJSTBL)	> 110 C	34	WARNING
Gearbox	" "	> 80 C	22	"
Compressor	" "		21	"
Dynamometer	" "		20	"
ENGINE coolant water press.	HERGA (NON-ADJ)	< 20 ft g	28	"
" " " temp.	" "	> 95 C	33	"
DYNO " " press.	" "	< 13 PSI	30	"
TURBINE air pressure	HERGA (NON-ADJ)	< 18 PSI	25	"
LEVEL INDICATIONs :				
Engine coolant	ASCO (NON-ADJ)		27	FUEL
Fuel tank	FLOAT in tank "		26	WARNING
Gearbox oil	" " " "		24	"
Comprressor oil	" " " "		23	"
Dynamometer oil	" " " "		29	"
				"

SD = Shutdown W = Warning NON-ADJ = Non-adjustable ADJSTBL = Adjustable

Table 8.4 Instrumentation and safety provisions of the laboratory DCE unit

OUTPUT		EXP. RES. (1)	PREDICTIONS ADJUSTED (2)	PREDICTIONS TENTATIVE (3)	EXP. RES. (1)	PREDICTIONS ADJUSTED (2)	PREDICTIONS TENTATIVE (3)	EXP. RES. (1)	PREDICTIONS ADJUSTED (2)	PREDICTIONS TENTATIVE (3)
Speed	rpm	682.00	[682.00]	[682.00]	700.00	[700.00]	[700.00]	1080.00	[1080.00]	[1080.00]
Torque	Nm	704.07	583.14	861.81	1021.74	946.34	1537.62	400.11	410.70	470.00
Power	kW	49.82	41.66	61.58	73.73	69.40	112.76	45.30	46.47	53.27
Thermal Eff	%	18.14	15.73	22.15	14.22	13.86	22.49	26.50	27.34	31.77
BSFC	g/kWh	466.15	530.00	377.00	594.66	602.00	371.00	319.08	305.00	263.00
ENGINE										
Speed	rpm	1200.00	[1200.00]	[1200.00]	1457.00	[1457.00]	[1457.00]	900.00	[900.00]	[900.00]
Torque	Nm	888.14	[888.14]	[888.18]	1350.90	[1350.91]	[1350.92]	735.20	[735.20]	[735.00]
Power	kW	111.70	111.44	111.54	206.15	205.94	206.05	69.30	69.24	69.00
Boost Ratio		2.57	2.62	2.52	3.79	3.74	3.82	2.33	2.36	2.24
BMEP	bar	13.60	13.56	13.57	20.69	20.64	20.65	11.26	11.23	11.20
Max Cyl Pres	bar	138.19	138.39	92.87	153.65	153.42	129.12	109.40	109.64	100.95
Dyn Inj deg	BTDC	15.13	13.70	7.20	9.96	12.10	8.00	11.88	7.20	11.30
Inj Duration	deg	18.73	15.80	16.40	31.13	25.80	25.90	15.39	12.00	11.90
Fuel/Shot	mg	107.42	102.26	96.60	167.17	159.20	159.46	89.23	87.50	86.33
Brk Th Eff	%	40.67	42.08	40.12	39.76	41.14	41.10	40.53	40.74	41.15
Air Flow	kg/min	12.08	11.79	12.28	24.37	18.38	21.44	8.08	8.65	8.31
Air/Fuel		31.21	32.03	31.77	33.35	26.41	30.76	33.54	36.62	35.66
Inl Man Temp	K	320.20	301.20	299.01	334.40	318.91	314.61	318.20	294.23	294.00
Exh Man Templ	K	719.00	732.60	783.32	879.00	905.62	858.99	661.00	659.71	678.30
" " " 2	K	726.00			885.00			670.00		
Inl Man Pres	barg	1.55			2.73			1.31		
Exh Man Pres	barg	1.13			2.49			1.38		
COMPRESSOR										
Speed	rpm	7300.00	7323.10	7323.00	9502.00	9506.10	9506.10	2752.00	2764.20	2764.20
Torque map	Nm	101.61	99.35	97.05	161.54	151.16	148.43	80.66	81.98	80.01
Power map	kW	78.08	76.22	74.45	161.18	150.54	147.82	23.25	23.74	23.17
Isen Eff T-S	%	82.06			77.26			76.65		
Overall Eff	%	67.26	65.50	70.00	61.85	59.70	68.50	60.83	61.00	61.50
Mass orif	kg/min	28.45			35.15			7.88		
Mass map	kg/min	29.35	29.42	32.48	36.74	36.65	42.27	10.02	10.15	10.29
Press Ratio		2.92	2.78	2.68	4.57	4.06	4.00	2.42	2.43	2.38
Inlet Dep	mbarg	70.67	[70.67]	0.00	107.17	[107.17]	0.00	5.35	[5.35]	0.00
Inlet Temp	K	298.40	[298.40]	[294.40]	297.40	[297.40]	[294.40]	294.40	[294.23]	[294.40]
Outlet Temp	K	428.00	453.00	431.28	505.00	540.00	502.31	404.00	434.21	428.84
Interclr DP	mbar	137.29	[137.29]		274.59	[274.59]		72.64	[72.64]	
Intercooler	kW	21.92			69.99			11.67		
Byp Flow	kg/min	17.27	17.63	20.21	12.37	18.27	20.83	1.93	1.50	1.98
TURBINE										
Speed	rpm	10002.89	10004.90	10004.90	10266.90	10269.00	10269.00	15840.36	15843.60	15843.60
Wheel Torque	Nm	33.74	17.34	29.92	64.15	31.22	61.35	13.43	6.89	7.25
Power	kW	35.02	18.17	31.36	67.90	33.59	66.00	22.32	11.44	12.03
Isen Eff	%	65.58	36.90	45.10	47.85	28.40	41.80	85.09	46.90	56.90
Mass flow	kg/min	30.48	29.79	32.88	38.61	37.35	42.97	10.94	10.38	10.52
Press Ratio		2.05	2.17	2.57	3.31	3.36	3.90	2.37	2.43	2.27
Back Pres	mbarg	30.45	[30.45]	0.00	50.88	[50.88]	0.00	7.07	[7.07]	0.00
Inlet Templ	K	534.00	572.06	573.69	731.00	735.00	693.73	539.00	628.87	633.75
" " 2	K	583.00			768.00			644.00		
Outlet Temp	K	495.00			658.00			537.00		
GEARBOX LOSSES										
Gbox Losses	kW	18.82	11.72	6.86	39.14	19.60	11.47	23.06	10.46	4.60
O/S Gearing	kW		2.72	1.21		3.72	1.61		3.84	1.72
Comp. "	kW		1.00	2.69		1.83	4.54		0.33	0.92
Turb. "	kW		8.27	3.06		14.31	5.48		6.33	2.26

Table 8.5,a Comparison of the experimental results (1) with the ' DCE2 ' predictions based on simulation of both the basic laboratory unit (2), and for some tentative values for gearbox and piping losses (3)

	EXP.	PREDICTIONS		EXP.	PREDICTIONS		EXP.	PREDICTIONS	
OUTPUT	RES. (1)	ADJUSTED (2)	TENTATIVE (3)	RES. (1)	ADJUSTED (2)	TENTATIVE (3)	RES. (1)	ADJUSTED (2)	TENTATIVE (3)
Speed rpm	1229.00	[1229.00]	[1229.00]	1195.00	[1195.00]	[1195.00]	1200.00	[1200.00]	[1200.00]
Torque Nm	200.99	203.54	221.72	400.84	327.28	398.00	901.30	869.25	1153.73
Power kW	25.79	26.21	28.55	50.02	40.97	49.94	113.15	109.28	145.04
Thermal Eff %	25.83	27.00	28.32	27.42	23.10	27.13	23.08	22.04	29.93
BSFC g/kWh	327.33	309.00	294.00	308.32	361.00	307.00	366.39	378.00	279.00
ENGINE									
Speed rpm	900.00	[900.00]	[900.00]	1200.00	[1200.00]	[1200.00]	1456.00	[1456.00]	[1456.00]
Torque Nm	401.98	[401.98]	[401.98]	575.21	[575.21]	[575.21]	1319.91	[1319.91]	[1319.87]
Power kW	37.92	37.52	37.83	72.31	72.19	71.84	201.44	201.04	201.23
Boost Ratio	1.60	1.62	1.50	1.78	1.79	1.70	3.70	3.60	3.66
BMEP bar	6.15	6.08	6.13	8.81	8.78	8.74	20.22	20.16	20.18
Max Cyl Pres bar	79.23	79.58	74.29	94.58	94.80	92.32	149.73	149.56	133.66
Dyn Inj deg BTDC	11.35	8.60	15.90	12.53	10.60	18.60	8.74	10.70	10.40
Inj Duration deg	9.18	8.50	8.70	12.53	11.90	12.20	30.43	25.60	25.10
Fuel/Shot mg	52.08	49.96	51.90	71.37	68.46	71.06	158.04	157.76	154.20
Brk Th Eff %	37.97	38.65	37.53	39.64	40.71	39.03	41.09	40.55	41.53
Air Flow kg/min	5.27	6.05	5.65	9.52	8.66	8.44	26.25	19.04	20.55
Air/Fuel	37.51	44.88	40.37	37.05	35.15	33.00	37.99	27.63	30.52
Inl Man Temp K	318.60	289.88	289.20	317.50	294.40	293.51	329.80	317.05	314.95
Exh Man Templ K	570.00	565.80	601.40	661.00	671.74	712.68	873.00	894.37	853.21
" " " 2 K	579.00			673.00			869.00		
Inl Man Pres barg	0.59			0.77			2.71		
Exh Man Pres barg	0.64			0.54			2.76		
COMPRESSOR									
Speed rpm	2056.00	2049.10	2049.10	4857.00	4861.30	4861.30	7085.00	7097.80	7097.80
Torque map Nm	46.04	44.75	43.11	66.09	64.27	62.36	155.40	147.68	144.98
Power map kW	9.97	9.61	9.25	33.69	32.73	31.76	115.44	109.81	107.81
Isen Eff T-S %	76.65			78.50			79.25		
Overall Eff %	54.38	57.90	58.50	61.51	61.10	63.00	62.56	61.50	65.50
Mass orif kg/min	5.45			18.94			27.24		
Mass map kg/min	7.01	7.05	7.26	19.92	19.95	20.92	27.98	28.24	30.47
Press Ratio	1.65	1.66	1.63	1.94	1.90	1.86	4.26	3.90	3.85
Inlet Dep mbarg	2.84	[2.84]	0.00	30.74	[30.74]	0.00	63.94	[63.94]	0.00
Inlet Temp K	298.80	[298.80]	[294.40]	297.00	[297.00]	[294.40]	300.45	[300.45]	[294.40]
Outlet Temp K	359.00	380.47	370.81	376.00	395.25	385.28	493.00	531.04	504.70
Interclr DP mbar	49.32	[49.32]		102.64	[102.64]		285.26	[285.26]	
Intercooler kW	3.59			9.38			72.12		
Byp Flow kg/min	1.73	0.99	1.60	10.39	11.29	12.48	1.73	9.19	9.92
TURBINE									
Speed rpm	18025.74	18029.40	18029.40	17527.06	17530.60	17530.60	17600.40	17604.00	17604.00
Wheel Torque Nm	6.42	2.97	2.01	15.67	6.80	8.23	31.75	24.40	34.46
Power kW	12.10	5.60	3.80	28.69	12.49	15.11	58.46	44.99	63.55
Isen Eff %	130.99	65.20	71.40	142.41	70.20	68.70	48.17	40.50	52.70
Mass flow kg/min	7.56	7.19	7.40	20.67	20.21	21.19	29.81	28.93	31.15
Press Ratio	1.62	1.67	1.53	1.50	1.54	1.75	3.59	3.65	3.75
Back Pres mbarg	11.34	[11.34]	0.00	13.45	[13.45]	0.00	29.27	[29.27]	0.00
Inlet Templ K	551.00	541.11	553.58	504.00	521.65	525.57	775.00	786.04	748.63
" " 2 K	557.00			545.00			790.00		
Outlet Temp K	469.00			447.00			683.00		
GEAR LOSSES									
Total Losses kW	14.25	7.31	3.82	17.28	10.97	5.25	31.30	26.93	11.92
O/S Gear " kW		3.21	1.49		3.71	1.69		6.27	2.71
Comp. " " kW		0.16	0.52		0.49	1.68		1.34	3.34
Turb. " " kW		4.31	1.89		6.94	1.43		19.62	5.97

Table 8.5,b As per table 8.5,a

	EXP. RES.	PREDICTIONS ADJUSTED	PREDICTIONS TENTATIVE	EXP. RES.	PREDICTIONS ADJUSTED	PREDICTIONS TENTATIVE	EXP. RES.	PREDICTIONS ADJUSTED	PREDICTIONS TENTATIVE
OUTPUT	(1)	(2)	(3)	(1)	(2)	(3)	(1)	(2)	(3)
Speed rpm	1472.00	[1472.00]	[1472.00]	1475.00	[1475.00]	[1475.00]	1568.00	[1568.00]	[1568.00]
Torque Nm	621.54	611.82	700.00	996.85	918.06	1221.46	403.59	412.82	467.95
Power kW	95.68	94.35	107.97	153.19	141.86	188.75	65.80	67.81	76.87
Thermal Eff %	28.36	28.61	33.52	22.92	22.50	30.90	29.35	29.71	34.26
BSFC g/kWh	298.13	292.00	249.00	386.91	371.00	270.00	288.07	281.00	243.00
ENGINE.....									
Speed rpm	1250.00	[1250.00]	[1250.00]	1785.00	[1785.00]	[1785.00]	1200.00	[1200.00]	[1200.00]
Torque Nm	1025.85	[1025.85]	[1025.85]	1313.85	[1313.85]	[1313.85]	730.51	[730.51]	[730.51]
Power kW	134.17	134.20	133.89	244.93	245.54	245.43	91.94	91.74	91.55
Boost Ratio	2.99	3.11	3.07	3.60	3.56	3.68	2.27	2.27	2.19
BMEP bar	15.71	15.68	15.64	20.13	20.09	20.08	11.19	11.16	11.14
Max Cyl Pres bar	117.56	117.48	112.45	153.56	152.94	130.04	124.51	124.64	101.21
Dyn Inj deg BTDC	8.84	5.80	8.50	20.72	13.90	10.70	18.02	12.70	13.10
Inj Duration deg	22.93	18.70	18.30	35.46	30.90	30.10	15.72	14.20	14.00
Fuel/Shot mg	126.88	122.26	119.40	176.36	163.63	158.53	87.62	88.13	86.63
Brk Th Eff %	39.77	40.69	41.57	36.65	38.95	40.18	41.01	40.20	40.80
Air Flow kg/min	14.65	15.05	15.27	23.96	21.84	24.81	10.27	10.87	10.72
Air/Fuel	30.83	32.79	34.11	25.44	24.92	29.22	32.52	34.29	34.36
Inl Man Temp K	323.10	306.74	305.34	335.20	323.56	321.38	318.10	299.32	298.11
Exh Man Templ K	793.00	782.43	766.79	963.00	990.05	905.90	678.00	715.73	720.17
" " " 2 K	789.00			978.00			695.00		
Inl Man Pres barg	1.97			2.62			1.25		
Exh Man Pres barg	2.13			2.81			1.37		
COMPRESSR.....									
Speed rpm	3954.00	3773.50	3973.50	8642.00	8683.20	8683.20	3069.00	3071.30	3071.30
Torque map Nm	113.60	114.67	112.34	155.92	147.00	144.32	81.31	81.32	79.45
Power map kW	47.16	47.73	46.77	141.24	133.72	131.28	26.69	26.17	25.56
Isen Eff T-S %	74.87			80.24			80.82		
Overall Eff %	62.84	63.80	66.00	63.67	62.00	68.20	62.73	62.30	63.10
Mass orif kg/min	13.74			33.24			9.77		
Mass map kg/min	14.95	15.04	15.67	34.42	34.69	38.28	11.55	11.33	11.80
Press Ratio	3.20	3.27	3.24	4.37	3.94	3.89	2.42	2.40	2.35
Inlet Dep mbarg	15.47	[15.47]	0.00	97.73	[97.73]	0.00	8.05	[8.05]	0.00
Inlet Temp K	300.15	300.15	294.40	297.45	[297.45]	294.40	301.45	[301.45]	[294.40]
Outlet Temp K	457.00	489.25	472.23	490.00	526.14	498.37	408.00	439.16	423.83
Interclr DP mbar	159.29	[157.00]		351.91	[351.91]		125.30	[125.30]	
Intercooler kW	33.03			62.44			15.55		
Byp Flow kg/min	0.29	-0.01	0.39	10.46	12.85	13.46	1.27	0.45	1.08
TURBINE.....									
Speed rpm	21589.82	21594.20	21594.20	21633.82	21638.30	21638.30	22997.85	23002.60	23002.60
Wheel Torque Nm	16.50	12.60	12.71	38.57	30.20	39.68	9.22	7.40	7.23
Enthalpy kW	37.27	28.49	28.75	86.93	68.46	89.88	22.07	17.82	17.42
Isen Eff %	63.48	49.40	52.00	54.49	48.20	56.90	72.65	60.60	66.10
Mass flow kg/min	16.33	15.49	16.11	36.55	35.57	39.13	12.50	11.65	12.11
Press Ratio	3.07	3.27	3.14	3.52	3.77	3.79	2.30	2.39	2.25
Back Pres mbarg	10.31	[10.31]	0.00	47.44	[47.44]	0.00	23.86	[23.86]	0.00
Inlet Templ K	763.00	782.43	760.00	830.00	833.99	774.23	670.00	705.62	695.36
" " 2 K	769.00			863.00			675.00		
Outlet Temp K	653.00			727.00			582.00		
GEAR LOSSES.....									
Total Losses kW	28.59	20.61	7.91	37.42	38.40	15.27	21.51	15.58	6.53
O/S Gear " kW		6.45	2.83		7.68	3.32		5.56	2.49
Comp. " " kW		0.61	1.59		1.63	4.07		0.36	1.01
Turb. " " kW		13.66	3.93		29.25	8.15		9.67	3.27

Table 8.5,c As per table 8.5,a

	EXP. RES.	PREDICTIONS ADJUSTED	TENTATIVE	EXP. RES.	PREDICTIONS ADJUSTED	TENTATIVE	EXP. RES.	PREDICTIONS ADJUSTED	TENTATIVE
OUTPUT	(1)	(2)	(3)	(1)	(2)	(3)	(1)	(2)	(3)
Speed rpm	1720.00	[1720.00]	[1720.00]	2090.00	[2091.00]	[2091.00]	2234.00	[2234.00]	[2234.00]
Torque Nm	200.37	202.45	213.62	313.44	303.95	329.27	403.23	394.66	442.00
Power kW	36.12	36.48	38.49	68.27	66.58	72.13	94.35	92.37	103.45
Thermal Eff %	27.02	28.20	28.50	30.37	29.47	31.49	31.09	29.63	33.64
BSFC g/kWh	312.91	296.00	293.00	278.39	283.00	249.00	271.98	282.00	248.00
ENGINE									
Speed rpm	1200.00	[1200.00]	[1200.00]	1520.00	[1520.00]	[1520.00]	1700.00	[1700.00]	[1700.00]
Torque Nm	400.74	[400.74]	[400.74]	568.06	[551.86]	[551.81]	675.41	675.41	675.41
Power kW	50.33	50.25	49.95	90.64	87.37	87.41	120.35	120.09	119.82
Boost Ratio	1.54	1.54	1.44	1.80	1.75	1.67	1.98	2.00	1.95
BMEP bar	6.13	6.12	6.08	8.70	8.39	8.39	10.34	10.32	10.29
Max Cyl Pres bar	76.49	76.85	76.05	87.47	78.56	96.86	104.59	104.76	106.42
Dyn Inj deg BTDC	11.51	9.10	19.70	11.06	7.20	24.40	17.35	12.30	21.10
Inj Duration deg	10.36	9.80	10.00	14.26	13.80	13.90	18.37	17.30	17.20
Fuel/Shot mg	52.35	49.96	52.16	69.30	68.86	69.83	83.78	84.96	83.80
Brk Th Eff %	37.66	38.85	36.97	40.33	38.67	38.16	39.66	38.52	38.97
Air Flow kg/min	7.61	7.62	7.19	11.13	10.65	10.38	13.12	13.26	13.33
Air/Fuel	40.41	42.40	38.32	35.16	33.91	32.61	30.67	30.60	31.19
Inl Man Temp K	317.60	291.88	291.37	320.30	297.46	297.27	320.00	303.35	302.21
Exh Man Templ K	598.00	612.28	643.56	697.00	743.67	742.76	733.00	814.30	789.25
" " " 2 K	609.00			698.00			748.00		
Inl Man Pres barg	0.53			0.79			0.96		
Exh Man Pres barg	0.62			0.93			1.14		
COMPRESSOR									
Speed rpm	2334.00	2341.90	2341.90	3390.00	3387.10	3387.10	4279.00	4290.20	4290.20
Torque map Nm	46.45	44.63	42.98	64.79	61.65	59.80	75.60	75.63	73.43
Power map kW	11.32	10.95	10.54	23.52	21.88	21.22	34.00	33.99	33.00
Isen Eff T-S %	76.26			78.42			80.80		
Overall Eff %	54.98	58.40	58.70	60.83	60.10	59.80	64.57	64.40	65.10
Mass orif kg/min	6.75			11.88			15.55		
Mass map kg/min	8.37	8.60	8.78	13.45	13.28	13.58	16.92	17.01	17.82
Press Ratio	1.63	1.63	1.59	1.96	1.89	1.85	2.23	2.21	2.15
Inlet Dep mbarg	4.12	[4.12]	0.00	11.88	[11.88]	0.00	20.53	[20.53]	0.00
Inlet Temp K	296.95	[296.95]	[294.40]	295.35	[295.35]	[294.40]	300.55	[300.55]	[294.40]
Outlet Temp K	355.00	373.20	366.37	380.00	393.87	387.92	396.00	419.89	405.19
Interclr DP mbar	84.64	[85.00]		140.63	[140.63]		203.28	[203.28]	
Intercooler kW	4.79			11.19			16.78		
Byp Flow kg/min	0.75	0.97	1.58	2.31	2.63	3.20	3.80	3.75	4.48
TURBINE									
Speed rpm	25227.24	25232.40	25232.40	30654.00	30675.00	30675.00	32766.07	32772.80	32772.80
Wheel Torque Nm	4.95	2.92	1.46	7.73	5.54	4.04	10.10	8.55	7.47
Power kW	13.10	7.71	3.87	24.71	17.80	12.99	34.68	29.35	25.66
Isen Eff %	120.93	73.70	62.40	97.16	74.10	71.30	90.85	73.80	74.20
Mass flow kg/min	8.99	8.78	8.97	14.30	13.60	13.91	18.03	17.45	18.25
Press Ratio	1.57	1.63	1.49	1.85	1.90	1.75	2.04	2.18	2.04
Back Pres mbarg	19.44	[29.44]	0.00	27.60	[27.60]	0.00	36.39	[36.39]	0.00
Inlet Templ K	583.00	587.04	597.03	639.00	680.08	666.07	664.00	735.33	700.88
" " 2 K	589.00			653.00			685.00		
Outlet Temp K	509.00			555.00			574.00		
GEAR LOSSES									
Total Losses kW	15.99	10.53	4.78	23.55	16.71	7.05	26.68	23.07	9.04
O/S Gear " kW		4.48	2.08		6.35	2.89		7.57	3.41
Comp. " " kW		0.18	0.59		0.33	0.98		0.48	1.36
Turb. " " kW		5.98	2.54		10.56	3.66		15.32	4.72

Table 8.5,d As per table 8.5,a

	EXP. RES.	PREDICTIONS ADJUSTED	PREDICTIONS TENTATIVE	EXP. RES.	PREDICTIONS ADJUSTED	PREDICTIONS TENTATIVE	EXP. RES.	PREDICTIONS ADJUSTED	PREDICTIONS TENTATIVE
OUTPUT	(1)	(2)	(3)	(1)	(2)	(3)	(1)	(2)	(3)
Speed rpm	2522.00	[2522.00]	[2522.00]	2700.00	[2700.00]	[2700.00]	2837.00	[2837.00]	[2837.00]
Torque Nm	200.98	207.75	205.45	612.27	625.32	726.81	404.60	413.20	456.81
Power kW	53.02	54.89	54.28	173.35	176.88	205.99	120.08	122.81	135.77
Thermal Eff %	26.60	27.23	25.73	31.37	31.34	38.06	31.40	30.87	35.17
BSFC g/kWh	317.89	306.00	324.00	269.52	266.00	219.00	269.27	270.00	237.00
ENGINE.....									
Speed rpm	1700.00	[1700.00]	[1700.00]	2107.00	[2107.00]	[2107.00]	2000.00	[2000.00]	[2000.00]
Torque Nm	423.07	[423.07]	[423.01]	980.64	[980.65]	[980.65]	714.12	[714.12]	[714.10]
Power kW	75.29	75.17	74.70	216.83	215.92	215.72	149.47	149.23	149.07
Boost Ratio	1.49	1.46	1.40	2.67	2.81	2.94	2.01	2.04	2.07
BMEP bar	6.48	6.46	6.42	15.02	14.97	14.95	10.94	10.90	10.88
Max Cyl Pres bar	80.89	81.20	84.43	148.62	148.21	123.57	105.50	105.80	111.08
Dyn Inj deg BTDC	14.78	12.70	28.50	20.39	18.40	16.40	15.59	13.40	22.00
Inj Duration deg	13.05	12.60	13.00	29.39	26.60	25.70	20.74	20.60	20.20
Fuel/Shot mg	55.10	54.93	57.50	122.93	124.13	118.80	89.90	92.16	89.43
Brk Th Eff %	37.77	37.29	35.41	39.24	38.25	39.94	39.09	37.52	38.62
Air Flow kg/min	9.96	9.99	9.74	21.35	21.39	23.63	15.64	15.52	16.33
Air/Fuel	35.45	35.65	33.23	27.42	27.26	31.46	29.03	28.07	30.44
Inl Man Temp K	319.00	295.94	295.38	324.80	317.17	317.43	321.20	308.48	307.40
Exh Man Templ K	656.00	721.71	735.16	873.00	935.34	848.01	796.00	892.05	824.24
" " " 2 K	671.00			886.00			811.00		
Inl Man Pres barg	0.48			1.63			0.99		
Exh Man Pres barg	0.64			2.02			1.30		
COMPRESSOR.....									
Speed rpm	2908.00	2908.10	2908.10	5618.00	5647.70	5647.70	4043.00	4045.50	4045.50
Torque map Nm	50.03	47.13	45.44	110.32	109.43	107.23	78.83	79.46	78.08
Power map kW	15.26	14.36	13.84	65.37	64.75	63.45	33.38	33.68	33.09
Isen Eff T-S %	76.84			79.11			80.58		
Overall Eff %	56.08	58.10	58.70	66.52	68.30	72.80	65.02	64.80	66.30
Mass orif kg/min	9.45			21.29			14.13		
Mass map kg/min	11.10	11.26	11.63	22.57	22.58	23.94	15.62	15.69	16.59
Press Ratio	1.66	1.62	1.59	3.17	3.21	3.18	2.34	2.34	2.29
Inlet Dep mbarg	7.36	[7.36]	0.00	38.70	[38.70]	0.00	17.09	[17.09]	0.00
Inlet Temp K	297.10	[297.25]	[294.40]	295.30	[295.45]	[294.40]	302.40	[302.55]	[294.40]
Outlet Temp K	357.00	373.57	365.73	440.00	466.26	452.49	405.00	430.66	413.62
Interclr DP mbar	153.29	[153.29]		367.91	[367.91]		278.59	[278.59]	
Intercooler kW	6.37			41.41			22.07		
Byp Flow kg/min	1.13	1.27		1.21	1.19	0.31	-0.01	0.17	0.26
TURBINE.....									
Speed rpm	36990.17	36997.70	36997.70	39600.90	39609.00	39609.00	41610.27	41618.80	41618.80
Wheel Torque Nm	5.23	2.22		17.03	16.71	16.43	10.03	8.39	7.05
Power kW	20.26	8.60		70.71	69.35	68.16	43.69	36.56	30.75
Isen Eff %	127.99	55.60		77.02	72.40	73.70	96.22	74.60	72.50
Mass flow kg/min	11.88	11.55		24.33	23.37	24.69	16.87	16.24	17.14
Press Ratio	1.56	1.63	1.48	2.85	3.22	3.07	2.17	2.36	2.19
Back Pres mbarg	41.35	[41.35]	0.00	48.23	[48.23]	0.00	44.89	[44.89]	0.00
Inlet Templ K	649.00	685.77	680.52	845.00	913.71	843.45	786.00	887.69	818.54
" " 2 K	653.00			854.00			791.00		
Outlet Temp K	562.00			706.00			659.00		
Gear Losses.....									
Total Losses kW	26.60	14.52	6.57	48.82	43.63	14.85	39.70	29.31	10.95
O/S Gear " kW		6.74	3.12		11.50	5.06		9.93	4.45
Comp. " " kW		0.24	0.75		0.84	2.20		0.47	1.32
Turb. " " kW		7.72	3.33		31.72	8.27		19.17	5.87

Table 8.5,e As per table 8.5,a

OUTPUT		EXP. RES. (1)	PREDICTIONS ADJUSTED (2)	PREDICTIONS TENTATIVE (3)	EXP. RES. (1)	PREDICTIONS ADJUSTED (2)	PREDICTIONS TENTATIVE (3)
Speed	rpm	3400.00	[3400.00]	[3400.00]	3409.00	[3409.00]	[3409.00]
Torque	Nm	400.54	410.58	460.89	533.95	547.73	629.49
Power	kW	142.41	146.25	164.17	189.99	195.61	224.82
Thermal Eff	%	30.06	30.75	34.47	30.48	31.61	36.31
BSFC	g/kWh	281.33	271.00	242.00	277.41	264.00	230.00
ENGINE.....							
Speed	rpm	2340.00	[2340.00]	[2340.00]	2435.00	[2435.00]	[2438.00]
Torque	Nm	720.98	[720.98]	[721.01]	896.63	[896.63]	[896.59]
Power	kW	176.59	176.27	176.58	228.89	227.82	228.46
Boost Ratio		1.98	1.99	2.06	2.35	2.46	2.53
BMEP	bar	11.04	11.00	11.02	13.73	13.66	13.68
Max Cyl Pres	bar	108.12	108.19	107.72	135.25	135.24	104.60
Dyn Inj deg BTDC		15.43	16.70	22.10	19.74	21.10	16.10
Inj Duration	deg	23.85	24.20	24.30	31.44	30.30	30.30
Fuel/Shot	mg	95.17	94.20	94.30	120.12	117.76	117.66
Brk Th Eff	%	37.27	37.06	37.08	36.72	36.81	36.90
Air Flow	kg/min	17.99	17.32	18.52	21.90	20.98	22.95
Air/Fuel		26.94	26.19	27.29	24.93	23.52	25.27
Inl Man Temp	K	318.40	308.73	313.59	325.30	322.12	324.82
Exh Man Templ	K	870.00	947.45	891.26	955.00	1014.05	957.24
" " " 2	K	890.00			974.00		
Inl Man Pres	barg	0.95			1.31		
Exh Man Pres	barg	1.32			1.77		
COMPRESSOR.....							
Speed	rpm	4321.00	4345.90	4345.90	5156.00	5141.60	5168.00
Torque map	Nm	80.76	80.12	78.72	100.59	99.97	98.09
Power map	kW	36.83	36.48	35.84	54.90	53.85	53.11
Isen Eff T-S	%	78.17			78.53		
Overall Eff	%	64.76	64.40	67.20	65.70	66.80	69.00
Mass orif	kg/min	15.68			20.00		
Mass map	kg/min	17.45	17.47	18.07	20.58	20.24	21.75
Press Ratio		2.39	2.35	2.31	2.91	2.94	2.79
Inlet Dep	mbarg	20.33	[20.33]	0.00	32.07	[32.07]	0.00
Inlet Temp	K	289.95	[289.95]	[294.40]	294.45	[294.45]	[294.40]
Outlet Temp	K	394.00	414.78	424.68	427.00	473.04	467.08
Interclr DP	mbar	346.58	[346.58]		438.55	[438.55]	
Intercooler	kW	22.90			37.49		
Byp Flow	kg/min	-0.54	0.15	0.45	-1.32	-0.74	-1.19
TURBINE.....							
Speed	rpm	49867.80	49878.00	49878.00	49999.80	50010.00	50010.00
Wheel Torque	Nm	9.91	7.70	7.08	14.57	12.89	12.58
Power	kW	51.70	40.22	37.00	76.06	67.52	65.90
Isen Eff	%	92.64	70.20	67.90	87.19	75.20	74.60
Mass flow	kg/min	18.88	18.14	18.75	22.46	21.10	22.62
Press Ratio		2.18	2.38	2.32	2.60	3.01	2.79
Back Pres	mbarg	56.18	[56.18]	0.00	62.86	[62.86]	0.00
Inlet Templ	K	858.00	943.53	891.26	940.00	1014.05	957.24
" " 2	K	866.00			946.00		
Outlet Temp	K	728.00			782.00		
GEAR LOSSES.....							
Total Losses	kW	49.04	33.76	13.57	60.06	45.88	36.66
O/S Gear "	kW		11.96	5.36		13.70	12.50
Comp. " "	kW		0.51	1.43		0.71	0.81
Turb. " "	kW		21.57	7.05		32.24	24.03

Table 8.5,f As per table 8.5,a

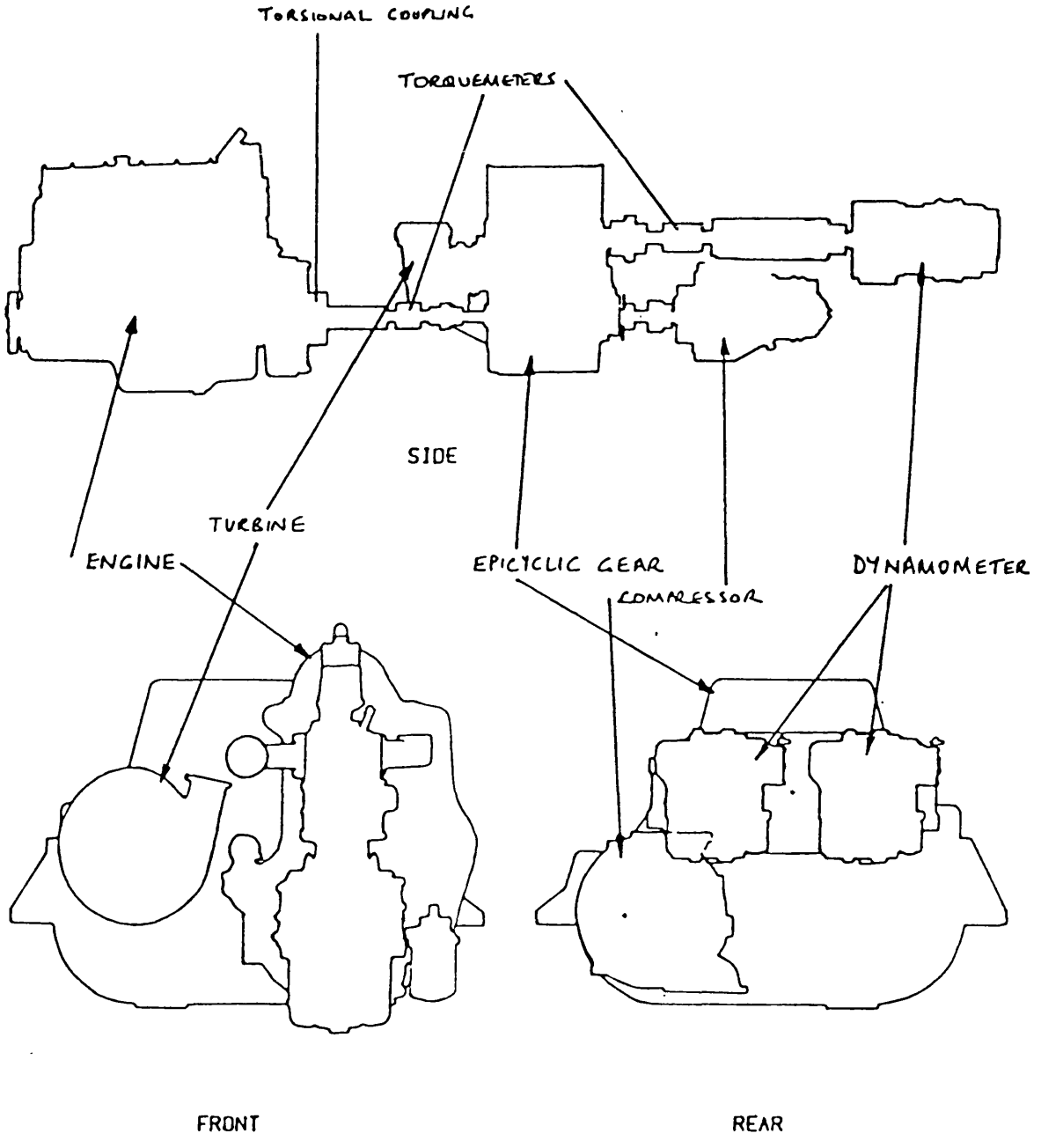

Fig. 8.1 Overall silhouette of the prototype

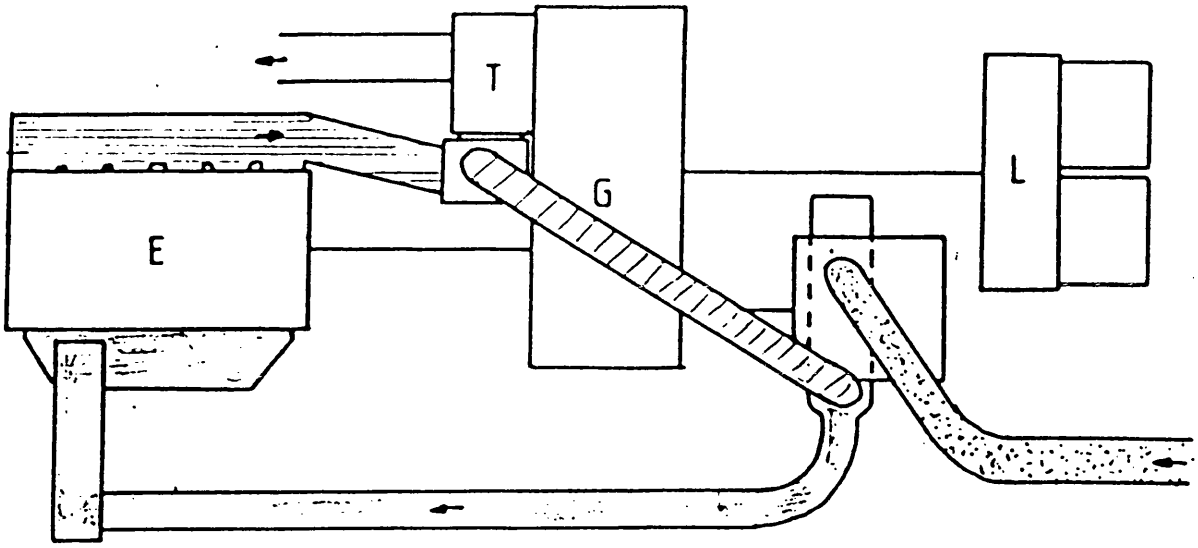

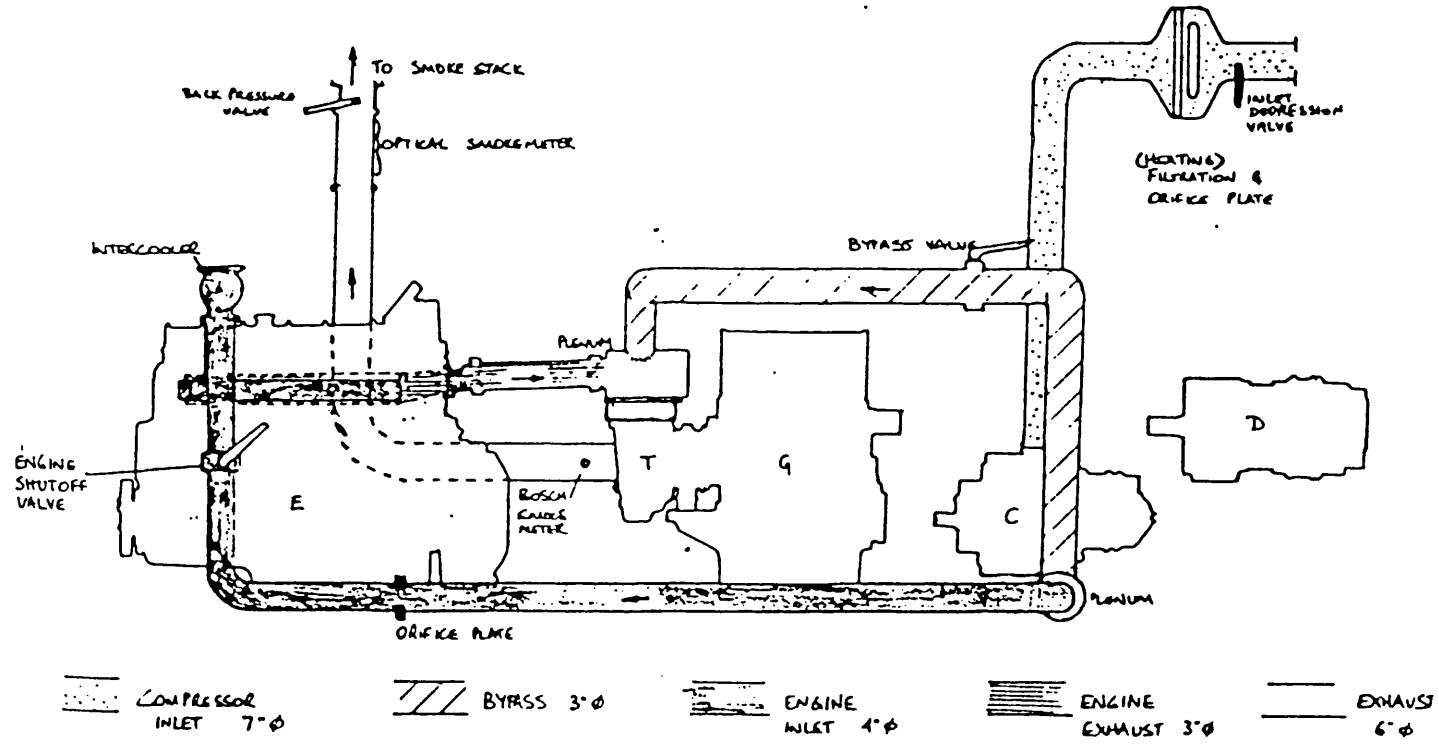

Fig. 8.2 Pipework arrangement of the prototype

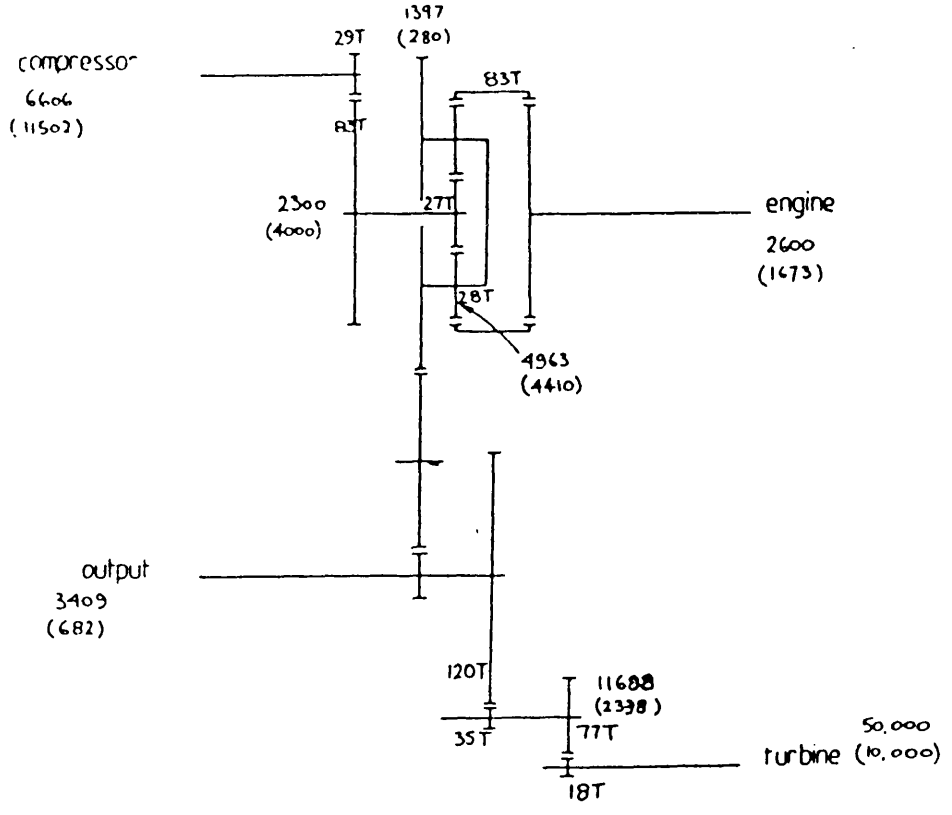

Speeds (RPM) at Rated and (Stall) conditions. T = no. of teeth

DJP 15.10.84

Fig. 8.3 Epicyclic gear together with turbine, compressor and output shaft geartrain arrangement

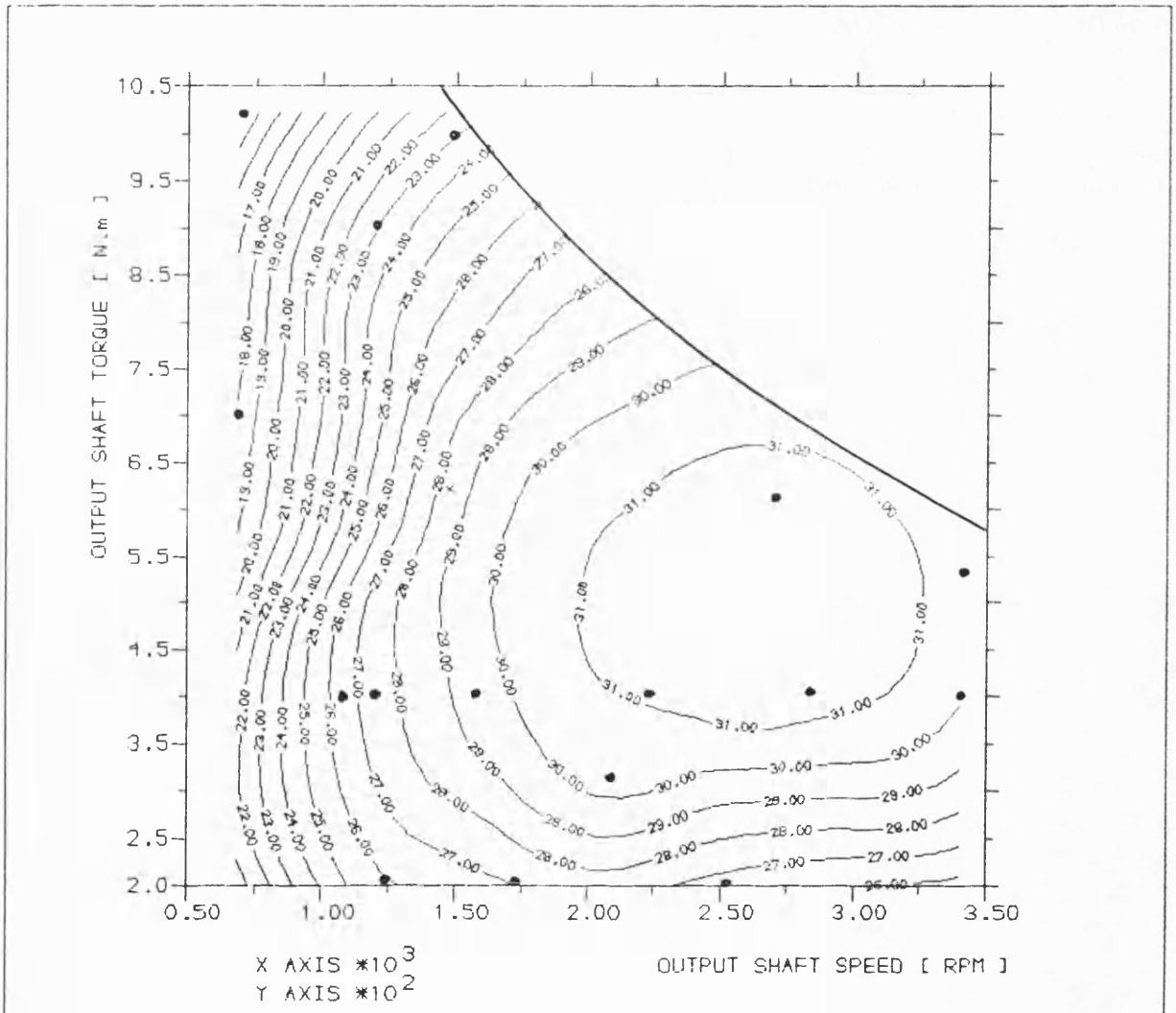

Fig. 8.4,a Contours of output shaft efficiencies (experimental)

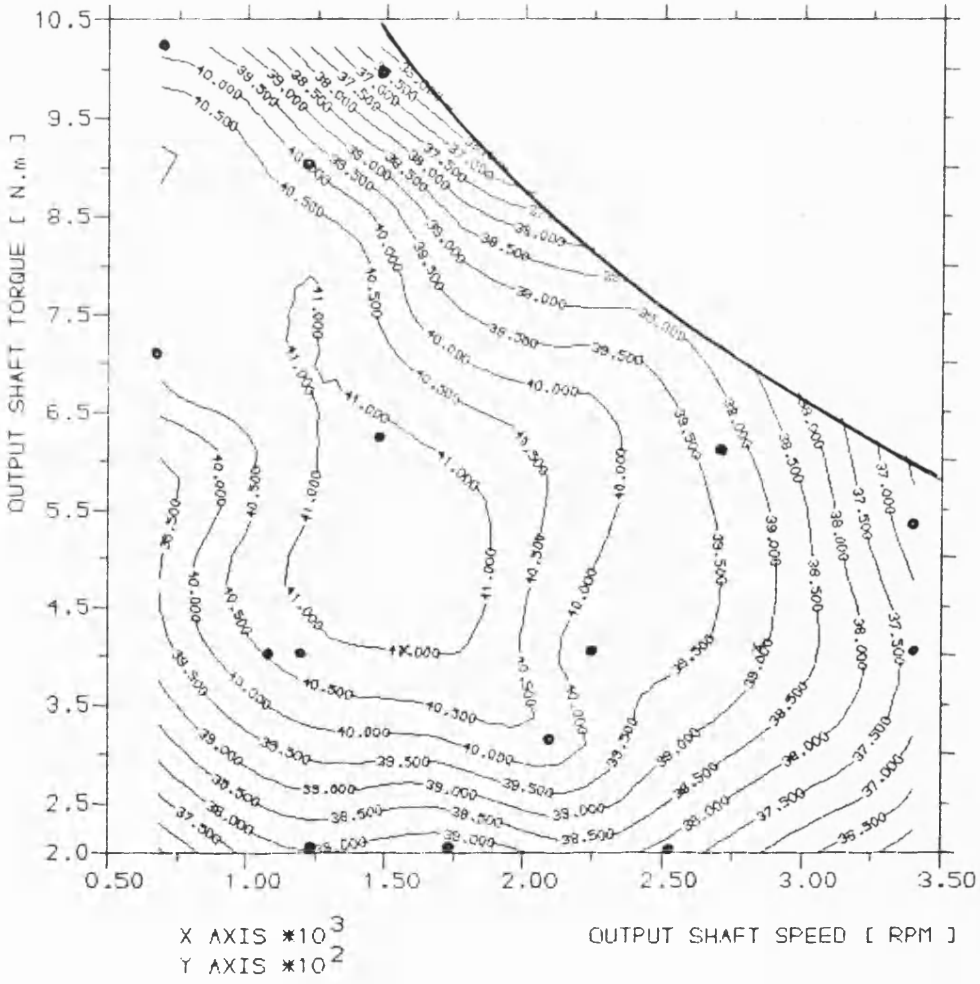

Fig. 8.4,b Contours of engine brake thermal efficiency (experimental)

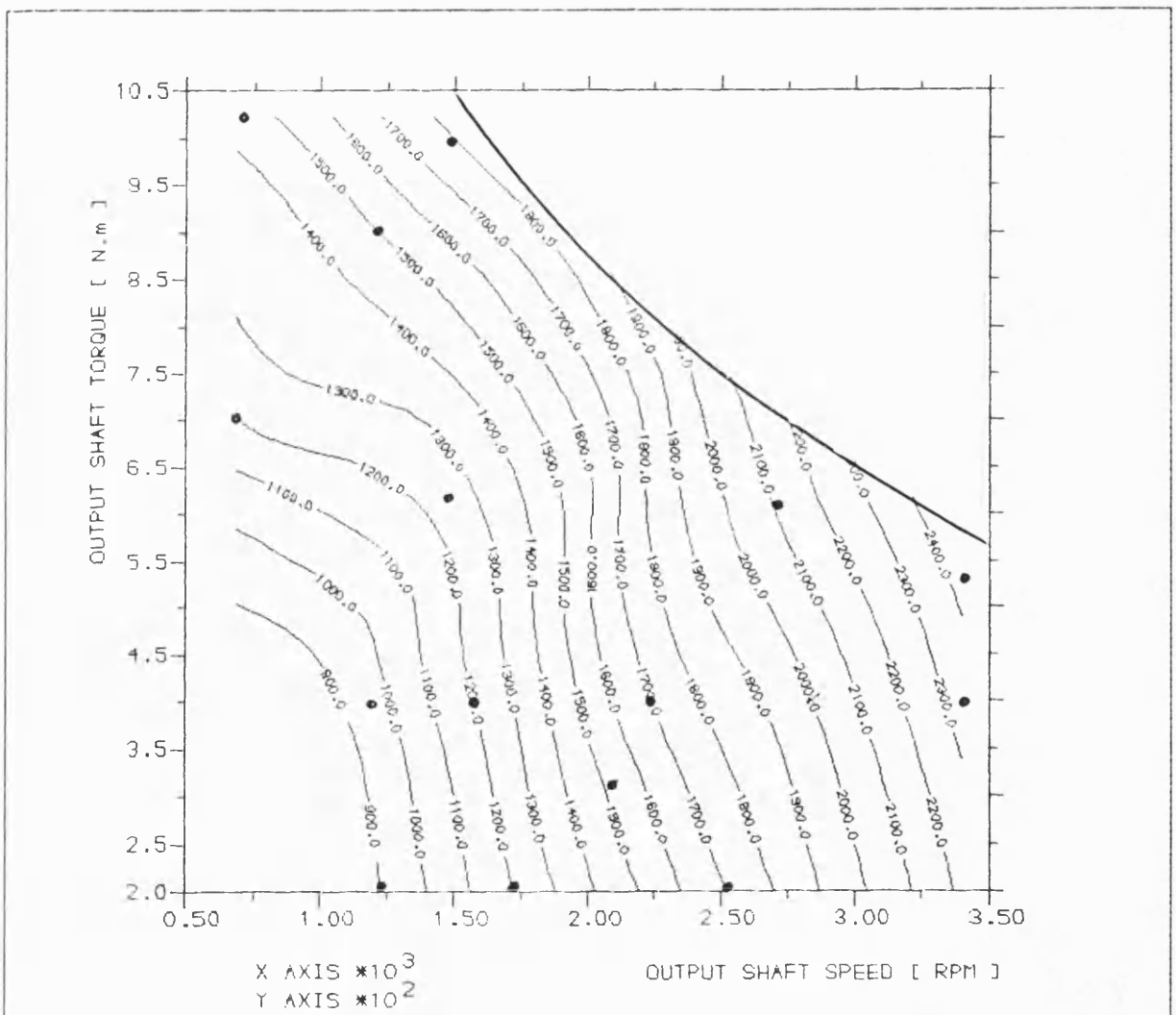

Fig. 8.4,c Contours of engine speed (experimental)

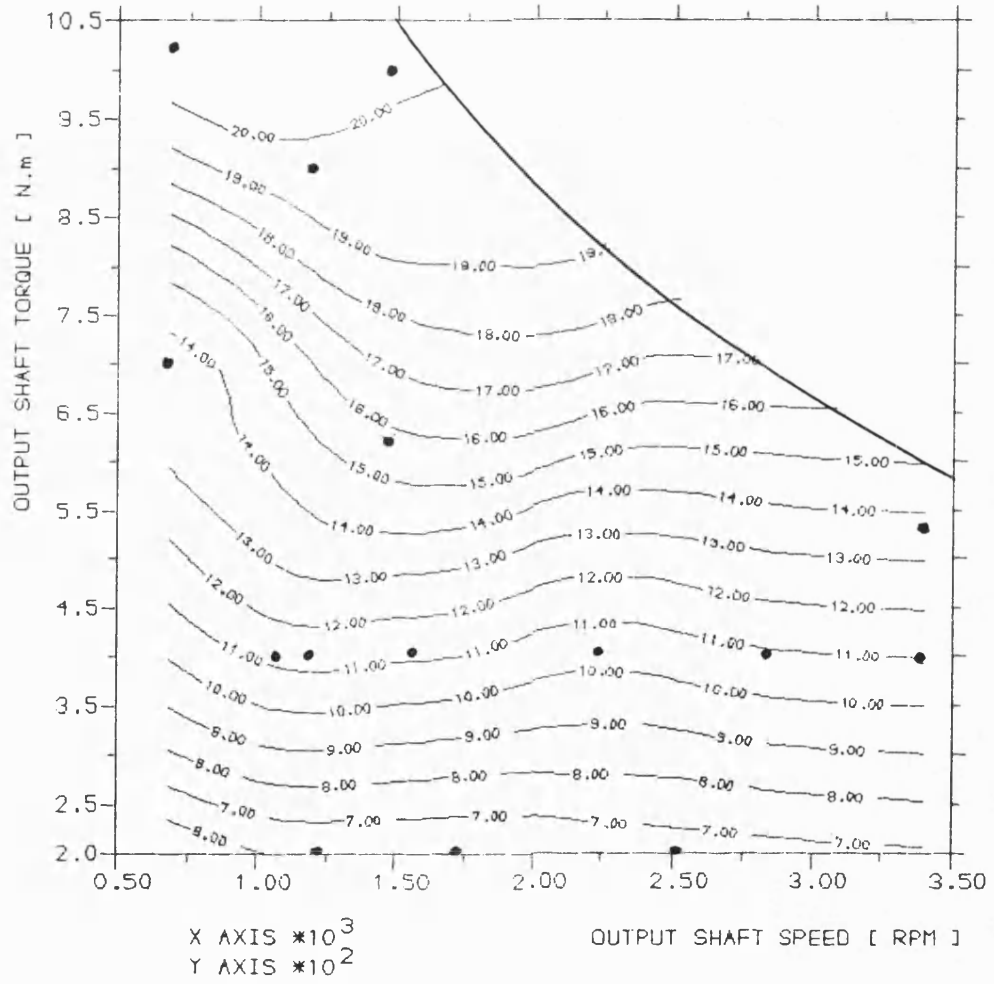

Fig. 8.4,d Contours of BMEP (experimental)

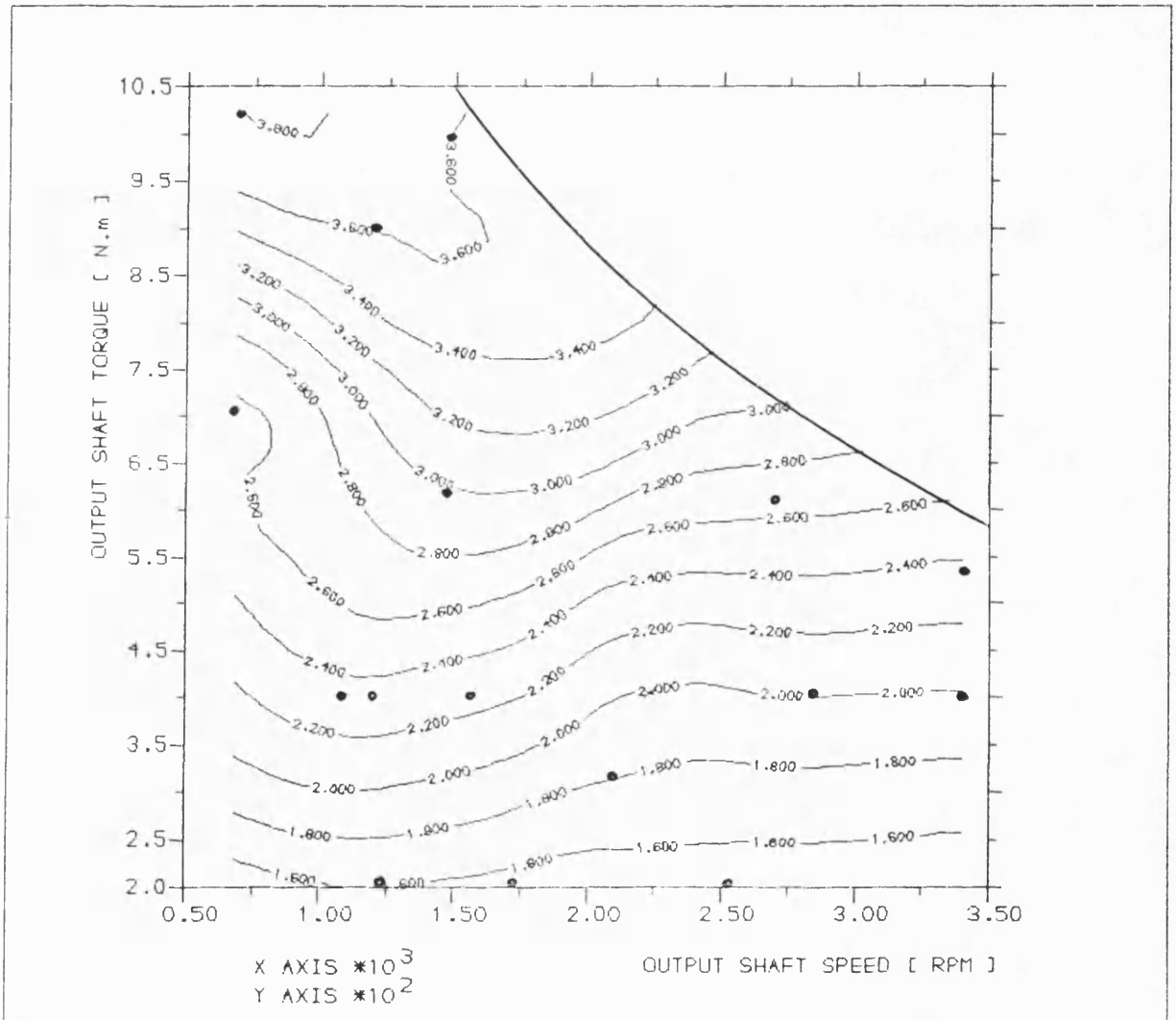

Fig. 8.4,e Contours of boost pressure ratio (experimental)

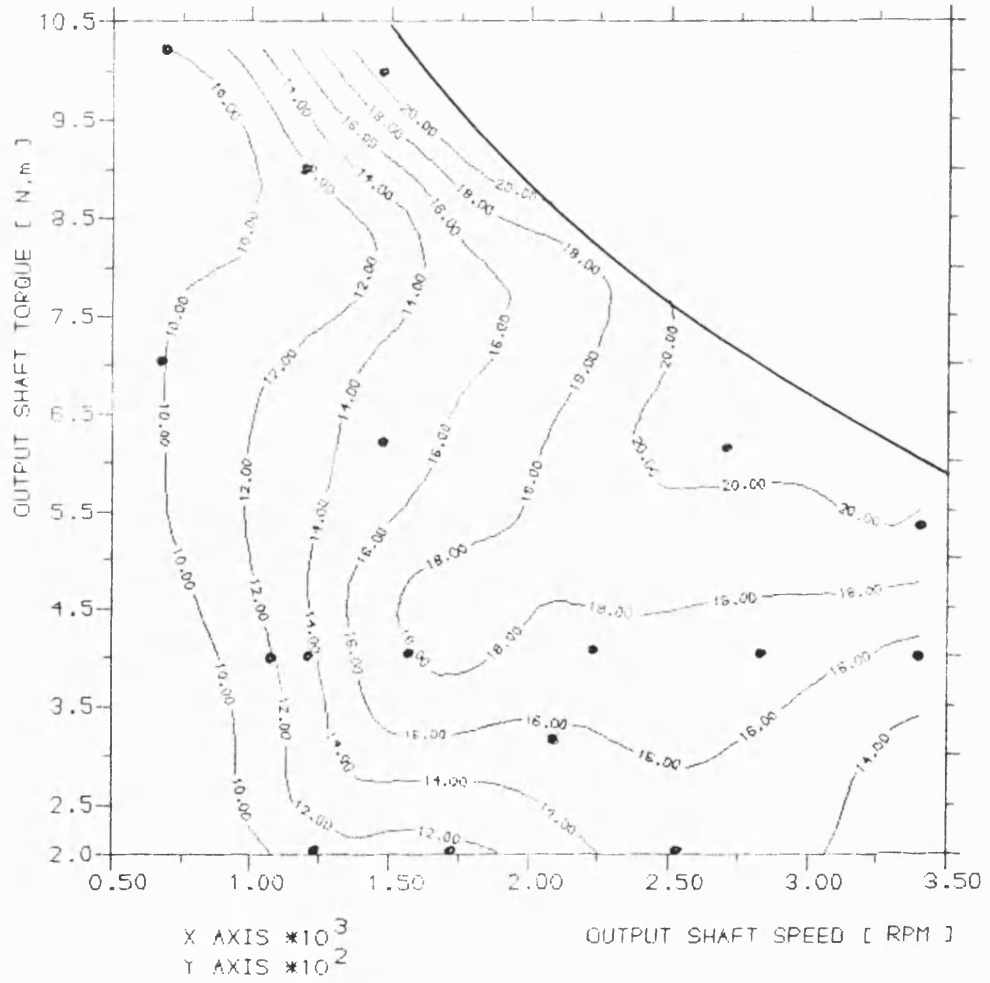

Fig. 8.4,f Contours of dynamic injection timing (experimental)

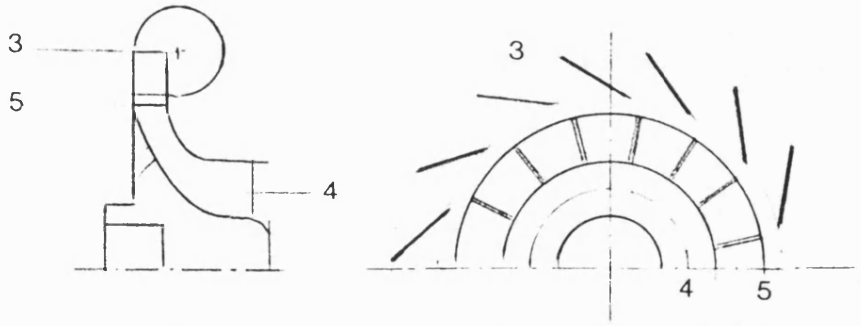

(a) Components of a radial flow turbine

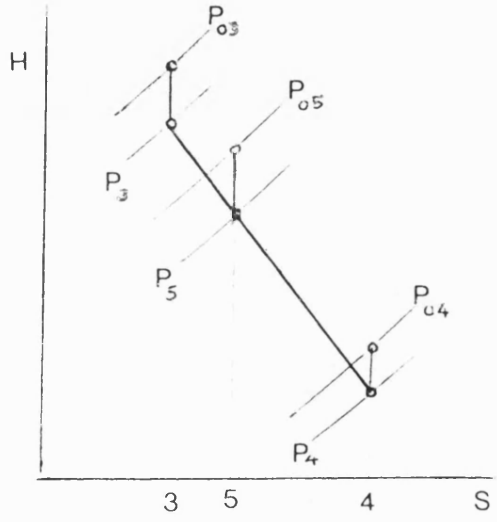

(b) Enthalpy-entropy diagram for a turbine stage

Fig. 8.5 Radial flow turbine

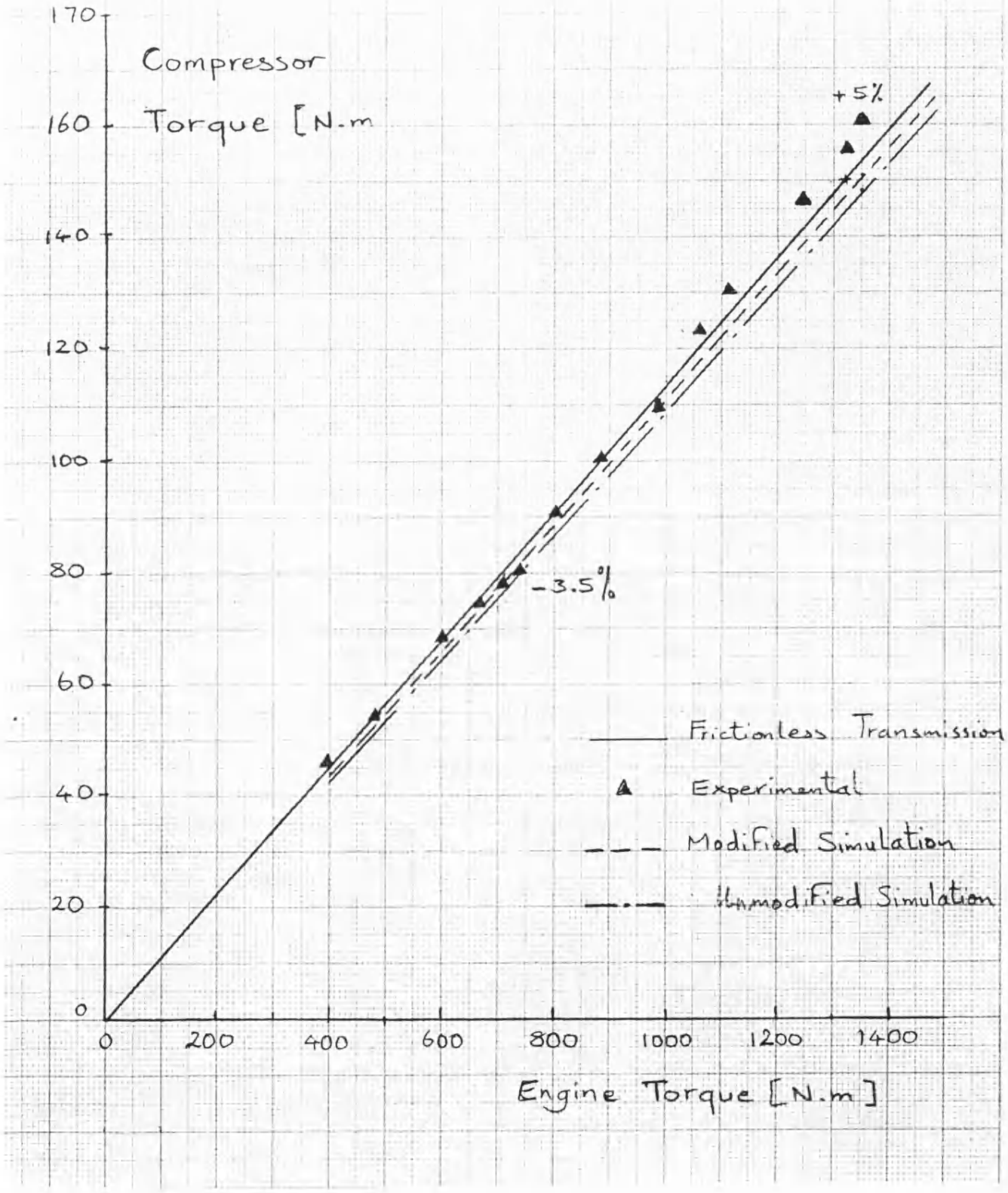

Fig. 8.6 Compressor torque versus engine torque (due to interposed epicyclic and step up geartrain)

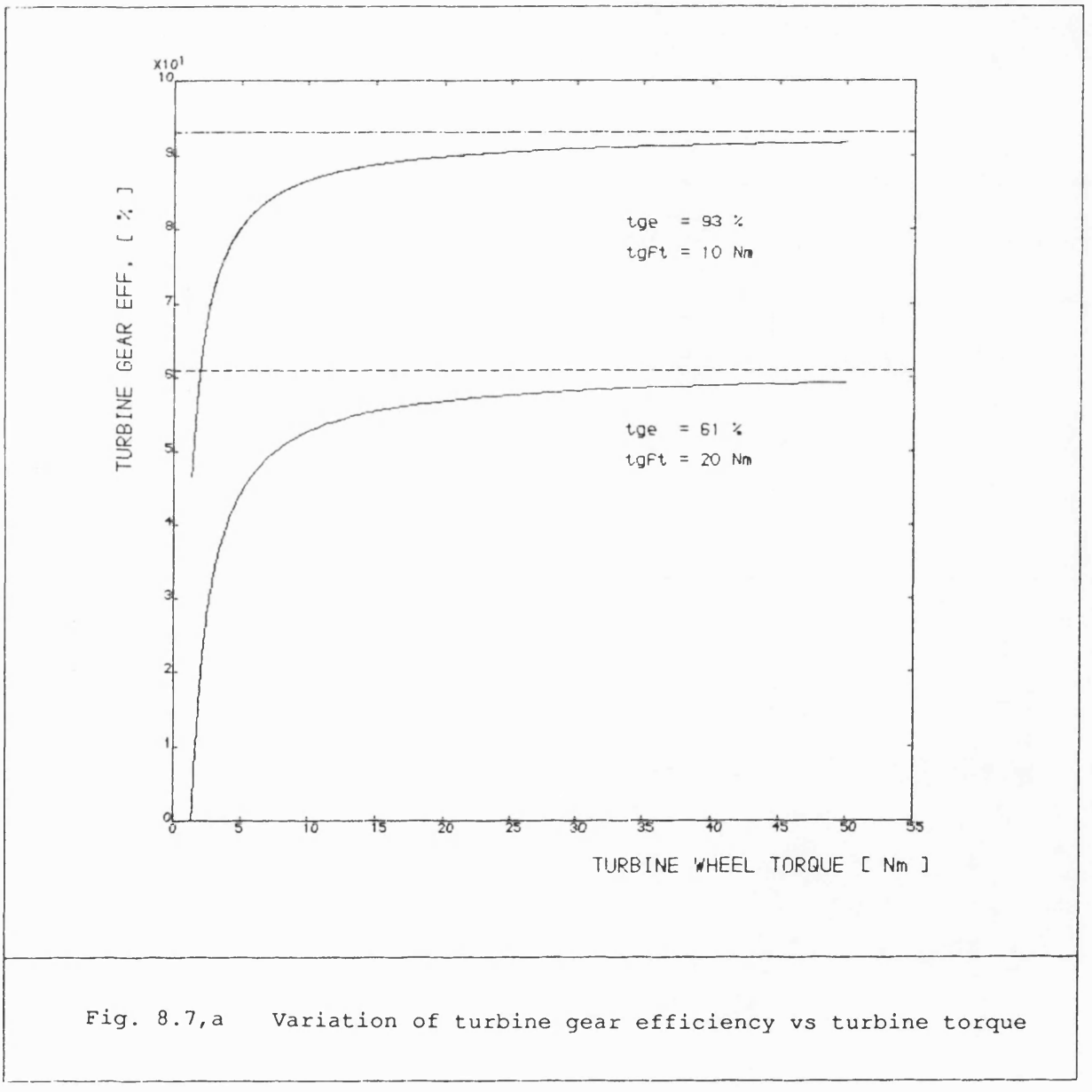

Fig. 8.7,a Variation of turbine gear efficiency vs turbine torque

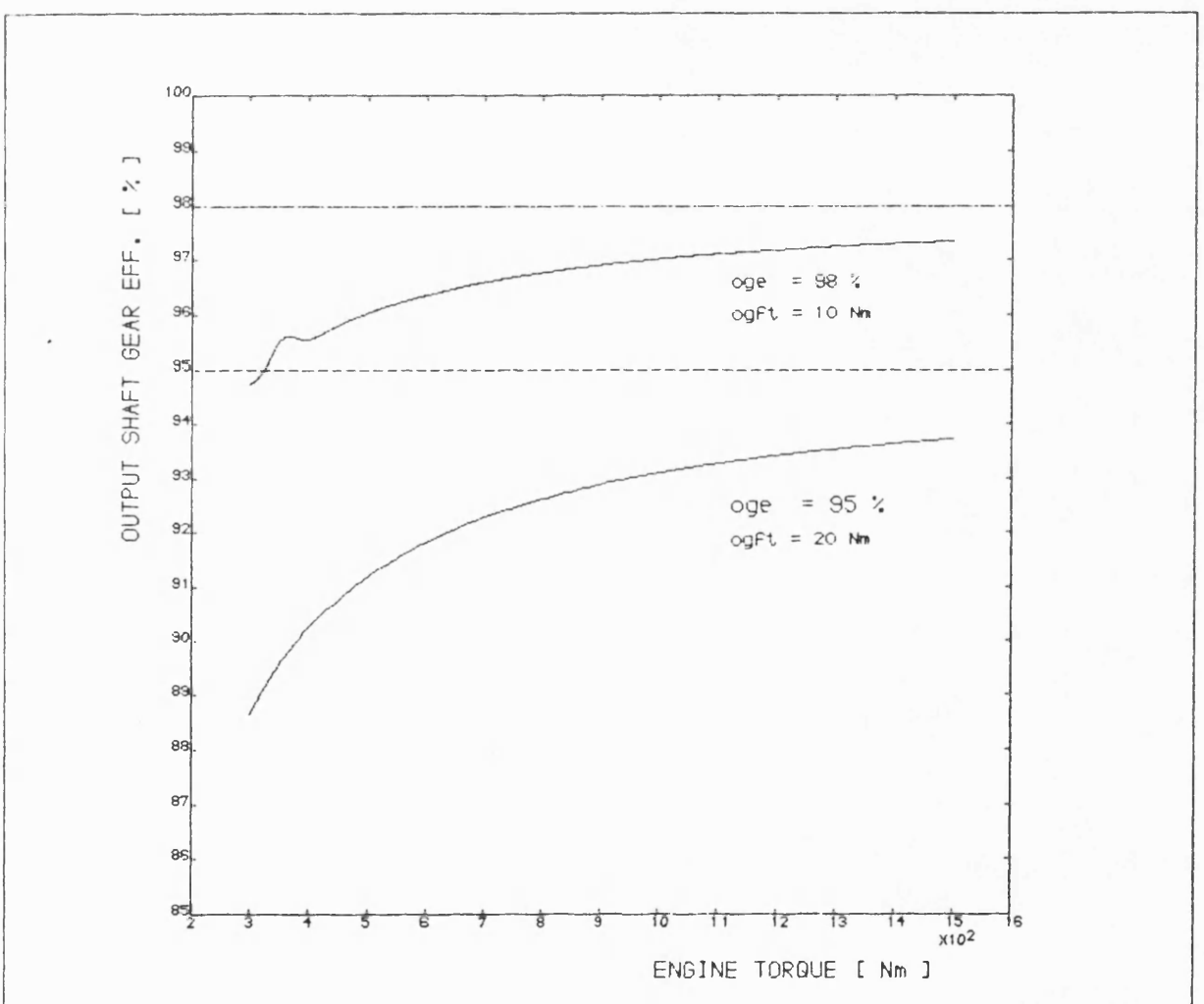

Fig. 8.7,b Variation of output shaft gear efficiency vs engine torque

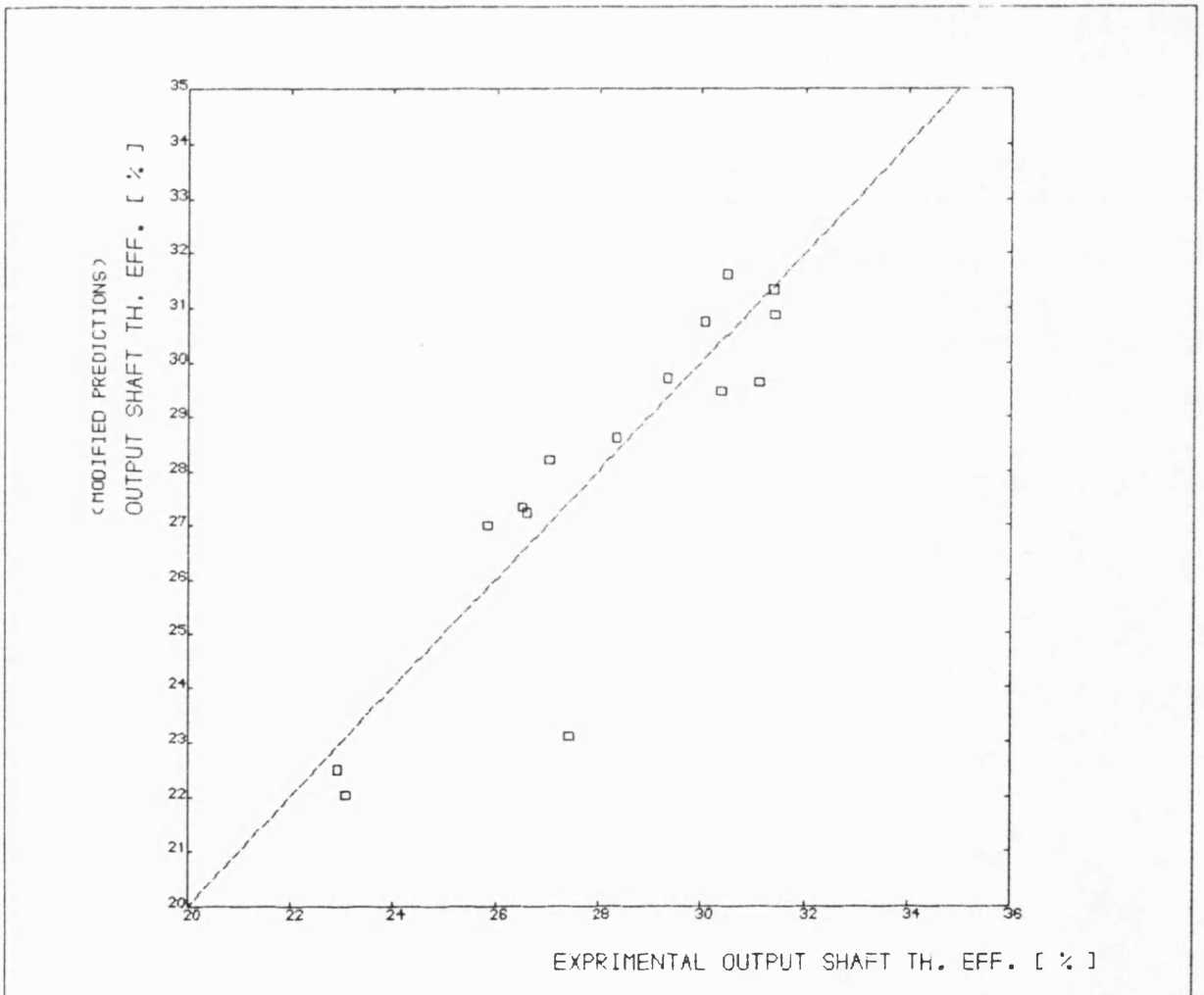

Fig. 8.8,a Comparison of output shaft torques obtained from experiments and from adjusted simulations

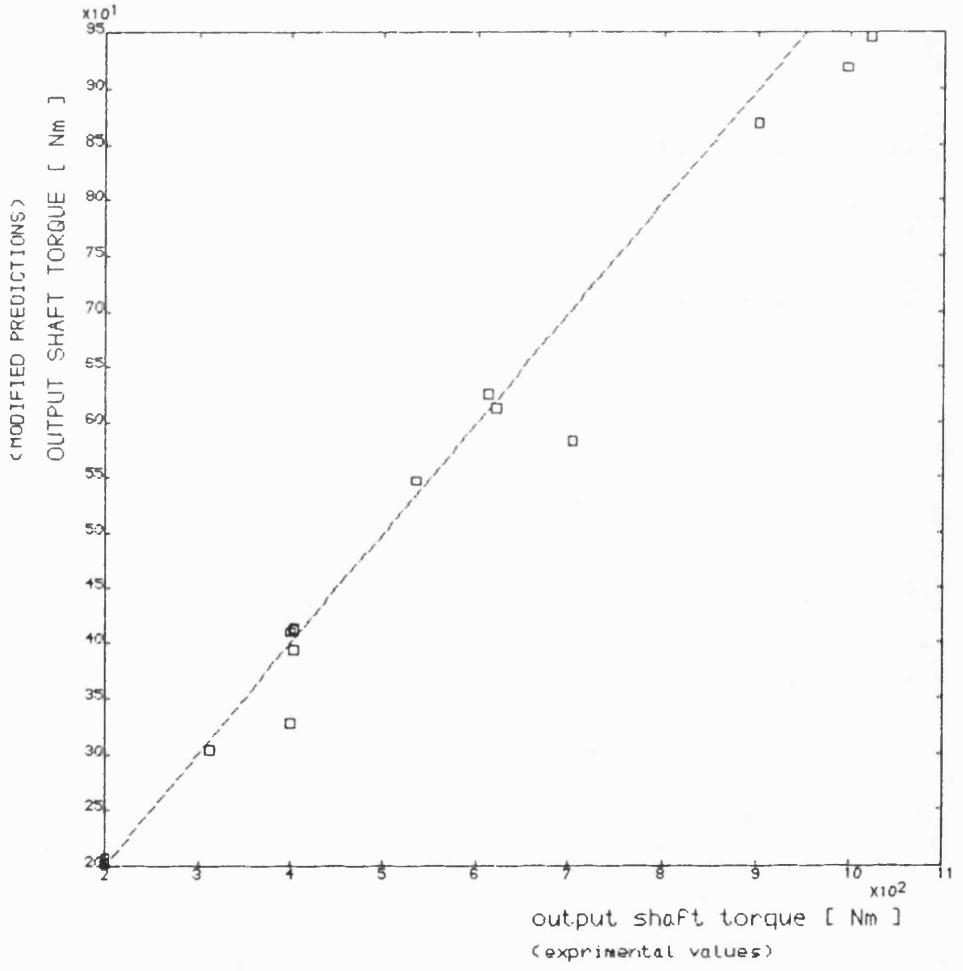

Fig. 8.8,b As per 'a' but for output shaft efficiencies

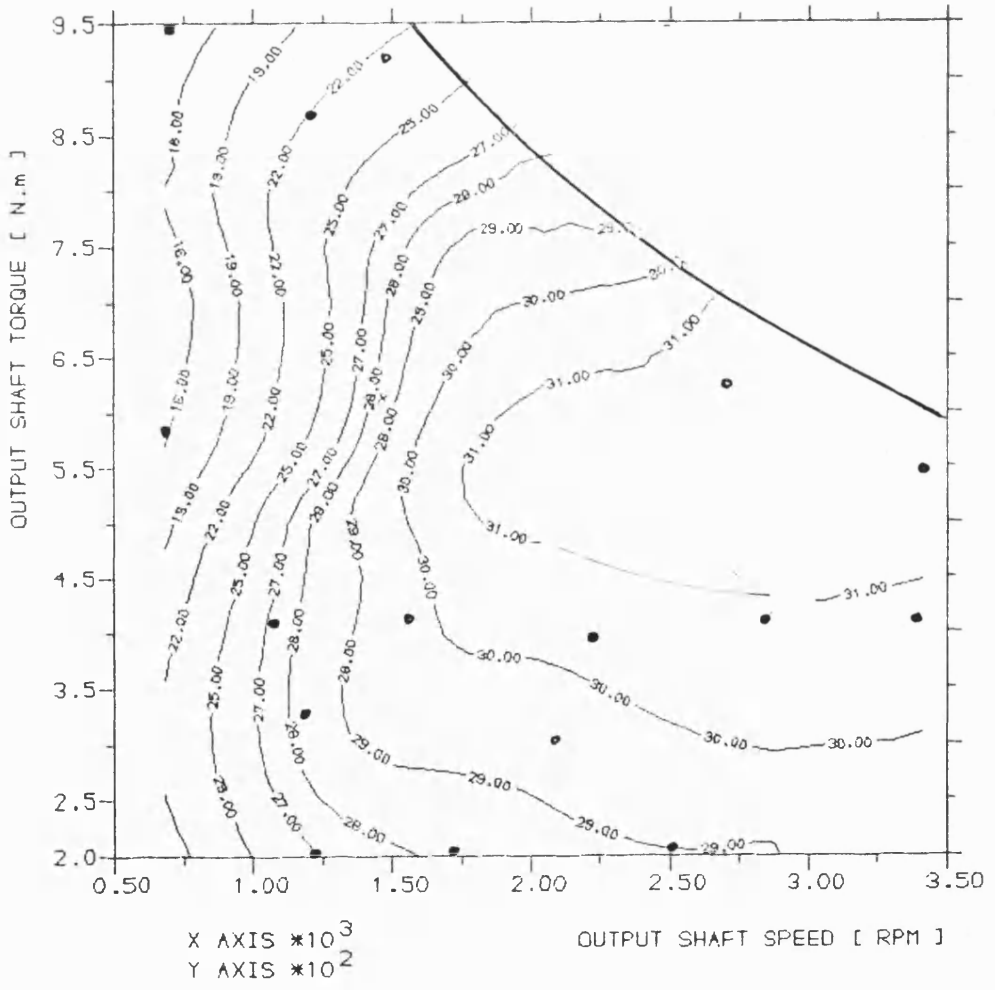

Fig. 8.9,a Contours of output shaft efficiences (adjusted simulation)

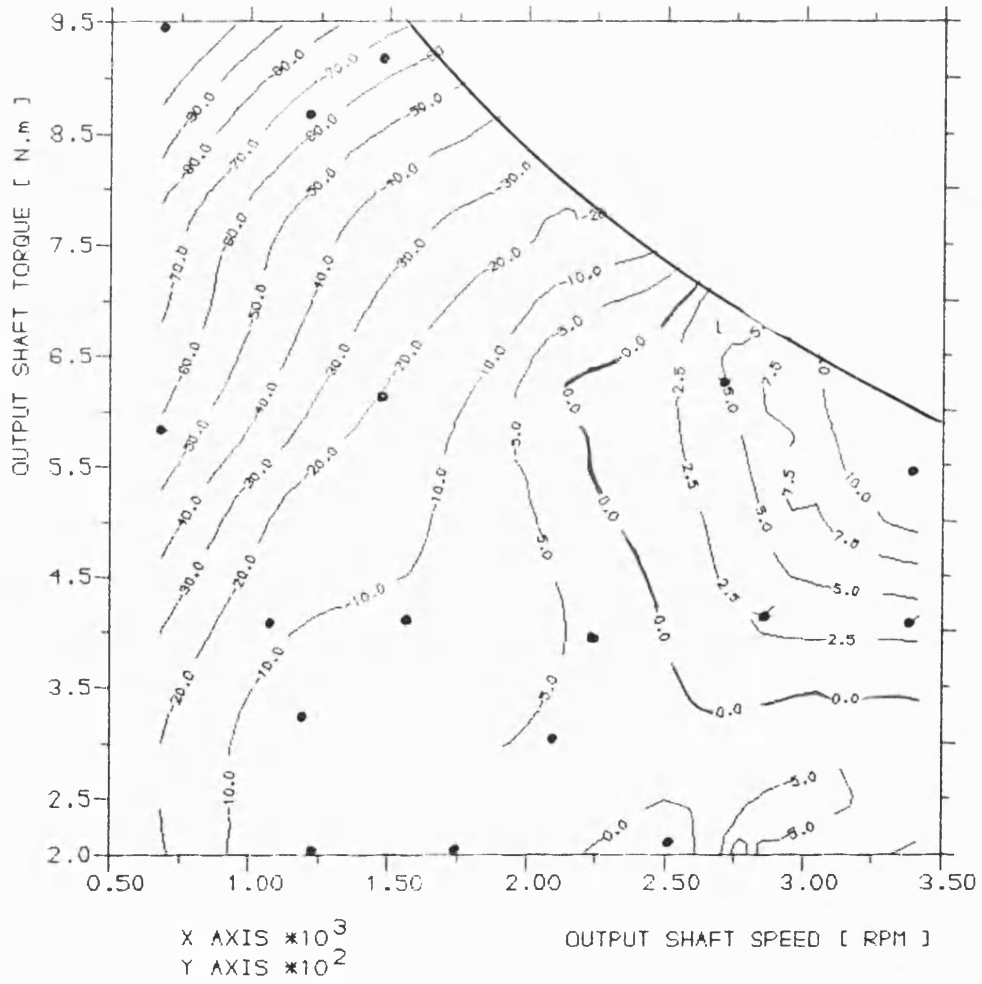

Fig. 8,9,b Contours of compounding effects (adjusted simulation)

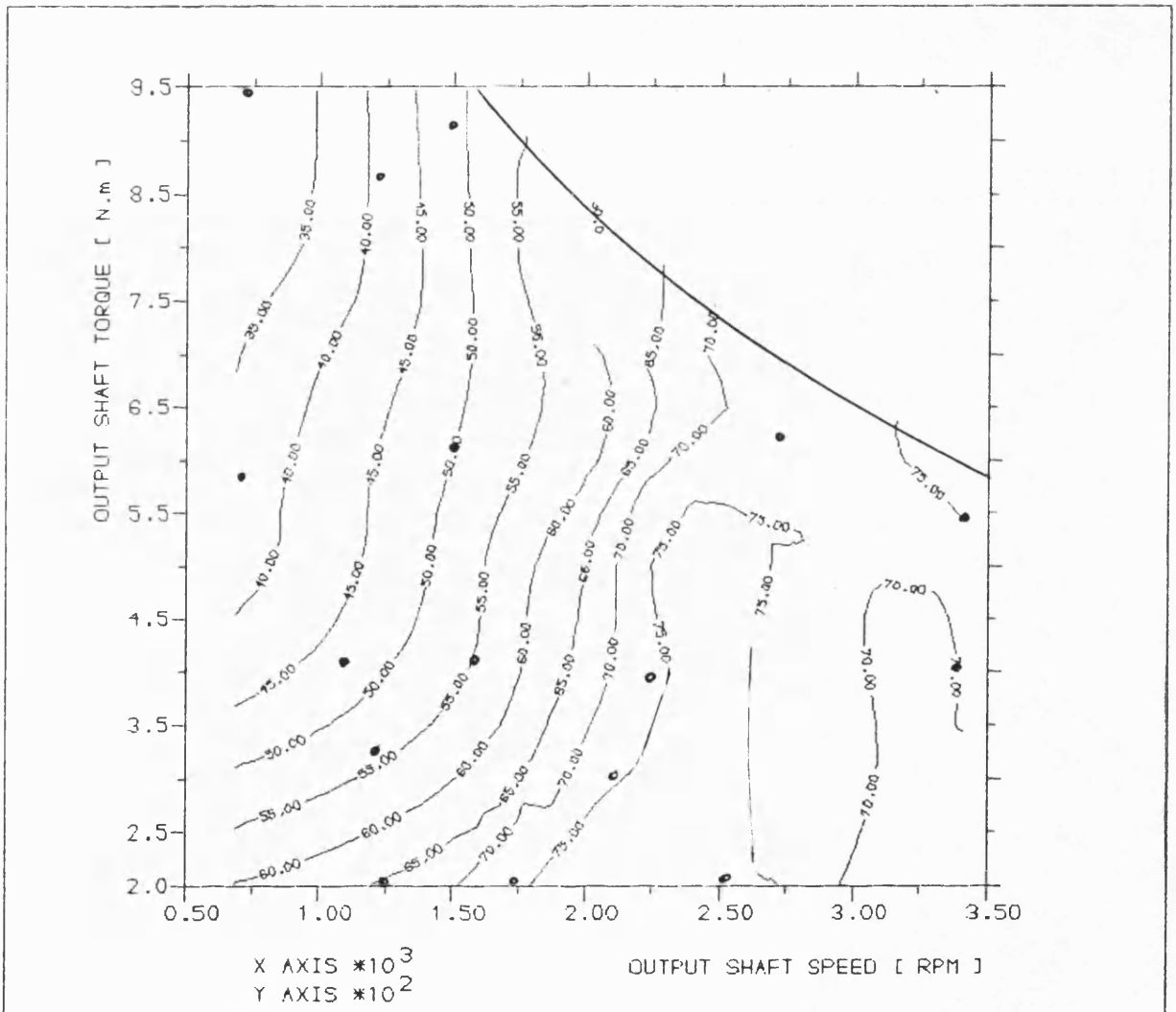

Fig. 8,9,c Contours of turbine efficiences (adjusted simulation)

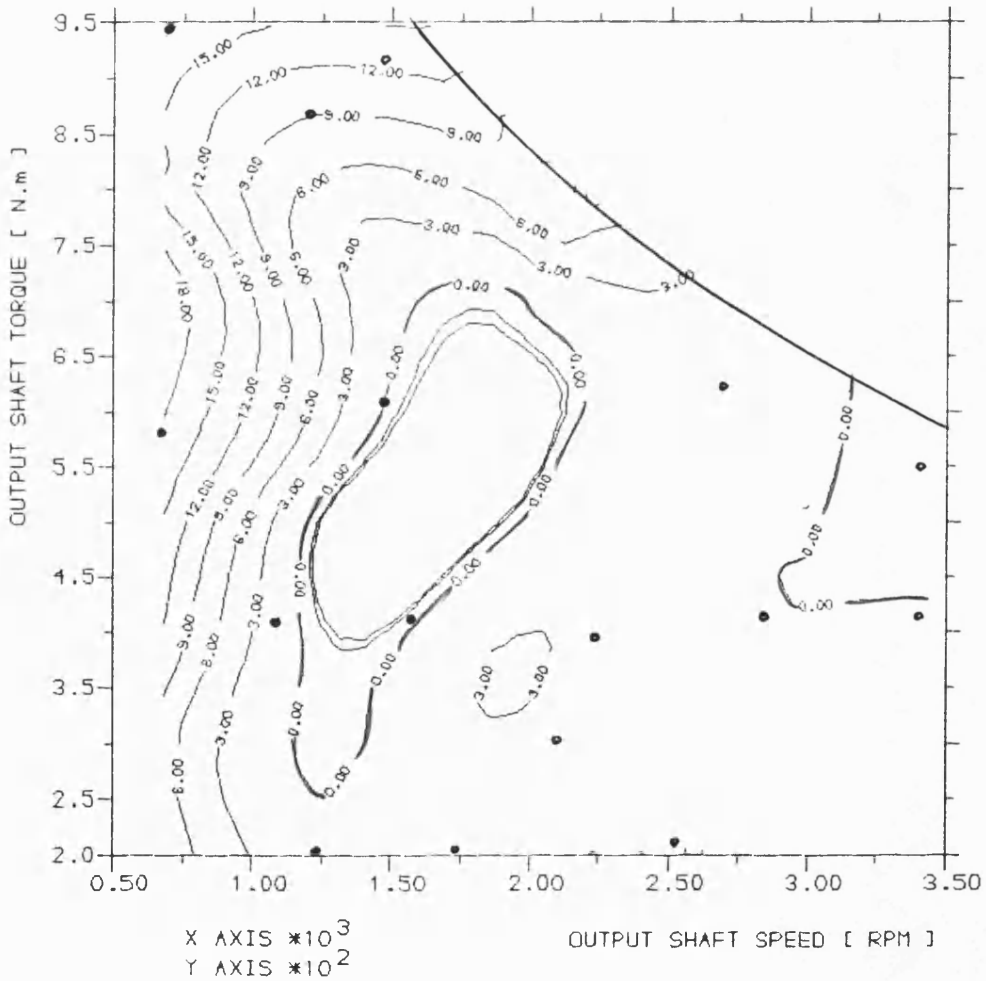

Fig. 8,9,d Contours of bypass flows (adjusted simulation)

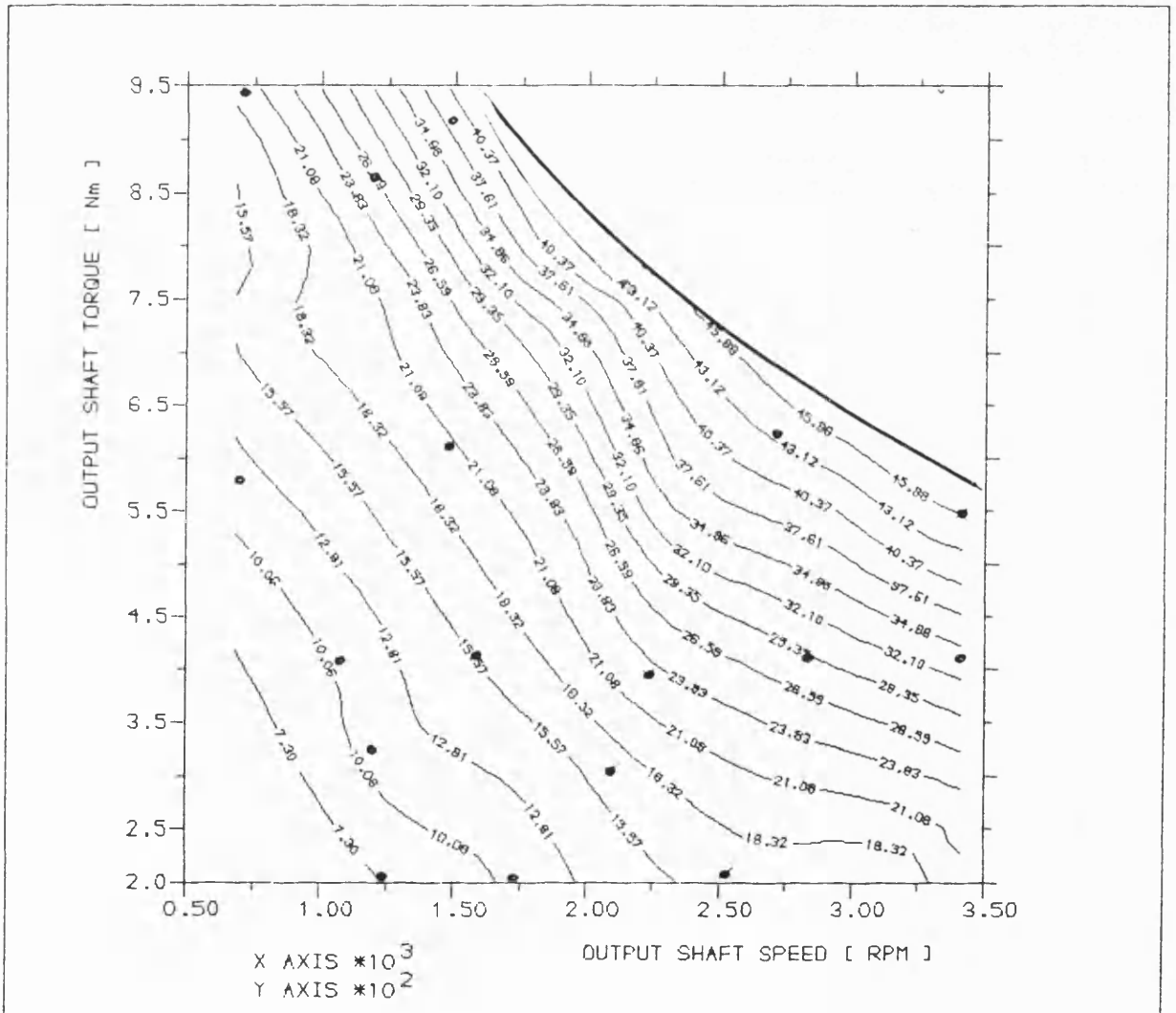

Fig. 8,9,e Contours of gear losses (adjusted simulation)

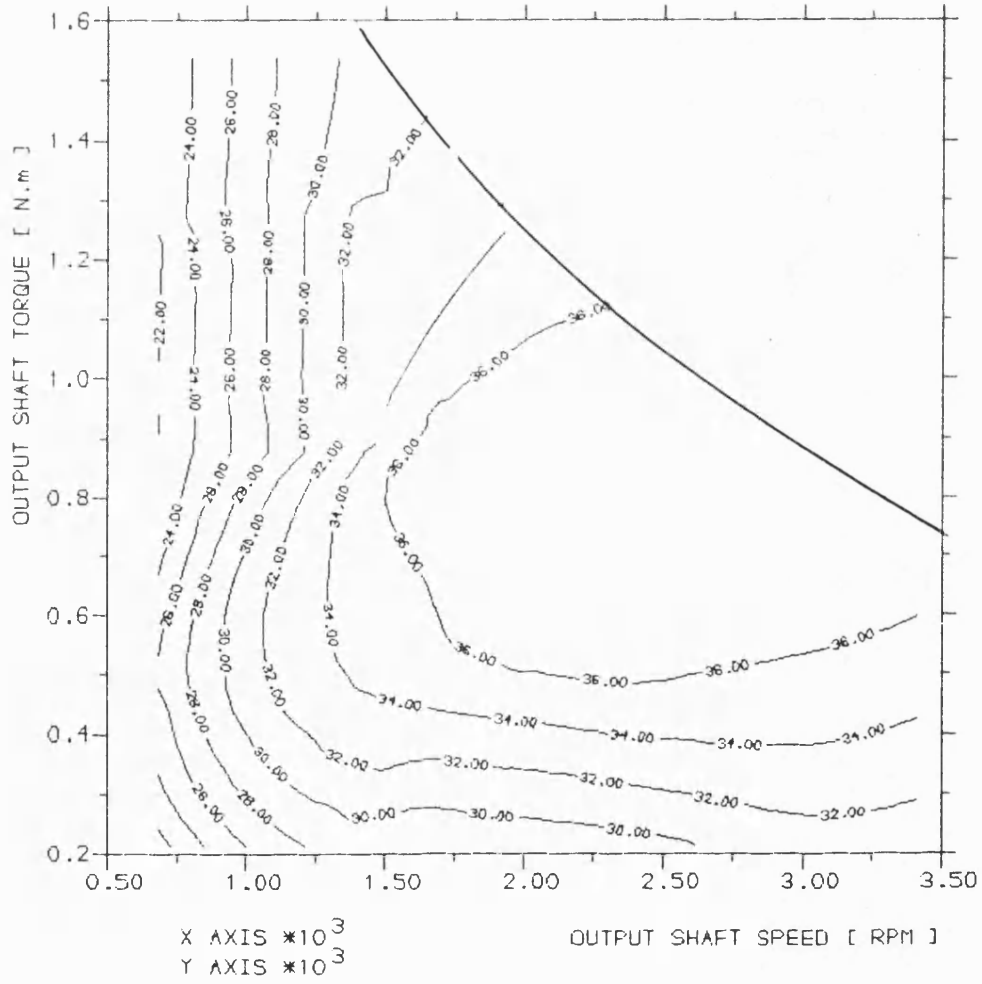

Fig. 8.10,a Contours of output shaft efficiencies (tentative gear losses)

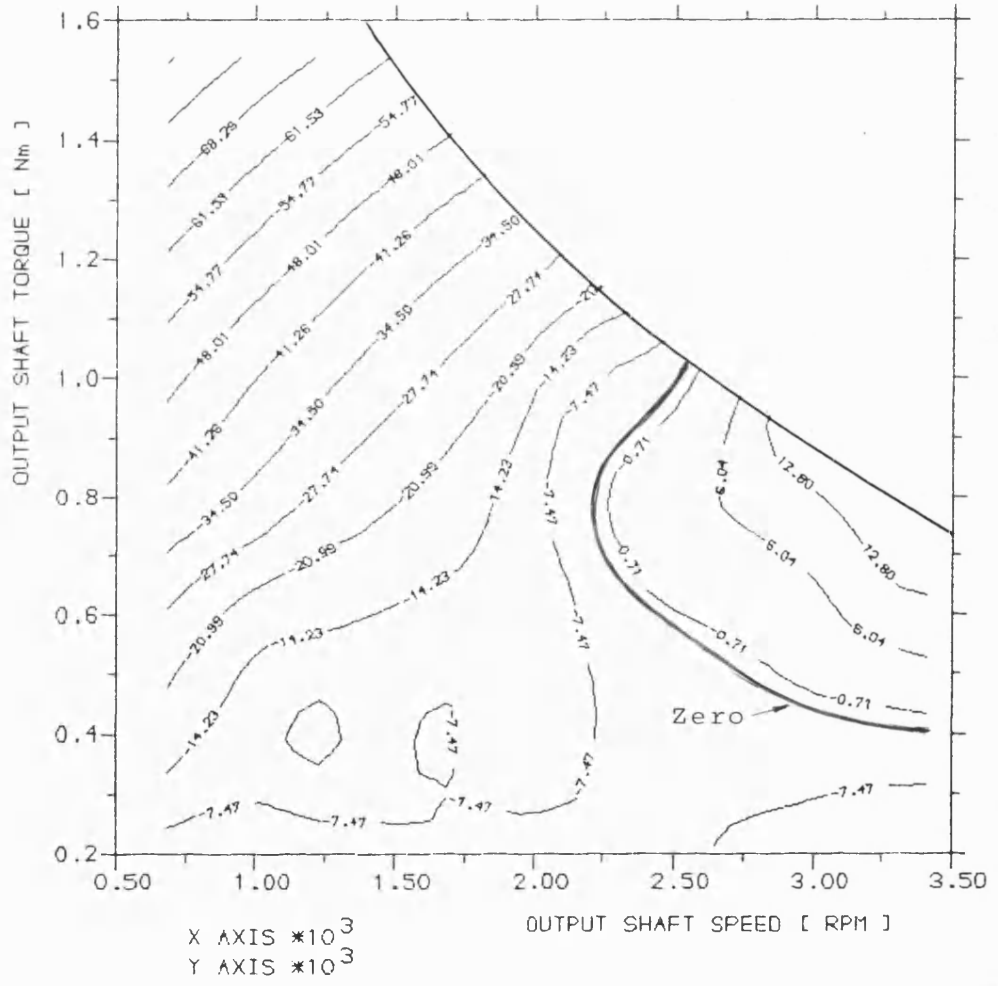

Fig. 8.10,b Contours of compounding effects (tentative gear losses)

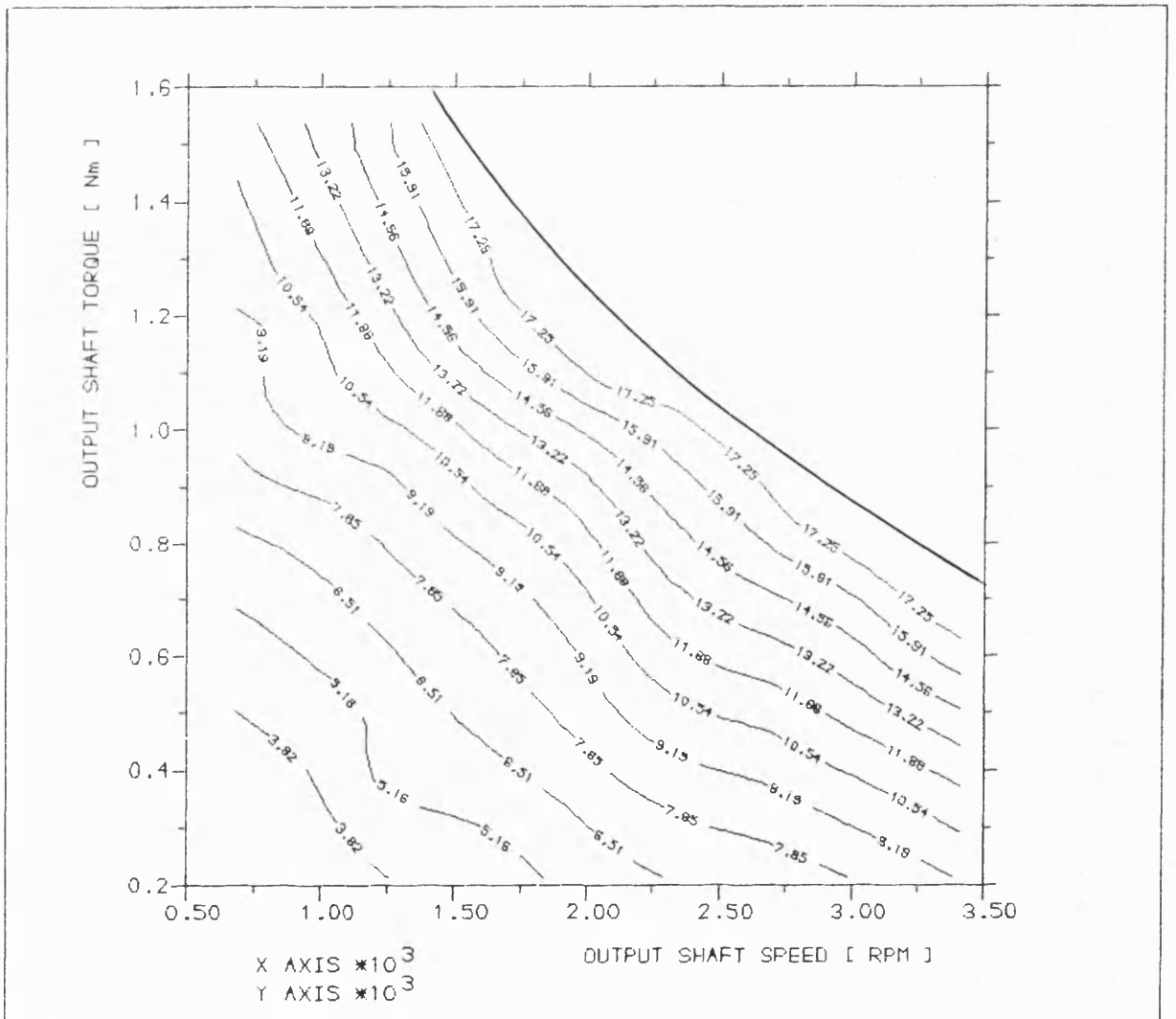

Fig. 8.10,c Contours of gear losses (tentative gear losses)

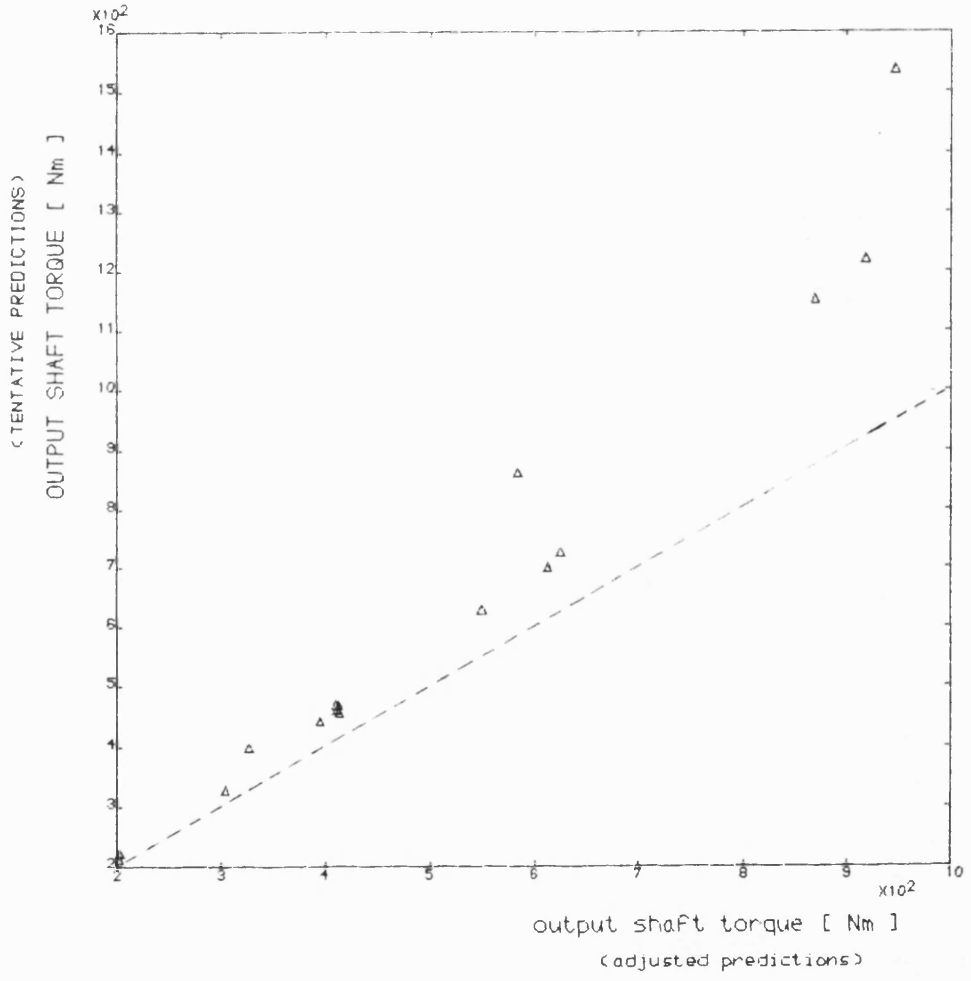

Fig. 8.11,a Comparison of output shaft torques obtained from simulations of prototype and those based on tentative gear losses

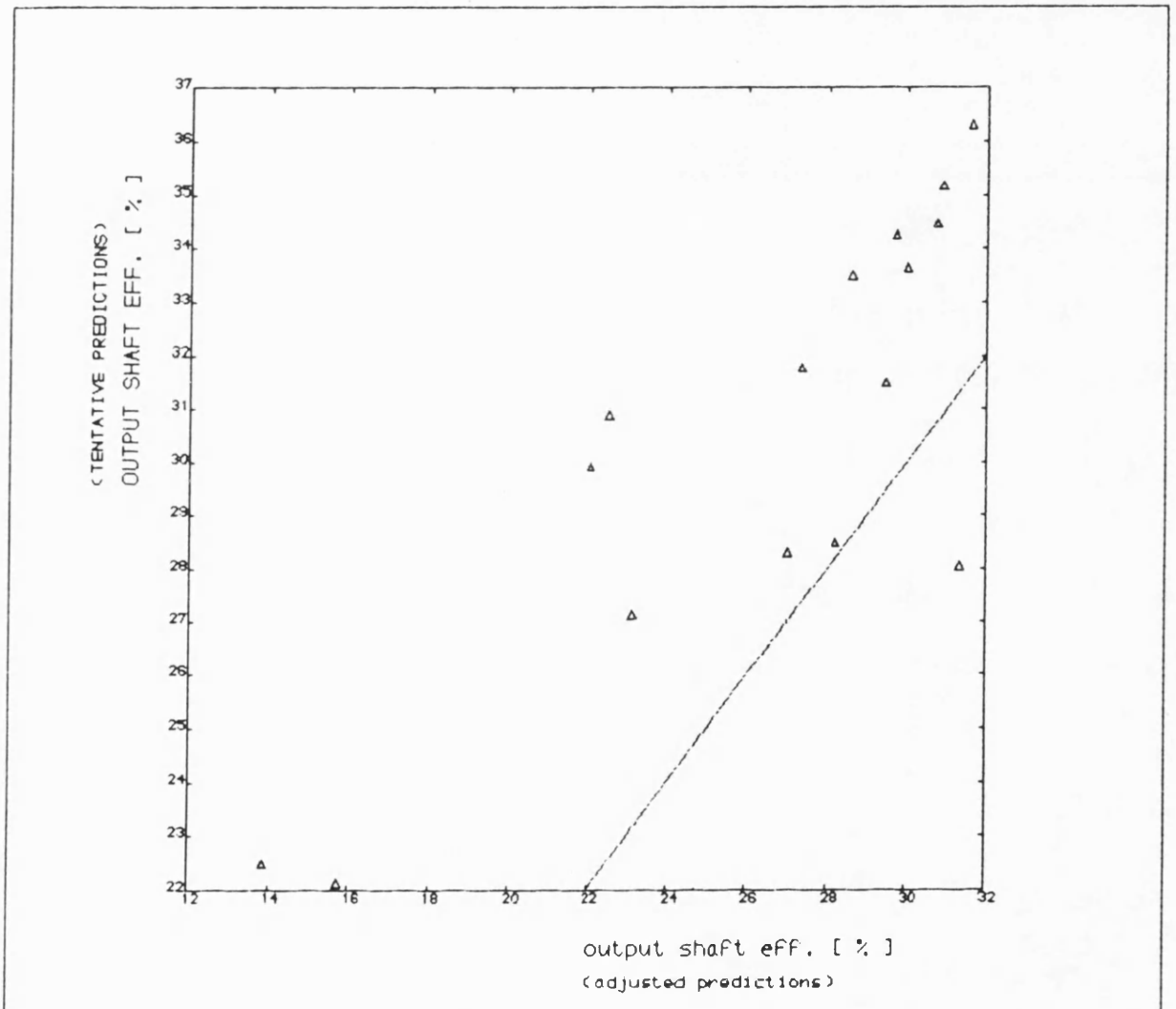

Fig. 8.11,b Comparison of output shaft efficiency obtained from simulations of prototype and those based on tentative gear losses

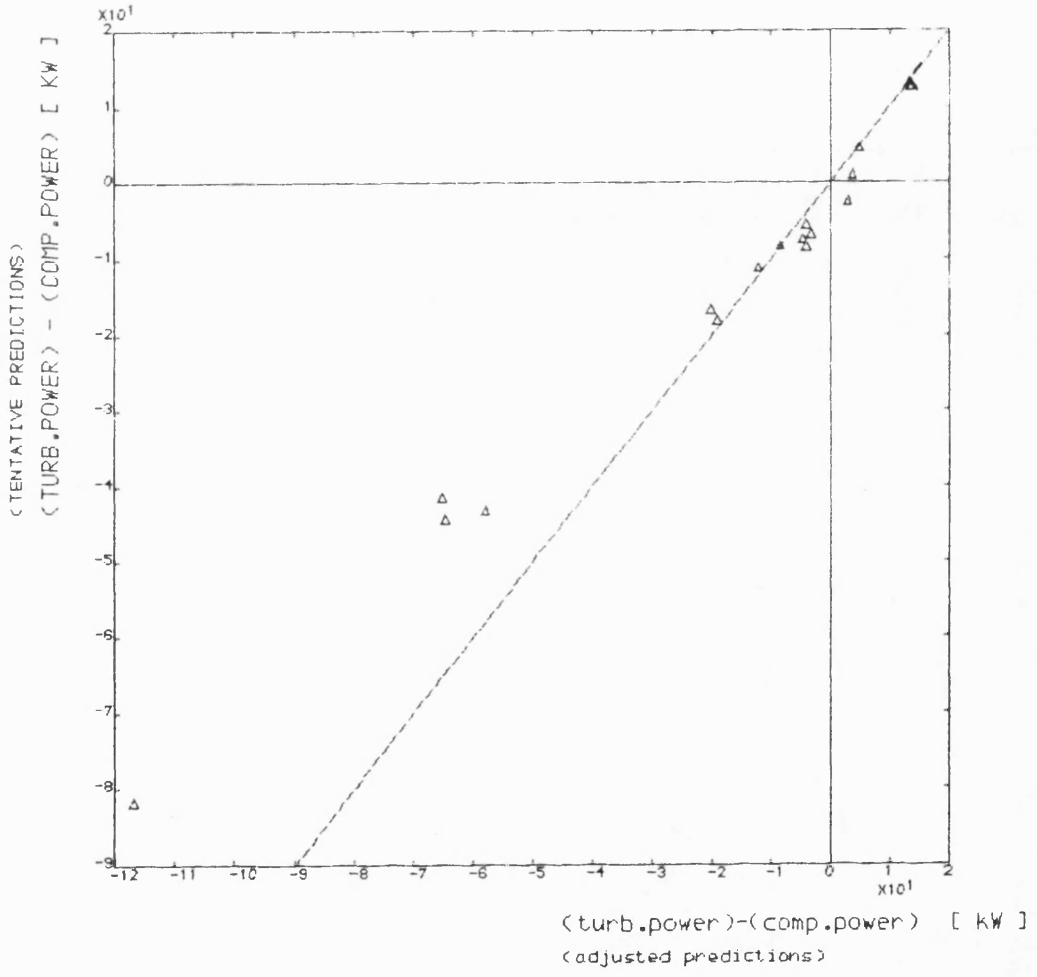

Fig. 8.11,c Comparison of compounding effect obtained from simulations of prototype and those based on tentative gear losses

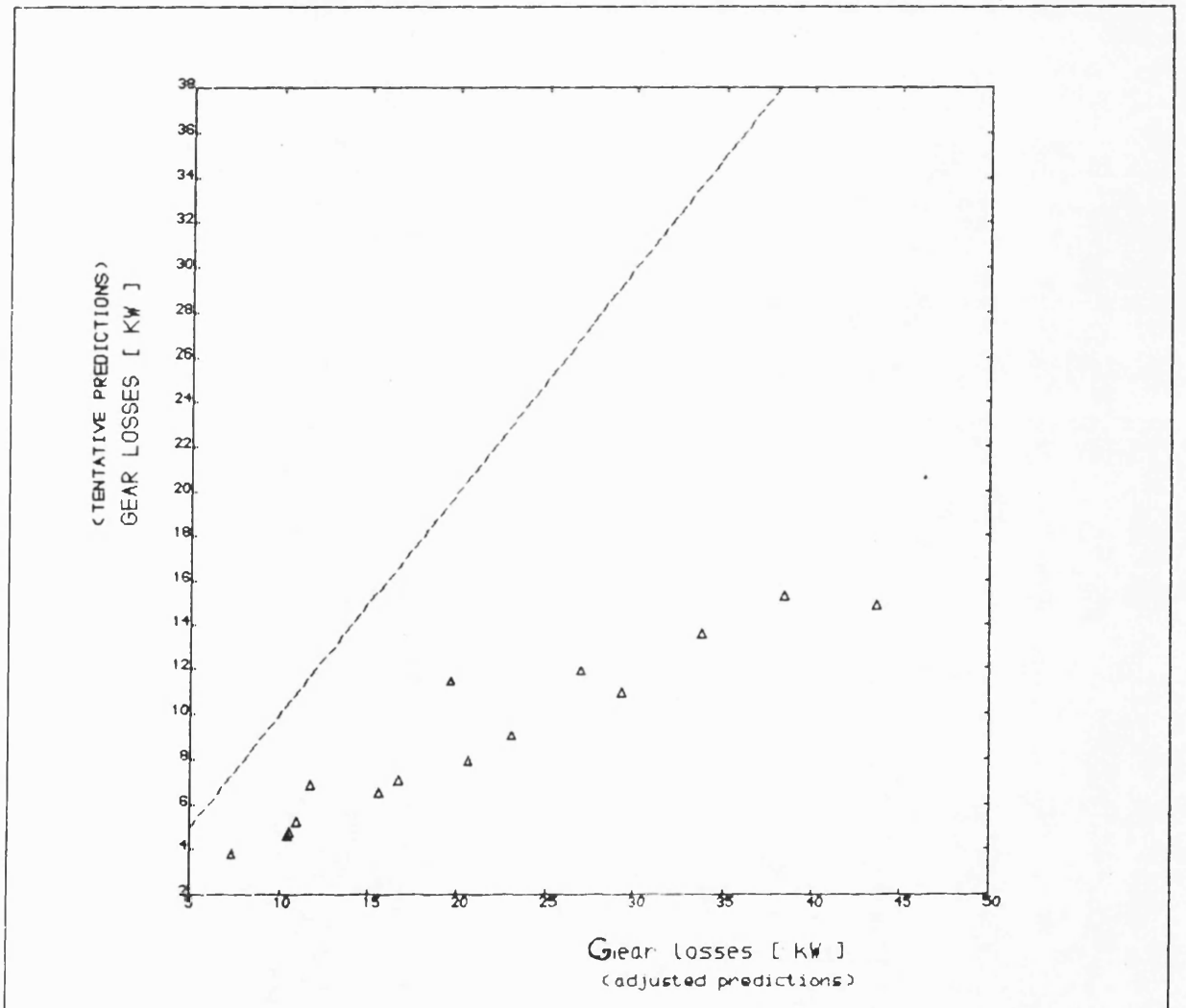

Fig. 8.11,d Comparison of gear losses obtained from simulations of prototype and those based on tentative gear losses

CHAPTER NINE

CONCLUSIONS AND RECOMMENDATIONS FOR FURTHER WORK

The thesis describes a predominantly theoretical investigation of the operating characteristics of a high output Diesel engine. (The Cummins L10) in two basic configurations, viz.

a) as an aftercooled turbocharged engine
b) as a differential compound engine

9.1 PROGRAMMING TECHNIQUES

Three basic programming techniques have been employed, viz.

a) a rapid prediction technique for steady state performance - programs EMAT and DCE2

b) a detailed step-by-step technique based on filling and emptying which can be used for both steady state and dynamic performance predictions, viz.
   program SPICE for the T/C engine
   " CSPDCE " " DCE

c) a rapid prediction technique for transient performance derived from(a) -
   program TRANIC for the T/C engine
   " DCETRAN " " DCE
   (The latter not included in this thesis)

The main conclusions from the use of these programs are :-

i) the rapid prediction programs EMAT and DCE2 yield results of acceptable accuracy provided the numerous empirical constraints are well matched against some initially available experimental results.

ii) the step-by-step programs SPICE and CSPDCE require much more

extensive input than EMAT and DCE2. While providing much more detailed information concerning thermodynamic and mechanical behaviour throughout the cycle, these programs still require calibration against initially available experimental results, especially with respect to heat release.

Since these detailed programs (SPICE and CSPDCE) are rather costly to run, they were used only to validate the predictions of the simple programs (EMAT and DCE2) for some selected points.

As regards the detailed simulation of the DCE, the program CSPDCE had to be modified as already described in Chapter 6, Section 6.4, the object being to run at predetermined shaft speeds and engine power, and thus to achieve direct comparability with the results of the rapid simulation program DCE2.

iii) the transient prediction program TRANIC is an effective tool for following the performance of the turbocharged engine under accelerating conditions, during gear change and when combined with a vehicle subroutine, for detailed analysis of the complete engine-transmission-vehicle system.

9.2 COMPARISONS BETWEEN THE TWO MAJOR ENGINE SYSTEMS, i.e. T/C and DCE

The present study has aimed at providing a comprehensive and balanced comparison of the performance characteristics of the two systems. For this purpose compatible simulations have been developed under the 3 headings already referred to, viz.

a) simplified steady state predictions
b) detailed step-by-step predictions
c) transient predictions

In order to ensure comparability of the two systems, identical engine ratings and similar torque back up characteristics were assumed. The use of a 7 speed gearbox with the turbocharged engine and a torque converter with the DCE gave similar output shaft torque envelopes. The following comparisons summarize the behaviour of the two systems :-

a) Steady state characteristics by simplified predictions

The DCE achieves the major objective of continuous torque back up combined with high efficiency over the major part of the operating range. Only at very low output shaft speeds does the thermodynamically wasteful bypassing of air cause a serious loss of system efficiency.

The engine in turbocharged form undoubtedly achieves high efficiencies, in this case extending into the low speed regime, but its torque characteristics necessitate a multi ratio gearbox.

From an emission standpoint it is significant that the DCE operates consistently with trapped air-fuel ratios in excess of 28:1 while the turbocharged engine operates, in general, at some 5 ratios below this.

b) Steady state charact eristics by step-by-step predictions

The step-by-step predictions were adopted in order to permit detailed comparisons for the two systems of cyclic pressure, mass flow and temperature fluctuations, as well as heat release and heat transfer characteristics. The aspects of greatest interest were :

i) bypass flow (in the DCE),

ii) pumping loop work (in the DCE),

iii) relative thermal loading.

i) Bypass flow fluctuations are pronounced and at high output shaft speeds can lead to nett negative flow, i.e. from the exhaust to the inlet manifold. At low output shaft speeds, with large excess air, the bypass flow is always positive, but the fluctuation amplitude is larger.

ii) Pumping loop work is substantial in the DCE due to the negative pressure gradient existing between the inlet and the exhaust manifold. This leads to some reduction in engine brake thermal efficiency compared with the turbocharged engine, amounting to approx. 1 percentage point at the design point, from approx. 41% to 40%.

iii) Thermal loading, as expressed by piston crown temperature, is not a serious problem in the DCE in spite of the high rating, rising from 249C under rated conditions to 257C under stall conditions at a BMEP of 21.46 bar.

c) Transient performance of the DCE is demonstrably greatly superior to that of the turbocharged engine, both for a simple step response at fixed output shaft speed, but more importantly when comparing vehicle response. The test case of a 65000 lb truck showed that after 10 sec. the DCE powered truck travels over twice as fast as the T/C powered truck, with speeds of 40 and 18 km/hr respectively, the corresponding figures after 50 sec. being 77.8 and 66.8 km/hr respectively. Similarly in terms of cumulative fuel consumption, the wasteful gear change procedure leads to a significant increase in consumption, particularly in the early stages of frequent gearchanges.

9.3 RECOMMENDATIONS FOR FURTHER WORK

a) The various simulation programs described in the thesis comprehensively cover the steady state and transient performance characteristics of the DCE and of turbocharged engines.

b) The complete vehicle simulations are limited, at present to acceleration from rest and should be supplemented by route simulations.

c) The experimental rig, although comprehensively instrumented, still has several shortcomings. In particular, the division of power within the epicyclic gearbox requires further instrumentation in the form of high speed torquemeters for the turbine and preferably also for the compressor.

d) The experimental optimization work would be greatly facilitated by the implementation of an on-line optimization routine as part of a microprocessor control system.

REFERENCES

1. Agres, R.V. and McKenna, R.P.
   "Alternatives to the Internal Combustion Engine"
   The John Hopkins University Press, Baltimore, M.D, 1972.

2. Myers, P.S.
   "The Diesel Engine for Truck Application"
   S.A.E. SP-391, Feb. 1975.

3. Holmer, E. and Häggh, B.
   "The Turbocharged Diesel as a Road Transporter Power Unit"
   Proc.I.Mech.E., Vol. 184, Part 3P, 1969-70.

4. Dinger, H. and Deutschmann, H.
   "Further Development of the MTU 956/1163 Series Engines"
   Paper D72 CIMAC, Helsinki, 1981.

5. Not obtainable

6. S.A.E. Handbook, Vol. 3.
   "Engines, Fuels, Lubricants, Emissions and Noise"
   Section 25, 1988.

7. Harris, C.M.
   "Handbook of Noise Control"
   McGraw Hill, Inc. 1979.

8. Janota, M.S.
   "Vehicle Engine Fuel Consumption and Air Polution"
   Paper : "Anti-Polution Legislation" by Draper, P.,
   1974.

9. Watson, N.
"Turbochargers and Turbocharged Engines"
S.A.E. SP-442, 1979.

10. Wallace, F.J., Ghadiri-Zareh, M.S. and Myers, J.
"Matching of Turbocharged Diesel Engines with Fluid Couplings and Multi-Speed Planetary Gearboxes for Best Efficiency",
I.Mech.E. Conf. on Land Transport Engines, Paper C22/77, p.221
Jan. 1977.

11. Dawson, J.G., Hayward, W.J. and Glamann, P.W.
"Some Experiences with a Differentially Supercharged Diesel Engine",
Proc.I.Mech.E. Automobile Div., Vol. 178, Part 2A, No.6, 1963-674.

12. Hooker, R.
"Orion, a Gas Generator, Turbo-Compound Engine",
S.A.E., 1957.

13. Chatteron
"The Diesel Engine in Association with the Gas Turbine",
Proc.I.Mech.E., Vol. 174, p.409, 1960.

14. Wallace, F.J.
"Operating Chargeristics of Compound Engine Schemes for Traction Purposes based on Opposed Piston Two Stroke Engines with Differential Gearing",
Proc.I.Mech.E, Vol.177, No.2, 1963.

15. Smyth, R. and Wallace, F.J.
"Comparative Performance Assessment of Various Compression Ignition Engine Configurations in Combination with Compressors and Turbines",
I.Mech.E, London, Dec. 1966.

16. Wallace, F.J., Few, P.C. and Cave, P.R.
"The Differential Compound Engine - Further Development",
S.A.E Congress, Detroit, Jan. 1971.

17. Wallace, F.J., Tarabad, M. and Howard, D.
"The Differential Compound Engine - a New Integrated Engine Transmission System Concept for Heavy Vehicles",
Proc.I.Mech.E, Vol.197A, Feb. 1983.

18. M.Sc. Notes, School of Mechanical Engineering, University of Bath.
"Engine Performance Analysis".

19. Tarabad, M.
"EMAT (Engine Matching Computer Program) User's Manul",
University of Bath, 1983.

20. Charlton, S.J.
"SPICE (Simulation Program for Internal Combustion Engine)",
University of Bath, 1985.

21. Wiebe, I.
"Halbempirische Formel für die Verbrennungs-geschwindigkeit",
Verlag de Akademic der Wissenschaften der VdSSR, Moscow, 1967.

22. Watson, N., Marzouk, M. and Pilley, A.D.
"A Combustion Correlation for Diesel Engine Simulation",
S.A.E 800029, Diesel Combustion and Emission SP86, Feb. 1980.

23. Wolfer, H.H.
"Ignition Lag in the Diesel Engine",
VDI-Forschungsheft No. 392, 1938, Trans. by Royal Aircraft Establishment, 1938.

24. Woschni, G.
"A Universally Applicable Equation for the Instantaneous Heat Transfer Coefficient in the Internal Combustion Engine",
S.A.E Report No. 670931, 1967.

25. Hohenberg, G.F.
"Advanced Approaches for Heat Transfer Calculations",
S.A.E Report No. 790825, 1979.

26. Eichelberg, G.
"Some New Investigations on Old Combustion Engine Problems",
Engineering, Oct-Dec. 1939.

27. Annand, W.J.D.
"Heat Transfer in the Cylinders of Reciprocating Internal Combustion Engines",
Proc.I.Mech.E, Vol.177, No.36, 1963.

28. Rogers, G.F.C. and Mayhew, Y.R.
"Engineering Thermodynamics : Work and Heat Transfer"
3rd ed., Longman Group Ltd., 1980, and
"Thermodynamic and Transfer Properties of Fluids",
3rd ed. The Camelot Press Ltd., 1980.

29. Chen, S.K. and Flynn, P.
"Development of a Compression Ignition Research Engine"
S.A.E 650733, 1965.

30. Shipinski, J., Uyehara, O.A. and Myers, P.S.
"Experimental Correlation between Rate of Injection and Rate of Heat Release in a Diesel Engine",
A.S.M.E Paper - 68 DGP11 (1968).

31. Not obtainable

32. Watson, N.
"Combustion and Gas Properties"
Presented at Dept. of Mechanical Engineering, Imperial College of Science and Technology, Sept. 1979.

33. Krieger, R.B. and Boreman, G.L.
"The Computation of Apparent Heat Release for Internal Combustion Engines",
A.S.M.E., Paper 66-WA/DGP-4, 1966.

34. Dutcher, F.J.
"The Friction of Reciprocating Engines",
Trans.A.S.M.E., Vol.60, April 1938.

35. Ricardo, H.R.
"The High-Speed Internal Combustion Engine",
Blackie and Son, Ltd. 1953.

36. Mueller, H.T. and Pfundstein, K.L.
"Survey of Engine Losses Reported"
S.A.E. Journal, pp. 42-45, March 1949.

37. Lilly, L.R.C.
"Diesel Engine Reference Book",
Butterworth and Co. Ltd., 1984.

38. Horlock, J.H.
"Thermodynamics and Gas Dynamics of the internal Combustion Engines"
Vol.2, Oxford Clarendon Press, 1982.

39. Prince, D.
"Design Build and Steady State Test of a Differential Compound Engine",
Ph.D Thesis, University of Bath, 1987.

40. Abdalla, E.A.
"Optimization and Control of the Differential Compound Engine",
Ph.D Thesis, University of Bath, 1983.

41. Roberts, E.W.
"Variable Geometry Turbocharging Optimization and Control",
Ph.D Thesis, University of Bath, 1984.